Understanding the role of PAX6 in Corneal Epithelial Regulation at the Limbal Niche

Thesis submitted for the degree of

DOCTOR OF PHILOSOPHY

To

THE DEPARTMENT OF ANIMAL BIOLOGY
SCHOOL OF LIFE SCIENCES
UNIVERSITY OF HYDERABAD
HYDERABAD – 500 046
INDIA

By

P. Vinay Kumar

Under the supervision of

Dr. Indumathi Mariappan

LV Prasad Eye Institute

Co supervisor

Dr. A. Bindu Madhava Reddy

University of Hyderabad

Sudhakar and Sreekanth Ravi Stem Cell Biology Laboratory
Prof. Brien Holden Eye Research Centre
L V Prasad Eye Institute
Hyderabad- 500 034

February 2022

Enrolment No: **15LAPH13**

University of Hyderabad
Hyderabad-500 046, India

CERTIFICATE

This is to certify that this thesis entitled "*Understanding the role of PAX6 in corneal epithelial regulation at the limbal niche*" submitted by **Mr. P Vinay Kumar** bearing registration number **15LAPH13** in partial fulfillment of the requirements for the award of Doctor of Philosophy in the Department of Animal Biology, School of Life Sciences, is a bonafide work carried out by him under my supervision and guidance. This thesis is free from plagiarism and has not been submitted previously in full or parts, have not been submitted to any other University or Institution for the award of any degree or diploma.

Parts of this thesis have been:

A. Published/Under review

1. Susaimanickam PJ, Maddileti S, **Pulimamidi VK**, Boyinpally SR, Naik RR, Naik MN, Reddy BG, Sangwan VS and Mariappan I. Generating minicorneal organoids from human induced pluripotent stem cells. *Development*. 2017 Jul 1;144(13):2338–51. DOI: 10.1242/dev.143040
2. **Kumar V**, Ali MJ, Ramachandran C. Effect of mitomycin-C on contraction and migration of human nasal mucosa fibroblasts: implications in dacryocystorhinostomy. *Br. J. Ophthalmol*. 2015 Sep; 99(9):1295-300. DOI: 10.1136/bjophthalmol-2014-306516
3. **Pulimamidi VK**, Maddileti S, Mariappan I. Human PAX6 and its target gene regulation by Wnt signals in ocular cells. Sci Rep. 2021; (Manuscript under review).

B. Presented in the following conferences

1. Poster presentation of a paper titled "**Human PAX6 promoter A and its regulation in LSCS**" at the Hy-Sci 2019-CCMB, Hyderabad.
2. Poster presentation of a paper titled "**Differential regulation of human PAX6 promoters in different ocular cell types**" at the IERG-ARVO 2019-Chennai.
3. Poster presentation of a paper titled "**Differential regulation of human Pax6 promoters and the surface ectoderm enhancer in different ocular cell types**" at the IERG-ARVO 2017-Madurai.

Further, the student has passed the following courses towards fulfillment of coursework requirements for Ph.D.

Name	Credits	Pass/Fail
Molecular Genetics	4	Pass
Research Ethics	2	Pass
Biostatistics	2	Pass
Cell Biology	4	Pass

Dr. Indumathi Mariappan
Supervisor

Dr. A. Bindu Madhava Reddy
Co-Supervisor

Dr. A. Bindu Madhava Reddy
Assistant Professor
Dept. of Animal Biology
School of Life Sciences
University of Hyderabad
Hyderabad-500 046.

K. Seeniraseth

Head,
Department of
Animal Biology

अध्यक्ष / HEAD
जंतु जैविकी विभाग
Department of Animal Biology

Dean,
School of Life
Sciences

DEAN
School of Life Sciences
University of Hyderabad
Hyderabad-500 046.

HYDERABAD EYE RESEARCH FOUNDATION
HYD.

University of Hyderabad
School of Life Sciences
Department of Animal Biology
Hyderabad-500 046, India

CERTIFICATE

This is to certify that this thesis entitled "***Understanding the role of PAX6 in corneal epithelial regulation at the limbal niche***" submitted by **Mr. P Vinay Kumar** bearing registration number 15LAPH13 for the degree of Doctor of Philosophy to the University of Hyderabad is a bonafide record of research work carried out by him at the L.V. Prasad Eye Institute, Hyderabad under my supervision. The contents of this thesis, in full or parts have not been submitted to any other University or Institution for the award of any degree or diploma. I hereby, recommend his thesis for submission, for the award of the degree of Doctor of Philosophy from the University.

Dr. Indumathi Mariappan
Supervisor

HYDERABAD EYE RESEARCH FOUNDATION HYD.

Dr. A. Bindu Madhava Reddy
Co-Supervisor
Dr. A. Bindu Madhava Reddy
Assistant Professor
Dept. of Animal Biology
School of Life Sciences
University of Hyderabad
Hyderabad-500 046.

Head,
Department of
Animal Biology
अध्यक्ष / HEAD
जंतु जैविकी विभाग
Department of Animal Biology

Dean,
School of Life Sciences
DEAN
School of Life Sciences
University of Hyderabad
Hyderabad-500 046.

University of Hyderabad
School of Life Sciences
Department of Animal Biology
Hyderabad-500 046, India

DECLARATION

I, **P Vinay Kumar** hereby declare that this thesis entitled "***Understanding the role of PAX6 in corneal epithelial regulation at the limbal niche***" submitted by me under the guidance and supervision of **Dr. Indumathi Mariappan**, is an original and independent research work. I also declare that it has not been submitted to any other University or Institution for the award of any degree or diploma.

P. Vinay Kumar

Date: 16th February 2022

P Vinay Kumar
15LAPH13

DEDICATED TO

MY LOVING AMMA

AND

DR. INDU

ACKNOWLEDGEMENTS

This Ph.D. thesis work is an important milestone in my life. I have carried out this work under the supervision of **Dr. Indumathi Mariappan** at LV Prasad Eye Institute. This work would not have been possible without the involvement of many brilliant minds and I would like to take this opportunity to extend my sincere gratitude and appreciation to all those who made this Ph.D. work possible and memorable.

First and foremost, I would like to express my sincere gratitude to my supervisor, **Dr. Indumathi Mariappan** for offering me this Ph.D. position. I am thankful to her for the constant support and guidance. Whenever I got stuck in any experiment, she was always available with her valuable suggestions. She is not just a supervisor, but also a real multitasker and plays multiple roles in the lab. She is a scientist, a troubleshooter and an advisor at the same time. If some experiment doesn't work even after multiple trials, she also turns herself into a student who performs the experiment in every possible way to make it work. She has this 'never give up' quality imbibed in her and has also taught us the same, both in science and life. Apart from science, she is also like a caring mother, who takes care of us, who never misses getting delicious food for us at festivals, and I must say, I am the only lucky one to relish lunches cooked by Ma'am during the lockdown. Her passion for science inspires me and keeps us all motivated in the lab. I feel very fortunate that I received an opportunity to train myself under her mentorship.

I would also like to thank **Dr. Bindu Madhav Reddy**, Department of Animal Biology, University of Hyderabad (UoH) for accepting to be my co-supervisor and helping me to move my thesis process more swiftly.

I would like to thank all HoDs of the Department of Animal Biology, University of Hyderabad (UoH) during the Ph.D. tenure: **Prof. B. Senthil Kumaran**, **Prof. Jagan Pongubala**, **Dr. Anita Jagota** and **Dr. Sreenivasulu Kurukuti**; The Deans, School of Life Sciences, UoH during the Ph.D. tenure: Prof. **A.S. Raghavendra**, **Prof. P. Redanna**, **Prof. K.V.A. Ramaiah**, **Prof. S. Dayananda**; the Controller of Examinations and the School Board for all the administrative help and access to the University infrastructures.

I would like to extend thanks to my DAC members **Dr. Chitra Kannabiran** and **Dr. S Shivaji** for their insightful advice on my research as well as on my career.

I would like to thank the founder of LV Prasad Eye Institute **Dr. Gullapalli Nageshwara Rao**, Chairman **Dr. Prashant Garg**, Director Emeritus **Prof. Dorairajan Balasubramanian** and Director of research **Dr. Sayan Basu**, LVPEI for providing world-class infrastructure and laboratory facilities and for granting me an opportunity to carry out my doctoral research

work. I thank LVPEI for arranging informative lectures, seminars, and occasions to meet eminent scholars from various fields.

My sincere thanks also goes to **Dr. Charanya Ramachandran** for introducing me to research for the first time in LVPEI and for teaching me all the basic cell culture techniques.

I would like to specially thank **Mrs. Savitri Maddileti** for her all-time immense support, encouragement and care, professionally and personally. She has always treated me like her family, and has been a part of every episode of my life in LVPEI, who always showered me with love and care. Savitri Garu has a very strong voice and is quite straightforward in her thoughts. Me being an introvert, she has always advised and helped me to present my point of view in front of Ma'am. Before I joined LVPEI, she was the one, who initiated Pax6 work, which I continued further. Without her efforts, I wouldn't have chosen this work for my Ph.D!! Thank you **Savitri Garu** for always being there like a rock-solid pillar of support for me and for always having my back.

Ph.D. is a long and overwhelming journey with many highs and lows, but if one has good company, then then no one can stop it from becoming a memorable one!!!… I can say that I have wonderful lab members who made this journey unforgettable, beautiful and easier. In this list, the first name has to be **Dr. Praveen Joseph**, my senior, and more of a buddy. I have spent the maximum of my time with him, be it in the lab or outside. I can't recall of any outing, party or get-together where he wasn't there with me. We were like two musketeers always hanging out together, who even share same birthday!! He has always encouraged me during my PhD. I am glad that I met you 'Mama' and had you as a friend in this journey, and I miss you being here after you left for U.S. **Ms. Sudipta Mahato** was constantly there to help me out with my wet lab work. I have not met anyone before who is equally bold and sensitive at the same time, whose energy is like a morning dose of caffeine that never gets out of charge. Thank you 'Pittu' for being the constant in my life. **Ms. Trupti Agrawal**, the 'chotu' of our lab, always carries a contagious smile on her face throughout the day. I have never seen her getting tired of work. Thank You 'chotu' for all your timely advice and support in the thesis write-up. But still, it doesn't make up for the fact that you never gave a single non-veg party to us. Our lab is incomplete without **Ms. Divya Pidishetty**, whose crazy jokes and humor always brought laughter and smiles in the lab. We are like 'Tom and Jerry', who had endless episodes of fights, but always ended up with patch-up. Thank you Divya for all the help, food, and fun at the same time. **Santhosh Damera** is the most diet conscious member in our lab. I cherished a brief period with him as a room-mate. The most recent one is **Sadab Khan**, who is always eager to learn new things. It's not an exaggeration if I mention that I couldn't have got any better labmates than them, who have become more of a family to me. Be it a

presentation, or meeting deadlines, or working on Sundays, or partying on weekends, they have always been by my side. I would like to thank to each one of them for always being there throughout these years.

I would like to thank the two people who were there when I joined LVPEI - **Dr. Pulla Rao Vendra** and **Dr. Praveen Kumar Balne**, my first roommates and very good seniors. In the room, it was fun to learn from them.

In this Ph.D. journey, I made friends for lifetime. I would like to thank **Meha**, **Satish**, **Shahana**, **Sonika**, **Praveen, Ranjith,** and **Rishi** for always being there. We formed a wonderful gang that I still cherish. The weekend masti restricted to Sunday was also enough for us as an LVPEIan. We used to cook, eat, and make fun of each other. These moments will be captured in my memories that I would cherish for lifetime!!

Dr. Abhinav Kethri and **Mr. Mukesh Damala**, these two people are the most calm and composed that I have met in LVPEI. I admire them for their determination in finishing the work they take up; being it related to the instrumental error correction or organizing SECRET SANTA to bring everyone close to celebrate.

I especially thank **Chandrika Garu** for her assistance and guidance in the confocal imaging.

I would like to thank my seniors, friends, and colleagues at LVPEI: **Dr. Pulla Rao Vendra**, **Dr. Ganeswara Rao Musada**, **Dr. Praveen K Balne**, **Dr. Srinivasu K**, **Mr. Nanda Shivshankar**, **Ms. Puja Sarkar**, **Mr. Rishikesh Gupta**, **Ms. Swatilekha Hazra**, **Ms. Jilu Jaffet**, **Ms. Jacquelyn**, **Ms. Sneha Isakala**, **Mr. Salman**, **Mr. Sameer**, **Mr. Goutham**, **Ms. Deeksha**, **Dr. Khatija Tabassum**, **Dr. Derin Thomas**, **Sushma Viswakarma, Ms. Jayashree Gandhi**, **Ms. Poonam Naik** and **Ms. Satyashree**.

I thank my current roommates **Shashi** and **Madhu** for cooking food for me and for the everyday fun we have during sleep time.

I would like to thank **Dr. Dilip. K. Mishra**, Consultant Pathologist, and **Mr. Sreedhar Rao Boyinpally** and **Chenchu Naidu**, for their support and providing the tissue sections on time.

I also thank Ramayamma international eye bank and **Mr. Srinivas** for providing cadaveric donor corneas for my experiments. Without those tissues, my work would not have run smoothly. I want to thank all the people who generously donated their eyes, and also my deep condolences to the family members who lost their loved ones.

I would like to thank the staff of LVPEI, **Ms. Elena D Roopchandra**, **Srinivas**, **Mr. K Poorna Chandar Rao** and **Mr. Ramulu** from BHERC for managing all the administrative and financial support over the years, **Ms. Neha Hasija** and **Mr. Yedukondalu** from Communication department for their help in scientific poster preparation.

I would also like to thank Hyderabad Eye Research Foundation (HERF) and Champalimaud Translational Centre for Eye Research and Prof. Brien Holden Eye Research Centre for extending financial and infrastructure support.

I thank **Ms. Sabera Banu**, **Mr. Sudhakar Kothapalli**, and **Mr. Quddus** from Library for helping me in getting all the books, articles, and photocopies needed for my research work.

I thank ISD (**Shiva**, **Sunil**) and the Purchase dept. (**Jagadesh**) for their constant support and services.

Last, but not the least, it would have been impossible for me to persue this if I wouldn't have had the immense and constant support from my family; my **Amma**, **brothers** and **sisters-in-law**. My amma is the source of energy and the ray of hope in my life. She had never imposed the burden of responsibility on me while growing up, fought against every odds in life, and stood by me to help me pursue higher studies. She has been Amma as well as Appa for me. After all your sacrifices and endless sleepless nights, hope I have made you proud Amma. Thank you amma for always holding my hand through all situations that life offered us.

And thank you God for being by my side!!

Vinay Kumar Pulimamidi

LVPEI, Hyderabad

ABSTRACT

Cornea is the transparent and avascular tissue on the anterior surface through which the light enters the eye. The corneal surface epithelial layer undergoes regular sloughing and is constantly replenished by the stem cells (LSCs) located at the corneal periphery called the "Limbus". It is well known that the PAX6 gene is the master regulator of eye development and is important for corneal epithelial fate determination and maintenance. Mutations in the *PAX6* gene are known to cause aniridia and results in limbal stem cell (LSC) failure and impaired anterior segment development. Conversely, the overexpression of PAX6 in the eye results in abnormal lens, retinal and corneal development, with marked defects in corneal epithelial proliferation and adhesion in adult corneas. But the exact involvement of PAX6 in regulating limbal stem cell proliferation vs differentiation fate decisions and its effects on cornea-specific gene targets remain unclear. Therefore, this study is aimed to understand the differential regulation of human *PAX6* promoters and the expression of different PAX6 isoforms in native ocular tissues and cell lines. Luciferase reporter assays confirmed that *PAX6* promoters are differentially regulated in different ocular cells and the distal *PAX6*-pA promoter was the predominant promoter that drives the expression of PAX6 in the eye. The earlier characterized ocular surface ectoderm (OSE) enhancer actually regulates corneal epithelial development by repressing the pA promoter in corneal epithelial cells and by enhancing its activity in lens and retinal epithelium. To maintain the stoichiometry and optimal levels of PAX6 in a cell, *PAX6* promoters are tightly regulated and maintained in a repressed state in ocular cells by the recruitment of HDACs (Histone deacetylases) and Kaiso repressor complexes. Upon stem cell activation, the canonical Wnt signals activates the *PAX6*-pA promoter in a sub-set of transiently amplifying cells (TACs), by the direct binding of β-catenin of to the TCF/LEF1 consensus site and increases PAX6 protein expression. The Wnt signals also induced the activity of TAp63, KRT3 and KRT12 expression and together promote TAC expansion and differentiation. A further increase in PAX6 protein levels triggers the terminal differentiation of TACs and induces post-mitotic arrest and the expression of mature corneal epithelial markers such as, KRT3 and KRT12. Apart from the three reported PAX6 variants (PAX6A, PAX6B, PAX6D), we have identified four novel alternately spliced PAX6 variants in eye tissues. These novel variants are generated by different splicing events involving the two major splicing hotspots near the Exon 6-7 and Exon 12-13 splice junctions. We have named them as, PAX6A-AS-Δ6, PAX6B-AS-Δ6, PAX6A-Δ6 and PAX6A-12a, which carry in-frame deletions, affecting either the N-terminal paired domain-mediated DNA binding or the C-terminal PST domain-mediated transactivation functions. The expression of these novel splice variants are

majorly driven by the pA promoter in all the ocular tissues and the expression was found to be significantly higher in the limbus and corneal epithelium. Luciferase reporter assays using recombinant PAX6 isoforms has confirmed negative auto-feedback regulation on the *PAX6*-pA promoter. While PAX6A could activate *KRT3* promoter, it had no effect on *KRT12*, *TAp63* and Δ*Np63* promoters. However, a paired domain truncated isoform significantly activated the Δ*Np63*, *KRT12* and *KRT3* promoters. *In situ* localization studies using RNA-FISH combined with ICC/IHC has confirmed that the novel variants are co-expressed along with PAX6A transcripts in a subset of cells that are predominantly located at the basal and supra-basal layers of the limbal and corneal epithelium. These cells are identified as $PAX6^{Low}$, $p63\alpha^{High}$, $BrdU^{+}$ and $KRT3/KRT12^{-}$ proliferating and migrating TACs. Therefore, the novel PAX6 splice variants seem to alter the relative stoichiometry of wild-type transcripts and ensure low levels of PAX6 expression in basal cells. This enables the self-renewal of activated LSC, proliferation and expansion of TACs, while preventing pre-mature differentiation, thus promoting optimal epithelial stratification during normal corneal development and wound healing.

Contents

List of Tables

List of Figures

List of Abbreviations

Abbreviations	Full forms
AGE	Agarose gel electrophoresis
ALP	Alkaline phosphatase
ATP	adenosine triphosphate
BDT	Big dye terminator
bFGF	basic Fibroblast growth factor
BMP4	Bone morphogenetic protein 4
bp	base pair
BrdU	Bromodeoxyuridine
BSA	Bovine serum albumin
CaCl2	calcium chloride
cDMEM	complete Dulbecco's Modified Eagle medium
cDNA	complementary DNA
ChIP	chromatin immunoprecipitation
CK	cytokeartin
CMV	Cytomegalovirus
DAB	3,3'-diaminobenzidine
DAPI	4',6-diamidino-2-phenylindole
DAVID	Database for Annotation, Visualization and Integrated Discovery
ddATP	dideoxyadenosine triphosphate
ddCTP	dideoxycytosine triphosphate
ddGTP	dideoxyguanosine triphosphate
ddNTPs	dideoxynucleotides triphosphates
ddTTP	dideoxythiamidine triphosphate

DMSO	dimethyl sulfoxide
DNA	deoxyribonucleic acid
dNTP	deoxyribonucleotide triphosphate
DTT	Dithiothreitol
EDTA	ethylenediaminetetraacetic acid
eEF1α	eukaryotic elongation factor 1α promoter
EFTFs	eye field transcription factors
EGF	epidermal growth factor
EGFP	enhanced green fluorescent protein
ESC	embryonic stem cell
EtBr	ethidium bromide
FBS	fetal bovine serum
FGF	fibroblast growth factor
FISH	fluorescent insitu hybridization
GO	gene ontology
H&E	hematoxylin and eosin
HDAC	histone deacetylase
hESC	human embryonic stem cell
hiPSC	human induced pluripotent stem cell
HRP	horseradish peroxidase
ICC	Immunocytochemistry
IHC	Immunohistochemistry
iPSCs	induced pluripotent stem cells
IRB	Institutional Review Board
IRES	internal ribosomal entry site
KCl	potassium chloride
LB	Luria-Bertani
LSC	Limbal stem cells
LSCD	Limbal stem cell deficiency
MgCl2	magnesium chloride
MITF	microphthalmia-associated transcription factor

NaB	sodium butyrate
NaCl	sodium chloride
NaH2PO4	sodium dihydrogen phosphate
NaHCO3	sodium bicarbonate
NaOH	sodium hydroxide
NCBI	National Centre for Biotechnology Information
NIH/3T3	Murine fibroblast cell line
PAX6	Paired box protein 6
P63α	Tumor protein 63 alpha variant
PBS	phosphate buffered saline
PCR	polymerase chain reaction
PFA	paraformaldehyde
PI	propidium iodide
Plat-A	Platinum-A
PVDF	polyvinylidene difluoride
qRT-PCR	Quantitative real time PCR
RNA	ribonucleic acid
RNP	Ribonucleoprotein
RPE	retinal pigment epithelium
rpm	revolutions per minute
RT	room temperature
RT-PCR	Reverse Transcriptase PCR
SDS	sodium dodecyl sulphate
TAE	Tris, Acetic acid and EDTA
TAC	transiently amplifying cells
TDC	terminally differentiating cells
TSS	transcription start site
UV	Ultraviolet

CHAPTER 1

INTRODUCTION

Chapter 1: Introduction

Cornea is the transparent and avascular tissue that forms the anterior most portion of the eye and acts as a protective barrier for its internal parts (DelMonte & Kim, 2011). It provides approximately two-thirds of the total ocular refractive power required for a clear vision. It consists of five layers: a stratified squamous epithelium on the outer surface, the Bowman's membrane, a thick stroma in the middle, the Descemet's membrane which is followed by a thin layer of endothelium on the inner surface (Chew, 2011).

The cornea and sclera have limbus at their junction, which acts as a niche for the stem cells of corneal epithelium located at the "Palisades of Vogt". This limbus forms a barrier and prevents conjunctival vasculatures to invade. The corneal epithelium is regularly replenished by the limbal stem cells which divide, differentiate and migrate centripetally from the limbus towards the central cornea (Lavker *et al.*, 2004; Schermer *et al.*, 1986). The limbal vasculatures, unique extracellular matrices, neuronal inputs (Polisetti *et al.*, 2017; Kameishi *et al.*, 2015; Echevarria *et al.*, 2011; Schlotzer-Schrehardt *et al.*, 2007), direct or indirect cell-cell interactions with niche cells such as corneal stromal stem cells (Kureshi *et al.*, 2015; Dziasko *et al.*, 2014) and melanocytes (Dziasko *et al.*, 2015) together support and regulate the functions of CESCs.

Chemical or thermal burns and diseases like aniridia and Steven-Johnson's syndrome can damage the limbus leading to limbal stem cell deficiency (LSCD). Patients with LSCD display loss of corneal epithelial regeneration, acute ocular surface inflammation, which in turn triggers conjunctivalisation and corneal neovascularization. This opaque and vascular pannus tissue growth on the ocular surface affects the corneal transparency and leads to partial or complete blindness (Dua *et al.*, 2003). Current therapeutic approaches to LSCD includes transplantation of autologous or allogenic limbal tissues and *ex vivo* cultured limbal epithelial cell sheets for ocular surface reconstruction. Around 60-70% success rate has been observed with this therapeutic approach (Gupta *et al.*, 2018; Basu *et al.*, 2016; Vazirani *et al.*, 2016; Sangwan *et al.*, 2012; Baylis *et al.*, 2011; Rama *et al.*, 2010). In majority of the cases observed, the clinical outcomes are related to the proportion of limbal stem cells (LSCs) present in the donor grafts and this explains the importance of LSCs in corneal regeneration (Rama *et al.*, 2010).

Maintaining limbal progenitors or LSCs in an undifferentiated state requires proper maintenance of the limbal niche. Limbal niche cells provide the necessary ECMs and paracrine support for the stem cells and regulate their self-renewal and differentiation behaviours. When a stem cell divides, the division is asymmetric where the niche cells are saved, and the divided cell enters a

differentiation pathway according to the specific genetic and environmental stimuli, thereby undergoing different cell fate decisions. However, the exact mechanism by which this regulation occurs is still unclear. Signaling pathways such as the Sonic hedgehog, Wnt/β-catenin, TGF-β, BMP, and Notch signaling have being implicated in mediating corneal homeostasis. However little is known about their exact roles in the LESC maintenance and fate regulation. Limbal stem cell failure is commonly implicated in patients suffering from Aniridia, an inherited eye disease caused due to mutations in *PAX6* gene. PAX6 has been shown to be important for corneal epithelial fate determination and maintenance (Sasamoto *et al.*, 2016; T. Ramaesh *et al.*, 2005; Ramaesh *et al.*, 2003; Collinson *et al.*, 2003). However, the mechanisms of PAX6-mediated corneal epithelial regulation is not well explored.

The *Pax6* gene is a part of the Pax family of homeobox transcription factors and its expression and regulation is highly conserved across species. It acts as a "master control" gene for the early development of brain, eye and pancreas. However, in many adult ocular tissues, Pax6 expression gets down regulated and is maintained only in the lens, corneal, conjunctival epithelium and in a subset of retinal cells. The *PAX6* gene is known to be regulated by two alternate promoters namely the proximal p1 or pB promoter and the distal p0 or pA promoter in mice and humans respectively (Okladnova *et al.*, 1998). A third promoter (pα or pC) located in intron 4 has also been identified in mammals, but its spatiotemporal expression within the eye is not well known (Kim & Lauderdale, 2008; Lakowski *et al.*, 2007; Kim & Lauderdale, 2006; Kammandel *et al.*, 1999). The pA and pB constitute the major promoters and initiate expression in most cells that express PAX6. Different PAX6 promoters (pA, pB and pC) may have diverse roles in regulating the expression of different isoforms during eye development and adult tissue homeostasis. The PAX6 locus encodes three known protein isoforms, viz; canonical PAX6A (Wt) and PAX6B (5a), as a result of alternate splicing and PAX6D (ΔPD) due to an alternate internal promoter usage (Shaham *et al.*, 2012; Chauhan *et al.*, 2004; J. A. Epstein *et al.*, 1994). During development, PAX6 regulation is complex which is mediated through differential selection of the promoters, enhancers, differential splicing to regulate spatio-temporal and tissue-specific gene expression in various tissues like brain, retina, pancreas, lens and ocular surface.

PAX6 is an important gene required for fate determination and maintenance of the corneal epithelium. Heterozygous mutations and haploinsufficiency in PAX6 protein leads to aniridia, which results in impaired iris and corneal development, breakdown of limbal barrier functions, leading to vascularization, corneal opacity and total LSCD (Lima Cunha *et al.*, 2019; Yokoi *et al.*, 2016; G. Li *et al.*, 2015; Douvaras *et al.*, 2013). Similarly, ectopic overexpression of Pax6 resulted

in thin and underdeveloped corneas, with severely impaired corneal wound healing responses(J. Davis & Piatigorsky, 2011; Mort *et al.*, 2011; Dora *et al.*, 2008; Manuel *et al.*, 2008; J. Ouyang *et al.*, 2006; J. Davis *et al.*, 2003; Duncan *et al.*, 2000). Thus, it is clear that the expression of Pax6 is tightly regulated to ensure correct spatio-temporal and optimal levels of protein expression during development and wound healing responses. However, the exact mechanisms of this regulation and its role in limbal stem cell (LSC) fate determination is still unclear. Although it is well known that PAX6 and its variants are important for brain, eye and pancreatic development, very little is known about its cornea-specific regulation and target specificities. Therefore, it is important to understand -How PAX6 maintains LSCs? How they regulate stem cell proliferation vs differentiation fate decisions?

Based on the above rationale, this study was aimed to elucidate the eye-specific mechanisms of regulation of different PAX6 promoters, expression and functions of different PAX6 variants and their effects on ocular tissue-specific gene targets.

Aims of the study

The two main aims of the study are:

1. To understand the differential regulation of human *PAX6* promoters in different ocular cell types.
2. To understand the expression patterns of different PAX6 isoforms in native ocular tissues and their effects on target gene regulation.

CHAPTER 2

REVIEW OF LITERATURE

2: Review of Literature

2.1 Anatomy of the human eye

The eye is the light sensory organ present on either side of the head, in cavities called the orbit. They are connected to the brain through the optic nerves. The outermost layer of the eyeball consists of sclera, limbus and cornea. The sclera comprises of dense collagen fibers making the tissue rigid and tough, which acts as a protective layer to prevent any damage to the inner structures of the eye. The cornea is the transparent layer which helps in light refraction and allows the light to fall on retina for image perception. The limbus is the region which marks the boundary between the sclera and cornea.

The middle layers of the eye is collectively termed as the "uvea" and is comprised of three structures namely, the iris in the front, followed by ciliary body and choroid at the back. The uveal tract is enriched with melanosomes and blood vessels. The iris acts like a diaphragm and regulates the amount of light that enters the eye through the central hole called the pupil. Sphincter and dilator muscles regulate the constriction or dilation of the iris, which in turn modulates the pupil size, based on the surrounding light and allows optimal light entry into the eye. The ciliary body is present in continuation with iris and comprises of ciliary muscle and ciliary processes. The epithelium of the ciliary processes is involved in production of aqueous humor and the zonular fibres connecting the ciliary processes and the lens facilitates accommodation by relaxing or flattening the lens. The rest of the uveal tract comprises of choroid, which is highly enriched with melanosomes and blood vessels and is located between the sclera and retina. The melanin pigments of the melanosomes absorb the excess light and prevents light scatter. It also helps in free radical scavenging and offers protection from photo oxidation and retinal inflammation. The blood vessels present in the choroid nourishes the light sensing photoreceptor cells of the retina.

The third and innermost layer of the eye is the retina which senses the light and communicates the signals to the brain via the optic nerve. Retina is highly light sensitive and comprises of photoreceptors cells, viz; rods and cones in the vertebrate retina, which converts the light signals into electrical impulses that are transmitted to the brain via the optic nerve. The lens is a transparent, biconvex structure present right behind the iris, held in place by the suspensory ligaments called the zonular fibers which are attached to ciliary body. The space between the iris and cornea is called as anterior chamber, which is filled with a clear watery substance called

aqueous humor, secreted by the ciliary epithelium. The space between the lens and retina is called as posterior chamber, which is occupied by a clear jelly like, cell-free substance called the vitreous body or vitreous humor. The vitreous body is held in place by adhesions to the ciliary body, zonular fibers and epithelial cells on the anterior side.

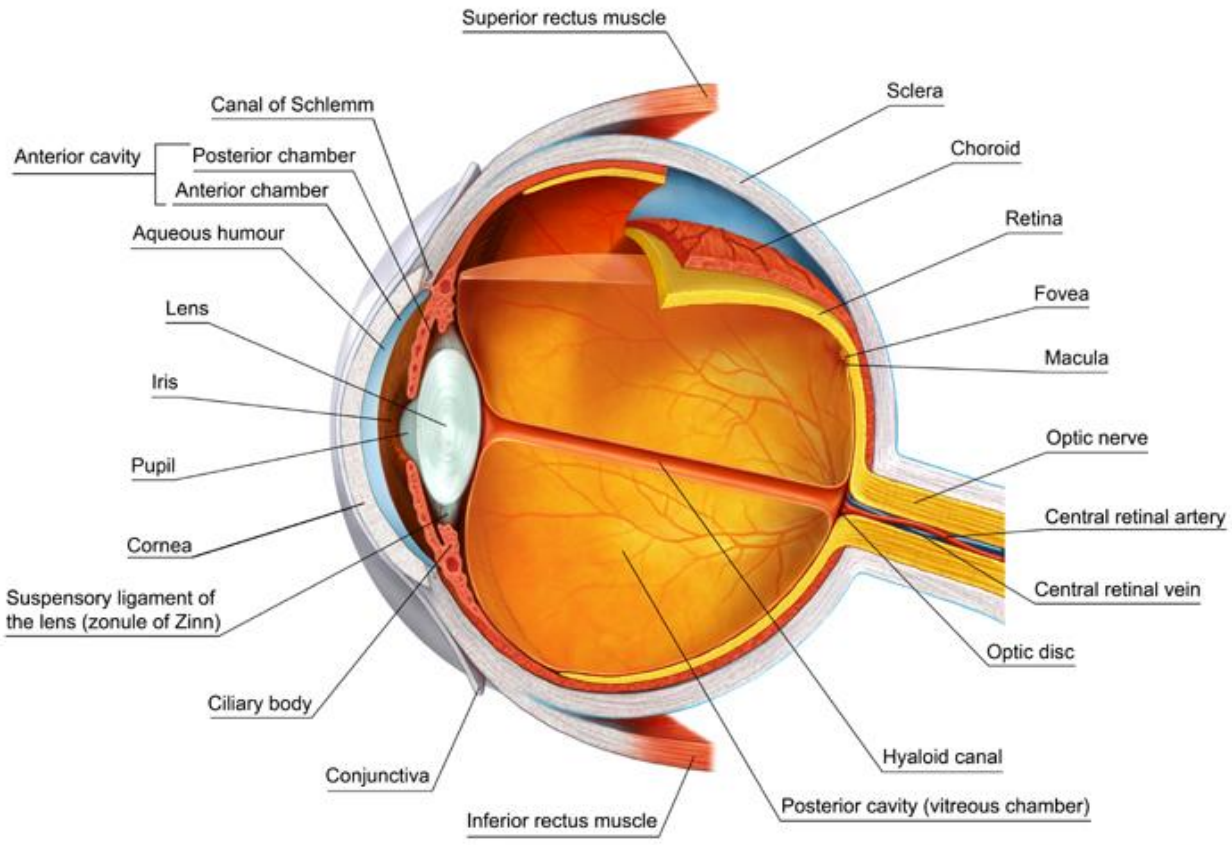

Figure 2.1: Cross section and anatomy of the human eye. Image is adapted from: http://www.myvmc.com/anatomy/the-eye-and-vision

2.2 Development of the vertebrate eye

The development of the vertebrate eye takes place between 3rd and 10th week, where it is formed from the three ectoderm derivatives of the embryo: head surface ectoderm, neural crest and neuroectoderm. These tissues interact with each other and dictate the development and positioning of different ocular tissues within an eye. The head surface ectoderm contributes to the development of cornea, conjunctival epithelia, eye lids, lens and the lachrymal apparatus. The neural ectoderm develops into optic cup and further differentiates to neural retina, RPE and optic nerve. The peripheral regions of the optic cup develop into

ciliary body and iris. The other eye tissues, viz; iris, orbit and eye lid sphincter muscles, choroidal and corneal stromal cells and the vasculatures are acquired from the ocular mesenchyme and neural crest cells. The vitreous humor is derived from the combined secretions of the mesenchymal, neural crest and neuro-ectodermal cells. The secretions of the ciliary epithelium form the aqueous humor.

2.2.1 Optic cup and lens vesicle development

Eye development initiates with the appearance of the optic grooves or optic sulci, on each side of the neural folds in the developing forebrain at day 22. (**Fig 2.2.A.i**). When the neural tube is closed, the optic grooves grow out as optic vesicles towards the surface ectoderm, through the surrounding mesenchymal cells (**Fig 2.2.A.ii**). During this process, the optic vesicle is connected to the forebrain and forms optic stalk, which eventually becomes the optic nerve. The optic vesicle induces pseudostratified thickening of the proximal surface ectoderm layers, which further undergoes proliferation and forms the lens placode (**Fig 2.2.A.iii**). The lens placode further invaginates forming the lens pit, leading to the detachment from the overlying surface ectoderm and triggering the formation of lens vesicle. The optic vesicle in close proximity to the lens placode also undergoes proliferation, stratification and invagination, thus forming a double layered optic cup, with an outer retinal layer (future RPE) and inner retinal layer (future neuro-retina). It takes the shape of a goblet, where the lens vesicle is floating at its open end. The optic cup and lens vesicle gains access to the blood vessels through a groove on their inferior surface called the choroidal fissure. The blood vessels from the hyaloid artery. Upon maturation of the fetal lens, the distal end of the hyaloid artery disintegrates and the proximal end becomes the central retinal artery.

2.2.2 Retinal development

Retina is formed from the two layers of the optic cup which undergoes differentiation to form the mature retina. The outer layer develops into a monolayer of retinal pigmented epithelium containing melanin granules. At around 5 weeks of development, the cells of the inner layer of the optic cups proliferate and form a thick neuroblastic layer, which undergoes proliferation and differentiation. The neuroblast cells on external side develops into mature rod and cone photoreceptor cells, while the internal cell layers gives rise to the muller glia, bipolar, amacrine and horizontal cells. By day 120, the retinal ganglion cell layer of the retina starts appearing. The axons of RGC layer forms the optic nerve bundle, which exits the eyeball at the fovea and connects with the neurons of the visual cortex of the brain. The space present between RPE

and neural retina is called as sub-retinal space. Most layers of the retina develops within 8 months, except the photoreceptors which continues to develop after birth. A fully mature retina consists of 10 layers and is almost transparent except the outer RPE layer. The light that enters the eye can therefore pass freely through all the layers of neuroretina till it hits the outermost photoreceptor cells.

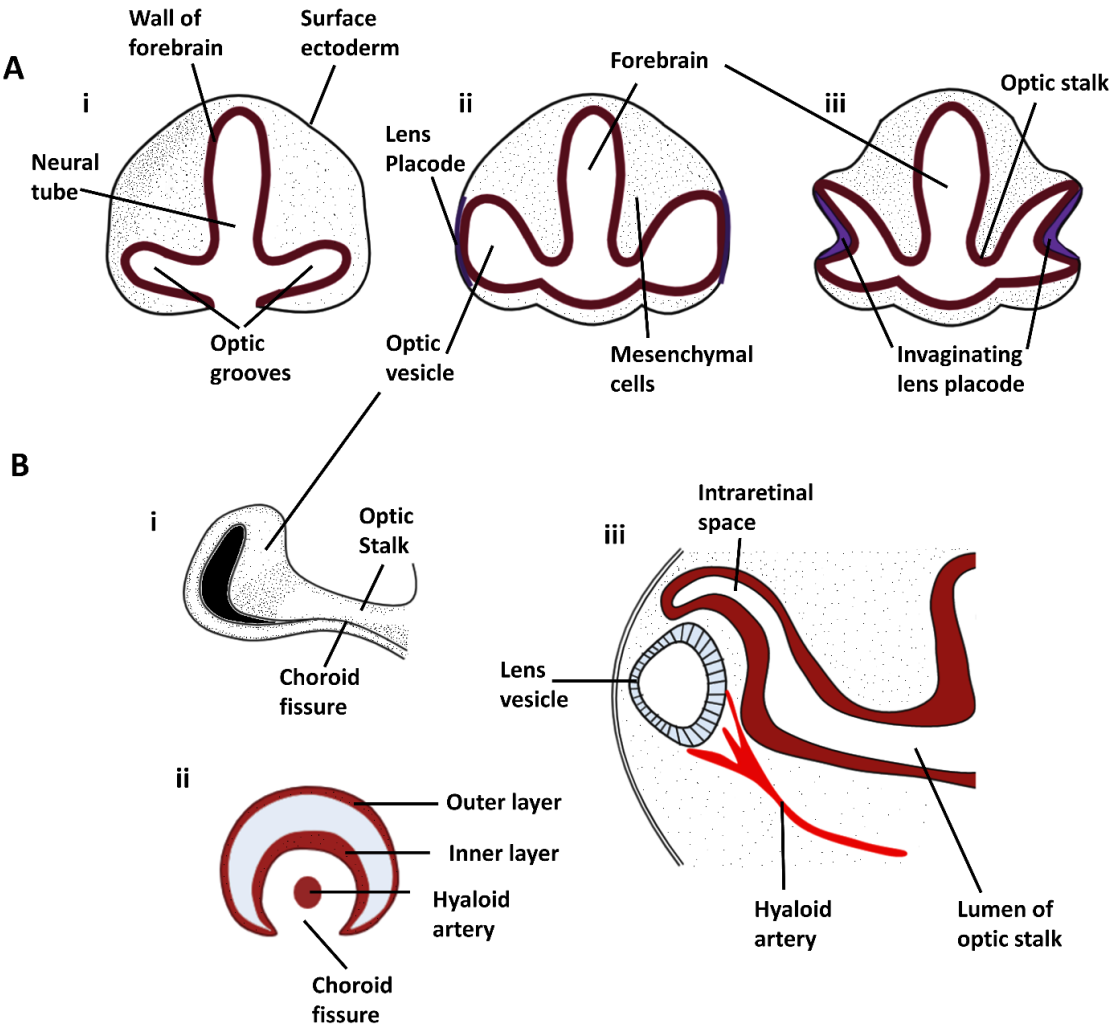

Figure 2.2: Development of the vertebrate eye cup A. *Early development of the optic cup and lens in vertebrates. Pictorial representation of the forebrain of a 22day old human embryo describing the migration of the optic grooves towards the surface ectoderm (**i**).Pictorial representation of the forebrain of a 28 days embryo. Upon close contact with overlying surface ectoderm, the optic vesicle induces the differentiation of ectodermal cells to form the lens placode (**ii**). Pictorial representation of the forebrain of a 5mm embryo. The lens placode and optic vesicle further undergoes invagination to form the lens vesicle and the inner neural retina and outer RPE layers.* ***B.*** *Ventrolateral view of the optic cup and the optic stalk of a 42 days embryo.*

*Transverse section through the optic stalk as indicated in (**i**). Hyaloid artery and the choroidal fissure (**ii**) Section through the lens vesicle, optic cup and optic stalk at the plane of the choroidal fissure (**iii**).*

2.2.3 Lens development

After detachment from the surface ectoderm, the lens vesicles gain polarized morphology and subsequently form the mature lens. The anterior lens epithelial cells proliferate to form the lens epithelium whereas the lens fibre are formed from posterior cells, which exit cell cycle and elongate towards the anterior side and differentiates into lens fibre cells. By the end of seven weeks, the primary lens fibres reach the anterior epithelium and completely fill the lumen, thus forming the lens nucleus. The lens nucleus has the highest protein concentration and optical density. Once the lens structure is completely formed, the epithelial cells above the transition zone keeps proliferating and differentiating and continuously add secondary lens fibres around the primary lens fibres. Finally, the fibres at the centre of the lens lose their cell organelles (anuclear) and compactly organize themselves and helps in maintaining the lens transparency (**Fig 2.3**). α, β, γ-crystallins, **lens fiber membrane intrinsic protein, LIM2,** intermediate filament proteins, CP49 and filensin are some of the fiber cell specific markers.

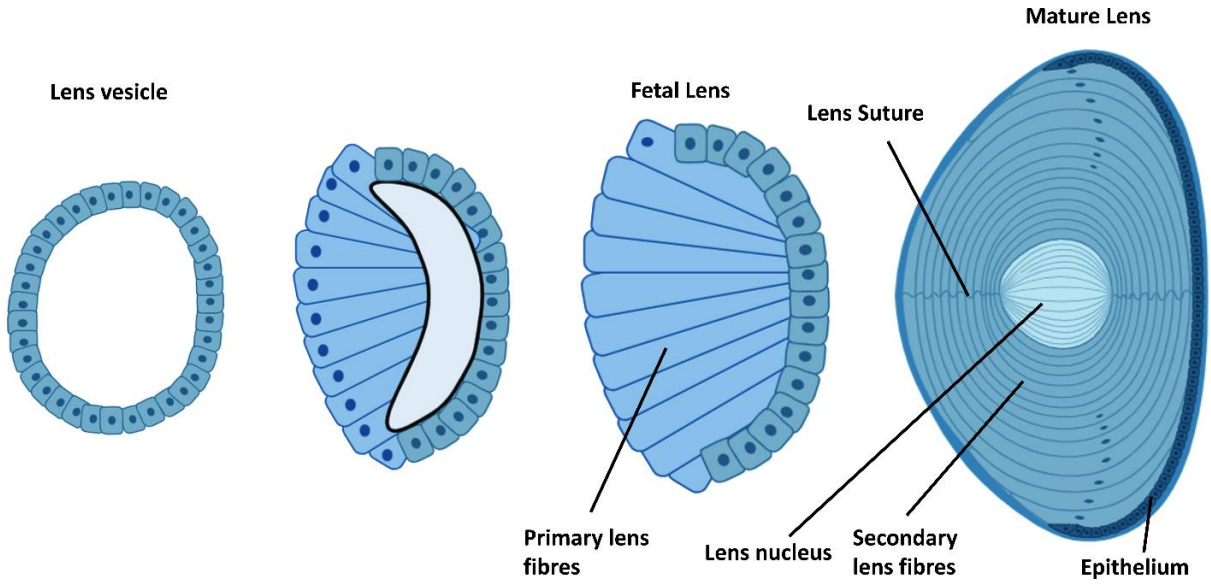

Figure 2.3: Cartoonic representation showing the development of the lens. 1. *A single layer of epithelial cells on the interior surface of lens vesicle invaginates from the lens placode; **2.** Cells on the posterior surface are induced by signals from the neural retina and undergo differentiation into primary lens fibers; **3.** The lens fibers further elongates towards the anterior side and fills the lumen of the vesicle. The cells produce different crystalline proteins and loss their nuclei; **4.** The epithelial cells on the anterior side undergo*

division continuously until they reach the equatorial region, where they undergo differentiation for the formation of new secondary lens fibers.

2.2.4 Iris and ciliary body development

The optic cup undergoes changes in conjunction with the lens and cornea formation. The outer layer differentiates to form the retinal pigmented epithelium (RPE), while the inner layer differentiates to form the neural retina. The neural retina and the pigmented epithelium meet at the peripheral margins of the optic cup, close to lens vesicle, which develops into iris and ciliary body. Extension of the outer layer of the optic cup is followed by the proliferation and migration of periocular mesenchymal and neural crest cells, which contributes to the formation of iris stroma (Davis-Silberman & Ashery-Padan, 2008).

Lens tissue plays an important role for the proper development of iris and ciliary body. Mechanical ablation or chemical ablation of lens using the cytotoxic diphtheria toxin A was found to disrupt the development of iris, cornea and ciliary body (Beebe & Coats, 2000).

The molecular mechanisms underlying this is still unknown. Studies have also shown that BMP signaling is very important for the development of iris and ciliary body. It was observed that the ciliary development was completely in transgenic mice with lens-specific overexpression of Noggin, a BMP antagonist (Zhao *et al.*, 2002). Also, the anti-parallel gradients of BMP and FGF signals define the development of ciliary margin in chicken (Dias da Silva *et al.*, 2007). When Wnt2b induced β-catenin signaling is constitutively activated in developing optic vesicles, the retinal identity was lost and found to be sufficient to induce the formation of iris and ciliary body in developing chick eyes (Cho & Cepko, 2006).

2.2.5 Corneal development

The ocular surface ectoderm contributes to the development of cornea and is comprised of three main layers. A stratified corneal surface epithelium forms the outermost layer. The central or the middle layer is the stroma which is comprised of neural crest derived keratocytes, which forms a thick collagenous and highly ordered matrix. The inner most lining is the monolayer of neural crest derived endothelial cells. The thick basement membranes of the epithelium and the endothelium are called the Bowman's layer (BM) and the Descemet's membrane (DM) respectively. They are composed of strong collagen fibrils and are sandwiched between the epithelial layer and the stroma; or the stroma and the endothelium respectively (**Fig 2.4**).

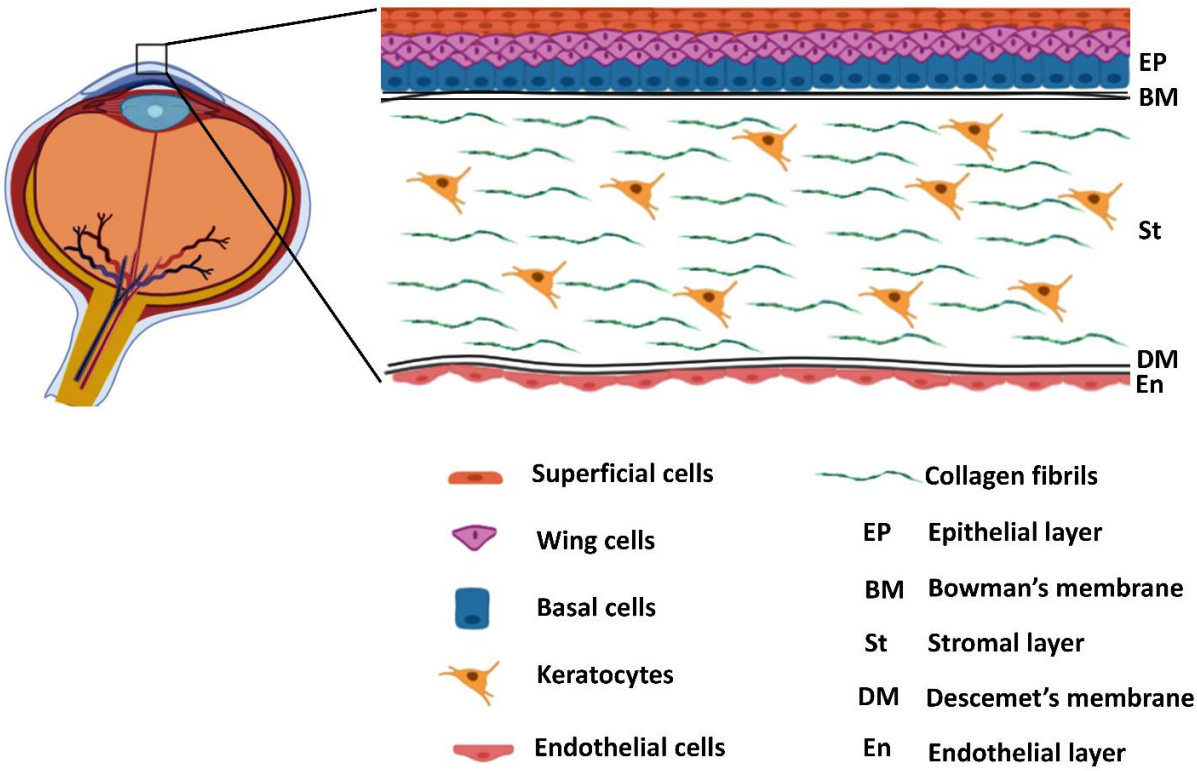

Figure 2.4: Diagrammatic representation of the cross section of the corneal layers. *A multi-layered, stratified squamous epithelium forms the outermost layer of the corneal epithelium (Ep), which remains adhered to the Bowman's membrane (BM). The middle connective tissue or the stromal layer (St) contains the keratocytes and a densely packed, thick collagenous matrix. The innermost layer of the cornea is the endothelium (En) and these cells stay adhered to a thick Descemet's membrane (DM).*

2.2.5.1 Corneal epithelium

The surface ectoderm present above the immature lens develops into corneal epithelium. A bi-layered primitive epithelium can be observed at 5 weeks of gestation in humans, while it can be seen at embryonic day 11 and 12 in mice. The expression of corneal epithelium specific markers K3 and K12 can be observed at embryonic day 15.5-17.5 (Wolosin *et al.*, 2004). The eyelid develops above the cornea and the corneal epithelium is contiguous with the lid surface epithelium. The space between the corneal epithelium and the lens is infiltrated with the migrating neural crest cells, which later differentiates into endothelial cells and the stromal keratocytes. The collagens and ECMs produced by the keratocytes forms the thick stroma. The eyelids open at 24 weeks of gestation in humans, while it opens only at 12 days post birth in mice. After the lid opening, the corneal epithelium undergoes stratification and complete maturation. The thickness of the corneal epithelium increases to about 6-7 cell layer. The basal

cell morphology changes from cuboidal to a columnar shape. However, the cells flatten up during stratification to form the suprabasal wing-like cells. These cells flatten further to form the superficial cells that are connected by tight junctions.

2.2.5.2 Corneal stroma

As discussed above, at around 7th week of gestation in humans, the space present between the immature corneal epithelium and the lens placode is filled with the migrating neural crest cells, which later differentiates to form corneal stroma, endothelium, trabecular meshwork and iris. The first wave of neural crest cell crest migration and differentiation contributes to the development of corneal and trabecular meshwork endothelium, whereas the keratinocytes are formed during the second wave (Zieske, 2004). The third wave of infiltrating neural crest cells and the periocular mesenchyme is responsible for the development of iris. The stromal keratocytes do not undergo terminal differentiation but remain in the G_0 stage. Any damage to cornea can trigger wound healing response mediated by the activation and proliferation of stromal keratocytes (Cvekl & Tamm, 2004). TGFβ and FOXC1 signaling are necessary for the neural crest cell migration, proliferation, differentiation and for modulating stromal development. Knockout mice models (TGF-β2$^{-/-}$ and FOXC1$^{-/-}$) are shown to be associated with corneal abnormalities such as corneal and stroma thinning, absence of corneal endothelium and the appearance of hyaline cells in excess in the vitreous. Also, the lens fail to detach from the corneal epithelium (Banh *et al.*, 2006; Saika *et al.*, 2001; Kidson *et al.*, 1999). Mutations in FOXC1 gene has been found to be associated with Peter's anomaly in humans.

The stroma contributes to about 80-85% of the total corneal thickness and is composed of flattened keratocytes embedded in a thick, well organized collagenous matrix made of different collagens (type I, III, V and VI) and keratin sulfate glycosaminoglycans, in addition to different matrix metalloproteases. Along with collagen, various other extracellular proteins like vitronectin, laminin and fibronectin are also present in the corneal stroma. The corneal keratocytes are majorly located in anterior stroma. The crystallins also contribute to about 30% percent of soluble protein in the cornea and help in reducing the light back scatter, thereby enhancing the corneal transparency (Jester *et al.*, 1999).

2.2.5.3 Corneal endothelium

Corneal endothelium is formed by the first wave of the neural crest cells and develops along with the stroma. Factors affecting stromal development also affect the development of corneal

endothelium. FOXC-1 and TGF-β2 null mice are associated with defect in endothelial development in addition to stromal thinning.

Corneal endothelium plays a major role in maintaining the cornea in a slightly dehydrated state, which is absolutely necessary for optical transparency of the cornea. The tight junctions, fluid pumps and solute transporters expressed by the endothelial cells ensure optimal hydration, solute transport and nourishment to the cells in an avascular corneal tissue. These are post-mitotic cells arrested in G1-phase of cell cycle and any cell loss during adulthood is compensated only by cell migration and volume expansion and not by cell proliferation or active regeneration (Zieske, 2004).

2.3 Pax6: Role in eye development

PAX6 is a paired box and homeobox containing transcription factor required for the normal development of brain, eye and pancreatic tissues. The importance of Pax6 in the development of the eye has been well documented in the past few decades. Mutation screening in aniridia patients, cre-transgenic mice, drosophila, zebrafish and *xenopus laevis* models have helped in the elucidation of mechanisms involved in eye development, specification and maintenance of adult tissue homeostasis.

2.3.1 Specification of the optic vesicle progenitors

A co-ordinated expression of the eye field transcription factors (EFTFs) in the vertebrate neural plate in the anterior region is necessary for the specification of neuroectodermal progenitors into eye field precursors. This specification has been extensively studied in *xenopus laevis* embryos (Zuber, 2010; Zuber *et al.*, 2003; H. Li *et al.*, 1997). The genes *SIX3, RAX (RX), LHX2, TBX3, OPTX2 (SIX6), NR2E1 (TLX)* and *PAX6* are some of the EFTFs, which works along with *OTX2* and together regulate head determination. These eye field genes are expressed in a spatial and temporal manner in a subset of neuroectodermal cells. When misexpressed in frog embryos, PAX6 was found to induce ectopic eyes (Zuber *et al.*, 2003). It is well established that EFTFs co-regulate each other when overexpressed in *Xenopus laevis* embryos. *Pax6* overexpression induced the expression of *Lhx2, Six3, Tlx* and *Optx2*, whereas Six3 overexpression upregulated *Pax6, Lhx2* and *Tll* (Zuber *et al.*, 2003). This EFTF gene regulatory network is highly conserved in invertebrates and vertebrates, even though significant evolutionary differences exist in the anatomy of eye structures (Xu *et al.*, 1999).

Pax6 is the first EFTF highly expressed in the anterior neural plate for neuroectoderm specification and also induces the expression of other EFTFs, viz; Rx, Tbx3 and Lhx2 (Zuber *et al.*, 2003). Expression of the eyeless gene in Drosophila resulted in the induction of ectopic eyes (Halder *et al.*, 1995). Similarly, in developing Xenopus embryos, overexpression PAX6 alone was sufficient for the induction of ectopic lens like structures, but not retina (Altmann *et al.*, 1997), while under different conditions, it could induce the formation of fully developed ectopic eyes (Chow *et al.*, 1999). The PAX6 transgene was shown to induce the expression of Rx, Otx2, Six3 and also the endogenous Pax6 to activate the complete eye program at ectopic sites. This confirmed that Pax6 is the master regulator that stimulates the eye program in co-ordination with other EFTFs in most vertebrates.

2.3.2 EFTFs and their role in partitioning of eye field

After gastrulation, a series of pattering events take place in neuroectoderm, specifying the ectodermal head region and the eye field. During the neurulation process, optic vesicle (OV) formation takes place by the lateral evagination of two extensions coming from the eye fields. Sonic hedgehog (Shh) signaling was shown to be involved in the partitioning of a single eye field into two bilateral OVs by inducing hypothalamic fates in the central diencephalon. Absence of *shh* signalling leads to the loss of fore brain structures (holoprosencephaly) and cyclopia (one eyed). Six3 is also involved in the formation of forebrain and eye, mainly by Wnt signalling inhibition, which in turn antagonizes Shh signalling. Also, *six3* directly regulates *shh*, and its misregulation leads to holoprosencephaly (Geng *et al.*, 2008).

Once the eye field undergoes partitioning, optic vesicles (OVs) evaginate and come in close proximity to the overlying surface ectoderm. Early studies in mice have demonstrated that *RX* is an essential EFTF involved in the morphogenesis of the OVs in both fish and mammals (Svoboda & O'Shea, 1987). During the optic vesicle evagination, dorsal-ventral and proximal-distal patterning takes place. Shh plays an essential role in ventral patterning of the optic vesicle by regulating the expression of ventralizing homeodomain transcription factors *Vax1* and *Vax2* (Take-uchi *et al.*, 2003; Sasagawa *et al.*, 2002). BMP4 is involved in dorsal patterning of the OV by driving the expression of *Tbx5*. Misexpression of Tbx5, results in failure of dorsalization of OVs (Sasagawa *et al.*, 2002; Koshiba-Takeuchi *et al.*, 2000). Shh signalling which induces distal and ventral patterning mediates the expression of Pax2 on the proximal side (develops into optic stalk) and Pax6 on the distal side (develops into optic cup). Pax2 and Pax6 coregulate each other and establish a boundary between the optic cup and optic stalk.

The progenitors for the retinal pigmented epithelium present at the periphery of OV expresses Microphthalmia-Associated Transcription Factor (MITF), which is responsible for the pigment cell-specific gene expression, melanogenesis and RPE specification. The cells at the distal end of the optic vesicle which is in close contact and exposed to the bFGF signalling from the surface ectoderm, express the homeodomain transcription factor, Vsx2 or Chx10, which is important for the proliferation and neuro-retinal specification of retinal progenitors. Both *Mitf* and *Vsx2 (Chx10)* mutually repress each other and regulates the establishment and maintenance of RPE and neuro-retinal fates respectively (Fuhrmann, 2010; Horsford *et al.*, 2005). Misexpression of Chx10 in the presumptive RPE layer induced neuro-retinal specification of RPE precursors (Wang *et al.*, 2016).

The specification or patterning of the OV into neuroretina and RPE is dependent on EFTFs. Using the Rx-Cre system, when *Six3* gene was deleted in OVs, the specification of neuroretina is abrogated, while the RPE development was normal. Elevated expression of Wnt8b suppresses neuroretinal specification and induces RPE formation. *Lhx2 is* a LIM homeodomain transcription factor, also involved in dorsal and ventral patterning of the OV. In *Lhx2* mutants, the OVs develop normally, but show defect in RPE and neuroretinal specification of retinal progenitors (Hagglund *et al.*, 2011; Yun *et al.*, 2009).

In *Pax6*$^{-/-}$mouse embryos, optic vesicle evaginates and EFTFs expression is maintained. Interestingly, the neuroretina and RPE progenitors gets specified normally and is independent of PAX6 expression (Baumer *et al.*, 2003; Marquardt *et al.*, 2001; Grindley *et al.*, 1995). However, further development of the optic vesicle is prevented. The retinal progenitor proliferation is drastically reduced and the neurogenesis takes place prematurely due to the upregulation of proneural gene, *Mash1* and the photoreceptor precursor marker, Crx. However, complete neurogenesis is inhibited in the absence of Pax6. Analysis of double mutants of *Pax6* and *Pax2* showed that both the transcription factors are important and regulate *Mitf* co-operatively, thus playing a crucial role in specifying the RPE fate (Baumer *et al.*, 2003). Additionally, Pax6 is required for the establishment of patterning in temporal-nasal and dorso-ventral domains of the OV.

Taken together, it is clear that Pax6 can independently trigger the early eye field commitment in neuro-ectodermal cells. However, the partitioning of eye fields, development of optic vesicles from the eye field, OV patterning and retinal fate commitment are collectively regulated by the EFTFs and specific transcription factors. Though OV morphogenesis is not

strictly dependant on PAX6 expression, it seems to play a critical role in the later development and maturation of retina, lens, cornea and other ocular structures.

2.3.3 Extrinsic signals involved in optic vesicle patterning

Apart from transcriptional regulators, secreted growth factors and morphogens also play an important role in neuro-epithelial patterning. As described in the previous section, Shh secreted from the ventral side is crucial for the partitioning of the central eye field. Shh signalling also stimulates the expression of Vax1 and Pax2 and inhibits Pax6 expression on the ventral side of the OV. Studies on chick embryos have demonstrated that growth factor signaling from the surrounding mesenchyme and ocular surface ectodermal cells regulate optic vesicle patterning into neuro-retina and RPE fates. The FGFs secreted by the surface ectoderm induce neuro-retinal fate in retinal progenitors located at the distal regions of the OV. Studies on chick have shown that the surgical removal of surface ectoderm reduced the expression of neuro-retinal progenitor markers. This can be rescued by the ectopic expression of FGF2, which induced Vsx2 and repressed Mitf expression (Hyer *et al.*, 1998). Additionally, Zhao *et al.* demonstrated that the loss of Fgf9 results in the expansion of RPE instead of neuroretina (Zhao *et al.*, 2001). This demonstrates the significant role of FGF signaling in OV patterning, where the surface ectodermal cells serve as the prime source of FGF ligands. Deletion of Pax6 in lens ectoderm (LE) using a Cre-LoxP system abrogated lens development but had no effect on neuroretinal and RPE fate (Smith *et al.*, 2009; Ashery-Padan *et al.*, 2000). However, OV morphogenesis was altered with abnormal retinal progenitor proliferation, resulting in a neuro-retina with multiple folds, instead a single symmetric cup. Similarly, the factors secreted by the periocular mesenchyme surrounding the OVs such as, the TGFβ, BMPs, activins and Wnt ligands induces the expression of Mitf in the retinal progenitors located at the proximal regions of the OV and induces RPE fate.

2.4 Pax6: An eye field master regulator

2.4.1 Evolutionarily conserved role of Pax6 in eye development

Pax6 is evolutionarily highly conserved through 400 million years of divergence. Homologs of pax6 are present in *Caenorhabditis elegans*, nemertean, mollusks, cnidarians, annelids, and arthropods, and play an important role in brain and eye development. Human PAX6 has 90% and 96% sequence similarity with *Drosophila melanogaster* and zebrafish, respectively. Alternative splicing of Pax6 is highly conserved in species, from zebrafish to humans. In drosophila, two

Pax6 genes, eyeless (ey) and twin-of-eyeless (toy), and two other Pax6-like genes, viz; eye gone (eyg) and twin of eye gone (toe), corresponds to the canonical PAX6 and PAX6-5a respectively, and it is thought to be the products of gene duplication. These four genes have important functions during the development of the eye (Jacobsson *et al.*, 2009). So far, seven genes namely, *ey, toy*, *eyg, eya, dac, optix* and *tsh* are considered as key genes involved in eye specification in Drosophila. Misexpression of any of these genes induced ectopic eyes (Czerny *et al.*, 1999). In notch mutants, the defect in eye growth was rescued only by *eyg* (mammalian ortholog is PAX6B) and not by *ey* or *toy* (mammalian ortholog is PAX6A). This demonstrates that while *ey* or *toy* regulates eye specification, *eyg* is crucial for regulating eye growth (Dominguez *et al.*, 2004).

2.4.2 Pax6 mutants and their phenotypes

In spontaneously emerged Drosophila mutants that failed to develop eyes, the mutant gene was first identified on chromosome 4 and was named as "eyeless" (Sturtevant, 1951). In humans, *PAX6* mutations was found to be linked to multiple eye disorders like aniridia, Peter's anomaly, Autosomal dominant keratitis and isolated foveal hypoplasia. Aniridia is caused by heterozygous mutations in one of the alleles, resulting in PAX6 haploinsufficiency and defective ocular surface development (van Heyningen & Williamson, 2002). The disease is bilateral and affects all the tissues of the eye (panocular), characterized by foveal hypoplasia, abnormal or complete absence of iris. It is often associated with corneal neovascularization, cataract, glaucoma and corneal abnormalities. The mechanism behind the corneal abnormalities is largely unknown, but speculated to be associated with limbal stem cell failure and corneal stromal defects (K. Ramaesh *et al.*, 2005; Tseng & Li, 1996; Nishida *et al.*, 1995).

Mutations in *Pax6* results in the formation of small eyes in mice (*sey* mice) and rats (Matsuo *et al.*, 1993; Hill *et al.*, 1991). Some abnormalities in the central nervous system have also been found to be related to SEY. These animals are excellent models to study aniridia and the progressive nature of corneal abnormalities. SEY mice strains with three different point mutations in *Pax6* and a separate deletion mutant have been generated so far (Lyon *et al.*, 2000; Schmahl *et al.*, 1993; Hill *et al.*, 1991; Hogan *et al.*, 1986; Theiler *et al.*, 1980). Homozygous SEY mice ($Pax6^{-/-}$) lacks eyes, have defective olfactory structures and they usually die after birth. The eyes of these animals are not completely formed. The Optic vesicle and the surface ectoderm fail to interact and subsequently, the lens placode and optic cup formation does not occur (Grindley *et al.*, 1995). The commonly observed abnormalities are microophthalmia,

defect in iris, lens and retina with variations in the disease severity (Callaerts *et al.*, 1997; Hill *et al.*, 1991). After birth, the SEY mice mutants develop cataract, glaucoma and corneal opacity. Phenotypic variations have been observed within mice carrying the same mutation and even between different eyes of same mice (Schedl *et al.*, 1996; Hill *et al.*, 1991). This confirms the pleiotropic effects of PAX6 gene mutations and the importance of spatio-temporal and dosage regulations of PAX6 expression during normal eye development and function.

2.4.3 Optic cup specification

2.4.3.1 Development of optic cup neuroepithelium

The progenitor cells present in the OV differentiate gradually into neuro-retina, RPE, ciliary body and iris. The neuro-retina is organized into three different cellular layers separated by neural synaptic connections sandwiched in-between. The outer nuclear layer (ONL) is comprised of rod and cone photoreceptors; the inner nuclear layer (INL) is made of horizontal, bipolar and amacrine inter neurons and the muller glial cells; and lastly the ganglion cells form the retinal ganglion cell layer (RGC). A single layer of Retinal pigmented epithelium (RPE) developed from the neuro-ectoderm is positioned adjacent to the photoreceptor cells. These are tightly packed pigmented, cuboidal cells that help in the nourishment and maintenance of photoreceptors and participate in the visual cycle.

Upon retinal progenitor differentiation, the RGCs, horizontal cells, cone photoreceptors and amacrine cells develop first, while the rod photoreceptors, bipolar cells and the Muller glial cells are formed the last. Retinal differentiation proceeds from the center towards the periphery, with the undifferentiated precursors occupying the ciliary margin zone (CMZ) at the retinal periphery. The retinal progenitor cells proliferate and contributes to the growth and increase in the size of optic cups. Different transcription factors expressed during the early stages viz. Sox2, Rx, Six6, Pax6, Six3, Chx10 and Lhx2 are crucial for this regulation. Pax6, Rx and Chx10 are expressed by every cell during the early optic cup stage. Upon retinal differentiation, the progenitors down regulate PAX6 expression and are retained only in a subset of early formed, retinal neurons namely, the horizontal cells, amacrine cells and the RGCs. Similarly, Chx10 regulates the bipolar cell fate and Rx triggers muller glial differentiation, while they are downregulated in rest of the retinal neurons.

Apart from homeobox genes, the co-expression of different basic helix loop helix (bHLH) genes in retinal progenitors also dictates different neuro-retinal cell fates. Mutation studies

have shown that Math5 & Brn3b double mutants are defective in RGC development (Moshiri *et al.*, 2008). Similarly, NeuroD or Math3 overexpression in retinal progenitors induces amacrine cell fate and a double knockout of NeuroD & Math3 showed selective ablation of amacrine cells. Also, overexpression of Foxn4 generates amacrine cells in retinal explants. Foxn4 knockout results in loss of horizontal cells and a reduction in amacrine cell number. Additionally, the transcription factor Prox1 plays an essential role in the generation of horizontal cells (Dyer *et al.*, 2003). Similarly, Mash1 and Math3 are crucial for the differentiation of bipolar cells and double knockouts results in complete loss of bipolar cells. The induction of both Otx2 and Crx expression triggers the photoreceptor precursor fate commitment. Knockout of either of these genes results in the conversion of photoreceptor precursors into amacrine cells.

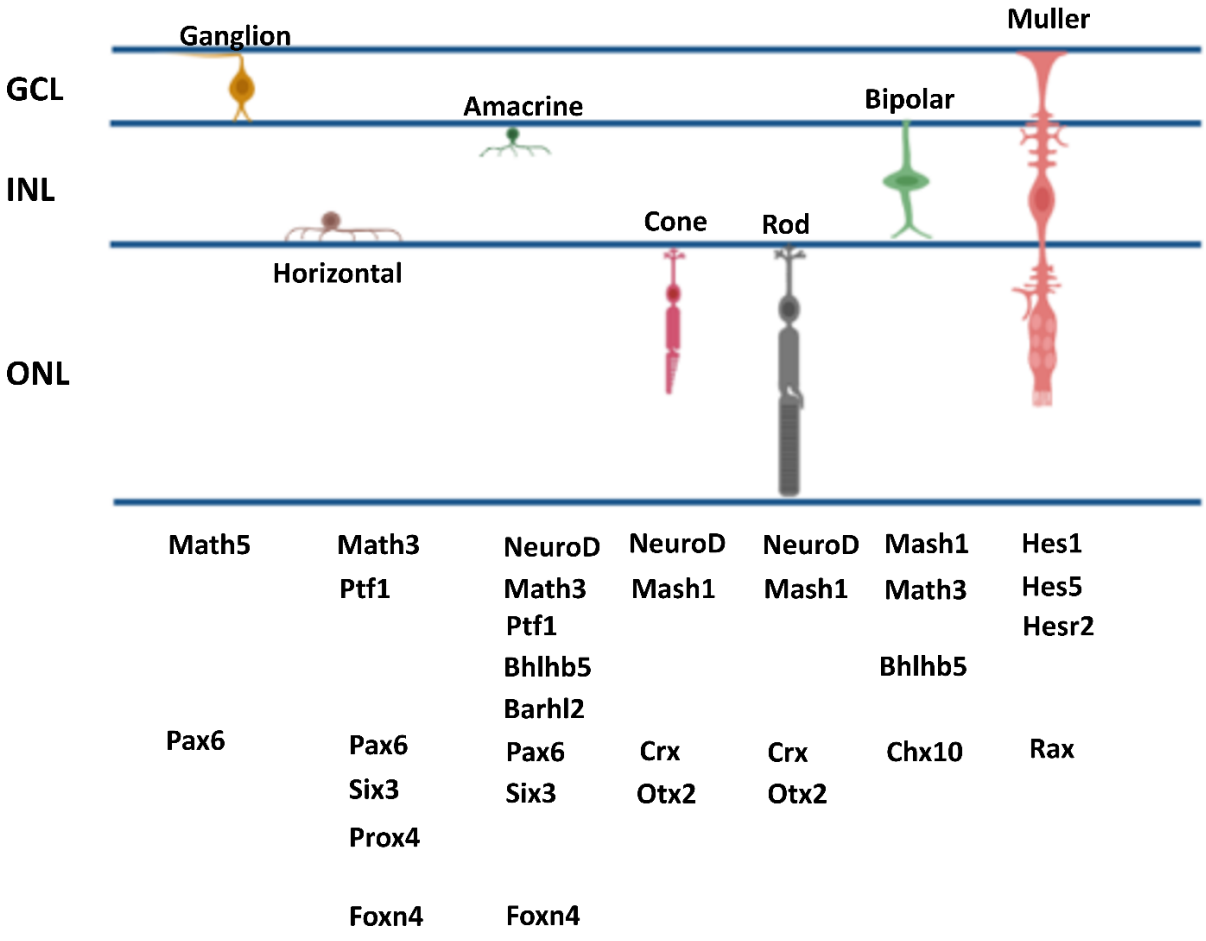

Figure 2.5: Transcription factors regulating neuro-retinal cell fate. *bHLH and Homeobox family of transcription factors and their combinations required for the specification of different retinal cell types.*

2.4.3.2 Role of Pax6 in the differentiation of optic cup progenitors

PAX6 induced during the early eye field specification is retained by the retinal precursor cells at the optic vesicle and optic cup stages (**Fig 2.6.A.B**). Once the optic cup differentiates, Pax6 expression is retained by the RPE cells and in a sub-set of neuro-retinal cells. The photoreceptors in the ONL and the bipolar cells in the INL lose PAX6 expression once they get committed and reach the post-mitotic maturation phase. Whereas the differentiated amacrine, horizontal and some of the retinal ganglion cells maintain Pax6 expression (**Fig 2.6.C**) (Hsieh & Yang, 2009; Oron-Karni *et al.*, 2008; Macdonald & Wilson, 1997).

During eye development, Pax6 is known to regulate diverse cellular functions. Pax6 knockdown is associated with ciliary body and iris developmental failure (N. Davis *et al.*, 2009; Marquardt *et al.*, 2001). The progenitor cells at the periphery of the optic cup undergo late differentiation. PAX6 expression in these peripheral progenitors prevents premature induction of differentiation by repressing CRX expression. Conversely, PAX6 promotes the differentiation of neuro-retinal progenitors located within the central retina by inducing Crx and other bHLH transcription factors. Thus PAX6 plays a dual role in regulating retinal development in two spatially separate sub-sets of retinal precursors. Pax6 ablation in the central retinal progenitors resulted in the exclusive generation of amacrine cells (Oron-Karni *et al.*, 2008). The loss of Pax6 in retinal progenitor cells results in the downregulation of bHLH transcription factors which are crucial for the specification of neurons. In the developing brain and endocrine cells of the pancreas, the pro-neural transcription factors are dependent on Pax6, where it directly binds to the enhancers and regulate the activity of bHLH factors such as *Mash1, Math5, Ngn2* and *Neurod1* (Gosmain *et al.*, 2010; Riesenberg *et al.*, 2009; Visel *et al.*, 2007; Marquardt *et al.*, 2001). Thus, retinal neurogenesis is differentially regulated by PAX6 in a spatio-temporal manner.

2.4.4 Specification of ocular surface ectoderm

The correct spatio-temporal patterning of PAX6 expression and its dosage are known to be critical for the normal development of eye and different ocular structures. Olfactory and optic placode are induced in the surface ectodermal regions that express Pax6 and are termed as pre-placodal region (PPR). Early studies have shown that the interaction of surface ectoderm with the optic vesicle sends the first signal for lens placode induction within the ocular surface ectoderm (Marquardt *et al.*, 2001; Ashery-Padan *et al.*, 2000; Callaerts *et al.*, 1997). Pax6 is

normally expressed in the surface ectoderm overlaying the optic vesicle and also in the lens and corneal placodes.

2.4.4.1 Role of Pax6 and its regulation during lens formation

PAX6 expression in the PPR and during lens development is regulated by various transcription factors and signaling such as Six3, FoxE3, Sox2, Sfrp2, BMP4, BMP7 and Prep1. Six3 is expressed in the eye field and pre placodal region prior to Pax6 and is shown to regulate PAX6 expression (H. Liu *et al.*, 2006; Goudreau *et al.*, 2002). The pinching of the invaginating lens placode (lens pit) and its detachment from the surface ectoderm is an important event during lens development. FoxE3 plays a critical role in the separation of lens vesicle from the surface ectoderm and also for the survival and proliferation of lens epithelium. In heterozygous PAX6 mutant models and in aniridia patients, the lens vesicle fail to separate from the overlying cornea and FoxE3 expression was completely down regulated in the lens pit (N. Davis *et al.*, 2009; Blixt *et al.*, 2000).

Pax6 activates the expression of several lens-specific genes namely, αA, αB, δ, and ζ crystallin (Cvekl *et al.*, 1995; Richardson *et al.*, 1995). Also, together with Sox2, it regulates δ1 crystallin and N-cadherin expression and supports lens morphogenesis (Pontoriero *et al.*, 2009; Kamachi *et al.*, 2001). Within the lens tissue, Pax6 expression is seen mostly in the proliferating epithelial cells at the anterior lens margin and in the cells of the transition zone at the lens periphery. However, Pax6 expression is downregulated in young differentiating lens fiber cells at the periphery and is completely lost in fully mature lens fibers. In *Pax6* mutant models, the lens epithelial cells fail to exit the cell cycle, undergo apoptosis and results in impaired lens fiber differentiation. Studies have shown that the suppression of canonical Wnt signaling is necessary for lens induction in surface ectodermal cells, crystalline gene expression and lens fiber differentiation. Pax6 inhibits Wnt signaling by directly regulating the wnt antagonist, *Sfrp1*, *Sfrp2*, and *Dkk1* in the presumptive lens, to induce cell cycle exit and differentiation of lens fiber cells (Machon *et al.*, 2010; Shaham *et al.*, 2009). Overexpression of β-catenin in the lens primordium suppressed Pax6 expression and prevented lens formation (Smith *et al.*, 2005). Similarly, mutations in BMP4 or BMP7 are also shown to inhibit lens placode development, independent of Pax6 involvement (Wawersik *et al.*, 1999; Furuta & Hogan, 1998).

The ocular surface ectoderm-specific enhancer also plays an important role in mediating the expression of PAX6 in the PPR (Dimanlig *et al.*, 2001; Kammandel *et al.*, 1999; Williams *et al.*,

1998). The transcription factor Prep1 binds to the lens enhancer and activates Pax6 expression in the lens (Rowan *et al.*, 2010).

Taken together, it is clear that expression PAX6 is critically regulated and is important both for the lens placode induction and also for the formation of a fully mature lens tissue.

2.4.4.2 Role of Pax6 in corneal development and homeostasis

Many studies have shown that the dosage of PAX6 is crucial for eye morphogenesis, since overexpression as well as haploinsufficiency or loss of expression of PAX6 disrupts normal eye development. During mice embryogenesis, Pax6 expression can be seen in discrete regions of the head surface ectoderm at embryonic day, E8.5. The regions that express PAX6 forms different ocular structures, namely, the lens, corneal and conjunctival epithelium, while the surrounding cells that lack PAX6 expression develops into head-surface epidermis (Ashery-Padan & Gruss, 2001). High level of Pax6 is expressed by the developing lens, RPE, corneal and conjunctival epithelium and in majority of the retinal progenitors (**Fig 2.6**). However, in adult eyes, the entire corneal, limbal and conjunctival epithelium, RPE cells and a sub-set of retinal inter neurons (amacrine and horizontal cells) and the RGCs retain Pax6 expression. The late emerging neurons such as photoreceptors in the ONL and the bipolar cells in the INL down regulate Pax6 expression upon differentiation and maturation (**Fig 2.6**).

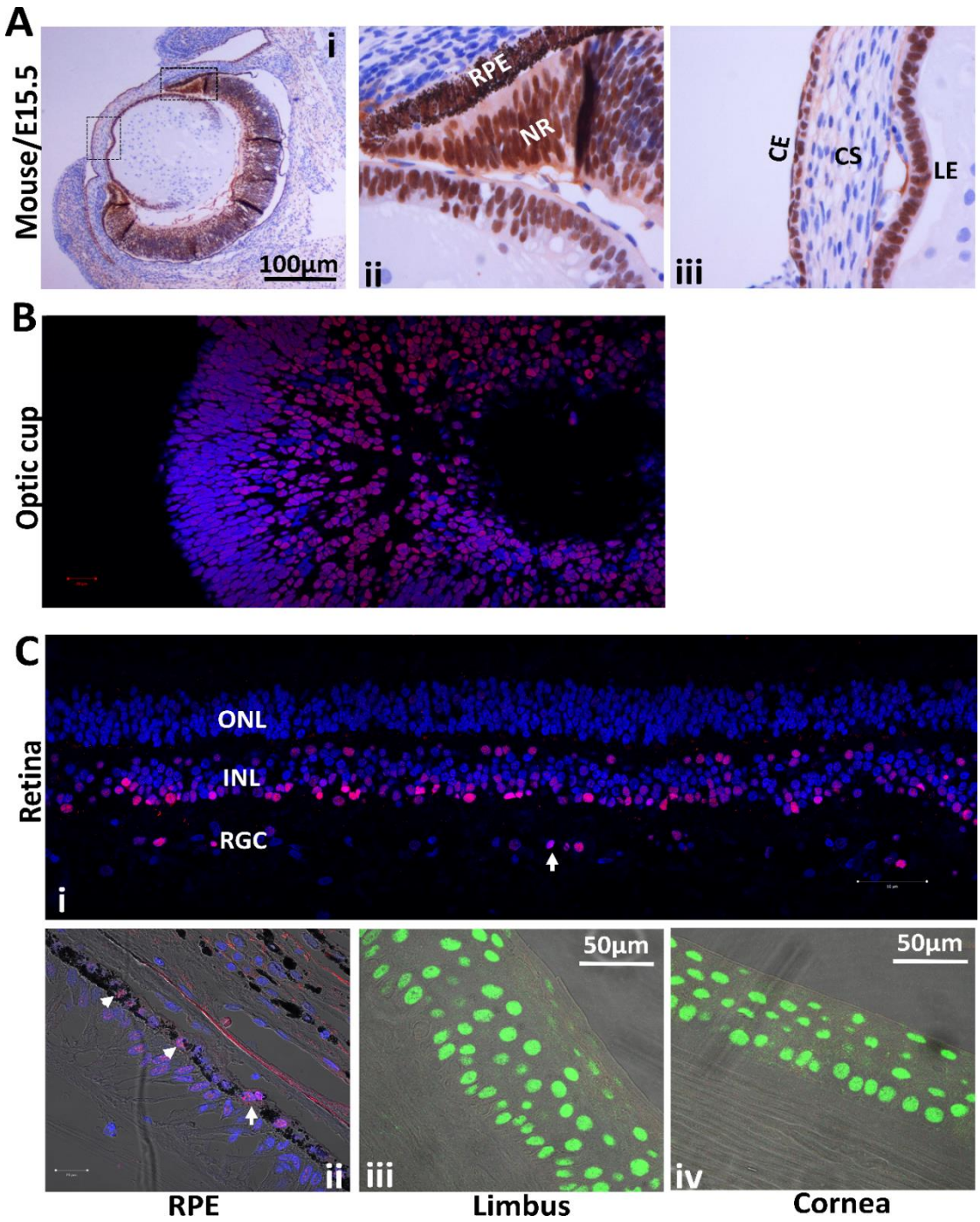

Figure 2.6: Expression of Pax6 in developing and adult ocular tissues. A*. Expression of Pax6 in the developing mouse embryos (E15.5). IHC images showing Pax6 expression in RPE, neural retina, corneal epithelium, and lens epithelium (i). Magnified images from the highlighted sections of A(i); (ii, iii).* ***B****. IHC section of iPSC-derived three dimensional neuro-retinal cups consisting of immature retinal progenitors expressing PAX6 (in red).* ***C****. Confocal images of adult ocular tissue sections. Pax6 expression can be seen in a subset of inner nuclear cells (horizontal and amacrine cells) and RGCs (arrows) of an adult human retina and RPE cells, in red (i-ii), limbus and corneal epithelium, in green (iii-iv).*

Heterozygous *Pax6*$^{+/-}$ mutant animals displayed thinning of corneal epithelial layers, reduced expression of desmoglein, β and α- catenin and keratin 12 resulting in cell-cell adhesion abnormalities and impaired corneal epithelial maturation (J. Davis *et al.*, 2003). Impaired lens formation and delayed corneal epithelial formation, maturation and differentiation was observed in Pax6 mutant cells and in Pax6$^{+/-}$ chimeras, thus indicating a role for Pax6 in controlling the proliferation and differentiation of corneal epithelial cells (T. Ramaesh *et al.*, 2005; Collinson *et al.*, 2003; Collinson *et al.*, 2001).

Pax6$^{+/-}$ mice and aniridia patients cannot secrete the soluble VEGF receptor 1 (sFLT1), which is responsible for blocking corneal vascularization. Supplementing Pax6 expression in Pax6$^{+/-}$ heterozygous animals restores the avascularity of the cornea (Ambati *et al.*, 2006). However, the involvement of Pax6 or the mechanisms involved in the cornea-specific regulation of sFlt1 secretion and maintenance of corneal avascularity is still unknown.

Studies have reported that Pax6 concentration is inversely correlated with cell proliferation and cell cycle progression in corneal epithelial cells (J. Ouyang *et al.*, 2006; T. Li & Lu, 2005). Loss of Pax6 has been shown to convert the corneal epithelial cells into epidermal-like cells similar to that of a skin, while the overexpression of Pax6 in epidermal cells can convert them into corneal epithelial-like cells (H. Ouyang *et al.*, 2014; Pearton *et al.*, 2005). In severe ocular surface diseases, the corneal surface epithelium gets keratinized, with the induction of skin-specific, keratin, K10 and reduced or completely diminished expression of PAX6 and the cornea-specific keratin, K12. Another study has shown that miR-450b-5p and Pax6 were reciprocally distributed in the presumptive epidermis and ocular surface epithelium, respectively. miR-450b-5p was shown to inhibit Pax6 expression and corneal epithelial fate *in vitro*, which suggest that by repressing Pax6, miR-450b-5p triggers epidermal specification of the ectoderm. Absence of miR-450b-5p allows Pax6 expression and ocular epithelial development. Additionally, miR-184 was detected during early eye development and point mutation in miR-184 leads to corneal dystrophy. Also, knockdown of miR-184 resulted in a decrease in Pax6 and K3 in corneal epithelial cells derived from differentiated iPSCs (Shalom-Feuerstein *et al.*, 2012). Thus, *PAX6* is regulated in multiple ways and it in turn regulates diverse cellular functions and mediates normal corneal development and homeostasis. Different Pax6 mutant models and documented abnormalities are listed in **table 2.1**.

2.4.4.3 Alternative splicing of *Pax6* and its role (s) in eye and corneal development

The importance of PAX6 alternative splicing in corneal development was first highlighted by naturally occurring point mutation at -3 position of the exon 5a splice acceptor site. This mutation (T to C) stabilizes the 3' splice acceptor site and favors the inclusion of exon 5a. When exon 5a splicing of *Pax6* pre-mRNA is predominant, it disturbs the balance in the stoichiometry between the levels of canonical PAX6 and PAX6 5a isoforms. PAX6 5a is mainly generated in the patient eye, which results in pannus formation and opaque corneas (J. A. Epstein *et al.*, 1994) . These studies have also shown that the two PAX6 isoforms could bind to their target genes distinctly via either the N' paired box (Pax6-Wt) or the C' homeobox domains (Pax6-5a), thus implicating different target specificities, which may differentially regulate Pax6 functions related to eye development, corneal epithelial differentiation and vascularization (J. Davis *et al.*, 2011; J. Epstein *et al.*, 1994). In another study, many heterozygous *Pax6* contiguous deletion mutants spanning the Pax6 genomic locus and the flanking upstream and downstream genes were generated and their eye phenotypes were examined. In Pax6 mutant line *Pax6*$^{11neu/+}$, along with *Pax6*, another gene located upstream namely, reticulocalbin 1 (*Rcn1*) was also deleted. Absence of this gene gave rise to severe eye phenotypes, as compared to the milder effects seen in *Pax6*$^{12neu/+}$ mutants, where *Pax6* and two other downstream genes namely, *Elp4* and *Immp1L* were deleted. Heterozygous *Pax6*$^{11neu/+}$showed microophthalmia and opaque cornea as compared to *Pax6*$^{12neu/+}$**.** Interestingly, in spite of the diverse phenotypes observed, the levels of different Pax6 isoform expression in the eyes of these two mutant lines were identical (Favor *et al.*, 2009). In mutant mice where exon 5a of Pax6 gene is deleted, loss of Pax6-5a isoform expression resulted in iris hypoplasia and defects in the cornea, lens, and retina, while the entire Pax6 null mice exhibited anopthalmia with central nervous system defects and lethality (Singh *et al.*, 2002). Another recent study has shown that different *PAX6* isoforms, PAX6A and PAX6B differentially regulate the corneal epithelium specific target genes, Keratin 3 & 12. PAX6A activated the expression of keratin, K3, whereas, PAX6B along with Klf4 and Oct4 activated the keratin, K12 (Sasamoto *et al.*, 2016). Different isoform specific functions of Pax6 are listed in **Table 2.2.**

Table 2.1: Mutant models and the role of PAX6 in eye development

S.No	Pax6 function	Technique	Phenotypes	Mechanism	References
1	Eye field formation	Overexpression of EFTFs including Pax6	Ectopic eye formation	PAX6 is one of the eye field marker genes	(Zuber *et al.*, 2003)
2	Survival of OV cells	Pax6 morpholinos	Death of OV cells and Small eye	Pax6 is important during HH stage 9-10 for OV and lens development in chicks	(Canto-Soler & Adler, 2006)
3	Lens forming pre-placodal region	*Pax6*$^{Sey/Neu}$, *Pax6*$^{Sey/Sey}$	No lens induction	BMP signaling-mediated Pax6 function for lens formation	(Wawersik *et al.*, 1999; Furuta *et al.*, 1998)
4	Formation of lens placode	Le-Cre, AP2-Cre-driven Pax6 flox	No lens formation	Cell autonomous function of Pax6 is important	(Ashery-Padan *et al.*, 2000)
5	Migration of neural crest derived cells	*Pax6*^{Sey}	Abnormal migration of neural crest derived cells	Mis-splicing due to insertion of G in exon	(Matsuo *et al.*, 1993)
6	Corneal tissue formation (epithelial, stromal, and endothelial)	*Pax6* hetero and homozygous mutant	Defect in corneal development	Expression of Pax6 is important for the maintenance of lens placode and lens epithelial formation	(Ramaesh *et al.*, 2003; Collinson *et al.*, 2001)
7	Corneal epithelium	*Pax6* heterozygous mutant	Thinning of corneal epithelium	Development of goblet cells in corneal epithelium	(Ramaesh *et al.*, 2003)
8	Corneal epithelium	Overexpression of Aldh3a1 promoter driven Pax6	Altered epithelium, neovascularization, immune cell invasion	Downregulation of KRT12 expression	(J. Davis *et al.*, 2011)
9	Corneal growth and development	*Pax77* mice transgenic line contains 5-7 copies of Pax6 locus	Impaired wound healing and microcornea	Different levels of PAX6 expression leading to various eye defects	(Dora *et al.*, 2008)
10	Cell adhesion in corneal epithelium	*Pax6*$^{+/-}$ mutant	Defects in cytoskeletal structure	Altered desmoplakin, and actin localization	(Ou *et al.*, 2010)

Table 2.2. Isoform-specific functions of Pax6 during eye and corneal development

S.NO	Function of *Pax6* isoforms	Technique	Phenotypes	Mechanism	References
1	Specification of neuroectoderm	Overexpression of canonical *PAX6*	Specially canonical PAX6 induces the differentiation of hESCs to neuroectoderm lineage but not PAX6 5a	PAX6 wt specifically binds to the gene promoters of neuroectoderm	(X. Zhang *et al.*, 2010)
2	Corneal development	Naturally occurring T>C mutation at position -3 of the alternative splice acceptor site of exon5a	Aniridia, opaque cornea and Pannus formation	Significant increase in alternate splicing and expression of PAX6-5a than PAX6-wt	(J. Epstein *et al.*, 1994; J. A. Epstein *et al.*, 1994)
3	Important role in the formation of cornea, retina and iris.	Deletion of 200 kb region upstream of *PAX6* gene including the neighboring *Rcn1* gene	Extreme microophthalmia, thickened cornea and lens-corneal adhesion	Changes in the ratios of Pax6 isoforms, that is higher due to inclusion of exon5a and by the deletion of *Rcn1* gene	(Favor *et al.*, 2009)
4	Along with *Klf4, PAX6-Wt* induced *KRT3* and *PAX6-5a* induced *KRT12* gene expression	Overexpression of canonical *PAX6* and *PAX6 5a* in oral mucosal epithelium	NA	Activation of *KRT3* and *KRT12* gene	(Sasamoto *et al.*, 2016)
5	Lens formation	Overexpression of Pax6 5a using α-A crystalline promoter	Cataract formation in the lens	Upregulation of Paxillin, p120 and α5β1 integrin's by *Pax6* 5a	(Duncan *et al.*, 2000)
6	Formation of iris, cornea, lens and retina	Naturally occurring mutation in exon 5a (Pax6-5a)	Peters anomaly, congenital cataract, Axenfeldt anomaly and foveal hypoplasia	V54D missense mutation unmasks the binding affinity to P6CON site	(Azuma *et al.*, 1999)
7	Maturation of retina	Misexpression of Pax6-5a under the control of CAG promoter in the developing retina	Foveal hypoplasia in a patient with having mutation in exon5a	Higher expression of Pax6 5a in the posterior retina	(Azuma *et al.*, 2005)
8	Formation of iris, lens, retina and cornea	Deletion of *Pax6* exon5a	Iris hypoplasia, defects in cornea, lens and retina	unknown	(Singh *et al.*, 2002)

2.5 Structure and regulation of Pax6 gene

The PAX6 gene codes for a member of the Pax family of transcription factors and a key transcriptional regulator, crucial for the development of eye, central nervous system, olfactory system and pancreas. It is located on chromosome 11p13 and its genomic organization and regulations are highly conserved across species, from flies to humans. The gene expression regulation is tightly controlled in a spatio-temporal manner, with complex regulations at the level of promoters, enhancers, repressors and through alternate splicing.

In Mammals, Pax6 gene consists of 16 exons, which spans 30 kb of genomic region: 14 exons include Exon 1(A & B), exons 2-13 and the other two intronic exons are exon α and exon 5a (**Fig 2.9**) (Kim *et al.*, 2006; Kammandel *et al.*, 1999; Glaser *et al.*, 1992). Different Pax6 transcripts are formed from the Pax6 locus based on promoter choice or by alternative splicing. P0 and P1 are the two main promoters encoding the two major transcripts that are 13 exons long, which gets translated into two known reported protein isoforms (PAX6A and PAX6B) (Walther & Gruss, 1991).

2.5.1 Differential regulation of human PAX6 by alternate promoter choice

Pax6 expression is driven by the activity of two major promoters, viz; P0 and P1 in quail and mouse (Anderson *et al.*, 2002; Plaza, Dozier, Langlois*, et al.*, 1995), whereas in humans they are known as pA and pB promoters respectively (Okladnova *et al.*, 1998). In humans, the distal pA promoter is 7 kb upstream of the transcription start site (TSS) of the proximal pB promoter. These alternate promoter derived transcripts carry unique exons namely the exon 1A or exon 1B and shares the remaining exons 2 to 13 (**Fig 2.7.A.B**).

During the development of eye and brain, P0 or pA and P1 or pB derived transcripts are differentially regulated and are expressed in a spatio-temporal manner (Anderson *et al.*, 2002; Xu *et al.*, 1999). The presence of alternate promoters, specific cis regulatory element/s and long range enhancer/s help in spatiotemporal and tissue specific gene expression of the gene in the pancreas, brain, retina, lens and the ocular surface. The P0 or pA derived transcripts are predominant expressed in the lens placode, cornea and conjunctiva. P1 or pB derived transcripts are mainly active in the developing lens placode, optic vesicle and in the brain (Xu *et al.*, 1999). Also, a third promoter termed as the Pα promoter has been identified within the intron 4 of mouse Pax6. The alternative transcript derived from this Pα promoter encodes an N-terminally truncated PAX6 isoform namely, Pax6ΔPD.

A

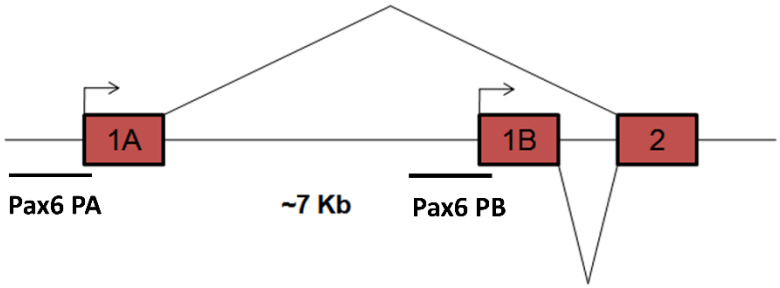

B

```
                                          CCAAT                                  TATA
agccgccatg acgtcacgcg ggccgggcag ccaatgagga cggcgctggc gtggatatta

          +1
aggaaagtta gcgcCTGCCT GAGCACCCTC TTTTCTTATC ATTGACATTT AAACTCTGGG
                                        exon 1a
GCAGGTCCTC GCGTAGAACG CGGCTGTCAG ATCTGCCACT TCCCCTGCCG AGCGGCGGTG
AGAAGTGTGG GAACCGGCGC TGCCAGGCTC ACCTGCCTCC CCGCCCTCCG CTCCCAGgta
                                        intron
accgcccggg ctccggcccc ggcccggctc ggggcccgcg.....~6.5kb..... ..... ggacca
                                      CCAAT
attgcaccag gcggggagag ggagcatcca atcggctggc gcgaggcccc ggcgctgctt

          TATA                    +1
tgcataaagc aatatttgt gtgagagcgA GCGGTGCATT TGCATGTTGC GGAGTGATTA
                                        exon 1b
GTGGGTTGAA AAGGGAACCG TGGCTCGGCC TCATTTCCCG CTCTGGTTCA GGCGCAGGAG
GAAGTGTTTT GCTGGAGGAT GATGACAGAG GTCAGGCTTC GCTAATGGGC CAGTGAGGAG
CGGTGGAGGC GAGGCCGGGC GCCGGCACAC ACACATTAAC ACACTTGAGC CATCACCAAT
CAGCATAGgt gtgctggctg cagccacttc cctcacccac actctttatc tctcactctc
cagccgctga cagcccattt tattgtcaat ctctgtctcc ttcccagGAA ATCTGAGAAT
                                        exon 2
TGCTCTCACA CACCAACCCA GCAACATCCG TGGAGAAAAC TCTCACCAGC AACTCCTTTA
```

Figure 2.7: *(**A**) Cartoonic representation of 5' regulatory region of the PAX6 gene and its alternate promoters. (**B**) Sequence alignment of the human PAX6 exons 1a and 1b. Sequences in lowercase represents intron. Sequences underlined are CCAAT and TATA box. Transcription start sites of the promoters PA and PB are indicated with +1. The 5' splice donor site (gt) and 3' splice acceptor site (ag) are marked in bold.*

The quail Pax6 P0 promoter (homolog of human pA promoter) was reported to be active during early neural differentiation, suggesting its involvement in early brain development (Plaza, Dozier, Turque, *et al.*, 1995). However, the pB promoter has been reported to be highly active and primarily controls the PAX6 gene expression in adult human brain (Okladnova *et al.*, 1998).

2.5.2 Alternative splicing and expression of different PAX6 variants

Pax6 is a tissue specific transcription factor and contains multiple functional domains that aid in DNA binding and protein-protein interactions. Alternate promoter activities and differential splicing enables a single gene to encode more than one transcript variants and protein isoforms, with or without a combination of different functional domains. Thus, mRNA transcripts with variable stabilities and protein isoforms with diverse functions are generated, to orchestrate complex cellular behaviour's.

Canonical Pax6 or PAX6A in mice and humans encodes a 422 amino acid protein with two DNA binding domains, namely the Paired Domain (PD) which is comprised of 128 amino acids and is present at the N terminus; the second Homeobox domain in the middle is comprised of 68 amino acids. The paired domain and the homeobox domain are separated by a 78 amino acids long, glycine-rich linker sequence. A proline-serine-threonine-rich (PST) transactivation domain (TAD) is located at the C-terminus that undergoes post-translational modifications such as phosphorylation and regulate target gene activations (**Fig 2.8.B**).

In mammals, paired domain of Pax6 is encoded by the exons 4-7. Crystallographic studies have shown that paired domain of human PAX6 protein is structurally and functionally separated into independent DNA binding sub-domains, termed as the N-terminal PAI domain and the C-terminal Red domain. Crystal structure analysis have showed that the PAX6 binds to a consensus DNA sequence, termed as P6CON, which is a bipartite site in which the 5' portion is strongly recognized by the PAI sub-domain and 3' portion is weakly recognized by the RED sub-domain (**Fig 2.8.C**).

The alternatively spliced forms in mice and humans are the Pax6-5a or PAX6B variants respectively, which is generated by the alternative splicing and in-frame insertion of 42 bases long exon 5a, located within the intronic region between exon 5 and exon 6 (**Fig 2.9.A**). Thus, the extra 14 aa encoded by exon 5a falls within the first helix of HTH region of the PAI subdomain of PAX6 and disrupts its DNA binding through PAI domain, without altering its interactions through the RED subdomain. The 5aCON consists of two half sites and PAX6-5a is predicted to bind as dimers through the RED domain (**Fig 2.8.C**) (J. A. Epstein *et al.*, 1994). Thus, PAX6A and PAX6B may have both common and unique set of target genes for regulation during brain and eye development and in adult tissue functions. Another possible mechanism by which alternative splicing of PAX6 can modulate PAX6 biological functions is through altered subcellular localization. An earlier study has showed that the alternately spliced isoform with 14 aa insertion and paired domain disruption is pan nuclear and

localized both in the nucleus and cytoplasm, whereas, the wild type isoform is completely nuclear (Carriere *et al.*, 1995).

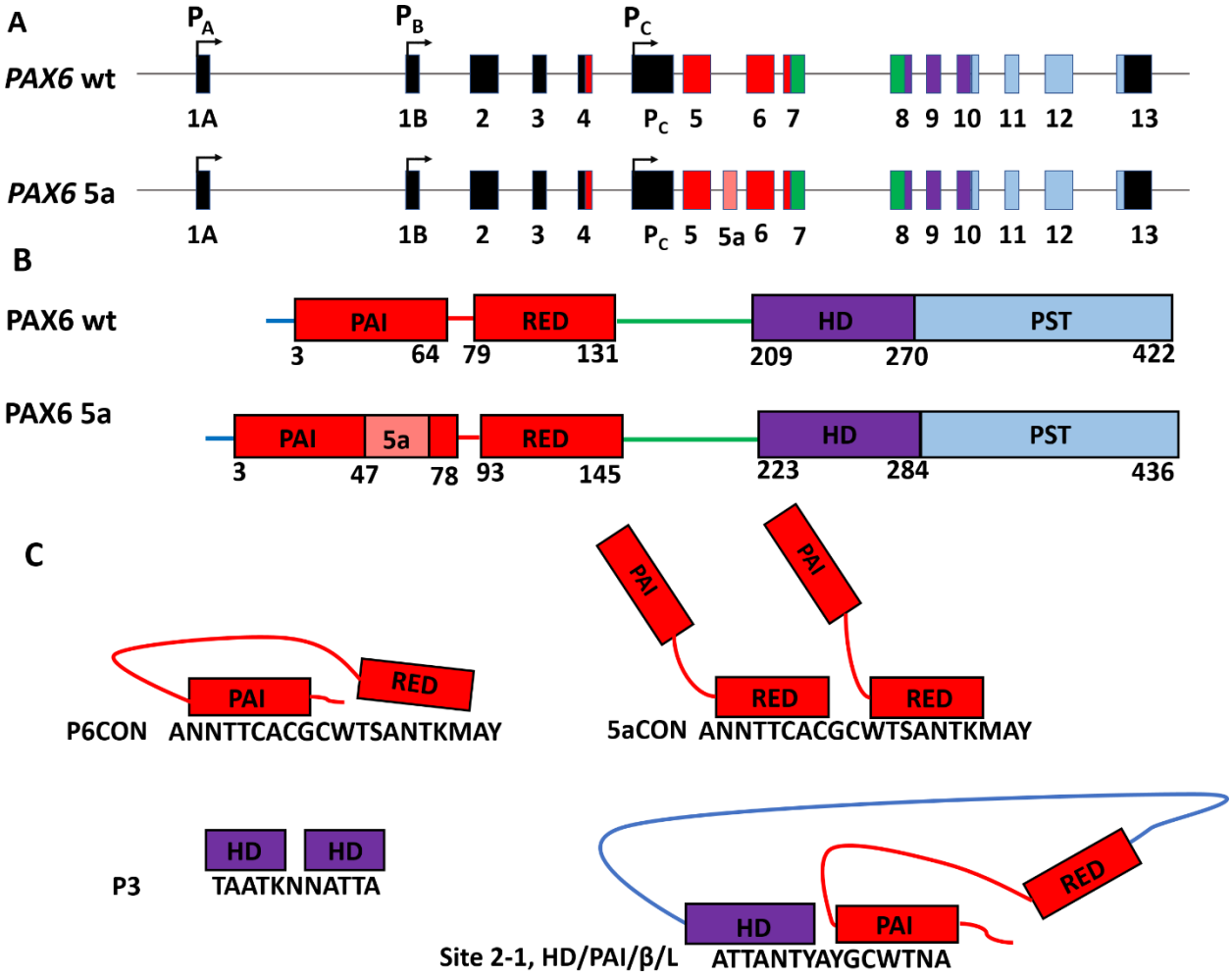

Figure 2.8: PAX6 genomic and protein structure. *PAX6 gene consists of 15 exons including exon a or Pc and alternative exon 5a. Coding exons are colored and noncoding exons are black in color. Transcription start sites of three different promoters are indicated by arrows. The pA, pB and pC promoters are differentially regulated to drive the expression of PAX6 transcripts (**A**). Exons coding for, paired domain are shown in red color, glycine rich linker are shown in green color, homeobox domain are represented in purple color and finally the PST domain are shown in light blue color (A, B). The two protein isoforms wt and 5a are generated by alternative splicing and they differ by 14 amino acid insertion within the PAI domain (**B**). Schematic representation of PAX6 domains and their consensus DNA binding sites; PAX6-wt (P6CON), PAX6-5a (5aCON) and homeodomain (P3) and site 2-1 is bound by HD, PAI, beta and linker regions (**C**). N is any nucleotide; Y is T or C; M is A or C; S is G or C; K is G or T; W is A or T.*

The ratio of canonical Pax6 and Pax6-5a varies from tissue to tissue. It is hypothesized that the canonical PAX6 is highly active during early cell fate determination and differentiation during the embryonic development, while PAX6 5a works in a spatially restricted manner and its role is important in regulating postnatal tissues. It has been found that the expression of canonical PAX6 is higher (8:1) as compared to PAX6-5a during embryonic development of the mouse lens. However, the ratio is just 1:1 in adult ocular tissues including lens, cornea and retina (W. Zhang *et al.*, 2001). Similarly, it has been observed in the chick embryonic retina that canonical Pax6 has higher expression in the lens primordium and lens placode whereas the expression of Pax6-5a increased in the later stages of the eye development, especially in lens and cornea (Azuma *et al.*, 2005). The gain of function and loss of function studies using transgenic models have showed that Pax6-5a is crucial for the development of lens and iris (N. Davis *et al.*, 2009; Singh *et al.*, 2002; Duncan *et al.*, 2000). Interestingly, no defect was noted in the retinal development of homozygous Pax6-5a deleted mice (Singh *et al.*, 2002). Pax6-5a is highly expressed in the foveal region and plays an essential role in the formation of cone cell rich fovea.

The homeobox domain is coded by the exons 8, 9 and 10 of PAX6 and is comprised of three α-helices with a HTH motif and it bind to the DNA cooperatively along with the paired domain and its target region is a palindromic sequence consisting of two inverted ATTA separated by 2 or 3 bases (**Fig 2.8.C**).

Apart from Pax6-Wt and Pax6-5a transcripts derived from the P0 and P1 promoters, the paired domain deleted Pax6-ΔPD or PAX6D is generated by the transcriptional activity of Pα or pC promoter. Pax6-ΔPD expression is observed in some of ocular tissues, but its normal physiological activities are not fully elucidated. Overexpression of this variant affects the development of the eye, disrupting lens and corneal development majorly and also results in microophthalmia (Kim *et al.*, 2008, 2006). A recent study has reported the involvement of PAX6D in the specification of neuroepithelium into neuro retina, through canonical wnt signaling regulation via the repression of Wnt8B (Tao *et al.*, 2020).

The C' terminal proline/serine/threonine-rich (PST) region of PAX6 is highly conserved and acts as the transactivation domain of Pax6 and is encoded by the exons 10-13 (**Fig 2.8.A**). All four exon encoded regions act synergistically to enable effective transcription of target genes, but none of them can act individually to stimulate the transcription of a heterologous GAL4 DNA binding domain

fusions (Tang *et al.*, 1998). The transactivation functions are mediated by the recruitment of multiple transcriptional co-activators via protein-protein interactions at the PST domain.

Apart from transcriptional functions, a recent study has reported a novel splice variant of Pax6 termed as Pax6(S), which interacts with Ca(2+) channel beta subunit (Ca(v)beta) and regulate the cell surface expression, localization and gating of high voltage-activated Ca(2+) channels. Pax6(S) contains the two paired domain and homeobox domains for DNA binding and a C' terminally truncated, PST rich transactivation domain. This novel variant is generated by the inclusion of intron 11 and encodes the unique C' terminal S tail (Y. Zhang, Y. Yamada*, et al.*, 2010). However, the detailed biological functions of this isoform during eye development are not known.

2.5.3 Tissue-specific enhancers of Pax6

Apart from alternate promoter choices (P0 or pA, P1 or pB and Pα or pC), the PAX6 gene is also controlled by multiple tissue specific, cis and trans-acting enhancer elements located either within the gene or at significant distances from the 5' and 3' ends of the coding region (**Fig 2.9**). Multiple regulatory sequences that control Pax6 gene expression have been identified based on sequence conservation, using transgenic reporter constructs and DNaseI protection assays (**Table 2.3**).

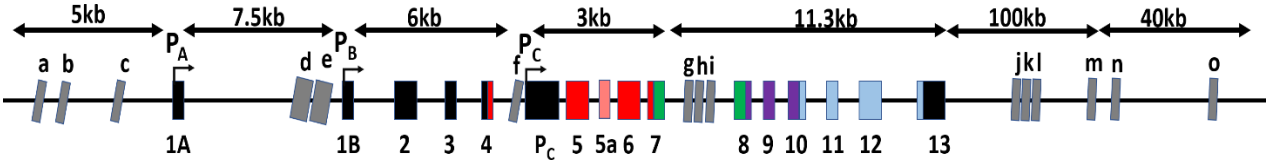

Figure 2.9: Schematic representation of Pax6 enhancers showing in the genomic regions of Pax6.

Table 2.3: Tissue specific enhancers in genomic region of Pax6

S.No	Regions of reporter expression	Approximate position coordinates from the TSS of the proximal P_0 promoter	Code in figure	References
1.	Islets of pancreas	-4.6 kb	a	(Kammandel *et al.*, 1999)
2	Pax6 ocular surface ectoderm enhancer	-3.9 kb	b	(Kammandel *et al.*, 1999)
3	cornea, lens, conjunctiva	~3.5 kb	b	(Williams *et al.*, 1998)

4	Pancreatic islets, retinal progenitor cells	-2.3 kb	c	(Xu *et al.*, 1999)
5	dorsal telencephalon, hindbrain, spinal cord	1.5-6.5 kb	d	(Kammandel *et al.*, 1999)
6	Photoreceptor progenitors	3.5 kb	e	(Xu *et al.*, 1999)
7	Ciliary body, iris, distal retina a, amacrine cells,	14 kb	f	(Xu *et al.*, 1999; Kammandel *et al.*, 1999; Plaza, Dozier, Turque*, et al.*, 1995)
8	Late eye development	17.5 kb	g	(Kleinjan *et al.*, 2004)
9	Diencephalon	19 kb	h	
	Rhombencephalon	21 kb	i	
10	Olfactory region, pretectum and neural retina	~105 kb, 106 kb, 107 kb	j, k, l	(Griffin *et al.*, 2002)
11	Lens, proximal retina, diencephalon, hindbrain and cerebellum	~110 kb	m	(Kleinjan *et al.*, 2006; Kleinjan *et al.*, 2001)
12	Neuroretina, RPE and telencephalon	~128 kb	n	(Kleinjan *et al.*, 2001)
13	Forebrain, diencephalon, pineal gland	~165 kb	o	(Kleinjan *et al.*, 2006)

Kammandel et al. identified tissue specific cis regulatory elements that control the expression of Pax6 in different mice tissues. The expression of Pax6 in cornea, lens, lacrimal gland, conjunctiva and pancreas is mediated through a 107 bp enhancer and a 1.1 kb 5' UTR region upstream of the P0 promoter (4.6 kb in total) (**regions a and b in Fig 2.9**). The Pax6 expression in neural retina and iris is mediated through a 530 bp fragment present downstream of the TSS (**region c in Fig 2.9**). A 5 kb fragment present in between promoter P0 and P1 regulates the expression of Pax6 in hind brain, spinal cord and dorsal telencephalon (**region d in Fig 2.9**). These cis-regulatory elements are highly conserved across species and provide binding sites for tissue-specific transcription factors and controls important events responsible for the development and homeostasis of different tissue types (Kammandel *et al.*, 1999). Another study has also reported that a highly conserved regulatory element of about 341 bp located 3.5 kb upstream of the proximal P0 promoter (**region b in Fig 2.9**) is required for Pax6 expression in lens and corneal epithelium (Williams *et al.*, 1998).

Another cis regulatory element present upstream of the P0 promoter (**region c in Fig 2.9**) mediates the expression of Pax6 in retinal progenitors and pancreas. A second regulatory element located upstream of the P1 promoter (**region e in Fig 2.9**) is also required for the expression of Pax6 in some of the post mitotic retinal neurons. A third element located within the intron 4 (**region f in Fig 2.9**) is also required for the expression in amacrine cells, ciliary body and iris tissues (Kammandel *et al.*, 1999; Xu *et al.*, 1999). Thus, the expression of Pax6 in the eye is differentially regulated by three different promoters and multiple cis acting regulatory elements or enhancers. By deleting the ectoderm enhancer region, a study has experimentally demonstrated that the Pax6 expression was diminished, but not completely eliminated, thus proving the combined activity of multiple regulatory elements in regulating PAX6 expression (Dimanlig *et al.*, 2001).

In addition to multiple cis-regulatory elements identified either upstream or within the intron/s, other distal regulatory elements have also been identified downstream of the Pax6 gene by analyzing the genomic regions of aniridia patients. Aniridia is usually caused by mutations or deletions in Pax6, and also a subset of patients carry two copies of PAX6 gene with chromosomal rearrangements. Kleinjan et al. have reported several putative cis regulatory elements using DNaseI hypersensitivity mapping and YAC reporter transgenic assays. A 420 kb YAC clone including the Pax6 coding sequence could rescue homozygous Pax6 sey/sey mice lethality, in the presence of the 3' region of Pax6 (Kleinjan *et al.*, 2001; Schedl *et al.*, 1996). This 3' region contains multiple regulatory elements that are functionally conserved between mice and humans (Tyas *et al.*, 2006) and are collectively named as downstream regulatory region (DRR) (**regions j-o in Fig 2.9**). The activity of DRR is essential for the expression of Pax6 in some but not for all tissues (Kleinjan *et al.*, 2006).

2.6 Corneal tissue maintenance

The cornea is an avascular and transparent tissue present on the outside of the ocular surface and contributes to more than 60% of the refractive power of the eye. It protects the eye from environmental damages by acting as a physical barrier between the internal structures of the eye and the external surrounding. The cornea is made of five distinct layers namely, the epithelium, Bowman's layer, the stroma, Descemet's membrane and the endothelium (**Fig 2.10**). The outermost layer of the cornea is the corneal epithelium and is continuously bathed by the tear film. It consists of 4-5 layers of stratified squamous non-keratinized epithelium of about 40-50 μm thickness and is comprised of

three types of cells, viz; superficial squamous cells, central suprabasal cells, also called as wing cells and the internal single layer of columnar basal cells.

The mucinous basal layer of the tear film ensures uniform spreading of the tear film on top of the differentiated superficial squamous epithelial cells via adhesions through the microvilli and microplicae and keeps the epithelial cells sufficiently hydrated and nourished. The suprabasal wing cells contain polyhedral cells which rarely undergo cell division. These cells migrate superficially to become terminally differentiated squamous cells. The basal cells of the corneal epithelium are mitotically active and act as a source for wing and superficial cells. The epithelial cells of cornea are connected to the basement membrane with the help of hemidesmosomes. Superficial and basal cells of the corneal epithelium are tightly joined together through tight junctions and provide the barrier function to the cornea. The stromal keratocytes secrete collagen and glycosaminoglycans to maintain the corneal thickness, strength and transparency. The monolayer of endothelial cells present at the posterior part of the cornea are enriched with ion and water channel pumps and helps in epithelial nourishment and in maintaining optimal corneal hydration and transparency. The Bowman's and the Descemet's layers serves as thick basement membranes for the corneal epithelium and the endothelium respectively and helps in maintaining the corneal structural integrity.

Unlike the endothelium and the stromal cell layers of the cornea, the surface epithelial cells continuously undergo slogging and get replenished by the mitotic activity of the stem cells residing at the limbus. The limbus acts as the niche for corneal epithelial stem cells and also acts a boundary between the corneal and conjunctival epithelium. The conjunctival epithelium is highly vascularized unlike the corneal epithelium. The non-keratinizing stratified epithelium of the conjunctiva is contiguous with the corneal epithelium. It also contains the goblet cells that secrete mucin, which constitutes about 10% of the total conjunctival cell population.

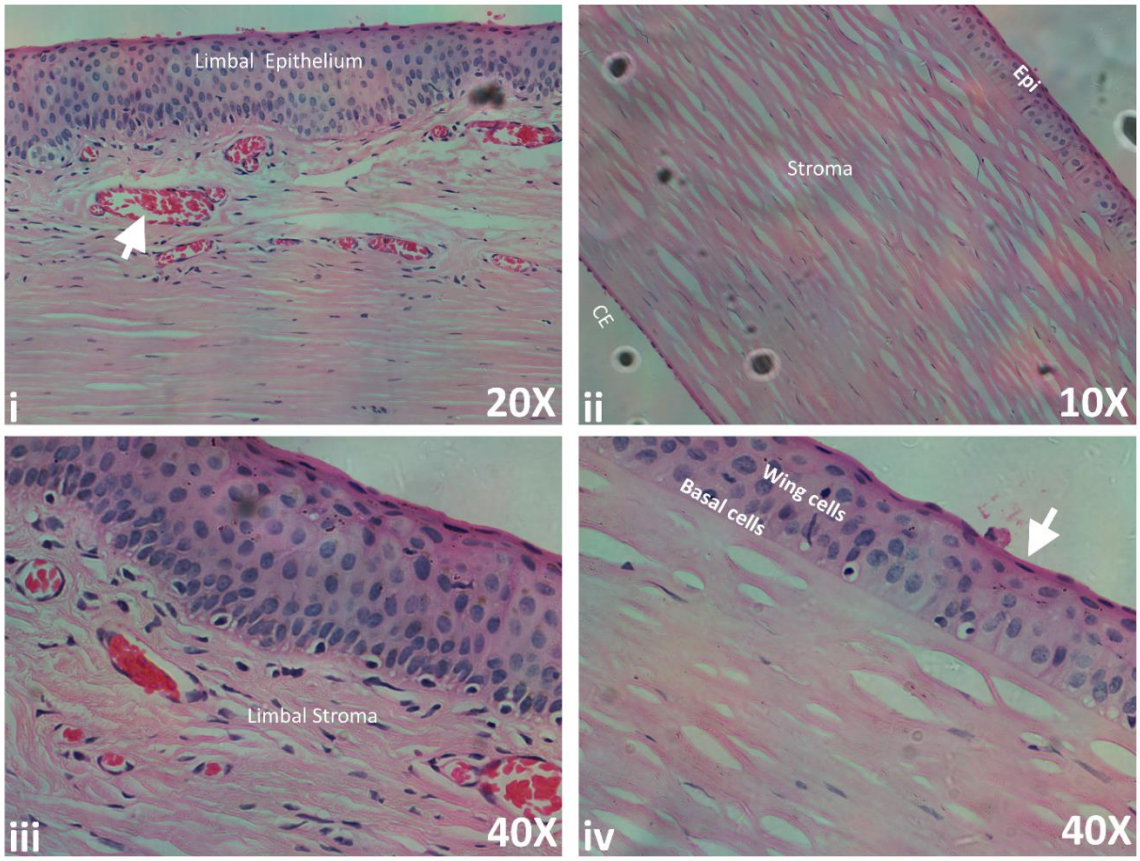

Figure 2.10. Cross-sectional view of an adult human corneal tissue. *Hematoxylin and eosin stained images of human corneal sections. (**i**) Adult limbal epithelium showing 7-8 layers of epithelial cells with crypt-like projections deep into the limbal stromal layer. Arrow points to the blood vessels in the limbal stroma.(**ii**) Adult central corneal epithelium showing 4-5 layers of epithelial cells; Bowman's membrane, stroma, Descemet's membrane and the inner endothelial monolayer; (**iii**) Magnified view of the limbal region. (**iv**) Magnified view of the central corneal epithelium showing columnar basal cells, suprabasal wing cells and the superficial flat epithelial cells (Arrow).*

2.6.1 Limbal epithelial stem cells (LESCs)

The limbus forms the boundary between the transparent cornea and the opaque sclera and serves as the niche for corneal epithelial stem cells and acts as a barrier for the conjunctival vasculatures. Limbal damage results in the migration of conjunctival cells onto the corneal surface, thus forming an opaque and vascularized pannus tissue in LSCD eyes.

Adult corneal epithelium undergoes regeneration and this is mediated by the limbal stem/progenitor cells present within the "palisades of vogt" at the limbus (Lavker *et al.*, 2004; Davanger & Evensen, 1971). Upon corneal surface injury, the quiescent LSCs residing at the basal regions of the limbus gets

activated and undergoes both asymmetric and symmetric cell division, for the self-renewal of daughter cells and also to produce transiently amplifying cells (TACs) respectively. The TACs migrate centripetally towards the basal layer of the corneal epithelium, from where they further migrate apically and undergo differentiation to finally become the post-mitotic, terminally differentiated cells (TDCs) or the mature corneal surface epithelium. During normal blinking and surface wear and tear, the senescent surface epithelial cells shed from the ocular surface, which in turn stimulates further cell division, migration and differentiation (**Fig 2.11**) (Schermer *et al.*, 1989).

The limbal stem cells are mitotically inactive; however they possess high proliferative abilities during the transiently amplifying stage. DNA labeling experiments have shown that the basal epithelial cells of the limbus retain the tritiated thymidine after long chase periods. The putative stem cells present in the basal layer of the limbal epithelium are smaller, with high nucleus to cytoplasmic ratio and the nucleus is rich in heterochromatin with no well-defined nucleoli. These putative limbal basal stem cells are shown to either uniquely or differentially express some of the markers such as: ΔNp63α, ABCG2, CK15, CK14, CK17, Frizzled 7 and ABCB5 (Mei *et al.*, 2014; Yoshida *et al.*, 2006; Di Iorio *et al.*, 2005; Watanabe *et al.*, 2004). The corneal basal TACs express Nestin, Connexin 43, E-cadherin, involucrin, integrin alpha9, TCF4, AQP1, p75NTR and are negative for the expression of mature corneal epithelium-specific keratins like CK3 and CK12 (Z. Chen *et al.*, 2004).

2.6.2 Limbal epithelial stem cell niche

The stem cell niche is a microenvironment that comprises of both the structural, cellular and extracellular matrix components that together helps to maintain stem cells (SCs) in an undifferentiated state (Schofield, 1983). Therefore, the corneo-limbal margin acts as an excellent model to study SCs. The regional demarcation, compartmentalization and the location of SCs exclusively within the limbal margin indicates the existence of specialized microenvironment at the limbus. The limbus is devoid of Bowman's layer that separates the epithelium and the underlying stroma and therefore enables direct interaction of the stromal niche cells (stromal keratocytes, melanocytes, vascular, neural and immune cells) and the limbal basal epithelial cells. Unlike the cornea, the "palisades of vogt" are supplied with blood vessels and lymphatics and this helps to nourish the stem cells and establishes the limbal niche. The niche cells that are in close association with the LSCs provide the necessary ECMs and paracrine support to regulate their self-renewal and differentiation behaviour's (W. Li *et al.*, 2007) (**Fig 2.11**).

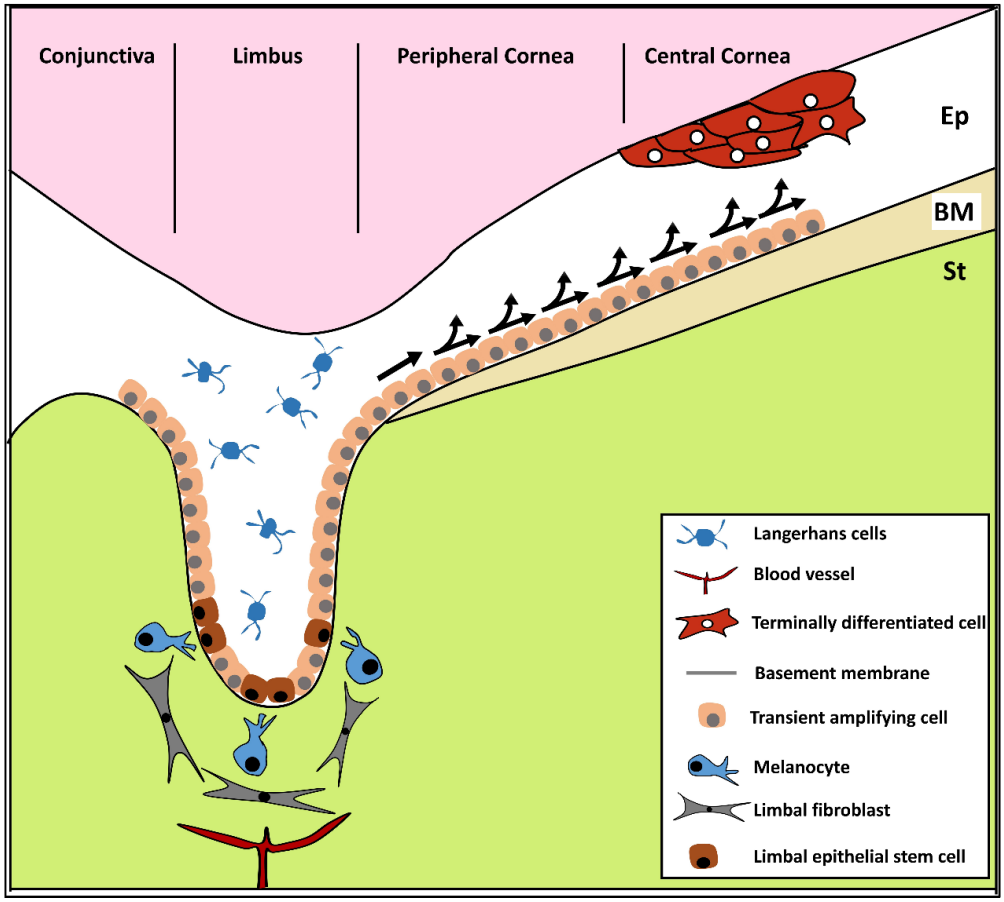

Figure 2.11: Cartoonic representation of the human limbus*. Limbal epithelial stem cells are present at the periphery of the cornea. Transient amplifying cells (TACs) that remain adhered to the Bowman's membrane in the epithelial basal layers (BM) undergo cell division and migrate centripetally towards the central cornea. The stroma of the limbus contains blood vessels, melanocytes and fibroblasts. Modified illustration based on (Notara et al., 2011).*

2.6.3 XYZ hypothesis of corneal epithelial maintenance

XYZ hypothesis of corneal epithelial migration was first proposed by Thoft and Friend in 1983 to describe the normal corneal epithelial homeostasis. As shown in figure 2.13, the XYZ hypothesis proposed that 'X' represents the proliferating cells at the limbal basal layers, 'Y' represents the centripetal migration of TACs from the limbal periphery towards the central cornea and 'Z' represents the loss of superficial cells from the corneal surface during normal desquamation (**Fig 2.12**). According to the hypothesis, the normal corneal homeostasis can be maintained only when X + Y = Z. In other words, the net cell loss should be compensated by a corresponding cell regeneration (Thoft & Friend, 1983). However, this hypothesis failed to describe the importance of LESCs, which plays a crucial role in the maintenance of corneal epithelium. To perfectly explain the corneal epithelial

homeostasis, Mort *et al.*, 2012 reinterpreted this model by taking into account the LESCs and TACs and proposed that, $Y_{SC} + X_{TAC} = Z_L$, where Y_{SC} is the production of basal epithelial cells from the limbus, X_{TAC} is the proliferation of basal TAC cells and Z_L is the loss of epithelial cells (Mort *et al.*, 2012).

Some elegant studies have observed the migration of corneal epithelial cells in chimeric and X-Gal reporter mosaic mice, where the pattern of adult corneal epithelium development was tracked and observed through LacZ expressing cells (Collinson *et al.*, 2002). The daughter cells produced from the LSCs were tracked by X-Gal staining and the observation of distinct striped mosaic patterns in the corneal epithelium clearly suggested the existence of a peripheral limbal niche and the centripetal migration of proliferating cells from the periphery towards the center during normal corneal development and wound healing. Nagasaki and Zhao, 2003 also followed the same technique to visualize the striped patterns of cell clones migrating from the periphery to the center in live animals, using the transgenic GFP mosaic mice, which expressed GFP constitutively under the control of β-actin promoter (Nagasaki & Zhao, 2003). Recently, Di Girolamo et al performed multiple cell lineage tracing experiments to visualize the independent stem cell clones and their progenies using multi-coloured fluorescent reporter protein expressing K14CreERT2 confetti mice, which contains the Brainbow 2.1 cassette (Di Girolamo *et al.*, 2015). All these studies confirmed that the long term maintenance of corneal epithelium depends on the stem cells residing at the limbal niche.

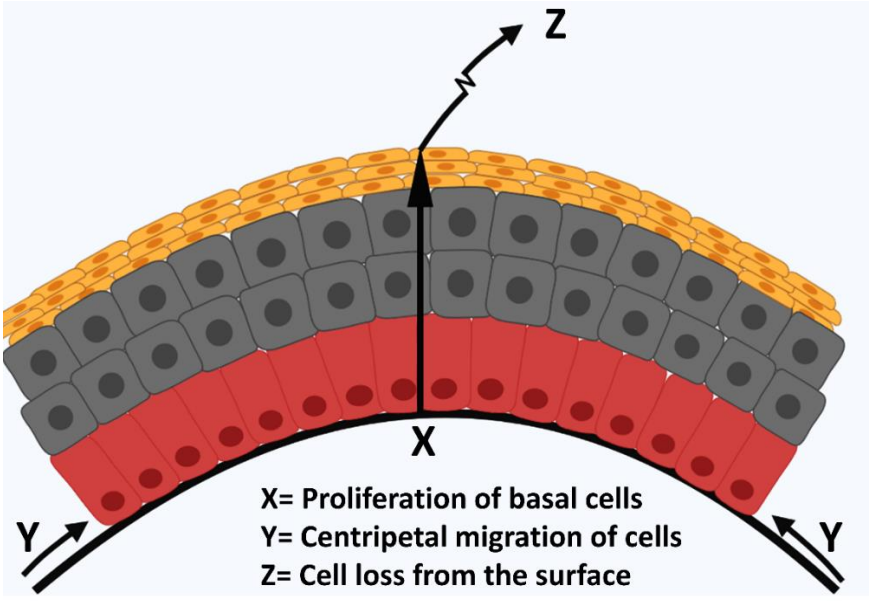

Figure 2.12: XYZ hypothesis of corneal epithelial homeostasis. *The proliferative, transiently amplifying basal columnar cells are represented in red color. The differentiating and migrating wing cells are shown in grey and the terminally differentiated and mature epithelial cells on the surface are shown in orange.*

2.6.4 Limbal stem cell deficiency (LSCD)

Limbal stem cell deficiency (LSCD) can occur as a primary cause or can happen as a result of acquired injury. Patients with hereditary aniridia usually suffer with primary LSCD. The stem cells/transient amplifying cells (TAC) are lost due to dysregulation of the stromal microenvironment, thus leading to LSCD and severe epithelial defects. External factors such as trauma, chemical injuries (acid or alkali burns) or thermal injuries or systemic auto-immune conditions such as the Stevens-Johnson syndrome (SJS) can cause damage to the LSCs and eventually leading to limbal stem cell deficiency (LSCD). LSCD patients display a total loss of corneal epithelial regeneration, conjunctivalization and neovascularization of corneal surface, leading to persistent inflammation. The opaque and vascular pannus tissue growth on the ocular surface affects the corneal transparency and leads to partial or complete blindness (**Fig 2.13**) (Dua *et al.*, 2003).

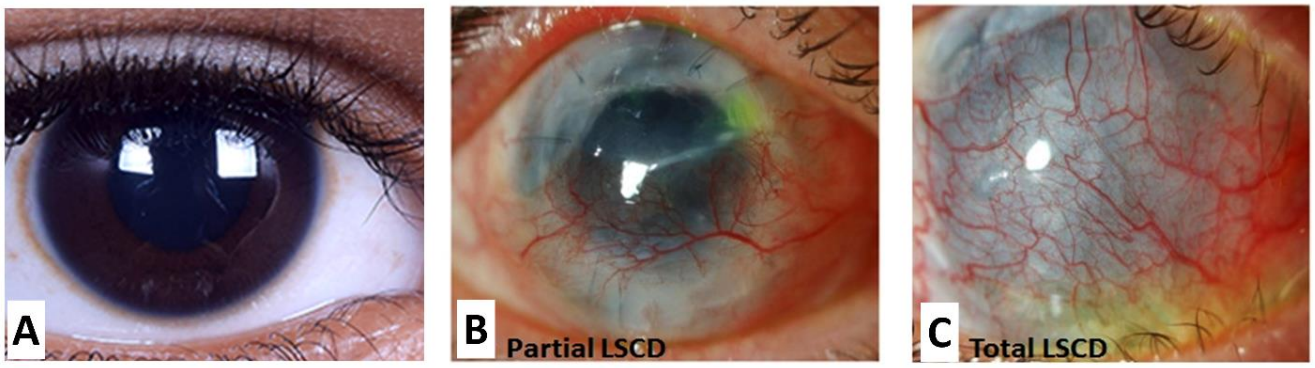

Figure 2.13: Corneal surface view of LSCD eyes: *A. Normal corneal surface, B. Partial LSCD eye with some part of the superior limbus being normal and healthy, C. Total LSCD eye with a complete 360° loss of limbal margin and the corneal surface is covered by the opaque and highly vascularized conjunctival epithelium.*

2.6.5 Therapeutic management of LSCD

Currently, LSCD is managed through autologous or allogeneic limbal tissue transplantation, or in cases where autologous or allogenic tissues are not available, ex vivo cultured limbal epithelial cell sheets are used to reconstruct damaged ocular surface. The success rate for these therapeutic approaches is around 60-70% (Basu *et al.*, 2012; Baylis *et al.*, 2011; Rama *et al.*, 2010). In most cases, the clinical

outcomes are directly related to the presence of limbal stem cells in the donor grafts and this further emphasizes the importance of limbal stem cells in corneal regeneration. For *ex vivo* expansion of limbal stem cells, various groups have used different substrates such as the recombinant collagen gels, fibrin gels, PLGA polymers, plasma polymer coated surfaces, thermo sensitive polymer coated surfaces, mitotically inactivated murine NIH-3T3 fibroblasts, human limbal stromal fibroblasts and human amniotic membrane (hAM) for preparing transplantable sheets of corneal epithelium (Mariappan *et al.*, 2010). To treat bilateral limbal stem cell deficiency, researchers are exploring stem cell derived corneal organoids or corneal epithelial-like cells derived from human embryonic stem cells (Ahmad *et al.*, 2007), induced pluripotent stem cells (Susaimanickam *et al.*, 2017; Foster *et al.*, 2017; Hayashi *et al.*, 2016) and also by transdifferentiation of dental pulp stem cells and hair follicle stem cells (Blazejewska *et al.*, 2009). Such approaches may provide alternate therapeutic modalities for the treatment of patients suffering from bilateral LSCD.

2.7 Signalling pathways and Pax6 regulation in the cornea

2.7.1 Role of Pax6 in corneal epithelial maintenance

Apart from the requirement of PAX6 for corneal tissue morphogenesis during early development, it is important for the normal tissue maintenance during adulthood (J. Davis *et al.*, 2003; Koroma *et al.*, 1997). As described earlier in Section 2.4.4.2, PAX6 is expressed in adult limbal and corneal epithelial cells and a conditional genetic knock out in adult corneal tissues disrupts corneal epithelial maintenance and normal homeostasis (Latta *et al.*, 2019; Kitazawa *et al.*, 2017; H. Ouyang *et al.*, 2014). Loss of PAX6 in LSCs downregulates the expression of corneal differentiation markers, KRT3 and KRT12 and the corneal epithelial gets transdifferentiated into skin-like epithelium coupled with hair follicle development (G. Li *et al.*, 2015; H. Ouyang *et al.*, 2014; Y. T. Chen *et al.*, 2013). A recent study had used CRISPR-Cas9 system to knock out PAX6 gene in human limbal cultures and shown that it resulted in the downregulation of KRT3, KRT12 and ALDH3A1 and a loss of corneal epithelial identity. These cells also upregulated the expression of keratin 10, keratin 1, involucrin (IVL), filaggrin (FLG) and attained a skin-like phenotype (Kitazawa *et al.*, 2017). Heterozygous ($Pax6^{+/-}$) mouse serves as an excellent model to study the importance of Pax6 dosage and its effects in corneal epithelial maintenance and wound healing (Ramaesh *et al.*, 2006; J. Davis *et al.*, 2003). Expression of Pax6 from both the alleles is required to maintain the normal corneal epithelial cell adhesion and migration in adult cornea. $Pax6^{+/-}$ heterozygous mice showed large gaps in the epithelial cells, with changes in the

appearance of hemidesmosomes and impaired cell adhesion (J. Davis *et al.*, 2003). Another study has shown that the expression of Pax6 is high in the epithelial cells at the migrating front, where it regulates the expression of MMP9 and aids in extracellular matrix modulation and wound closure (Sivak *et al.*, 2004). Thus, Pax6 plays a crucial role in maintaining corneal epithelium throughout adulthood.

2.7.2 Spatial and temporal expression of Pax6 isoforms in the eye

Differential expression of Pax6 isoforms in ocular tissues is very well described in many organisms from drosophila to humans. Jang et al. demonstrated that Pax6 drosophila homologs, eyg and ey are expressed in different regions of eye discs (Jang *et al.*, 2003). The ratio of the expression of the two isoforms of Pax6 i.e. wt and 5a is differentially, tightly and temporally regulated in a tissue specific manner during the chick eye development. The expression level of Pax6-5a is high in the temporal and posterior part of retinal tissues during early eye development, while the Pax6-wt is expressed throughout the retina. Also, upon overexpression it induced the development of retina-like structures (Azuma *et al.*, 2005). Pax6-wt is mainly expressed in the lens and retina, whereas Pax6 5a is preferentially expressed in the iris and cornea in bovine eyes (Jaworski *et al.*, 1997). During early neurogenesis, Pax6-wt transcripts are expressed at 6-10 times more abundant than the Pax6-5a transcripts in murine telencephalon, diencephalon and hindbrain and this ratio was observed to reduce significantly to about 3:1 during later development (Pinson *et al.*, 2005). Similarly, Pax6 expression is differentially expressed in adult corneal epithelium. Frozen section of the human corneal epithelium was micro dissected into four zones namely: limbal-apical, limbal-basal, central-apical and central-basal and the expression level of PAX6 isoform was assessed. The study observed that both isoforms were co-expressed in individual cells and were relatively highly expressed in the central-apical region. Interestingly, the PAX6A expression was higher both in the central-apical and limbal-apical region, whereas PAX6B expression was higher only in central-apical region (Sasamoto *et al.*, 2016).

2.7.3 Effects of gain or loss of function of Pax6 isoforms in the eye

The right dosage and spatio-temporal expression of different Pax6 isoforms is tightly regulated and is critical for normal eye development. This is evident from the observation that haploinsufficiency of Pax6 ($Pax6^{+/-}$) in mice and humans results in aniridia. In contrast, the Pax77 transgenic mouse that overexpressed PAX6, by the insertion of 5-7 copies of a human PAX6, exhibited opaque microcorneas, with normal looking stroma and without the development of goblet cells or blood

vessels (Schedl *et al.*, 1996). In brain, graded expression of Pax6 is important for the correct specification in major areas of the developing neurocortex (Bishop *et al.*, 2002).

Overexpression of Pax6-wt in normal mice corneas under the control of a cornea-specific, Aldh3a1 promoter resulted in corneal opacification, neovascularization, changes in corneal thickness and immune cell invasion in the stromal region. Additionally, the expression of cornea-specific keratin, CK12 was found to be drastically reduced in PAX6 overexpressing cells (J. Davis *et al.*, 2003). This confirms that both the loss of expression and overexpression of Pax6 can cause severe eye and corneal abnormalities.

Similarly, the lens development is also critically regulated by PAX6 levels and spatio-temporal expression. Overexpression of human or mouse PAX6-wt in transgenic mice, under the control of mouse alphaA-crystallin promoter was reported to be associated with lens fiber cell differentiation defects. The formation of lens placode is delayed and the cells fail to express N-cadherin and undergo apoptosis. The lens cup fails to completely detach from the surface ectoderm and develops abnormally (Duncan *et al.*, 2004; van Raamsdonk & Tilghman, 2000). Similarly, overexpression of human Pax6-5a resulted in cataract and the disintegrating lens fiber cells showed upregulated expression of α5 and β1 integrin's, Paxillin and p120 (Duncan *et al.*, 2000). Overexpression of Pax6-5a in the eyes of chicken embryos induced the formation of differentiated retina-like structure, thus indicating the involvement of Pax6-5a in retinal differentiation (Azuma *et al.*, 2005).

In Drosophila melanogaster, ectopic expression of human PAX6-5a variant resulted in tissue overgrowth / hyperplasia, whereas the Pax6-wt had no effect (Dominguez *et al.*, 2004). Elegant experiments using different PAX6 mutant mice models have shown that the paired domain is necessary for the regulation of neurogenesis, cell proliferation and brain tissue patterning. However mutations within the homeodomain only resulted in minor defects in forebrain development. Similarly, retroviral vector mediated expression of Pax6-5a in neural progenitors inhibited cell proliferation, without influencing cell fate decisions, while the PAX6-wt affected both cell proliferation and cell fate (Haubst *et al.*, 2004). Suppression of pluripotency genes and the induction of neuro ectodermal genes are required for the differentiation of embryonic stem cells (ESCs) into neuronal cells. While the knock out PAX6 gene blocked neuro-ectodermal lineage specification of human ESCs, it did not affect the differentiation of mouse ESCs into neurons. This confirms the species-specific roles of PAX6 and its importance for neuro-ectodermal specification in humans. Also,

overexpression studies have shown that both PAX6A and PAX6B isoforms can regulate pluripotency genes and induce ectodermal differentiation. However, only PAX6A could regulate the neuro-ectodermal genes and trigger neural fate commitment (X. Zhang *et al.*, 2010). Another study has shown that the two PAX6 isoforms differentially regulate the expression of the two key cornea-specific genes namely, KRT3 and KRT12, when overexpressed in oral mucosal epithelial cells that do not express PAX6. Mutation in either KRT3 or KRT12 causes Meesmann corneal dystrophy, an autosomal dominant disorder. It was observed that the overexpression of PAX6B, along with KLF4 and OCT4 stimulated the expression of KRT12. However, PAX6A induced the expression of KRT3 and this was further induced in co-operation with KLF4 (Sasamoto *et al.*, 2016).

This indicates that PAX6 isoforms have different functional roles during neuroectodermal specification, brain and eye development and in adult corneal epithelial homeostasis. Based on these evidences, we hypothesize that PAX6-wt may be responsible for stem cell differentiation and cell fate specification, whereas, PAX6-5a may be involved in gene regulation during progenitor cell proliferation and expansion.

2.7.4 Autoregualtion of Pax6

Transcription of PAX6 is mainly controlled by two promoters namely, the distal P0/pA and the proximal P1/pB in mouse and humans respectively. Studies on quail gene have shown that, Pax6 can bind to its own promoter at multiple sites and regulates its expression (Plaza, Dozier, Turque*, et al.*, 1995; Plaza *et al.*, 1993). The quail Pax6-P0 promoter-driven CAT reporter activity in neuroretinal cells was positively autoregulated and induced by the co-expression of quail Pax6 (Plaza, Dozier, Turque*, et al.*, 1995; Plaza *et al.*, 1993). Another study has reported both negative and positive autoregulation of human pB promoter by Pax6-wt, when co-expressed in COS-7 and JAR cells respectively (Okladnova *et al.*, 1998). Grocott et al. 2007 reported that the expression of human Pax6 gene is controlled by TGFβ/Smad3 signaling in lens epithelial cells. TGFβ suppresses the activity of Pax6 by the translocation of Smad3 from the cytoplasm to nucleus. In nucleus, the MH1 domain of Smad3 interacts with the RED subdomain within the paired domain of Pax6 and releases it from its own DNA binding site on the human PAX6-pA promoter and inhibits its transcription and in turn blocks its effect on downstream target genes. Smad3 may differ in its interaction with Pax6-5a due to the insertion of 14 amino acids within the paired domain, which might disrupt this protein-protein

interaction (Grocott *et al.*, 2007). Thus, the auto-regulatory loop of PAX6A is targeted and repressed by the TGFβ signaling in lens epithelium.

2.7.5 Role of Wnt signalling in corneal epithelial maintenance

Wnt signaling plays a very important role in the regulation of cell proliferation, migration, fate commitment, differentiation, cell polarity and in determining the neural patterning and organogenesis during early development and in tissue repair during adult homeostasis. The canonical Wnt/β-catenin signaling in turn regulates other signal transduction cascades, including the non-canonical planar cell polarity pathway and the BMP/TGFβ signaling and regulates various complex cellular behaviours. The Wnts are secreted glycoprotein ligands that bind to the frizzled (Fz) family of transmembrane receptors and mediate signal transduction from outside to inside of the cell.

When the Wnt ligands binds to their cognate receptors, the external signals gets transmitted to the cytosolic phosphoprotein, Dishevelled (Dsh/Dvl). Dsh acts downstream of Wnts and play a pivotal role in regulating the three branches of Wnt signaling namely, the canonical Wnt/β-catenin signaling, the non-canonical planar cell polarity (PCP) pathway and the Wnt-Calcium pathway. To antagonize the Wnt signaling, a number of secreted antagonistic proteins present in extracellular matrix competes and prevents the binding of Wnts to the Frizzled receptors or the LRP5/6 co-receptors. Some of the Wnt ligand antagonists are Dickkopf family of proteins (DKKs), Wnt inhibitory factor 1 (WIF1) and the soluble/secreted Frizzled-related proteins (SFRPs). The secreted wnt ligands and antagonists together set the localized Wnt signalling gradients and regulate tissue patterning during embryogenesis.

The canonical or the Wnt/β-catenin dependent pathway was first identified in drosophila and is highly conserved across all species such as, plants, flies, worms, frog, fish and mouse and higher order mammals. The downstream signal effector in the canonical pathway is the translocation of β-catenin from the cytoplasm to the nucleus. When the canonical signaling is absent, the destruction complex [which includes the Axin, Protein Phosphatase 2A (PP2A), Adenomatosis Polyposis Coli (APC), glycogen synthase kinase 3β (GSK3β) and casein kinase 1α (CK1α)] sequesters and phosphorylates the cytosolic β-catenin and targets it for proteosomal degradation. When Wnt signaling is active, the Wnt ligand binds to its cognate Fz receptor along with the co-receptors LRP5/6 and initiates a series of downstream signal transduction events that disrupts the cytosolic β-catenin degradation complex. This includes Axin mediated activation of Dsh which further gets phosphorylated by casein kinase 1 and 2, inhibits the GSK3β enzyme activity and prevents the phosphorylation and degradation of β-

catenin. The stabilized β-catenin accumulates in the cytoplasm and further translocates to the nucleus, where it binds to wnt target promoters along with the TCF/LEF1 co-activators and acts as a transcriptional factor to regulate gene expression.

Wnt signaling plays an important role in the regulation of different types of stem cells residing at various stem cell niches and dictate their proliferation and differentiation decisions. In the intestinal crypts or the epithelial stem cell niche, the myofibroblasts secrete Wnt ligands and regulate stem cell proliferation and self-renewal. Wnt inhibition abrogates stem cell activation and proliferation and results in the destruction and loss of intestinal crypts (S. Y. Chen *et al.*, 2011; Pinto *et al.*, 2003). Also, in the epidermis, specific depletion of β-catenin in the basal layers disrupts the hair follicle morphogenesis during development. However, when β-catenin is ablated postnatally, it results in the loss of hair follicles in mice, which further emphasizes the importance of Wnt/β-catenin signaling in stem cell regulation and epithelial maintenance (Huelsken *et al.*, 2001). In human cornea, multiple wnt ligands such as Wnt2, Wnt11, Wnt16b; wnt antagonists such as DKK1, WIF1, SFRP2, SFRP5, FRZB; Wnt receptors such as frizzled 7 and the transcription factor, TCF4 are predominantly expressed in the limbus and the basal epithelial layers, where the corneal epithelial stem cells reside (Mei *et al.*, 2014; Lu *et al.*, 2012; Nakatsu *et al.*, 2011; Kulkarni *et al.*, 2010). However, the nuclear localized β-catenin was detected only in a subset of limbal supra-basal cells.

Lithium chloride or small molecules like BIO or CHIR99021 treatment inhibits GSK3β, and activates the canonical wnt-β-catenin signaling in ex vivo limbal primary cultures. Studies have shown that lithium chloride treatment of limbal cultures induced the nuclear localization of β-catenin and activation of canonical wnt signaling, which resulted in increased cell proliferation and colony forming efficiency. These cells expressed higher levels of stem cell markers such as ABCG2 and ΔNp63 and lower levels of corneal differentiation marker, CK12 (Nakatsu *et al.*, 2011). The same group has shown that the stem cell proliferation and expansion is enhanced upon activation of wnt signals by blocking DKK2 using the small molecule, IIIC3 in ex vivo human limbal cultures. Alternately, inhibition of wnt signals using the small molecule, IC15 significantly affected the colony forming efficiency and total cell yield (Gonzalez *et al.*, 2019). Similarly, shRNA mediated knock down of TCF4 resulted in reduced limbal epithelial cell proliferation (Lu *et al.*, 2012; Lu *et al.*, 2011). Conditional expression of the stabilized form of β-catenin in CK12 expressing corneal epithelium resulted in hyperplastic transformation in transgenic mouse corneas, wherein the abnormally proliferating epithelial cells

organized into nodules and lost the expression of corneal markers such as Pax6 and CK12 (Y. Zhang, M. K. Call*, et al.*, 2010). Conversely, conditional expression of stabilized β-catenin in Keratocan expressing corneal stromal keratocytes significantly affected the stratification of corneal epithelium. These epithelial cells showed down regulated expression of ΔNp63 and BMP4, without any effects on PAX6, CK12 and CK14 expression (L. Zhang *et al.*, 2019). Another study has shown that Wnt7a and its cognate receptor, FZD5 induces PAX6 gene expression, which together with p63 regulates the differentiation of corneal epithelial cells. Knockdown of either Wnt7a or FZD5 reduced the expression levels of PAX6 and resulted in skin-like transformation of corneal epithelium, without affecting cell proliferation (H. Ouyang *et al.*, 2014). The limbal basal stem cells expressed Frizzled 7 (Fz7) and shRNA mediated knockdown resulted in significantly decreased expression of stem cell markers such as ABCG2, ΔNp63α and K14 (Mei *et al.*, 2014).

Similarly, the soluble wnt antagonist, Dkk2 plays an important role in regulating the corneal fate of ocular surface epithelium, by repressing the canonical wnt signaling during development. Loss of DKK2 expression results in epidermal-like transformation and conjunctivalization of corneal epithelium. The cornea of Dkk2 knockout mice appears completely opaque with hair outgrowths, sebaceous glands and conjunctiva-specific goblet cells (Mukhopadhyay *et al.*, 2006). Another study has shown that the DKK2 expression is lost in the neural-crest derived, periocular mesenchymal cells in Pitx2 null mice. Also, in DKK2 null mice, the Pitx2 expression persists in these cells, which suggests that Pitx2 directly induces DKK2, which in turn negatively regulates both Pitx2 and canonical wnt signals in neural crest cells and ocular surface ectoderm. Similar to DKK2 null mice, the Pitx2 null mice also show aberrant wnt activation and proliferation of ocular surface cells, with epidermal transformations and ectopic blood vessel formation (Gage *et al.*, 2008). Another study has shown that both PAX6A and PAX6B can directly bind to the DKK3 promoter and regulate its expression (Forsdahl *et al.*, 2014).

2.7.6 Wnt and BMP signaling cross talk in corneal epithelial differentiation

Many studies have shown that the canonical BMP and wnt signals regulate each other and dictate epithelial stem cell maintenance, self-renewal and differentiation decisions. The limbal basal epithelial cells were shown to express several BMPs such as BMP1, BMP2, BMP3, BMP4, BMP5 and its receptors, BMPRIA, BMPRIB and BMPRII (Maruyama-Koide *et al.*, 2017; Han *et al.*, 2014). A recent study has shown that during the mouse CE stratification from PN12 to PN20, BMP6 and its receptors

BMPR1A and BMPR2 were upregulated and the antagonist, Noggin was downregulated. Also, exogenous application BMP6 inhibited cell proliferation and induced the expression of differentiation markers like Klf4, p21 and desmosomal cadherins to promote corneal epithelial cell stratification (Tiwari *et al.*, 2020).

The limbal niche cells expresses Noggin and DKK1/2 which are antagonists for the canonical BMP and wnt/β-Catenin signaling respectively. Blocking of BMP signals with Noggin treatment resulted in significant downregulation of Wnt7A and upregulation of DKK1, DKK2 and also induced the nuclear localization of β-Catenin and activation of wnt signals in limbal epithelial stem cells. Similarly, blocking wnt signals with XAV939, which inhibits tankyrase and promote the degradation of β-catenin, resulted in the upregulation of BMP signals, repressed noggin expression in niche cells and induced the nuclear localization SMAD 1/5/8 in both limbal epithelial and stromal cells. Both BMP and wnt activation induced the expression of CK12 and CK15 without affecting p63α and promoted corneal epithelial differentiation. Thus, a balanced regulation of both BMP and Wnt signals at the limbus regulate the clonal expansion and differentiation of limbal epithelial cells (Han *et al.*, 2014). Conditional knockout of β-Catenin or the wnt co-receptors LRP5/6 resulted in the upregulation of BMP4 and Smad1/5 phosphorylation in corneal stromal keratocytes and a corresponding precocious stratification of the corneal epithelium. Conversely overexpression of the stabilized form of β-Catenin mutant inhibited corneal epithelium stratification. Sub-conjunctival injection of BMP4 and its conditional ablation replicated the β-Catenin knockout and overexpression phenotypes respectively. β-Catenin was also shown to directly bind and regulate the BMP4 promoter activity (Y. Zhang *et al.*, 2015). Another study has reported that the neuro-ectodermal cells secrete the two wnt antagonists, DKK1 and SFRP2 and dictate the differentiation of iPSCs into non-neural ectodermal cells. Further, the BMP4 signaling was shown to drive the differentiation of non-neural ectodermal cells in corneal surface epithelial lineage. Therefore, a combined treatment of iPSCs with a wnt inhibitor (IWP, to block both canonical and non-canonical wnt signaling) and BMP4 during the first four days of differentiation was shown to be necessary to generate higher percentages of ocular surface ectodermal cells. Conversely, the treatment of iPSCs with either the GSK3β inhibitor/canonical wnt activator (CHIR99021) or BMP4 inhibitor (LDN193189) or TGFβ inhibitor (SB431542) significantly affected the differentiation of p63 positive ocular surface epithelial cells (Kobayashi *et al.*, 2020).

Taken together, it is clear that a tightly regulated wnt signaling, in co-operation with the BMP signaling is crucial for the proper development and maintenance of the corneal tissue. While some of the mechanisms of regulations are well understood, it is not clear if either of the signaling can directly influence the expression of the master regulatory gene, PAX6 at the limbal niche. Though PAX6 is a key cornea-specific gene important for the initiation of corneal epithelial differentiation and maturation, its spatio-temporal expression and the dosage needs to be tightly regulated and this mechanism is largely unknown.

As a part of this thesis, we therefore aim to understand the promoter-level regulation of PAX6 in different ocular cells, limbal primary cultures and in human iPSC derived, in vitro developed early eye field tissues. Also, we examined the effects of alternate splicing and elucidated the roles of different PAX6 isoforms in critically regulating limbal stem cell proliferation and differentiation decisions.

CHAPTER 3

METHODOLOGY

3: Methodology

3.1 Ethics and regulatory statements

All experiments were performed in accordance to the tenets of the declaration of Helsinki and were approved by our Institutional Review Board and Institutional human Ethics Committee (IRB & IEC), Institutional Committee for Stem Cell Research (IC-SCR) and the Institutional Bio-Safety Committee (IBSC).

3.2 Construction of a human *PAX6*-pA promoter driven luciferase reporter plasmid

3.2.1 Blood genomic DNA isolation

Genomic DNA was isolated from blood using the phenol-chloroform method. Briefly, from a healthy individual, 5 mL blood was collected in EDTA containing vacutainer and was stored at -30°C until further use. For genomic DNA isolation, blood was thawed on ice and collected in a centrifuge tube. For 1 mL of blood, 3 mL of cold 1X PBS was added and mixed well on ice and the tube was vortexed till the solution appeared clear. The tube was incubated on ice for 10 mins, followed by centrifugation at 3000 rpm for 15 min. The supernatant was discarded without disturbing the pellet. This washing step was repeated until a pale pink pellet appeared.This pellet was suspended in 0.75 mL of extraction buffer containing 0.4 mg/mL of proteinase K and 75 μg/mL RNase and was incubated at 37°C overnight. The next day, 0.3 mL of Tris saturated phenol (pH 7.8-8.2) was added and mixed well. To this, 0.3 mL of chloroform: isoamyl alcohol (24:1 ratio) was added and mixed gently by inversion until an emulsion was formed. The tube was centrifuged at 3000 rpm for 15 min. The top aqueous layer was collected in a fresh tube without disturbing the bottom layer. To the aqueous phase, equal volumes of chloroform: isoamyl alcohol (24:1 ratio) was added and mixed gently. The tube was spun at 2500 rpm for 10 min. The top aqueous phase was collected in a fresh eppendorf tube and two volumes of chilled 100% ethanol and 10 μL of 10M ammonium acetate were added. The precipitated genomic DNA appeared as a white cloudy lump which was transferred to a fresh eppendorf tube. DNA was washed with 0.5 mL of 70% chilled ethanol by centrifuging at 3000 rpm for 15 min. The supernatant was discarded and the pellet was air-dried. The dried pellet was suspended in 200 μL of TE (Tris-EDTA) buffer (pH 8) and allowed to dissolve at room temperature overnight.

3.2.2 Agarose gel electrophoresis (AGE) of DNA samples

Agarose gel electrophoresis (AGE) is one of the most common molecular techniques used to check the quality or integrity of the DNA samples. In agarose gels, the DNA molecules get

separated based on their molecular size i.e. the smaller fragments migrate faster than the larger ones. To check the quality of the DNA isolated from cultured cells/tissues or those amplified by PCR, 1% agarose gel was prepared in 1X **TAE buffer** by heating and melting it in a microwave oven. When the agarose solution is cooled down to ~60-65°C, 2 μL of 10 mg/mL ethidium bromide per 100 mL was added and mixed gently to avoid frothing. The solution was then poured into a gel casting tray with a suitable comb and care was taken to avoid any air bubbles. Upon cooling and solidification, the agarose gel, along with the casting tray was transferred into the electrophoresis tank containing 1X TAE buffer. The comb was then gently removed and the wells were cleared by flushing with the tank buffer. The DNA samples mixed with the DNA loading dye (6X) was loaded into the wells of the agarose gel. A suitable DNA ladder (250 ng of 1 Kb or 100 bp ladder) was loaded on to a separate well to help with size comparisons. The gel was then run at 80-120V until the dye front reached half the distance of the complete gel and then visualized under a UV trans-illuminator and a gel documentation system (Bio-Rad, USA).

3.2.3 Quantification of genomic DNA

The concentration of DNA can be estimated approximately by running a molecular marker (250 ng) and the test DNA side by side in the same gel. When the DNA sample was run, the intensity of the DNA (diluted DNA 1:10) was compared with the known band intensity of the resolved molecular marker and the test DNA was quantified approximately.

NanoVue™ was used alternatively, for the better quantification of DNA which works on the principle of Beer-Lamberts law on the absorption of light by different biomolecules. TE buffer was used as blank control in which the DNA samples were dissolved. A diluted DNA sample in 2 μL volume was loaded onto the sample loading area and the DNA was quantified by measuring the optical density (OD) at 260 and 280 nm. The OD at 260 nm was used to quantify the DNA yield and the DNA quality was also checked by measuring the ratio of OD at 260/280 nm. A good quality DNA and RNA should have an OD ratios of ~1.8 and ~2 at 260/280 nm respectively. Values less than 1.8 indicate that the DNA is contaminated with either phenol or protein.

3.2.4 PCR amplification of human *PAX6*-pA promoter

The sequence of the genomic region upstream to the *PAX6*-pA promoter was obtained from the NCBI nucleotide database and analysed using the Genomatix-Matinspector software to

identify the key transcription factor binding motifs. Primers were designed to span *PAX6*-pA promoter (-862 bp to +72 bp) (**Annexure V**) for region-specific PCR amplification.

Polymerase chain reaction (PCR) is a common technique used in the lab to make multiple copies of the genomic region of interest. During the replication process *in vivo*, DNA helicase is the enzyme involved in the unwinding of the DNA, and priming is done by RNA primase. Whereas, all the above processes are taken care of by a thermal cycler under laboratory conditions *in vitro*. The thermal cycler has a thermostat that can heat up and cool down very fast. Five major components are required to amplify DNA targets by PCR using a thermal cycler. These includes (i) a template DNA source, which contains the target region to be amplified. (ii) region-specific primers (forward and reverse primers), which are a short stretches of DNA nucleotides to initiate the PCR. They are designed to bind to either strands of the template DNA, but in opposite directions and thus spans the target region to be amplified. (iii) dNTPs for incorporation into the newly synthesized DNA (iv) a reaction buffer to provide the optimal conditions for the enzyme reaction and finally (v) the Taq DNA polymerase (from Thermus aquaticus), an enzyme that adds dNTPs to the growing chain of the DNA and is stable at high denaturing temperatures of around 95°C. Each PCR cycle results in double the number of target DNA fragments amplified. Each amplicon in turn acts as templates in subsequent cycles, thus leading to an exponential increase in the number of DNA fragments after every cycle. Hence this reaction is named as polymerase chain reaction (PCR). The formula used to calculate the number of DNA amplicons present after every PCR reaction cycle is: $N \times 2^n$, where, 'N' represents the number of copies of DNA molecules present initially, and 'n' is the number of amplification cycles. The concentration of different components used in a PCR reaction mix is shown in **table 3.1**. Once the PCR reaction mix is ready, the reaction tubes are placed in the thermal cycler and the temperature conditions used are mentioned in the table below.

3.1: Preparation of PCR master mix

S.No.	Reagents	Concentration	Volume (µL)
1	Genomic DNA	100 ng	1
2	Taq buffer	10X	2
3	dNTPs	2 mM	2
4	Forward primer	5 pmol/µL	1

5	Reverse primer	5 pmol/µL	1
6	Taq polymerase	5 U/µL	0.2
7	Deionized water	-	12.8
	Total volume		20

Table 3.2: Thermal cycler program

S.No.	Amplification steps	Temperature (ºC)	Duration
1	Initial denaturation	95	5 mins
2	Denaturation	95	30 secs
3	Annealing	58	30 secs
4	Extension	72	60 secs per Kb of the amplicon
Steps 2-4 for 35 cycles			
5	Final extension	72	10 mins
6	Hold	4	10 mins

Note: For the purpose of cloning, the *PAX6*-pA region was amplified with the Phusion DNA polymerase, a high fidelity polymerase with 3'to 5' proof reading activity. Unlike the Taq DNA polymerase, this high fidelity enzyme does not create any 3' A-overhangs and enables direct blunt ended cloning of PCR amplicons. The PCR products were then analysed on agarose gels, as described under **Section 3.2.2.**

3.2.5 Modification of DNA ends

The proximal *PAX6*-pA region selected for amplification has an internal PstI site towards the 5' end. The amplicon of size 934 bp was digested with PstI enzyme that resulted in an insert of about 881 bp size with a sticky 5' end and a blunt 3' end. The digested PCR amplicon was run on agarose gel and the DNA band was cut and eluted using NucleoSpin Gel and PCR Clean-up kit (Takara). The DNA elute was further checked and quantified using agarose gels or a Nanodrop.

3.2.6 Linearization of the vector

pMOS-Blue vector was used to clone the Pst I digested *PAX6*-pA amplicon. The vector was linearized by double digestion with PstI and EcoRV restriction enzymes. The reaction was set as follows:

Table 3.3: Restriction digestion reaction mixture

S.No.	Reagents	Concentration	Volume (µL)
1	10X buffer 3.1	10X	2
2	PstI	20000 U/mL	0.5
3	EcoRV-HF	20000 U/mL	0.5
4	pMOS vector	1 µg/µL	1
5	Nuclease free water	-	16
	Total volume		20

The reaction mixture was incubated at 37°C for 3 hrs and then, electrophoresed on an agarose gel. The linearized vector band was excised and gel extraction was performed as per the manufacturer's instructions. The concentration of elute was checked on an agarose gel, followed by quantification using a Nanodrop.

3.2.7 Vector and insert ligation

Ligation involves the formation of a phosphodiester bond between the two ends of DNA molecules. The reaction is catalyzed by T4 DNA ligase and was set as follows in a 0.5 mL microcentrifuge tube and incubated at 16°C for overnight, followed by bacterial transformation the following day

Table 3.4: Ligation reaction mixture

S.No.	Reagents	Concentration	Volume (µL)
1	T4 DNA ligase buffer	10X	1.5
2	Linearized Vector (pMOS)	300 ng	3
3	Insert (Prom A amplicon-881 bp)	274 ng	5
4	T4 DNA ligase	1.0 U	1
5	Nuclease free water	-	4.5
	Total volume		15

3.2.8 Transformation of plasmid DNA into *E. coli*

Transformation is the process by which a laboratory E. coli strain (DH5α or STBL3) takes up the foreign DNA under stress or suitable extracellular microenvironment such as, thermal or electric shock or chemical treatments. The most common method for transformation is the heat-shock method, where the ligation reaction mixture or the plasmid DNA is added to the competent cells and incubated on ice for 30 mins. Then, a brief heat shock was given at 42°C for 90 sec and again incubated on ice for 2-3 mins. LB (Luria Bertini) broth was then added to the cells and allowed to grow for 1 h on a shaker at 37°C. This culture was then spread on to LB agar plates containing suitable antibiotics [Ampicillin (LB-Amp)/Kanamycin LB-Kan)] and incubated at 37°C overnight for the emergence of recombinant colonies.

3.2.9 Clonal inoculation of bacterial recombinants and preparation of replica plates

Individual bacterial colonies on culture plates were picked using a micropipette tip and the tip was used to make a small streak/patch on LB-Amp plate, to prepare a replica plate. The same tip was then dropped into a 15 mL culture tube containing 2 mL of sterile LB-Amp broth for clonal inoculation. All culture handling were done under sterile environment, inside a BSL-II laminar hood. The replica plate and broth culture tubes were then incubated overnight at 37°C, in a shaker cum incubator.

3.2.10 Plasmid isolation from 2 mL bacterial culture (miniprep)

The broth cultures that were incubated overnight and showing nice bacterial growth were processed for plasmid DNA isolation as follows. The liquid broth culture was transferred into 1.5 mL microcentrifuge tubes and centrifuged at 12,000 rpm for 10 min and the supernatant (spent media) was discarded into a beaker containing sodium hypochlorite solution. The bacterial pellet was resuspended in 150 µL of the glucose containing **Buffer 1 (Annexure-II),** which creates a hypotonic condition. The tube is then vortexed vigorously to prepare a homogenous bacterial cell suspension. This helps to swell the cells and prepares them for uniform lysis during the next steps. Later, 150 µL of the alkaline lysis **Buffer 2** was added and mixed gently by inverting the tubes 5-6 times to achieve uniform cell lysis and denaturation of cellular proteins, without shearing the genomic DNA. The SDS solubilizes the cell membrane and helps in the lysis of bacterial cells and the release of cellular contents. NaOH denatures all the proteins and DNA (genomic and plasmid DNA) at alkaline pH. Immediately after the complete cell lysis, 150 µL of **Buffer 3** was added and mixed gently by 5-6 inversions and incubated on ice at 4°C for 10 min. The potassium acetate in Buffer 3 neutralizes the alkalinity

of the mixture, resulting in the renaturation of bacterial proteins. This forms a white curd-like precipitate along with the trapped genomic DNA and cell debris. This white precipitate is pelleted by centrifuging the tubes at 12,000 rpm for 10 min. The low molecular weight, supercoiled plasmid DNA gets partitioned into the supernatant, which was then aspirated and transferred into a fresh 1.5 mL microcentrifuge tube. To the supernatant, equal volumes of 100% isopropanol (600 µL) was added and mixed gently for 10 min to precipitate the plasmid DNA at room temperature. The precipitated DNA was pelleted by centrifugation at 12,000 rpm for 10 min. The DNA pellet was then washed with 70% ethanol and centrifuged at 12,000 rpm for 5 min. The supernatant was aspirated out and discarded. The plasmid DNA pellet was briefly air-dried at room temperature, to remove the left over ethanol. The dried DNA appears transparent and was resuspended in 50 µL of TE (pH 8.0), containing 1 µg/mL of RNase and incubated for one hour at 37ºC to digest and eliminate all the contaminating bacterial RNAs. The quality and quantity of the plasmid DNA yield was checked using AGE and a Nanodrop.

3.2.11 Confirmation of plasmid constructs by restriction digestion

To confirm the positive recombinants with inserts cloned in right orientation, the pMOS_*PAX6*-pA plasmids from individual clones were subjected to restriction digestion using HindIII and BamHI enzymes, to release a fragment of 902 bp. The restriction enzyme reaction mixture was prepared as mentioned in **table 3.5**. The digested products were run on an agarose gel for visual analysis.

Table 3.5: Restriction digestion reaction mixture

S.No.	Reagents	Concentration	Volume (µL)
1	Cutsmart buffer	10X	2
2	HindIII	20000 U/mL	0.5
3	BamHI	20000 U/mL	0.5
4	Plasmid DNA	1 µg/µL	1
5	Nuclease free water	-	16
	Total volume		20

3.2.12 Sub cloning of *PAX6*-pA promoter into pGL3-Basic vector

The sequence confirmed recombinant clone 15 of pMOS_*PAX6*-pA was chosen for subcloning. The plasmid was double digested with HindIII and BamHI, which released an insert of 902 bp with sticky ends. The digested product was run on agarose gel, the insert DNA

band in the gel was cut and eluted using the NucleoSpin Gel and PCR Clean-up kit (Takara). The gel-purified elute was incubated with T4 DNA polymerase for end-filling.

T4 DNA polymerase helps in removing the 3'overhangs and filling the 5' overhangs to form blunt ends. The reaction was set as follows:

Table 3.6: T4 DNA polymerase reaction mixture

S.No.	Reagents	Concentration	Volume (µL)
1	Insert		16
2	Buffer	10X	2
3	dNTPs	2 mM	1
4	T4 DNA polymerase	3000 U/mL	1
5	Nuclease free water	-	-
	Total volume		20

The reaction was incubated at 12°C for 15 mins, followed by the addition of 2 µL of 100 mM EDTA to stop the reaction. The reaction mixture was run on an agarose gel and purified by gel extraction. The pGL3-Basic vector was digested with SmaI enzyme for 3 hrs at 37°C to accommodate the blunt ended *PAX6*-pA insert. The linearized plasmid DNA was ran on a gel and the DNA band was cut, gel eluted and purified. The restriction enzyme reaction was set as follows:

Table 3.7: Vector digestion reaction mixture

S.No.	Reagents	Concentration	Volume (µL)
1	Cut smart buffer	10X	2
2	SmaI	20000 U/mL	0.5
3	pGL3-Basic vector	1 µg/µL	1
4	Nuclease free water	-	16.5
	Total volume		20

After purification of vector and insert DNA, their concentrations were checked using Nanodrop. Ligation reaction was set up as below.

Table 3.8: Ligation reaction mixture

S.No.	Reagents	Concentration	Volume (µL)
1	T4 DNA ligase buffer	10X	1.5
2	Vector (pGL3-Basic)	300 ng	3

	4818 bp		
3	Insert (Pax6-pA) 902 bp	130 ng	5
4	T4 DNA ligase	1.0 U	1
5	Nuclease free water	-	4.5
	Total volume		20

The reaction was incubated at 16°C overnight and the next day the ligation mix was transformed into ultra-competent E. coli and plated on Amp selection plates. The recombinant colonies were picked for plasmid isolation, restriction enzyme checks (**Section 3.2.11, 3.2.12**), followed by Sanger sequencing to confirmation the cloned DNA sequence.

3.3 Cloning of OSE enhancer upstream to the *PAX6*-pA promoter in pGL3-Basic vector

Using genomic DNA as a template, the OSE enhancer was PCR amplified. The primers used for amplifying the OSE region are listed in **Annexure-V**. The amplified PCR product was cloned into the pMOS-Blue vector at the EcoRV site to prepare the pMOS-OSE construct. To clone the OSE enhancer upstream to the pA promoter, the OSE and *PAX6* pA fragments cloned into the respective pMOS clones were digested using KpnI-PstI and PstI-BamHI respectively. pGL3-basic vector was digested with KpnI-BglII. The digested products were run on agarose gel, the insert DNA bands of OSE and *PAX6-pA* were cut and eluted for ligation together with the KpnI-BglII digested pGL3-Basic vector to obtain the pGL3_OSE_*PAX6*-pA construct. These reporter constructs were further used in luciferase reporter assays in different mammalian cell lines.

3.4 Cloning of *PAX6*-pC in pGL3-Basic vector

The human PAX6-pC was PCR amplified using the primers listed in **Annexure V** and was cloned into the EcoRV site of the pMOS-Blue vector to obtain the pMOS-h*PAX6*-pC. This *PAX6*-pC region from the pMOS vector was further digested with BamHI and subcloned directly into the BglII digested and CIP treated pGL3-Basic vector to obtain the pGL3_h*PAX6*-pC promoter construct. The right orientation of the clones were confirmed by HindIII digestion.

3.5 Site-directed mutagenesis and generation of TCF/LEF1 site mutation in *PAX6*-pA

The *PAX6*-pA has a consensus TCF/LEF1 binding site and two half-sites flanking the consensus. To create mutation within the consensus site, point mutations were introduced in

the primers as follows (mutated nucleotides are indicated in bold letters): forward-5' CAACAGTTAA**GC**CAAAGTCAAAGATAAATACA3'; and reverse-5' CTTTGACTTTG**GC**TTAACTGTTGACTTTGTGA 3'. The mutagenic internal primer sets and the flanking, T7 and M13-F vector backbone specific sequencing primer combinations (in pMOS-*PAX*6-pA construct) were used in overlap-extension PCRs, to generate amplicons encoding a mutant promoter sequence with disrupted TCF/LEF1 binding sites. The PCR amplicon was cut with BamHI and sub-cloned into the KpnI cut, end-filled and BglII cut sites of the pGL3-Basic vector to generate the pGL3-*PAX6*-pA mutant construct.

3.6 Maxi preparation and purification of plasmid DNA

After the confirmation of plasmid constructs by restriction digestion and sequencing, the best recombinant plasmid clone was amplified by maxi prep using a 100 mL bacterial culture and purified using a nuclease free, silica column based, plasmid DNA isolation kit based on manufacturer's instructions (Nucleobond® Xtra Midi Kit, MN, Cat no. 740410.100). For this, 100 µL of starter culture was inoculated in 100 mL of LB-broth media with 100 µg/mL of ampicillin and was incubated at 37°C in a shaking incubator for 16 hours or till the cultures reached an optical density at 600 nm of 2.0 (for high copy number plasmids) or 8 (for low copy number plasmids).

The bacterial culture was then transferred from the conical flask to the 50 mL centrifuge tubes (x2) and centrifuged at 7500 rpm for 20 min at 4°C. The supernatant of bacterial growth media was discarded in a sodium hypochlorite solution containing discard container. The bacterial pellet was suspended in a total of 8 mL of resuspension buffer containing RNase A by vigorous vortexing. To this, 8 mL of lysis buffer was added and mixed gently by inverting the tube 5-6 times until the solution became blue. The tube was incubated for 5 min at room temperature. Meanwhile, the Nucleobond® Xtra column and the filter were equilibrated with 12 mL of equilibration buffer. To the plasmid-containing tube, 8 mL of neutralization buffer was added and mixed gently by inverting the tube 5-6 times until the solution became transparent with a white precipitate. The precipitated solution was centrifuged at 4000-7500 rpm for 10 min and the supernatant was loaded onto the Nucleobond® Xtra column. When the solution is passed through the column, the plasmid DNA binds to the silica-based anion exchange resin packed within the column. At acidic pH, the positively charged column binds to the negatively charged nucleic acids with high affinity. The column and filter were again equilibrated with 5 mL of equilibration buffer. Once the column became empty, the filter was discarded and the column

was washed with 8 mL of wash buffer. After this, the plasmid DNA was eluted in 5 mL of elution buffer. At alkaline pH, the affinity of the column with nucleic acid is lost and the plasmid DNA is released from the column. To precipitate the plasmid DNA present in the eluted sample, 3.5 mL of isopropanol was added and incubated at room temperature for 10 min. The precipitated DNA with isopropanol was centrifuged at 12,000 rpm for 30 min at 4°C. The supernatant was discarded and the pellet was washed with 2 mL of 70% ethanol. The pellet was air-dried and resuspended in TE buffer, pH 7.4 and allowed to dissolve slowly at room temperature. The quality and quantity of the concentrated stock and the diluted plasmid DNA was checked by AGE and quantified using a Nanodrop.

3.7 Assay of human *PAX6* promoter activity in cell lines

3.7.1 Transfection of mammalian cells

To check the *PAX6* promoter activity, the reporter constructs were transfected into different ocular cell lines (HCE, ARPE19, 661w and HLE-3B). For this, the respective cells were seeded at a density of 80,000 cells/well in 12 well plates and were allowed to adhere. Once the cells became 60 to 70% confluent, transient transfection was done using Lipofectamine 3000 (Invitrogen cat no. L3000-008). The reaction mixtures in tubes A and B, as mentioned in **Table 3.9**, were mixed and incubated at room temperature for 30 min. The transfection mixture containing the DNA trapped lipid complexes was slowly added directly on top of the cells grown in 12 well plates and incubated in a CO2 incubator at 37°C.

Table 3.9: Transfection reaction mixture

Vial A	
DMEM medium	50 µL
Purified reporter plasmid	0.5 µg
p3000 transfection reagent	1 µL
Vial B	
DMEM medium	50 µL
Lipofectamine 3000	1.5 µL
Total volume	100 µL

3.7.2 Assay of luciferase reporter activity

After 48 hours of transfection, the cells were washed with 1X PBS for 2-3 times. The assay was carried out using the Promega Luciferase Assay System (Cat No. E1500), as per the manufacturer's instruction. About 100 µL of the 1X lysis buffer was added to the cells in each

well of the 12-well plates and incubated on ice for 15 min. Cells were scraped from the dish and the suspension was transferred to 1.5 mL microcentrifuge tubes. These tubes were centrifuged at 12,000 rpm for 5 min at 4°C and the supernatant was transferred to fresh Eppendorf tubes. About 20 µL of the clear cell lysate was mixed with 30 µL of the luciferin containing substrate solution and mixed well by brief vortexing. The luminescence emitted in the solution was measured using a luminometer. The amount of light produced is directly proportional to the promoter activity. Fold change was calculated based on the basal activity of the promoterless pGL3-Basic vector.

3.8 Characterization of human *PAX6* promoters in primary limbal cultures

3.8.1 Establishment and maintenance of human primary limbal epithelial cultures

Human rejected donor corneal tissues were obtained from the Ramayamma International Eye Bank located at the L.V Prasad Eye Institute, Hyderabad. The corneo-scleral rims were processed in the laboratory to isolate the limbal tissue within 48-72 hours after harvesting the tissue from the donors. For limbal explant cultures, the inner surface of the corneal tissues was gently scraped with no. 15 blades to remove the pigmented iris. The corneal tissue was washed with 1X PBS (phosphate-buffered saline) containing double-strength antibiotics. The sclera and the cornea were excised out using the No. 21 surgical blade, leaving the limbal tissue intact with the surface epithelium. The limbal tissue was further processed under the dissection microscope, where the superficial stroma was excised along with the limbal epithelium. The limbal tissue was chopped into small pieces of around 1-2 mm size and explanted onto the surface of sterilized glass coverslips. These coverslips with limbal explants were placed in the incubator for 30 min to allow their adhesion. After adhesion, the limbal explant cultures were maintained in complete human corneal epithelial media (CHCE) and incubated at 37°C. Media was changed on alternate days until 70-80% confluency was attained.

To establish the limbal suspension cultures, the whole limbal rim was cut into two to four pieces and incubated with basal media containing 1.2 IU/mL Dispase and 0.3 mg/mL Collagenase type IA at 37°C for one hour. The limbal epithelium was scraped gently using a scalpel blade and the stroma was removed. The limbal epithelial suspension was collected in 15 mL media and the enzymatic reaction was terminated by adding the serum containing, complete HCE media (CHCE). The limbal epithelial cell suspension was then triturated well using a 1 mL pipette to prepare a well dispersed single-cell suspension. This suspension was then centrifuged at 1000 rpm for 1 min. The final cell pellet was seeded on Mitomycin C

treated, mitotically inactive, NIH3T3 feeder cells and cultured in complete HCE media for approximately 1-2 weeks in a CO2 incubator at 37°C, before processing the cultures for further analysis. The composition of CHCE media is described in **Annexure I**.

3.8.2 Cloning of PAX6-pA, pC and OSE-pA promoters upstream of GFP reporter in a lentiviral construct

The pMOS clones of *PAX6*-pA, pC and OSE-pA (described in sections 3.2, 3.3 and 3.4) were further mobilized upstream to the GFP reporter in a promoter less lentiviral vector, pHR-SIN to obtain the pHR-SIN_*PAX6*-pA_GFP, pHR-SIN_*PAX6*-pC_GFP and pHR-SIN_OSE-*PAX6*-pA_GFP reporter constructs. After restriction digestion to assess the right orientation of inserts in positive clones, the recombinant plasmids were further checked by Sanger sequencing to confirm the correctness of cloned DNA sequences.

3.8.3 Preparation and purification of recombinant lentiviral vectors

Platinum A (Plat-A) cell line was used to produce the recombinant lenti or retroviruses that can deliver the transgene into the host cell DNA. Plat-A cell line is a modified form of HEK 293T cells, which stably encodes a copy of the viral replication and envelope genes such as, the gag, pol and env genes that is amphotropic and allows transduction into most mammalian cell lines. The retroviral construct is either transfected into Plat-A cells alone or can be cotransfected with the packaging constructs that carries the *gag, pol* and *VSVG* genes [pDR8.2_GPRT (Addgene Cat. NO 8455), pCMV VSV-G (Addgene cat No. 8454)] in HEK 293T cells, to prepare a VSVG psedotyped recombinant lentiviral particles. After transfection into packaging cells, the transgene encoding plasmids express the mRNA and proteins. Gag encodes for the group of proteins that forms the structure of the viral core. Pol encodes for reverse transcriptase and integrase, which are important proteins for the reverse transcription of the viral mRNA. The env/VSV-G codes for the envelope protein and confers amphotropic/pantropic ability (to infect a wide range of species) to the virus. Since the helper plasmids are devoid of packaging signals (Psi Ψ), their mRNA will not be packed within the viral genome. However, the plasmid constructs carrying the desired transgenes encode a packaging signal Ψ, thus allowing only the transgene and any DNA sequences spanning the 5' and 3' LTRs gets packaged and forms the core genome of the recombinant viral particles. These third generation recombinant viral vectors are therefore infectious, but cannot replicate once they integrate into the host cell genome.

About 2×10^5 cells were seeded into a well of a 6-well plate and were allowed to adhere. Once the cells reach 60-70% confluency, lipofection was done using Lipofectamine 3000 (Invitrogen cat no. L3000-008) to deliver the transgene and helper plasmid constructs into packaging cells. The reaction components of the vial A and B (as mentioned in Table **3.10**) were mixed and incubated at room temperature for 30 mins to prepare the cell transfection complex.

Table 3.10: Transfection reaction mixture

Vial A	
Basal DMEM medium	100 µL
Purified plasmid DNA of interest	1 µg
pCMV_VSV-G	250 ng
pDR8.2_GPRT	750 ng
p3000 transfection reagent	2 µL
Vial B	
Basal DMEM medium	100 µL
Lipofectamine 3000	3 µL
Total volume	200 µL

The cells were washed and 0.5 mL of serum free medium was added. The transfection mixture was added slowly on top of the cells and mixed by gently swirling motion for even distribution. After 24 hours of transfection, 1 mM sodium butyrate (an HDAC inhibitor) was added to increase the viral production and packaging.

Culture supernatant / spent medium containing the recombinant viral particles was collected at 36 hours post-transfection and passed through a 0.45 µm syringe filter to get rid of all cell debris. Fresh media was added to the cells and the spent media was collected at every 12 hours intervals until 60 hrs post-transfection. The filtered supernatant containing the viral particles was aliquoted into 0.5-1.0 mL volumes in cryovials, snap-frozen in liquid nitrogen and stored at -80ºC until use.

3.8.4 Lentiviral transductions in mammalian cells

When the primary limbal epithelial cells reach 40% confluency, the viral supernatant containing the recombinant lentiviruses was added to the cells, along with equal volumes of fresh culture medium and 10 µg/mL Polybrene. The infected cultures were incubated at 37°C in a CO2 incubator. At 12 hrs after transduction, the spent media was replaced and the cells were cultured further till 72 hrs. The virus takes around 3-6 hours for transduction, while complete

expression of the viral transduced genes takes around 72 hours. Therefore, the transduction efficiency can be checked after 72 hrs of transduction and the cells can be processed for different downstream molecular or cytological analysis.

3.8.5 BrdU labelling of cultured cells

To identify the proliferating cells in primary limbal epithelial cultures, pulse labeling was done using 5-Bromo-2'-deoxyuridine (BrdU). When the cells were 50% confluent, BrdU (10 μM/mL) was added to the culture media and incubated for 30 min. Exactly after this time, the cells were washed with 1X PBS and fixed using 4% paraformaldehyde. Triton-X 0.5% was used to permeabilize the cells for 10 min and was then washed with 1X PBS. To denature the DNA, cells were treated with 2N HCl for 30 minutes followed by neutralization with 1 mg/mL sodium borohydride for 30 Sec. Blocking was done with 10% FBS for an hour. BrdU incorporated cells were identified using an anti-BrdU antibody. A secondary antibody tagged with fluorophore was used to detect the anti-BrdU antibody labelled cells. The fluorescently labelled samples were then imaged using a fluorescence microscope.

3.8.6 Immunofluorescence staining of cultured cells

To know the identity of *PAX6*-pA driven GFP expressing cells, immunofluorescence was performed on primary limbal epithelial cultures transduced with lentiviral vectors. For this, the limbal explants were cultured on glass coverslips placed inside a 12 well plate. Once the limbal cultures reached 60-70% confluent, the cells were washed 2-3 times with 1X PBS and fixed with 4% formaldehyde for ten minutes at RT, followed by 3 washes with 1X PBS for five minutes each. Later, permeabilization of cells was done with 0.5% Triton-X for ten minutes and washed with 1X PBS thrice. To avoid the non-specific binding of the antibody, cells were incubated with blocking buffer (10% FBS or 2.5% BSA) for one hour. The primary antibodies (Annexure VI) were diluted in the blocking buffer at required concentrations and incubated for one hour at room temperature (RT) or at 4°C overnight in a moist chamber to prevent the evaporation of antibody. The cells were then washed thrice with 1X PBS for ten minutes each. The secondary antibody tagged with a suitable fluorophore or a biotin label was added at required concentrations and incubated for 30-45 min at RT. In case of biotinylated secondary antibodies, an additional step was included wherein; a suitable fluorophore conjugated streptavidin was added at required concentrations and incubated for further 45 min at RT, followed by three 1X PBS washes. The nuclei were counterstained with either PI or DAPI for 10-15 minutes at RT. Finally, the coverslips are mounted on a clean glass slide, using a

homemade mountant containing sterile 90% glycerol and 10% 1X PBS. The slides were then observed under a fluorescent microscope and further imaged using a laser scanning confocal microscope (Zeiss LSM880).

3.9 Characterization of cornea-specific markers in human corneal tissues

Donor corneas that do not meet the inclusion criterion for clinical use are accessible for basic research use. Such rejected eye tissues were obtained from the Ramayamma international eye bank, LV Prasad Eye Institute, Hyderabad.

3.9.1 Preparation of paraffin-embedded tissue

The corneal tissues were fixed in 10% formalin overnight and processed in an automated tissue processor, which involves a series of alcohol dehydrations and xylene washes and finally the tissues are embedded in paraffin wax and allowed to dry. Thin sections of about 4-5 μm thickness was taken using a microtome and the sections were collected on positively charged microscopic slides. The slides with paraffin embedded tissue sections are stored in the fridge at 4°C or at room temperature until further use.

3.9.2 Deparaffinization of paraffin-embedded tissue sections

Deparaffinization was done by heating the slides in a hot air oven at 70°C, followed by treating the slides with series of three xylene changes, for three minutes each, to remove the paraffin completely. Incomplete removal of paraffin results in poor staining of the sections and higher noise. After deparaffinization, the slides were hydrated in series using different percentages of ethanol (100%, 90% and 80% ethanol), for 3 min each. Later, the slides were rinsed with distilled/MilliQ water and processed further for hematoxylin and eosin staining (**section 3.9.3**) and immunohistochemistry (**section 3.9.4**).

3.9.3 Hematoxylin and Eosin staining

After completion of deparaffinization and hydration, the sections on the slides were processed for hematoxylin staining by incubating the slides in hematoxylin solution for 3-5 min, followed by water wash in running tap water for 5-10 min. After washing the slides under tap water, the tissue slides were dipped in 1% acid alcohol for 30 seconds to remove the non-specific binding of the hematoxylin. The tissue on slides were washed in running tap water thoroughly and further counterstained with Eosin Y for 2 min, dehydrated with 95% and 100% ethanol. Sections were cleared with two changes of Xylene for 5 minutes each, dried, and mounted with DPX (Dibutylphthalate Polystyrene Xylene) mounting medium. The sections were then analyzed under a light microscope.

3.9.4 Immunohistochemistry

Before proceeding with antigen retrieval, a Coplin jar with sodium citrate buffer (pH 6) was preheated in a microwave oven until it reached 95°C to 100°C. Coplin jars containing the tissue slides were heated in the microwave oven for 15 min. Coplin jar was taken out from the microwave oven and placed at room temperature and allowed to cool down, after which the sections were given 2-3 1X PBS washes. The sections were blocked for endogenous peroxidase with a mixture of methanol and H_2O_2 at 1:1 ratio. After giving PBS washes, the slides were then incubated with 0.5% Triton-X100 for 15 minutes. To block the non-specific binding of the primary antibody, the sections were incubated with a blocking buffer containing 10% FBS in 1X PBS, for a maximum of 1 hour. This was followed by primary antibody incubation for 1-2 hours at room temperature or overnight at 4°C, followed by three sequential washes with 1X PBS, for 3-5 minutes each to remove the unbound antibody. A suitable fluorophore or biotin or HRP conjugated secondary antibody was added and incubated for 45 min. After three PBS washes, the section were further incubated with fluorophore conjugated streptavidin-conjugates to capture fluorescence signals or processed for DAB staining. In case of HRP conjugated secondary antibodies, a chromogenic substrate called the DAB (3-3- diamidino benzidine) was added and incubated for approximately for 8-10 mins and washed under a running tap water for 1 minute. The nucleus was counterstained with either DAPI/PI/ hematoxylin and mounted using a resinous (DPX) mountant or with 90% glycerol. The slides were then imaged using a light microscope (in case of DAB staining) or the Carl Zeiss LSM 880 confocal laser scanning microscope (in case of fluorescence-based signals).

3.10 Chromatin Immunoprecipitation (ChIP)

Chromatin Immunoprecipitation is a form of *in vivo* binding assay used to evaluate protein-DNA interactions, in the context of an intact chromatin. In primary limbal epithelial cultures, the protein-DNA interactions *in situ* were preserved by cross linking reactions, with the addition of 137 µL of 37% formaldehyde to 5 mL of the cell culture media (final concentration 1%) and incubated for 10 min at room temperature. To quench the formaldehyde, 500 µL of 10X glycine was added and incubated for 10 min at room temperature. The cells were then washed with ice-cold 1X PBS along with protease inhibitor, scraped and collected into a 1.5 mL Eppendorf tube and pelleted by centrifuging at 12,000 rpm for 10 min. The cells were then lysed using an SDS lysis buffer, where 1 mL of buffer along with 1X protease inhibitor was added and incubated on ice for 10 min. For every 1×10^7 cells (10 million), 1 mL of SDS lysis

buffer was used. The ratio of lysis buffer to the cell density is crucial for proper lysis of the cells. After sufficient cell lysis, the chromatins were sonicated (20 Seconds "ON" and 60 Seconds "OFF" in 20 cycles), to achieve sheared genomic fragments predominantly of 200-1000 bp size. The sheared chromatin fragments were centrifuged at 12000 rpm for 10 min at 4°C. The supernatant was collected and about 50 µL volume was taken and stored separately at -80°C, to be used later as input or internal control sample. To reduce the non-specific background, the supernatant containing the sheared chromatins was subjected to pre-clearing using 40 µL of protein A/G beads (Santacruz, USA) and incubated for 60 min at 4°C with constant mixing on a rotator. The samples were then centrifuged at 1000 rpm for 2 min at 4°C to pellet the protein A/G beads. The pre-cleared chromatin containing supernatant was transferred to a fresh 1.5 mL tube and diluted with 10 folds of ChIP dilution buffer containing 1X Protease inhibitor and further divided into two halves and used for incubation with a control IgG antibody or a target protein-specific antibody for immuno precipitation. The samples were then incubated at 4°C with primary and anti-IgG antibodies and maintained overnight, with constant mixing on a rotator. Next morning, about 60 µL of protein A/G beads was added to the sample tubes and incubated for 1 hour at 4°C on rotation to pull down the proteins bound to the antibody complex. The antibody-protein complex bound beads were pelleted by centrifugations at 1000 rpm for 2 min at 4°C. The supernatant comprising of the unbound protein and chromatin was discarded. The pelleted A/G bead complex containing the antibody/protein complex was sequentially washed using 1 mL of ice-cold washing buffers (Low salt buffer, High salt buffer, LiCl salt buffer, 1X TE). Elution of the bound protein from the antibody complex was done by adding 250 µL of elution buffer to the A/G beads, vortexed gently for uniform suspension and incubated at room temperature for 15 min. The tube was spun at 1000 rpm for 2 min at 4°C and the supernatant elute fraction was transferred into a fresh tube. The above elution steps are repeated once and the elute 2 was collected. 20 µL of 5M NaCl was added to the eluted samples and also the frozen input samples and heated at 65°C for 6 hours to reverse the protein-DNA crosslinks. Further, 10 µL of EDTA (0.5M), 20 µL of Tris (1M) pH 6.5 and 2 µL of proteinase K (10 mg/mL) was added and incubated for 1 hrs at 45°C. The immunoprecipitated genomic DNA fragments were then isolated and purified by phenol-chloroform-isoamyl method. To confirm the region-specific binding of transcription factors on target gene promoters, targeted PCR was carried out subsequently, using the ChIP isolated DNA as templates and target site flanking primers. Primers used for ChIP-PCR amplification are listed in **Annexure V.**

3.11 Evaluating the expression of PAX6 variants

3.11.1 RNA isolation

RNA was isolated from ocular tissues and ocular cell lines for cDNA synthesis to confirm the expression of novel PAX6 splicing variants. Briefly, ocular cell lines (ARPE19, 661W, HLE-3B, and HCE) and ocular tissues (corneal epithelium, limbus, retina, and human iPSC-derived optic cups) were washed with ice-cold 1X PBS. Cells/tissues were properly minced, lysed in 1 mL of TRIzol™ reagent (Invitrogen life technologies Cat No. 15596026) and nicely triturated for about 5 min to disrupt and disperse the cellular contents. The lysed solution was transferred into fresh 1.5 mL tubes and 0.2 mL of chloroform was added and mixed by inverting the tubes 5-10 times and kept at room temperature for 3 min and then centrifuged at 12000 rpm for 15 min at 4°C. This forms a clear upper aqueous phase that contains the RNA, an interphase containing the cell debris, membrane lipids, DNA and proteins and then the organic phase of phenol-chloroform at the bottom. The top aqueous phase (0.6 mL) was carefully transferred into fresh 1.5 mL tubes and 0.5 mL of isopropanol was added. The tubes were inverted gently for proper mixing and incubated at room temperature for 10 min to precipitate the RNA. The precipitated RNA was pelleted by spinning down at 12000 rpm for 10 min at 4°C. The pellet was washed with 70% ethanol and air-dried on ice. The dried RNA pellet was resuspended in nuclease-free DEPC treated water.

3.11.2 cDNA synthesis by reverse transcription for RT-PCR

For semi-quantitative gene expression analysis, the mRNAs obtained from the Trizol method were converted into cDNA using SuperScript III Reverse Transcriptase (Thermo Fisher Scientific Cat no 18080051). The reaction mixture mentioned in **Table 3.11** was prepared in 0.1 mL PCR tubes and heated in a PCR machine set to 65°C for 5 min for denaturation and opening of RNA secondary structures, followed by hold at 4°C.

Table 3.11: Reaction mixture for cDNA preparation

S.No.	Reagents	Concentration	Volume in µL
1	Oligo(dT)$_{20}$	50 µM	1
2	Total RNA	10 pg - 5 µg	5
3	dNTP mix	10 mM	1
4	Nuclease free water	-	3
	Total volume		10

Once the above reaction reaches 4°C, the reaction mixture detailed in the **Table** (**3.12**) was added to the tubes and mixed well by brief vortexing and centrifuging and incubated at 50°C for 30-60 min.

Table 3.12: Reaction mix

S.No.	Reagents	Concentration	Volume in µL
1	RT buffer	10X	2
2	DTT	0.1M	2
3	$MgCl_2$	25 mM	4
3	RNase out	40 U/µL	1
4	Reverse transcriptase	200 U/µL	1
	Total volume		10

At the end of the reaction, the reverse transcriptase was inactivated by heating at 70°C for 14 min. The resulting cDNA was used as a template for semi-quantitative PCR analysis to quantify the expression levels of different mRNA targets in different ocular cell lines and tissues. The gene-specific and PAX6-variant-specific primers used for qRT-PCR experiments are listed in **Annexure V**. The PCR reaction mixture was similar to the reaction cocktail detailed in **section 3.2.4**. The PCR amplicons were analyzed by agarose gel electrophoresis.

3.11.3 Sanger sequencing: ddNTP chain termination method

To check the sequence of short DNA fragment and PCR amplicons, we performed DNA sequencing by Sanger's chain termination method. In this method, only one primer (either forward or reverse primer) is used in a reaction mixture. The DNA amplicons do not increase exponentially as we see in a normal PCR with a pair of primers. Here, the number of amplicons increases linearly (N+1) with each cycle. Also, the reaction mix contains fluorescently labelled ddNTPs (ddATP, ddGTP, ddTTP, and ddCTP, with each dideoxy nucleotide being labelled with different fluorophore) along with the normal dNTPs, to enable chain termination at all possible sites along the length of the amplicons. The components of the reaction mixture and the amplification conditions of the sequencing PCR are mentioned in **Table 3.13** and **Table 3.14** respectively. Here, the primer annealing and extension steps are similar to that of the normal PCR, until the dideoxynucleotide is incorporated which results in the termination of chain elongation at all possible nucleotide positions. The prematurely terminated single stranded amplicons carry a specific fluorescently labelled nucleotide at the 3' end, which are read by the automated DNA sequencer and decodes the DNA sequence in the read out.

Table 3.13: Sequencing reaction mixture

S.No.	Reagents	Concentration	Volume (µL)
1	PCR product	5-20 ng	0.5-1
2	Sequencing buffer	5X	2
3	BigDye Terminator	-	0.2
4	Forward/Reverse primer	5 pmol	1
5	Deionized water	-	5.8-6.3
	Total volume		10

Table 3.14: Thermal cycling conditions for a sequencing reaction

S.No.	Amplification steps	Temperature (°C)	Duration (Secs)
1	Initial denaturation	96	120
2	Denaturation	96	10
3	Annealing	56	6
4	Extension	72	240
Steps 2-4 for 30 cycles			
5	Hold	4	300

3.11.4 Precipitation of sequencing reaction products

The terminated DNA fragments of different lengths obtained from the sequencing reaction were purified before subjecting them to capillary electrophoresis. It is important to remove the unused primers and unincorporated ddNTPs and dNTPs from the sequencing reaction mixture. If they are not removed, they may result in noisy signals in the chromatogram.

The precipitation of PCR products was carried out directly in the 0.1 mL PCR tubes or the PCR plate. To the sequencing reaction product, 1 µL of 125 mM EDTA (pH 8.0) and 1 µL of 3 M potassium acetate (pH 5.2) was added. The tube/plate was subjected to a short spin to bring all the solution to the bottom and 50 µL of 100% ice-cold ethanol was added to precipitate the DNA. Later, the tubes/plate was covered with aluminum foil and placed on a rocker for 20 min at room temperature. The plate/tubes were then centrifuged at 4000 rpm for 30 min at 4°C to precipitate the DNA. The plate/tube was inverted on a tissue paper to discard the supernatant, without disturbing the DNA pellet. The pellet was then washed with

50 µL of 70% ethanol and centrifuged at 4000 rpm for 20 min. The tube/pellet was inverted on a paper towel to remove the ethanol and air-dried for 15-20 min. The washed pellet was then re-suspended in10 µL of HiDi (Formamide solution) and heated at 95°C to denature the single stranded DNA and to maintain it in an open confirmation. The samples were then subjected to capillary electrophoresis using the 3130 Genetic Analyzer, (Applied Biosystems, USA).

3.11.5 Capillary gel electrophoresis: Automated reading

The precipitated sequencing PCR product is comprised the amplicons of all possible length, with a unique fluorescently labelled ddNTP at the 3' terminus end. During capillary electrophoresis, the amplicons differing by 1 bp length were separated based on their sizes. The shorter fragments run faster at the front, followed by the longer ones. The fluorescent dyes are excited by lasers at different wavelengths and their specific emission spectrum are detected by the analyser, which converts the signals it into digital data which are presented in the form of a chromatogram, with different colours representing each of the four bases.

3.11.6 Sequence analysis

The chromatogram files obtained from the Sanger Sequence Analyzer are in the form of .abi files. These were analyzed using the Chromas software. The textual sequence was extracted, converted into FASTA format and analyzed using various bioinformatics tools and software for sequence alignment and comparisons with published gene sequences available at various public databases.

3.12 Absolute quantification of PAX6 variants by quantitative PCR

PAX6 variants were quantified by real-time PCR (qRT-PCR). SYBR green chemistry was used to perform the qRT-PCR, which binds to the double-stranded DNA by intercalating between the bases, and the PCR amplicons are quantified by measuring the overall fluorescence emission throughout the cycle. Stringent variant-specific primers were designed to specifically recognize and amplify individual PAX6 variants (as listed in **Annexure V**) and their specificity was confirmed by semi-quantitative PCR before proceeding with qRT-PCR.

For absolute quantification, reported and novel alternatively spliced *PAX6* transcript variants were cloned into the mammalian expression vector, pEGFP-C1 (**Section 3.15.1**). Concentrations of the plasmid DNA preparations were assessed by NanoDrop and copy number of plasmid per µL (copies/µL) was calculated using the following formula:

$$\text{Copies}/\mu\text{L} = \frac{\text{Plasmid DNA concentration (ng}/\mu\text{L)} \times 6.02\times10^{14}}{660 \times (\text{Vector length+Insert DNA length})}$$

Serial dilutions of plasmid DNA ranging from 1×10^{9} to 1×10^{1} copies per µL was prepared and used as templates in qRT-PCR, in triplicate reactions. The resulting Ct values were plotted against the gradually increasing concentrations of plasmid DNA templates, to establish a standard curve. Such standard curves were prepared for each plasmid encoding different PAX6 variants. The qRT-PCR reaction mixture was prepared as follows:

Table 3.15 (A): Preparation of qRT-PCR reaction mix for standard curve

S.No.	Reagents	Concentration	Volume (µL)
1	SYBR green master mix	2X	5
2	Forward primer	5 pmol/µL	1
3	Reverse primer	5 pmol/µL	1
4	Plasmid DNA (Serial dilutions)	-	1
5	Deionized water	-	2
	Total volume		10

Table 3.15 (B): Preparation of qRT-PCR reaction mix for the test sample

S.No.	Reagents	Concentration	Volume (µL)
1	SYBR green master mix	2X	5
2	Forward primer	5 pmol/µL	1
3	Reverse primer	5 pmol/µL	1
4	cDNA	10 ng	1
5	Deionized water	-	2
	Total volume		10

The qPCR reaction was executed in 96-well format on Applied Biosystems 7900HT Fast Real-Time PCR system (SDS 2.4.0 software). Run was performed with an initial hold at 50 ºC for 2 min and at 94 ºC for 10 min followed by 40 cycles of denaturation at 94 ºC for 15 sec, annealing at 55 ºC for 1 min and extension at 72ºC for 30 sec. After the run, raw fluorescence data were

automatically processed into C_T value by SDS software. The standard curves of the C_T values generated using the plasmid DNA standards was used to compare the test sample CT values, to estimate the copy number of specific transcripts present in 10 ng of tissue-specific cDNA and was further extrapolated to calculate the absolute copy numbers per μg of total RNA from different ocular tissues.

3.13 Relative quantification of transcripts using quantitative real-time PCR (qRT-PCR)

To determine the expression of different transcripts in different ocular tissues, as compared to a test control, relative quantification was performed using the $2^{-\Delta\Delta CT}$ method. C_T value of different test samples from different ocular tissues was normalized with β-actin as the internal/housekeeping gene control. The relative expression levels of a specific transcript in different test tissues were compared with that of a control tissue, and the fold change in expression was calculated as follows:

$$\Delta C_T \text{ (Test)} = C_T \text{ (test)} - C_T \text{ (housekeeping gene)}$$

$$\Delta C_T \text{ (Control)} = C_T \text{ (control)} - C_T \text{ (housekeeping gene)}$$

$$\Delta\Delta C_T = \Delta C_T \text{ (Test)} - \Delta C_T \text{ (Control)}$$

$$\text{Fold change} = 2^{-\Delta\Delta CT}$$

3.14 Assessment of *in situ* expression and localization of PAX6 variants within cells and tissues

RNA transcript expression and their localization within cultured cells and native corneal tissues were assessed using the BaseScope assay from Advanced Cell Diagnostics (ACD Biotech Pvt Ltd). It is a form of RNA *in situ* Hybridization (RNA-ISH) technique used to localize the RNA of different splice variants using variant specific short RNA probes. This technology enables amplification of signals from the bound probes and allows easier identification of low abundant RNAs, splice variants with small insertions or deletions, point mutations and even the short RNA targets such as miRNAs. Also, the BaseScope duplex assay can identify two RNA targets simultaneously and can be combined with immunohistochemistry for the simultaneous detection of both the RNA and protein targets within the same cell or tissue samples.

3.14.1 RNA fluorescent *in situ* hybridization (RNA-FISH) by BaseScope assay in cultured cells

Primary limbal epithelial cells were cultured on sterilized coverslips, as described in **section** (**3.7.1**). The BaseScope duplex assay was performed according to the manufacturer's

recommended protocol (Advanced Cell Diagnostics, New York, USA) (**Note:** All reagents required for the BaseScope assay are included in the kit; Cat No: 323800).

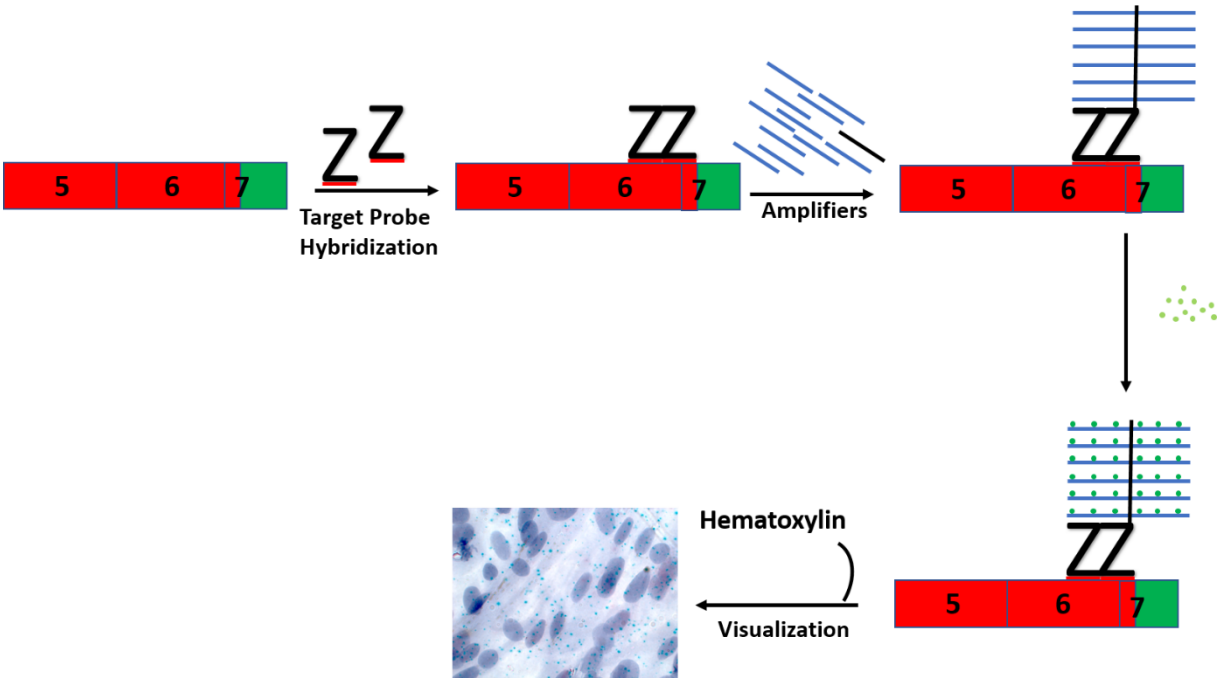

Figure 3.1: Cartoon representation of the BaseScope assay workflow. *The custom-made gene-specific Z pair RNA probes were first added to the cells or tissues to enable specific binding or hybridization to the target mRNAs. To amplify the signals from the bound probe, signal amplifying complementary probes and detection reagents are added, followed by stringent washes to remove the unbound probes and detection reagents, as per the manufacturer's instructions. The amplifiers are either horse radish peroxidase (HRP) or the alkaline phosphatase (ALP) enzyme conjugates, which upon addition of respective substrates, produces either the green/blue colored (Fast green label, C1 channel) and red/pink colored (Fast red label, C2 channel) chromogenic products, respectively. Finally, the samples were counterstained using hematoxylin, to mark all cell nuclei. The signals can be visualized under a bright field or fluorescent microscope in the form of cytoplasmic and nuclear dots, where each dot represents an individual mRNA molecule within the cells and tissues.*

3.14.1.1 Fixation and pre-treatment of cultured cells

Once the cells reached 70-80% confluency, they were washed twice with1X PBS and fixed with 4% formaldehyde by incubating at room temperature for 30 min. The cells were dehydrated using different percentages of ethanol (50%, 70%, 100% ethanol) at room temperature for 1 min (Note: the coverslips with cultured cells can be stored in 100 % ethanol at -20°C for up to 3-4 months). To rehydrate the coverslips, the cells were incubated with different percentages of ethanol (100%, 70%, and 50% ethanol). The cells were then

permeabilized by incubating with 0.1% Tween 20 in 1X PBS at room temperature for 10 min. To block the endogenous peroxidase, 1X PBS was replaced with hydrogen peroxide and incubated at room temperature for 10 min. The hydrogen peroxide solution was then removed and the cells are washed with 1X PBS, followed by the addition of 1-3 drops of Protease III (at 1:15 dilution) and incubated at room temperature for 10 min.

3.14.1.2 RNA-FISH probe hybridization

The sequences of the custom designed RNA probes for Basescope duplex assay targeting different splice junctions of PAX6 and p63 (TAp63 and dNp63) are listed in **Table: 3.17.** A positive control probe targeting the housekeeping gene, POLR2A was used to ensure the optimization of treatment conditions of each tissue. A negative control probe targeting dihydrodipicolinate reductase B (DapB), a bacterial gene was used to ensure that there is no background staining. The target probes consist of short oligonucleotides designed to bind to variant-specific RNAs. These target RNA probes were designed for two channels (C1 and C2) (**Table 3.16**). In the BaseScope duplex assay, the red color (C2) was developed by adding the substrate for Alkaline Phosphatase and the green color (C1) was developed by adding the substrate for Horseradish Peroxidase.

Table 3.16: BaseScope probes

Probe channel ID	Chromogenic Labels	
	Enzyme	**Color**
C1 probe	Horseradish Peroxidase (HRP)	Green
C2 Probe	Alkaline Phosphatase (AP)	Red

The duplex probe hybridization mix was prepared by mixing and dilution of C2 probe (50X) with the ready to use C1 probe in 1:50 ratio and gently mixed by pipetting. If only a single C2 probe was used, it was diluted with the BaseScope probe diluent buffer (Cat No. 700011). After dilution, ~4 drops were added onto the coverslip containing the cells, to cover it entirely and incubated in a humidified chamber at 40°C for 2 hours. After incubation, the coverslips are stored in **5X SSC buffer** at room temperature for overnight. The coverslips are then washed twice with **1X washing buffer** before proceeding with the signal amplification steps.

Table 3.17: BaseScope RNA probes and their chromogenic labels

S.No	Probe	Entrez Gene ID	Accession No	Target region	No of Z pairs	Channel (Green/Red)
1	PAX6-Wt-E6-E7	5080	NM_001604.5	826-868	1	C1 (Green)
2	PAX6-E5a-ΔE6-E7	5080	NM_001368921.1	637-678	1	C2 (Red)
3	PAX6-E12-E12a	5080	-	176-222	1	C2 (Red)
4	PAX6-Wt-E6-E7	5080	NM_001604.5	826-868	1	C2 (Red)
5	TA-p63-E2-E3	8626	NM_003722.4	119-163	1	C2 (Red)
6	ΔN-p63-E3a-E4	8626	NM_001114980.2	151-195	1	C2 (Red)
7	POLR2A	20020	NM_009089.2	2802 - 3678	3	C1 (Green)
8	DapB	#	EF191515	414-862	3	C1 (Green)

3.14.1.3 Signal Amplification

After probe hybridization, the targeted RNA-specific signals in the test samples (cultured cells on glass coverslips or tissue sections on glass slides) are amplified by a series of signal amplification steps (AMP 1-AMP13). After completion of each amplification step, the coverslips were washed twice with 1X washing buffer. Briefly, 4-5 drops of AMP1 solution were added onto the coverslip and incubated at 40°C for 30 min followed by washing with 1X wash buffer twice. Likewise, AMP 2 (30 min at 40°C), AMP 3 (15 min at 40°C), AMP 4 (30

min at 40°C), AMP 5 (30 min at 40°C), AMP 6 (15 min at 40°C), AMP 7 (30 min at RT), AMP 8 (15 min at RT) were sequentially added, with a wash in between each steps. The signals are detected by using Fast Red and Fast Green based enzyme substrates or detection reagents, in the following steps. To detect the red signal, the Red working solution was prepared by adding 2 μL of Red-B to 120 μL of Red-A reagent in a microfuge tube, mixed gently and added onto the coverslip and incubated at room temperature for 15 min, followed by a wash with 1X wash buffer. Subsequently, the coverslips were incubated with AMP 9 (15 min at 40°C), AMP 10 (15 min at 40°C), AMP 11 (30 min at RT), and AMP 12 (15 min at RT). The green signal was then detected by adding 2.4 μL Green B to 120 μL of Green A reagent in a microfuge tube, mixed gently and added onto the coverslips and incubated for 15 min at room temperature. The coverslips or slides are then washed twice with 1X wash buffer, followed by a quick MilliQ water wash to remove the excess wash buffer.

3.14.2 BaseScope assay on formalin-fixed, paraffin-embedded tissue sections

Paraffin-embedded tissues were sectioned into 5 μm thick sections using a microtome and the sections were collected onto SUPERFROST PLUS slides. The sections on the slides were dried overnight at RT. Deparaffinisation was carried out by baking the slides in an oven for 15 min at 60°C. Sections were then transferred to a xylene containing dish, where they were slightly agitated by dipping down and lifting up motions for about 10 times, followed by a second and third xylene wash steps. Later, the tissue sections are dehydrated by incubating in 100% ethanol with slight agitation (3 mins each). The slides are drained on an adsorbent paper and dried in an oven for 5 min at 60°C.

To prepare the tissue sections for RNA probe hybridization, the sections are treated with three different reagents. To block the endogenous peroxidase, the sections were incubated with 5-8 drops of RNAscope H_2O_2 solution at room temperature for 10 mins. Washing was done 3-5 times with distilled water, by gentle dipping down and lifting up motions. Target retrieval was done by placing the slides in a Coplin jar containing 1X target retrieval reagent and by heating at 99°C for 10 min. Once the target retrieval was done, slides are washed with distilled water and transferred in 100% ethanol for 3 min, and then air-dried at room temperature for 10-15 mins. Using a hydrophobic pen, a circular barrier was drawn around the sections and the slide was not disturbed until the barrier is dried completely. To permeabilize the cell membrane and to degrade and remove all RNA-associated proteins for better probe access and hybridization, 5 drops of Protease III was added to cover the entire section and incubated at 40°C for 30

min. The slides were then washed with distilled water to remove excess enzyme solution. Probe hybridization, signal amplification and staining was performed as described in sections **3.14.1.2 and 3.14.1.3**.

3.14.3 Counterstaining, mounting and imaging

The samples are counterstained using 50% hematoxylin solution for 1 min at RT, to mark all cell nuclei. Washing of the slides/coverslips was done under a running tap water, followed by fresh distilled water until only the sections remained purple, followed by 0.02% ammonia water wash until the sections turned blue, followed by 2-3 freshwater washes. Slides/coverslips are then dried in a hot air oven at 60°C for 15 min and rinsed once with fresh xylene. Mounting was done by adding 2-3 drops of vectamount on the slide and a glass coverslip was placed over the sections without trapping any air bubbles. The slides are dried overnight at room temperature.

3.14.4 Imaging and quantification

The stained cell or tissue samples are then analyzed using a bright-field or fluorescent microscope or a confocal laser scanning microscope. (Note: The red color, C2 BaseScope probes can be visualized under Cy3 filter in a fluorescence microscope and DAPI can be used as a counter stain instead of hematoxylin). Quantification was done by manually counting of cells (at least 300 cells) based on positive or negative signals using randomly acquired images covering multiple areas within the test samples. The values are presented as mean percentage of cells ± standard deviations.

3.15 Effects of PAX6 variants on target gene promoters

3.15.1 Cloning of PAX6 variants in the mammalian expression vector

To make GFP fusion constructs, different human PAX6 variants were PCR amplified using the primers listed in **Annexure V** and the amplicons were cloned into the EcoRV site of pMOS-Blue vector, by blunt end ligations and the positive clones are sequence confirmed. The PAX6 variant encoding regions were then subcloned into pEGFP-C1 mammalian expression vector, as in-frame EGFP fusions, to obtain pEGFP-PAX6A or pEGFP-PAX6B or pEGFP-PAX6B-ASΔ6 or pEGFP-PAX6A-12a constructs.

3.15.2 Confirmation of expression of cloned PAX6 isoforms by western blotting

The EGFP-PAX6 constructs were transfected into HEK293T cells, as described in section **3.15.1**. After 48 hours of transfection, the cells are washed with ice-cold 1X PBS containing

1X protease inhibitor cocktail (Sigma; catalog no. S8820). The PBS was aspirated out and ice-cold SDS lysis buffer (2x Laemmli Buffer) was added and the plate was incubated on ice for 10 min (for every 1×10^7 cells, 1 mL of SDS lysis buffer were used). The cells were then scraped out using a cell scraper and the cell lysate was transferred into a 1.5 mL microfuge tube. Gentle syringing was done through a 30 gauge needle for uniform lysis of the cells. The lysate was then centrifuged at 12,000 rpm for 10 min at 4°C. The supernatant was collected and transferred in a fresh 1.5 mL microfuge tube and heated on a boiling water at 98-100°C for 5-10 min and allowed to cool at room temperature.

For western blotting, about 50-100 μg of total protein sample was loaded onto 8-10% SDS-Polyacrylamide gel along with a molecular weight marker (The percentage of the gel required depends on the size of the protein of interest). The gel was allowed to run at 100V until the dye front reached the bottom of the gel. The proteins in the gel are then transferred onto a PVDF membrane (Cat NoIPVH00010) equilibrated with western blot transfer buffer and using a semi-dry transfer system (Amersham) at 40 mA for 2 hours. The PVDF membrane blots, with the transferred proteins are blocked using 5% non-fat dry milk or a blotting grade blocking reagent (Cat No. 1706404) diluted in 1X TBST for one hour on a shaker, with gentle rocking. After this, the membrane was incubated with a specific primary antibody at appropriate dilutions in blocking buffer, with overnight incubations on a shaker at 4°C. The blots were then intensely washed thrice with 1X TBST for 15-20 mins and incubated with a suitable HRP-conjugated secondary antibody (1:5000 dilutions in blocking buffer) for one hour. The blots are then washed with 1X TBST for three to four times and the final wash was given with 1X TBS (without Tween 20). For the visualization of the desired protein bands, an equal volume of ECL-chemiluminescent substrate reagent A and B (Cat No.WP20005) was mixed and added to the membrane blot. This was incubated for 1-2 min. The luminol or acridan based ECL substrate are metabolized by the antibody conjugated HRP (horseradish peroxidase) and produces excited intermediates which release photons and the luminescence intensity is directly proportional to the amount of antibody bound to the membrane, and in turn the protein levels. These light signals are captured by exposing the blot to X-ray films and the duration of exposure was decided by the signal intensities. Finally, X-ray films are developed and fixed to visualize the desired protein bands and the blot image was documented using a gel documentation system (Biorad).

3.15.3 Cloning of ΔNp63 and TAp63 promoters into pGL3-Basic vector

The genomic sequences immediately upstream of the human *TA-p63* and *ΔNp63* genes were obtained from the NCBI nucleotide database and analysed for potential TCF/LEF1 and PAX6 binding sites, using the Genomatix-Matinspector software.

The *ΔNp63* full length (-1987 to +86 bp) and the minimal promoter (-233 to +86 bp) regions were PCR amplified using human genomic DNA as a template. Primers to amplify the above genomic regions were designed to carry XhoI and HindIII restriction enzyme sites into the forward and reverse primers respectively. The PCR product were digested with XhoI and HindIII and directly cloned into the XhoI and HindIII digested pGL3-Basic vector, upstream of the luciferase reporter gene to obtain the pGL3_ *ΔNp63*P-FL and pGL3_*TAp63*P-M constructs.

Similarly, the primers for the human *TAp63* full length (-1829 to +13 bp) and the minimal (-671 to +13 bp) promoters were designed to carry SmaI site-specific overhangs at their 5' ends and the PCR amplicons were directly cloned into the SmaI cut site of the pGL3-Basic vector, upstream of the luciferase reporter gene, to obtain the pGL3_*TAP63*P-FL and pGL3_*TAP63*P-M constructs.

The primers used for different promoter region amplifications are listed in **Annexure V**. The positive clones are confirmed by restriction enzyme digestions and sequencing. These reporter constructs are then transfected into HCE and NIH3T3 cells, with or without co-transfection of either of the GFP-PAX6 variant constructs to assess the effect of PAX6 variants on different p63 promoter activities. The transfected cells are lysed after 48 hours of transfection and the lysates are used to carry out the luciferase reporter assay, as described in section **3.6.2**.

3.15.4 Cloning of *KRT3* and *KRT12* promoters into pGL3-Basic vector

The genomic sequences immediately upstream of the human *KRT3* and *KRT12* genes were obtained from the NCBI nucleotide database and analysed for potential TCF/LEF1 and PAX6 binding sites, using the Genomatix-Matinspector software.

Region-specific primers were designed for the PCR amplification of the human *KRT3* full length 1621 to +65 bp) and the minimal (-514 to +65 bp) promoters; and also the human *KRT12* full length (-1045 to +19 bp) and the minimal (-539 to +19 bp) promoters. The primers were designed to carry EcoRV site-specific overhangs at their 5' ends and the PCR amplicons were directly cloned into the SmaI cut site of the pGL3-Basic vector, upstream of the luciferase

reporter gene, as blunt ended ligations, to obtain the pGL3_*KRT3P*-FL, pGL3_ *KRT3P*-M, pGL3_*KRT12P*-FL, pGL3_ *KRT12P*-M constructs respectively.

The primers used for different promoter region amplifications are listed in **Annexure V**. The positive clones are confirmed by restriction enzyme digestions and sequencing. These reporter constructs are then transfected into HCE and NIH3T3 cells, with or without co-transfection of either of the GFP-PAX6 variant constructs to assess the effect of PAX6 variants on *KRT3* and *KRT12* promoter activities. The transfected cells are lysed after 48 hours of transfection and the lysates are used to carry out the luciferase reporter assay, as described in section **3.6.2**.

3.16 Differential global gene expression analysis of cells expressing individual PAX6 isoforms

3.16.1 Cloning of human PAX6 variants into a retroviral vector

The cDNA of *PAX6* isoforms PAX6A, PAX6B, PAX6B-ASΔ6, and PAX6A-12a were PCR amplified using isoform-specific primers (listed in **Annexure V**) and cloned into the pMOS-Blue vector and the positive clones are confirmed by restriction enzyme digestion and the insert DNA was sequence confirmed. The PAX6 variant encoding inserts are then sub-cloned into the pLNCX2-CMV-IRES-GFP retroviral vector downstream of the CMV promoter using the BglII-BamHI restriction sites, as in-frame HA tag fusions at the N' end. The recombinant retroviral particles were prepared by transfecting these constructs into Plat A cells, as described under **Section 3.7.3**.

3.16.2 Generation of stable HCE cell lines expressing individual PAX6 isoforms

Along with the human PAX6 genes, the retroviral vectors encode a neomycin resistance gene which allows G418/Geneticin antibiotic selection to select for stable recombinant cells. HCE were treated with variable concentrations of G418 antibiotic (0, 50, 100, 200, 300, and 400 μg/mL) and cultured for about 7 days to assess the optimal concentration (MIC) that can kills all the untransfected cells within 1 week. A concentration of 100 μg/mL of G418 was found to be optimal, which was further used to select for recombinant HCE cells after recombinant retroviral vector transductions. To establish HCE cells stably expressing an individual PAX6 variant, 2×10^5 HCE cells/well were seeded in a 6-well plate. The cells were then cultured for about 12 hrs and allowed to adhere and attain their normal morphology. Once the HCE cells reached 60% confluency, a transduction mix consisting of the recombinant retroviral vectors encoding a specific PAX6 variant and 10 μg/mL of polybrene in 2 mL of culture medium was added to the cells. After 48 hours of transduction, the cells were cultured in G418 antibiotic

(100 μg/mL) containing complete HCE medium, with media changes on alternate days for up to one week. During this period, most of the cells underwent apoptosis due to cytotoxicity, except the transduced cells that stably expressed the transgene cassette. These surviving stable cells were further maintained in G418 containing medium until they reach confluence. They were further passaged and cryopreserved for the long term use. Total RNA isolated from the stable HCE cell lines expressing each of the human PAX6 variants are subjected to comparative whole genome expression profiling, using the Agilent 60K microarrays.

3.16.3 Analysis of global gene expression using Microarrays

The gene expression library probes were prepared for three biological repeat samples, for each of the PAX6 variant expressing cells and for a HCE cell line control. The labelled probes were hybridized on to the Agilent 60K microarrays and processed as per the manufacturer's protocols and the slides were imaged using the GCOS software. The fluorescent intensity of the images was normalized for background correction and data was analysed using the Gene spring 12.5 software. The untransduced HCE cell line control was used for data normalization and for the identification of differentially expressed genes in different PAX6 variant expressing sample sets. Student's unpaired t-test was used for the analysis of gene expression data across different sample sets and p-values were calculated for testing the statistical significance. Genes that exhibited $\geq$ 2.0 fold increase or decrease in expression and $p<0.05$ were considered as significant differentially regulated gene sets, which were considered for further downstream analysis such as, cluster analysis, gene ontology mapping and pathway analysis.

3.17 Statistical analysis of experimental data

All experimental values were reported as mean ± standard deviations. Group means were compared using the Student's unpaired t-test; $P < 0.05$ was considered statistically significant (*), $P < 0.01$ was considered highly significant (**), $P < 0.005$ was considered very highly significant (***) and $P > 0.05$ was considered statistically insignificant (#).

CHAPTER 4

RESULTS

4: Results

4.1. Differential regulation of human *PAX6* promoters in different ocular cell types

4.1.1. Cloning of human *PAX6* promoters and the ocular surface ectoderm enhancer

To study the eye-specific regulation of human *PAX6,* the distal PAX6 promoter, the retina-specific intronic promoter and the ocular surface ectoderm (OSE) enhancer regions were identified based on published reports. To understand the potential transcription factor binding sites of human *PAX6* pA promoter, we analyzed the full length distal pA promoter using Genomatix-Matinspector software. The results revealed some of the key transcription factor binding sites within the *PAX6* pA region (-800 to +73 bp) such as PAX6, Kaiso, TATA box, CCAAT box, C/EBP and TCF/LEF1 sites upstream to the reported transcription start site (**Fig 4.1.B**). Region specific primers were designed and *PAX6* pA (-800 to +73 bp) and *PAX6* pC (1.2 kb) regions were PCR amplified and cloned upstream to the luciferase reporter gene in pGL3 basic vector (**Fig 4.1.C**). As mentioned earlier, enhancers are crucial for PAX6 regulation. The OSE enhancer region is highly conserved across species and is located approximately 3.5 kb upstream to the transcription start site of the proximal pA promoter. Earlier reports have demonstrated that OSE enhancer in *PAX6* is important for lens formation (Williams *et al.*, 1998). To know the enhancer specific regulation of pA in ocular cells, OSE enhancer (-4179 to -3603 bp) was also cloned upstream to the pA promoter in pGL3 basic vector (**Fig 4.1.C**).

4.1.2. Characterization of *PAX6* promoters and the OSE enhancer in different ocular cell types

To check the relative activity and strength of these promoters (pA, OSE-pA and pC), the reporter constructs were transfected into different ocular cell lines viz; HCE (human corneal epithelium), ARPE19 (human retinal pigmented epithelium), 661W (mice cone photoreceptor precursor) and HLE-3B (human lens epithelium). The luciferase reporter activity confirmed that pA promoter is highly active in the corneal epithelial cells (HCE; 429 fold), retinal pigmented epithelial cells (ARPE-19; 455 fold), neuro-retinal/cone precursor cells (661W; 231 fold) and lens epithelial cells (HLE-3B; 268 fold) when compared to the basal activities of the pGL3-Basic vector (**Fig 4.1.D**). This confirms that pA promoter is ubiquitously active in many parts of the eye. When compared to *PAX6*-pA, *PAX6*-pC was found to be a weak promoter in all the ocular cell lines tested (**Fig. 4.1.D**). When the pA promoter was supplemented with the OSE enhancer, there was no significant change in the activity of pA promoter in HCE

cells, whereas it significantly induced the activity of pA in ARPE19, 661W and HLE-3B cells to about 1.9, 1.5 and 2.9 folds respectively (**Fig. 4.1.D**). This suggests that the OSE enhancer is truly a lens-specific enhancer and has no significant role in regulating the pA promoter in other ocular surface ectoderm derived tissues such as the corneal and conjunctival epithelium.

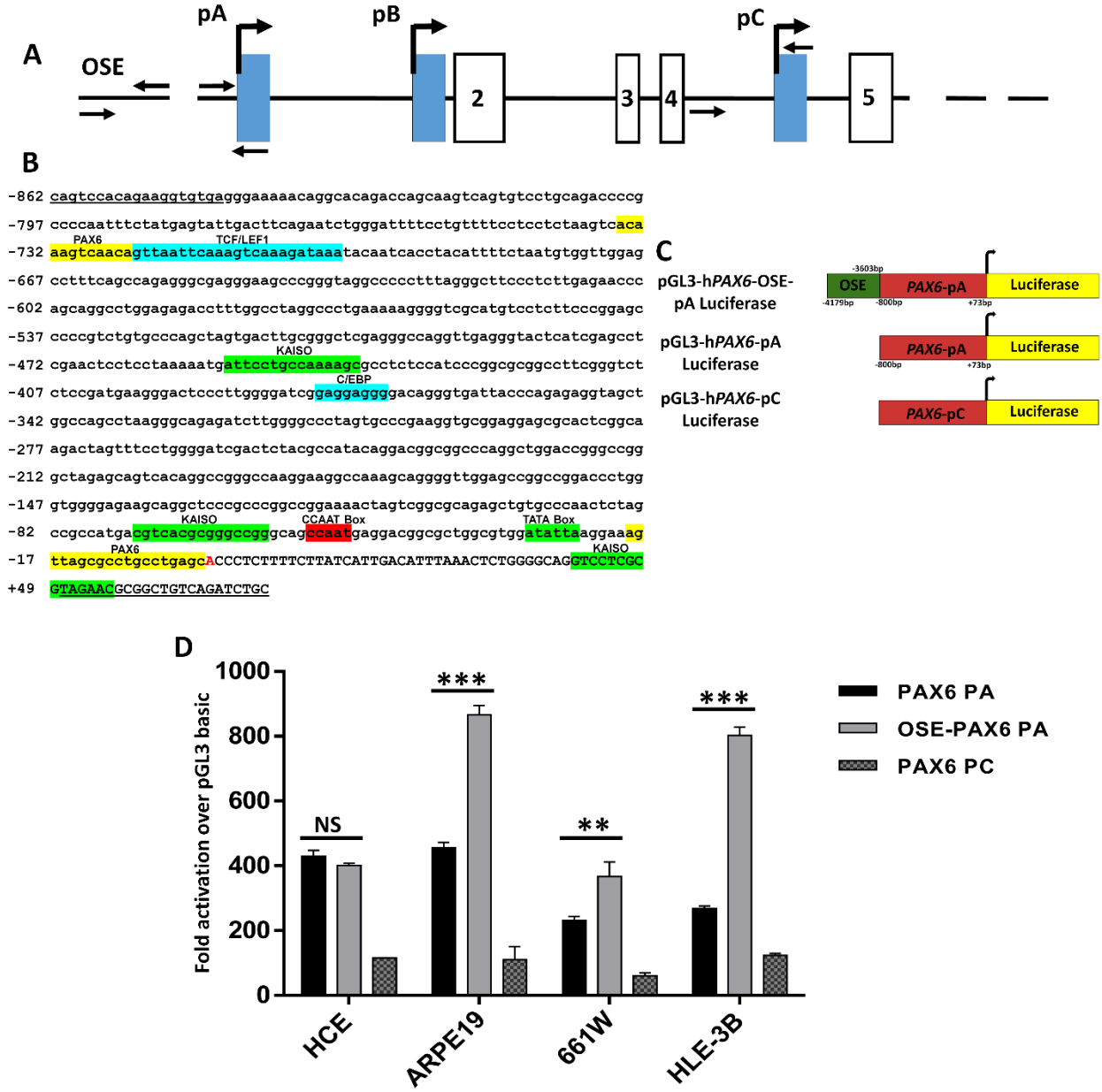

Figure 4.1: Human PAX6 promoter cloning and characterization in different ocular cell lines. ***A****. Cartoon representation of human PAX6 genomic locus and the positions of primer sets spanning different PAX6 promoter regions that were cloned into luciferase and GFP reporter constructs.* ***B****. 5' upstream region of the human PAX6 pA promoter (-800 to +73 bp) highlighted with important cis-regulatory elements in different colours, with transcription start site in red.* ***C****. Pictorial representation of human PAX6-OSE-pA and PAX6 pA and PAX6 pC promoters cloned upstream to the luciferase reporter gene in the pGL3-Basic vector.* ***D****. Histogram representation of human PAX6 promoter activities in different PAX6 expressing ocular*

*cell lines viz; HCE, ARPE19, 661W and HLE-3B. Normalized reporter values were plotted as fold activation over pGL3-Basic control values. The data is represented as mean ± standard deviations, with N=3. *P<0.05, **P<0.005 and ***P<0.0005.*

4.1.3. *PAX6* pA and pC activity in primary limbal epithelial cultures

We further went ahead and checked the activity of *PAX6* pA and pC promoters in primary cultures of human limbal epithelial cells, established both as suspension and explant cultures. The human pA (-800 to +73 bp) and pC promoter regions were cloned into pHR-SIN lentiviral vector upstream of the EGFP reporter gene and recombinant lentiviral particles were prepared (**Fig 4.2.A**). These recombinant lenti-virus were transduced in the primary cultures of human limbal epithelial cells. In explant cultures, we observed that the cells at the leading edge showed intense pA driven GFP expression while rest of the cells were negative or showed weak GFP expression (**Fig 4.2.B.i**). In cell suspension culture on NIH 3T3 feeders, most of the cells within the clonally expanding colonies expressed GFP. Also, the 3D sphere clusters showed highly intense pA driven GFP expression (**Fig 4.2.B.ii**). These sphere clusters represent the proliferating stem cell clones. This suggests that pA is highly active in proliferating limbal epithelial cells. However, the pC promoter driven GFP expression was not observed in the limbal explant cultures, indicating that pC is inactive in the limbal and corneal epithelium (**Fig 4.2.C**).

4.1.4. *PAX6* promoter activity in iPSC derived ocular tissues

PAX6 is a critical master regulatory gene important for eye formation. In order to check the activity of *PAX6* pA and pC promoters during early eye development, we differentiated human induced pluripotent stem cells (iPSCs) into ocular lineage using the standard protocols established in our lab (Susaimanickam *et al.*, 2017) and generated different ocular cell types such as the retinal/optic cups, retinal pigmented epithelium, ocular surface epithelium and lens primordium/lentoids. The differentiating cultures at the eye field stage were then transduced with lentiviral vectors encoding the GFP reporter driven by different *PAX6* promoters (*PAX6* pA, OSE-*PAX6* pA and *PAX6* pC). After 72 hours of transduction, the cultures were checked for GFP reporter expression under a fluorescence microscope. As shown in figure ***4.3.B***, pA activity, as indicated by GFP reporter expression was seen in the neuro-retina or optic cups, pigmented RPE cells with cobble stone morphology, and in the migrating ocular surface ectoderm cells, thus indicating pA activity in all the three cell types (**Fig 4.3.B**). OSE enhancer linked pA promoter was found to be highly active in the gamma crystalline expressing lentoid structures formed adjacent to the neuro-retina, indicating the lens specific role of OSE

enhancer in regulating pA activity (**Fig 4.3.C**). In contrast, the *PAX6* pC was inactive most ocular cell types such as the lens and corneal epithelium (data not shown). However, the pC driven GFP was highly expressed in the retinal neurons of the iPSC derived optic cups, indicating that the pC is retina specific in developing eyes (**Fig 4.3.D**).

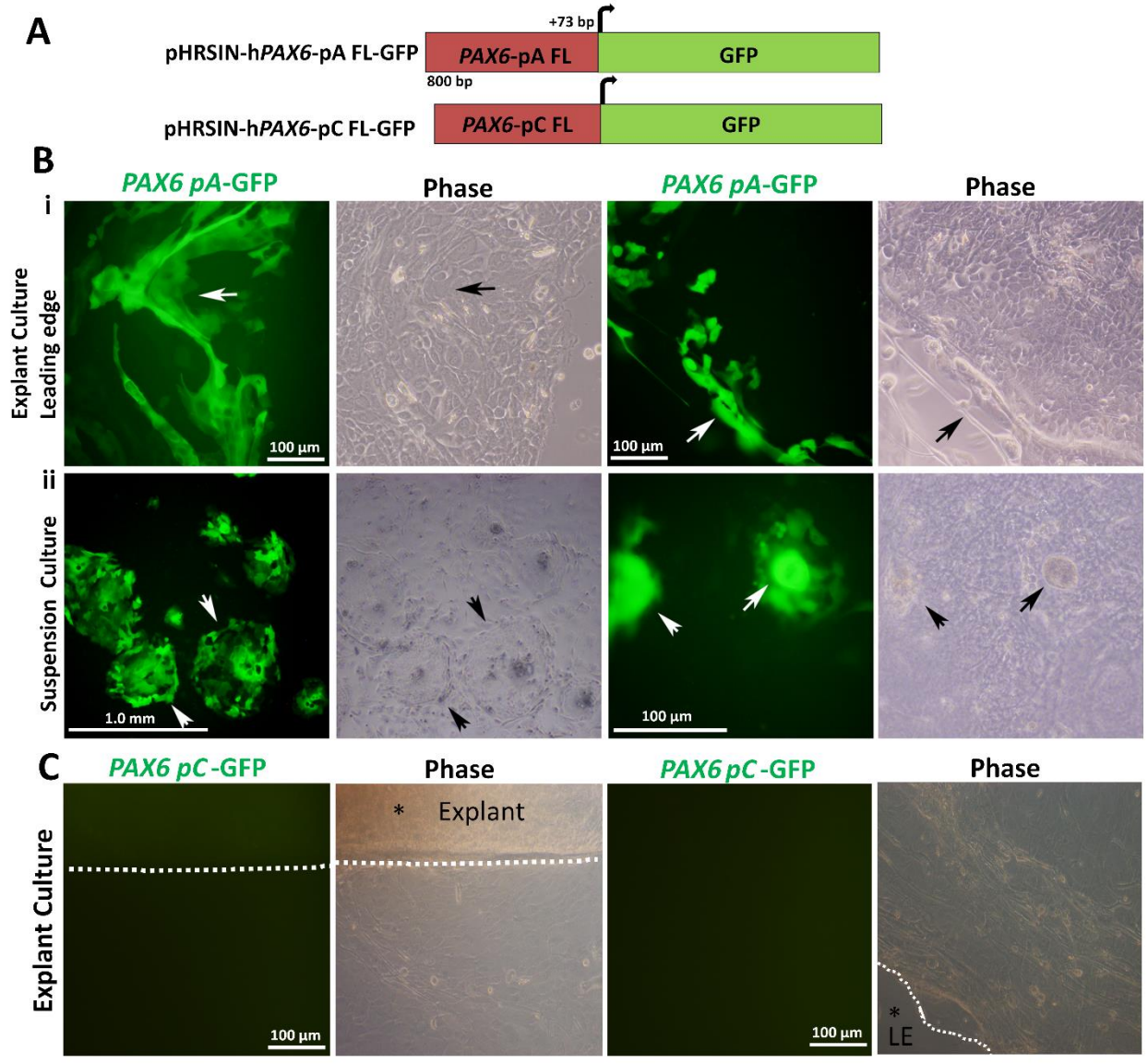

Figure 4.2: Activity of PAX6 promoters in primary limbal epithelial cultures. A. *Cartoon representation of PAX6 pA and pC promoters cloned upstream of the GFP reporter gene in pHR-SIN lentiviral vector.* ***B.*** *GFP reporter expression in primary limbal epithelial cultures transduced with PAX6 pA and pC EGFP encoded lentivectors.* ***Bi.*** *Leading edge of cell outgrowths showing intense GFP expression (arrows) in explant cultures.* ***Bii.*** *Clonally expanding cells and 3D sphere clusters containing activated stem cells show intense GFP expression (arrows) in suspension cultures.* ***C.*** *pC promoter shows no activity or GFP expression in the primary limbal epithelial cells. Dotted line marks the boundary of the explants and the leading edge of the migrating cells. Scale bar- 100 µm.*

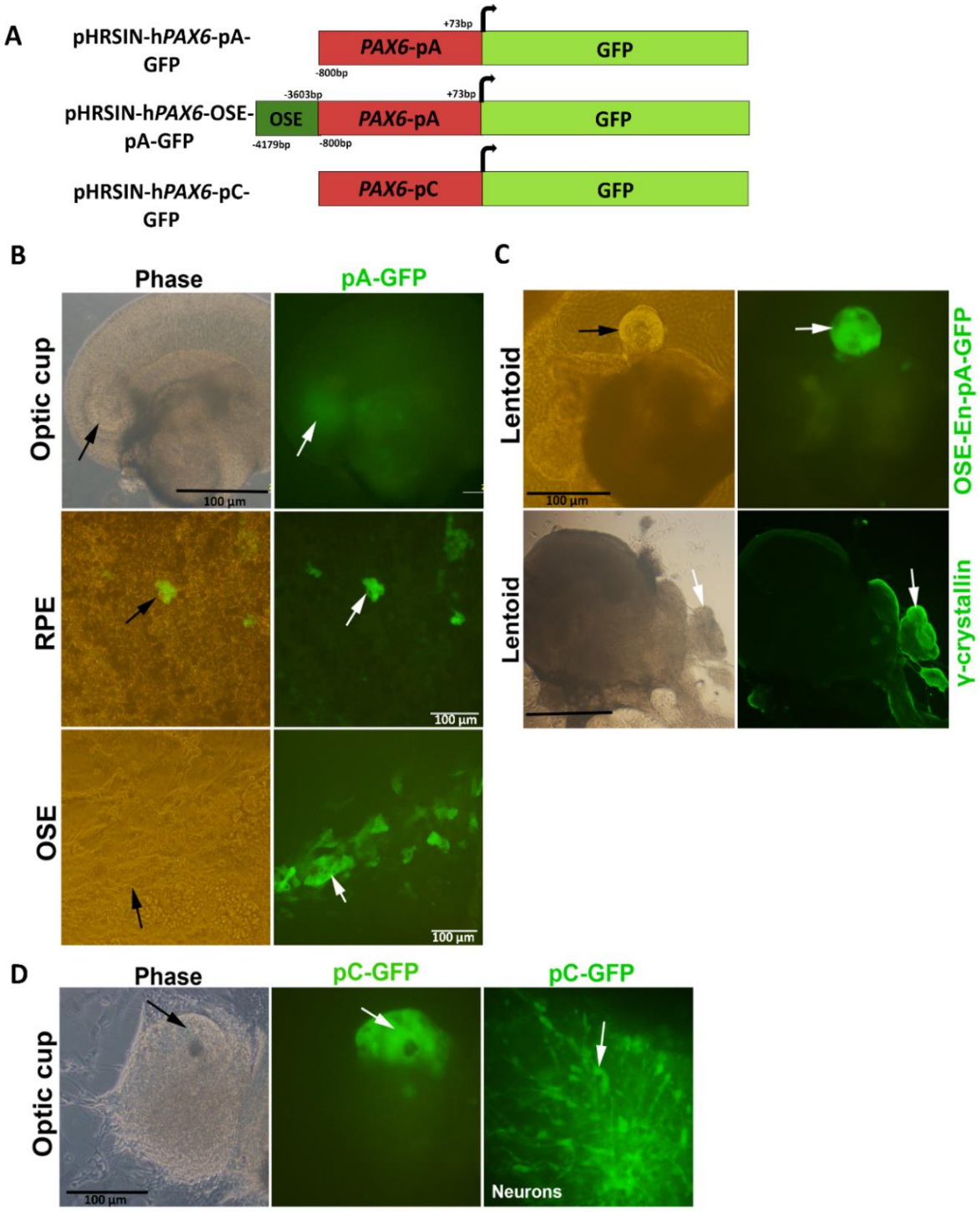

Figure 4.3: Activity of PAX6 promoters in human iPSC-derived ocular cell types. A. *Cartoon representation of PAX6 pA, pC and OSE enhancer driven pA promoters cloned upstream to the EGFP reporter gene in pHR-SIN lentiviral vector.* ***B.*** *Activity of pA in iPSC derived neuro-retinal cups, RPE and ocular surface ectodermal cells is marked by GFP reporter expression.* ***C.*** *OSE influenced pA activity in iPSC derived lentoids, which also expressed γ – crystallin (in green).* ***D.*** *pC activity in hiPSC derived neuro-retinal cups and retinal neurons. Scale bar- 100 µm.*

4.1.5. Characterization of *PAX6* pA expressing primary limbal epithelial cells

To identify the nature of pA expressing cells, lentiviral vectors encoding the GFP reporter driven by *PAX6* pA was transduced into limbal primary cultures and immunostained using antibodies against different corneal epithelial and stem cell markers. The results confirmed that most of the transduced cells that expressed GFP had moderate levels of PAX6 (**Fig 4.4.i**). The GFP^+ cells were also found to express high levels of p63, an epithelial stem cell and proliferating cell marker, thus confirming the activity of pA promoter in the TACs (**Fig 4.4.ii**). To distinguish between the TACs and terminally differentiated cells, the cultures were also evaluated for the expression KRT3/KRT12 proteins which are mature corneal epithelial markers. We observed that the GFP^+ cells are negative for K3/K12 expression, which indicates that pA promoter is not active in terminally differentiated cells (**Fig 4.4.iii**). The proliferative nature of the transduced cultures was evaluated by BrdU pulsing them for 30 mins, followed by immunostaining them with BrdU. All the pA expressing cells were found to be actively proliferating and incorporated the BrdU label (**Fig 4.4.iv**). Taken together, we confirm that the *PAX6* pA is highly active in transiently amplifying limbal epithelial cells.

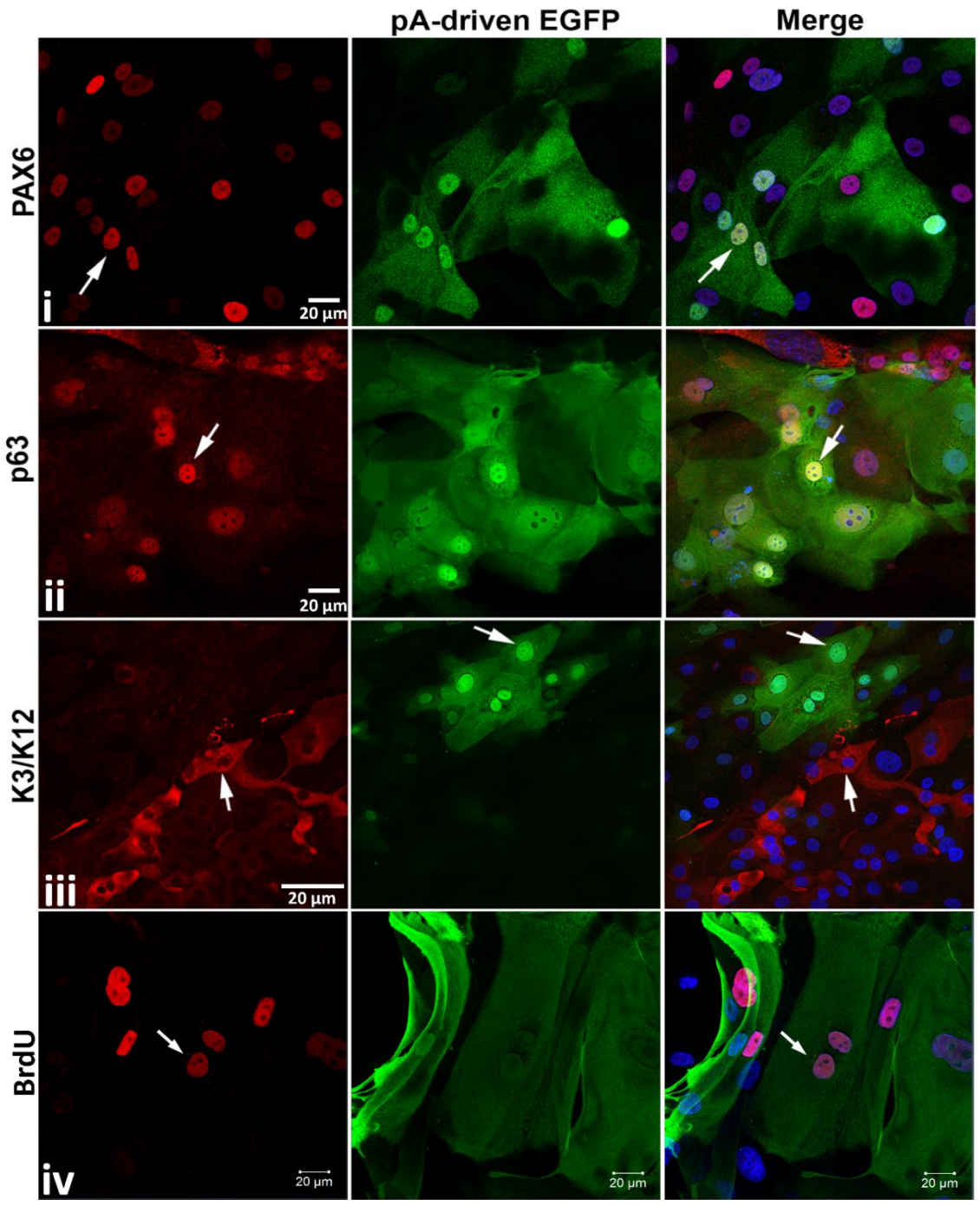

Figure 4.4: Characterization of primary limbal epithelial cultures transduced with the lentivector encoding PAX6-pA-GFP reporter. *Transduced corneal epithelial cells expressing pA promoter driven GFP co-expressed PAX6* ***(i)*** *and the epithelial stem cell and TAC marker, p63* ***(ii)****. However, they did not express the corneal differentiation and mature cell markers K3/K12* ***(iii)****. The GFP expressing cells were also proliferating and incorporated the BrdU label* ***(iv)****. All cell nuclei are counterstained with DAPI (Blue). Arrow heads indicate the cells coexpresing GFP along with different markers tested. (Scale bar- 20 µm).*

4.1.6. Role of Wnt/β-catenin signaling in regulating PAX6 expression

Wnt signaling is known to play an important role in regulating corneal epithelial development and wound healing responses (Gonzalez *et al.*, 2019; Sasamoto *et al.*, 2016; Lu *et al.*, 2012; Nakatsu *et al.*, 2011; Mukhopadhyay *et al.*, 2006). An earlier report has shown that Wnt signaling is involved in the regulation of limbal epithelial stem cells. Treatment of limbal cultures with lithium chloride was shown to activate Wnt signaling and increased cell proliferation and promoted clonal expansion.

Based on this knowledge, we hypothesized that Wnt signaling could be influencing PAX6 expression, which in turn can regulate some of the known targets genes such as, KRT3/KRT12 (important for corneal epithelial differentiation) and ΔNp63/TAp63 (epithelial stem cell/TAC marker) and together mediate the limbal stem cell proliferation vs differentiation decisions (**Fig 4.5**).

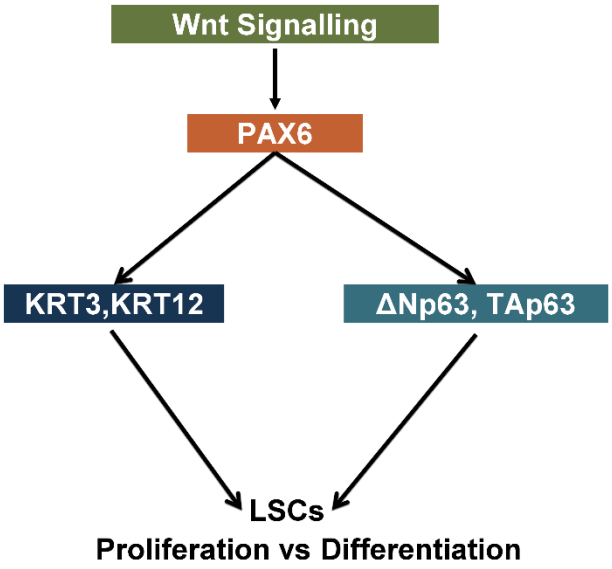

Figure 4.5: Hypothetical representation of PAX6 regulation through Wnt signaling.

To check the effect of Wnt activity on PAX6 regulation, the cells were treated with BIO (6-bromoindirubin-3'-oxime, a small molecule inhibitor of GSK3β, which helps to stabilize β-catenin and promote its nuclear accumulation and transcriptional activity. Also, in the absence of Wnt signals, the Wnt responsive promoters are known to get repressed in a histone deacetylase (HDAC) repressor dependent manner. Therefore, we also checked for the effects of HDAC inhibition on PAX6 regulation by treating the cells with Valproic acid (VPA). The effect of BIO (2.5 μM for 12 hrs) and/or VPA (1 mM for 12 hrs) treatments on pA promoter activity was tested in different ocular cell lines viz; HCE, HLE-3B, ARPE-19 and 661W. The

reporter constructs of *PAX6* pA promoter with or without the OSE enhancer (*PAX6* pA, OSE_*PAX6* pA) was transfected into ocular cell lines to carryout luciferase reporter assays at 48 hrs post transfection.

The normalized reporter activity values are represented as fold activation over pGL3-Basic. Upon Wnt activation (BIO treatment), pA activity was significantly increased by 8.8 and 4.34 folds in HCE and HLE-3B cells respectively (**Fig 4.6.A, B**). However, it repressed the activity of pA promoter in ARPE19 and 661W cells by 0.74 and 0.6-folds respectively (**Fig 4.6.C, D**). This confirms that Wnt signals activate pA in corneal and lens epithelium, while it represses the promoter in retinal cells. Upon HDAC inhibition (VPA treatment), pA activity was found to significantly increase (5, 7, 3.2 and 13 fold respectively) in all the ocular lines HCE, HLE-3B, ARPE19 and 661W cell lines (**Fig 4.6.A-D**). This suggests that the pA promoter is tightly regulated and maintained in a highly repressed state in a HDAC dependent manner, in the absence of Wnt signals.

However, when the Wnt was activated in the presence of OSE enhancer, there was upregulation in the activity of pA in all the cell lines except ARPE-19. Upon HDAC inhibition, there was a synergistic effect that resulted in 28 fold increased *PAX6* pA activity in HCE cells and 1.9, 2.54 and 6 fold respectively in other ocular cell lines (**Fig 4.6.A-D**).

Thus, the *PAX6* pA promoter is differentially regulated by Wnt signals in different ocular cell types. Apart from Wnt signals, it is also tightly regulated by repressor complexes by HDAC-dependent mechanisms.

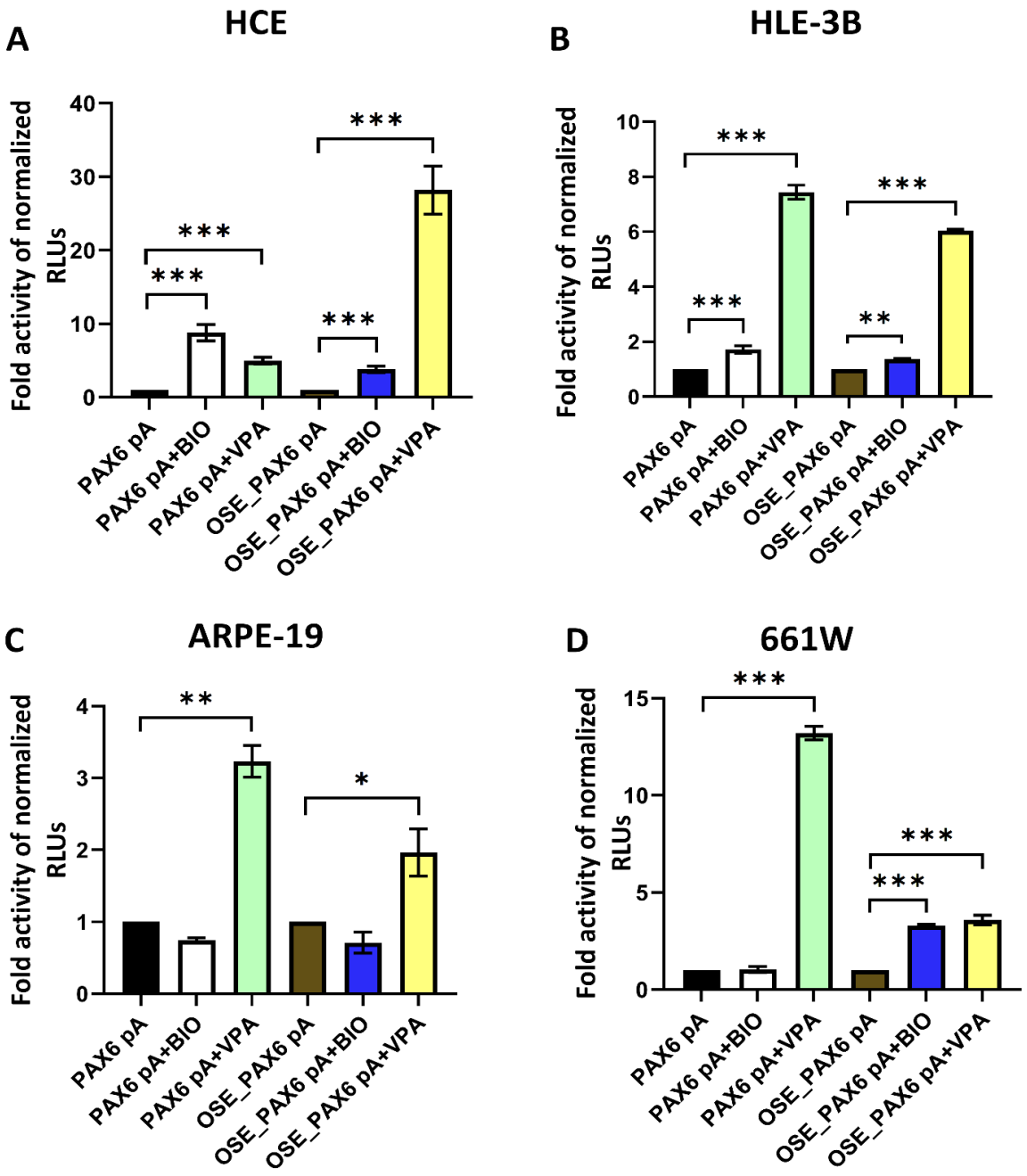

Figure 4.6: Effect of Wnt activation and HDAC inhibition on PAX6 promoters in different ocular cell lines. *Different PAX6 promoter driven luciferase constructs were transfected into HCE, ARPE19, 661w and HLE-3B cell lines, followed by BIO (GSK3β blocker) and VPA (HDAC inhibitor) treatments. The cell lysates were used to carry out luciferase reporter assays. Normalized reporter values were used to calculate the relative luciferase units. The mean fold changes over the PAX6-pA promoter activities are plotted for A. HCE, B. HLE3B, C. ARPE-19, D. 661W cells. Error bars represents ± standard deviations. N=3.*P<0.05, **P<0.005 and ***P<0.0005.*

4.1.6.1. *PAX6* pA promoter is a direct target of Wnt/β-Catenin signaling

While analyzing for putative transcriptional factor binding sites by Genomatix-Matinspector software, we observed that the *PAX6* pA promoter has a highly conserved TCF/LEF1 binding site, along with two half sites on either sides with a very high Matinspector score (>0.95) (**Fig 4.7.A**). Here, we hypothesized that pA promoter could be a direct transcriptional target for Wnt/β catenin signaling in ocular cells.

To check if the TCF/LEF1 site within the pA promoter can recruit β-catenin, we performed chromatin Immunoprecipitation (ChIP) of primary limbal epithelial cultures using a ChIP grade β-catenin antibody, using the protocols described in the methods. The DNA from the antibody-protein-DNA complex containing ChIP pellet was purified and used as template for region specific PCRs. Region specific PCR primers were designed to flank the putative TCF/LEF1 site within the *PAX6* pA promoter. Positive amplification of the TCF/LEF1 site containing region has confirmed that the β-catenin binds to and regulate the *PAX6*-pA promoter, thereby suggesting the direct involvement of Wnt signaling in regulating *PAX6* expression (**Fig 4.7.B**).

The results of the luciferase reporter assays and the effects of valproic acid treatment clearly suggested the involvement of HDAC-mediated repressive mechanism in the regulation of *PAX6* pA promoter. Also, the Matinspector analysis has indicated a KAISO repressor binding site close to the TCF/LEF1 site within the pA promoter (**Fig 4.7.A**). Kaiso is a transcriptional regulator that can recruit N-CoR repressor complex to promote histone deacetylation and repression of Wnt signaling and other target genes promoters. Therefore, we checked whether the HDACs and Kaiso repressors are directly binding and regulating the pA promoter using ChIP assay. For this, primary limbal epithelial cells were lysed, sonicated and immunoprecipitated using either the KAISO or HDAC antibody. Primers flanking the TCF/LEF1 and Kaiso consensus motifs within the *PAX6* pA promoter was used to carry out region specific PCR. The Kaiso and HDAC ChIP complex DNA was used as a template to amplify the region of interest. Positive amplification from both the HDAC and KAISO ChIP samples has confirmed the direct binding of these repressors close to the TCF/LEF1 site of pA promoter (**Fig 4.7.B**). This clearly suggests that the *PAX6* pA promoter is tightly regulated by Wnt-dependant activation and Kaiso-HDAC-dependant repressive mechanisms to ensure optimal spatio-temporal gene expression.

In order to assess the response of canonical Wnt signals in corneal cells, the HCE cells were transfected with TOP/Flash and FOP/Flash Wnt reporter constructs. The TOP/Flash construct encode a luciferase reporter driven by a basal promoter and a synthetic DNA element encoding 6X TCF/LEF1 consensus sites. The FOP/Flash construct carries the mutated 6X TCF/LEF1 consensus. The cells were treated with 10 mM BIO, 1 mM Valproic acid (VPA) and 1 mM Sodium butyrate (SB) respectively for 12 hrs and the lysates were prepared for luciferase assay. The reporter activities are represented as TOP/FOP relative luciferase units (RLU). The results revealed that the HCE cells respond to Wnt signals and show more than 120 fold activation of the Wnt reporter expression upon BIO treatment. However HDAC inhibition has no effect on the reporter activity (Fig. 7D). This suggests that the HCE cells are permissive and respond to canonical Wnt signals significantly (**Fig 4.7.D**). However, the weaker effects of Wnt signals on *PAX6* pA activation in HCE cells may be attributed to the existence of other repressor mediated negative regulation.

To further confirm the direct role of canonical Wnt signals on PAX6 pA promoter regulation, we created TCF/LEF1 site mutations by site directed mutagenesis, wherein the consensus TCF/LEF1 site was disrupted by two base pair changes (TTCAAAG to GCCAAAG) (**Fig 4.7.C**). To assess the effect of this mutation on pA promoter activity, we carried out luciferase reporter assay in HCE cells transfected with Wt and mutant pA promoter constructs respectively. We observed that TCF/LEF1 site mutation significantly abolished the promoter activity (**Fig 4.7.E**), which suggests that the canonical Wnt signals plays a direct role in regulating the *PAX6* pA promoter activity in HCE cells. To further activate the canonical Wnt pathway, the cells were treated with BIO. This resulted in significant activation of Wt pA but the mutant promoter continued to remain inactive (**Fig 4.7.E**). Upon HDAC inhibition, the Wt pA promoter got significantly activated. Interestingly, the mutant promoter also showed significant activation (**Fig 4.7.E**). This again confirmed that the *PAX6*-pA promoter is a direct target of Wnt signals and also tightly regulated by HDAC dependent repressive mechanisms.

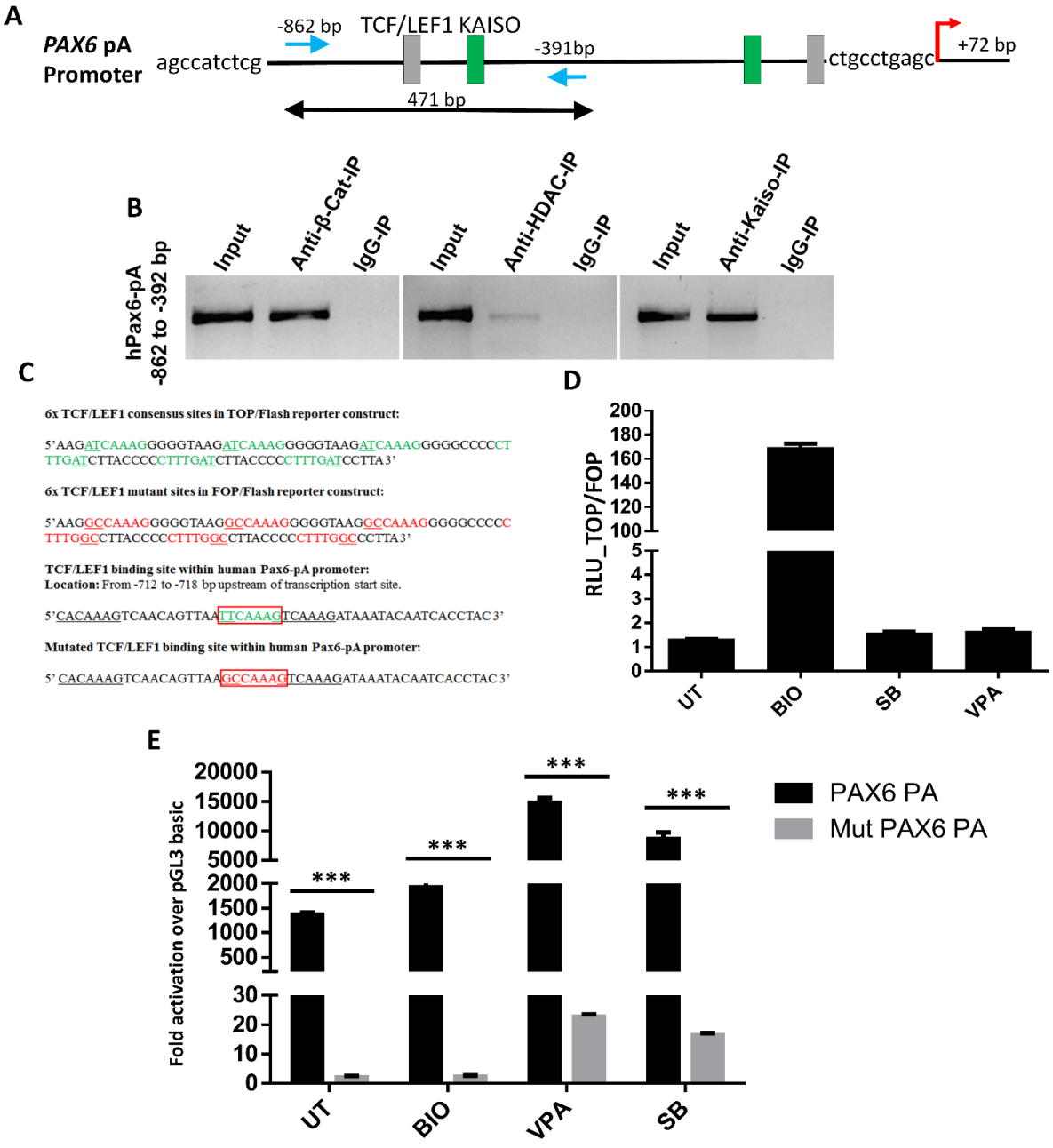

Figure 4.7: Effect of β-catenin, HDAC and Kaiso repressors on pA promoter activity. ***A****. Cartoon representation of the predicted TCF/LEF1 and Kaiso binding sites (-862 to -391 bp) on the pA promoter.* ***B.*** *Agarose gel image of chromatin immunoprecipitation (ChIP) and pA promoter region specific PCR amplicons. Chromatin preparation of primary limbal epithelial cells was immunoprecipitated using antibodies against β-catenin, HDAC1 and Kaiso respectively and pA promoter region was PCR amplified using the DNA templates purified from the chromatin inputs (positive controls), antibody-specific ChIP (test sample) and IgG ChIP complexes (negative controls).* ***C.*** *TCF/LEF1 consensus and the mutant sequences in TOP/Flash, FOP/Flash and PAX6 pA promoter-reporter constructs.* ***D.*** *Histogram representation of the relative TOP/FOP luciferase reporter activities in HCE cells treated with or without BIO, Valproic acid (VPA) and sodium butyrate (SB).* ***E.*** *Histogram representation of the Wt pA and TCF/LEF1 mutant*

*pA promoter activities in HCE cells treated with or without BIO, VPA and SB. Normalized luciferase reporter values were plotted as fold activation over the pGL3-Basic vector activities. Error bars represents mean ± standard deviations. N=3. *P<0.05, **p<0.005 and ***p<0.0005.*

4.1.6.2. Effects of Wnt signaling on PAX6 target genes

Next, we checked the effect of Wnt signaling on some of the known PAX6 target genes such as, KRT12/KRT3 and p63 (ΔNp63 and TAp63).

KRT12 and KRT3 are the early and late corneal differentiation marker respectively. p63 is a key epithelial specific transcription factor, which has its transactivation domain at the N-terminus, DNA binding domain in the middle and an oligomerization domain at the C-terminus. It exists in two different isoforms, namely, TAp63 and ΔNp63, depending on the alternate promoter usage. The full length protein that has the N terminal transactivation domain is the TAp63 isoform that is predominantly expressed by the transiently amplifying cells (TACs) of the limbus and cornea. Whereas, the p63 protein that lacks the N-terminus transactivation domain is the ΔNp63 isoform that is predominantly expressed by the basal limbal stem cells (LSCs) and play a crucial role in maintaining their quiescent state.

Using Genomatix-Matinspector software, the human promoters of *KRT3* (-4000 to +66 bp), *KRT12* (-4000 to +25 bp), *ΔNp63* (-1996 to +86 bp) and *TAp63* (-2000 to +1 bp) upstream of the transcription start site was analyzed and multiple TCF/LEF1 binding sites were identified (**Fig 4.8.A.i**). In order to check the binding of β-catenin on the promoter regions of *KRT12*, *KRT3* and *p63* (TAp63 and ΔNp63) in primary limbal epithelial cells, we performed ChIP using an antibody against β-catenin. ChIP PCR primers were designed to span the genomic regions predicted to have the TCF/LEF1 binding sites. The primary limbal epithelial cell culture lysates were used to check the binding of β-catenin at TCF/LEF1 sites using ChIP. Region specific PCR of ChIP complex DNA confirmed direct binding of β-catenin on the *KRT3*, *KRT12*, *ΔNp63* and *TAp63* promoter regions (**Fig 4.8.A.ii**).

Further, we cloned the proximal promoter regions of *KRT12* (2.5 kb), *KRT3* (1.6 kb), *ΔNp63* (2 kb) and *TAp63* (1.8 kb) in a promoter less pGL3 basic vector upstream of the luciferase gene and checked the effects of Wnt signals in regulating these promoter activities. HCE cells were transiently transfected with *KRT12*, *KRT3* and *p63* promoter constructs and treated with BIO and/or VPA to assess the effects of Wnt activation and HDAC inhibition on these promoter activities. At 48 hours post transfection and 12 hrs of drug treatment, the cells lysates were prepared for luciferase reporter assay. In HCE cells, the luciferase reporter activity of

KRT12 and *KRT3* promoters showed 63 and 116 fold activation over the pGL3-Basic vector (**Fig 4.8.B, C**). Upon activation of Wnt signals, there was a significant increase in the luciferase activity, with 1.6 fold increase with *KRT12* and 2.3 fold increase with *KRT3* promoter activities (**Fig 4.8.B, C**). However, HDAC inhibition did not have any influence on both *KRT12* and *KRT3* promoters in HCE cells (**Fig 4.8.B, C**). This indicates that the *KRT3* and *KRT12* promoters responds positively to Wnt signals and may help in inducing corneal epithelial differentiation, while HDAC inhibition has no effect on these differentiation and maturation specific genes.

In contrast, Wnt activation resulted in 1.9 fold increase in the *TAp63* promoter activity, but there was no effect on *ΔNp63* promoter in HCE cells. HDAC inhibition significantly induced the activation of *TAp63* and *ΔNp63* promoters to about 3 and 3.5 fold respectively in HCE cells (**Fig 4.8.D, E**). This suggests that Wnt activation supports the expansion of TAp63 expressing TA cell populations, while simultaneously inducing K3/K12 genes and enables their differentiation. Whereas, HDAC inhibition promotes both TAp63 and ΔNp63 expression without any effect on K3/K12 genes, which suggests the usefulness of this strategy to promote stem cell maintenance and to allow the expansion TA cell population without precocious differentiation. This need to be further validated in clonal assays to compare the effects of BIO and VPA treatments in terms of limbal stem cell preservation and holoclone forming efficiencies.

To validate this further, primary limbal epithelial cells treated with BIO and VPA were used to check the levels of expression of mRNAs of different Wnt target genes, limbal stem cell and corneal differentiation specific genes by semi quantitative RT-PCR. In accordance with luciferase assay, RT-PCR data also showed that Wnt activation upregulated the expression of CCND1, LEF1, PAX6A, PAX6B, KRT3, KRT12 and TA-p63, as compared to untreated control. However, HDAC inhibition has moderately induced the expression of PAX6A, PAX6B and p63 genes with no effect keratin gene expression. (**Fig 4.8.F**).

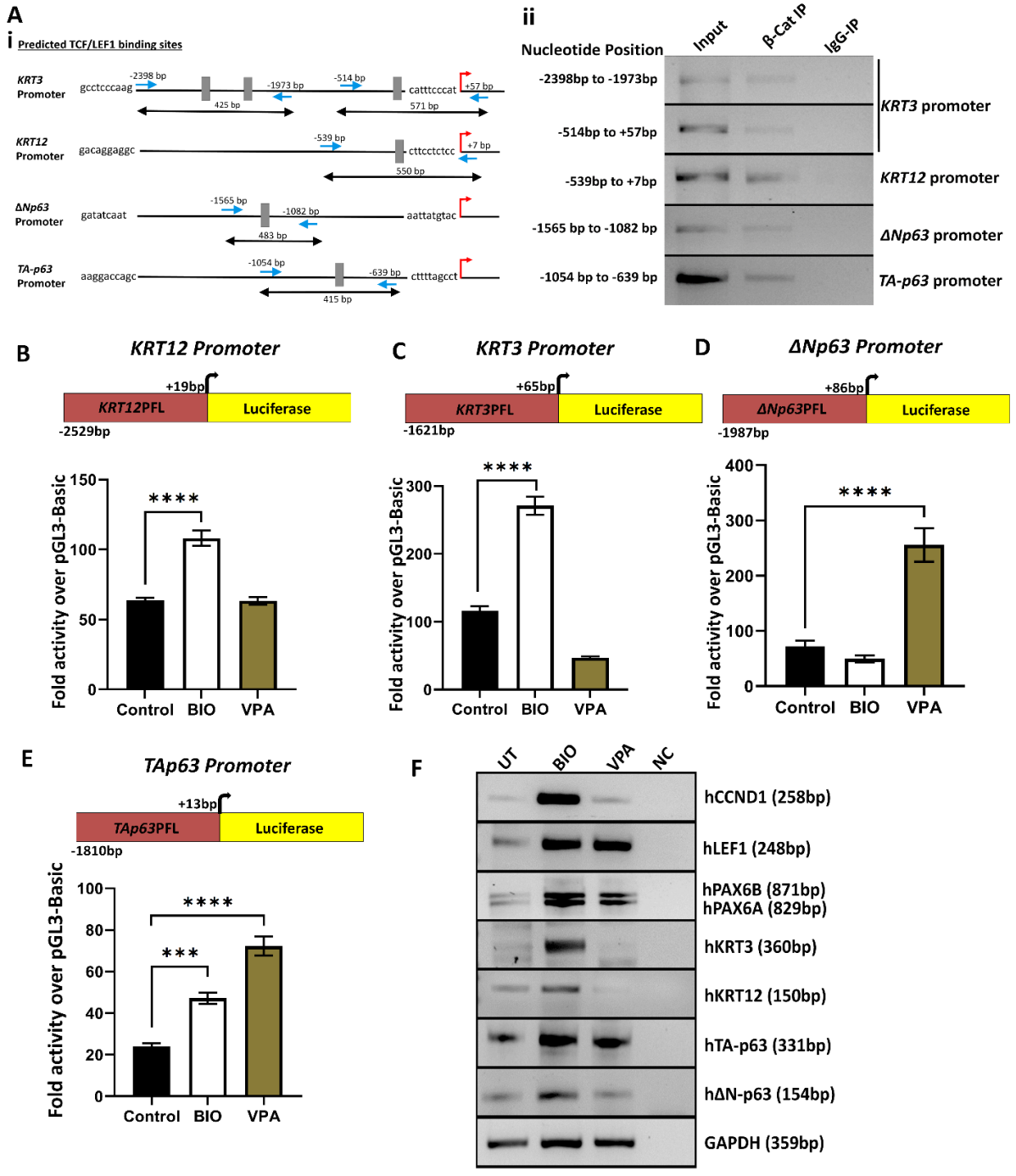

Figure 4.8: Effect of Wnt activation and HDAC inhibition on PAX6 target genes. A (i). *Cartoon representation of the predicted TCF/LEF1 binding sites on the KRT3, KRT12, ⊿Np63 and TAp63 promoters. Red arrow mark indicates the transcription start sites (TSS).* ***A (ii).*** *Agarose gel image of chromatin immunoprecipitation (ChIP) and KRT3, KRT12, ⊿Np63 and TAp63 promoter region specific PCR amplicons. Chromatin preparation of primary limbal epithelial cells was immunoprecipitated using an antibody against β-catenin and respective promoter regions were PCR amplified using the DNA templates purified from the chromatin inputs (positive controls), antibody-specific ChIP (test sample) and IgG ChIP complexes (negative controls).* ***B-E.*** *Histogram representation of the KRT3, KRT12, ⊿Np63 and TAp63*

*promoter activities in HCE cells treated with or without BIO and VPA. Normalized luciferase reporter values were plotted as fold activation over the pGL3-Basic vector activities. Error bars represents mean ± standard deviations. N=3. *P<0.05, **p<0.005 and ***p<0.0005.* ***F****. Agarose gel images of semi-quantitative RT-PCR products of CCND1, LEF1, PAX6B, PAX6A, KRT3, KRT12, TA-p63 and ⊿N-p63 genes, amplified using the cDNAs prepared from total RNAs of primary limbal epithelial cultures, treated with or without the BIO and VPA. The cDNAs were normalized using GAPDH expression as the internal loading control.*

Overall, the results suggest that Wnt activation induces KRT3, KRT12, and TAp63 gene expression in primary limbal cultures, thus promoting TA cell expansion and differentiation. Conversely, the HDAC inhibition enables TA cell expansion in an undifferentiated state.

4.1.7. Expression of cornea-specific markers in native limbus and corneal tissues

Native expression of cornea specific markers was checked in human corneal tissues by immunohistochemistry. Though PAX6 is expressed by all the cells of limbus and cornea, the levels were relatively less in the basal cells (**Fig 4.9.A.i**). Suprabasal and apical cells are known to be in a differentiated state and were found to express high levels of KRT3/12. The basal epithelial layers are comprised of either stem cells at the limbus or the undifferentiated progenitor and TA cells which are completely negative for KRT3/12 expression (**Fig 4.9.A.ii**). The stem and progenitor cells at the basal layers of the limbus and cornea are marked by the expression of p75NTR (NGF receptor) (**Fig 4.9.A.iii**).

Further, we checked for the co-expression of PAX6 along with the epithelial stem cell marker, p63α. We clearly observed that the basal stem/progenitor cells expressing high levels of p63α expressed low levels of PAX6 (**Fig 4.9.B.i**) and they were completely negative for the corneal differentiation marker KRT3/12 (**Fig 4.9.B.ii**). This suggests that the low levels of PAX6 seem to be critical for maintaining the stemness and proliferating status of the basal cells. The basal cells that were in close proximity to the niche cells at the limbus are believed to be the putative stem cells. Further, using an antibody against Melan A to mark the melanocytes (a sub-set of niche cells), we evaluated the expression of PAX6 and p63 in the proximal limbal stem cells. We observed that the niche associated putative stem cells expressed low levels of PAX6, while the suprabasal cells away from the niche, expressed high levels of PAX6 (**Fig 4.9.C.i**). Similarly, the cells in close proximity to the niche cells were found to express high levels of p63α (**Fig 4.9.C.ii**). Taken together, the results confirmed that the putative stem cells located at the basal layers of the limbal epithelium expressed low levels of PAX6 and high levels of p63α.

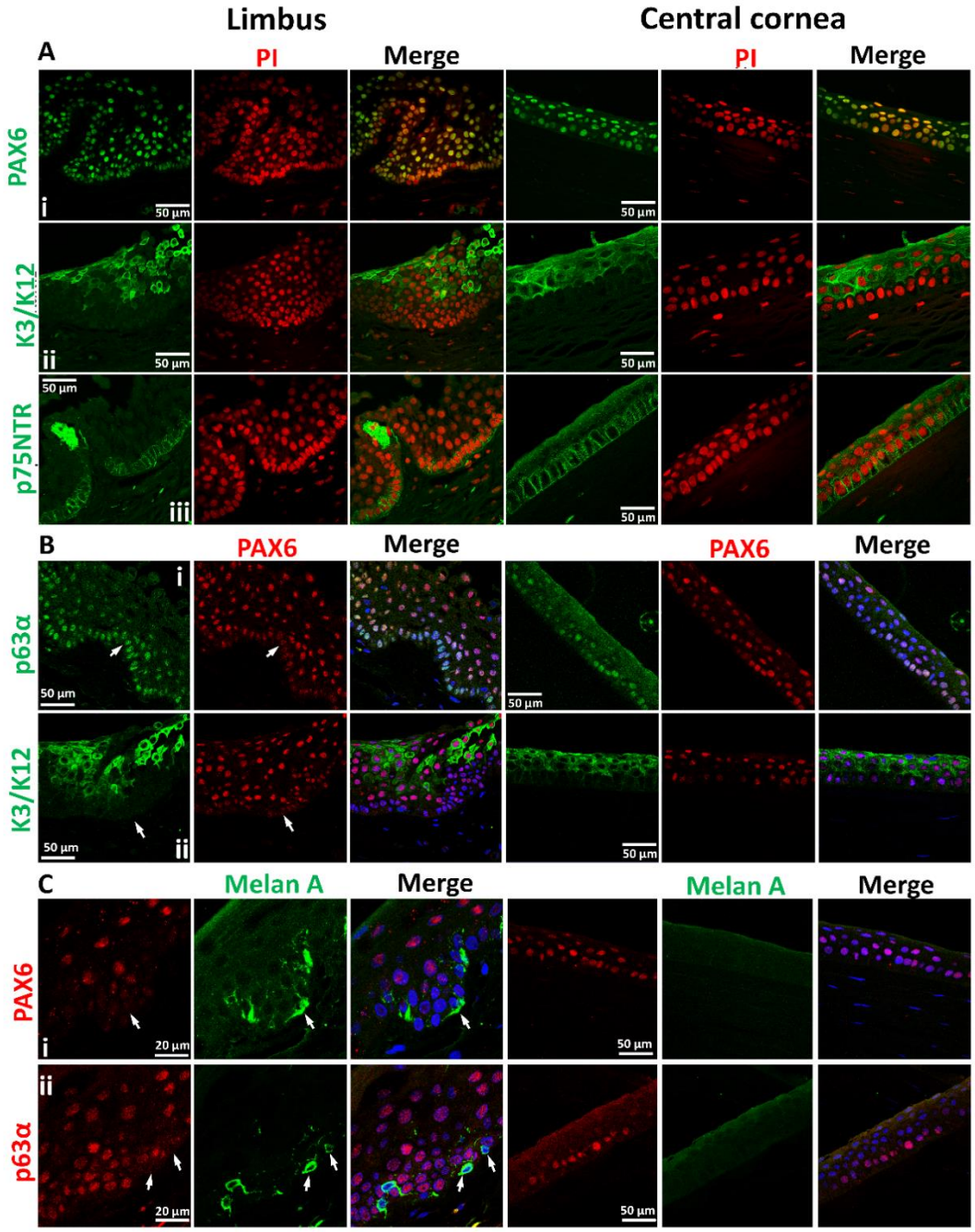

Figure 4.9: Expression of cornea specific markers in limbus and corneal tissues. *Confocal images of adult human limbal and corneal tissues showing the expression of various cornea-specific markers. A. Single marker images showing the expression of different corneal markers such as,* ***Ai.*** *PAX6,* ***Aii.*** *K3/K12 and* ***Aiii.*** *p75NTR (in green). The basal epithelial cells are PAX6^{Low}, K3/K12^{-} and p75NTR^{+}. All cell nuclei are marked by PI (in red). B. Double marker images showing the co-localization of PAX6 (in red) with* ***Bi.*** *P63a or* ***Bii.*** *K3/K12 (in green). The basal epithelial cells are PAX6^{Low} P63a^{High} and K3/K12^{-}, while the apical cells are PAX6^{High} P63a^{-} K3/K12^{+}. All cell nuclei are marked by DAPI (in blue). C. Double marker images showing the niche cells expressing Melan A (in green) and the proximal putative limbal stem cells expressing* ***Ci.*** *PAX6 or* ***Cii.*** *P63a (in red). The LSCs that are proximal to Melan A expressing*

niche cells are PAX6^{Low} P63a^{High}. All cell nuclei are marked by DAPI (in blue). Scale bar 50 μm or as specified.

4.1.8. Expression of canonical Wnt signaling markers in native limbus and corneal tissues

To check for the activity of Wnt canonical pathway in native corneal tissues, we checked for the expression of β-catenin in intact limbal tissues by IHC. We observed that the β-catenin was localized to the cell membranes in basal cells and in most of the supra basal and apical cells of the limbus and central cornea. However, a subset of supra basal cells at the limbus alone expressed β-catenin in the nucleus (**Fig 4.10.i**), which suggests that the Wnt signals are active only in a subset of proliferating TACs in the supra basal layers, while it is mostly inactive in the basal and apical layers. Further, we observed that DKK2, an antagonist of Wnt/beta-catenin signaling was distinctly expressed by the limbal basal cells. This indicates that Wnt signaling is actively blocked at the limbal niche and basal epithelial layers to ensure proper maintenance of stem cells in a quiescent state (**Fig 4.10.ii**).

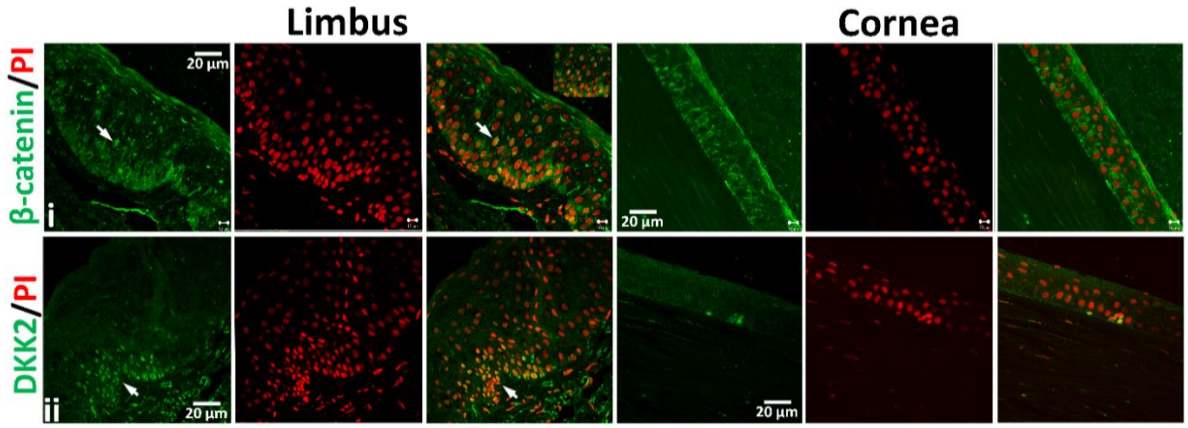

Figure 4.10: Expression of canonical Wnt signalling proteins in human limbus and cornea. i*. Confocal images showing the nuclear localization of β-catenin (in green) in a sub-set of cells at the supra basal layers of the limbal epithelium (marked by an arrow). However, the β-catenin was found to be membrane localized in rest of the cells.* ***ii****. Confocal images showing the expression of DKK2 (in green) in limbal basal epithelial cells (marked by an arrow). All cell nuclei are marked by PI (in red). Scale bar – 20 μm.*

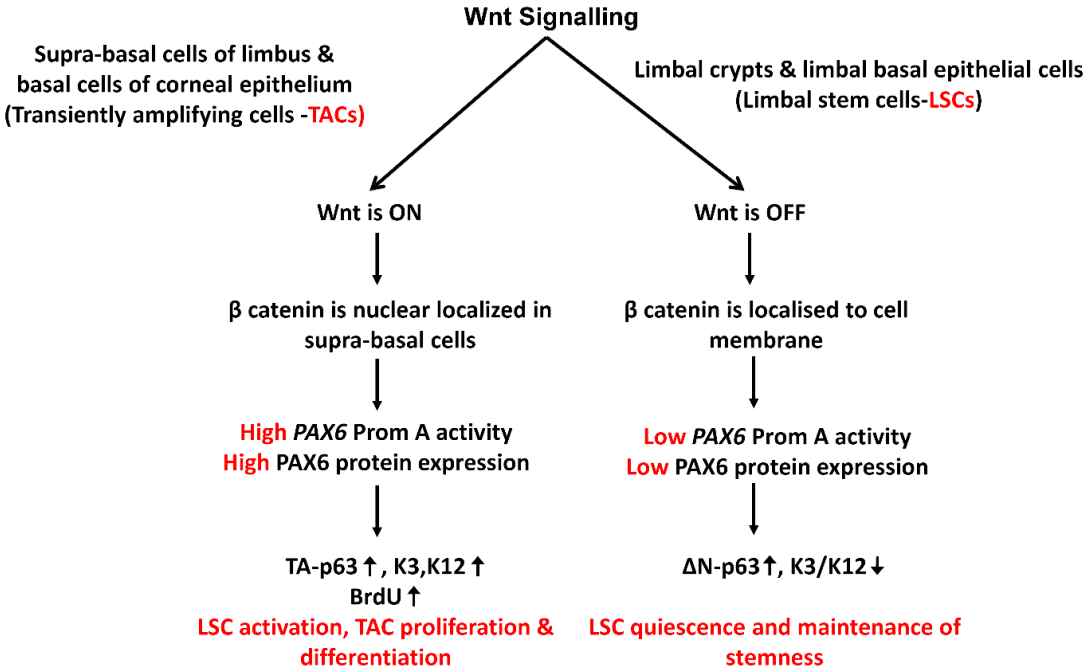

Figure 4.11: Schematic representation of Wnt signaling in corneal epithelial regulation.

Based on the observations from all the experiments discussed above, we conclude that the canonical Wnt signaling is active only in a subset of suprabasal TA cells at the limbus, which directly induces the *PAX6* pA promoter activity and increases the cellular PAX6 protein levels. Wnt signals also induce the expression of TAp63, KRT3 & KRT12 and together with *PAX6* promoter TA cell expansion and differentiation. An increase in PAX6 levels beyond a critical threshold possibly triggers cell cycle arrest and terminal differentiation of TA cells, to form the apical mature corneal epithelium. However, the expression of Wnt antagonists such as the DKK2 represses the canonical Wnt signals at the limbal niche. Reduced Wnt signals in turn results in reduced *PAX6* pA promoter activity and low PAX6 protein expression in basal epithelial cells. Optimal Wnt stimulation in turn triggers the proliferation and expansion of basal cells and help in normal wound healing and tissue homeostasis.

Taken together, we declare the following molecular code for different types of limbal epithelial cells. The putative stem cells and the activated progenitor cells at the limbal basal epithelial layers are Wnt^{Low}, $PAX6^{Low}$, $\Delta Np63^{High}$, $K3^{-}$, $K12^{-}$. The proliferating TACs at the suprabasal epithelial layers are Wnt^{High}, $PAX6^{Low}$, $TAp63^{High}$, $K3^{-}$, $K12^{-}$. The fully mature and differentiated post-mitotic cells at the apical epithelial layers are Wnt^{-}, $PAX6^{High}$, $TAp63^{Low/-}$, $K3^{+}$, $K12^{+}$.

4.2. Expression patterns of different PAX6 isoforms in native ocular tissues and their effects on target gene regulation

The human *PAX6* gene is of 30 kb size and comprises of 16 exons and 15 introns (**Fig 2.9**). Two transcripts have been already reported for this gene, of which the PAX6A variant (NM_001604.5) encodes for 13 exons, whereas the PAX6B variant (NM_001368894.2) has an additional exon 5a which encodes 14 amino acids in frame within the paired domain region (**Fig 2.8**). The translation initiation codon (ATG) is located within exon 4. Structurally, exon 4 to 7 encodes for the paired domain, exon 8 to 10 encodes for the homeodomain, and exons 10 to 13 encodes for the transactivation domain. PAX6A and PAX6B transcripts codes for 422 and 436 amino acids respectively (**Fig 2.8**). Two well characterized promoters differentially drives the expression of PAX6 in different tissues. The proximal pB promoter was reported to be brain-specific and the distal pA promoter (about 7 kb upstream of pB) was reported to be eye-specific. The promoter-specific exon 1 (1A & 1B) is unique and this further generates variants differing in their 5' UTRs, encoded from exon 1 to 4.

4.2.1. Cloning of PAX6A gene into mammalian expression and retroviral vectors

In order to study PAX6 gene targets and also to employ it as the "master regulator" to induce iPSC differentiation into ocular lineages, we attempted to clone the complete PAX6A cDNA, prepared using the total RNA isolated from a human limbal tissue. For the full length gene amplification by RT-PCR, primers were designed to span the entire coding region from exon 4 to exon 13 (**Fig 4.12.i**). The specific RT-PCR product was cloned into a mammalian expression vector (pEGFP-C1) as C' EGFP fusion and also into a retroviral vector (pLNCX2) as C' HA-tag fusion constructs. While confirming the positive clones by Sanger sequencing, a subset of clones was identified to carry a unique 3' end terminal sequence, apart from the reported full length PAX6A variant. This variant had extra 38 bases which arose from the intronic region of exon 12, and has not been reported so far (sequences submitted to NCBI) (**Fig 4.12.ii.iii**). As shown in **fig 4.12**, sequence chromatogram of PAX6A cDNA has exon 12 and exon 13 in continuation, while in the novel variant exon 12a was included between exon 12 and 13 due to alternative splicing of the 3' end of the transcript, which included the intronic sequence that was 38 bp immediately upstream of exon 13. Insertion of exon 12a results in the inclusion of a unique 11 amino acid sequence at the C' terminus followed by an in frame stop codon (**Fig 4.12.iv.v**). Inclusion of a stop codon just before the exon 13 coding region will result in the truncation of about 27 amino acids at the C' terminus. We therefore named this

novel variant as PAX6A-12a. The predicted isoform is expected to be defective in the transactivation domain functions and will encode a shorter protein of about 406 amino acids, instead of the 422 amino acids long wild type protein (PAX6A) (**Fig 4.12.vi**).

In order to reconfirm the novel PAX6A-12a transcript variant, semi-quantitative RT-PCR was performed using the cDNA from the ocular tissues and cell lines. The forward primer was designed in exon 11 and the reverse primer was designed in exon 12a (**Fig 4.12.viii**). Specific amplifications confirmed the native existence, with limbus and cornea expressing this novel variant predominantly, as compared to other ocular tissues and cell lines (**Fig 4.12.ix**).

4.2.2. Cloning of PAX6B gene into mammalian expression and retroviral vectors

In order to clone the other known variant, PAX6B (5a variant), we adopted a partial cloning strategy of replacing only the N' terminus of PAX6A construct with the PAX6B-specific PCR amplicons. The primers were designed to span the PAX6 exon 5 to exon 7 (**Fig 4.13.i**). The RT-PCR products of the N' terminus region specific primer sets gave rise to multiple fast migrating bands just below the two prominent doublets corresponding to PAX6A (327 bp) and PAX6B (367 bp) variants in different ocular tissues and also cell lines (**Fig 4.13.ii**). To know the identity of these unexpected bands and also to confirm the sequence of the expected bands, the entire PCR product was purified and cloned in the pMOS-Blue vector at the EcoRV restriction site. Sequencing of the top two bands of the expected size confirmed the presence of the reported variants PAX6A and PAX6B (**Fig 4.13.iii.iv**). The other three bands were found to be the novel alternatively spliced transcript variants generated by differential selection of alternate splice sites around the exon 5-exon 6 junctions, during the pre-mRNA processing (**Fig 4.14**).

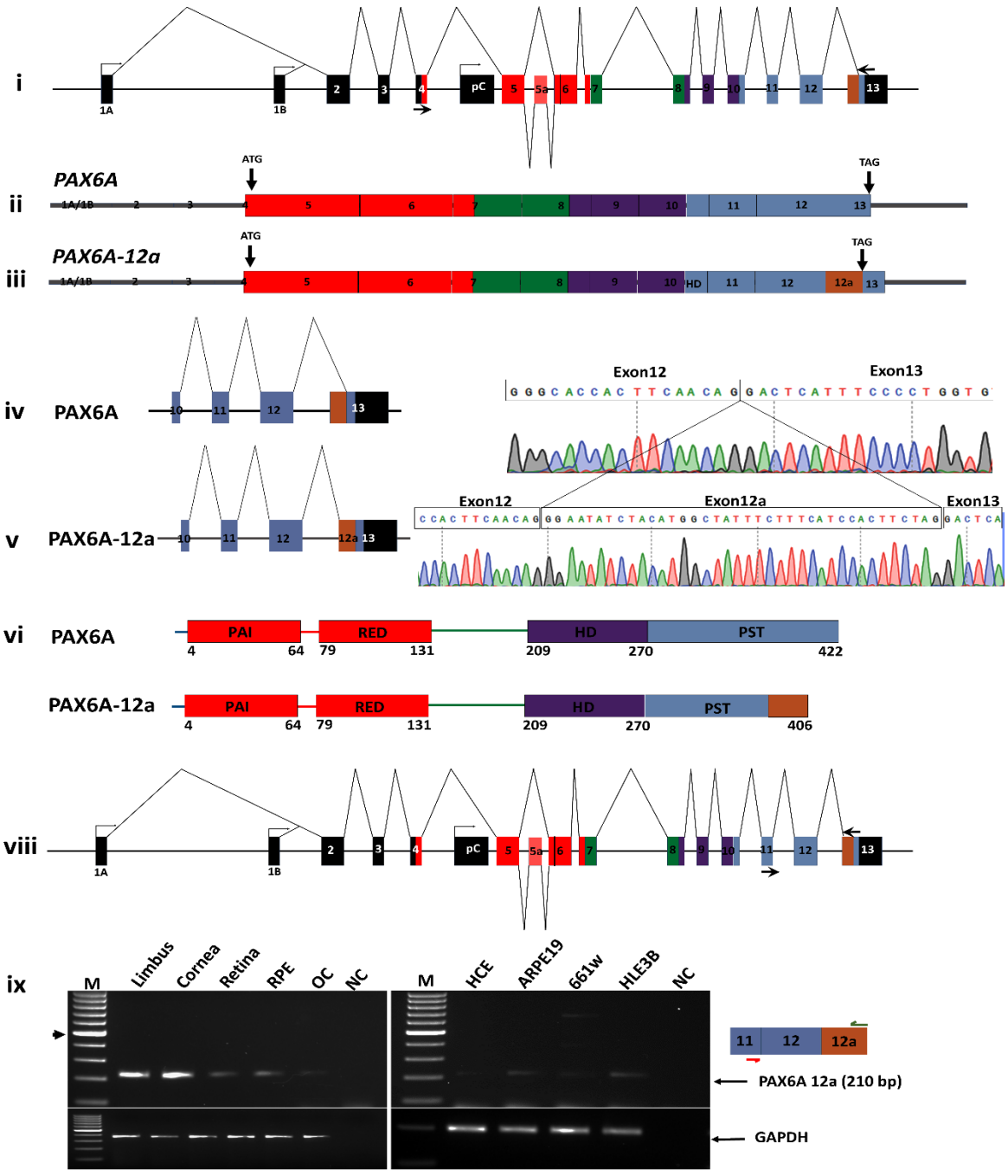

Figure 4.12: Novel alternative splicing at the C' terminus of PAX6 gene. *(**i**) Cartoon representation of the human PAX6 gene. Rectangular boxes indicate the exons (the dimensions of boxes are drawn proportionate to the size of each exon). Arrow mark indicates the approximate location of primers spanning the coding regions from exon 4 to exon 13. (**ii**) PAX6A transcript with ATG representing the translation start codon and TAG representing the stop codon. (**iii**) Novel c-terminus alternatively spliced PAX6A transcript which includes the 12a region of intron 12. (**iv**) Sequence chromatogram of PAX6A transcript. (**v**) Sequence chromatogram of PAX6A-12a variant where the exon 12 sequence is followed by a 38 bp sequence from the C' terminal end of intron 12 (exon 12a), followed by the exon 13 sequence. (**vi**) PAX6A variant encodes for a 422 aa long protein that comprises of three important domains viz; paired*

*domain, homeodomain and transactivation domain. (**vi**) PAX6A-12a variant is predicted to encode a protein of around 406 aa with a c-terminus truncation in the transactivation domain. (**viii**) Cartoon representation of the PAX6 gene indicating the location of variant specific primers spanning the exon 12 and 12a. (**ix**) Agarose gel image of PAX6A-12a variant specific RT-PCR amplicons in human limbus, cornea, retina, RPE, hiPSC-derived optic cups (OC); and also in ocular cell lines such as HCE, ARPE19, 661w and HLE-3B. Marker indicates 100 bp DNA ladder.*

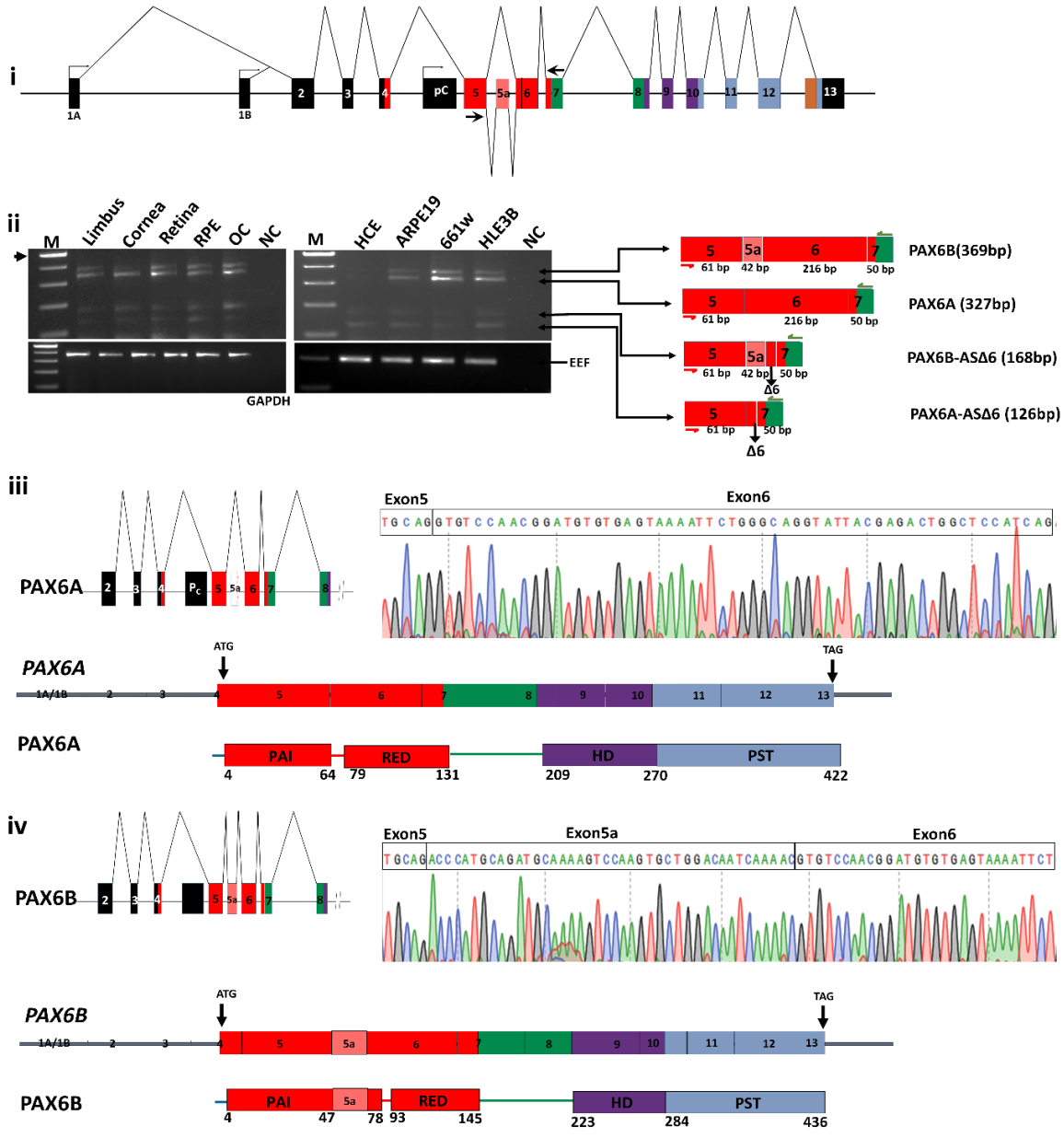

Figure 4.13: RT-PCR analysis of the N-terminus of human PAX6 gene. *(**i**) Cartoon representation of the human PAX6 gene. Arrows mark the location of primers spanning from exon 5 to exon 7. (**ii**) Agarose gel image of the semi quantitative RT-PCR products of the N-terminus of PAX6 in different ocular tissues and cell lines. On the right is the pictorial representation of all possible alternately spliced transcripts. Arrows in red and green marks the forward and reverse primer binding sites respectively and the*

*corresponding amplicon sizes for each of the variants are given in brackets. (**iii & iv**) Sequence chromatograms of the expected, top two bands seen in the agarose gel that corresponds to the reported variants PAX6A and PAX6B. PAX6A transcript encodes for 422 aa long protein. In PAX6B, there is an inclusion exon 5a in between exon 5 and 6 due to alternative splicing, thus encoding a 436 aa long protein. Note the presence of multiple bands, below the expected top two doublets which corresponds to the novel splice variants. Marker indicates 100 bp DNA ladder.*

Two of the novel variants are homologous to PAX6A (Wt) and PAX6B (5a) sequence respectively. However, the exon 6 of these two variants was alternatively spliced using a cryptic splice donor site after +15 position within exon 6 and was spliced on to the putative splice acceptor site of exon 7 and results in the internal deletion of 201 nucleotides or 67 amino acids (**Fig 4.14.i.ii**). However, this internal deletion in exon 6 does not disturb the coding frame, allowing in-frame translation of exon 7 to 13. These transcripts were predicted to code for a protein of 355 (39 kDa) and 369 amino acids (41 kDa) respectively (**Fig 4.14.i.ii**). We therefore named these two novel variants as PAX6A-ASΔ6 and PAX6B-ASΔ6 respectively. The third novel transcript was found to be homologous to PAX6A sequence, but with a complete skipping of exon 6, by the direct splicing of exon 5 on to the exon 7. This results in the internal in frame deletion of 216 nucleotides or 72 amino acids and allows in-frame translation of exon 7 to 13. This transcript was predicted to code for a protein of 350 amino acids (~38 kDa) (**Fig 4.14.iii**). We therefore named this third novel variant as PAX6A-Δ6.

If all three novel transcripts undergo translation, the resulting protein isoforms with or without 5a insertions and exon 6 internal deletions would result in protein isoforms with both PAI and RED domain disruptions (PAX6A-Δ6, PAX6A-ASΔ6, PAX6B-ASΔ6), as opposed to that of the known PAX6B isoform, with only PAI domain disruption.

Thus, altogether we have found four novel human PAX6 variants (PAX6A-Δ6, PAX6A-ASΔ6, PAX6B-ASΔ6 and PAX6A-12a) with either PAI-RED domain or PST domain disruptions leading to possible dominant negative effects on the wild type PAX6A protein functions. Sequences of all these variants have been submitted to the NCBI database.

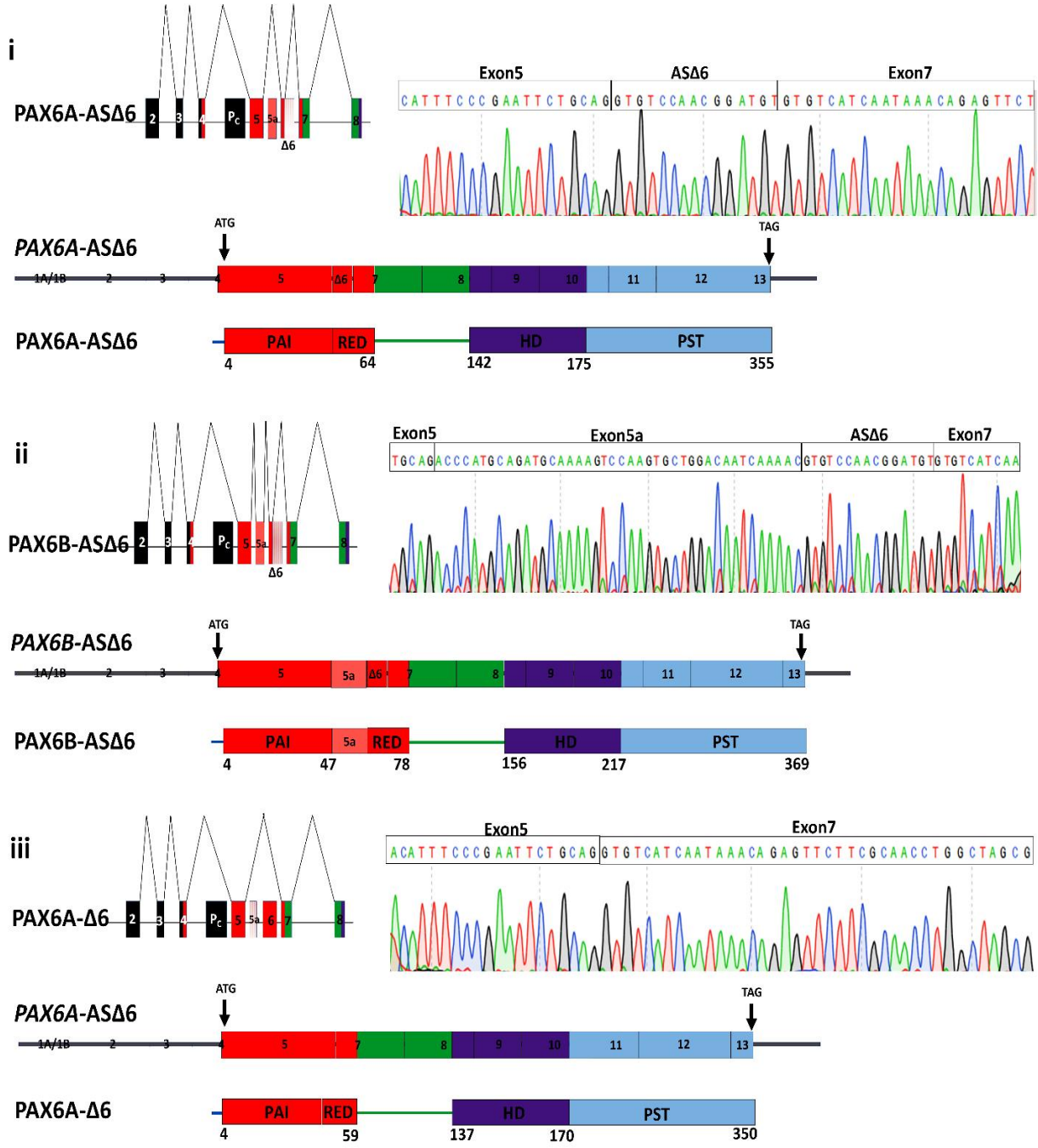

Figure 4.14: Novel alternate splicing at the N' terminus of PAX6 gene. *Sequence analysis of the smaller amplicons detected in* ***Fig 4.13 ii****. On the left is the cartoon representation of the alternate splicing pattern identified in respective variants. On the right is the sequence chromatogram spanning the splicing junction. Three novel splice variants (PAX6A-AS⊿6, PAX6B-AS⊿6 and PAX6A-⊿6) were generated via alternate splicing near the exon 6 splice acceptor locus and were predicted to encode a protein of about 355, 369 and 350 aa long (****i, ii, iii****).*

4.2.3. Validation of newly identified alternatively spliced transcripts by semi quantitative nested RT-PCR

To validate the existence of full length form of alternatively spliced PAX6 transcripts, semi-quantitative RT-PCR was performed using cDNA of different human ocular tissues. To amplify the full-length PAX6 transcript, end primers were designed to span exon 4 to exon 13 (**Fig 4.15.A**). RT-PCR using this primer set resulted in only two visible bands, possibly corresponding to PAX6A and PAX6B with an anticipated band size of 1289 and 1331 bp respectively (**Fig 4.15.B**). To validate the presence of other novel PAX6 transcripts, a second round of PCR was carried out using region-specific internal primer sets, as described earlier.

The PCR product from the first round of amplification using the end primers was diluted 1:10 and used as a template for the next round of PCRs. The primer set spanning the exon 5 to exon 7 region was used to amplify all possible N' terminus PAX6 transcript variants, and the primer set spanning exon 11 to exon 12a region was used to amplify the variant PAX6A-12a. Agarose gel electrophoresis of the semi-nested PCR products revealed the presence of variant-specific bands in all the ocular tissues. The amplicons corresponding to the known transcripts such as, PAX6A (327 bp) and PAX6B (367 bp) and also the novel transcripts PAX6A-ASΔ6 (126 bp), PAX6B-ASΔ6 (168 bp) and PAX6A-12a (210 bp) were detected in all ocular tissues tested in more than 3 biological replicate experiments (**Fig 4.15.C.D**). However, we couldn't clearly distinguish and identify the PAX6A-Δ6 variant (111 bp) on the agarose gel, possibly due to only 15 bp difference between this variant and the PAX6A-ASΔ6 (126 bp) variant. The PCR products were cut eluted from the agarose gel, cloned in the PCR product cloning vector, pMOS-Blue and the positive clones with inserts of different sizes were identified and sequenced to confirm the presence of all four novel variants, as explained earlier.

4.2.4. Differential expression of pA, pB and pC promoter derived PAX6 transcripts in ocular tissues

In humans, PAX6 transcription is regulated by three distinct alternative promoters viz; the proximal pB, the distal pA, and the internal pC promoter, as explained earlier. The pA and pB promoters have unique transcription start sites resulting in the unique first exon 1A and 1B respectively. Transcripts derived from these two promoters differ only in their exon 1 and share all the remaining common exons 2-13. However, the pC promoter lies in the intron 4 and its unique transcription start site generates the exon 1C. The pC derived transcripts share all the remaining common exons 5-13 (**Fig 4.16.A**). These alternate promoters are regulated

in a tissue-specific manner and produce promoter-specific and differentially spliced mRNAs of reported variants namely, PAX6A, PAX6B and PAX6D.

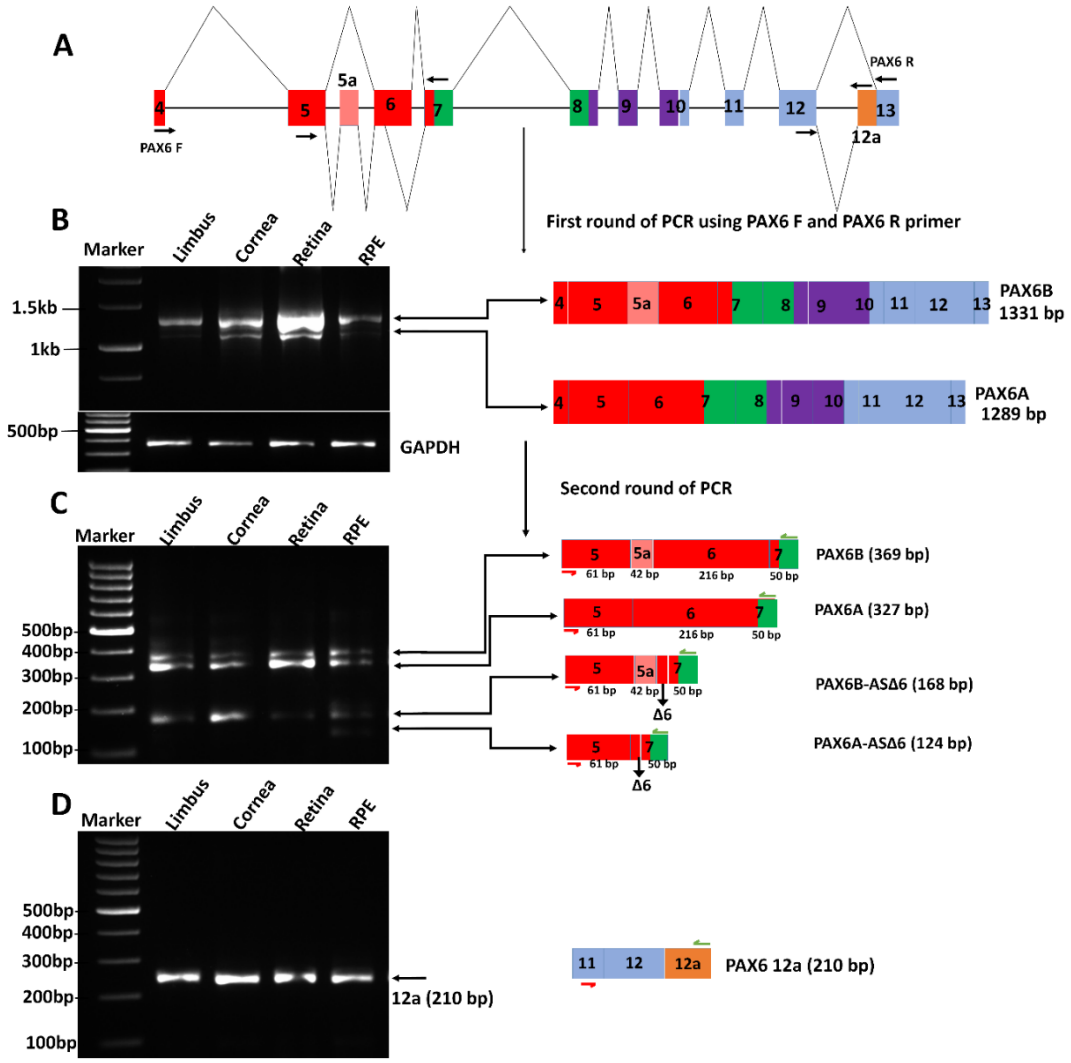

Figure 4.15. Agarose gel image of two-step RT-PCR amplifications of PAX6 transcripts in different ocular tissues and cell lines. *(**A**) Cartoon representation of different alternatively spliced transcripts of PAX6 gene. (**B**) First step, full length amplification of the PAX6 transcripts by semi quantitative RT-PCR using the forward and reverse primers spanning from exon 5 to exon 13. Amplicons of sizes 1331 bp and 1289 bp in all the lanes correspond to the two known variants, PAX6B and PAX6A respectively. Marker indicates 1 kb DNA ladder. (**C**) Second step nested PCR using internal primers at the N' terminus, which spans from exon 5 to exon 7. Amplicons of sizes 367 bp and 327 bp corresponds to the two known variants, PAX6B and PAX6A respectively. Amplicons of sizes 168 bp and 124 bp corresponds to the newly identified alternately spliced variants, PAX6B-AS⊿6 and PAX6A-AS⊿6 respectively in all the tissues examined. (**D**) Second step nested PCR using internal primers at the C' terminus, which spans from exon 11 to exon 12a. Amplicon of 210 bp size corresponds to the alternately spliced variant, PAX612a in all the tissues examined. On the right is the cartoon representation of the respective splice variant specific PCR products. Arrows in red and green marks the forward and reverse primer binding sites respectively and the*

corresponding amplicon sizes for each of the variants are given in brackets. Marker indicates 100 bp DNA ladder.

To determine the tissue-specific expression of pA, pB, and pC promoter-derived transcripts and also to check the promoter(s) associated with the expression of novel variants, semi-quantitative RT-PCR was performed using mRNA isolated from different ocular tissues.

Firstly, to check the pA-derived transcripts, a forward primer was designed within the unique exon 1A, downstream of the TSS. Similarly, for the amplification of the pB and pC derived transcripts, the forward primer was designed within the unique exon 1B and exon 1C, downstream of their respective TSS. A common reverse primer was designed within the exon 7 coding region (**Fig 4.16.A**). Amplified RT-PCR products were electrophoresed on an agarose gel where multiple pA initiated transcripts namely PAX6B (871 bp), PAX6A (829 bp), PAX6B-ASΔ6 (670 bp) and PAX6A-ASΔ6 (628 bp) were identified in all the ocular tissues tested (**Fig 4.16.B**). Among these, the known PAX6A and PAX6B transcripts are highly expressed and seem to be the major variants. The sequence chromatogram of pA derived transcripts confirmed that the exon 1A is spliced on to exon 2, as expected (**Fig 4.16.B**). Thus, we confirm that the alternate splicing of pA-derived pre-mRNA, results in the generation of all the PAI-RED domain disrupted, novel alternately spliced variants, apart from the two known PAX6A (wt) and PAX6B (5a) variants.

As shown in the figure **4.16.C**, the pB promoter was found to be weekly active in most adult ocular tissues. However, the pB derived transcripts such as PAX6B (790 bp), PAX6A (748 bp), PAX6B-ASΔ6 (589 bp), and PAX6A-ASΔ6 (547 bp) respectively are detectable in the stem cell containing limbal tissues and in iPSC derived neuro-retinal cups (**Fig 4.16.C**). This clearly confirms that pA is the major promoter that drives the expression of all PAX6 variants in most adult ocular cell types. However, the brain-specific pB promoter seem to be weekly active and drives the expression of all PAX6 variants at low levels, specifically in developing ocular tissues such as the neuro-retina and in the stem cell and progenitor cell containing limbal epithelium. The sequence chromatogram of pB derived transcripts confirmed that the exon 1B is spliced on to exon 2, as expected (**Fig 4.16.C**).

Similarly, the pC promoter was found to be weakly active and the transcripts derived from this minor promoter were detected only in retinal cell types. Also, among all the variants, only PAX6B (462 bp) and PAX6A (420 bp) expression was confirmed in the retina (**Fig 4.16.D**).

The sequence chromatogram of pC derived transcripts confirmed that the exon 1C is spliced on to exon 5, as expected (**Fig 4.16.D**).

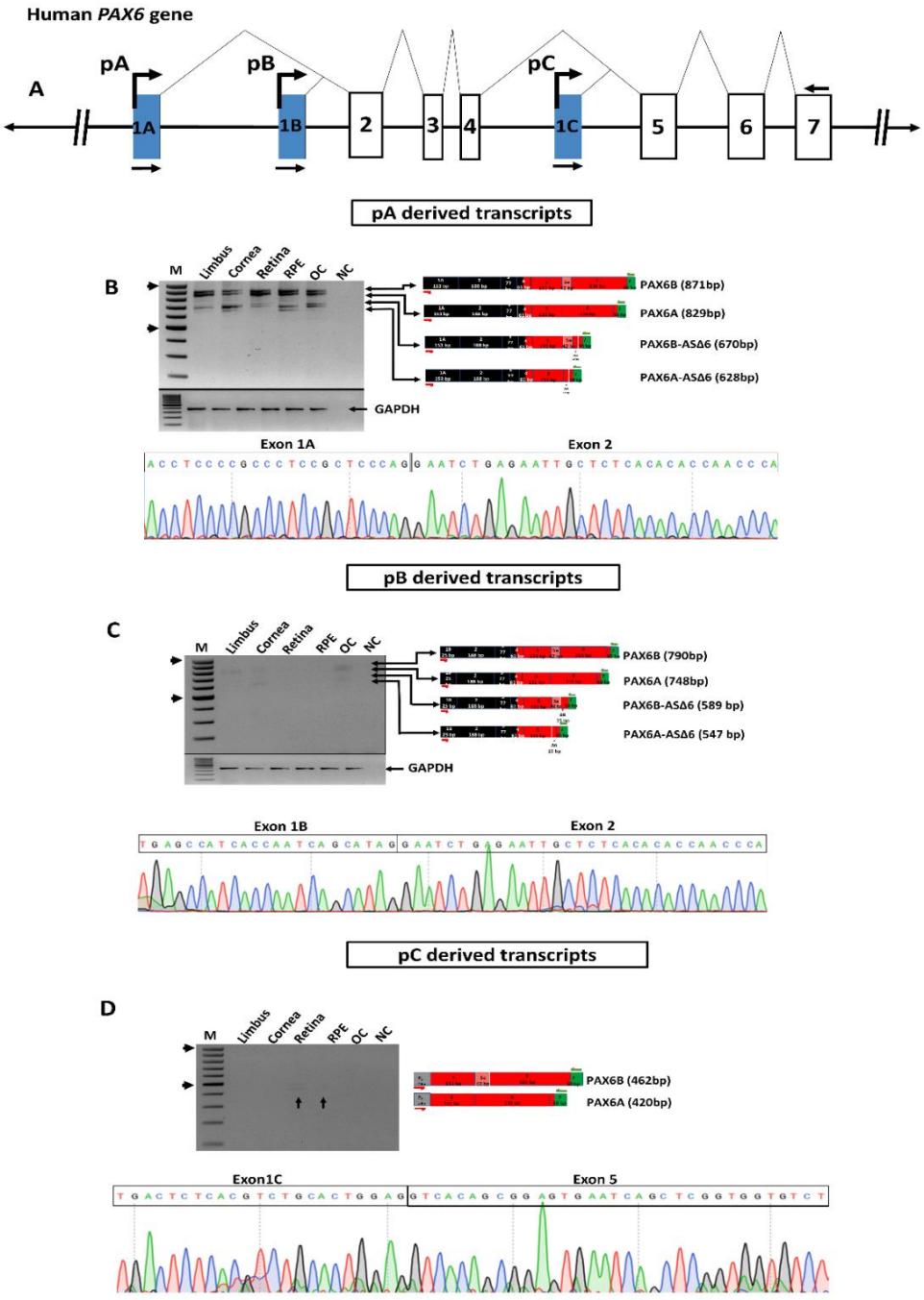

Figure 4.16: Promoter-specific expression of PAX6 variants. *(**A**) Cartoon representation of the PAX6 gene along with the promoter positions. pA, pB and pC marks the distal, proximal and internal promoters respectively (blue boxes). Exons and introns are indicated with rectangular boxes and horizontal lines respectively. Positions of primers used for RT-PCR are indicated with arrows. (**B, C, D**) Agarose gel image of semi-quantitative RT-PCR amplicons using pA, pB and pC specific primer pairs spanning from the unique exon 1 to the common exon 7 region in different ocular tissues. On the right is the cartoon representation*

*of the variant specific amplicons with arrows indicating the position of specific primer sets. Sequence chromatogram of pA derived transcript where the exon 1a is immediately followed by exon 2 (**B**). Sequence chromatogram of pB derived transcript where the exon 1b is immediately followed by exon 2 (**C**). Sequence chromatogram of pC derived transcript where the exon 1c is immediately followed by exon 5 (**D**). All cDNA samples were normalized using GAPDH as the equal loading control.*

4.2.5. Absolute quantification of PAX6 variants expressed in different ocular tissues

For absolute quantifications, variant-specific primer sets were designed to exclusively amplify only the specific transcripts (refer to Annexures.V for primer details). We further prepared standard curves of copy number vs CT values for all variants, using 10 fold serial dilutions of cloned, variant-specific plasmid constructs as templates in qPCRs. Total RNA isolated from different ocular tissues (50 ng each) was converted into cDNA by reverse transcription reactions, Nanodrop quantified and used in qRT-PCR reactions, using variant-specific primer sets. The CT values of variant-specific qRT-PCR reactions were then compared with the standard curves established for each of the variants, to work out their copy numbers in native tissue derived mRNA samples. The absolute copy number was worked out by normalizing for dilution factors, if any. The results confirmed that the PAX6A is the predominant and highly expressed transcript in all ocular tissues tested. The copy number was found to be higher in the limbus ($1.6X10^4$ copies per ng of total mRNA), followed by the cornea, retina and RPE cells (**Fig 4.17.A**). The PAX6B-ASΔ6 was expressed at significantly higher levels, exclusively in the corneal epithelium, while the copy numbers were minimal in other ocular tissues tested. The copy number of PAX6B-ASΔ6 ($6.4X10^4$ copies per ng of total mRNA) was higher than that of the PAX6A transcript ($8.5X10^3$ copies per ng of total mRNA) in the corneal epithelium (**Fig 4.17.B**). This suggests a crucial role for PAX6B-ASΔ6 variant in corneal epithelium. However, the PAX6A-12a variant is expressed at low copy numbers in all ocular tissues, with relatively higher expression in the limbal and corneal epithelium ($1.4X10^3$ copies per ng of total mRNA) (**Fig 4.17.C**).

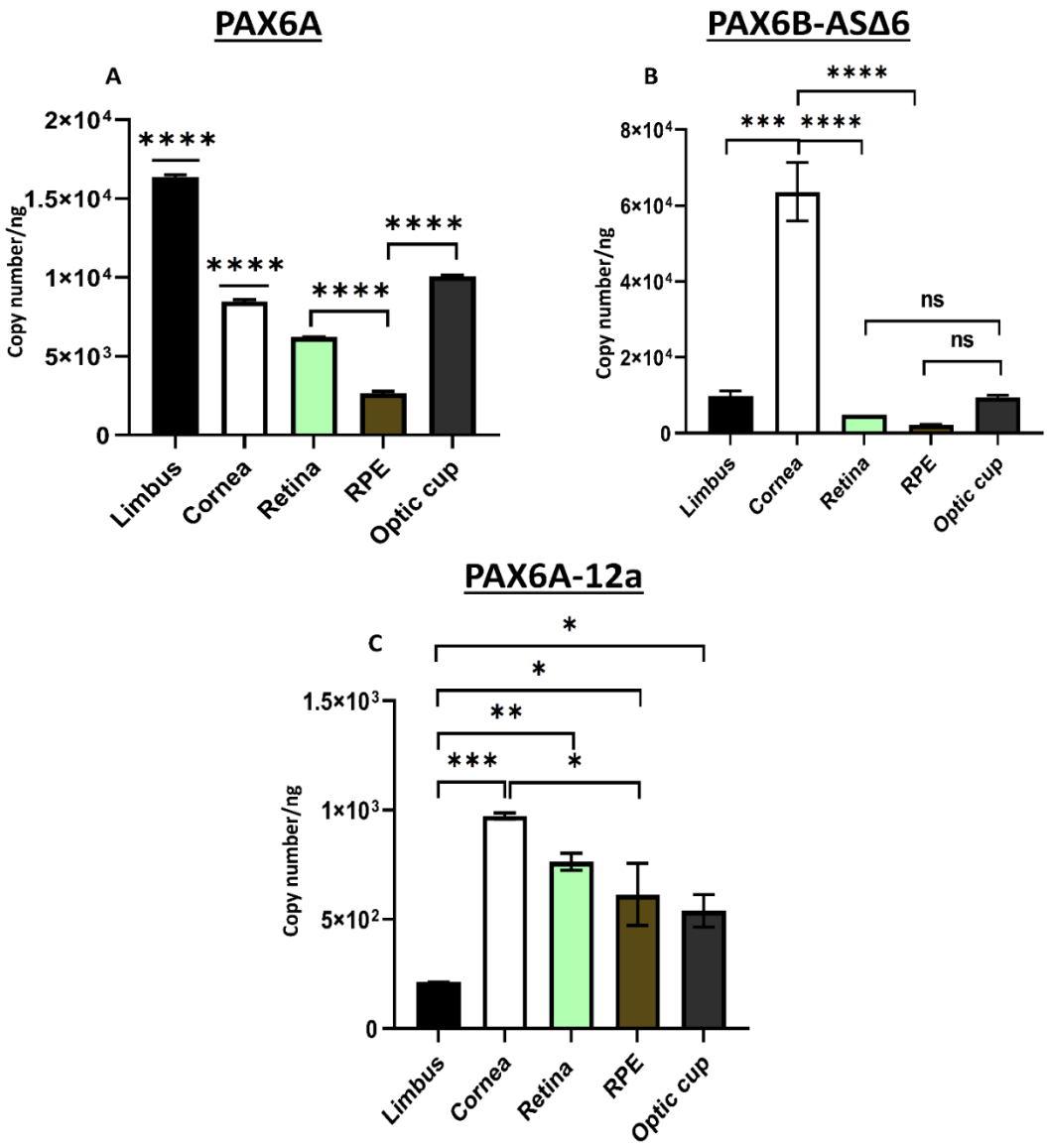

Figure 4.17: Absolute quantification of PAX6 variants in different ocular tissues. *Quantitative RT-PCR and absolute copies of PAX6A (**A**), PAX6B-AS⊥6 (**B**) and PAX6A-12a (**C**) transcripts in different ocular tissues was worked out from the respective Ct values, using the standard curve prepared with Ct values of tenfold serial dilutions of corresponding plasmid DNA templates. The graph indicates the number of copies/ng of total RNA isolated from respective ocular tissues. The data is represented as mean ± SD, N=3. *P<0.05, **p<0.005 and ***p<0.0005.*

4.2.6. Relative quantification of PAX6 variants in different ocular tissues

To check the relative expression levels of alternately spliced PAX6 variants when compared to the wild type transcript (PAX6A), we performed quantitative real time PCR using variant specific primers. The wild type PAX6A variant was used as the reference control to quantify the relative mRNA levels of other variant transcripts. The results confirmed that the PAX6A

forms the major variant and other variants are expressed at relatively lower levels in most ocular cells tested. Interestingly, the expression level of PAX6B variant was found to be significantly higher than PAX6A only in the corneal epithelium (2.8 folds) and iPSC-derived RPE cells (1.6 folds) (**Fig 4.18.A**). Similarly, the expression level of the novel splice variant, PAX6B-ASΔ6 was found to be significantly higher than PAX6A only in the corneal epithelium (1.6 folds) (**Fig 4.18.B**). The expression level of the minor variant, PAX6A-12a variant was found to be significantly lower than the PAX6A levels in all ocular tissues tested. Interestingly, the relative level of PAX6A-12a was significantly higher in the corneal epithelium when compared to that of the limbal epithelium (4.5 folds) (**Fig 4.18.C**). Taken together, the results suggest some critical role(s) for PAX6B-ASΔ6 and PAX6A-12a variants in the corneal epithelium.

4.2.7. Splice donor-acceptor sites of pA-derived PAX6 transcripts

The genomic sequence of the PAX6 gene was further analyzed to check the presence of donor GT and acceptor AG dinucleotide in all the alternatively spliced exon-intronic junctions. We found that all the exons of the reported and novel variants were flanked by splice donor GT and splice acceptor AG dinucleotides, thus confirming alternate splicing consensus (**Fig 4.19**). The exon AS-Δ6 of PAX6B-ASΔ6 and PAX6A-ASΔ6 transcripts; and the exon 12a of PAX6A-12a transcript codes for in-frame sequences. Thus, successful translation of these transcripts would result in protein isoforms of variable sizes namely, PAX6A (422 aa), PAX6B (436 aa), PAX6A-ASΔ6 (355 aa), PAX6B-ASΔ6 (369 aa), PAX6A-Δ6 (350 aa) and PAX6A-12a (406 aa), with the translation start codon (ATG) in the common exon 4.

4.2.8. Comparative analysis of the reported and novel PAX6 variants

We further compared the predicted amino acid sequences of the novel PAX6 splice variants with that of the wild type PAX6A variant using the web-based tool ClustalW. The multiple sequence alignment of different PAX6 variant encoded proteins (**Fig 4.20**) revealed that the PAI-RED domain is intact only in the isoforms PAX6A and PAX6A-12a, whereas the PAX6B isoform has 15 aa insertion at the C terminus of the PAI domain, possibly disrupting only the PAI domain functions. However, the PAX6A-ASΔ6, PAX6B-ASΔ6 and PAX6A-Δ6 isoforms showed disruptions at C' terminus of PAI domain and also the N' terminus of RED domain, thus resulting in the total disruption of both the PAI and RED domain functions. The homeodomain was found to be intact in all the reported and novel transcript variants. The

transactivation domain was intact in all the variants except PAX6A-12a, with a truncated C' terminus due to the premature stop codon at the end of exon 12a.

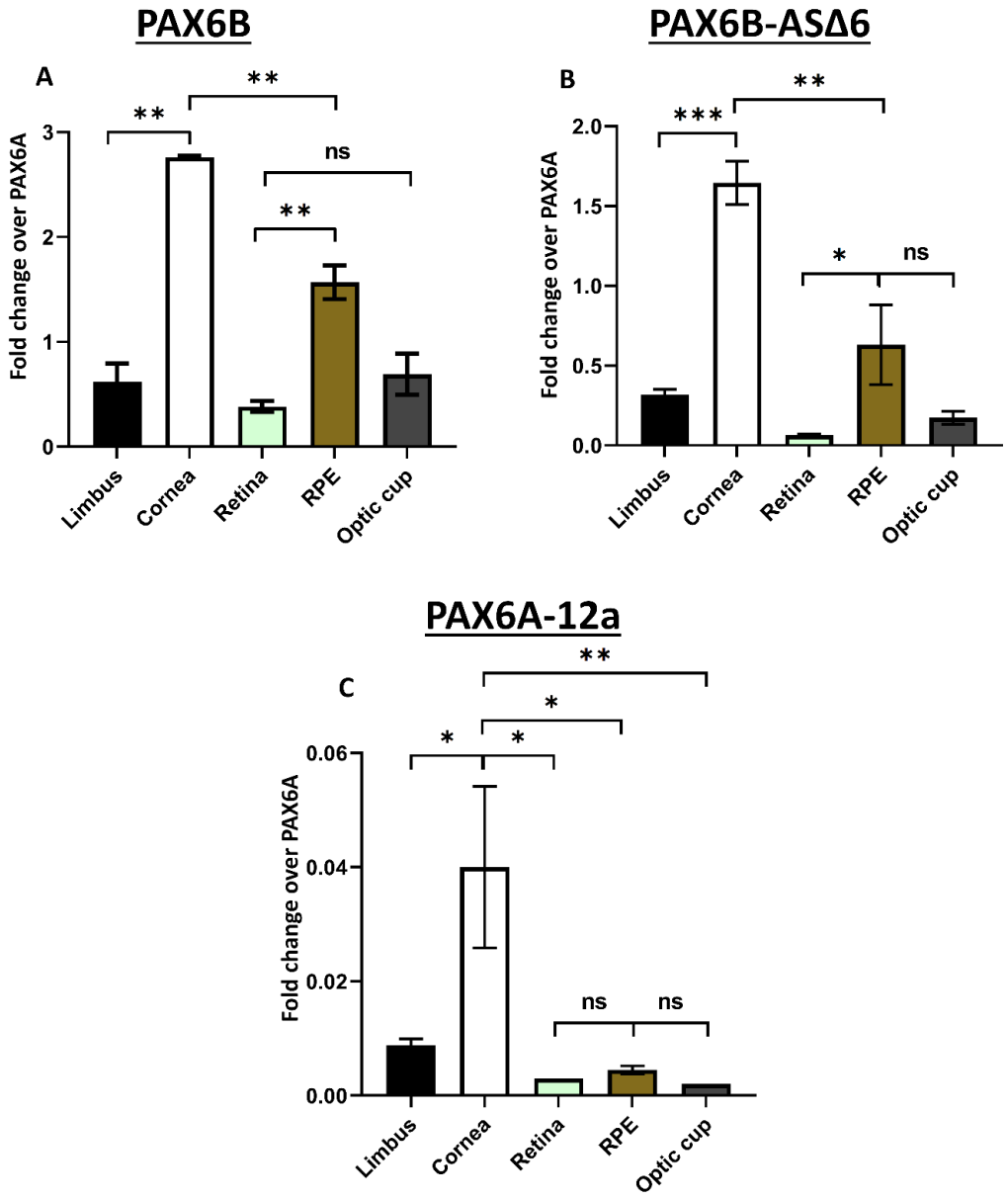

Figure 4.18: Relative abundance of PAX6 splice variants in different ocular tissues. *The relative fold change in the expression levels of different splice variants as compared to the wild type PAX6A variant is plotted for PAX6B (**A**), PAX6B-AS⊿6 (**B**) and PAX6A-12a (**C**). The data is represented as mean ± SD, N=3. *P<0.05, **p<0.005 and ***p<0.0005.*

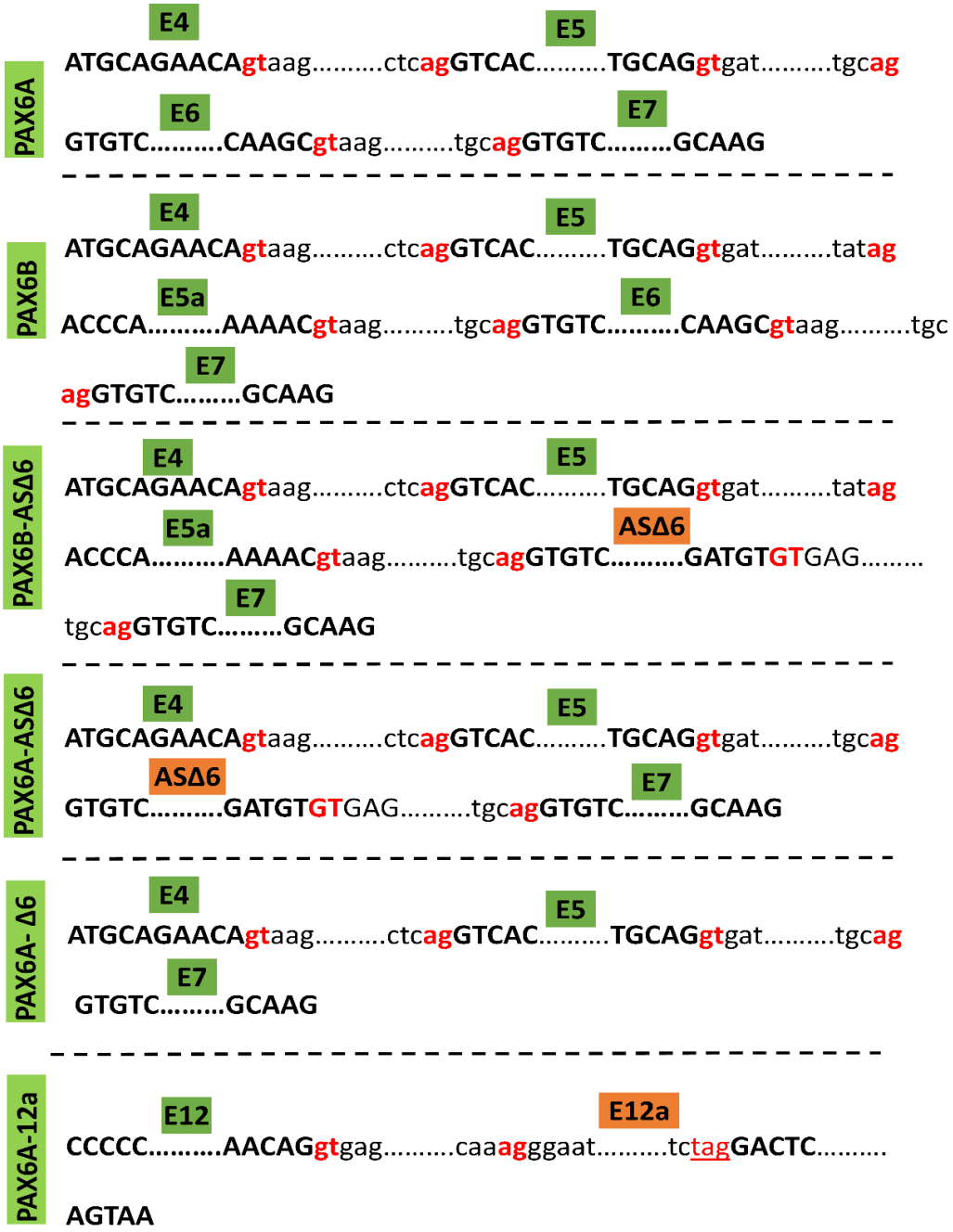

Figure 4.19. Splice donor and acceptor sites at different exons of PAX6 variants. *The donor GT and the acceptor AG splice site dinucleotide bases are shown in red and are italicized. The identity of PAX6 exons are mentioned above their sequences, in green, while the alternatively spliced newly identified exons are indicated in red color. Exons and introns are shown in capital and lower case letters respectively. The identities of transcripts are indicated adjacent to the sequence, in green colour.*

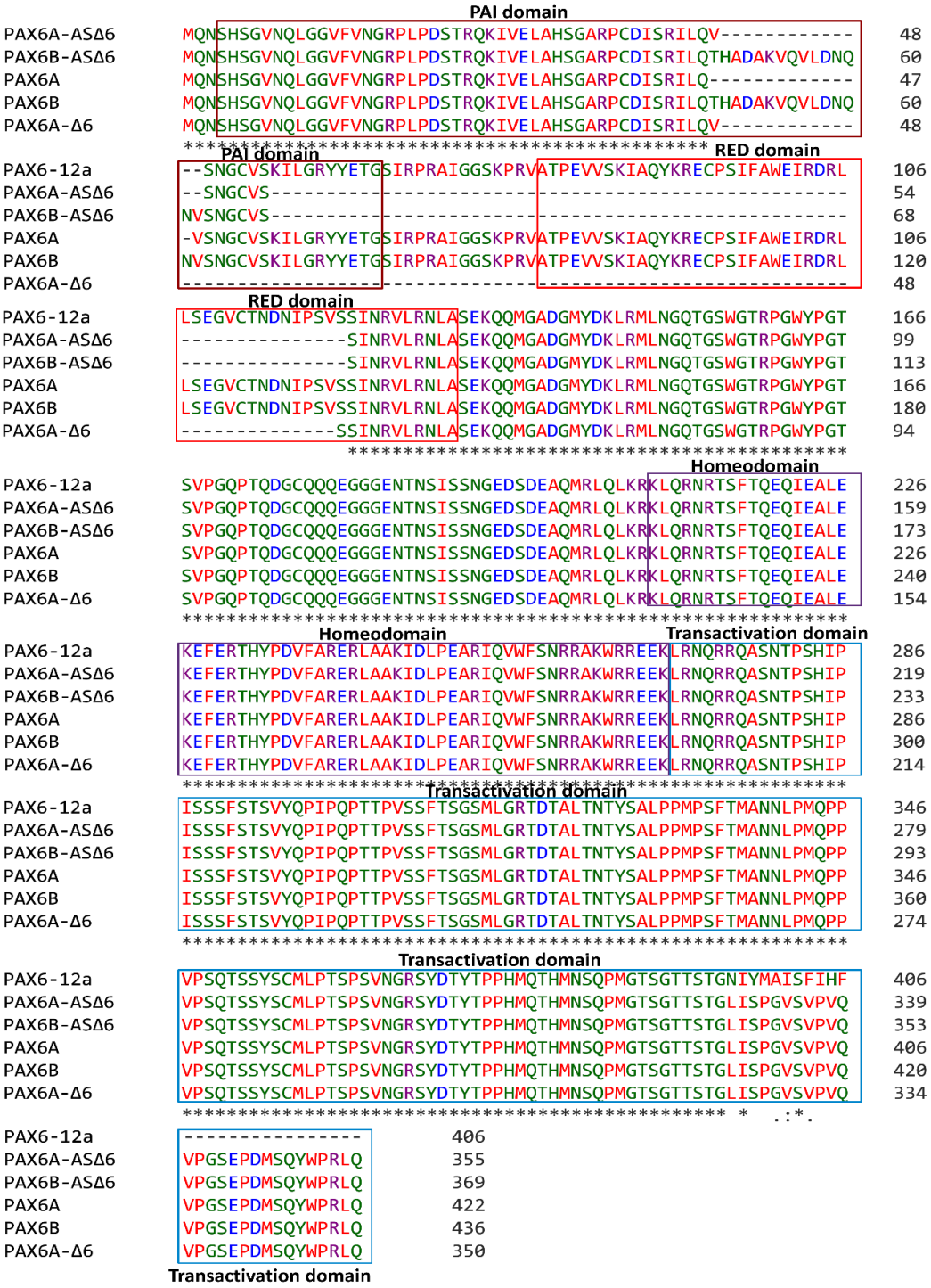

Figure 4.20. Multiple sequence alignment (ClustalW) of deduced amino acid sequence of the reported transcripts PAX6A, B and newly identified transcripts (PAX6B-ASΔ6, PAX6A-ASΔ6 and PAX6A-12a). *The names of the respective protein isoforms are indicated at the beginning of the sequence. The alignment of amino acid sequences clearly indicate differences at the N' terminus region (for PAX6B, PAX6B-AS⊿6, PAX6A-AS⊿6 isoforms) and C' terminus region (for PAX6A-12a isoform) of PAX6 protein. Asterisk (*), colon (:) and hyphen (-) indicates identical, or similar amino acids or no residues respectively.*

4.2.9. RNA-FISH: BaseScope RNA probe assay detection and localization of RNA within cells and tissues

RT-PCR is a simpler and effective technique used for the detection and quantification of transcribed RNAs in cultured cells and human ocular tissues. However, it fails to provide any spatial information such as the cell-type restricted expression and *in situ* visualization capabilities of IHC or RNA-FISH. It is possible that the novel variants may remain as regulatory RNAs and do not undergo translation. However, if they generate smaller protein isoforms, then the routine antibody based detection becomes a challenge, to uniquely detect and localize them by IF or IHC. This is mainly because the epitopes of most commercial antibodies fall within the common region and cannot distinguish individual variants differing by a few internal residues. While it is feasible to distinguish the protein isoforms, PAX6A and PAX6B, based on their sizes by western blotting, it proved to be a challenge to detect the other smaller and minor variants with overlapping sizes, differing by only a few kilodaltons. However, we could successfully test a monoclonal antibody raised against a short peptide mapping to the C' terminus of PAX6 (from Biolegend) and confirmed that it specifically recognize the recombinant PAX6A and PAX6B, but not PAX6A-12a. Nevertheless, the lack of reactivity was not useful to detect and localize the protein in native tissues. Recently, the reproducibility and reliability of RNA florescence in-situ hybridization (RNA-FISH or shortly RISH) has significantly advanced with the advent of novel FISH-based single molecule localizations techniques, such as the Stellaris™ probe technology developed by LGC Biosearch technologies; RNAscope™ and BaseScope™ technology developed by ACD biotech. These technologies employ unique signal amplification strategies that allow the visualization of target RNAs as discrete dots, where each dot represents an individual RNA molecule. When combined with suitable image analysis software, it enables both localization and quantifications of cellular RNAs within cells and tissues. The key advantage of the BaseScope assay is its high sensitivity due to signal amplification and unique probe design that minimizes any nonspecific off-target signals. This technology has been further optimized for the detection of small RNAs such as miRNA and differentially spliced transcripts. With this rationale, we employed BaseScope assay to elucidate the cell type-specific expression of the wild type and novel PAX6 transcripts in limbal basal cells, TACs and differentiated cells of the cornea.

To localize the PAX6 splice variants in limbal and corneal cells, we designed BaseScope probes to uniquely detect the wild type isoform either alone or in combination with one of the N' terminus splice variant (PAX6B-ASΔ6) or the C' terminus splice variant PAX6A-12a. To

recognize PAX6A in native tissues, BaseScope single Z pair probe targeting exon 6/7 junction was designed (**Fig 4.21.A.i**). To detect the expression of the novel PAX6B-ASΔ6 and PAX6A-12a transcripts, a single Z pair probe was designed to target the junctions of the exon 5a/Δ6/E7 and 12/12a/13 respectively (**Fig 4.21.A.ii, iii**). Using this unique probe design strategy, we could successfully identify and localize the novel splice variants PAX6B-ASΔ6 and PAX6A-12a and distinguish them from PAX6A transcripts.

4.2.9.1. BaseScope™ *in Situ* hybridization work flow

The schematic workflow of the BaseScope assay using the Z pair probes is explained in figure **3.1** and is summarized in detail in section **3.14.1**. Briefly, the procedure consists of four parts where the ocular tissues or primary limbal epithelial cultures were permeabilized with target retrieval and protease III treatment, followed by the hybridization of the target RNA, signal amplification using Pre-amplifiers and amplifiers, followed by the visualization of the signal.

BaseScope Assay Kit was purchased from Advanced Cell Diagnostics (ACD Biotech) and was designed for tissues as well as adherent cultures. Specific to this experiment, a positive control probe targeting the mRNA of RNA polymerase II subunit A (POLR2a) and a negative control probe which recognizes *Bacillus subtilis* dihydrodipicolinate reductase (DapB) mRNA was also used. The test RNA probes were specifically designed to target PAX6 transcripts. Each probe encompassed about 30-40 oligonucleotides, with a double Z configuration. One side of the Z was complementary to the target mRNA molecule and other side of the Z was complimentary to the preamplifier DNA sequence (**Fig 4.21.B**). Sequential addition of the preamplifier and amplifier molecules led to the amplification of the signal. Further addition of the chromogenic substrate led to the labelling of individual target mRNAs. Finally, the signal was visualized under a bright field or fluorescence microscope (**Fig 4.21.B**). If the two oligonucleotide Z pairs are not bound immediately adjacent to each other on the target mRNAs, the signals will not get amplified, thus ensuring specificity that minimizes false positive detections. The mRNA expression levels within individual cells can be either quantified manually or using any image analysis software tool, based on the number of dots counted per cell.

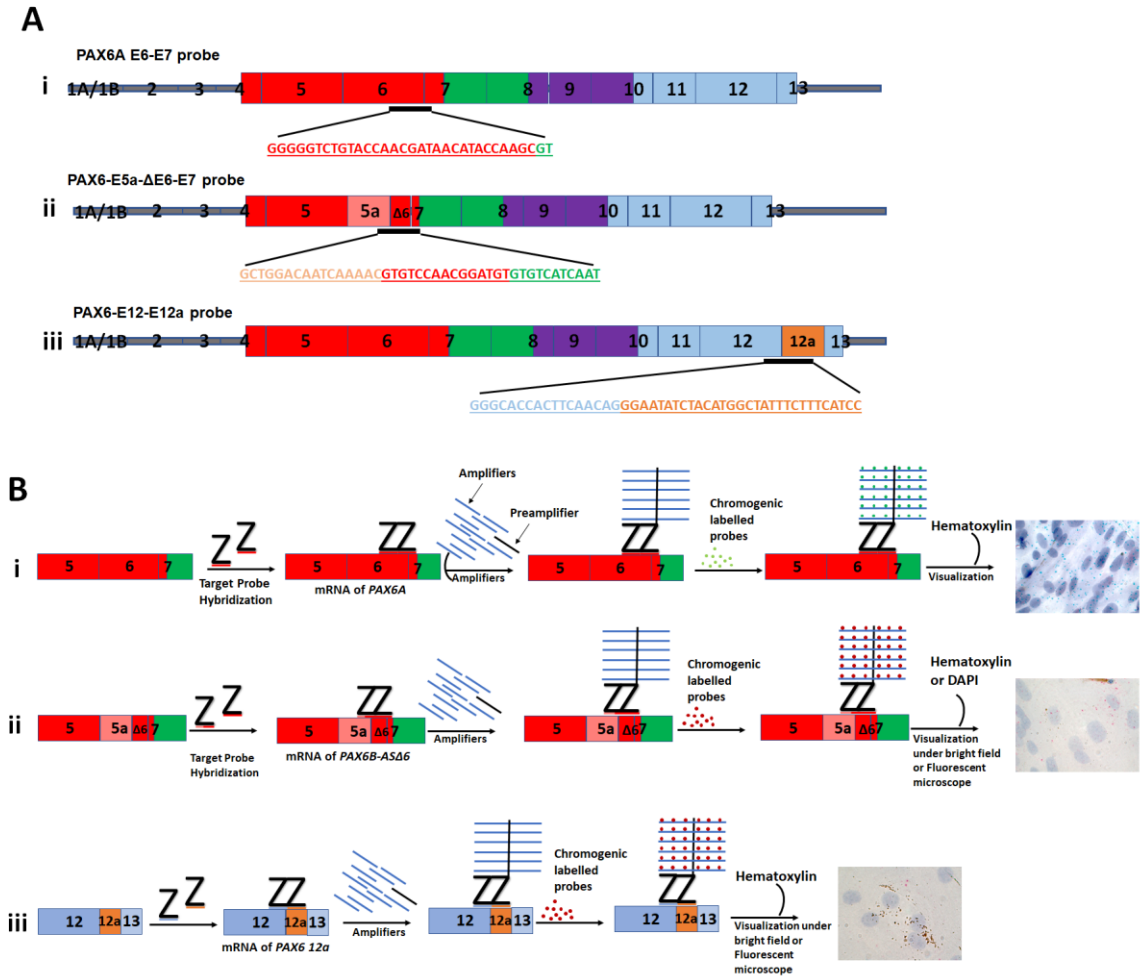

Figure 4.21: Design and workflow of BaseScope assay using PAX6 RNA-FISH probes. ***(A)*** *Cartoon representation of the design of PAX6A, PAX6B-AS⊿6 and PAX6A-12a RNA probes to uniquely detect the novel alternatively spliced PAX6 transcripts. The probes consists of a single ZZ pair oligonucleotides. (**Ai**) The E6-E7 probe is designed to detect the junction between exon 6 and exon 7 and detects only the PAX6A transcript. (**Aii**) E5a-⊿E6-E7 probe spans the junction between exon 5a, AS⊿6 and exon 7 and detects only the PAX6B-AS⊿6 transcript. (**Aiii**) E12-12a probe spans the junction of exon 12 and 12a and detects only the PAX6A-12a transcript. **(B)** Cartoon representation of the workflow of Basescope assay. Firstly, the target specific individual Z probes bind next to each other on the targeted RNA, the preamplifier then binds to the complimentary sequences on the top of the double Z probe. The preamplifier contains multiple binding sites for the amplifiers. The amplifiers carry either the horse radish peroxidase (HRP) or the alkaline phosphatase (ALP) enzyme conjugates, which upon addition of respective substrates, produces either the green/blue and red/pink (Fast green or Fast red labelled) chromogenic products, respectively. This allows for the signal amplification and detection of single RNA molecules in the form of discrete spots within cells and tissues. (**Bi**) The E6-E7 probe detects PAX6A transcripts in green color, (**Bii**) the E5a-⊿E6-E7 probe detects PAX6B-AS⊿6 transcripts in red color and (**Biii**) the E12-12a probe detects PAX6A-12a transcripts in red color. The cells and tissue sections are counterstained with DAPI or hematoxylin. The labelled transcripts are visualized as discrete green or red coloured punctas under a bright field microscope.* ***Note:*** *The*

red colored of BaseScope probes can also be visualized using the Cy3 detector in a fluorescent or confocal microscope.

4.2.9.2. Confirmation of variant specificity of PAX6 RNA probes

To check the specificity of the PAX6A variant-specific RNA probes, NIH3T3 cells were transfected with PAX6A, PAX6B, PAXB-ASΔ6 and PAX6A-12a constructs respectively. The PAX6 E6-E7 targeting probe detected PAX6A as discrete blue colored dots indicating the expression and localization of individual mRNAs (**Fig 4.22.i**). However this probe failed to detect PAX6B-ASΔ6 with exon 6 region deleted, thus confirming the specificity of the probe (**Fig 4.22.ii**). Similarly, the cells transfected with PAX6B or PAX6B-ASΔ6 were probed with the E5a-ΔE6-E7 probe. As expected, the probe failed to detect PAX6B, though it carried the exon 5a region (**Fig 4.22.iii**). However, the cells transfected with PAX6B-ASΔ6 showed several red colored dots indicating the expression and localization of individual mRNAs (**Fig 4.22.iv**). Next, the cells transfected with PAX6A or PAX6A-12a were probed with the E12-12a probe and observed that it failed to detect PAX6A (**Fig 4.22.v**). However, in the cells transfected with PAX6A-12a, the probe could clearly recognize the mRNA and showed several red colored dots, thus confirming the expression and localization of individual mRNAs (**Fig 4.22.vi**). Taken together, we confirmed that the wild type, positive control probe (E6-E7) and the two novel variant-specific test probes (E5a-ΔE6-E7 and E12-12a) are absolutely target specific.

4.2.9.3. Localization of novel PAX6 variants in primary limbal cells using BaseScope assay

BaseScope assay validation was done by using bacterial E. coli gene, DapB and a human RNA polymerase III gene, POLR2A, as negative and positive controls respectively, in limbal epithelial cells. As expected, DapB did not show any signal, since it is a bacterial gene and therefore not expressed in limbal epithelial cells (**Fig 4.23.A.i**). POLR2A, encodes the polymerase, which is ubiquitously expressed in all vertebrate cells and showed multiple discrete punctas marking individual mRNAs (**Fig 4.23.A.ii**), thus successfully validated the BaseScope probes assay.

Endogenous expression of PAX6A, PAX6B-ASΔ6, and PAX6-12a was checked in limbal epithelial cells using the probes E6-E7, E5a-ΔE6-E7 and E12-12a respectively. PAX6A is the Wt isoform and the gene was found to be highly expressed using the E6-E7 BaseScope probe that spans the exon 6 and 7 junction (**Fig 4.23.A.iii**).

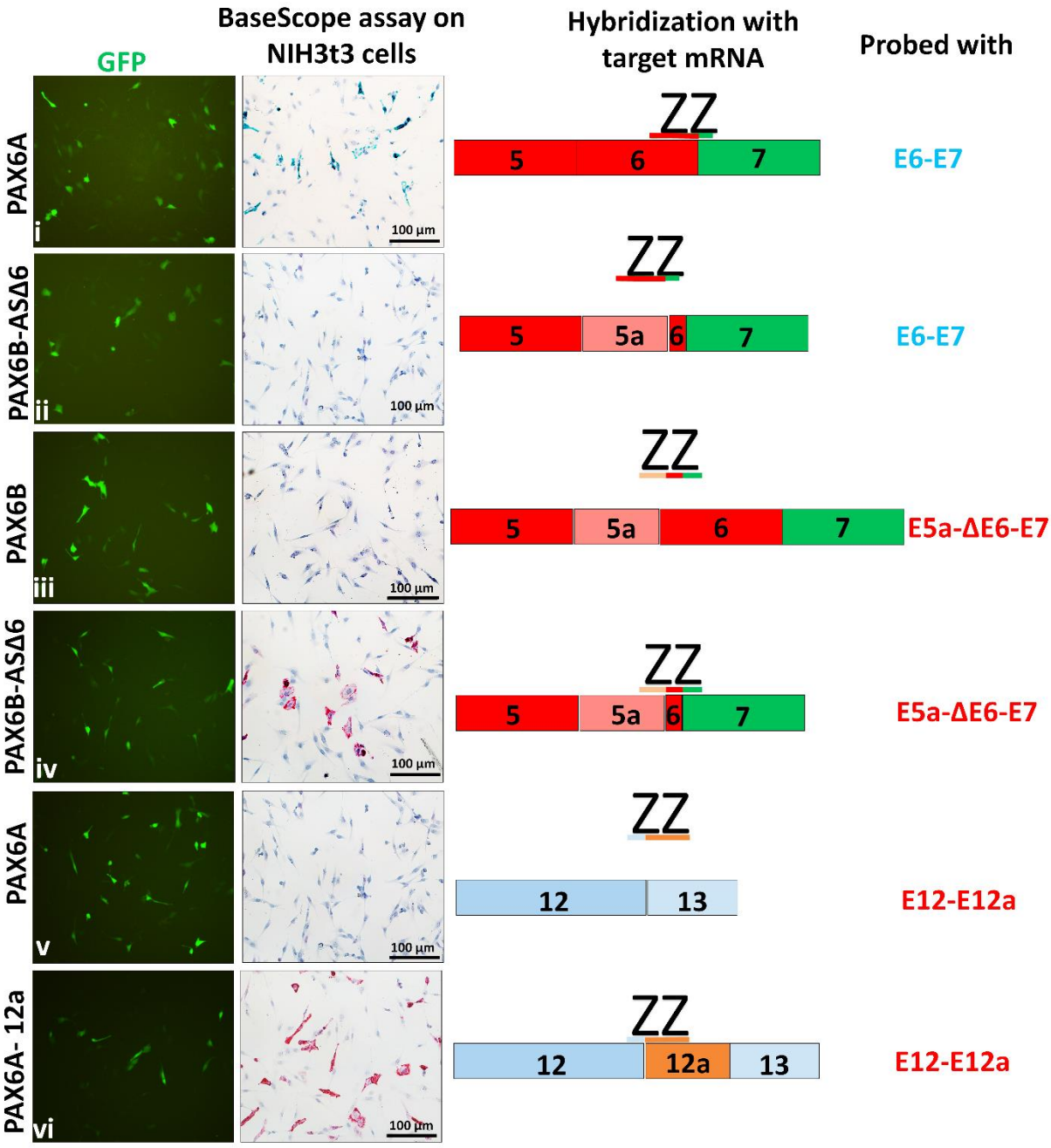

Figure 4.22: Validation of the specificity of variant-specific RNA-FISH BaseScope probes. *BaseScope assay was carried out in NIH3T3 cells transfected with different PAX6 variant encoded constructs. Cells transfected with (**i**) PAX6A (positive control) and (**ii**) PAX6B-AS⊥6 (negative control) were probed with the E6-E7 probe. Green punctas indicate PAX6A transcript-specific signals. No signals were detected with PAX6B-AS⊥6 transcripts. Cells transfected with (**iii**) PAX6B (Negative control) and (**iv**) PAX6B-AS⊥6 (Positive control) were probed with the E5a-⊥E6-E7 probe. Red punctas indicate PAX6B-AS⊥6 transcript-specific signals. No signals were detected with PAX6B transcripts. Cells transfected with (**v**) PAX6A (Negative control) and (**vi**) PAX6A-12a (Positive control) were probed with the E12-E12a probe. Red punctas indicate PAX6A-12a transcript-specific signals. No signals were detected with PAX6A transcripts. On the right is the cartoon representation of the location of the specified ZZ probes. The cells are counterstained with haematoxylin to mark the nucleus in blue. Scale bar: 100 µm.*

The novel PAX6B-ASΔ6 transcript was found to be moderately expressed only in a subset of limbal epithelial cells using the E5a-ΔE6-E7 BaseScope probe that spans the exon 5a/Δ6/7 junction (**Fig 4.23.B.i**). Similarly, using the E12-12a BaseScope probe that spans the exon 12 and 13 junction, we found that the novel PAX6A-12a variant was moderately expressed only in a subset of limbal epithelial cells (**Fig 4.23.B.ii**). Thus we confirm that the novel human PAX6 variants are expressed at optimal levels, but only in a subset of cultured limbal cells, as compared to the ubiquitously expressed PAX6A isoform.

In order to identify whether these novel alternately spliced transcripts are exclusively expressed or co-expressed along with the native variant, we performed the dual BaseScope assay. We observed that the novel variants were co-expression along with the wild type PAX6A variant in the smaller subset of cultured limbal cells (**Fig 4.23.B.iii, iv**).

To quantify the expression levels of novel variants, the labeled punctas within a single cell were counted. A minimum of 300 cells were counted for each type of transcript. In a single cell, the number of punctas of PAX6A was higher than those of PAX6B-ASΔ6 or PAX6A-12a (**Fig 4.23.C**). We also observed that the percentage of cells expressing PAX6A was higher when compared with PAX6B-ASΔ6 and PAX6A-12a (**Fig 4.23.D**; $p=0.02$). Collectively, this suggests that PAX6A is the highly expressed and dominant transcript, followed by PAX6B-ASΔ6 and PAX6A-12a in limbal epithelial cells.

4.2.9.4. Co-localization of mRNAs of PAX6 variants and other cellular antigens in limbal cultures

To understand the significance of alternate splicing of PAX6 transcripts, it becomes important to evaluate its effects on PAX6 protein expression, target gene expression and normal cellular functions. This can be partly checked by the simultaneously detection of novel transcripts, along with other limbal marker proteins in cultured cells.

As mentioned above, we observed that the novel transcripts are co-expressed along with the wild type PAX6A transcript. This suggests that the alternate splicing of pre mRNA may directly influence the relative abundance of wild type transcripts and the novel spliced forms. This can in turn dictate the PAX6 protein abundance and accumulation within specific cell types.

In order to identify whether these novel transcripts have any impact on the native PAX6 protein expression, we performed colocalization of both the protein and the transcripts, by combining immunocytochemistry and BaseScope RNA-FISH assay.

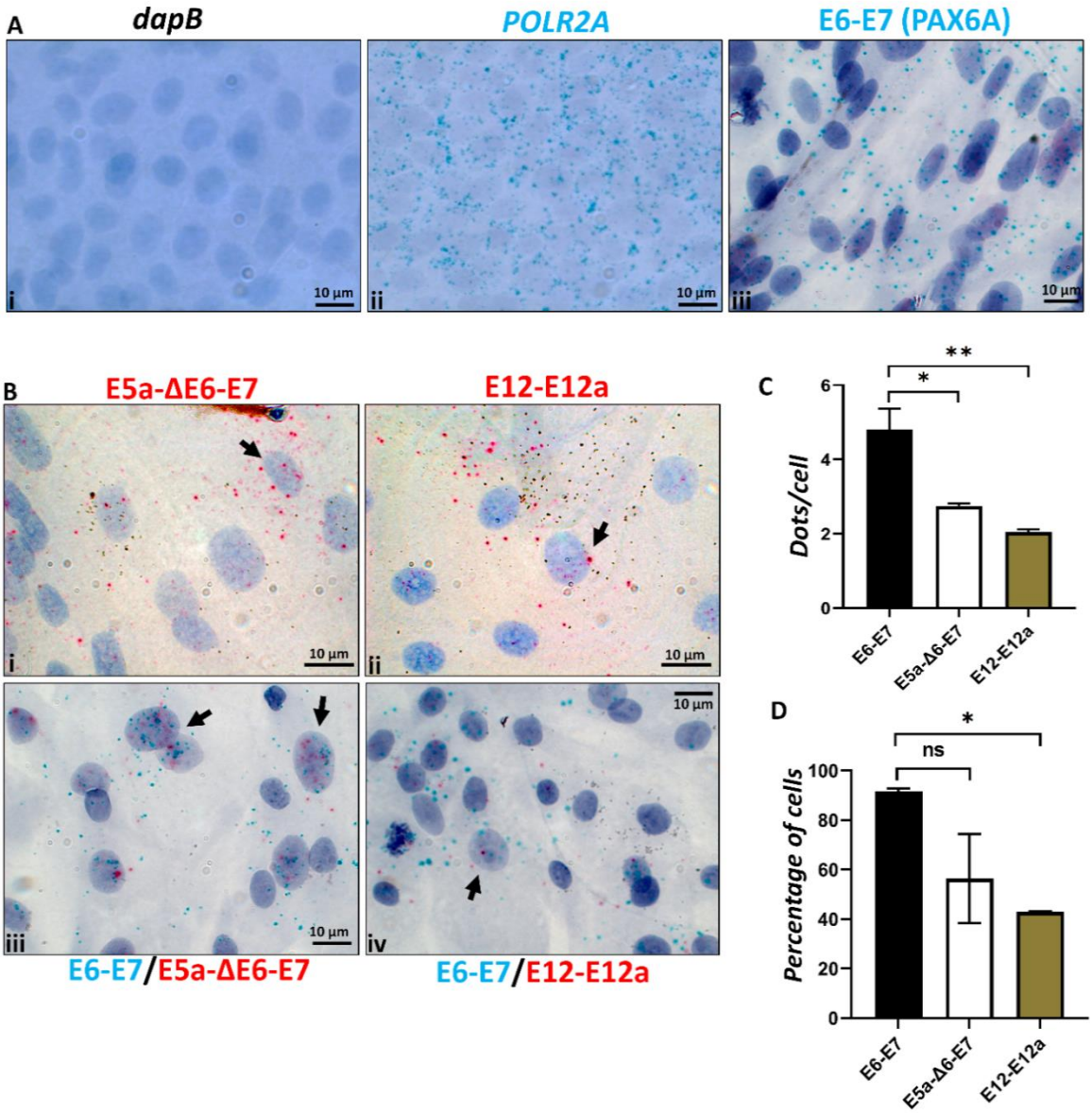

Figure 4.23: Localization of PAX6A (blue), PAX6B-ASΔ6 (Red) and PAX6A-12a (Red) transcripts in primary limbal epithelial cultures. (Ai) *A probe against the bacterial gene, dapB was used as a negative control. (**Aii**) A probe against the human housekeeping gene, POLR2A was used as a positive control. (**Aiii**) Detection of the ubiquitously expressed PAX6A transcripts in limbal cultures using the E6-E7 BaseScope probe (in green). (**Bi**) Detection of PAX6B-AS⊿6 transcripts in a sub-set of limbal cells, using E5a-⊿6-E7 BaseScope probe (in red). (**Bii**) Detection of PAX6A-12a transcripts in a sub-set of limbal cells, using E12-12a BaseScope probe (in red). (**Biii, iv**) Dual detection of both PAX6A (in green) and PAX6B-AS⊿6 (in red) or PAX6A-12a (in red) transcripts. Arrows marks the cells expressing specific transcripts. The cells are counter stained with hematoxylin to mark the nuclei in blue. Scale bar: 10 µm. (**C**) Histogram plot showing the average number of dots/cells detected for PAX6A, PAX6B-AS⊿6 and PAX6A-12a transcripts (**D**) Histogram plot showing the mean percentage of positive cells expressing*

*PAX6A, PAX6B-AS⊿6 and PAX6A-12a transcripts. The data is represented as mean ± SD, N=3. *P<0.05 and **p<0.005.*

The results confirmed that the PAX6A mRNA specific punctas were found to be uniformly distributed in all PAX6 expressing cells (**Fig 4.24.A.i**), whereas, the PAX6B-ASΔ6 mRNA specific punctas were abundantly observed only in a subset of cells with low levels of PAX6 protein ($PAX6^{Low}$ cells) (**Fig 4.24.A.ii**). In contrast, PAX6A-12a mRNA transcript was expressed in a subset of cells with variable levels of PAX6 protein (both $PAX6^{High}$ and $PAX6^{Low}$ cells) in growing limbal primary cultures (**Fig 4.24.A.iii**). However, further evaluation in native corneal tissues would help to confirm the identity and spatial positioning of these cells expressing the novel splice variants.

The mRNA punctas were also quantified and compared with dual labeled cells having lower or higher levels of PAX6 protein expression. The results revealed that higher percentage of PAX6A transcript expressing cells, expressed higher levels of PAX6 protein. Conversely, higher percentage of PAX6B-ASΔ6 transcript expressing positive cells, expressed lower levels of PAX6. However, the cells positive for PAX6-12a transcript had both low levels and also high levels of PAX6 in an equal proportion (**Fig 4.24.B**). This suggests that the novel splice variants seem to be influencing the relative abundance of wild type variant transcripts and in turn the PAX6A protein levels within individual cells.

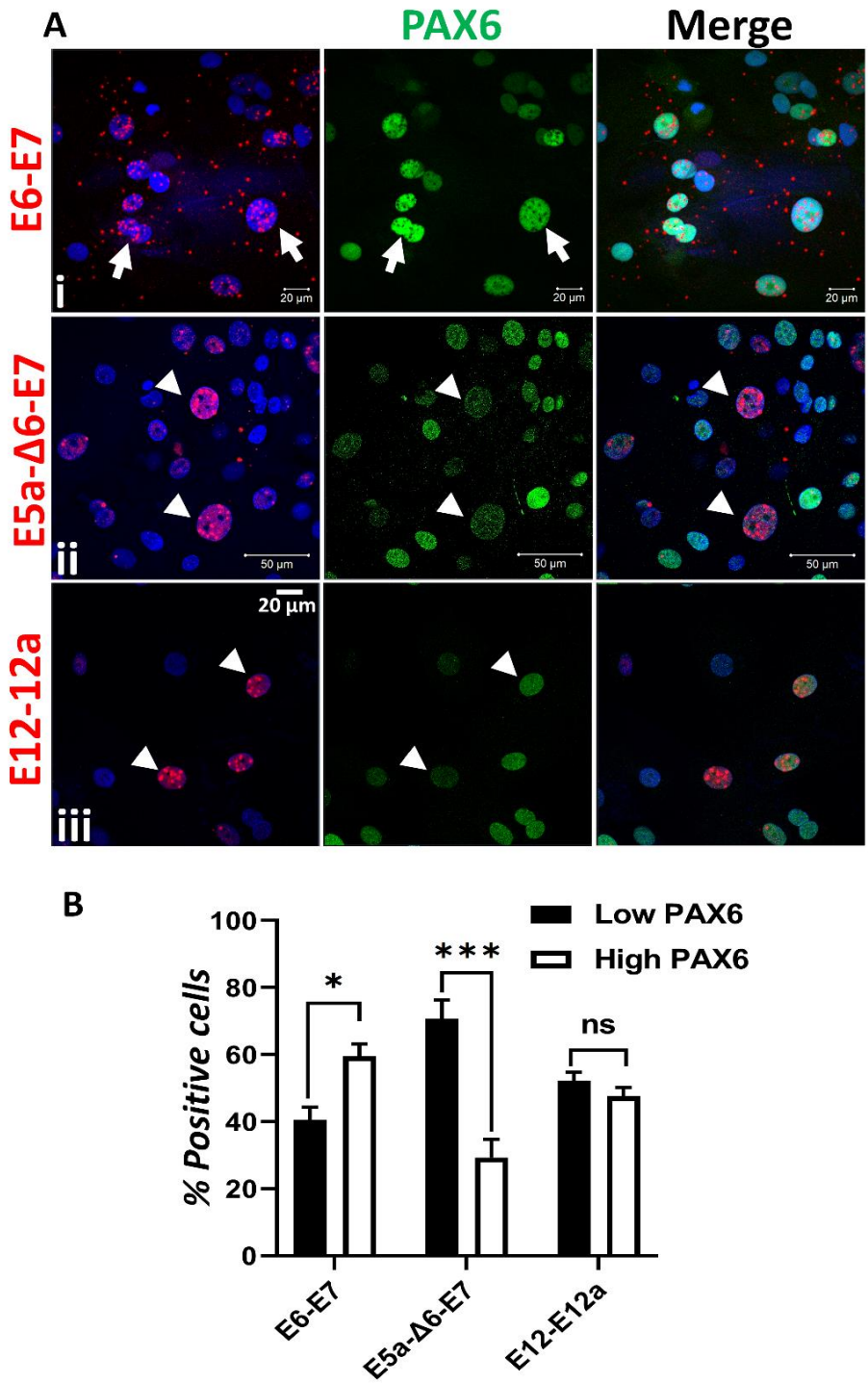

Figure 4.24: Co-localization of PAX6 transcripts and the protein in primary limbal epithelial cells. *(**A**) A combined BaseScope probe assay and immunostained images primary limbal epithelial cultures showing PAX6A, PAX6B-AS⊿6 and PAX6A-12a transcript expression (as red dots) in cells co-stained with anti-PAX6 antibody (in green). (**Ai**) PAX6A transcript is ubiquitously expressed. Cells expressing higher levels of transcripts showed intense PAX6 antibody staining. (**Aii**) Cells expressing higher levels of PAX6B-AS⊿6 transcripts have low levels of PAX6 protein expression, corresponding to a*

*weaker antibody staining. (**Aiii**) PAX6A-12a transcript expressing cells have both high and low levels of PAX6 protein expression. The cells are counterstained with DAPI to mark all cell nuclei (in blue). Arrows point to high PAX6 expressing cells; arrow heads points to low PAX6 expressing cells. Scale bar: 20 μm or as specified. (B) Histogram plot showing the mean percentage of different PAX6 transcript expressing cells, with high or low levels of PAX6 protein expression. The data is represented as mean ± SD, N=3.*P<0.05, **p<0.005 and ***p<0.0005.*

4.2.9.5. Localization of novel PAX6 variants in limbal and corneal tissues using BaseScope assay

For spatial visualization and to understand the cell type specific expression of the novel transcripts, PAX6B-ASΔ6 and PAX612a in native tissues, we employed BaseScope assay on formalin fixed, paraffin embedded ocular tissues.

As expected, with PAX6A specific BaseScope probe (E6-E7), targeted mRNA-specific intracellular signals were seen as discrete punctas in all the cells of the apical and basal layers of the central corneal epithelium. However, only the cells in the supra basal and apical layers showed specific signals in the limbal epithelium. The limbal basal cells were found to have low levels of PAX6A transcript expression (**Fig 4.25.i**). These basal cells with low PAX6A transcript were found to have high levels of PAX6B-ASΔ6 mRNA in limbus and central cornea (**Fig 4.25.ii**). The basal layers of the limbus and cornea contain the putative stem cells and the progenitor cells that give rise to the proliferating TA cells respectively. However, majority of the differentiated cells reside in the apical layers of the limbus and cornea and only a few of them expressed low levels of PAX6B-ASΔ6 mRNA (**Fig 4.25.ii**). On the other hand, PAX6A-12a mRNA expressing cells were found to be distributed throughout the suprabasal and apical layers of the corneal epithelium. Similarly, majority of the cells in the limbus expressed the 12a variant, except a single layer of basal cells and the top most wing cells (**Fig 4.25.iii**). This confirms that the PAX6 novel transcripts are differentially expressed in different cell types of the limbus and cornea.

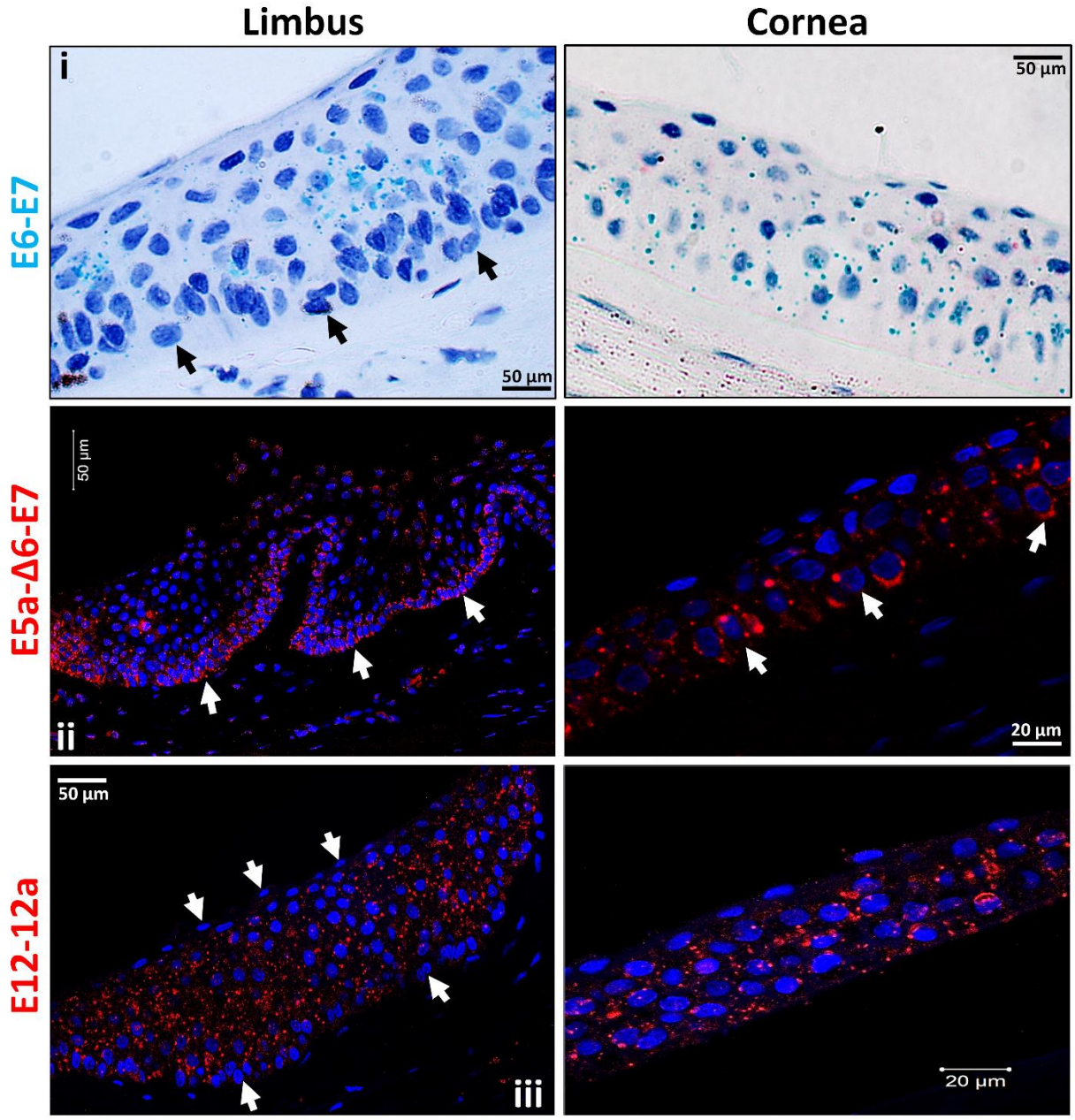

Figure 4.25: Localization of PAX6 transcripts in limbus and corneal tissues using BaseScope assay. *(**i**) Discrete punctas representing the PAX6A transcripts (in green) are localized to most of the suprabasal and apical cells of the limbus and the entire corneal epithelium. (**ii**) Discrete punctas representing the PAX6B-AS⊿6 transcripts (in red) are localized mainly to the basal cells of the limbus and cornea. (**iii**) Discrete punctas representing the PAX6A-12a transcript (in red) is seen distributed throughout the suprabasal and apical cells of the limbus and the entire corneal epithelium. The cells are counterstained with haematoxylin or DAPI to mark all the nuclei in blue. Scale bar: 50 µm or as specified.*

4.2.9.6. Co-localization of PAX6 RNA variants and the translated protein in corneal tissues

In corneal tissues, the level of expression of PAX6 protein determines the fate of corneal epithelial cells. To check the effects of novel splice variants on PAX6 protein expression and abundance in native corneal tissues, we combined immunohistochemistry and BaseScope RNA-FISH assay, as described in the methods. The results further confirmed that PAX6B-ASΔ6 mRNA is highly expressed in the $PAX6^{Low}$ basal epithelial cells of the limbus and cornea (**Fig 4.26.i, ii**). Most of the suprabasal cells of the limbus and cornea expressed very high levels of PAX6 protein. However, only a few of these $PAX6^{High}$ cells expressed the PAX6B-ASΔ6 transcript (**Fig 4.26.i, ii**). In contrast, the expression of the PAX6A-12a transcript was observed both in the $PAX6^{Low}$ suprabasal TA cells and $PAX6^{High}$ apical differentiated and mature epithelial cells of the limbus and cornea (**Fig 4.26.iii, iv**).

We also did dual labeling experiment to co-localize the novel PAX6 transcripts along with the basal stem cell marker, p75NTR/ LNGFR. We observed that the PAX6B-ASΔ6 transcript was highly expressed in p75NTR expressing basal epithelial cells of the limbus and cornea. The suprabasal cells lacked the expression of both the novel transcript and p75NTR, thus confirming the stem and progenitor cell-specific expression of PAX6B-ASΔ6 transcripts (**Fig 4.27.i, ii**). The intense expression of PAX6A-12a transcript was observed mostly in the suprabasal TA cells of the limbus and cornea. The cells in the basal layers expressing low levels of PAX6A-12a co-localized with p75NTR, thus confirming that the proliferating progenitors in the limbus and the expanding TA cells of the cornea expresses the PAX6A-12a transcripts (**Fig 4.27.iii, iv**).

Further, we did dual labeling experiment to co-localize the novel PAX6 transcripts along with the cornea-specific, differentiation/mature cell marker, Keratin 3. We observed that a majority of the differentiated supra basal cells expressing KRT3 failed to express either the PAX6B-ASΔ6 or PAX6A-12a transcripts. Similarly, the undifferentiated basal and supra basal cells expressing high levels of the novel transcripts did not express KRT3 (**Fig 4.28.i-iv**).

Taken together, the combined results of the BaseScope RNA-FISH & ICC/IHC experiments confirmed that the novel, alternately spliced, PAX6 transcripts are differentially expressed in different cell types within the limbal and corneal epithelium. While, the expression of PAX6B-ASΔ6 transcript is limbal stem cell and proliferating progenitor cell-specific, the PAX6A-12a

transcript is predominantly expressed by the expanding, undifferentiated TA cells in the supra basal layers.

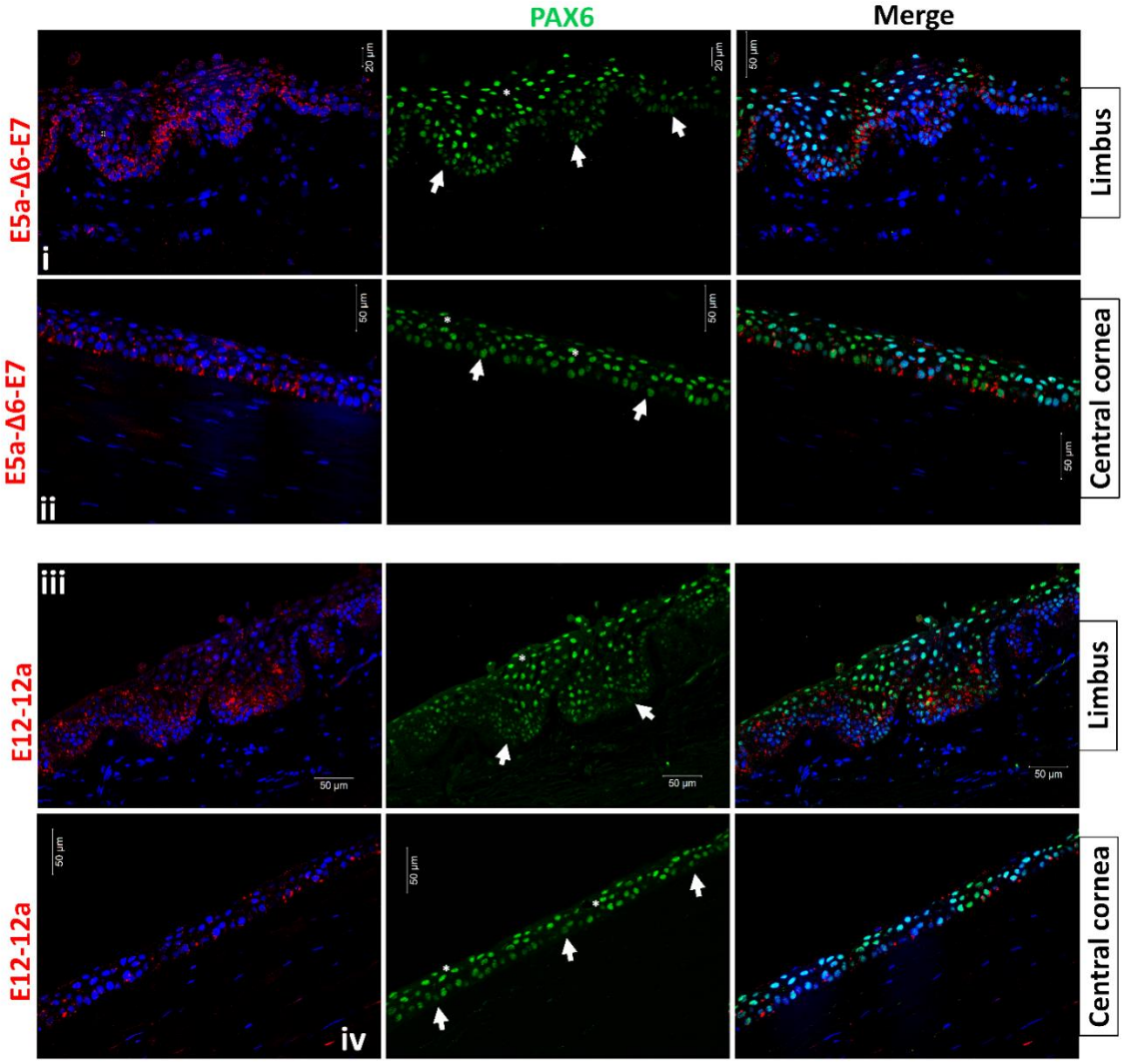

Figure 4.26: Co-localization of PAX6 transcripts and the protein in limbus and corneal tissues. *The tissue sections are dual labelled with transcript-specific Basescope RNA probes (in red) and IHC with anti-PAX6 antibody (in green). Representative confocal images show the PAX6B-AS⊿6 RNA and PAX6 protein expression and localization in the limbal (**i**) and corneal epithelium (**ii**). The PAX6^{low} basal cells express high levels of PAX6B-AS⊿6 RNA and the PAX6^{high} suprabasal and apical cells show negligible expression of PAX6B-AS⊿6 RNA. Representative confocal images showing PAX6A-12a RNA and PAX6 protein expression and localization in the limbal (**iii**) and corneal epithelium (**iv**). Most of the suprabasal cells of the limbus and cornea with moderate levels of PAX6 protein expressed the PAX6A-12a RNA. Arrows indicate the basal cells expressing low levels of PAX6 at the limbus and cornea. Aster risk indicates the cells expressing high levels of PAX6. The sections are counterstained with DAPI to mark all cell nuclei in blue. Scale bar- 50 μm or as specified.*

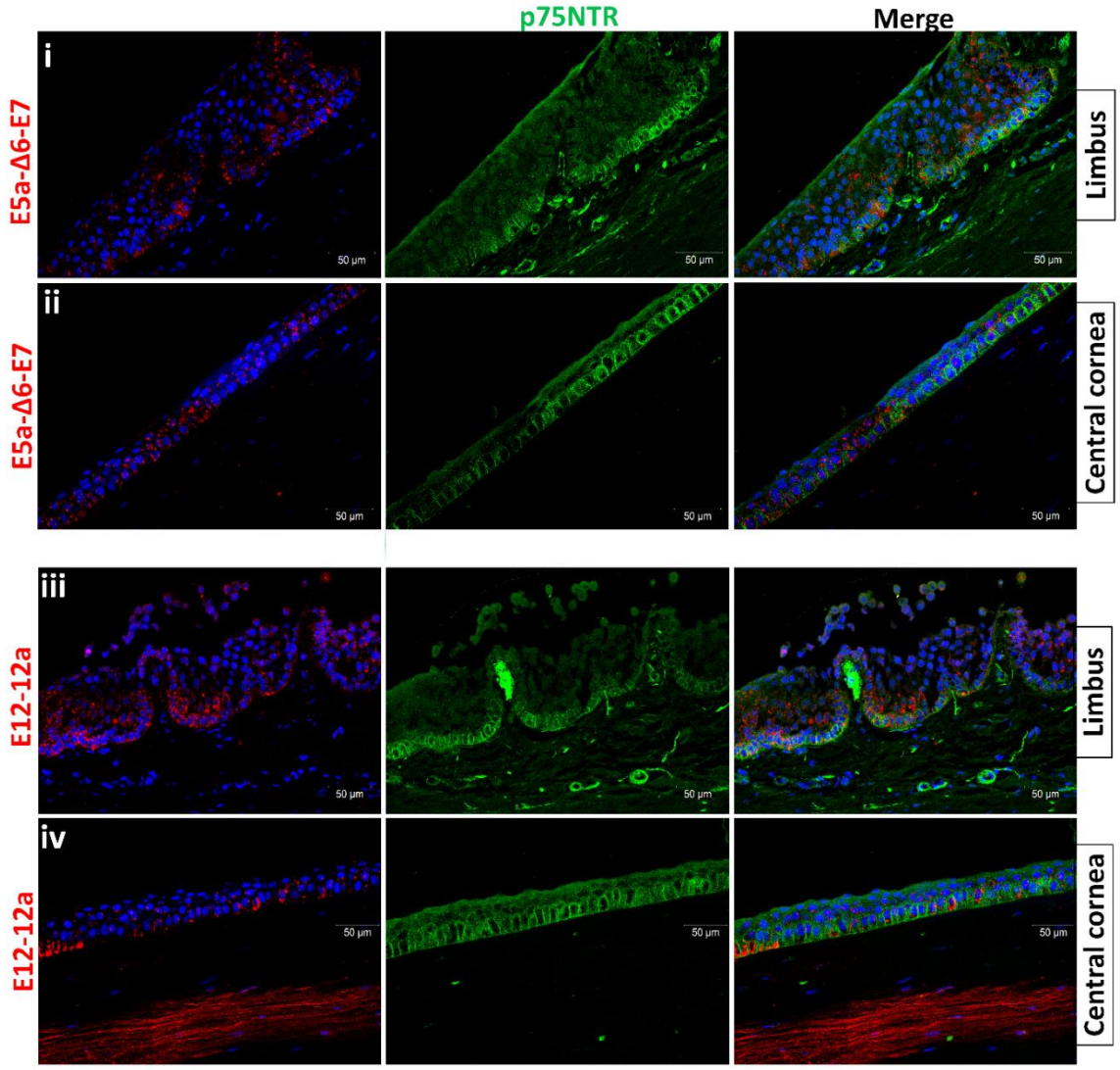

Figure 4.27: Co-localization of PAX6 transcripts and p75NTR protein in limbus and corneal tissues. *The tissue sections are dual labelled with transcript-specific BaseScope RNA probes (in red) and IHC with anti-p75NTR antibody (in green). Representative confocal images show the PAX6B-AS⊿6 RNA and p75NTR protein expression and localization in the limbal (**i**) and corneal epithelium (**ii**). The basal cells of the limbus and the cornea co-expressed both the PAX6B-AS⊿6 RNA and the progenitor cell-specific p75NTR protein. Representative confocal images showing PAX6A-12a RNA and p75NTR protein expression and localization in the limbal **(iii)** and corneal epithelium **(iv).** Most of the suprabasal cells and a subset of p75NTR expressing basal cells of the limbus and cornea expressed the PAX6A-12a RNA. The sections are counterstained with DAPI to mark all cell nuclei in blue. Scale bar- 50 µm.*

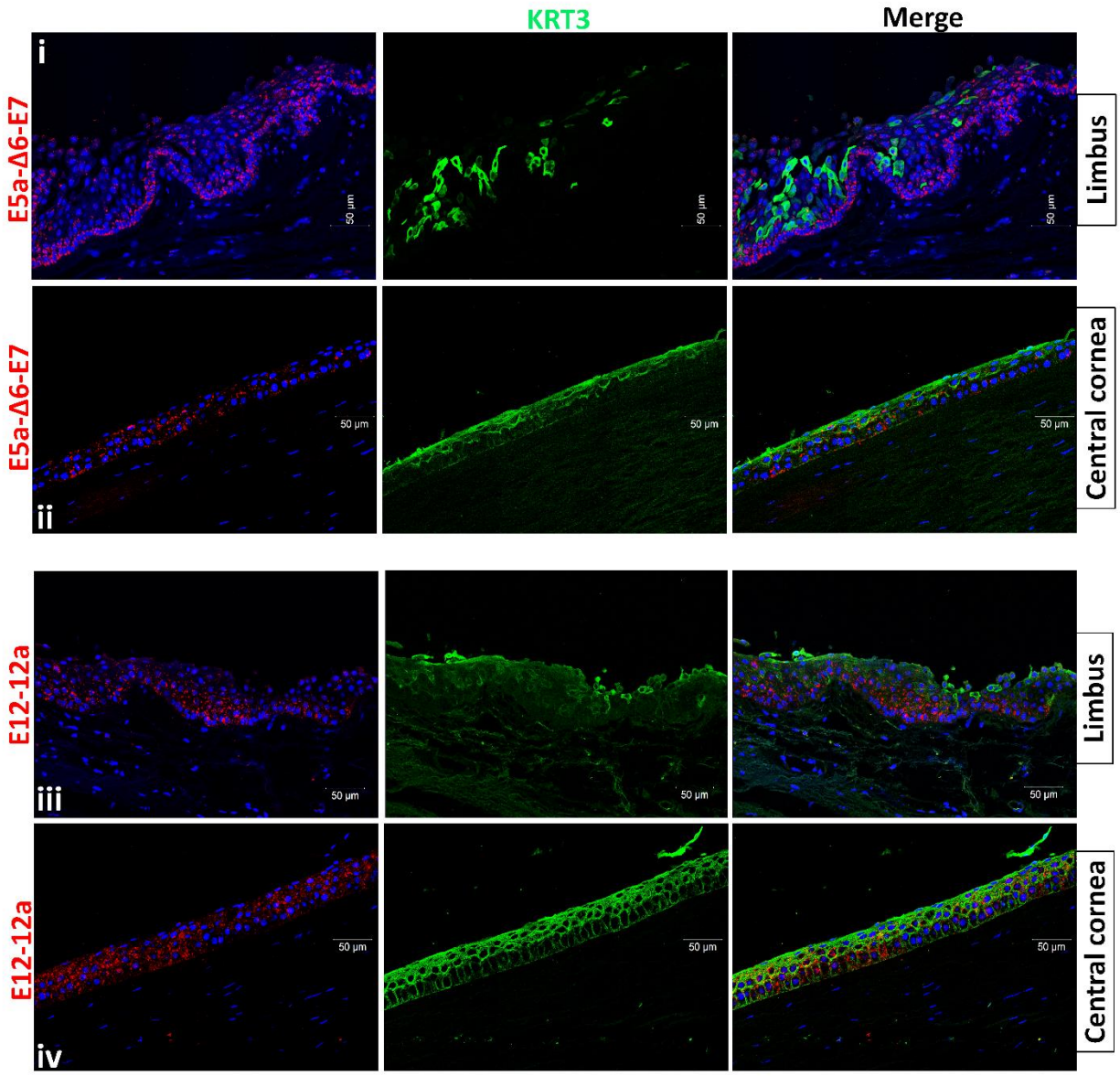

Figure 4.28: Co-localization of PAX6 transcripts and KRT3 protein in limbus and corneal tissues. *The tissue sections are dual labelled with transcript-specific Basescope RNA probes (in red) and IHC with anti-KRT3 antibody (in green). Representative confocal images show PAX6B-AS⊿6 RNA and KRT3 protein expression and localization in the limbal (**i**) and corneal epithelium (**ii**). The supra basal and apical cells expressed the mature corneal epithelial marker protein, KRT3. These cells did not express PAX6B-AS⊿6 RNA. Conversely, the basal cells that express high levels of PAX6B-AS⊿6 RNA did not express KRT3. Representative confocal images showing PAX6A-12a RNA and KRT3 protein expression and localization in the limbal (**iii**) and corneal epithelium (**iv**). Most of the suprabasal cells expressing the PAX6A-12a RNA, co-expressed the KRT3 protein. The sections are counterstained with DAPI to mark all cell nuclei in blue. Scale bar- 20 µm.*

4.2.9.7. Detection of ΔNp63 and TAp63 transcripts in limbal cultures and in corneal tissues

To identify and localize the two alternate promoter driven p63 transcripts, we performed BaseScope assay in primary limbal cultures. We designed the BaseScope RNA-FISH probes to specifically recognize the unique Exon 1 regions of the ΔNp63 and TAp63 transcripts. In explant cultures, the ΔNp63 transcripts (stem cell-specific epithelial marker) were found to be highly expressed in the cells at the explant edge (**Fig 4.29.A.i**) and the leading edge (**Fig 4.29.A.iii**). This indicates that the stem cells at the explant edge and the quiescent progenitors migrating at the leading edge express the ΔNp63 variants. Whereas, the TAp63 transcripts (TA cell-specific epithelial marker) was found to be highly expressed by the expanding TA-cells in the middle region of the explant outgrowth (**Fig 4.29.A.v**). This confirms that the middle region is comprised of actively proliferating TA cells, while the explant edge and the leading edges are comprised of activated stem cells and quiescent precursors, as reported earlier (Mekala et al. 2015).

Further, to confirm the spatial localization and cell type specific expression of ΔNp63 and TAp63 transcripts in native corneal tissues, we performed BaseScope assays on corneo-scleral tissue sections. As expected, the basal cells of the limbus and corneal epithelium expressed high levels of ΔNp63 transcripts (**Fig 4.29.B.i**) whereas, the TAp63 transcripts were expressed at high levels in majority of the suprabasal cells of the limbus and corneal epithelium (**Fig 4.29.B.ii**).

4.2.9.8. Triple labeling and co-localization of novel PAX6 transcripts along with PAX6 and p63 proteins in limbal cultures

To further validate the nature of novel PAX6 transcript expressing cells, we checked for the colocalization of PAX6 transcripts (using BaseScope probes) along with PAX6 and p63α proteins (using specific primary antibodies) in limbal epithelial cultures. PAX6A transcript was found to be expressed abundantly in cells with high PAX6 and low p63α protein, indicating the PAX6A variant to be highly expressed in terminally differentiated cells (**Fig 4.30.i**). In contrast, PAX6B-ASΔ6 and ΔNp63 transcripts were expressed abundantly in a subset of cells with low PAX6 and high p63α protein levels, indicating that these variants are highly expressed in proliferating TACs (**Fig 4.30.ii, iv**). The PAX6A-12a and TAp63 transcripts were highly expressed in cells with variable levels of PAX6 and p63α protein, indicating that these two variants are expressed in proliferating TACs as well as in TDCs (**Fig 4.30.iii, v**).

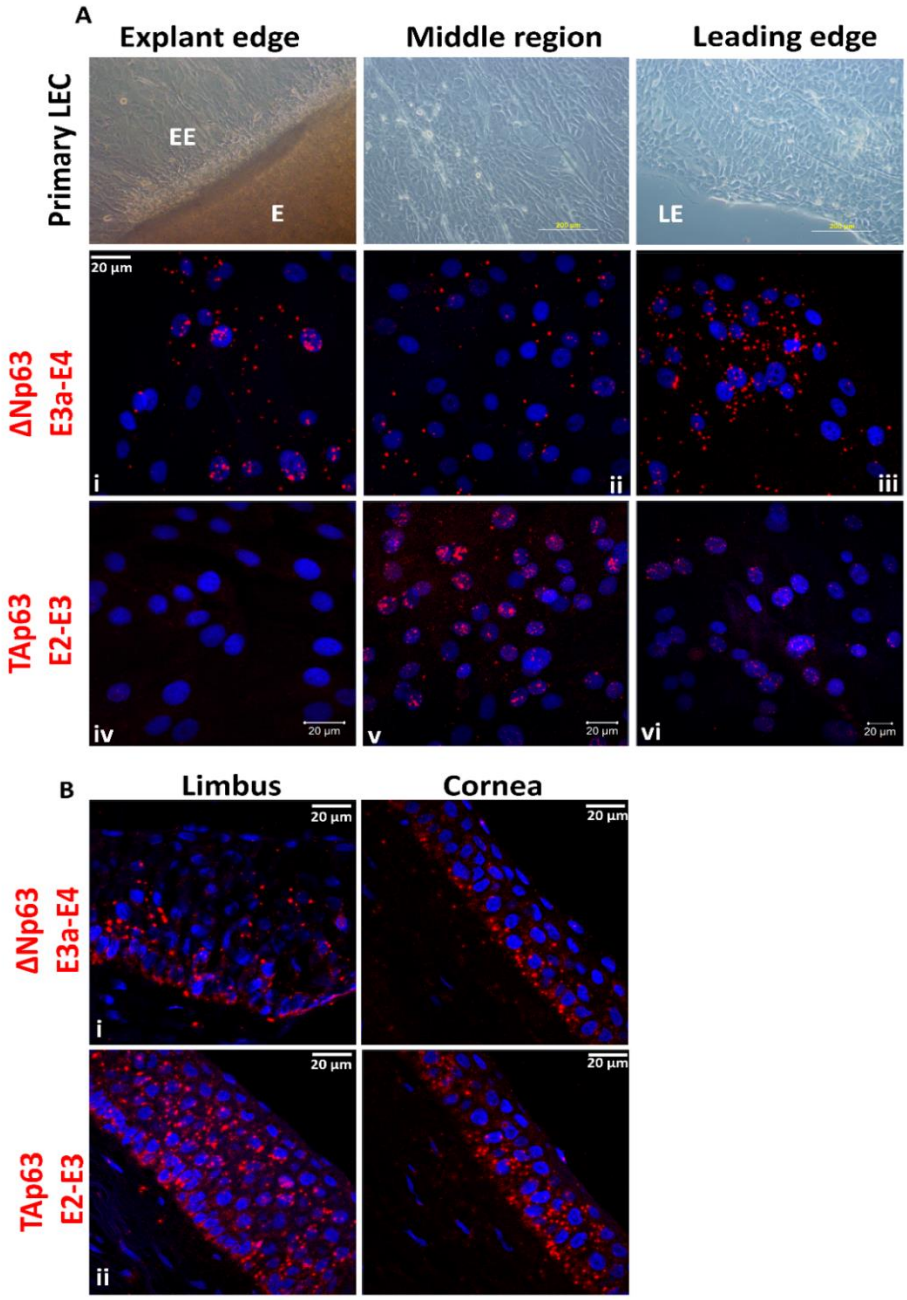

Figure 4.29: Localization of p63 transcripts in primary limbal epithelial cultures and in corneal tissue sections. *(**A**) Localization of ΔNp63 and TAp63 transcripts in limbal explant cultures. Phase contrast images showing limbal epithelial cells at different regions (explant edge, middle zone and the leading edge). The stem cell specific ⊿Np63 transcripts are expressed predominantly by the activated cells located at the explant edge (**Ai**) and also by the quiescent precursors migrating at the leading edges (**Aiii**). The TAp63 transcript is mostly expressed by the actively proliferating and expanding TACs occupying the middle zone of the cell outgrowths (**Av**). (**B**) Localization of ⊿Np63 and TAp63 transcripts in corneal tissue sections. (**Bi**) ⊿Np63 transcript is localized to the basal cells of the limbus and cornea. (**Bii**) TAp63 transcript is expressed*

in most of the suprabasal cells of the limbus and corneal epithelium. The cells and tissue sections are counterstained with DAPI to mark all cell nuclei in blue. Scale bar- 20 μm.

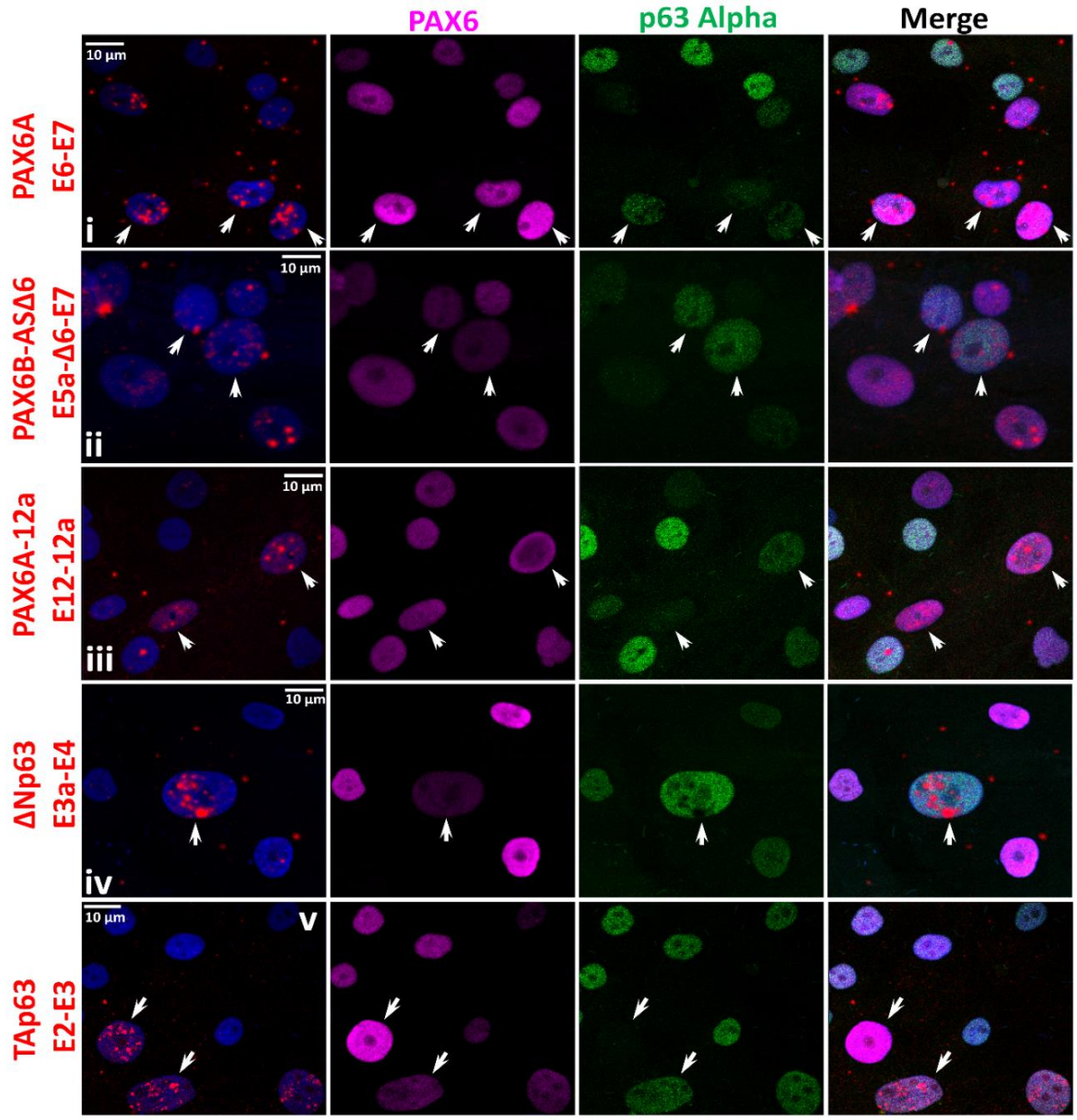

Figure 4.30: Co-localization of PAX6 transcripts along with PAX6 and p63α protein in cultured limbal epithelial cells. *BaseScope RNA-FISH combined with dual immunostained images of cultured limbal epithelial cells expressing specific PAX6 or p63 transcripts (in red) and localized with the transcription factors, PAX6 (in magenta) and p63a (in green). (**i**) Abundant PAX6A transcript expressing cells are $PAX6^{High}$ and $p63d^{Low}$. (**ii**) Abundant PAX6B-AS⊿6 transcript expressing cells are $PAX6^{Low}$ and $p63d^{High}$. (**iii**) Abundant PAX6A-12a transcript expressing cells have moderate levels of Pax6 and p63a protein expression. (**iv**) Abundant ⊿Np63 transcript expressing cells are $PAX6^{Low}$ and $p63d^{High}$. (**v**) Abundant TAp63 transcript expressing cells have both moderate to high levels of PAX6 and low to moderate*

levels of p63a protein expression. The cells are counterstained with DAPI to mark all cell nuclei in blue. Scale bar: 10 μm.

4.2.9.9. Proliferation status of cells expressing the novel PAX6 transcripts in primary limbal cultures

To mark all proliferating cells that enter the S-phase of cell cycle, limbal cultures were pulsed with 25 mM BrdU for 12-24 hrs, followed by immunolabeling using anti-PAX6 and anti-BrdU antibodies. We observed that most of the proliferating cells that incorporated the BrdU label were expressing low levels of PAX6 protein (**Fig 4.31.i**). To check the proliferation status of novel PAX6 variant expressing cells, the cultures were pulsed with BrdU and analyzed for specific PAX6 splice variant expression using BaseScope assay probes and also subsequently immunostained using anti-BrdU antibody. Majority of the PAX6B-ASΔ6 and PAX6A-12a transcript expressing cells were found to co-localize with BrdU antibody staining (**Fig 4.31.ii, iii**). This confirmed that the cells expressing the novel PAX6 splice variant are the proliferating TACs.

Taken together, the results confirm that maintaining low PAX6 protein levels is important for the maintenance of stemness, self-renewal of activated progenitors and for TAC expansion. Similarly, accumulation of high levels of PAX6 protein is required to promote the differentiation and cell cycle arrest of TACs and complete maturation of TDCs. We provide evidence that the regulated expression of novel PAX6 splice variants could play a very important role in modulating the cellular stoichiometry and relative abundance of wild type PAX6A transcripts and in turn can alter the cellular PAX6 protein levels and their fate decisions

4.2.9.10. Localization of novel PAX6 transcripts in human retina, lens and hiPSC-derived neuro-retinal cups

To check the expression of novel variants in other PAX6 expressing ocular tissues, we performed dual BaseScope staining of PAX6A transcript with PAX6B-ASΔ6 or PAX6A-12a transcript in human adult retina, lens and also in human iPSC-derived neuro-retinal cups. Only a subset of cells in the inner nuclear layer (horizontal and amacrine cells) and the retinal ganglion cell layer of the retina expressed the PAX6A variant.

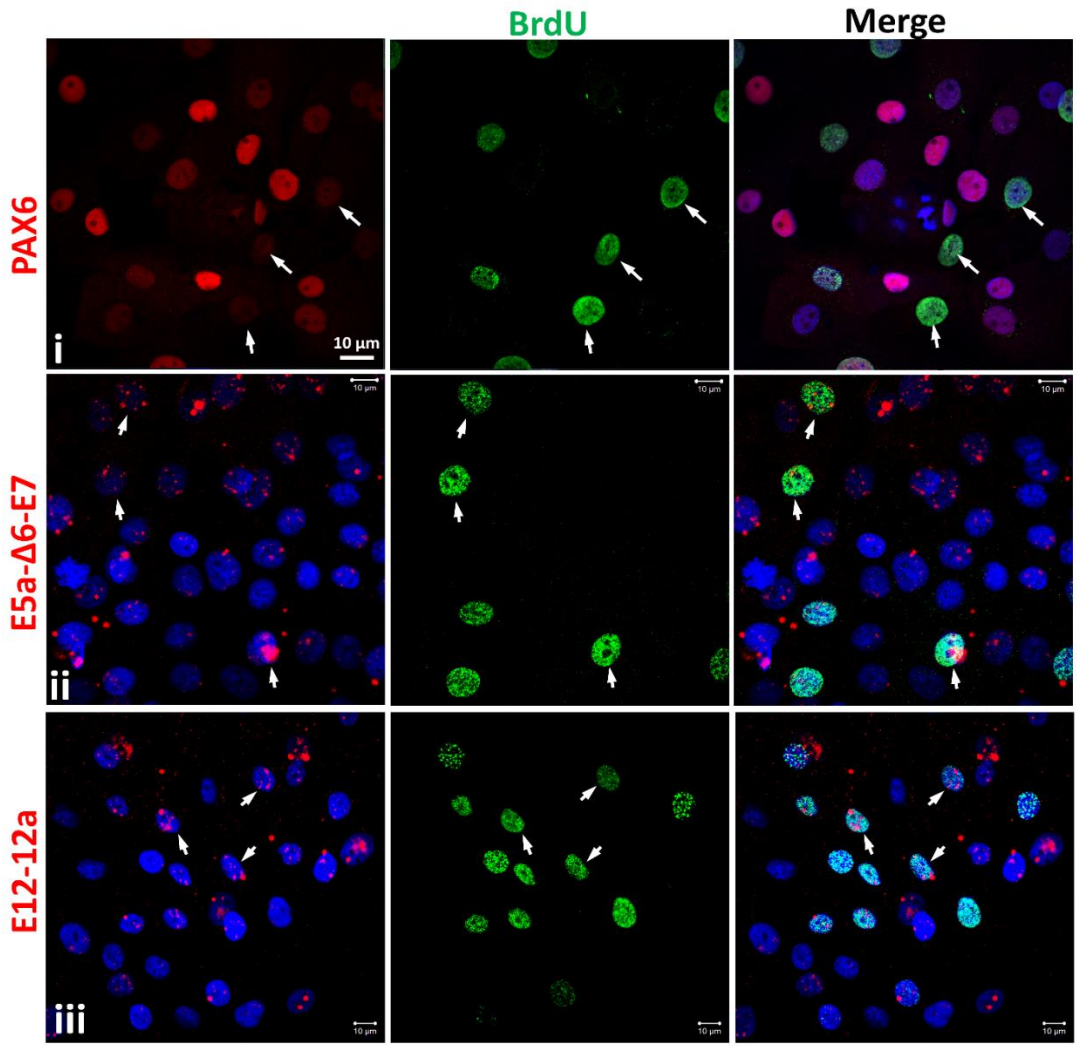

Figure 4.31: Co-localization of PAX6 transcripts and the BrdU label in cultured limbal epithelial cells. *BaseScope RNA-FISH and immunostained images showing PAX6BAS-⊿6 and PAX6-12a transcripts (in red) co-stained with anti-Brdu (in green) in primary limbal epithelial cultures. (**i**) $Pax6^{Low}$ cells are $BrdU^{+}$, $Pax6^{High}$ cells are $BrdU^{-}$. (**ii, iii**) Cells expressing either PAX6BAS-⊿6 or PAX6-12a transcripts are actively proliferating and incorporated the BrdU label. The cells are counterstained with DAPI to mark all cell nuclei in blue. Scale bar: 10 µm.*

We did not detect any signals in the outer nuclear layer, thus confirming the absence of PAX6 expression in photoreceptor cells and the specificity of BaseScope probes used in the study (**Fig 4.32.i-ii**). However, most cells of the lens epithelium majorly expressed the wild type PAX6A variant (**Fig 4.32.iii-iv**). As observed in corneal tissues, only a smaller subset of cells in the lens epithelium, INL and RGC layers of the retinal tissues expressed very low levels of the novel variants, PAX6B-ASΔ6 and PAX6A-12a, either exclusively or along with the PAX6A variant. Interestingly, in human iPSC-derived optic cups with early neuro-retinal progenitors,

the PAX6A variant was ubiquitously and abundantly expressed in all the cells. Only rare cells showed weaker signals for the novel variants, suggesting adult tissue specific roles for these variants.

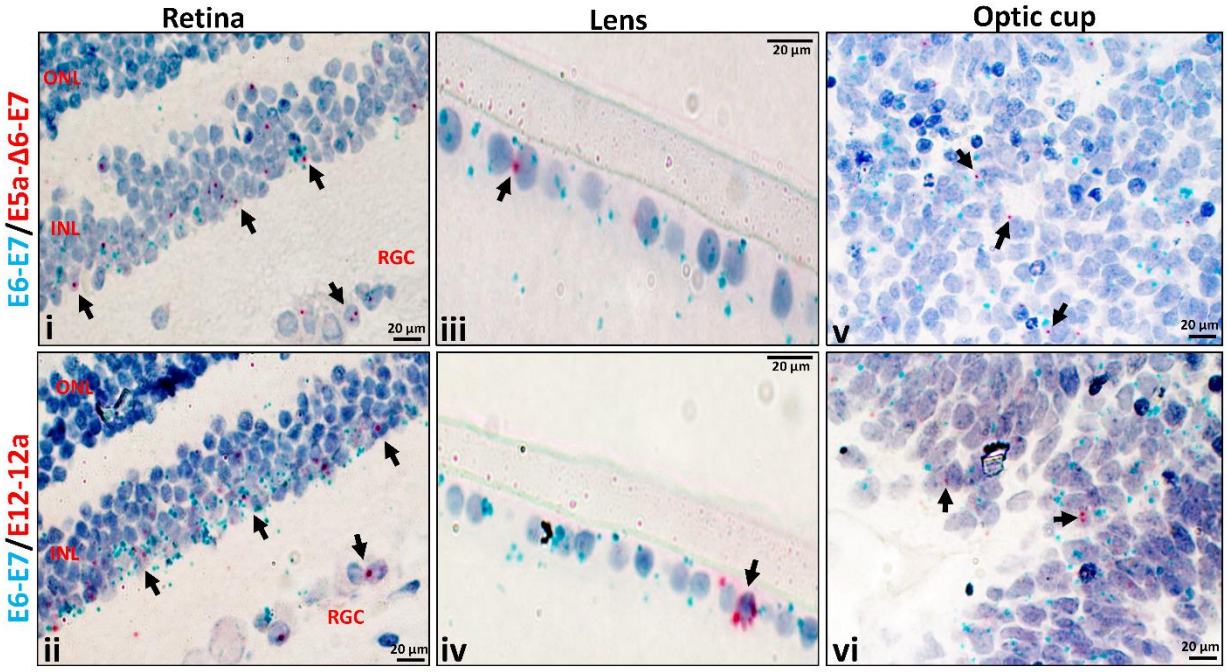

Figure 4.32: Localization of PAX6 transcripts in histological section of human retina, lens and hiPSC-derived optic cups. *Representative bright field images showing the dual expression of PAX6A transcripts (in green) and PAX6B-AS⊿6 or PAX6A-12a transcripts (in red) in the histological sections of adult human retina* ***(i, ii),*** *lens* ***(iii, iv)*** *and human iPSC-derived neuro-retinal cups/ optic cups* ***(v, vi).*** *Rare cells in the retinal inner nuclear layer, RGC layer, lens epithelium and hiPSC-OCs expressed the novel PAX6 splice variants (marked by arrows). The sections are counterstained with hematoxylin to mark all cell nuclei in blue. Scale bar- 20 µm.*

4.2.10. Cloning and expression of PAX6 isoforms as EGFP fusion proteins

To further characterize the canonical (PAX6A, PAX6B) and novel PAX6 variants (PAX6B-ASΔ6 and PAX6A-12a) at protein level, the cDNA of all PAX6 variants were cloned between XhoI and BamHI restriction sites of pEGFP-N1 vector (eukaryotic expression vector) as EGFP fusions. To validate the expression and in frame GFP fusion of all PAX6 isoforms, the constructs were transfected into NIH3T3 or HEK293T cell lines, which does not express PAX6. After 48 hours of transfection, the cells were processed for immunostaining using an anti-PAX6 antibody which can recognize all PAX6 isoforms. Similar to the canonical isoforms, the GFP fusion proteins of the novel PAX6 isoforms were stably expressed and got localized to the nucleus (**Fig 4.33.A**). The transfected cell lysates were further validated by western

blotting to detect the ectopically expressed isoforms. We employed two different antibodies to recognize the N' terminal and C' terminal regions of PAX6. The anti-PAX6 antibody with N' terminal region epitope recognized all the PAX6 isoforms with corresponding difference in their protein sizes (**Fig 4.33.B**). The anti-PAX6 antibody with C' terminal peptide epitope recognized all PAX6 isoforms, except the 12a isoform, which differs in the C' terminal end residues (**Fig 4.33.C**). Thus, the synthetic transgene constructs of the novel variants were successfully expressed *in vitro* and the GFP fusion proteins localize normally to the nucleus. However, it remains to be confirmed if the novel transcripts detected in corneal tissues also get translated into functional proteins *in vivo* or they remain as regulatory RNAs in the nucleus and influence wild type transcript abundance, translation and protein function.

4.2.10.1. Autoregualtion of *PAX6* gene expression

PAX6 expression is controlled by the pA and pB promoters and earlier studies have suggested the involvement of auto regulation of the pB promoter in brain tissues. In reporter assays, PAX6A was shown to activate the pB promoter when co-expressed together in HEK or COS1 cells (Grocott *et al.*, 2007; Okladnova *et al.*, 1998; Plaza *et al.*, 1993). We therefore aimed to evaluate the effects of different PAX6 variants in regulating the activity of eye-specific, human pA promoter. Genomatix-Matinspector analysis revealed the presence of putative PAX6 binding sites within the cloned 0.9 kb pA promoter. We further confirmed the direct binding by chromatin Immunoprecipitation assay (ChIP) of HCE cells overexpressed with GFP fusion constructs of PAX6 variants (PAX6A, PAX6B, PAX6B-ASΔ6). PCR amplification of the immuno-precipitated samples using region specific flanking primers confirmed the direct binding of PAX6A, PAX6B and PAX6B-ASΔ6 on the pA promoter (**Fig 4.33.D**). To investigate the role of PAX6 variants on its own promoters, the pA promoter-reporter construct was co-transfected along with the mammalian expression constructs encoding different PAX6 variants and was assayed in different ocular cell lines, viz; HCE, ARPE19, 661W and HLE3B. Cells lysates were prepared 48 hours post transfection to carry out luciferase reporter assay. Luciferase reporter activities revealed that the overexpression of all PAX6 isoforms (PAX6A, PAX6B, PAX6B-ASΔ6 and PAX6A-12a) repressed the pA activity significantly in all ocular cells tested (**Fig 4.33.E**), thus confirming the existence of a negative auto-feedback regulation. This could be an additional stringent regulatory mechanism that ensures optimal levels of PAX6 expression in ocular cell types.

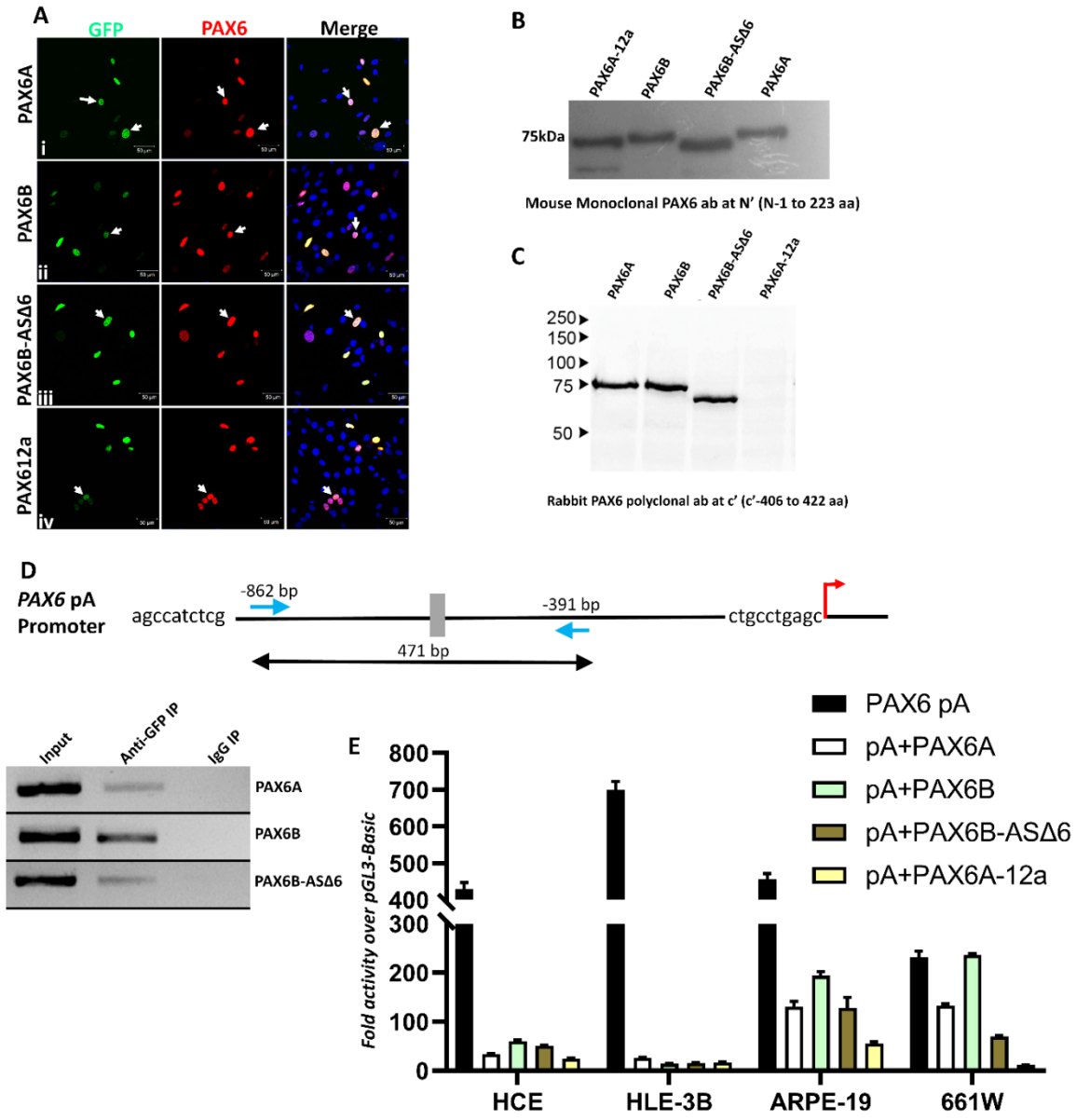

Figure 4.33: Effects of different PAX6 variants on human PAX6 pA promoter activity. *(**A**) NIH3T3 cells transfected with EGFP fusion constructs encoding different PAX6 isoforms (PAX6A, PAX6B, PAX6B-AS⊥6 and PAX6A-12a) (in green) and immunostained with anti-PAX6 antibody (in red). The cells are counter stained with DAPI to mark all cell nuclei (in blue). The GFP fusion proteins localized to the nucleus and are recognized by the antibody in all transfected cells (arrows). (**B, C**) Western blot analysis of different PAX6 isoform expressing cell lysates using a mouse monoclonal antibody raised against the N' terminal region of human PAX6 (**B**) and a rabbit polyclonal antibody raised against a short, synthetic C' terminal end peptide region of human PAX6 (**C**). (**D**) Agarose gel image of chromatin immunoprecipitation (ChIP) and pA promoter region specific PCR amplicons. Chromatin preparations of HCE cells expressing EGFP fusions of different PAX6 isoforms was immunoprecipitated using an anti-GFP antibody and the pA promoter region spanning the predicted PAX6 binding sites was PCR amplified using region specific primer sets and DNA templates purified from the chromatin inputs (positive controls), antibody-specific ChIP (test sample) and IgG ChIP complexes (negative controls). (**E**) Histogram representation of the PAX6 pA promoter*

*driven luciferase reporter activities in HCE, HLE-3B, ARPE19 and 661W cells transfected with or without gene expression constructs encoding different PAX6 isoforms. Normalized luciferase reporter values were plotted as fold activation over the pGL3-Basic vector activities. Error bars represents mean ± standard deviations. N=3. *P<0.05, **p<0.005 and ***p<0.0005.*

4.2.10.2. PAX6 isoforms and their effects on p63 promoters

p63 is a transcription factor and a key regulator of most epithelial cell types. The p63 protein exists as two different types of isoforms namely, TAp63 and ΔNp63 isoforms, depending on the alternate promoter usage. The isoforms derived from the immediate upstream promoter are the full length transcripts that encode TAp63 isoforms that has an intact N' terminal transactivation domain. Whereas, the isoforms derived from an intronic promoter encodes for the ΔNp63 isoforms, which are N' terminally truncated proteins that lacks the transactivation domain. ΔNp63α is a stem cell specific isoform and is expressed by the limbal stem cells and plays a crucial role in regulating stem cell proliferation and self-renewal (Di Iorio *et al.*, 2005; Pellegrini *et al.*, 2001). The TAp63 is mainly expressed by the activated progenitor cells and proliferating TACs of the limbus and cornea (Wang *et al.*, 2005; Lehrer *et al.*, 1998). An earlier report has also shown that PAX6 can bind to and positively regulate a 0.72 kb long rabbit ΔNp63 promoter in limbal epithelial cells (Hsueh *et al.*, 2013).

We therefore wanted to check the relative effects of PAX6A and other novel isoforms on p63 promoter regulation. For this, we PCR amplified and cloned the full length and minimal promoters of human *ΔNp63* (-1987 to +86 bp and -233 to +86 bp) and *TAp63* (-1810 to +13 bp and -671 to +13 bp) into a promoter less pGL3-Basic vector, upstream of the luciferase reporter gene, to prepare the human *ΔNp63* FL, *ΔNp63* Minimal, *TAp63* FL, *TAp63* Minimal promoter constructs (**Fig 4.34**). Each of the promoter construct was then co-transfected along with the gene expression constructs that encode different PAX6 isoforms as EGFP fusion proteins in NIH3T3 cells. The results confirmed that the PAX6B and PAX6B-ASΔ6 significantly enhanced the activity of *ΔNp63* full length promoter by 2 and 3.6 folds respectively, whereas the PAX6A and PAX6A-12a caused only marginal activation, which was not significant (**Fig 4.34.A**). In contrast, *ΔNp6*3 minimal promoter activity was uniformly repressed by all the PAX6 isoforms, indicating the absence of necessary regulatory elements within the cloned *ΔNp63* minimal promoter region (**Fig 4.34.B**). However, none of the PAX6 isoforms had any effect on the *TAp63* FL promoter, except PAX6B which significantly repressed its activity (**Fig 4.34.C**). The *TAp63* minimal promoter got moderately activated by PAX6A and PAX6B-ASΔ6 (**Fig 4.34.C, D**).). These results suggest that when compared to

the wild type PAX6A isoform, the novel splice isoforms (PAX6B and PAX6B-ASΔ6) positively regulate *ΔNp63* promoter while the *TAp63* promoter either does not respond or get repressed by PAX6B. This further suggests that the novel splice variants promote progenitor and TAC expansion.

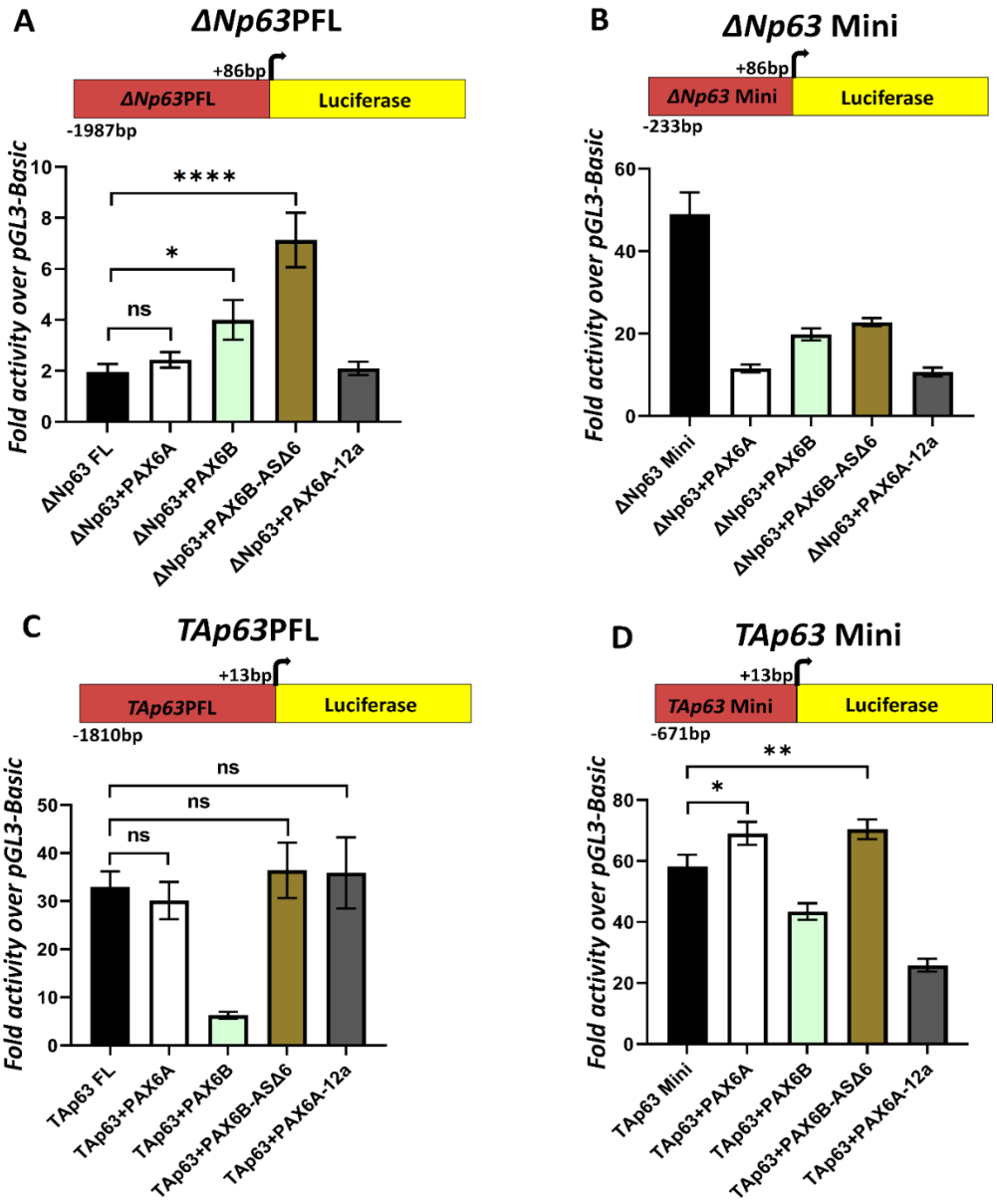

Figure 4.34: Effects of PAX6 variants on human p63 promoter activity in NIH3T3 cells. *Histogram plots representing the human ΔNp63 promoter (full length and minimal) (**A, B**) and TAp63 promoter (full length and minimal) (**C, D**) driven luciferase reporter activities, in HCE cells transfected with or without gene expression constructs encoding different PAX6 isoforms. Normalized luciferase reporter values were plotted as fold activation over the pGL3-Basic vector activities. Error bars represents mean ± standard deviations. N=3. *P<0.05, **p<0.005 and ***p<0.0005.*

4.2.10.3. PAX6 isoforms and their effect on *KRT12* and *KRT3* promoters

PAX6 is crucial for the development and maintenance of corneal epithelium and it directly regulates the expression of epithelial maturation markers such as the cornea-specific keratins, KRT3 and KRT12. An earlier report has also shown that PAX6 can bind to and positively regulate a 1 kb long mouse K12 promoter in HCE cells (Liu *et al.*, 1999). However, the differential roles of PAX6A, PAX6B and other novel splice isoforms in regulating KRT3 and KRT12 genes are largely unknown.

To check for the direct promoter binding of PAX6 variants (PAX6A, PAX6B, PAX6B-ASΔ6 and PAX6A-12a) on *KRT3* and *KRT12* promoters, we performed ChIP assay using chromatins preps obtained from HCE cells transfected with EGFP fusion constructs encoding different PAX6 isoforms. Anti-GFP antibody was used for the chromatin pull down and the total genomic DNA in the final pull down complex was purified and used a template for region-specific PCR amplifications. Using Genomatix-Matinspector software, we have identified putative PAX6 binding sites on *KRT3* (-4000 to +66 bp) and *KRT12* (-4000 to +25 bp) promoters (**Fig 4.35.A**) and designed region-specific, spanning primers for PCR amplification of the immunoprecipated DNA.

The results confirmed that all the four PAX6 isoforms tested could successfully bind and regulate the *KRT3* promoter at regions viz. -2398 to -1973 bp and -514 to +57 bp, with respect to TSS. However, PAX6A-12a uniquely binds within the -3207 to -2911 bp region (**Fig 4.35.B-E**). Similarly, all the four PAX6 isoforms tested could successfully bind and regulate the *KRT12* promoter within the region spanning -539 to +7 bp, with respect to TSS. However, only PAX6A could uniquely bind within the -3192 to -2693 bp region (**Fig 4.35.B-E*)*** and differentially regulate the K12 promoter. Taken together, the results confirmed that all PAX6 isoforms can bind directly and regulate *KRT3* and *KRT12* promoter activities.

Since we confirmed direct binding, we further analyzed the effects of PAX6 variants on KRT3 and KRT12 promoter activities. For this, we PCR amplified the full length promoters of human *KRT12* (-1045 to +19 bp) and *KRT3* (-1621 to +65 bp) genes and cloned them upstream of the luciferase reporter gene in the pGL3-Basic promoter less, reporter construct (**Fig 4.35**). These *KRT12* and *KRT3* reporter constructs were then co-transfected along with the gene expression constructs that encode different PAX6 isoforms as EGFP fusion proteins in NIH3T3 cells. After 48 hours of transfection, the cell lysates were checked for the luciferase activity. The results confirmed that only the PAX6B-ASΔ6 isoform could significantly enhance

the activity of *KRT12* promoter to about 2 folds over the basal promoter activity, while PAX6-12a repressed the promoter activity. However, the *KRT12* promoter did not respond to PAX6A and PAX6B isoforms expression (**Fig 4.35.F**). Interestingly, all the PAX6 isoforms significantly enhanced the activity of *KRT3* full length promoter by 1.93, 1.93, 3.12, 2.7 and 1.32 folds over the basal promoter activity respectively (**Fig 4.35.G**).

Taken together, we conclude that PAX6A had no effect on p63 promoters, while it significantly induced the mature-cell specific K3 promoter activity. Similarly, PAX6B uniquely repressed the TAC-specific TAp63 promoter and also activated the mature cell specific K3 promoter, suggesting the roles of PAX6A & PAX6B in promoting terminal differentiation. Interestingly, PAX6B-ASΔ6 uniquely activated the ΔNp63 promoter and also the K3 and K12 gene promoters significantly. Similarly, the PAX6A-12a uniquely repressed the K12 promoter with no effect on p63 and K3 promoters. This suggests that the PAX6B-ASΔ6 and PAX6A-12a seem to support the proliferation of activated stem cells, optimal TAC expansion without pre-mature differentiation, thus promoting proper corneal development and wound healing.

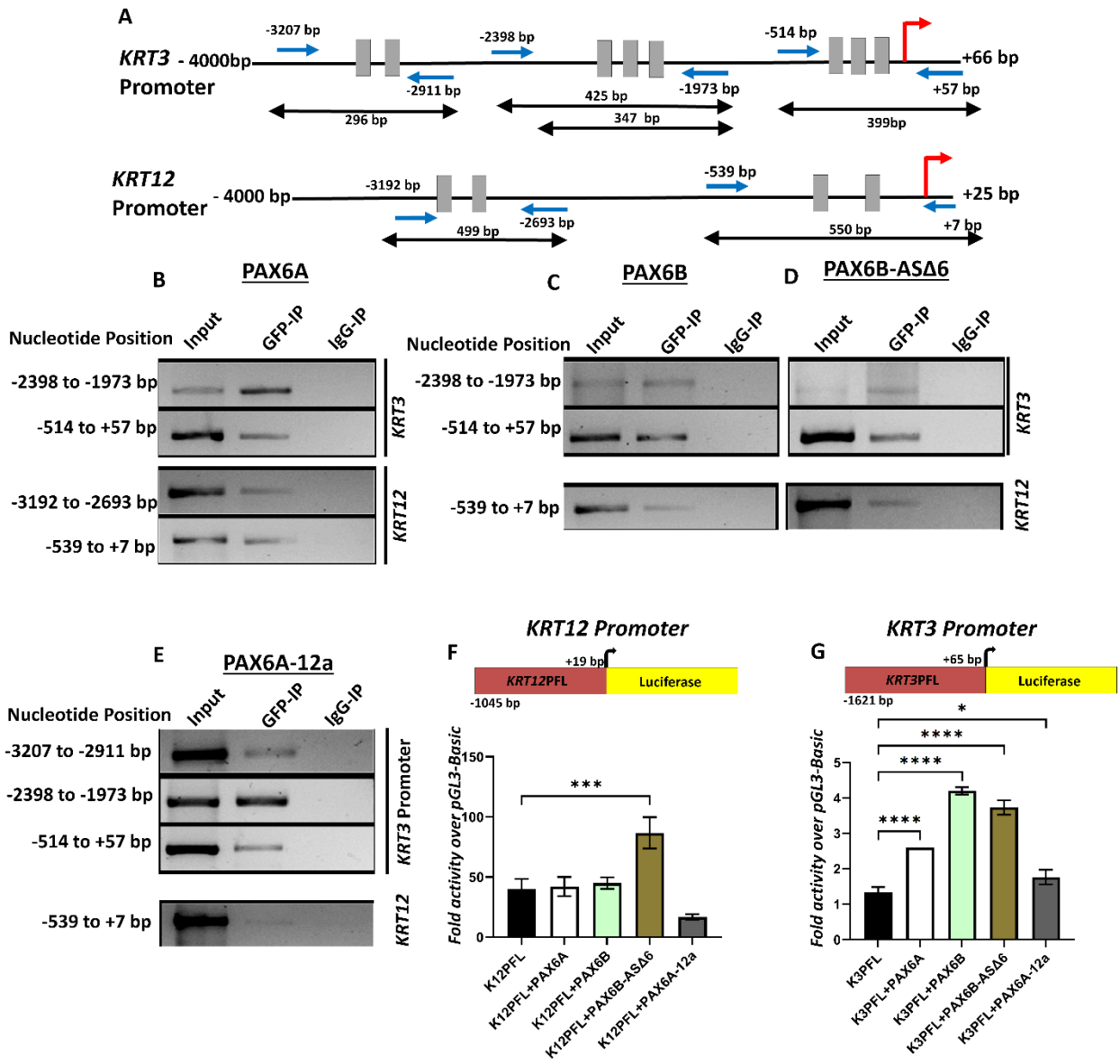

Figure 4.35: Effects of PAX6 variants on human KRT3 and KRT12 promoter activity. *(**A**) Cartoon representation of the KRT3 and KRT12 promoter regions. The boxes indicate the in silico predicted PAX6 binding sites at appropriate position within the respective promoters. The numbers indicate the nucleotide position in relation to the transcription start site. Arrow indicates the location of primers used for amplifying the immunoprecipated DNA in ChIP experiments. (**B-E**) Agarose gel images of ChIP assays to detect the direct binding of different PAX6 isoforms at different regions of KRT3 and KRT12 promoters. Chromatin preparations of HCE cells expressing EGFP fusions constructs of different PAX6 isoforms namely, PAX6A (**B**), PAX6B (**C**), PAX6B-AS⊿6 (**D**) and PAX6A-12a (**E**) was immunoprecipitated using anti-GFP antibody. Different regions of KRT3 and KRT12 promoters, spanning the predicted PAX6 binding site was PCR amplified using region specific primer sets and DNA templates purified from the chromatin inputs (as positive controls), GFP antibody-specific ChIP (test sample) and IgG ChIP complexes (as negative controls).The nucleotide positions relative to the TSS are indicated on the left side of the gel images. (**F, G**) Histogram plots representing the human KRT12 promoter (**F**) and KRT3 promoter (**G**) driven*

*luciferase reporter activities, in HCE cells transfected with or without gene expression constructs encoding different PAX6 isoforms. Normalized luciferase reporter values were plotted as fold activation over the pGL3-Basic vector activities. Error bars represents mean ± standard deviations. N=3. *P<0.05, **p<0.005 and ***p<0.0005.*

4.2.11. Global gene expression analysis and identification of differentially expressed genes in PAX6 isoform expressing HCE cells

In order to identify the differentially expressed genes upon overexpression of each of the PAX6 isoforms, we cloned the PAX6 variants into a retroviral vector, pLNCX2 downstream of the CMV promoter at the BglII and BamHI site, as N' terminus HA-tag fusion constructs (**Fig 4.36.A**). To validate the expression and in frame HA-tag fusion of PAX6 retroviral constructs, the HCE cells were transfected with individual pLNCX2_PAX6 isoform constructs. The expression and nuclear localization of HA-PAX6 fusion proteins was confirmed by immunostaining using anti-PAX6 and anti-HA-tag antibodies, where PAX6 was confirmed to co-localize with the HA-tag (**Fig 4.36.B**). The expression of the fused protein was further confirmed by transfecting the constructs into HEK293T cells, followed by cell lysis after 48 hours of transfection. Western blotting with anti-PAX6 antibody recognized HA-tag fused PAX6 isoforms of respective sizes (**Fig 4.36.C**). This confirmed that all novel and canonical variants gets expressed as stable PAX6 protein isoforms in the cell lines tested.

We further established PAX6 variant expressing stable lines of HCE cells by transducing 50% confluent cultures with recombinant retroviruses prepared from pLNCX2-CMV-PAX6 variant encoded constructs. The stably transduced cells were screened by selecting with G418 (100 μg/mL) between 4-12 days post transduction. After G418 selection, all the HCE cells showed GFP reporter expression (**Fig 4.36.D**). These stable cells were further evaluated by immunostaining using anti-PAX6 antibody (**Fig 4.36.E**).

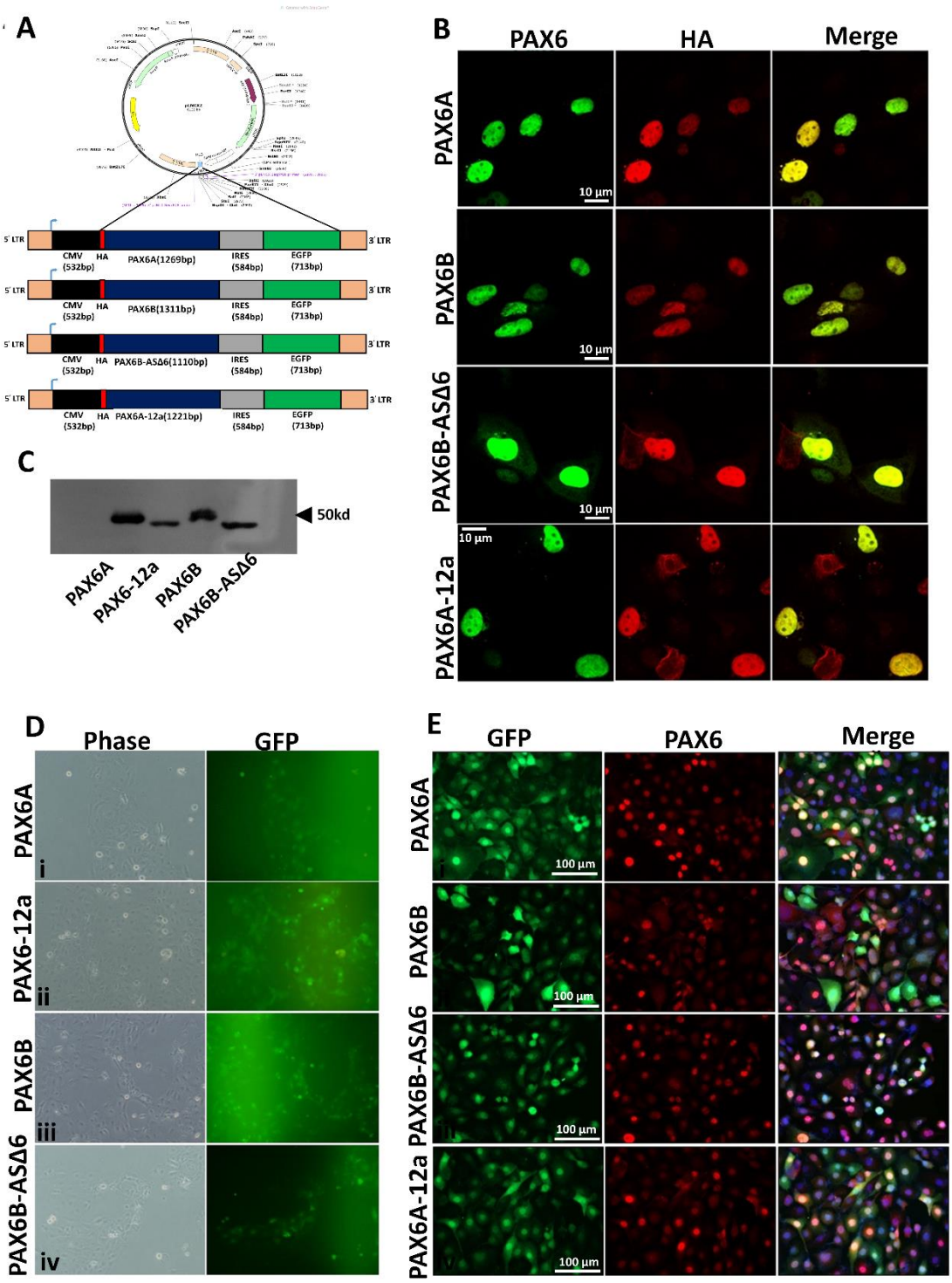

Figure 4.36: Generation of HCE cell lines stably expressing different PAX6 variants. *(**A**) Cartoon representation of retroviral gene expression constructs encoding different human PAX6 variants. CMV promoter drives the expression of N' terminally HA-tagged fusion proteins of different PAX6 variants and an IRES drives the independent GFP reporter gene expression. (**B**) Validation of different gene expression constructs and HA-PAX6 fusion protein expression in NIH-3T3 cells stained with anti-PAX6 (in green) and anti-HA (in red). (**C**) Western blot validation of HA-PAX6 fusion protein expression using cell lysates*

*prepared from HEK293T cells transfected with different PAX6 constructs and immunoblotted with anti-PAX6 antibody. (**D**) Phase contrast and green fluorescence images of HCE stable lines expressing different PAX6 variants. (**E**) Fluorescence microscopic images of HCE stable cells immunostained using anti-PAX6 antibody. All GFP positive cells (in green) stably express HA-PAX6 in the nucleus (in red). Scale bar 100 μm.*

To assess the global differences in gene regulation by individual PAX6 variants, total RNA was isolated from native HCE cells and stable lines expressing PAX6A, PAX6B, PAX6B-ASΔ6 and PAX6A-12a. The cDNAs were prepared and processed for microarray analysis using Agilant 60K gene expression arrays. cDNA samples from three biological replicates of HCE stable lines (N=3) expressing either of the PAX6 variants were independently processed for hybridization using human microarray chip. Analysis of the microarray data of HCE stable cell line expressing PAX6A and the untransduced HCE control line (lacks PAX6 expression) indicated that a total of 1155 genes were differentially expressed (491 were up and 664 genes were downregulated) with a $p \leq 0.05$ and fold change ≥ 2.0 (**Fig 4.37.A**).

HCE stable line expressing PAX6B showed 1235 genes to be differentially expressed compared to the HCE control line, 475 being downregulated and 760 being upregulated (**Fig 4.37.B**). PAX6B-ASΔ6 showed 1800 differentially expressed genes, of these 1034 genes were downregulated and 766 genes were upregulated (**Fig 4.37.C**). PAX6A-12a showed 1913 genes to be differentially expressed, of these 1107 genes were downregulated and 806 genes were upregulated (**Fig 4.37.D**).

A Venn diagram projects the number of common and differentially expressed genes (upregulated and down regulated DEGs) among all the four PAX6 variants. There were 358 (29.1%) and 213 (12.6%) commonly upregulated and downregulated genes respectively among all the four PAX6 variants (**Fig 4.37.E, F**). However, each of the individual PAX6 isoforms were also found to regulate unique set of genes (91 up and 116 downregulated genes for PAX6A, 83 up 69 downregulated genes for PAX6B, 142 up and 268 downregulated genes for PAX6B-ASΔ6, 137 up and 321 downregulated genes for PAX6A-12a) (**Fig 4.37.E, F**).

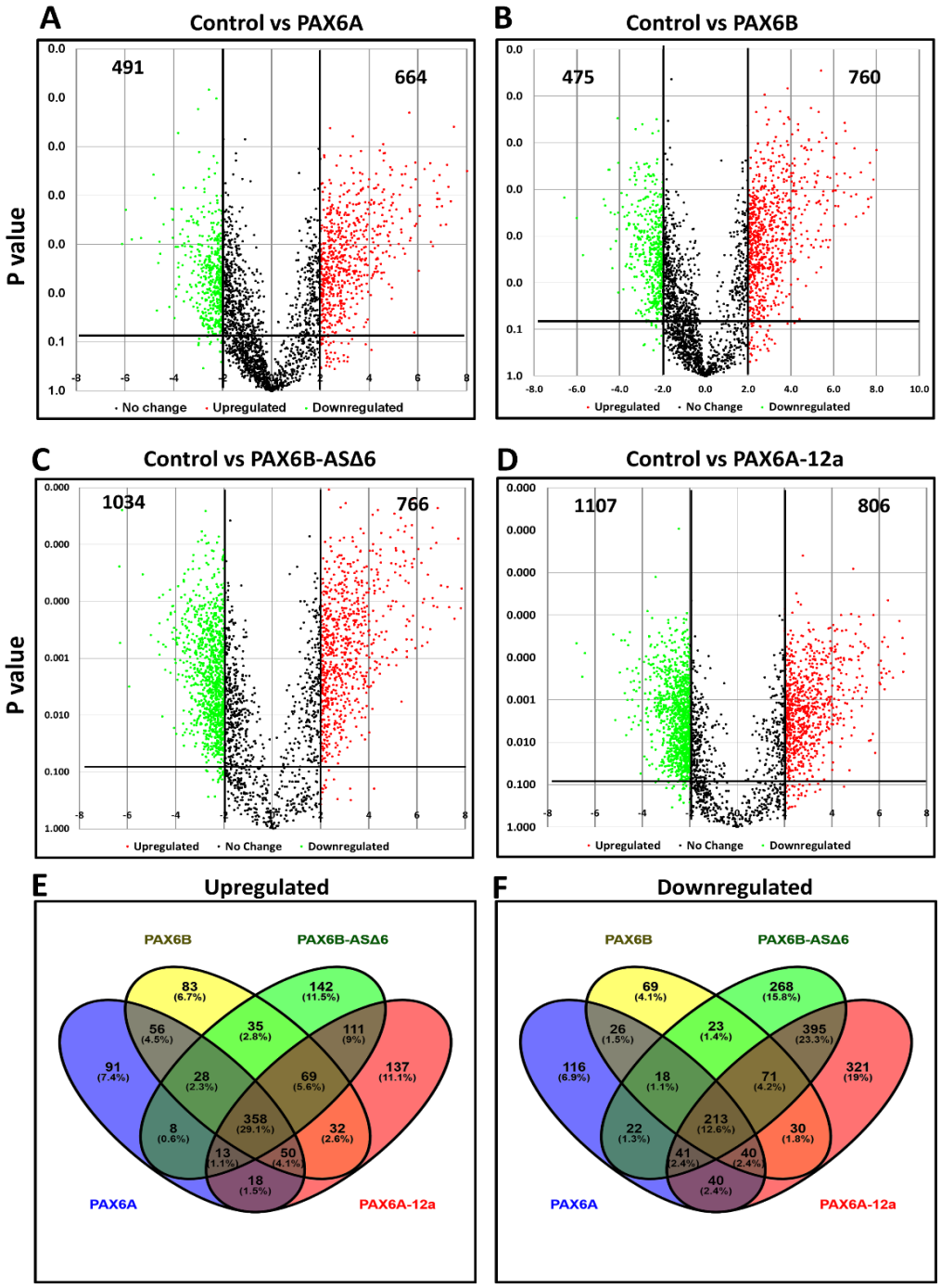

Figure 4.37: Differentially expressed genes in HCE cells stably expressing different PAX6 variants. (A-D) *Volcano plots representing the differentially expressed gene sets in different PAX6 variant expressing HCE cells when compared to the control or parental HCE cells. Genes that are up-regulated are on the right side of the axis and those that are down-regulated are on the left side of the axis. (**A**) HCE_PAX6A^{+} is compared with control HCE_PAX6^{-} (**B**) HCE_PAX6B^{+} is compared with control HCE_PAX6^{-} (**C**) HCE_PAX6B-AS⊿6^{+} is compared with control HCE_PAX6^{-} (**D**) HCE_PAX6A-12a^{+} is compared with control HCE_PAX6^{-}. Y axis represents the p value and the X axis represents fold change. Each dot represents a gene. A threshold of ≥2 fold change and P values ≤0.05*

*was considered to filter out differentially expressed genes for further analysis. Green dots represent the significantly downregulated genes; Red dots represent the significantly upregulated genes and Black dots represent the genes that are expressed similarly between the two samples compared. (**E-D**) Venn diagrams showing the common or uniquely expressed genes that are significantly upregulated or downregulated in different PAX6 variant expressing cells.*

The differentially expressed genes identified in the microarray data was further subjected to the principal component analysis (PCA) and heat map analysis. We observed that the three replicates were grouped together in the PCA plot, thus confirming that the triplicates of the control samples and all the four test samples showed similar gene expression profiles and were comparable. Also, the replicates of each of the test samples formed distinct clusters, which suggest clear differences in the global gene expression targets among the PAX6 isoforms tested (**Fig 4.38.A**). Heat map and hierarchical cluster analysis confirmed that the differentially regulated gene sets of PAX6A are different from that of PAX6A-12a, followed by PAX6B and PAX6B-ASΔ6 (**Fig 4.38.B**).

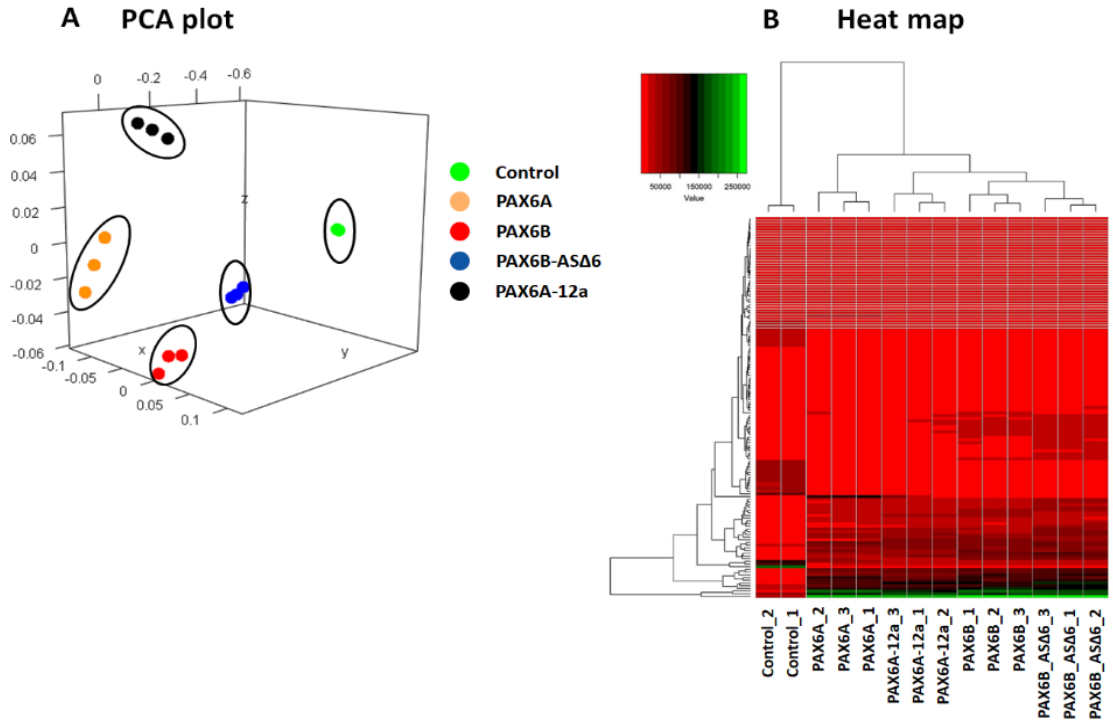

***Figure 4.38: Principal component analysis (PCA) plot and heat map of differentially expressed gene sets: (A)** Three dimensional PCA scatter plot representing the differential gene expression patterns of different samples tested. Each dot represents a single sample and dots of the same colour represent identical sample replicates namely, HCE parental control cells (green), or the HCE stable cells expressing PAX6A (orange), PAX6B (red), PAX6B-AS⊿6 (blue) and PAX6A-12a (black). (**B**) Hierarchical cluster analysis of differentially expressed genes in different samples analysed. Green color represents the*

downregulated genes, red color represents the upregulated genes and black colour indicates no change in gene expression levels.

The top twenty differentially regulated, unique gene sets corresponding to each of the PAX6 isoforms tested are given in the list of tables shown below.

Table 4.1: Top up-regulated and down-regulated genes uniquely expressed in PAX6A expressing HCE cells (≥2.0 fold change and p<0.05)

PAX6A up-regulated			
S.No	**Gene name**	**Fold change**	**P_Value**
1	*CCM2L*	5.71	0.000
2	*CD69*	4.86	0.001
3	*H2AFY*	4.65	0.000
4	*UBR4*	4.59	0.000
5	*FAM174B*	4.28	0.000
6	*ITM2A*	3.86	0.001
7	*DACH1*	3.60	0.002
8	*TPD52*	3.58	0.000
9	*KLF6*	3.36	0.000
10	*KLHL13*	3.25	0.002
11	*DHRS9*	3.24	0.019
12	*SPATA5L1*	3.20	0.002
13	*KIF3A*	3.17	0.002
14	*MED20*	2.99	0.002
15	*ZC2HC1A*	2.99	0.089
16	*COL4A4*	2.97	0.001
17	*DNAJC12*	2.69	0.000
18	*lnc-SEPT9-3*	2.64	0.007
19	*DMD*	2.62	0.002
20	*lnc-SNX18-1*	2.60	0.052

PAX6A down-regulated			
S.No	**Gene name**	**Fold change**	**P_Value**
1	*CDO1*	-2.69	0.028
2	*CLMP*	-2.66	0.008
3	*SUSD5*	-2.61	0.035
4	*PYGO1*	-2.60	0.001
5	*SAMD3*	-2.55	0.046
6	*TMPRSS15*	-2.53	0.003
7	*WSCD1*	-2.52	0.032
8	*GPC6*	-2.51	0.001
9	*PNMA2*	-2.51	0.020
10	*SOX9-AS1*	-2.48	0.034
11	*NUGGC*	-2.48	0.010
12	*OR4F15*	-2.46	0.001
13	*WFDC9*	-2.44	0.032
14	*UST*	-2.41	0.071
15	*SNORD56B*	-2.40	0.012
16	*MARK1*	-2.36	0.010
17	*SLC4A8*	-2.35	0.046
18	*CHGB*	-2.34	0.114
19	*SENCR*	-2.33	0.006
20	*MATK*	-2.31	0.018

Table 4.2: Top up-regulated and down-regulated genes uniquely expressed in PAX6B expressing HCE cells (≥2.0 fold change and p<0.05)

PAX6B up-regulated			
S.No	**Gene name**	**Fold change**	**P_Value**
1	*OTOG*	4.32	0.008
2	*PSKH2*	4.06	0.033
3	*COMMD6*	4.06	0.000
4	*CBX3*	4.04	0.000
5	*POTEM*	3.77	0.000
6	*TNK2*	3.50	0.000
7	*ARGLU1*	3.08	0.000
8	*ZNF605*	3.06	0.080
9	*BMF*	2.78	0.000
10	*RANBP2*	2.73	0.000
11	*SPINK6*	2.72	0.000
12	*HSPB9*	2.62	0.009
13	*PAIP2B*	2.38	0.002
14	*IFT74*	2.32	0.006
15	*OR5A1*	2.31	0.007
16	*SYNRG*	2.26	0.002
17	*CIRBP*	2.25	0.000
18	*OSBPL6*	2.21	0.000
19	*EPG5*	2.20	0.001
20	*MYLK*	2.20	0.000

PAX6B down-regulated			
S.No	**Gene name**	**Fold change**	**P_Value**
1	*CAMK4*	-3.11	0.000
2	*GEM*	-2.45	0.027
3	*ITGA2*	-2.43	0.083
4	*LPP*	-2.42	0.011
5	*ASB9P1*	-2.37	0.022
6	*SPACA5*	-2.30	0.021
7	*DPP9-AS1*	-2.30	0.001
8	*MEX3B*	-2.26	0.003
9	*EFNB2*	-2.22	0.006
10	*EML6*	-2.22	0.007
11	*MLLT4-AS1*	-2.22	0.013
12	*FRMD6*	-2.21	0.026
13	*TMEM170B*	-2.21	0.027
14	*SHISA2*	-2.20	0.001
15	*TRAM2*	-2.18	0.021
16	*SLC9A2*	-2.14	0.005
17	*GPR17*	-2.12	0.024
18	*STARD4*	-2.12	0.001
19	*PEG10*	-2.11	0.015
20	*PRKDC*	-2.07	0.003

Table 4.3: Top up-regulated and down-regulated genes uniquely expressed in PAX6B-ASΔ6 expressing HCE cells (≥2.0 fold change and p<0.05)

PAX6B-ASΔ6 up-regulated			
S.No	**Gene name**	**Fold change**	**P_Value**
1	*NLRP10*	3.93	0.000
2	*SSU72*	3.79	0.000
3	*PIK3AP1*	3.64	0.000
4	*GSDMC*	3.59	0.001
5	*CA3*	3.48	0.001

PAX6B-ASΔ6 down-regulated			
S.No	**Gene name**	**Fold change**	**P_Value**
1	*HMX1*	-4.09	0.000
2	*SLC30A5*	-3.17	0.094
3	*ZNF268*	-3.17	0.000
4	*NRSN1*	-3.08	0.000
5	*SH2D1A*	-3.06	0.000

6	*NR4A1*	3.40	0.001
7	*CCR1*	3.38	0.002
8	*BC021693*	3.37	0.000
9	*LGALS17A*	3.29	0.000
10	*DOK5*	3.26	0.003
11	*LRRIQ4*	3.25	0.001
12	*KCNT2*	3.13	0.009
13	*KLF3-AS1*	3.12	0.002
14	*KIAA1524*	3.07	0.001
15	*HOXB2*	3.03	0.000
16	*APOBEC3G*	3.02	0.001
17	*TRIM15*	2.99	0.006
18	*EGR4*	2.95	0.001
19	*WEE2-AS1*	2.93	0.007
20	*APCDD1*	2.92	0.018

6	*ATP11AUN*	-3.39	0.009
7	*SV2C*	-2.95	0.005
8	*MRGPRX4*	-2.95	0.000
9	*POLM*	-2.94	0.000
10	*SAMM50*	-2.94	0.227
11	*OR1A2*	-2.84	0.000
12	*PARVB*	-2.80	0.002
13	*SLC17A4*	-2.78	0.018
14	*KPNA7*	-2.75	0.009
15	*FNDC5*	-2.67	0.011
16	*P2RX6P*	-3.06	0.000
17	*RXFP3*	-2.55	0.002
18	*TNNI1*	-2.54	0.004
19	*CPXM2*	-2.53	0.001
20	*TTTY13*	-2.52	0.000

Table 4.4: Top up-regulated and down-regulated genes uniquely expressed in PAX6A-12a expressing HCE cells (≥2.0 fold change and p<0.05)

PAX6A-12a Upregulated			
S.No	**Gene name**	**Fold change**	**P_Value**
1	*TAP2*	4.36	0.000
2	*SUV420H2*	4.26	0.000
3	*BPIFB1*	3.66	0.064
4	*FAM65C*	3.54	0.001
5	*AK7*	3.50	0.003
6	*TCAM1P*	3.42	0.003
7	*CAMP*	3.31	0.002
8	*ATP2A3*	3.30	0.002
9	*GLYAT*	3.26	0.002
10	*TAF10*	3.24	0.001
11	*IFFO1*	3.14	0.000
12	*CATIP*	3.09	0.046
13	*TRAM1L1*	2.94	0.001
14	*FAM198B*	2.89	0.006
15	*IGSF9B*	2.82	0.051

PAX6A-12a downregulated			
S.No	**Gene name**	**Fold change**	**P_Value**
1	*CD72*	-4.35	0.001
2	*RNF6*	-3.30	0.003
3	*OLFML3*	-3.28	0.005
4	*DAW1*	-3.20	0.000
5	*PTPRJ*	-3.17	0.000
6	*LY6G5B*	-3.06	0.000
7	*SNORA2A*	-2.96	0.010
8	*TG*	-2.92	0.025
9	*FOSB*	-2.91	0.005
10	*RGPD4-AS1*	-2.78	0.003
11	*SLA*	-2.71	0.021
12	*CCND2-AS1*	-2.65	0.000
13	*HIGD2B*	-2.62	0.006
14	*SNORD91B*	-2.61	0.065
15	*ATAD3B*	-2.61	0.004

16	*CLEC2A*	2.80	0.112	16	*FRY-AS1*	-2.60	0.049
17	*PADI4*	2.77	0.037	17	*OR13A1*	-2.60	0.001
18	*MGAT3*	2.77	0.002	18	*OR3A3*	-2.59	0.015
19	*ALDH1A1*	2.76	0.004	19	*VN1R10P*	-2.58	0.086
20	*DMTN*	2.70	0.011	20	*CFP*	-2.54	0.009

4.2.11.1. Gene ontology analysis of the differentially expressed genes in each of the PAX6 isoform expressing cells

The DEGs were analyzed using the DAVID software to identify the enriched functional terms among upregulated and downregulated genes in HCE stables lines expressing each of the PAX6 isoforms. Genes that could not be annotated were removed from the differentially expressed gene list. The DEGs were divided into three categories of ontologies including the biological process, cellular components and molecular functions.

David analysis revealed functional clusters of genes that are involved in various biological process (**Fig 4.39.A**), molecular functions (**Fig 4.39.B**) and cellular components (**Fig 4.39.C**) and differentially expressed in individual isoform expressing cells, when compared to the HCE control cells. We examined a select list of differentially expressed and significant genes that are involved in cell cycle, cell signaling, growth factors and extracellular matrix/cell migration. Briefly, the observations confirmed the down regulation of several cell cycle genes, BMP and TGFβ signaling in PAX6A and/or PAX6B overexpressing cells. Conversely, genes involved in growth factor signalling, ECM modulation, cell adhesion and migration were up regulated in PAX6B-ASΔ6 and PAX6A-12a overexpressing cells (**Table 4.5**). This suggests that the wild type PAX6A variant seem to induce terminal cell cycle arrest and promotes terminal differentiation of TACs, whereas the novel splice variants seem to promote TAC cell proliferation and migration.

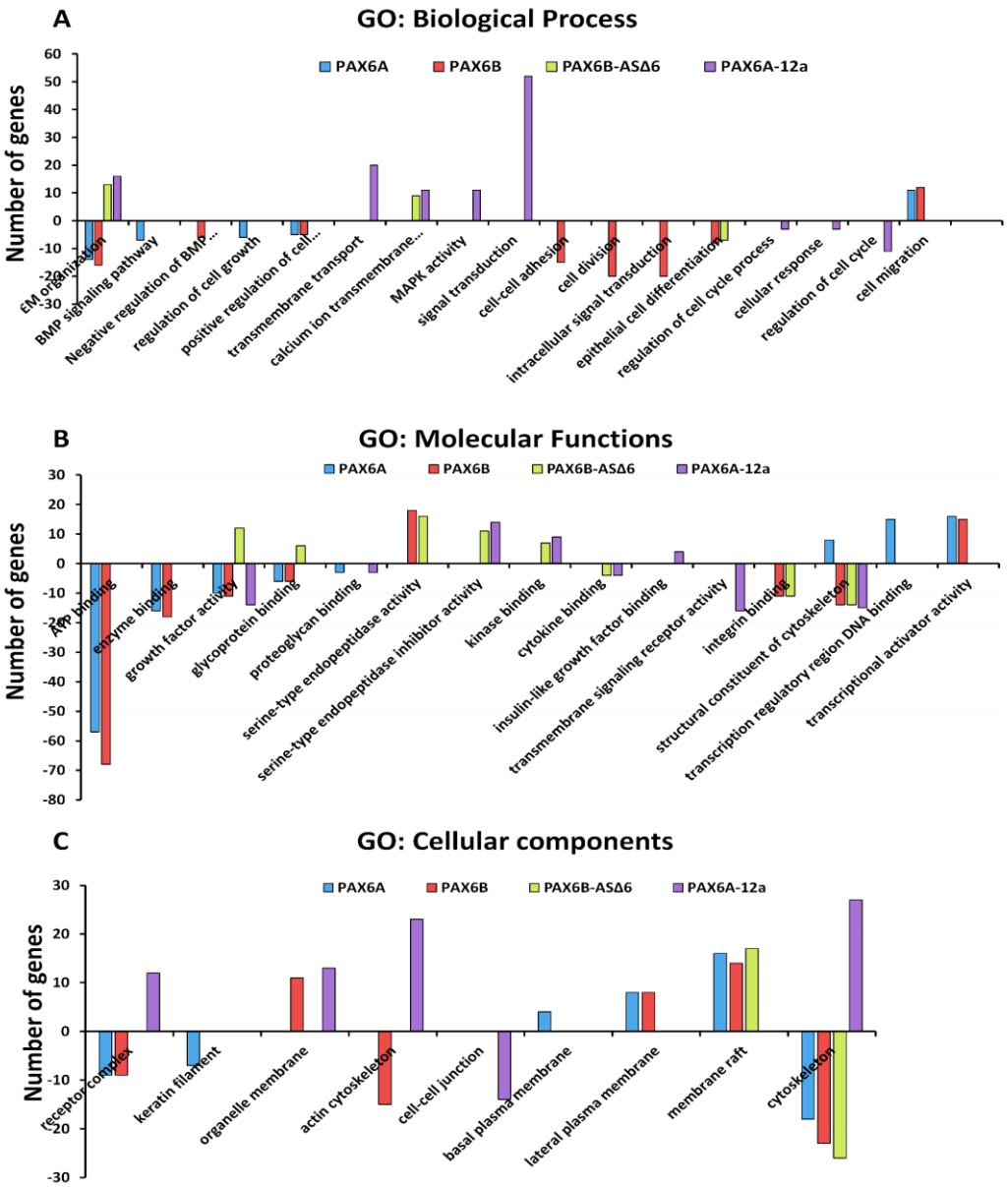

Figure 4.39: Gene ontology and functional group enrichment analysis of differentially expressed genes sets. *Histogram plots representing the number of up or downregulated genes that belongs to different functional groups such as (**A**) Biological process (**B**) Molecular functions (**C**) Cellular components, in PAX6A or PAX6B or PAX6B-AS⊿6 or PAX6A-12a expressing HCE cells.*

Taken together, we provide evidence that the choice of alternate promoters and tissue-specific enhancers, unique splicing mechanisms leading to the expression of novel dominant negative variants together tightly regulate PAX6 levels and cellular functions and ensures normal corneal development and homeostasis.

Table 4.5: Select list of genes under different biological processes that are differentially regulated in different PAX6 isoform expressing cells

	PAX6A	PAX6B	PAX6B-ASΔ6	PAX6A-12a
Cell cycle genes				
Cyclin A2(CCNA2)		down		
Cyclin B1(CCNB1)		down		down
Cyclin D2(CCND2)		down		
Cyclin dependent kinase 6(CDK6)		down		
Cell division cycle 20(CDC20)		down		
BUB1 mitotic checkpoint serine/threonine kinase(BUB1)		down		
Polo like kinase 1(PLK1)				down
Growth arrest specific 2 like 1(GAS2L1)				down
WNT5B			down	
WNT3A				up
Cell signalling				
Noggin(NOG)	down			down
Bone morphogenetic protein 5(BMP5)	down			down
Bone morphogenetic protein 1(BMP1)			up	
Transforming growth factor alpha(TGFA)			up	
Transforming growth factor beta receptor 1(TGFBR1)		down		
Growth factors				
Growth differentiation factor 10(GDF10)	down	down		down
Growth differentiation factor 11(GDF11)	down	down		down
Growth differentiation factor 6(GDF6)	down	down		down
Growth differentiation factor 15(GDF15)			up	up
Colony stimulating factor 2(CSF2)	down		up	up
Epithelial mitogen(EPGN)	down			
ECM/Cell Migration				
WNT1 inducible signaling pathway protein 2(WISP2)				up
MMP1				up
MMP3				up
Matrix metallopeptidase 11(MMP11)			up	up
Matrix metallopeptidase 13(MMP13)			up	up

Matrix metallopeptidase 7(MMP7)			up	up
TNF alpha induced protein 3(TNFAIP3)			up	
TNF receptor superfamily member 11b(TNFRSF11B)			up	
Tumor necrosis factor superfamily member 10(TNFSF10)			up	up
Tumor necrosis factor superfamily member 9(TNFSF9)			up	up
Collagen type IV alpha 3 chain(COL4A3)			up	
Extracellular matrix protein 2(ECM2)			up	
Integrin subunit alpha L(ITGAL)			up	
Intercellular adhesion molecule 1(ICAM1)			up	up
Intercellular adhesion molecule 4 (ICAM4)			up	up
Collagen type V alpha 1 chain(COL5A1)	down	down		
Collagen type V alpha 3 chain(COL5A3)	down			
Collagen type XIX alpha 1 chain(COL19A1)	down			
Collagen type XIII alpha 1 chain(COL13A1)		down		
Fibrillin 1(FBN1)	down	down		
Fibrillin 2(FBN2)	down	down		
Integrin subunit alpha 10(ITGA10)	down			
Integrin subunit alpha E(ITGAE)	down	down		
Integrin subunit alpha 6(ITGA6)		down		
Thrombospondin 1(THBS1)	down	down		
Lysyl oxidase like 1(LOXL1)		down		
Lysyl oxidase(LOX)		down		
Serpin family E member 1(SERPINE1)		down		
Junctional adhesion molecule 3(JAM3)		down		

CHAPTER 5

DISCUSSIONS

5: Discussions

Pax6 is a well-studied member of the paired box family of transcription factors and a master regulator of eye development. Mutations in the gene and loss of protein expression in developing embryos resulted in severe eye developmental anomalies (Quiring *et al.*, 1994; Hill *et al.*, 1991). Conversely, ectopic expression of Pax6 induced eye-like structures in lower vertebrates. Also, overexpression in rodent eyes resulted in abnormal lens and corneal development and affected adult tissue homeostasis (Onuma *et al.*, 2002; Chow *et al.*, 1999; Altmann *et al.*, 1997; Halder *et al.*, 1995). Thus, it is clear that a critical regulation of PAX6 dosage and spatio-temporal expression is important during embryonic eye development and in adult tissue homeostasis. This is mediated by complex gene regulatory mechanisms involving the usage of multiple alternate promoters, enhancers and the expression of different protein isoforms. Here, we aimed to elucidate the mechanisms of PAX6 gene regulation, specifically in the corneal surface epithelium.

Distal PAX6-pA promoter and Wnt signals regulate PAX6 expression in the eye

To study the promoter level regulation of human PAX6, the distal *PAX6* pA (-800 to +73 bp) (Okladnova *et al.*, 1998) and the intronic *PAX6* pC (1.2 kb) regions (Kim *et al.*, 2008; Lakowski *et al.*, 2007; Kim *et al.*, 2006) were PCR amplified from human genomic DNA and cloned upstream to the luciferase reporter gene in pGL3 basic vector (**Fig 4.1.C**). To know the enhancer specific regulation of pA in ocular cells, a previously reported OSE enhancer region (-4179 to -3603 bp) (Dimanlig *et al.*, 2001; Kammandel *et al.*, 1999; Williams *et al.*, 1998) was also cloned upstream to the pA promoter in pGL3-Basic vector (**Fig 4.1.C**).

The luciferase reporter assays confirmed that *PAX6*-pA is the dominant promoter in the eye and is highly active in human corneal epithelial cells (HCE), human retinal pigmented epithelial cells (ARPE-19), mice cone precursor cells (661W) and in human lens epithelial cells (HLE-3B). In most of these ocular cell lines, *PAX6*-pC was found to be a weak promoter, suggesting its minor role in the regulation of PAX6 expression in adult ocular tissues. On the other hand, OSE enhancer was found to mildly repress *PAX6*-pA activity in HCE cells, whereas, it significantly induced the activity of *PAX6*-pA in lens and retinal cell types (**Fig 4.1.D**). This confirms that the OSE enhancer positively regulates pA activity to induce PAX6 expression in lens epithelium, while it simultaneously represses the promoter in corneal epithelium, thus ensuring proper anterior segment development. It is possible that the pA promoter repression

by OSE enhancer may be crucial in regulating PAX6 levels for proper corneal epithelial cell proliferation and differentiation and needs further validation.

In primary limbal epithelial cells, *PAX6* pA was highly active in the migrating cells at the leading edge of explant cultures and in the 3D sphere clusters in suspension cultures (**Fig 4.2.B.i.ii**). These cells were confirmed to be TACs with positive expression of p63, PAX6 and BrdU, while were negative for the corneal differentiation marker KRT3, indicating that pA promoter is highly active in proliferating transiently amplifying limbal epithelial cells (**Fig 4.4**). However, pC activity was not observed in primary limbal cultures, thus confirming that this alternate promoter has no major role in regulating corneal epithelium (**Fig 4.2.B.iii**).

The activity of pA was also evaluated during early eye development in hiPSC derived ocular structures. The pA promoter was found to be highly active in iPSC derived neuro-retinal cups, RPE cells, ocular surface ectodermal cells and in lens like structures (**Fig 4.3.B.C**). In contrast, the pC promoter was found to be exclusively active in developing optic cups and neuro-retinal cells, thus confirming it's specific role in early retinal development (**Fig 4.3.D**).

Wnt signaling has diverse effects on different cell types and tissues. In human and mouse ESCs, Wnt activation helps in the self-renewal of hESCs (Anton *et al.*, 2007; Sato *et al.*, 2004). In adult tissues, Wnt specific proteins are involved in the regulation of self-renewal and differentiation of neural SCs (Kalani *et al.*, 2008; Lie *et al.*, 2005), skin SCs (Huelsken *et al.*, 2001; Zhou *et al.*, 1995) and intestinal SCs (Fevr *et al.*, 2007; Pinto *et al.*, 2003). Wnt signaling is also known to play an important role in regulating several genes at different stages of eye development and also in regulating limbal stem cell proliferation and differentiation (Gonzalez *et al.*, 2019; Lu *et al.*, 2012; Nakatsu *et al.*, 2011; Mukhopadhyay *et al.*, 2006). Therefore, in this study the consensus binding sites of key transcription factors and co-factors such as, PAX6, Kaiso, TATA box, CCAAT box, C/EBP and TCF/LEF1 immediately upstream of the reported transcription start site of cloned human PAX6 pA promoter was predicted using Genomatix-Matinspector software (**Fig 4.1.B**). An earlier study has reported that the mouse Pax6 proximal promoter is a direct target of canonical wnt signaling in radial glial stem cells (Gan *et al.*, 2014). In this study also, we observed that Wnt activation upregulates the expression of *PAX6* pA and OSE_*PAX6* pA activity in corneal (HCE) and lens epithelial cell (HLE-3B) types, but was repressed in retinal cells (ARPE19 and 661w) (**Fig 4.6**). In cornea and lens epithelial cells, activation of pA promoter by Wnt could possibly be mediated by binding of β-

catenin to the TCF/LEF1 site. This indicates the differential regulation of *PAX6* pA and OSE enhancer by Wnt signals in different ocular tissues.

In the absence of β-catenin, TCFs are known to recruit HDACs (Histone deacetylases) to the TCF/LEF1 consensus sites, and maintains the target promoters in a repressed state. Repression of HDACs therefore resulted in significant activation of *PAX6* pA in all the ocular cell types, with synergistic enhancement in the activity of pA in the presence of OSE enhancer (**Fig 4.6**). This confirmed that *PAX6* pA and OSE enhancer are tightly regulated by HDAC-dependant mechanisms and are maintained in a highly repressed state in HCE cells.

The direct interaction between the β-catenin and TCF/LEF1 sites of pA promoter was further validated by Chromatin Immunoprecipitation (ChIP) of β-catenin bound chromatins followed by region specific PCR of ChIP complex, thereby suggesting the direct involvement of Wnt signaling in regulating the pA promoter in primary limbal cells (**Fig 4.7.B**). Matinspector analysis also revealed a couple of KAISO repressor binding sites within the pA promoter. The repression of pA through Kaiso was checked by ChIP-PCR, thereby confirming the direct binding of HDACs and Kaiso within the *PAX6* pA promoter (**Fig 4.7.B**). Therefore, *PAX6* pA promoter is tightly regulated and is maintained in a repressed state by the recruitment of HDACs and Kaiso repressor complexes in the absence of Wnt signals.

Further, to investigate the direct effect of Wnt on *PAX6* pA promoter regulation, the consensus TCF/LEF1 site was disrupted by site directed mutagenesis. The mutant *PAX6* pA was found to be significantly repressed as compared to Wt *PAX6* pA promoter. Upon activation of canonical Wnt pathway using BIO, the Wt *PAX6* pA showed significant activation, while the mutant *PAX6* pA failed to respond. Upon HDAC inhibition using VPA, the Wt as well as the mutant *PAX6* pA promoter was significantly activated (**Fig 4.7.E**). This again suggests that *PAX6* pA promoter is regulated both by Wnt signals and HDAC dependent mechanisms directly through TCF/LEF1. These results demonstrate that the distal *PAX6*-pA promoter is a direct downstream target of Wnt/β-catenin signalling in the corneal epithelium and suggest its possible involvement in LSC regulation. The existence of an additional repressor complex mediated regulation may be necessary to enforce a tight control on the promoter activity and to allow only optimal levels of PAX6 expression in proliferating limbal stem cells. An earlier study has also demonstrated that the constitutive activation of wnt signals in β-catenin gain of function mutants have resulted in the downregulation of PAX6 and

cornea-specific keratin, CK12, thereby severely affecting normal corneal epithelial maintenance (Zhang *et al.,* 2010).

Wnt signaling also induced the activity of PAX6 target gene promoters *KRT12* and *KRT3* (the corneal epithelium-specific keratins). However, HDAC inhibition had no effect on the basal promoter activities. (**Fig 4.8.B.C**). Similarly, Wnt activation resulted in significant activation of *TAp63* promoter, but had no effect on the stem cell specific *ΔNp63* promoter (**Fig 4.8.D.E**). In contrast, HDAC inhibition significantly induced the activation of both *TAp63* and *ΔNp63* promoters in HCE cells (**Fig 4.8.D.E**). This suggests that Wnt activation enables the expansion of TACs and also promote their differentiation, whereas HDAC inhibition promotes the expansion and maintenance of stem/progenitor cells, without inducing their differentiation.

The dosage and expression levels of PAX6 are critically regulated and any alterations severely affect progenitor cell proliferation and specification during development (Hsieh *et al.*, 2009). In corneal tissues, the fully mature post-mitotic cells forms the apical layers and the proliferating and differentiating transiently amplifying cells (TACs) forms the suprabasal layers of the stratified squamous epithelium and they express high levels of PAX6 and KRT3/12 (**Fig 4.9.A.i.ii**). Majority of the basal cells are known to be the activated stem cells and undifferentiated TACs that are completely negative for KRT3/12. These undifferentiated basal cells express high levels of the epithelial stem cell marker, p63α and the NGF receptor, p75NTR (**Fig 4.9.A.iii, B.i**). Though PAX6 is ubiquitously expressed in all cells of limbal and corneal epithelium, the undifferentiated basal cells expressed relatively low levels of the protein. Also, the putative stem cells at the limbus that are in close proximity to the stromal cells and melanocytes (the niche cells) expressed high levels of p63α and low levels of PAX6 (**Fig 4.9.C.i.ii**). This suggests that the maintenance of low PAX6 levels is critical to allow sufficient expansion of the activated stem cells, before they undergo terminal differentiation.

We also observed that β-catenin is mostly membrane localized and only a small fraction of cells in the limbal suprabasal layers express it in the nucleus (**Fig 4.10.i**). This suggests that canonical Wnt signaling is only transiently active in the limbal suprabasal cells, which allows for stem cell self-renewal and the expansion of activated TACs. Wnt activation in turn induced the pA promoter mediated expression of PAX6, TA promoter mediated expression of p63 (marker for TAC cells) and also activates the KRT3/KRT12 genes (marker for corneal epithelial differentiation), thus enabling TAC proliferation and differentiation. Localized expression of secreted wnt inhibitory proteins such as Dickkopf (DKKs), secreted Frizzled

Related Proteins (sFRPs) and Wnt inhibitory factor 1 (Wif1) are known to negatively regulate and block canonical wnt signals. DKK2 null mice shows impaired corneal development, with skin-like epithelial transformations (Mukhopadhyay *et al.*, 2006). Our histology studies have confirmed the expression of DKK2 at the limbus, which could ensure low wnt signals at the basal cells (**Fig 4.10.ii**). Earlier studies have shown that the ciliated and non-ciliated cells respond differently towards wnt stimulation and KIF3A, a ciliary protein was shown to destabilize β-catenin and dampen the canonical wnt signals in ciliated, quiescent cells (Corbit *et al.*, 2008). Interestingly, the neatly arranged columnar basal cells at the limbus expressed primary cilium (data not shown). This suggests that the stem cells at the limbal niche are ciliated and this could be another redundant mechanism to block wnt signals and to maintain their quiescent state.

An earlier study has shown that lithium chloride treatment of limbal cultures activated the wnt signals and enabled the expansion of limbal stem cells (Nakatsu *et al.*, 2011). Another report has established a role for WNT7a and FZD5 in regulating limbal stem cells upstream of PAX6 (Ouyang *et al.*, 2014). Here, we establish that the *PAX6*-pA is a direct target of canonical wnt signaling and it gets transiently activated in a sub-set of PAX6 Low limbal supra-basal cells, which induces their proliferation, migration and differentiation. Wnt-induced expression of PAX6, TA-p63, K3 and K12 in turn triggers post-mitotic arrest and terminal differentiation of TACs. However, the Wnt signals are inactive at the limbal niche and this helps to maintain the stem cells in a quiescent state. Conversely, the constitutive activation of wnt signals at the limbus (or in primary cultures) would result in complete activation of stem cells, high levels of PAX6 expression, insufficient TAC expansion and premature terminal differentiation. This would result in total depletion of the reserve stem cell pool and defective corneal epithelial development, as seen in DKK2 null mice and PAX6 overexpressing (PAX77) mice (Manuel *et al.*, 2008; Mukhopadhyay *et al.*, 2006). However, a Wnt-independent activation of PAX6-pA by VPA treatment enables sufficient TAC expansion without triggering differentiation.

Taken together, we conclude that *PAX6*-pA is the major promoter that drives PAX6 expression in the eye and is directly regulated by canonical Wnt signaling in a sub-set of limbal supra-basal cells, which are the activated stem cells and mediate their expansion and differentiation.

Novel splice variants modulate PAX6 protein levels and regulate limbal epithelial proliferation and differentiation:

The relative stoichiometry of two known alternately spliced forms of PAX6 (PAX6A and PAX6B) (Fig 4.13.ii-iv) gets altered during the course of brain and lens development and are known to differentially regulate target genes and cellular functions (N. Davis *et al.*, 2009; Azuma *et al.*, 2005; Singh *et al.*, 2002; W. Zhang *et al.*, 2001). Here, we aimed to understand the relative expression and cell type specific expression of different PAX6 isoforms in stem cell derived and adult ocular tissues.

By tissue-specific transcript analysis, we identified four more novel transcripts of PAX6 in addition to PAX6A and PAX6B mRNA in human eye tissues. These novel transcripts that are generated by alternative splicing events at two major splicing hotspots near Exon 6-7 and Exon 12-13 splice junctions (**Fig 4.12, 4.13, 4.14**). We have named them as PAX6A-AS-Δ6, PAX6B-AS-Δ6, PAX6A-Δ6 and PAX6A-12a, which carry in-frame deletions, affecting either the N-terminal paired domain-mediated DNA binding or the C-terminal PST domain-mediated transactivation functions. Singh et al showed that any structural change/s in the N or C terminus of paired domain influences the DNA binding of homeodomain of PAX6 (Singh *et al.*, 2000). All these predicted PAX6 AS variant proteins could have distinct DNA binding activities and different target genes. In Pax6 5a isoform, insertion of 14 amino acids disrupts the PAI subdomain, while the intact Red subdomain and homeodomain for DNA binding regulates a different set of downstream target genes (Kozmik *et al.*, 1997; J. A. Epstein *et al.*, 1994). Presence of alternatively spliced transcripts of Pax6 exon 6 have also been reported in the neuroretina of quail and bovine eyes (Jaworski *et al.*, 1997; Carriere *et al.*, 1995). This indicates that splice donor site is conserved across all the species. Paired less Pax6 variant has been demonstrated to be highly expressed in brain (Mishra *et al.*, 2002), neural retina, but not the developing lens and cornea (Kim *et al.*, 2008, 2006). Another novel splicing variant Pax6 (s) has been reported by Zhang et al in 2010, in which PST rich transactivation domain is truncated (Y. Zhang, Y. Yamada*, et al.*, 2010). Splicing mutations in intron 12 have also been identified in aniridia patients that results in disturbance of splicing and could lead to elongation of 3' mRNA due to skipping of stop codon (Weisschuh *et al.*, 2012; Aggarwal *et al.*, 2011). We have also confirmed that these novel splice variants were majorly driven by the pA promoter in most ocular tissues, with significantly higher expression in the limbus and cornea (**Fig 4.16.B**). Some basal expression was also found to be driven by the pB promoter, but was

significantly less as compared to pA (**Fig 4.16.C**). The pC promoter activity in retinal cells resulted in only the PAX6A and PAX6B transcripts (**Fig 4.16.D**).

Many alternatively spliced variants are weakly expressed in most tissues. This low abundance is a feature of many transcription factors that are involved in the regulation of important cellular processes (Vaquerizas *et al.*, 2009). In this study, we analyzed the native expression levels and the relative abundance of different PAX6 variants in different ocular tissues. When we checked for their absolute expression, PAX6A was highly expressed in all ocular cells tested except the corneal epithelium (**Fig 4.17.A**). Interestingly, the alternately spliced PAX6B-ASΔ6 was found to be abundantly expressed only in the corneal epithelium (**Fig 4.17.B**). The PAX6A-12a variant was found to be the least abundant form and was expressed at 10-fold lower levels when compared to PAX6A and PAX6B. In spite of low abundance, PAX6A-12a expression was significantly higher in the limbal and corneal epithelium (**Fig 4.17.C**). When the relative abundance of all transcripts was compared with PAX6A expression, we observed that the alternatively spliced variants viz; PAX6B, PAX6B-ASΔ6 and PAX6A-12a are expressed at significantly higher levels in the native corneal epithelium, while the wild type PAX6A variant forms the major transcript in native limbal epithelium and the neuro-retina. Similarly, when we checked the expression of these variants in developing human iPSC-derived retinal cell types, the RPE cells expressed significantly higher amounts of PAX6B when compared to PAX6A. However, PAX6A forms the major transcript in iPSC-derived neuro-retinal cups (**Fig 4.18**).

Overexpressed of Pax6-wt and Pax6-5a isoforms could positively autoregulate the endogenous Pax6 promoter in NIH3T3, Neuro2D cell lines and in developing telencephalon (Manuel *et al.*, 2007; Pinson *et al.*, 2006). This autoregulation was mediated by the direct binding of PAX6 protein to the Pax6 response elements within the OSE enhancer region (Aota *et al.*, 2003). In this study, the novel and reported isoforms were found to be directly interacting with the endogenous pA promoter, and when co-expressed, they significantly repressed the *PAX6*-pA promoter activity, suggesting the existence of a tight negative auto-feedback regulation to maintain optimal PAX6 levels in the cells (**Fig 4.33**).

Using RNA-FISH (BaseScope assay) experiments, the novel PAX6B-ASΔ6 and PAX6A-12a transcripts were found to be expressed only in a subset of limbal epithelial cells and co-expressed along with the Wt transcripts (**Fig 4.23**). This suggests that their relative abundance

within cells could influence important cellular functions and may have positive or negative effects on the wild type variant translation and cellular function.

The novel splice transcript variants (PAX6B-AS-Δ6 and PAX6A-12a) were majorly localized to the basal and suprabasal cells of the limbus and cornea, where the activated stem cells and the proliferating TACs reside (**Fig 4.25**). These cells were found to be proliferating and incorporated BrdU and expressed low levels of PAX6 and high levels of p63α (**Fig 4.24, 4.26, 4.31**). This again suggests that alternative spliced transcripts may have a dominant negative effect on PAX6 expression. With increased alternate splicing and generation of novel variants, at the expense of the wild type transcript, the relative stoichiometry of the wild type transcripts within specific cells will get altered. This could explain the low levels of PAX6 protein in basal epithelial cells, which enables the proliferation and self-renewal of activated stem cells and the expansion of TACs. TAC expansion promotes corneal epithelial stratification and formation of a thick and normal cornea during development. The PAX6-Wt transcript expression gets upregulated in suprabasal and apical cells of the limbus and cornea, which is known to induce cell cycle arrest and inhibit the proliferation of TACs and promote terminal differentiation and maturation of corneal epithelium.

The two known isoforms of PAX6 cooperatively regulate the expression of corneal keratins, KRT3 and KRT12 (Sasamoto *et al.*, 2016). Dosage insufficiency in PAX6 heterozygous mice results in marked cell adhesion defects and loss of CK12 expression in corneal epithelium (J. Davis *et al.*, 2003). Similarly, knockdown of PAX6 in limbal epithelium down regulated the expression of KRT3, KRT12 and ALDH3A1. These cells lost their corneal identity and were transdifferentiated into skin-like epithelium (H. Ouyang *et al.*, 2014; Y. T. Chen *et al.*, 2013). PAX6 was also shown to directly bind to and regulate the promoters of both KRT12 (Shiraishi *et al.*, 1998) and ALDH3A1 (J. Davis *et al.*, 2008). When we co-expressed the PAX6 variants along with target gene promoter constructs, PAX6A had no effect on p63 promoters, while it significantly induced the mature-cell specific K3 promoter activity (**Fig 4.34, 4.35.G**). Similarly, PAX6B uniquely repressed the TAC-specific TAp63 promoter and also activated the mature cell specific K3 promoter (**Fig 4.34, 4.35.G**), suggesting the roles of PAX6A & PAX6B in promoting terminal differentiation. Interestingly, PAX6B-ASΔ6 uniquely activated the ΔNp63 promoter and also the K3 and K12 gene promoters significantly (**Fig 4.34, 4.35.F.G**). Similarly, the PAX6A-12a uniquely repressed the K12 promoter with no effect on p63 and K3 promoters (**Fig 4.34, 4.35**). This suggests that the PAX6B-ASΔ6 and PAX6A-12a seem to be

enabling the proliferation of activated stem cells, optimal TAC expansion without pre-mature differentiation, thus promoting proper corneal development and wound healing.

Microarray analysis of the transcriptome of HCE stable lines expressing either PAX6A or PAX6B, PAX6B-ASΔ6 and PAX6A-12a revealed the down regulation of several cell cycle genes, BMP and TGFβ signaling in PAX6A overexpressing cells. Conversely, genes involved in growth factor signalling, ECM modulation, cell adhesion and migration were upregulated in PAX6B-ASΔ6 and PAX6A-12a overexpressing cells. This suggests that the wild type PAX6A variant induces terminal cell cycle arrest and promotes differentiation, whereas the novel splice variants seem to promote cell proliferation and migration.

In ocular surface diseases like SJS, chemical burn, aniridia and recurrent pterygium, Pax6 expression was completely downregulated in corneal surface cells. In pannus cultures, the epithelial cells lost the expression of both PAX6 and CK12 and displayed an abnormal skin epithelium-like phenotype. Transient transfection of PAX6 upregulated the expression of CK12 in pannus cultures (W. Li *et al.*, 2008). It may be interesting to check the effects of overexpression of the novel PAX6 isoforms in pathogenic tissues and cultured cells. This will allow us to gain more insight on their unique roles in regulating different corneal epithelial genes at the limbal niche.

Taken together, we provide evidence that the choice of alternate promoters, tissue-specific enhancers, unique splicing mechanisms and the expression of novel dominant negative variants, together tightly regulate PAX6 levels and cellular functions and ensures normal corneal development and homeostasis.

CHAPTER 6

CONCLUSIONS

6: Conclusions

Cloning of different human *PAX6* promoters, its ocular surface enhancer region and other cornea-specific target gene promoters and their detailed characterizations on promoter strength, cell type-specific activities and regulation by the canonical Wnt/β-Catenin signaling has revealed the following:

1. The human *PAX6* gene promoter is differentially regulated in different ocular cells. *PAX6* pA is the dominant and strong promoter in most of the ocular cell types tested. *PAX6* pC is specifically active only in developing retinal tissues and plays a minor role in regulating PAX6 expression in adult ocular cells.
2. OSE enhancer is purely a lens enhancer and activates pA promoter in lens and retinal epithelium, but has no significant effect in corneal epithelium.
3. *PAX6*-pA is highly active in the proliferating transiently amplifying cells, while the activity is minimal in terminally differentiated cells.
4. Canonical Wnt signals directly and positively regulate pA promoter activity in corneal and lens epithelial cells and negatively in RPE and photoreceptor cells.
5. Apart from Wnt signaling, the *PAX6*-pA promoter is also tightly regulated by HDAC and Kaiso repressor complex dependant mechanisms to ensure optimal spatio-temporal gene expression.
6. Apart from *PAX6*-pA, Wnt signaling induced the activity of *TAp63*, *KRT3* and *KRT12* promoters, thus suggesting their key role in regulating corneal epithelial differentiation.
7. The putative stem cells and the TACs form the basal layers of the limbus and corneal epithelium respectively. Wnt signals are inactive in these cells and they express low levels of PAX6 and high levels of p63α, thereby maintaining their stemness.
8. The canonical Wnt signaling is active mainly in the supra-basal cells of the limbus, which promotes TAC expansion and differentiation.

The identification and cloning of different alternately spliced transcripts of the human *PAX6* gene and their characterizations on cell type specific expression and localization in native ocular tissues and their effects on *PAX6* and other target gene promoters has revealed the following:

1. Apart from the two known variants of PAX6 (PAX6A and PAX6B), four other novel variants namely, PAX6A-AS-Δ6, PAX6B-AS-Δ6, PAX6A-Δ6, PAX6A-12a are expressed in ocular tissues.
2. *PAX6*-pA is the dominant promoter in ocular tissues and it drives the expression of both the reported and novel transcripts.
3. The novel variants are co-expressed along with PAX6A in a subset of cells and their relative abundance within cells seem to regulate their fate decisions.
4. PAX6B-ASΔ6 and PAX6A-12a variants are expressed in the limbus and cornea, with significantly higher expression in the cornea. PAX6B-ASΔ6 is localized to the basal TACs, whereas, PAX6A-12a variant is localized to the basal and suprabasal TACs and TDCs of the limbus and cornea.
5. In limbal primary cultures, the PAX6A transcript is exclusively expressed in $PAX6^{High}$, $p63^{Low}$, $BrdU^{Neg}$ TDCs. PAX6B-ASΔ6 and PAX6A-12a transcripts are co-expressed along with the PAX6A transcript in $PAX6^{Low}$, $p63^{High}$, $BrdU^{Positive}$ proliferating TACs.
6. Wnt activation induced the expression of all the novel splice variants and suggests their role in TAC proliferation and expansion.
7. Expression of all PAX6 variants repressed the activity of *PAX6*-pA, suggesting a negative, auto-feedback regulation.
8. PAX6A and PAX6B had no effect or repressed the p63 promoters, while they activated the corneal keratin genes K3, K12, which suggest their role in promoting terminal differentiation of TACs.
9. PAX6B-ASΔ6 uniquely activates Δ*Np63* promoter and also the *KRT3* and *KRT12* gene promoters which suggest its role in promoting TAC expansion and differentiation.
10. Alternately spliced novel variants alter the relative stoichiometry of wild type transcripts and ensure low levels of PAX6 protein expression in the basal epithelial cells. This enables the proliferation and optimal expansion of TACs and promotes epithelial stratification, normal corneal development and wound healing.

CHAPTER 7

CONTRIBUTIONS

7. Contributions

1. This study has identified that the human PAX6 gene is a direct target of Wnt signaling and it directly regulates the activity of the eye-specific pA promoter.
2. This study confirmed that the activation of Wnt signaling in early TACs promotes their proliferation and differentiation into mature corneal epithelium. Whereas, HDAC inhibition aids in limbal stem cell maintenance and expansion without inducing differentiation. This knowledge will be useful to optimize the culture conditions suitable for the *ex vivo* culture and expansion of limbal stem cells, both for basic research and for translational applications.
3. This study has identified and validated the expression of four novel alternately spliced transcripts of the human PAX6 gene in ocular tissues and elucidated their possible roles in regulating the activated limbal epithelial stem cell expansion and differentiation fate decisions.

CHAPTER 8

LIMITATIONS OF THE STUDY

8: Limitations of the study

In this study, we could not validate if the mRNA transcripts of the novel PAX6 variants are translated into functional proteins in native tissues. This was not possible due to the lack of suitable antibodies that can uniquely detect the novel isoforms.

CHAPTER 9

FUTURE SCOPES

9: Future scopes

1. To identify differential gene targets of the novel PAX6 isoforms by genome-wide ChIP-Seq analysis.
2. To create PAX6 null iPSCs by CRISPR editing and then ectopically express the individual splice variants to elucidate their unique roles in regulating early eye development and tissue-specific lineage differentiation and maturation decisions.

REFERENCES

Aggarwal, S., Jinda, W., Limwongse, C., Atchaneeyasakul, L. O., & Phadke, S. R. (2011). Run-on mutation in the PAX6 gene and chorioretinal degeneration in autosomal dominant aniridia. *Mol Vis* 17, 1305-1309.

Ahmad, S., Stewart, R., Yung, S., Kolli, S., Armstrong, L., Stojkovic, M.*, et al.* (2007). Differentiation of human embryonic stem cells into corneal epithelial-like cells by in vitro replication of the corneal epithelial stem cell niche. *Stem Cells* 25(5), 1145-1155. doi:10.1634/stemcells.2006-0516

Altmann, C. R., Chow, R. L., Lang, R. A., & Hemmati-Brivanlou, A. (1997). Lens induction by Pax-6 in Xenopus laevis. *Dev Biol* 185(1), 119-123. doi:10.1006/dbio.1997.8573

Ambati, B. K., Nozaki, M., Singh, N., Takeda, A., Jani, P. D., Suthar, T.*, et al.* (2006). Corneal avascularity is due to soluble VEGF receptor-1. *Nature* 443(7114), 993-997. doi:10.1038/nature05249

Anderson, T. R., Hedlund, E., & Carpenter, E. M. (2002). Differential Pax6 promoter activity and transcript expression during forebrain development. *Mech Dev* 114(1-2), 171-175. doi:10.1016/s0925-4773(02)00051-5

Anton, R., Kestler, H. A., & Kuhl, M. (2007). Beta-catenin signaling contributes to stemness and regulates early differentiation in murine embryonic stem cells. *FEBS Lett* 581(27), 5247-5254. doi:10.1016/j.febslet.2007.10.012

Aota, S., Nakajima, N., Sakamoto, R., Watanabe, S., Ibaraki, N., & Okazaki, K. (2003). Pax6 autoregulation mediated by direct interaction of Pax6 protein with the head surface ectoderm-specific enhancer of the mouse Pax6 gene. *Dev Biol* 257(1), 1-13. doi:10.1016/s0012-1606(03)00058-7

Ashery-Padan, R., & Gruss, P. (2001). Pax6 lights-up the way for eye development. *Curr Opin Cell Biol* 13(6), 706-714. doi:10.1016/s0955-0674(00)00274-x

Ashery-Padan, R., Marquardt, T., Zhou, X., & Gruss, P. (2000). Pax6 activity in the lens primordium is required for lens formation and for correct placement of a single retina in the eye. *Genes Dev* 14(21), 2701-2711. doi:10.1101/gad.184000

Azuma, N., Tadokoro, K., Asaka, A., Yamada, M., Yamaguchi, Y., Handa, H.*, et al.* (2005). The Pax6 isoform bearing an alternative spliced exon promotes the development of the neural retinal structure. *Hum Mol Genet* 14(6), 735-745. doi:10.1093/hmg/ddi069

Azuma, N., Yamaguchi, Y., Handa, H., Hayakawa, M., Kanai, A., & Yamada, M. (1999). Missense mutation in the alternative splice region of the PAX6 gene in eye anomalies. *Am J Hum Genet* 65(3), 656-663. doi:10.1086/302529

Banh, A., Deschamps, P. A., Gauldie, J., Overbeek, P. A., Sivak, J. G., & West-Mays, J. A. (2006). Lens-specific expression of TGF-beta induces anterior subcapsular cataract formation in the absence of Smad3. *Invest Ophthalmol Vis Sci* 47(8), 3450-3460. doi:10.1167/iovs.05-1208

Basu, S., Ali, H., & Sangwan, V. S. (2012). Clinical outcomes of repeat autologous cultivated limbal epithelial transplantation for ocular surface burns. *Am J Ophthalmol* 153(4), 643-650, 650 e641-642. doi:10.1016/j.ajo.2011.09.016

Basu, S., Sureka, S. P., Shanbhag, S. S., Kethiri, A. R., Singh, V., & Sangwan, V. S. (2016). Simple Limbal Epithelial Transplantation: Long-Term Clinical Outcomes in 125 Cases of Unilateral Chronic Ocular Surface Burns. *Ophthalmology* 123(5), 1000-1010. doi:10.1016/j.ophtha.2015.12.042

Baumer, N., Marquardt, T., Stoykova, A., Spieler, D., Treichel, D., Ashery-Padan, R.*, et al.* (2003). Retinal pigmented epithelium determination requires the redundant activities of Pax2 and Pax6. *Development* 130(13), 2903-2915. doi:10.1242/dev.00450

Baylis, O., Figueiredo, F., Henein, C., Lako, M., & Ahmad, S. (2011). 13 years of cultured limbal epithelial cell therapy: a review of the outcomes. *J Cell Biochem* 112(4), 993-1002. doi:10.1002/jcb.23028

Beebe, D. C., & Coats, J. M. (2000). The lens organizes the anterior segment: specification of neural crest cell differentiation in the avian eye. *Dev Biol* 220(2), 424-431. doi:10.1006/dbio.2000.9638

Bishop, K. M., Rubenstein, J. L., & O'Leary, D. D. (2002). Distinct actions of Emx1, Emx2, and Pax6 in regulating the specification of areas in the developing neocortex. *J Neurosci* 22(17), 7627-7638.

Blazejewska, E. A., Schlotzer-Schrehardt, U., Zenkel, M., Bachmann, B., Chankiewitz, E., Jacobi, C.*, et al.* (2009). Corneal limbal microenvironment can induce transdifferentiation of hair follicle stem cells into corneal epithelial-like cells. *Stem Cells* 27(3), 642-652. doi:10.1634/stemcells.2008-0721

Blixt, A., Mahlapuu, M., Aitola, M., Pelto-Huikko, M., Enerback, S., & Carlsson, P. (2000). A forkhead gene, FoxE3, is essential for lens epithelial proliferation and closure of the lens vesicle. *Genes Dev* 14(2), 245-254.

Callaerts, P., Halder, G., & Gehring, W. J. (1997). PAX-6 in development and evolution. *Annu Rev Neurosci* 20, 483-532. doi:10.1146/annurev.neuro.20.1.483

Canto-Soler, M. V., & Adler, R. (2006). Optic cup and lens development requires Pax6 expression in the early optic vesicle during a narrow time window. *Dev Biol* 294(1), 119-132. doi:10.1016/j.ydbio.2006.02.033

Carriere, C., Plaza, S., Caboche, J., Dozier, C., Bailly, M., Martin, P.*, et al.* (1995). Nuclear localization signals, DNA binding, and transactivation properties of quail Pax-6 (Pax-QNR) isoforms. *Cell Growth Differ* 6(12), 1531-1540.

Chauhan, B. K., Yang, Y., Cveklova, K., & Cvekl, A. (2004). Functional interactions between alternatively spliced forms of Pax6 in crystallin gene regulation and in haploinsufficiency. *Nucleic Acids Res* 32(5), 1696-1709. doi:10.1093/nar/gkh334

Chen, S. Y., Hayashida, Y., Chen, M. Y., Xie, H. T., & Tseng, S. C. (2011). A new isolation method of human limbal progenitor cells by maintaining close association with their niche cells. *Tissue Eng Part C Methods* 17(5), 537-548. doi:10.1089/ten.TEC.2010.0609

Chen, Y. T., Chen, F. Y., Vijmasi, T., Stephens, D. N., Gallup, M., & McNamara, N. A. (2013). Pax6 downregulation mediates abnormal lineage commitment of the ocular surface epithelium in aqueous-deficient dry eye disease. *PLoS One* 8(10), e77286. doi:10.1371/journal.pone.0077286

Chen, Z., de Paiva, C. S., Luo, L., Kretzer, F. L., Pflugfelder, S. C., & Li, D. Q. (2004). Characterization of putative stem cell phenotype in human limbal epithelia. *Stem Cells* 22(3), 355-366. doi:10.1634/stemcells.22-3-355

Chew, H. F. (2011). Limbal stem cell disease: Treatment and advances in technology. *Saudi J Ophthalmol* 25(3), 213-218. doi:10.1016/j.sjopt.2011.04.012

Cho, S. H., & Cepko, C. L. (2006). Wnt2b/beta-catenin-mediated canonical Wnt signaling determines the peripheral fates of the chick eye. *Development* 133(16), 3167-3177. doi:10.1242/dev.02474

Chow, R. L., Altmann, C. R., Lang, R. A., & Hemmati-Brivanlou, A. (1999). Pax6 induces ectopic eyes in a vertebrate. *Development* 126(19), 4213-4222.

Collinson, J. M., Morris, L., Reid, A. I., Ramaesh, T., Keighren, M. A., Flockhart, J. H.*, et al.* (2002). Clonal analysis of patterns of growth, stem cell activity, and cell movement during the development and maintenance of the murine corneal epithelium. *Dev Dyn* 224(4), 432-440. doi:10.1002/dvdy.10124

Collinson, J. M., Quinn, J. C., Buchanan, M. A., Kaufman, M. H., Wedden, S. E., West, J. D.*, et al.* (2001). Primary defects in the lens underlie complex anterior segment abnormalities of the Pax6 heterozygous eye. *Proc Natl Acad Sci U S A* 98(17), 9688-9693. doi:10.1073/pnas.161144098

Collinson, J. M., Quinn, J. C., Hill, R. E., & West, J. D. (2003). The roles of Pax6 in the cornea, retina, and olfactory epithelium of the developing mouse embryo. *Dev Biol* 255(2), 303-312. doi:10.1016/s0012-1606(02)00095-7

Corbit, K. C., Shyer, A. E., Dowdle, W. E., Gaulden, J., Singla, V., Chen, M. H.*, et al.* (2008). Kif3a constrains beta-catenin-dependent Wnt signalling through dual ciliary and non-ciliary mechanisms. *Nat Cell Biol* 10(1), 70-76. doi:10.1038/ncb1670

Cvekl, A., Kashanchi, F., Sax, C. M., Brady, J. N., & Piatigorsky, J. (1995). Transcriptional regulation of the mouse alpha A-crystallin gene: activation dependent on a cyclic AMP-responsive element (DE1/CRE) and a Pax-6-binding site. *Mol Cell Biol* 15(2), 653-660. doi:10.1128/mcb.15.2.653

Cvekl, A., & Tamm, E. R. (2004). Anterior eye development and ocular mesenchyme: new insights from mouse models and human diseases. *Bioessays* 26(4), 374-386. doi:10.1002/bies.20009

Czerny, T., Halder, G., Kloter, U., Souabni, A., Gehring, W. J., & Busslinger, M. (1999). twin of eyeless, a second Pax-6 gene of Drosophila, acts upstream of eyeless in the control of eye development. *Mol Cell* 3(3), 297-307. doi:10.1016/s1097-2765(00)80457-8

Davanger, M., & Evensen, A. (1971). Role of the pericorneal papillary structure in renewal of corneal epithelium. *Nature* 229(5286), 560-561. doi:10.1038/229560a0

Davis-Silberman, N., & Ashery-Padan, R. (2008). Iris development in vertebrates; genetic and molecular considerations. *Brain Res* 1192, 17-28. doi:10.1016/j.brainres.2007.03.043

Davis, J., Davis, D., Norman, B., & Piatigorsky, J. (2008). Gene expression of the mouse corneal crystallin Aldh3a1: activation by Pax6, Oct1, and p300. *Invest Ophthalmol Vis Sci* 49(5), 1814-1826. doi:10.1167/iovs.07-1057

Davis, J., Duncan, M. K., Robison, W. G., Jr., & Piatigorsky, J. (2003). Requirement for Pax6 in corneal morphogenesis: a role in adhesion. *J Cell Sci* 116(Pt 11), 2157-2167. doi:10.1242/jcs.00441

Davis, J., & Piatigorsky, J. (2011). Overexpression of Pax6 in mouse cornea directly alters corneal epithelial cells: changes in immune function, vascularization, and differentiation. *Invest Ophthalmol Vis Sci* 52(7), 4158-4168. doi:10.1167/iovs.10-6726

Davis, N., Yoffe, C., Raviv, S., Antes, R., Berger, J., Holzmann, S.*, et al.* (2009). Pax6 dosage requirements in iris and ciliary body differentiation. *Dev Biol* 333(1), 132-142. doi:10.1016/j.ydbio.2009.06.023

DelMonte, D. W., & Kim, T. (2011). Anatomy and physiology of the cornea. *J Cataract Refract Surg* 37(3), 588-598. doi:10.1016/j.jcrs.2010.12.037

Di Girolamo, N., Bobba, S., Raviraj, V., Delic, N. C., Slapetova, I., Nicovich, P. R.*, et al.* (2015). Tracing the fate of limbal epithelial progenitor cells in the murine cornea. *Stem Cells* 33(1), 157-169. doi:10.1002/stem.1769

Di Iorio, E., Barbaro, V., Ruzza, A., Ponzin, D., Pellegrini, G., & De Luca, M. (2005). Isoforms of DeltaNp63 and the migration of ocular limbal cells in human corneal regeneration. *Proc Natl Acad Sci U S A* 102(27), 9523-9528. doi:10.1073/pnas.0503437102

Dias da Silva, M. R., Tiffin, N., Mima, T., Mikawa, T., & Hyer, J. (2007). FGF-mediated induction of ciliary body tissue in the chick eye. *Dev Biol* 304(1), 272-285. doi:10.1016/j.ydbio.2006.12.033

Dimanlig, P. V., Faber, S. C., Auerbach, W., Makarenkova, H. P., & Lang, R. A. (2001). The upstream ectoderm enhancer in Pax6 has an important role in lens induction. *Development* 128(22), 4415-4424.

Dominguez, M., Ferres-Marco, D., Gutierrez-Avino, F. J., Speicher, S. A., & Beneyto, M. (2004). Growth and specification of the eye are controlled independently by Eyegone and Eyeless in Drosophila melanogaster. *Nat Genet* 36(1), 31-39. doi:10.1038/ng1281

Dora, N., Ou, J., Kucerova, R., Parisi, I., West, J. D., & Collinson, J. M. (2008). PAX6 dosage effects on corneal development, growth, and wound healing. *Dev Dyn* 237(5), 1295-1306. doi:10.1002/dvdy.21528

Douvaras, P., Mort, R. L., Edwards, D., Ramaesh, K., Dhillon, B., Morley, S. D.*, et al.* (2013). Increased corneal epithelial turnover contributes to abnormal homeostasis in the Pax6(+/-) mouse model of aniridia. *PLoS One* 8(8), e71117. doi:10.1371/journal.pone.0071117

Dua, H. S., Joseph, A., Shanmuganathan, V. A., & Jones, R. E. (2003). Stem cell differentiation and the effects of deficiency. *Eye (Lond)* 17(8), 877-885. doi:10.1038/sj.eye.6700573

Duncan, M. K., Kozmik, Z., Cveklova, K., Piatigorsky, J., & Cvekl, A. (2000). Overexpression of PAX6(5a) in lens fiber cells results in cataract and upregulation of (alpha)5(beta)1 integrin expression. *J Cell Sci* 113 (Pt 18), 3173-3185.

Duncan, M. K., Xie, L., David, L. L., Robinson, M. L., Taube, J. R., Cui, W.*, et al.* (2004). Ectopic Pax6 expression disturbs lens fiber cell differentiation. *Invest Ophthalmol Vis Sci* 45(10), 3589-3598. doi:10.1167/iovs.04-0151

Dyer, M. A., Livesey, F. J., Cepko, C. L., & Oliver, G. (2003). Prox1 function controls progenitor cell proliferation and horizontal cell genesis in the mammalian retina. *Nat Genet* 34(1), 53-58. doi:10.1038/ng1144

Dziasko, M. A., Armer, H. E., Levis, H. J., Shortt, A. J., Tuft, S., & Daniels, J. T. (2014). Localisation of epithelial cells capable of holoclone formation in vitro and direct interaction with stromal cells in the native human limbal crypt. *PLoS One* 9(4), e94283. doi:10.1371/journal.pone.0094283

Dziasko, M. A., Tuft, S. J., & Daniels, J. T. (2015). Limbal melanocytes support limbal epithelial stem cells in 2D and 3D microenvironments. *Exp Eye Res* 138, 70-79. doi:10.1016/j.exer.2015.06.026

Echevarria, T. J., Chow, S., Watson, S., Wakefield, D., & Di Girolamo, N. (2011). Vitronectin: a matrix support factor for human limbal epithelial progenitor cells. *Invest Ophthalmol Vis Sci* 52(11), 8138-8147. doi:10.1167/iovs.11-8140

Epstein, J., Cai, J., Glaser, T., Jepeal, L., & Maas, R. (1994). Identification of a Pax paired domain recognition sequence and evidence for DNA-dependent conformational changes. *J Biol Chem* 269(11), 8355-8361.

Epstein, J. A., Glaser, T., Cai, J., Jepeal, L., Walton, D. S., & Maas, R. L. (1994). Two independent and interactive DNA-binding subdomains of the Pax6 paired domain are regulated by alternative splicing. *Genes Dev* 8(17), 2022-2034. doi:10.1101/gad.8.17.2022

Favor, J., Bradley, A., Conte, N., Janik, D., Pretsch, W., Reitmeir, P.*, et al.* (2009). Analysis of Pax6 contiguous gene deletions in the mouse, Mus musculus, identifies regions distinct

from Pax6 responsible for extreme small-eye and belly-spotting phenotypes. *Genetics* 182(4), 1077-1088. doi:10.1534/genetics.109.104562

Fevr, T., Robine, S., Louvard, D., & Huelsken, J. (2007). Wnt/beta-catenin is essential for intestinal homeostasis and maintenance of intestinal stem cells. *Mol Cell Biol* 27(21), 7551-7559. doi:10.1128/MCB.01034-07

Forsdahl, S., Kiselev, Y., Hogseth, R., Mjelle, J. E., & Mikkola, I. (2014). Pax6 regulates the expression of Dkk3 in murine and human cell lines, and altered responses to Wnt signaling are shown in FlpIn-3T3 cells stably expressing either the Pax6 or the Pax6(5a) isoform. *PLoS One* 9(7), e102559. doi:10.1371/journal.pone.0102559

Foster, J. W., Wahlin, K., Adams, S. M., Birk, D. E., Zack, D. J., & Chakravarti, S. (2017). Cornea organoids from human induced pluripotent stem cells. *Sci Rep* 7, 41286. doi:10.1038/srep41286

Fuhrmann, S. (2010). Eye Morphogenesis and Patterning of the Optic Vesicle. *Current Topics in Developmental Biology* 93, 61-84. doi:doi.org/10.1016/B978-0-12-385044-7.00003-5

Furuta, Y., & Hogan, B. L. (1998). BMP4 is essential for lens induction in the mouse embryo. *Genes Dev* 12(23), 3764-3775. doi:10.1101/gad.12.23.3764

Gage, P. J., Qian, M., Wu, D., & Rosenberg, K. I. (2008). The canonical Wnt signaling antagonist DKK2 is an essential effector of PITX2 function during normal eye development. *Dev Biol* 317(1), 310-324. doi:10.1016/j.ydbio.2008.02.030

Gan, Q., Lee, A., Suzuki, R., Yamagami, T., Stokes, A., Nguyen, B. C.*, et al.* (2014). Pax6 mediates ss-catenin signaling for self-renewal and neurogenesis by neocortical radial glial stem cells. *Stem Cells* 32(1), 45-58. doi:10.1002/stem.1561

Geng, X., Speirs, C., Lagutin, O., Inbal, A., Liu, W., Solnica-Krezel, L.*, et al.* (2008). Haploinsufficiency of Six3 fails to activate Sonic hedgehog expression in the ventral forebrain and causes holoprosencephaly. *Dev Cell* 15(2), 236-247. doi:10.1016/j.devcel.2008.07.003

Glaser, T., Walton, D. S., & Maas, R. L. (1992). Genomic structure, evolutionary conservation and aniridia mutations in the human PAX6 gene. *Nat Genet* 2(3), 232-239. doi:10.1038/ng1192-232

Gonzalez, S., Oh, D., Baclagon, E. R., Zheng, J. J., & Deng, S. X. (2019). Wnt Signaling Is Required for the Maintenance of Human Limbal Stem/Progenitor Cells In Vitro. *Invest Ophthalmol Vis Sci* 60(1), 107-112. doi:10.1167/iovs.18-25740

Gosmain, Y., Marthinet, E., Cheyssac, C., Guerardel, A., Mamin, A., Katz, L. S.*, et al.* (2010). Pax6 controls the expression of critical genes involved in pancreatic {alpha} cell differentiation and function. *J Biol Chem* 285(43), 33381-33393. doi:10.1074/jbc.M110.147215

Goudreau, G., Petrou, P., Reneker, L. W., Graw, J., Loster, J., & Gruss, P. (2002). Mutually regulated expression of Pax6 and Six3 and its implications for the Pax6 haploinsufficient lens phenotype. *Proc Natl Acad Sci U S A* 99(13), 8719-8724. doi:10.1073/pnas.132195699

Griffin, C., Kleinjan, D. A., Doe, B., & van Heyningen, V. (2002). New 3' elements control Pax6 expression in the developing pretectum, neural retina and olfactory region. *Mech Dev* 112(1-2), 89-100. doi:10.1016/s0925-4773(01)00646-3

Grindley, J. C., Davidson, D. R., & Hill, R. E. (1995). The role of Pax-6 in eye and nasal development. *Development* 121(5), 1433-1442.

Grocott, T., Frost, V., Maillard, M., Johansen, T., Wheeler, G. N., Dawes, L. J.*, et al.* (2007). The MH1 domain of Smad3 interacts with Pax6 and represses autoregulation of the Pax6 P1 promoter. *Nucleic Acids Res* 35(3), 890-901. doi:10.1093/nar/gkl1105

Gupta, N., Joshi, J., Farooqui, J. H., & Mathur, U. (2018). Results of simple limbal epithelial transplantation in unilateral ocular surface burn. *Indian J Ophthalmol* 66(1), 45-52. doi:10.4103/ijo.IJO_602_17

Hagglund, A. C., Dahl, L., & Carlsson, L. (2011). Lhx2 is required for patterning and expansion of a distinct progenitor cell population committed to eye development. *PLoS One* 6(8), e23387. doi:10.1371/journal.pone.0023387

Halder, G., Callaerts, P., & Gehring, W. J. (1995). Induction of ectopic eyes by targeted expression of the eyeless gene in Drosophila. *Science* 267(5205), 1788-1792. doi:10.1126/science.7892602

Han, B., Chen, S. Y., Zhu, Y. T., & Tseng, S. C. (2014). Integration of BMP/Wnt signaling to control clonal growth of limbal epithelial progenitor cells by niche cells. *Stem Cell Res* 12(2), 562-573. doi:10.1016/j.scr.2014.01.003

Haubst, N., Berger, J., Radjendirane, V., Graw, J., Favor, J., Saunders, G. F.*, et al.* (2004). Molecular dissection of Pax6 function: the specific roles of the paired domain and homeodomain in brain development. *Development* 131(24), 6131-6140. doi:10.1242/dev.01524

Hayashi, R., Ishikawa, Y., Sasamoto, Y., Katori, R., Nomura, N., Ichikawa, T.*, et al.* (2016). Co-ordinated ocular development from human iPS cells and recovery of corneal function. *Nature* 531(7594), 376-380. doi:10.1038/nature17000

Hill, R. E., Favor, J., Hogan, B. L., Ton, C. C., Saunders, G. F., Hanson, I. M.*, et al.* (1991). Mouse small eye results from mutations in a paired-like homeobox-containing gene. *Nature* 354(6354), 522-525. doi:10.1038/354522a0

Hogan, B. L., Horsburgh, G., Cohen, J., Hetherington, C. M., Fisher, G., & Lyon, M. F. (1986). Small eyes (Sey): a homozygous lethal mutation on chromosome 2 which affects the differentiation of both lens and nasal placodes in the mouse. *J Embryol Exp Morphol* 97, 95-110.

Horsford, D. J., Nguyen, M. T., Sellar, G. C., Kothary, R., Arnheiter, H., & McInnes, R. R. (2005). Chx10 repression of Mitf is required for the maintenance of mammalian neuroretinal identity. *Development* 132(1), 177-187. doi:10.1242/dev.01571

Hsieh, Y. W., & Yang, X. J. (2009). Dynamic Pax6 expression during the neurogenic cell cycle influences proliferation and cell fate choices of retinal progenitors. *Neural Dev* 4, 32. doi:10.1186/1749-8104-4-32

Hsueh, Y. J., Kuo, P. C., & Chen, J. K. (2013). Transcriptional regulators of the DeltaNp63: their role in limbal epithelial cell proliferation. *J Cell Physiol* 228(3), 536-546. doi:10.1002/jcp.24160

Huelsken, J., Vogel, R., Erdmann, B., Cotsarelis, G., & Birchmeier, W. (2001). beta-Catenin controls hair follicle morphogenesis and stem cell differentiation in the skin. *Cell* 105(4), 533-545. doi:10.1016/s0092-8674(01)00336-1

Hyer, J., Mima, T., & Mikawa, T. (1998). FGF1 patterns the optic vesicle by directing the placement of the neural retina domain. *Development* 125(5), 869-877.

Jacobsson, L., Kronhamn, J., & Rasmuson-Lestander, A. (2009). The Drosophila Pax6 paralogs have different functions in head development but can partially substitute for each other. *Mol Genet Genomics* 282(3), 217-231. doi:10.1007/s00438-009-0458-2

Jang, C. C., Chao, J. L., Jones, N., Yao, L. C., Bessarab, D. A., Kuo, Y. M.*, et al.* (2003). Two Pax genes, eye gone and eyeless, act cooperatively in promoting Drosophila eye development. *Development* 130(13), 2939-2951. doi:10.1242/dev.00522

Jaworski, C., Sperbeck, S., Graham, C., & Wistow, G. (1997). Alternative splicing of Pax6 in bovine eye and evolutionary conservation of intron sequences. *Biochem Biophys Res Commun* 240(1), 196-202. doi:10.1006/bbrc.1997.7623

Jester, J. V., Moller-Pedersen, T., Huang, J., Sax, C. M., Kays, W. T., Cavangh, H. D.*, et al.* (1999). The cellular basis of corneal transparency: evidence for 'corneal crystallins'. *J Cell Sci* 112 (Pt 5), 613-622.

Kalani, M. Y., Cheshier, S. H., Cord, B. J., Bababeygy, S. R., Vogel, H., Weissman, I. L.*, et al.* (2008). Wnt-mediated self-renewal of neural stem/progenitor cells. *Proc Natl Acad Sci U S A* 105(44), 16970-16975. doi:10.1073/pnas.0808616105

Kamachi, Y., Uchikawa, M., Tanouchi, A., Sekido, R., & Kondoh, H. (2001). Pax6 and SOX2 form a co-DNA-binding partner complex that regulates initiation of lens development. *Genes Dev* 15(10), 1272-1286. doi:10.1101/gad.887101

Kameishi, S., Sugiyama, H., Yamato, M., Sado, Y., Namiki, H., Kato, T.*, et al.* (2015). Remodeling of epithelial cells and basement membranes in a corneal deficiency model with long-term follow-up. *Lab Invest* 95(2), 168-179. doi:10.1038/labinvest.2014.146

Kammandel, B., Chowdhury, K., Stoykova, A., Aparicio, S., Brenner, S., & Gruss, P. (1999). Distinct cis-essential modules direct the time-space pattern of the Pax6 gene activity. *Dev Biol* 205(1), 79-97. doi:10.1006/dbio.1998.9128

Kidson, S. H., Kume, T., Deng, K., Winfrey, V., & Hogan, B. L. (1999). The forkhead/winged-helix gene, Mf1, is necessary for the normal development of the cornea and formation of the anterior chamber in the mouse eye. *Dev Biol* 211(2), 306-322. doi:10.1006/dbio.1999.9314

Kim, J., & Lauderdale, J. D. (2006). Analysis of Pax6 expression using a BAC transgene reveals the presence of a paired-less isoform of Pax6 in the eye and olfactory bulb. *Dev Biol* 292(2), 486-505. doi:10.1016/j.ydbio.2005.12.041

Kim, J., & Lauderdale, J. D. (2008). Overexpression of pairedless Pax6 in the retina disrupts corneal development and affects lens cell survival. *Dev Biol* 313(1), 434-454. doi:10.1016/j.ydbio.2007.10.043

Kitazawa, K., Hikichi, T., Nakamura, T., Sotozono, C., Kinoshita, S., & Masui, S. (2017). PAX6 regulates human corneal epithelium cell identity. *Exp Eye Res* 154, 30-38. doi:10.1016/j.exer.2016.11.005

Kleinjan, D. A., Seawright, A., Childs, A. J., & van Heyningen, V. (2004). Conserved elements in Pax6 intron 7 involved in (auto)regulation and alternative transcription. *Dev Biol* 265(2), 462-477. doi:10.1016/j.ydbio.2003.09.011

Kleinjan, D. A., Seawright, A., Mella, S., Carr, C. B., Tyas, D. A., Simpson, T. I.*, et al.* (2006). Long-range downstream enhancers are essential for Pax6 expression. *Dev Biol* 299(2), 563-581. doi:10.1016/j.ydbio.2006.08.060

Kleinjan, D. A., Seawright, A., Schedl, A., Quinlan, R. A., Danes, S., & van Heyningen, V. (2001). Aniridia-associated translocations, DNase hypersensitivity, sequence comparison and transgenic analysis redefine the functional domain of PAX6. *Hum Mol Genet* 10(19), 2049-2059. doi:10.1093/hmg/10.19.2049

Kobayashi, Y., Hayashi, R., Shibata, S., Quantock, A. J., & Nishida, K. (2020). Ocular surface ectoderm instigated by WNT inhibition and BMP4. *Stem Cell Res* 46, 101868. doi:10.1016/j.scr.2020.101868

Koroma, B. M., Yang, J. M., & Sundin, O. H. (1997). The Pax-6 homeobox gene is expressed throughout the corneal and conjunctival epithelia. *Invest Ophthalmol Vis Sci* 38(1), 108-120.

Koshiba-Takeuchi, K., Takeuchi, J. K., Matsumoto, K., Momose, T., Uno, K., Hoepker, V.*, et al.* (2000). Tbx5 and the retinotectum projection. *Science* 287(5450), 134-137. doi:10.1126/science.287.5450.134

Kozmik, Z., Czerny, T., & Busslinger, M. (1997). Alternatively spliced insertions in the paired domain restrict the DNA sequence specificity of Pax6 and Pax8. *EMBO J* 16(22), 6793-6803. doi:10.1093/emboj/16.22.6793

Kulkarni, B. B., Tighe, P. J., Mohammed, I., Yeung, A. M., Powe, D. G., Hopkinson, A.*, et al.* (2010). Comparative transcriptional profiling of the limbal epithelial crypt demonstrates its putative stem cell niche characteristics. *BMC Genomics* 11, 526. doi:10.1186/1471-2164-11-526

Kureshi, A. K., Dziasko, M., Funderburgh, J. L., & Daniels, J. T. (2015). Human corneal stromal stem cells support limbal epithelial cells cultured on RAFT tissue equivalents. *Sci Rep* 5, 16186. doi:10.1038/srep16186

Lakowski, J., Majumder, A., & Lauderdale, J. D. (2007). Mechanisms controlling Pax6 isoform expression in the retina have been conserved between teleosts and mammals. *Dev Biol* 307(2), 498-520. doi:10.1016/j.ydbio.2007.04.015

Latta, L., Nordstrom, K., Stachon, T., Langenbucher, A., Fries, F. N., Szentmary, N.*, et al.* (2019). Expression of retinoic acid signaling components ADH7 and ALDH1A1 is reduced in aniridia limbal epithelial cells and a siRNA primary cell based aniridia model. *Exp Eye Res* 179, 8-17. doi:10.1016/j.exer.2018.10.002

Lavker, R. M., Tseng, S. C., & Sun, T. T. (2004). Corneal epithelial stem cells at the limbus: looking at some old problems from a new angle. *Exp Eye Res* 78(3), 433-446. doi:10.1016/j.exer.2003.09.008

Lehrer, M. S., Sun, T. T., & Lavker, R. M. (1998). Strategies of epithelial repair: modulation of stem cell and transit amplifying cell proliferation. *J Cell Sci* 111 (Pt 19), 2867-2875.

Li, G., Xu, F., Zhu, J., Krawczyk, M., Zhang, Y., Yuan, J.*, et al.* (2015). Transcription Factor PAX6 (Paired Box 6) Controls Limbal Stem Cell Lineage in Development and Disease. *J Biol Chem* 290(33), 20448-20454. doi:10.1074/jbc.M115.662940

Li, H., Tierney, C., Wen, L., Wu, J. Y., & Rao, Y. (1997). A single morphogenetic field gives rise to two retina primordia under the influence of the prechordal plate. *Development* 124(3), 603-615.

Li, T., & Lu, L. (2005). Epidermal growth factor-induced proliferation requires down-regulation of Pax6 in corneal epithelial cells. *J Biol Chem* 280(13), 12988-12995. doi:10.1074/jbc.M412458200

Li, W., Chen, Y. T., Hayashida, Y., Blanco, G., Kheirkah, A., He, H.*, et al.* (2008). Down-regulation of Pax6 is associated with abnormal differentiation of corneal epithelial cells in severe ocular surface diseases. *J Pathol* 214(1), 114-122. doi:10.1002/path.2256

Li, W., Hayashida, Y., Chen, Y. T., & Tseng, S. C. (2007). Niche regulation of corneal epithelial stem cells at the limbus. *Cell Res* 17(1), 26-36. doi:10.1038/sj.cr.7310137

Lie, D. C., Colamarino, S. A., Song, H. J., Desire, L., Mira, H., Consiglio, A.*, et al.* (2005). Wnt signalling regulates adult hippocampal neurogenesis. *Nature* 437(7063), 1370-1375. doi:10.1038/nature04108

Lima Cunha, D., Arno, G., Corton, M., & Moosajee, M. (2019). The Spectrum of PAX6 Mutations and Genotype-Phenotype Correlations in the Eye. *Genes (Basel)* 10(12). doi:10.3390/genes10121050

Liu, H., Thurig, S., Mohamed, O., Dufort, D., & Wallace, V. A. (2006). Mapping canonical Wnt signaling in the developing and adult retina. *Invest Ophthalmol Vis Sci* 47(11), 5088-5097. doi:10.1167/iovs.06-0403

Liu, J. J., Kao, W. W., & Wilson, S. E. (1999). Corneal epithelium-specific mouse keratin K12 promoter. *Exp Eye Res* 68(3), 295-301. doi:10.1006/exer.1998.0593

Lu, R., Bian, F., Zhang, X., Qi, H., Chuang, E. Y., Pflugfelder, S. C.*, et al.* (2011). The beta-catenin/Tcf4/survivin signaling maintains a less differentiated phenotype and high proliferative capacity of human corneal epithelial progenitor cells. *Int J Biochem Cell Biol* 43(5), 751-759. doi:10.1016/j.biocel.2011.01.018

Lu, R., Qu, Y., Ge, J., Zhang, L., Su, Z., Pflugfelder, S. C.*, et al.* (2012). Transcription factor TCF4 maintains the properties of human corneal epithelial stem cells. *Stem Cells* 30(4), 753-761. doi:10.1002/stem.1032

Lyon, M. F., Bogani, D., Boyd, Y., Guillot, P., & Favor, J. (2000). Further genetic analysis of two autosomal dominant mouse eye defects, Ccw and Pax6(coop). *Mol Vis* 6, 199-203.

Macdonald, R., & Wilson, S. W. (1997). Distribution of Pax6 protein during eye development suggests discrete roles in proliferative and differentiated visual cells. *Dev Genes Evol* 206(6), 363-369. doi:10.1007/s004270050065

Machon, O., Kreslova, J., Ruzickova, J., Vacik, T., Klimova, L., Fujimura, N.*, et al.* (2010). Lens morphogenesis is dependent on Pax6-mediated inhibition of the canonical Wnt/beta-catenin signaling in the lens surface ectoderm. *Genesis* 48(2), 86-95. doi:10.1002/dvg.20583

Manuel, M., Georgala, P. A., Carr, C. B., Chanas, S., Kleinjan, D. A., Martynoga, B.*, et al.* (2007). Controlled overexpression of Pax6 in vivo negatively autoregulates the Pax6 locus, causing cell-autonomous defects of late cortical progenitor proliferation with little effect on cortical arealization. *Development* 134(3), 545-555. doi:10.1242/dev.02764

Manuel, M., Pratt, T., Liu, M., Jeffery, G., & Price, D. J. (2008). Overexpression of Pax6 results in microphthalmia, retinal dysplasia and defective retinal ganglion cell axon guidance. *BMC Dev Biol* 8, 59. doi:10.1186/1471-213X-8-59

Mariappan, I., Maddileti, S., Savy, S., Tiwari, S., Gaddipati, S., Fatima, A.*, et al.* (2010). In vitro culture and expansion of human limbal epithelial cells. *Nat Protoc* 5(8), 1470-1479. doi:10.1038/nprot.2010.115

Marquardt, T., Ashery-Padan, R., Andrejewski, N., Scardigli, R., Guillemot, F., & Gruss, P. (2001). Pax6 is required for the multipotent state of retinal progenitor cells. *Cell* 105(1), 43-55. doi:10.1016/s0092-8674(01)00295-1

Maruyama-Koide, Y., Mikawa, S., Sasaki, T., & Sato, K. (2017). Bone morphogenetic protein-4 and bone morphogenetic protein receptors expressions in the adult rat eye. *Eur J Histochem* 61(3), 2797. doi:10.4081/ejh.2017.2797

Matsuo, T., Osumi-Yamashita, N., Noji, S., Ohuchi, H., Koyama, E., Myokai, F.*, et al.* (1993). A mutation in the Pax-6 gene in rat small eye is associated with impaired migration of midbrain crest cells. *Nat Genet* 3(4), 299-304. doi:10.1038/ng0493-299

Mei, H., Nakatsu, M. N., Baclagon, E. R., & Deng, S. X. (2014). Frizzled 7 maintains the undifferentiated state of human limbal stem/progenitor cells. *Stem Cells* 32(4), 938-945. doi:10.1002/stem.1582

Mishra, R., Gorlov, I. P., Chao, L. Y., Singh, S., & Saunders, G. F. (2002). PAX6, paired domain influences sequence recognition by the homeodomain. *J Biol Chem* 277(51), 49488-49494. doi:10.1074/jbc.M206478200

Mort, R. L., Bentley, A. J., Martin, F. L., Collinson, J. M., Douvaras, P., Hill, R. E.*, et al.* (2011). Effects of aberrant Pax6 gene dosage on mouse corneal pathophysiology and corneal epithelial homeostasis. *PLoS One* 6(12), e28895. doi:10.1371/journal.pone.0028895

Mort, R. L., Douvaras, P., Morley, S. D., Dora, N., Hill, R. E., Collinson, J. M.*, et al.* (2012). Stem cells and corneal epithelial maintenance: insights from the mouse and other animal models. *Results Probl Cell Differ* 55, 357-394. doi:10.1007/978-3-642-30406-4_19

Moshiri, A., Gonzalez, E., Tagawa, K., Maeda, H., Wang, M., Frishman, L. J.*, et al.* (2008). Near complete loss of retinal ganglion cells in the math5/brn3b double knockout elicits severe reductions of other cell types during retinal development. *Dev Biol* 316(2), 214-227. doi:10.1016/j.ydbio.2008.01.015

Mukhopadhyay, M., Gorivodsky, M., Shtrom, S., Grinberg, A., Niehrs, C., Morasso, M. I.*, et al.* (2006). Dkk2 plays an essential role in the corneal fate of the ocular surface epithelium. *Development* 133(11), 2149-2154. doi:10.1242/dev.02381

Nagasaki, T., & Zhao, J. (2003). Centripetal movement of corneal epithelial cells in the normal adult mouse. *Invest Ophthalmol Vis Sci* 44(2), 558-566. doi:10.1167/iovs.02-0705

Nakatsu, M. N., Ding, Z., Ng, M. Y., Truong, T. T., Yu, F., & Deng, S. X. (2011). Wnt/beta-catenin signaling regulates proliferation of human cornea epithelial stem/progenitor cells. *Invest Ophthalmol Vis Sci* 52(7), 4734-4741. doi:10.1167/iovs.10-6486

Nishida, K., Kinoshita, S., Ohashi, Y., Kuwayama, Y., & Yamamoto, S. (1995). Ocular surface abnormalities in aniridia. *Am J Ophthalmol* 120(3), 368-375. doi:10.1016/s0002-9394(14)72167-1

Notara, M., Schrader, S., & Daniels, J. T. (2011). The porcine limbal epithelial stem cell niche as a new model for the study of transplanted tissue-engineered human limbal epithelial cells. *Tissue Eng Part A* 17(5-6), 741-750. doi:10.1089/ten.TEA.2010.0343

Okladnova, O., Syagailo, Y. V., Mossner, R., Riederer, P., & Lesch, K. P. (1998). Regulation of PAX-6 gene transcription: alternate promoter usage in human brain. *Brain Res Mol Brain Res* 60(2), 177-192. doi:10.1016/s0169-328x(98)00167-3

Onuma, Y., Takahashi, S., Asashima, M., Kurata, S., & Gehring, W. J. (2002). Conservation of Pax 6 function and upstream activation by Notch signaling in eye development of frogs and flies. *Proc Natl Acad Sci U S A* 99(4), 2020-2025. doi:10.1073/pnas.022626999

Oron-Karni, V., Farhy, C., Elgart, M., Marquardt, T., Remizova, L., Yaron, O.*, et al.* (2008). Dual requirement for Pax6 in retinal progenitor cells. *Development* 135(24), 4037-4047. doi:10.1242/dev.028308

Ou, J., Lowes, C., & Collinson, J. M. (2010). Cytoskeletal and cell adhesion defects in wounded and Pax6+/- corneal epithelia. *Invest Ophthalmol Vis Sci* 51(3), 1415-1423. doi:10.1167/iovs.09-4023

Ouyang, H., Xue, Y., Lin, Y., Zhang, X., Xi, L., Patel, S.*, et al.* (2014). WNT7A and PAX6 define corneal epithelium homeostasis and pathogenesis. *Nature* 511(7509), 358-361. doi:10.1038/nature13465

Ouyang, J., Shen, Y. C., Yeh, L. K., Li, W., Coyle, B. M., Liu, C. Y.*, et al.* (2006). Pax6 overexpression suppresses cell proliferation and retards the cell cycle in corneal epithelial cells. *Invest Ophthalmol Vis Sci* 47(6), 2397-2407. doi:10.1167/iovs.05-1083

Pearton, D. J., Yang, Y., & Dhouailly, D. (2005). Transdifferentiation of corneal epithelium into epidermis occurs by means of a multistep process triggered by dermal developmental signals. *Proc Natl Acad Sci U S A* 102(10), 3714-3719. doi:10.1073/pnas.0500344102

Pellegrini, G., Dellambra, E., Golisano, O., Martinelli, E., Fantozzi, I., Bondanza, S.*, et al.* (2001). p63 identifies keratinocyte stem cells. *Proc Natl Acad Sci U S A* 98(6), 3156-3161. doi:10.1073/pnas.061032098

Pinson, J., Mason, J. O., Simpson, T. I., & Price, D. J. (2005). Regulation of the Pax6 : Pax6(5a) mRNA ratio in the developing mammalian brain. *BMC Dev Biol* 5, 13. doi:10.1186/1471-213X-5-13

Pinson, J., Simpson, T. I., Mason, J. O., & Price, D. J. (2006). Positive autoregulation of the transcription factor Pax6 in response to increased levels of either of its major isoforms, Pax6 or Pax6(5a), in cultured cells. *BMC Dev Biol* 6, 25. doi:10.1186/1471-213X-6-25

Pinto, D., Gregorieff, A., Begthel, H., & Clevers, H. (2003). Canonical Wnt signals are essential for homeostasis of the intestinal epithelium. *Genes Dev* 17(14), 1709-1713. doi:10.1101/gad.267103

Plaza, S., Dozier, C., Langlois, M. C., & Saule, S. (1995). Identification and characterization of a neuroretina-specific enhancer element in the quail Pax-6 (Pax-QNR) gene. *Mol Cell Biol* 15(2), 892-903. doi:10.1128/mcb.15.2.892

Plaza, S., Dozier, C., & Saule, S. (1993). Quail Pax-6 (Pax-QNR) encodes a transcription factor able to bind and trans-activate its own promoter. *Cell Growth Differ* 4(12), 1041-1050.

Plaza, S., Dozier, C., Turque, N., & Saule, S. (1995). Quail Pax-6 (Pax-QNR) mRNAs are expressed from two promoters used differentially during retina development and neuronal differentiation. *Mol Cell Biol* 15(6), 3344-3353. doi:10.1128/mcb.15.6.3344

Polisetti, N., Sorokin, L., Okumura, N., Koizumi, N., Kinoshita, S., Kruse, F. E.*, et al.* (2017). Laminin-511 and -521-based matrices for efficient ex vivo-expansion of human limbal epithelial progenitor cells. *Sci Rep* 7(1), 5152. doi:10.1038/s41598-017-04916-x

Pontoriero, G. F., Smith, A. N., Miller, L. A., Radice, G. L., West-Mays, J. A., & Lang, R. A. (2009). Co-operative roles for E-cadherin and N-cadherin during lens vesicle separation and lens epithelial cell survival. *Dev Biol* 326(2), 403-417. doi:10.1016/j.ydbio.2008.10.011

Quiring, R., Walldorf, U., Kloter, U., & Gehring, W. J. (1994). Homology of the eyeless gene of Drosophila to the Small eye gene in mice and Aniridia in humans. *Science* 265(5173), 785-789. doi:10.1126/science.7914031

Rama, P., Matuska, S., Paganoni, G., Spinelli, A., De Luca, M., & Pellegrini, G. (2010). Limbal stem-cell therapy and long-term corneal regeneration. *N Engl J Med* 363(2), 147-155. doi:10.1056/NEJMoa0905955

Ramaesh, K., Ramaesh, T., Dutton, G. N., & Dhillon, B. (2005). Evolving concepts on the pathogenic mechanisms of aniridia related keratopathy. *Int J Biochem Cell Biol* 37(3), 547-557. doi:10.1016/j.biocel.2004.09.002

Ramaesh, T., Collinson, J. M., Ramaesh, K., Kaufman, M. H., West, J. D., & Dhillon, B. (2003). Corneal abnormalities in Pax6+/- small eye mice mimic human aniridia-related keratopathy. *Invest Ophthalmol Vis Sci* 44(5), 1871-1878. doi:10.1167/iovs.02-0576

Ramaesh, T., Ramaesh, K., Leask, R., Springbett, A., Riley, S. C., Dhillon, B.*, et al.* (2006). Increased apoptosis and abnormal wound-healing responses in the heterozygous Pax6+/- mouse cornea. *Invest Ophthalmol Vis Sci* 47(5), 1911-1917. doi:10.1167/iovs.05-1028

Ramaesh, T., Ramaesh, K., Martin Collinson, J., Chanas, S. A., Dhillon, B., & West, J. D. (2005). Developmental and cellular factors underlying corneal epithelial dysgenesis in the Pax6+/- mouse model of aniridia. *Exp Eye Res* 81(2), 224-235. doi:10.1016/j.exer.2005.02.002

Richardson, J., Cvekl, A., & Wistow, G. (1995). Pax-6 is essential for lens-specific expression of zeta-crystallin. *Proc Natl Acad Sci U S A* 92(10), 4676-4680. doi:10.1073/pnas.92.10.4676

Riesenberg, A. N., Le, T. T., Willardsen, M. I., Blackburn, D. C., Vetter, M. L., & Brown, N. L. (2009). Pax6 regulation of Math5 during mouse retinal neurogenesis. *Genesis* 47(3), 175-187. doi:10.1002/dvg.20479

Rowan, S., Siggers, T., Lachke, S. A., Yue, Y., Bulyk, M. L., & Maas, R. L. (2010). Precise temporal control of the eye regulatory gene Pax6 via enhancer-binding site affinity. *Genes Dev* 24(10), 980-985. doi:10.1101/gad.1890410

Saika, S., Saika, S., Liu, C. Y., Azhar, M., Sanford, L. P., Doetschman, T.*, et al.* (2001). TGFbeta2 in corneal morphogenesis during mouse embryonic development. *Dev Biol* 240(2), 419-432. doi:10.1006/dbio.2001.0480

Sangwan, V. S., Basu, S., MacNeil, S., & Balasubramanian, D. (2012). Simple limbal epithelial transplantation (SLET): a novel surgical technique for the treatment of unilateral limbal stem cell deficiency. *Br J Ophthalmol* 96(7), 931-934. doi:10.1136/bjophthalmol-2011-301164

Sasagawa, S., Takabatake, T., Takabatake, Y., Muramatsu, T., & Takeshima, K. (2002). Axes establishment during eye morphogenesis in Xenopus by coordinate and antagonistic actions of BMP4, Shh, and RA. *Genesis* 33(2), 86-96. doi:10.1002/gene.10095

Sasamoto, Y., Hayashi, R., Park, S. J., Saito-Adachi, M., Suzuki, Y., Kawasaki, S.*, et al.* (2016). PAX6 Isoforms, along with Reprogramming Factors, Differentially Regulate the Induction of Cornea-specific Genes. *Sci Rep* 6, 20807. doi:10.1038/srep20807

Sato, N., Meijer, L., Skaltsounis, L., Greengard, P., & Brivanlou, A. H. (2004). Maintenance of pluripotency in human and mouse embryonic stem cells through activation of Wnt signaling by a pharmacological GSK-3-specific inhibitor. *Nat Med* 10(1), 55-63. doi:10.1038/nm979

Schedl, A., Ross, A., Lee, M., Engelkamp, D., Rashbass, P., van Heyningen, V.*, et al.* (1996). Influence of PAX6 gene dosage on development: overexpression causes severe eye abnormalities. *Cell* 86(1), 71-82. doi:10.1016/s0092-8674(00)80078-1

Schermer, A., Galvin, S., & Sun, T. T. (1986). Differentiation-related expression of a major 64K corneal keratin in vivo and in culture suggests limbal location of corneal epithelial stem cells. *J Cell Biol* 103(1), 49-62. doi:10.1083/jcb.103.1.49

Schermer, A., Jester, J. V., Hardy, C., Milano, D., & Sun, T. T. (1989). Transient synthesis of K6 and K16 keratins in regenerating rabbit corneal epithelium: keratin markers for an alternative pathway of keratinocyte differentiation. *Differentiation* 42(2), 103-110. doi:10.1111/j.1432-0436.1989.tb00611.x

Schlotzer-Schrehardt, U., Dietrich, T., Saito, K., Sorokin, L., Sasaki, T., Paulsson, M.*, et al.* (2007). Characterization of extracellular matrix components in the limbal epithelial stem cell compartment. *Exp Eye Res* 85(6), 845-860. doi:10.1016/j.exer.2007.08.020

Schmahl, W., Knoedlseder, M., Favor, J., & Davidson, D. (1993). Defects of neuronal migration and the pathogenesis of cortical malformations are associated with Small eye (Sey) in the mouse, a point mutation at the Pax-6-locus. *Acta Neuropathol* 86(2), 126-135. doi:10.1007/BF00334879

Schofield, R. (1983). The stem cell system. *Biomed Pharmacother* 37(8), 375-380.

Shaham, O., Menuchin, Y., Farhy, C., & Ashery-Padan, R. (2012). Pax6: a multi-level regulator of ocular development. *Prog Retin Eye Res* 31(5), 351-376. doi:10.1016/j.preteyeres.2012.04.002

Shaham, O., Smith, A. N., Robinson, M. L., Taketo, M. M., Lang, R. A., & Ashery-Padan, R. (2009). Pax6 is essential for lens fiber cell differentiation. *Development* 136(15), 2567-2578. doi:10.1242/dev.032888

Shalom-Feuerstein, R., Serror, L., De La Forest Divonne, S., Petit, I., Aberdam, E., Camargo, L.*, et al.* (2012). Pluripotent stem cell model reveals essential roles for miR-450b-5p and miR-184 in embryonic corneal lineage specification. *Stem Cells* 30(5), 898-909. doi:10.1002/stem.1068

Shiraishi, A., Converse, R. L., Liu, C. Y., Zhou, F., Kao, C. W., & Kao, W. W. (1998). Identification of the cornea-specific keratin 12 promoter by in vivo particle-mediated gene transfer. *Invest Ophthalmol Vis Sci* 39(13), 2554-2561.

Singh, S., Mishra, R., Arango, N. A., Deng, J. M., Behringer, R. R., & Saunders, G. F. (2002). Iris hypoplasia in mice that lack the alternatively spliced Pax6(5a) isoform. *Proc Natl Acad Sci U S A* 99(10), 6812-6815. doi:10.1073/pnas.102691299

Singh, S., Stellrecht, C. M., Tang, H. K., & Saunders, G. F. (2000). Modulation of PAX6 homeodomain function by the paired domain. *J Biol Chem* 275(23), 17306-17313. doi:10.1074/jbc.M000359200

Sivak, J. M., West-Mays, J. A., Yee, A., Williams, T., & Fini, M. E. (2004). Transcription Factors Pax6 and AP-2alpha Interact To Coordinate Corneal Epithelial Repair by Controlling Expression of Matrix Metalloproteinase Gelatinase B. *Mol Cell Biol* 24(1), 245-257. doi:10.1128/MCB.24.1.245-257.2004

Smith, A. N., Miller, L. A., Radice, G., Ashery-Padan, R., & Lang, R. A. (2009). Stage-dependent modes of Pax6-Sox2 epistasis regulate lens development and eye morphogenesis. *Development* 136(17), 2977-2985. doi:10.1242/dev.037341

Smith, A. N., Miller, L. A., Song, N., Taketo, M. M., & Lang, R. A. (2005). The duality of beta-catenin function: a requirement in lens morphogenesis and signaling suppression of lens fate in periocular ectoderm. *Dev Biol* 285(2), 477-489. doi:10.1016/j.ydbio.2005.07.019

Sturtevant, A. H. (1951). http://www.dnaftb.org/11/bio.html.

Susaimanickam, P. J., Maddileti, S., Pulimamidi, V. K., Boyinpally, S. R., Naik, R. R., Naik, M. N.*, et al.* (2017). Generating minicorneal organoids from human induced pluripotent stem cells. *Development* 144(13), 2338-2351. doi:10.1242/dev.143040

Svoboda, K. K., & O'Shea, K. S. (1987). An analysis of cell shape and the neuroepithelial basal lamina during optic vesicle formation in the mouse embryo. *Development* 100(2), 185-200.

Take-uchi, M., Clarke, J. D., & Wilson, S. W. (2003). Hedgehog signalling maintains the optic stalk-retinal interface through the regulation of Vax gene activity. *Development* 130(5), 955-968. doi:10.1242/dev.00305

Tang, H. K., Singh, S., & Saunders, G. F. (1998). Dissection of the transactivation function of the transcription factor encoded by the eye developmental gene PAX6. *J Biol Chem* 273(13), 7210-7221. doi:10.1074/jbc.273.13.7210

Tao, Y., Cao, J., Li, M., Hoffmann, B., Xu, K., Chen, J.*, et al.* (2020). PAX6D instructs neural retinal specification from human embryonic stem cell-derived neuroectoderm. *EMBO Rep* 21(9), e50000. doi:10.15252/embr.202050000

Theiler, K., Varnum, D. S., & Stevens, L. C. (1980). Development of Dickie's small eye: an early lethal mutation in the house mouse. *Anat Embryol (Berl)* 161(1), 115-120. doi:10.1007/BF00304672

Thoft, R. A., & Friend, J. (1983). The X, Y, Z hypothesis of corneal epithelial maintenance. *Invest Ophthalmol Vis Sci* 24(10), 1442-1443.

Tiwari, A., Swamynathan, S., Campbell, G., Jhanji, V., & Swamynathan, S. K. (2020). BMP6 Regulates Corneal Epithelial Cell Stratification by Coordinating Their Proliferation and Differentiation and Is Upregulated in Pterygium. *Invest Ophthalmol Vis Sci* 61(10), 46. doi:10.1167/iovs.61.10.46

Tseng, S. C., & Li, D. Q. (1996). Comparison of protein kinase C subtype expression between normal and aniridic human ocular surfaces: implications for limbal stem cell dysfunction in aniridia. *Cornea* 15(2), 168-178. doi:10.1097/00003226-199603000-00010

Tyas, D. A., Simpson, T. I., Carr, C. B., Kleinjan, D. A., van Heyningen, V., Mason, J. O.*, et al.* (2006). Functional conservation of Pax6 regulatory elements in humans and mice demonstrated with a novel transgenic reporter mouse. *BMC Dev Biol* 6, 21. doi:10.1186/1471-213X-6-21

van Heyningen, V., & Williamson, K. A. (2002). PAX6 in sensory development. *Hum Mol Genet* 11(10), 1161-1167. doi:10.1093/hmg/11.10.1161

van Raamsdonk, C. D., & Tilghman, S. M. (2000). Dosage requirement and allelic expression of PAX6 during lens placode formation. *Development* 127(24), 5439-5448.

Vaquerizas, J. M., Kummerfeld, S. K., Teichmann, S. A., & Luscombe, N. M. (2009). A census of human transcription factors: function, expression and evolution. *Nat Rev Genet* 10(4), 252-263. doi:10.1038/nrg2538

Vazirani, J., Ali, M. H., Sharma, N., Gupta, N., Mittal, V., Atallah, M.*, et al.* (2016). Autologous simple limbal epithelial transplantation for unilateral limbal stem cell deficiency: multicentre results. *Br J Ophthalmol* 100(10), 1416-1420. doi:10.1136/bjophthalmol-2015-307348

Visel, A., Carson, J., Oldekamp, J., Warnecke, M., Jakubcakova, V., Zhou, X.*, et al.* (2007). Regulatory pathway analysis by high-throughput in situ hybridization. *PLoS Genet* 3(10), 1867-1883. doi:10.1371/journal.pgen.0030178

Walther, C., & Gruss, P. (1991). Pax-6, a murine paired box gene, is expressed in the developing CNS. *Development* 113(4), 1435-1449.

Wang, Z., Ge, J., Huang, B., Gao, Q., Liu, B., Wang, L.*, et al.* (2005). Differentiation of embryonic stem cells into corneal epithelium. *Sci China C Life Sci* 48(5), 471-480. doi:10.1360/04yc0050

Wang, Z., Yasugi, S., & Ishii, Y. (2016). Chx10 functions as a regulator of molecular pathways controlling the regional identity in the primordial retina. *Dev Biol* 413(1), 104-111. doi:10.1016/j.ydbio.2016.03.023

Watanabe, K., Nishida, K., Yamato, M., Umemoto, T., Sumide, T., Yamamoto, K.*, et al.* (2004). Human limbal epithelium contains side population cells expressing the ATP-binding cassette transporter ABCG2. *FEBS Lett* 565(1-3), 6-10. doi:10.1016/j.febslet.2004.03.064

Wawersik, S., Purcell, P., Rauchman, M., Dudley, A. T., Robertson, E. J., & Maas, R. (1999). BMP7 acts in murine lens placode development. *Dev Biol* 207(1), 176-188. doi:10.1006/dbio.1998.9153

Weisschuh, N., Wissinger, B., & Gramer, E. (2012). A splice site mutation in the PAX6 gene which induces exon skipping causes autosomal dominant inherited aniridia. *Mol Vis* 18, 751-757.

Williams, S. C., Altmann, C. R., Chow, R. L., Hemmati-Brivanlou, A., & Lang, R. A. (1998). A highly conserved lens transcriptional control element from the Pax-6 gene. *Mech Dev* 73(2), 225-229. doi:10.1016/s0925-4773(98)00057-4

Wolosin, J. M., Budak, M. T., & Akinci, M. A. (2004). Ocular surface epithelial and stem cell development. *Int J Dev Biol* 48(8-9), 981-991. doi:10.1387/ijdb.041876jw

Xu, P. X., Zhang, X., Heaney, S., Yoon, A., Michelson, A. M., & Maas, R. L. (1999). Regulation of Pax6 expression is conserved between mice and flies. *Development* 126(2), 383-395.

Yokoi, T., Nishina, S., Fukami, M., Ogata, T., Hosono, K., Hotta, Y.*, et al.* (2016). Genotype-phenotype correlation of PAX6 gene mutations in aniridia. *Hum Genome Var* 3, 15052. doi:10.1038/hgv.2015.52

Yoshida, S., Shimmura, S., Kawakita, T., Miyashita, H., Den, S., Shimazaki, J.*, et al.* (2006). Cytokeratin 15 can be used to identify the limbal phenotype in normal and diseased ocular surfaces. *Invest Ophthalmol Vis Sci* 47(11), 4780-4786. doi:10.1167/iovs.06-0574

Yun, S., Saijoh, Y., Hirokawa, K. E., Kopinke, D., Murtaugh, L. C., Monuki, E. S.*, et al.* (2009). Lhx2 links the intrinsic and extrinsic factors that control optic cup formation. *Development* 136(23), 3895-3906. doi:10.1242/dev.041202

Zhang, L., Wang, Y. C., Okada, Y., Zhang, S., Anderson, M., Liu, C. Y.*, et al.* (2019). Aberrant expression of a stabilized beta-catenin mutant in keratocytes inhibits mouse corneal epithelial stratification. *Sci Rep* 9(1), 1919. doi:10.1038/s41598-018-36392-2

Zhang, W., Cveklova, K., Oppermann, B., Kantorow, M., & Cvekl, A. (2001). Quantitation of PAX6 and PAX6(5a) transcript levels in adult human lens, cornea, and monkey retina. *Mol Vis* 7, 1-5.

Zhang, X., Huang, C. T., Chen, J., Pankratz, M. T., Xi, J., Li, J.*, et al.* (2010). Pax6 is a human neuroectoderm cell fate determinant. *Cell Stem Cell* 7(1), 90-100. doi:10.1016/j.stem.2010.04.017

Zhang, Y., Call, M. K., Yeh, L. K., Liu, H., Kochel, T., Wang, I. J.*, et al.* (2010). Aberrant expression of a beta-catenin gain-of-function mutant induces hyperplastic transformation in the mouse cornea. *J Cell Sci* 123(Pt 8), 1285-1294. doi:10.1242/jcs.063321

Zhang, Y., Yamada, Y., Fan, M., Bangaru, S. D., Lin, B., & Yang, J. (2010). The beta subunit of voltage-gated Ca2+ channels interacts with and regulates the activity of a novel isoform of Pax6. *J Biol Chem* 285(4), 2527-2536. doi:10.1074/jbc.M109.022236

Zhang, Y., Yeh, L. K., Zhang, S., Call, M., Yuan, Y., Yasunaga, M.*, et al.* (2015). Wnt/beta-catenin signaling modulates corneal epithelium stratification via inhibition of Bmp4 during mouse development. *Development* 142(19), 3383-3393. doi:10.1242/dev.125393

Zhao, S., Chen, Q., Hung, F. C., & Overbeek, P. A. (2002). BMP signaling is required for development of the ciliary body. *Development* 129(19), 4435-4442.

Zhao, S., Hung, F. C., Colvin, J. S., White, A., Dai, W., Lovicu, F. J.*, et al.* (2001). Patterning the optic neuroepithelium by FGF signaling and Ras activation. *Development* 128(24), 5051-5060.

Zhou, P., Byrne, C., Jacobs, J., & Fuchs, E. (1995). Lymphoid enhancer factor 1 directs hair follicle patterning and epithelial cell fate. *Genes Dev* 9(6), 700-713. doi:10.1101/gad.9.6.700

Zieske, J. D. (2004). Corneal development associated with eyelid opening. *Int J Dev Biol* 48(8-9), 903-911. doi:10.1387/ijdb.041860jz

Zuber, M. E. (2010). Eye field specification in Xenopus laevis. *Curr Top Dev Biol* 93, 29-60. doi:10.1016/B978-0-12-385044-7.00002-3

Zuber, M. E., Gestri, G., Viczian, A. S., Barsacchi, G., & Harris, W. A. (2003). Specification of the vertebrate eye by a network of eye field transcription factors. *Development* 130(21), 5155-5167. doi:10.1242/dev.00723

ANNEXURES

I. Media compositions

cDMEM

DMEM-F12 basal medium containing 10% fetal bovine serum (FBS), 100 U/mL Penicillin-Streptomycin solution and 2 mM GlutaMax™

Cryopreservation medium

DMEM-F12 basal medium containing 40% FBS and 10% DMSO.

Human corneal epithelial medium, HCEM

DMEM/F12 basal medium containing 10% FBS, 2 mM GlutaMax™, 100 U/mL Penicillin-Streptomycin solution, 10 ng/mL human recombinant EGF, 5 µg/mL human recombinant insulin.

II. Reagent compositions

Reagents used in molecular biology work

Genomic DNA extraction buffer

Tris-Cl – pH 8.0 (0.1 mM), EDTA – pH 8.0 (0.1 M), Sodium dodecyl sulphate (0.025%) in de-ionized water.

TAE (Tris acetate EDTA) buffer 50X Stock solution, pH 8.5

Tris (2 M), glacial acetic acid ( ), EDTA, pH 8.0 (50 mM) in de-ionized water.

Plasmid isolation solution I

Glucose (50 mM), Tris-Cl – pH 8.0 (25 mM), EDTA – pH 8.0 (10 mM) in de-ionized water.

Plasmid isolation solution II

Sodium hydroxide (0.2 N), Sodium dodecyl sulphate (1%) in de-ionized water.

Plasmid isolation solution III

Potassium acetate (5 M) in de-ionized water and adjusted to pH 5.5 with glacial acetic acid.

SDS lysis buffer

1% SDS, 10 mM EDTA, Tris-HCl-pH 8.1 (50 mM) in de-ionized water.

ChIP Dilution Buffer

0.01% SDS, 1.1% Triton X-100, 1.2 mM EDTA, Tris-HCl-pH 8.1(16.7 mM), 167 mM NaCl, 1X PI in deionoized water.

Low Salt Immune Complex Wash Buffer

0.1% SDS, 1% Triton X-100, 2 mM EDTA, Tris-HCl-pH 8.1 (20 mM), 150 mM NaCl in de-ionized water.

High Salt Immune Complex Wash Buffer

0.1% SDS, 1% Triton X-100, 2 mM EDTA, Tris-HCl-pH 8.1 (20 mM), 500 mM NaCl in de-ionized water.

LiCl Immune Complex Wash Buffer

0.25 M LiCl, 1% NP-40, 1% deoxycholic acid (sodium salt), 1 mM EDTA, Tris-HCl-pH 8.1 (10 mM) in de-ionized water.

Elution Buffer for ChIP

1%SDS, 0.1M NaHCO3 in de-ionized water.

Wash buffer for immunoprecipitation

1X PBS pH 7.4, 0.1% Triton-X 100 and protease inhibitor cocktail in de-ionized water.

Modified RIPA Buffer

Tris-HCl-pH 7.4 (25 mM**)**, 150 mM Nacl**,** 1X protease inhibitor cocktail and 0.1% Triton-X 100 in deionized water.

Resolving gel composition

30% Acrylamide-Bisacrylamide, Tris-HCl-pH 8.8 (1.5 M), 10% SDS, 10% APS and TEMED in de-ionized water.

Stacking gel composition

30% Acrylamide-Bisacrylamide, Tris-HCl-pH 6.8 (1.5 M), 10% SDS and TEMED in de-ionized water.

Running Buffer

48 mM Tris, 39 mM Glycine and 0.04% SDS in de-ionized water.

CBB staining solution

0.025% CBB R-250 in 40% methanol and 10% acetic acid in de-ionized water.

Destaining solution

30% methanol and 10% acetic acid in de-ionized water.

Transfer Buffer

48 mM Tris base, 39 mM Glycine, 0.04% SDS and 20% methanol in de-ionized water.

TBST

1M Tris (pH 7.5), 5M NaCl and 0.1% Tween 20 in de-ionized water.

TE buffer

Tris-Cl – pH 8.0 (10 mM), EDTA – pH 8.0 (1 mM) in de-ionized water.

TE-RNase

RNase A (400 μg/mL) in TE buffer.

Phosphate buffered saline 1X solution

Sodium chloride (137 mM), Potassium chloride (2.7 mM), Disodium phosphate (8 mM), Potassium dihydrogen phosphate (2 mM) in de-ionized water.

Luria Bertani agar plates with Ampicillin

Luria Bertani agar powder (40 g) suspended in 1000 ml distilled water. Heated to boiling to dissolve the medium completely. Sterilized by autoclaving at 15 lbs pressure (121°C) for 15 minutes. 100 μg/mL Ampicillin was added once the solution came down to 50-60° C. Mixed well and 20 ml of the media was poured onto sterile Petridishes (85 mm).

Luria-Bertani broth with Ampicillin

Luria Bertani broth powder (25 g) suspended in 1000 ml distilled water. Sterilized by autoclaving at 15 lbs pressure (121°C) for 15 minutes. 100 g/mL Ampicillin was added prior to use.

Hematoxylin staining solution (Stock)

Hematoxylin (0.5%), absolute ethanol (5%), ammonium aluminum sulphate (10%), Mercuric oxide (0.037%) in de-ionized water.

Hematoxylin staining solution (Working)

To 50 ml of the stock add 2-3 drops of glacial acetic acid.

Hydrochloric acid (1%) - ethanol solution

Add 1 ml of Hydrochloric acid (12 N) in 99 ml of isopropyl alcohol (70%).

Eosin stain (Stock)

Eosin (1%) in 75% ethanol.

Eosin staining solution (Working)

Add 25 ml of stock to 75 ml of 80% ethanol and 0.5ml of glacial acetic acid to obtain 100 ml of working solution of Eosin stain.

Sodium citrate buffer – pH 6.0

Sodium citrate (10 mM), Tween 20 (0.05%) in de-ionized water. pH adjusted to 6.0 using 1N HCl..

Ringer's solution

Potassium chloride (5 mM), Magnesium chloride (0.8 mM), Sodium chloride (113.4 mM), Sodium bi-carbonate (26.2 mM), Sodium dihydrogen phosphate (1 mM), Glucose (5.6 mM) and Calcium chloride (1.8 mM)

Lysis buffer

Tris – pH 8.0 (10 mM), sodium dodecyl sulphate (1%) and EDTA (50 mM)

II. Reagents used in cell culture work

10X Trypsin/EDTA

Trypsin (0.25%) and EDTA (1 mM) in 100 mL of 1X PBS solution, filtered and sterilized using 0.22 μM syringe filter.

100X Glutamine

Glutamine (200 mM) in 10 mL of sterile 1X PBS, filtered and sterilized using 0.22 μM syringe filter.

2000X Insulin

10 mg in 1 mL of sterile 1% HCl solution

2000X EGF

20 μg in 1 mL of sterile 1X PBS containing 0.1% BSA

Dispase

10 mg in 10 mL of sterile basal DMEM medium, filtered and sterilized using 0.22 μM syringe filter

IV. Chemicals/Materials used in the study

Reagent / Materials	Company / Catalog number
0.45 µm filters	PALL Acrodisc / PN4614
1 mL syringes	DISPO-VAN / 1 mL
1.5 mL centrifuge tubes	Tarson / 500010
100 mm petridish	Laxbro / PD-100
15 mL centrifuge tubes	Tarson / 546021
15 mL centrifuge tubes, cell-culture grade	BD / 352196
200 µL PCR tubes	ThermoFisher Scientific / AB0620
50 mL centrifuge tubes	Tarson / 546041
6-well plate	TPP / 92006
85 mm petridish	Laxbro / PD-85
Acetic acid, glacial	SRL / 60363
Agarose	Lonza / 50004
Ammonium Acetate	Sigma / A1542
Ammonium aluminium sulphate	Sigma / A2140
Ampicillin	Himedia / MB104
BamHI	NEB / R0136S
BglII restriction enzyme	NEB / R0144S
Big Dye Terminator	Applied Biosystems / 4337455
Bleach (1% hypochlorite solution)	Loba chemie / 283
Bovine Serum Albumin	Sigma / A7906
Cell scraper	Corning® Costar® / 3010

Chloroform	Merck / 1.94506.0521
Calf Intestinal Phosphatase (CIP)	NEB / M0525S
Coplin jar	Tarson / 480000
Cryovials	Nunc / V7884
DAB, 3-3- diamidino benzidine	DAKO / K0673
DAPI	Invitrogen™ / D1306
DEPC	Sigma / D5758
Disodium hydrogen phosphate	Sigma / S5136
DMEM-F12	Gibco / 10565-018
DMSO	Sigma / D8418
DNA ladder, 100 bp	Thermo Fisher Scientific / SM0241
DNA ladder, 1 kb	Thermo Fisher Scientific / SM0313
dNTPs	Bioline / BIO-39049
DPX mountant	SD fine chemicals / 46029-L02
Dulbecco's phosphate-buffered saline, DPBS	Sigma / D5652
EcoRV	NEB / R0195S
EcoRI	NEB / R0101S
EDTA	Sigma / E5134
EDTA, cell-culture grade	Gibco / 13151014
EGF, human recombinant protein	Biosource / PHG0311
Eosin - Y	Sigma / E4382
Ethanol	Changshu hongshen fine chemical ltd.
Ethidium bromide	Sigma / E7673

Fetal Bovine Serum, US origin	Gibco / 26140079
Formaldehyde Solution	Merck / 1.94950.0521
Glass coverslip, round, 18 mm	Blue star / 000871
Glucose	SRL / 42738
GlutaMAX™	Gibco / 35050061
L- Glutamine	Sigma / G6392
Glycerol	Sigma / G2025
Hematoxylin	Sigma / H3136
Hemocytometer	ROHEM INDIA / B.S. 748
Hi-Di Formamide	Applied Biosystems / 4311320
Hydrochloric acid	Thermo Fisher Scientific / A142-212
Hydrogen peroxide	Thermo Fisher Scientific / 18706
Insulin, human recombinant protein	Sigma / I2643
Isoamyl alcohol	Merck / 1.94608.0521
Isopropanol	Thermo Fisher Scientific / 26895
Lipofectamine 3000 Transfection Reagent	Invitrogen / L3000008
Luria Bertani agar	HIMEDIA / M1151
Luria Bertani broth	Himedia / M1245
Magnesium chloride	Merck / 1.93663.0521
Methanol	Thermo Fisher scientific / 43637G
NEB buffer 2.1	NEB / B7202S
NEB buffer 3.1	NEB / B7203S
No. 21 surgical blade	SURGEON / AF-055/2
NucleoBond® Xtra Midi kit	MN / 740410.100

Paraformaldehyde	EMS / 19200
pCMV_VSV-G	Addgene / 8454
pDR8.2_GPRT	Addgene / 8455
Penicillin-Streptomycin solution	Gibco / 15140122
Penicillin	Sigma / P3032-10 MU
pGL3 basic vector	Promega / E1751
Phenol	Sigma-Aldrich / P1037
Phusion DNA polymerase	NEB / M0530S
pIRES2-EGFP vector	Clontech / 6029-1
pLNCX2 vector	Clontech / 6102-1
pMOS-Blue blunt cloning vector	Sigma / GERPN5110
Polybrene	Sigma / TR1003
Potassium acetate	Sigma / P1190
Potassium chloride	SRL / 38630
Potassium dihydrogen phosphate	Sigma / P5655
Propidium iodide, PI	Sigma / P4170
Proteinase K	Genei / 2150180251730
RNase A	Sigma / R6513
SalI restriction enzyme	NEB / R0138S
Sequencing buffer	Applied Biosystems / 4336697
SmaI	NEB / R0141S
Sodium acetate	Sigma / S2889
Sodium bicarbonate	Sigma / S5761
Sodium butyrate	Sigma-Aldrich / B5887

Sodium chloride	SRL / 33205
Sodium dodecyl sulphate	SRL / 54468
Sodium hydroxide	Thermo Fisher Scientific / S320-1
Streptomycin	Sigma / S9137
SuperScript™ III Reverse Transcriptase	Thermo Fisher Scientific / 18080051
T4 DNA ligase	NEB / M0202S
T4 Polynucleotide Kinase	NEB / M0201S
T4 DNA Polymerase	NEB / M0203S
Taq Polymerase	Invitrogen / 610602400051730
TRIS base	Thermo Fisher Scientific / BP152-1
Triton™ X-100	Sigma-Aldrich / X100
TRIzolTM	Invitrogen / 15596026
Trypsin	Sigma / T4799
Xylene	Thermo Fisher Scientific / 35417

V. Primers used in the study

Genes	Primer sequence	Product Size in (bp)	NCBI Accession number
Primers used in PAX6 gene and promoters cloning			
hPAX6 PromA hPAX6 PromA-F hPAX6 PromA-R	**5'** CAGTCCACAGAAGGTGTGA 3' 5' GCAGATCTGACAGCCGCGTTCTA 3'	934	NC_000011.10
hPAX6 PromC hPAX6 PromC-F hPAX6 PromC-R	**5'** ATCTATTAGTTGCTTCGCGGTCGAGTTC 3' **5'** ATTCTCTAAGGTTGGACCACAGGGATCC 3'	1245	NC_000011.10
hPax6-OSE hPax6-OSE-EN-F hPax6-OSE-EN-R	5' GAATTCGATCACATGGACCTTTTGGG 3'	586	NC_000011.10

	5' AAGCTTCGGACCTCTGTGGAAAATCTCCAA 3'		
RT-PCR loading controls			
eEF1α	F: 5' GAAGTCTGGTGATGCTGCCATTGT 3' R: 5' TTCTGAGCTTTCTGGGCAGACTTG 3'	198	NM_001402.6
GAPDH	F: 5' CGTGGAAGGACTCATGACCACA 3' R: 5' TGTCGCTGTTGAAGTCAGAGGA 3'	359	NM_001357943.2
hACTB	F: 5' TGGCATCCACGAAACTACCT 3' R: 5' TGCTTGCTGATCCACATCTG 3'	264	NM_001101.5
Sequencing Primers			
M13-Fwd	5' GTTTTCCCAGTCACGAC 3'		
T7-Rev	5' TAATACGACTCACTATAGGG 3'		
hPAX6 PAX6-F PAX6-R	5' GCCAGCATGCAGAACAGTCACAG 3' 5' TTACTGTAATCTTGGCCAGTATTG 3'	1331 (5a) 1289 (Wt)	NM_001368892.2
hPAX6 hPax6-E5-F: hPax6-E7-R	5' GAAGATTGTAGAGCTAGCTCACAGCG 3' 3' TGTTGCTTTTCGCTAGCCAGGTTG 3' Amplifies all isoforms	369(5a), 327(wt) 168(5a-ASΔ6) 126(wt-ASΔ6) 111(wt-Δ6)	NM_000280 NM_001604
hPAX6A specific hPax6-E5-F: hPax6-5-6-R1:	5'GAAGATTGTAGAGCTAGCTCACAGCG 3' 5' TACTCACACATCCGTTGGACACCTG 3'	83	
hPAX6B specific hPax6-E5-F: hPax6-5a-6-R1:	5'GAAGATTGTAGAGCTAGCTCACAGCG 3' 5' TACTCACACATCCGTTGGACACGTT 3'	125	
hPAX6B-ASΔ6 specific hPax6-del6-7-F: hPax6-E7-R:	5' AAACGTGTCCAACGGATGTGTGTCATCA 3' 5' CACCGAAGTCCCCGGATACCAAC 3'	166	
hPAX6A-Δ6 specific hPax6-E5-7-F: hPax6-E7-R:	5' CCCGAATTCTGCAGGTGTCATCAATA 3' 5' CACCGAAGTCCCCGGATACCAAC 3'	161	
hPAX6-12a specific hPax6-E11-F: hPax6-12a-R:	5' CTATGCCCAGCTTCACCATGGCAAAT 3' 5' TAGCCATGTAGATATTCCCTGTTG 3'	210	
hPax6-pA specific hPax6-pA-E1-RT-F: hPax6-E7-R:	5' CGTAGAACGCGGCTGTCAGAT 3' 5'TGTTGCTTTTCGCTAGCCAGGTTG 3	871 (5a), 829 (wt) 670 (5a-ASΔ6) 628 (wt-ASΔ6) 613 (wt-Δ6)	

hPax6-pB specific hPax6-pB-E1-RT-F: hPax6-E7-R:	5' CTTGAGCCATCACCAATCAGCA 3' 5'TGTTGCTTTTCGCTAGCCAGGTTG 3'	790 (5a), 748 (wt) 589 (5a-ASΔ6) 547 (wt-ASΔ6) 532 (wt-Δ6)	
hPax6-pC specific hPax6-pC-E1-RT-F: hPax6-E7-R:	5' TGACTCTCACGTCTGCACTGGA 3' 5'TGTTGCTTTTCGCTAGCCAGGTTG 3'	462 (5a), 420 (wt) 261 (5a-ASΔ6) 219 (wt-ASΔ6) 204 (wt-Δ6)	
Primers used in p63 gene and promoters cloning			
ΔNp63 FL Prom XhoI- ΔNp63-F1 ΔNp63-R	5' GATCTCGAGACTTGGGACCCTGAGCCTTA 3' 5' CCAAAGCTTCCACCCCGAGACCCTTACAAT 3'	2082	NC_000003.12
ΔNp63 Mini Prom ΔNp63-F2 ΔNp63-R	5' CTTATGCTCGAGACAGGGAAAGTTTTACC 3' 5' CCAAAGCTTCCACCCCGAGACCCTTACAAT 3'	331	NC_000003.12
TA-p63 FL Prom TA-p63-Prom-F1 TA-p63-Prom-R1	5' GGGAGCATCAAGTAACCTGGGAACGTG 3' 5' GGGATATAAAGCCGGGAGGCTAAAAGCA 3'	1829	NC_000003.12
TA-p63 Mini Prom TA-p63-Prom-F2 TA-p63-Prom-R1	5' GGGAGGCAAAGCTTCTAAGGGGATGTGAAA 3' 5' GGGATATAAAGCCGGGAGGCTAAAAGCA 3'	690	NC_000003.12
hΔN-p63-RT	F: 5' TGGCAAAATCCTGGAGCCAGAAG 3' R: 5' GTTCTGAATCTGCTGGTCCATGCT 3'	154	NM_001329149.2
hTA-p63-RT	F: 5' CCCTTACATCCAGCGTTTCGTAGA 3' R: 5' GTTCTGAATCTGCTGGTCCATGCT 3'	331	NM_001329148.2
Primers used in *KRT3*, *KRT12* gene and promoters cloning			
KRT3 FL Prom hK3-Prom-F1 hK3-Prom-R1	5'ATCCAAGGCTGGTCTGAAACTCCTG3' 5'ATCTTGGCGAAGAGAAGAGTGTAAGTTAAGCAG 3'	2379	NC_000012.12
KRT3 Mini Prom hKRT3-Prom-F3 hKRT3-Prom-R1	5'ATCTGGGCACATACTGTGCACTCAGTCA 3'	571	NC_000012.12

	5'ATCTTGGCGAAGAGAAGAGTGTAAGTTAAGCAG 3'		
KRT12 FL Prom hKRT12-Prom-F1: hKRT12-Prom-R1:	5' ATCTCTGCTATTGAAGTGTCCA 3' 5' ATCACAACTGGAGAGGAAGTTGTGC 3'	2554	NC_000017.11
KRT12 Mini Prom hKRT12-Prom-F3: hKRT12-Prom-R1:	5' ATCCAGTGCATTTCACAGCTGCTTC 3' 5' ATCACAACTGGAGAGGAAGTTGTGC 3'	550	NC_000017.11
hKRT12-RT	F: 5' ATTGGAAATGCCCAGCTCCT 3' R: 5' TCTGCTCAGCGATGGTTTCA 3'	352	NM_000223.4
hKRT3-RT	F: 5' AGGCATGGGGATGACCTAAGA 3' R: 5' CACGGAGATGCTGACAGCACT 3'	360	NM_057088.3
hKRT12-RT	F: 5' ACATGAAGAAGAACCACGAGGATG 3' R: 5' TCTGCTCAGCGATGGTTTCA 3'	150	NM_000223.4
Canonical Wnt signalling Primers			
hCCND1	F: 5' TCCGGGTCACACTTGATCACTCT 3' R: 5' CCCGCACGATTTCATTGAACACT 3	258	NM_053056.3
hLEF1	F: 5' AGCGAATGTCGTTGCTGAGTGT 3' R: 5' CAGCTGTCATTCTTGGACCTGT 3'	248	NM_001130713.3
Chromatin Immunoprecipitation Primers			
Delta N-p63αF1 **Delta N-p63αR1**	5' ACTTGGGACCCTGAGCCTTA 3' 5' TGTGTCTAAATTCTACACCT 3'	377	
Delta N-p63αF2 **Delta N-p63αR2**	5' TTTGCCTTCTAGGCAGTGCT 3' 5' TCAGGGACCCAATTTCCTCTAT 3'	483	
EcoRV-ΔNp63-F **EcoRV-ΔNp63-R**	5' CATCAGGGTGCATTTCATCTCC 3' 5' CTGCACGTGATGCATCTATGT 3'	164	
TA-p63-Prom-F1 **p63_TA Prom_ChIP-R**	5' GGGAGCATCAAGTAACCTGGGAACGTG 3' 5' AGCGGCTAACATCTGTGAATTGTG 3'	415	
p63_TA Prom ChIP-F **EcoRV-TA-p63-Prom-R2**	5' CCAGGATAAGTTTACAGCCCATATTC 3' 5' ATCCCTTTCACATCCCCTTAGAAGC 3'	415	
hK12-Prom_ChIP-F1 **hK12-Prom_ChIP-R1**	5' AGCAGTAAACTACGGGGAATCT 3' 5' AAGACACTGGGCAAATGGACTA 3'	499	

hK12-Prom-F3 **hK12-Prom-R1**	ATCCAGTGCATTTCACAGCTGCTTC ATCACAACTGGAGAGGAAGTTGTGC	550	
hK3-Prom_ChIP-F1 **hK3-Prom_ChIP-R1**	5' GGAGTAAACACTTAGGGCGCTT 3' 5' GGAGTAAACACTTAGGGCGCTT 3'	296	
hK3-Prom-F1: **hK3-Prom_ChIP-R2**	5'ATCCAAGGCTGGTCTGAAACTCCTG3' 5' TGAAGTTAGCCCAGGCCTAGAGT 3'	347	
hK3-Prom_ChIP-F2 **hK3-Prom_ChIP-R2**	5' CACCTGGGTCTACAGGCACAT 3' 5' TGAAGTTAGCCCAGGCCTAGAGT 3'	425	
hK3-Prom-F2 **hK3-Prom_ChIP-R3**	ATCCAGTATAAGGGCTTAACCATTAGT 5' GCTGCACATTGGGCCCTTCTAA 3'	399	
hK3-Prom-F3 **hK3-Prom-R1**	ATCTGGGCACATACTGTGCACTCAGTCA CTGCTTAACTTACACTCTTCTCTTCGCCAAG AT	571	

VI. Antibodies used in the study

Antigen	Antibody	Manufacturer	Catalogue No.	Conc.	Dilution
P63	Mouse monoclonal	Santa Cruz	sc-8431	0.2 mg/mL	1:100
PAX6	Mouse monoclonal	Santa Cruz	sc-81649	0.2 mg/mL	1:100
Melan A	Mouse monoclonal	abcam	ab731	1 mg/mL	1:300
PAX6	Rabbit polyclonal	abcam	ab5790	1 mg/mL	1:300
K3/12	Mouse monoclonal	abcam	ab68260	1 mg/mL	1:300
BrdU	Mouse monoclonal	abcam	ab8152	1 mg/mL	1:300
β-Catenin	Rabbit polyclonal	abcam	ab6302	1 mg/mL	1:300
Kaiso	Mouse monoclonal	abcam	ab12723	1 mg/mL	1:200
TCF4	Goat polyclonal	Santa Cruz	sc-8631	200 µg/ml	1:100
p75NTR	Rabbit monoclonal	Cell signalling	8238		1:300

HDAC1	Rabbit polyclonal	Santa Cruz	sc-7872		1:200
Ki 67	Mouse monoclonal	Dako	M724029	0.05 mg/mL	1:100
Acetylated tubulin	Mouse monoclonal	Sigma	T6793	Ascites fluid	1:500
GFP	Mouse monoclonal	abcam	ab1218	1 mg/mL	1:1000
GFP	Rabbit monoclonal	abcam	ab290	100µg	1:1000
Secondary Antibodies					
Alexa Fluor® 488-anti-Mouse IgG	Goat polyclonal	Invitrogen	A11001	2 mg/mL	1:300
Alexa Fluor® 488-anti-Rabbit IgG	Goat polyclonal	Invitrogen	A-11008	2 mg/mL	1:300
Alexa Fluor® 594-anti-Mouse IgG	Goat polyclonal	Invitrogen	A-11005	2 mg/mL	1:300
Alexa Fluor® 594-anti-Rabbit IgG	Goat polyclonal	Invitrogen	A-11012	2 mg/mL	1:300
Alexa Fluor® 488-anti-Goat IgG	Donkey polyclonal	Invitrogen	A-11055	2 mg/mL	1:300
Anti-Mouse IgG Biotin	Goat Polyclonal	Invitrogen	B-2763626540	2 mg/ml	1:300
Anti-Rabbit IgG Biotin	Goat Polyclonal	Invitrogen	B-2770656140	2 mg/ml	1:300
Streptavidin-Alexa 488	-	Invitrogen	S-11223	1 mg/mL	1:300
Streptavidin-Alexa 594	-	Invitrogen	S-11227	1 mg/mL	1:300
Propidium iodide, PI	NA	Sigma	P4170	1 mg/mL	1:1000
DAPI	NA	Sigma	D8417	1 mg/mL	1:1000
Hoechst	NA	Sigma	382061	1 mg/mL	1:1000

Awards and Honors

National Awards

1. Received CSIR Senior Research Fellowship for PhD tenure.

2. Received IERG ARVO-India Travel Grant to attend the conference at Sankara Nethralaya, Chennai, India, Jul 27th – 28th 2019.

3. Received Prerna award for the recognition of service beyond the call of duty, L V Prasad Eye Institute on 31 March 2017

List of Presentations

- Vinay Kumar Pulimamidi, Vivek Pravin Dave, Praveen Joseph Susaimanickam, Savitri Maddileti, Sreedhar Rao Boyinpally, Subhadra jalali, Taraprasad Das, Indumathi Mariappan. **Assesment of in vivo survival and safety ogf human induced pluripotent stem cells (iPSC) derived retinal pigmented epithelial (RPE) cells in dystrophic RCS rat eyes.** Indian Eye Research Group-ARVO, 27th Annual Meeting organized by the LV Prasad Eye Institute, Hyderabad, Indian, Oct 7th -10th (Virtual)
- Vinay Kumar Pulimamidi, Savitri Maddileti, Indumathi Mariappan. **Human PAX6 promoter A and its regulation in LSCS**. Hy-Sci 2019 organized by CCMB, Hyderabad, India, 29th Aug-2019.
- Vinay Kumar Pulimamidi, Savitri Maddileti, Indumathi Mariappan. **Human PAX6 promoter A and its regulation in LSCS. Indan Eye Research Group**-ARVO organized by the Sankara Nethralaya, Chennai, India, Jul 27th – 28th 2019.
- Vinay Kumar Pulimamidi, Savitri Maddileti, Indumathi Mariappan. **Differential regulation of human PAX6 promoters in different ocular cell types**. Indan Eye Research Group-ARVO organized by the LV Prasad Eye Institute, Hyderabad, India, Jul 15th 2018.
- Vinay Kumar Pulimamidi, Savitri Maddileti, Indumathi Mariappan. **Differential regulation of human Pax6 promoters and the surface ectoderm enhancer in different ocular cell types**. Indan Eye Research Group-ARVO organized by the Aravind Eye Hospital, Madurai, India, Jul 29th – 30th 2017.
- Vinay Kumar Pulimamidi, Savitri Maddileti, Indumathi Mariappan. **Establishment of limbal stromal cell line**. Indan Eye Research Group-ARVO organized by the LV Prasad Eye Institute, Hyderabad, India, Jul 26th – 27th 2016.

List of Publications

Original research articles

- Susaimanickam PJ, Maddileti S, Pulimamidi VK, Boyinpally SR, Naik RR, Naik MN, Reddy GB, Sangwan VS, Mariappan I. Generating minicorneal organoids from human induced pluripotent stem cells. **Development.** 2017 Jul 1;144(13):2338-2351. DOI: 10.1242/dev.143040
- Kumar V**,** Ali MJ, Ramachandran C**.**. Effect of mitomycin-C on contraction and migration of human nasal mucosa fibroblasts: implications in dacryocystorhinostomy. **Br J Ophthalmol** 2015 Sep; 99(9):1295-300. DOI: 10.1136/bjophthalmol-2014-306516
- Pulimamidi VK, Maddileti S, Mariappan I. Human PAX6 and its target gene regulation by Wnt signals in ocular cells. Sci Rep. 2022; (Manuscript under review).
- Pulimamidi VK, Maddileti S, Mariappan I. Novel PAX6 variants and their roles in corneal epithelial regulation and homeostasis. Stem cells. 2022; (Manuscript under review).

Book chapter

- Pulimamidi VK, Maddileti S, Mariappan I. Induced pluripotent stem-cell-derived corneal grafts and organoids. IPSCs in tissue engineering, 99-127. https://doi.org/10.1016/B978-0-12-823809-7.00005-0.

© 2017. Published by The Company of Biologists Ltd | Development (2017) 144, 2338-2351 doi:10.1242/dev.143040

Generating minicorneal organoids from human induced pluripotent stem cells

Praveen Joseph Susaimanickam[1,*], Savitri Maddileti[1,*], Vinay Kumar Pulimamidi[1], Sreedhar Rao Boyinpally[2], Ramavat Ravinder Naik[3], Milind N. Naik[4], Geereddy Bhanuprakash Reddy[5], Virender Singh Sangwan[1,6] and Indumathi Mariappan[1,6,‡]

ABSTRACT

Corneal epithelial stem cells residing within the annular limbal crypts regulate adult tissue homeostasis. Autologous limbal grafts and tissue-engineered corneal epithelial cell sheets have been widely used in the treatment of various ocular surface defects. In the case of bilateral limbal defects, pluripotent stem cell (PSC)-derived corneal epithelial cells are now being explored as an alternative to allogeneic limbal grafts. Here, we report an efficient method to generate complex three-dimensional corneal organoids from human PSCs. The eye field primordial clusters that emerged from differentiating PSCs developed into whole eyeball-like, self-organized, three-dimensional, miniature structures consisting of retinal primordia, corneal primordia, a primitive eyelid-like outer covering and ciliary margin zone-like adnexal tissues in a stepwise maturation process within 15 weeks. These minicorneal organoids recapitulate the early developmental events *in vitro* and display similar anatomical features and marker expression profiles to adult corneal tissues. They offer an alternative tissue source for regenerating different layers of the cornea and eliminate the need for complicated cell enrichment procedures.

KEY WORDS: Human induced pluripotent stem cells, Ocular differentiation, Organogenesis, Corneal organoids

INTRODUCTION

Cornea is the transparent, avascular tissue on the ocular surface through which light enters the eye. Any damage to its epithelial, stromal or endothelial cell layers can lead to visual impairment. The annular limbus surrounding the cornea harbors adult stem cells that regenerate different parts of the cornea (Schermer et al., 1986; Cotsarelis et al., 1989). Cell replacement therapy using autologous or allogeneic adult limbal grafts has been the standard treatment for patients with severe limbal stem cell deficiency (LSCD) (Rama et al., 2010; Sangwan et al., 2011; Basu et al., 2016). However, in the case of bilateral epithelial defects and for the treatment of conditions affecting the stromal and endothelial cell layers, alternative stem cell sources such as embryonic stem cells (ESCs) and induced pluripotent stem cells (iPSCs) have been explored with a view to generating the various corneal cell types (Ahmad et al., 2007; Shalom-Feuerstein et al., 2012; Hayashi et al., 2012; Sareen et al., 2014; Mikhailova et al., 2014; Chan et al., 2013; Zhang et al., 2014; Chen et al., 2015; McCabe et al., 2015).

A recent report has shown coordinated development of corneal epithelium, neural crest cells, lens epithelium and retinal cells from iPSCs in a two-dimensional (2D) culture system and employed FACS to establish pure cultures of corneal epithelial cells (Hayashi et al., 2016). However, the requirement of rigorous cell enrichment protocols imposes a major hurdle in tissue-specific cell expansion, but can be overcome by establishing three-dimensional (3D) culture systems. This method exploits the inherent self-organizing capacity of differentiating progenitor cell populations, together with the surrounding niche cells, to generate complex tissue structures *in vitro*. This has been demonstrated successfully with the generation of neuroretinal tissues using PSCs (Eiraku et al., 2011; Gonzalez-Cordero et al., 2013; Assawachananont et al., 2014; Reichman et al., 2014; Zhong et al., 2014; Hiler et al., 2015; Kaewkhaw et al., 2015; Völkner et al., 2016). A recent report has described a method of generating immature corneal organoids from human iPSCs and shown them to express a few corneal markers (Foster et al., 2017). We report here a much simpler and efficient culture method that can generate complex 3D corneal organoids from both human ESCs and iPSCs. We report the establishment of long-term cultures and the characterization of these organoids at different stages of maturation. The mature organoids developed into complex, multilayered, minicornea-like 3D tissues and recapitulated the early developmental events *in vitro*. We also show that they offer an alternative tissue source for various ocular cell types and report the generation of transplantable sheets of corneal epithelium suitable for regenerative applications.

RESULTS

Derivation and characterization of human iPSCs

As pluripotent stem cells are valuable cell sources for generating various ocular cell types and for the study of organ development *in vitro*, we derived and characterized several human iPSC lines from human dermal fibroblasts as described earlier (Takahashi et al., 2007). As shown in Fig. S1A, the hiPSC-F2-3F1 line formed typical ESC-like colonies both on mouse embryonic fibroblast (MEF) feeders and on Matrigel-coated surfaces. This line expanded well under standard human iPSC culture conditions and the cells were passaged more than 25 times. They remained pluripotent and expressed the stem cell markers OCT4 (POU5F1), SOX2, SSEA4 and alkaline phosphatase (Fig. S1B). When passage 25 cells were transplanted into the subcutaneous space of nude mice, they

[1]Sudhakar and Sreekanth Ravi Stem Cell Biology Laboratory, Prof. Brien Holden Eye Research Centre, Hyderabad Eye Research Foundation, L.V. Prasad Eye Institute, Hyderabad 500 034, India. [2]Ophthalmic Pathology Laboratory, L.V. Prasad Eye Institute, Hyderabad 500 034, India. [3]National Centre for Laboratory Animal Sciences, National Institute of Nutrition, Hyderabad 500 007, India. [4]Department of Ophthalmic Plastic and Facial Aesthetic Surgery, L.V. Prasad Eye Institute, Hyderabad 500 034, India. [5]Biochemistry Division, National Institute of Nutrition, Hyderabad 500 007, India. [6]Tej Kohli Cornea Institute, Centre for Ocular Regeneration, L.V. Prasad Eye Institute, Hyderabad 500 034, India.
*These authors contributed equally to this work

‡Author for correspondence (indumathi@lvpei.org)

P.J.S., 0000-0002-1567-1312; V.K., 0000-0002-1365-878X; S.R.B., 0000-0002-2136-4415; R.R.N., 0000-0003-3884-157X; I.M., 0000-0001-7059-3030

Received 30 July 2016; Accepted 19 May 2017

Development (2017) 144, 2338-2351 doi:10.1242/dev.143040

proliferated and developed into teratomas comprising all three germ layers within 6 weeks (n=8, 6/8 animals developed teratomas) (Fig. S1C). The gross karyotype of this female line was found to be normal at passage 20 (Fig. S1D). Genotype analysis confirmed the presence of integrated copies of the three transgenes *OCT4*, *SOX2* and *KLF4*, but not *cMYC*. The endogenous copies of all four genes were active in passage 25 cells and were expressed at levels comparable to that of the human ESC line BJNhem20 (Inamdar et al., 2009; Mariappan et al., 2015) (Fig. S1E).

Eye field differentiation of iPSCs and the development of corneal primordial structures

To induce ocular differentiation, the iPSCs and ESCs were grown to 70-80% confluence under feeder-free conditions and differentiation was initiated *in situ* as described in Fig. 1A. At 4 weeks of differentiation, distinct clusters of raised, circular to oval-shaped eye field primordial (EFP) clusters (or 'EFPs') had developed (Fig. S2A). Starting from 1×10^6 PSCs, an average of 27.33±13.63 EFP clusters could be generated from a well of a 6-well plate (n=6). To confirm that these are EFPs, we manually collected the clusters for total RNA isolation and marker expression analysis by reverse transcription PCR (RT-PCR). As shown in Fig. S2B, the expression of *PAX6*, *OTX2*, *SIX6* and *RX* (*RAX*) confirmed that these 3D clusters consisted of eye field-committed progenitor cells. When the EFPs were allowed to differentiate further *in situ*, they gave rise to lens epithelial clusters (Fig. S2C) and a SEAM (self-formed ectodermal autonomous multizone) of ocular surface epithelium by 6-8 weeks, as described by Hayashi et al. (2016). The central island of neuroretinal (NR) cells was CHX10 $(VSX2)^+$ and $RCVRN^+$, and the SEAM of ocular surface ectodermal (OSE) sheets was P63 $(TP63)^+$ (Fig. 1Bi,ii). A wave of $SOX10^+$ pigmented neural crest cells (NCCs) marked the boundary between NR and OSE cell zones (Fig. 1Biv). Retinal pigmented epithelial (RPE) cells emerged as a compact, non-pigmented epithelium surrounding the NR clusters and later matured to acquire pigmentation. Lentoid clusters expressing gamma-crystallin developed at a precise location adjacent to NR clusters (Fig. 1Bv, Fig. S2C). The NR clusters developed into optic cups and $CHX10^+$ precursors self-organized to form the NR layer (Fig. S2D). Pigmented melanocytes were also observed interspersed within the zone of migrating epithelial cells (Fig. 1Bvi, Fig. S2E).

Apart from the emergence of SEAMs, rare EFP clusters developed into 3D, miniature eyeballs, with transparent anterior-segment-like structures on the surface and complex NR structures beneath. A wave of pigmented NCCs set the boundary for the cornea-like structures (Fig. 2Aiii,iv). When the EFPs at 4 weeks were manually collected and cultured under suspension in non-adherent dishes, 40.05±3.89% gave rise to distinct corneal primordial (CP) structures distinct from the generally observed retinal primordia (RP) (n=6; Fig. 2Avi-ix). In the earlier method described by Hayashi et al. (2016), the corneal epithelial cell enrichment was achieved by approximate zoning of cell outgrowths within the SEAM region and by FACS of $SSEA4^+$ and $ITGB4^+$ cells. However, the method described here enables the self-organization of different CP cells (OSE cells and NCCs) into 3D minicorneal organoids that can directly serve as valuable tissue sources to study corneal development *in vitro* and also to establish pure cultures of different corneal cell types.

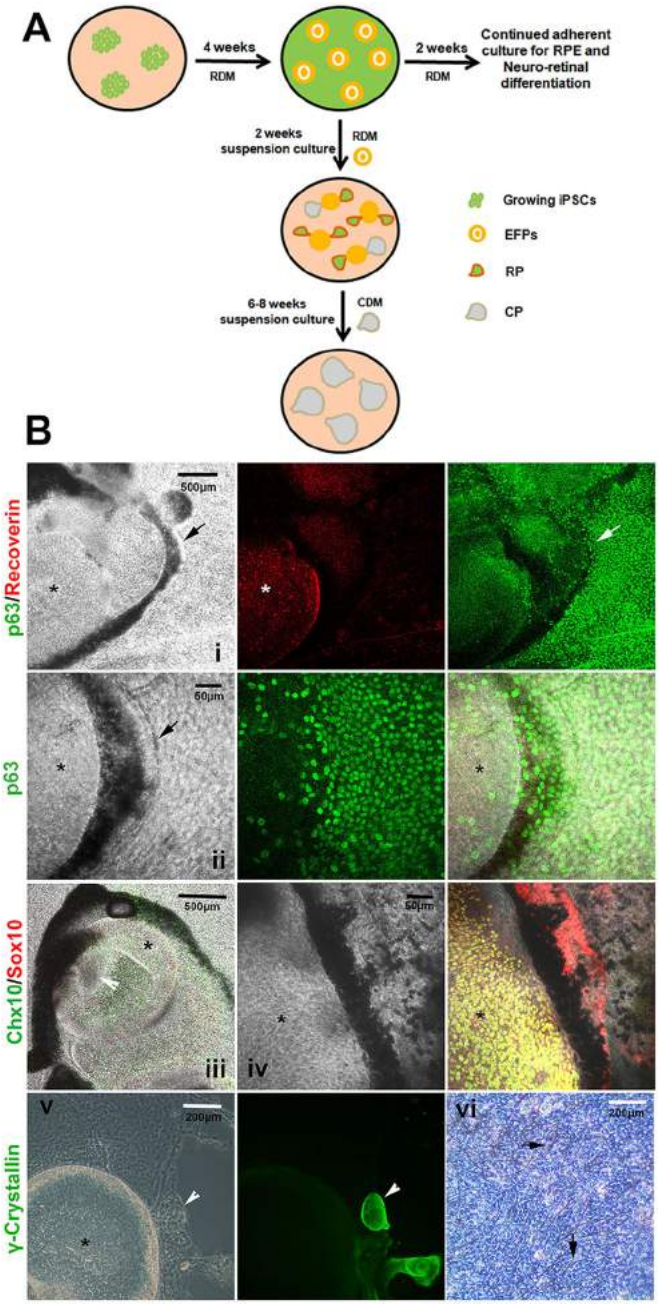

Fig. 1. Characterization of iPSC-derived eye field primordial (EFP) clusters. (A) Schematic representation of the stepwise differentiation of human iPSCs into retinal and corneal organoids. Growing iPSCs are first differentiated into EFPs, which upon isolation and suspension culture give rise to both retinal primordia (RP) and corneal primordia (CP). The dissected-out CP are cultured under corneal differentiation conditions for further maturation. CDM, corneal differentiation medium; RDM, retinal differentiation medium; RPE, retinal pigmented epithelium. (B) Distinct circular to oval-shaped EFPs encompassed a centrally located $CHX10^+$ $RCVRN^+$ neuroretinal (NR) cup (asterisks) (i). Pigmented neural crest-derived cells and $P63^+$ ocular surface ectodermal (OSE) cells appear to differentiate from the edges of EFP clusters. Arrows point to a distinct margin comprising a spindle-shaped melanocyte enriched-zone between the NR and OSE cells (i-iv). Arrowheads point to $crystallin^+$ lentoid clusters adjacent to NR cups (v) and a phase image showing the presence of pigmented melanocytes (arrows) over a layer of epithelial sheet within the migratory cell zone (vi).

Morphological features of minicorneas

The minicorneas (MCs) ranged from ~1-7 mm in diameter (Table S3). A magnified view of MCs revealed the presence of a uniform epithelial cell lining (Fig. 2Aix, Movie 1). Transmission electron microscopy images of an 8-week-old MC revealed the presence of a layer of epithelium with tight junctions and numerous

Development (2017) 144, 2338-2351 doi:10.1242/dev.143040

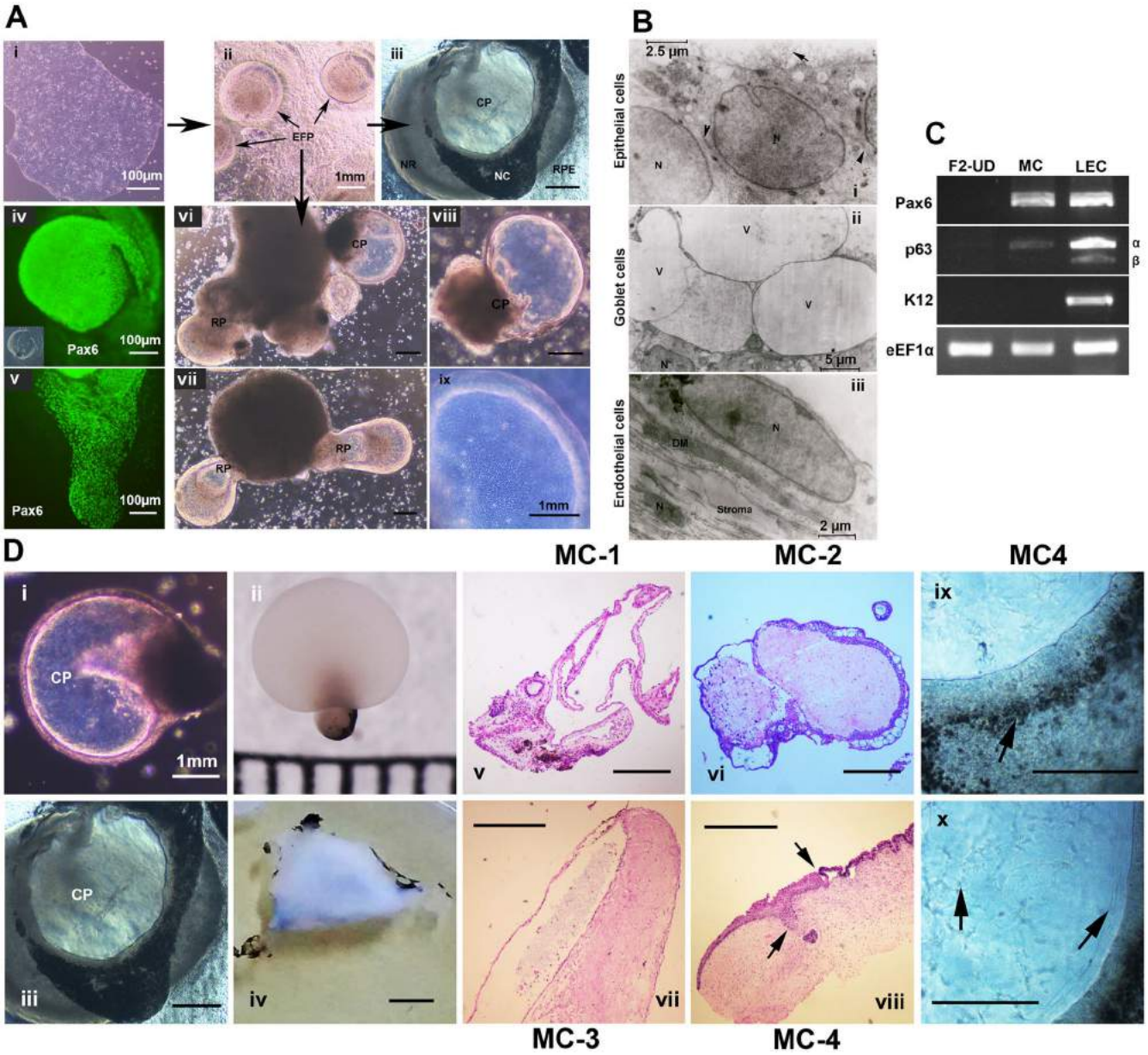

Fig. 2. Morphology of developing corneal organoids. (A) Growing iPSCs (i) differentiate into EFP clusters (ii), which further mature to form whole eyeball-like structures, with transparent CP on the surface and NR cup on the basal side. Pigmented neural crest (NC) cells mark the corneal boundary (iii). Pigmented RPE-like cells are seen migrating out of the NR tissue on the basal side. A subset of PAX6^{+} NR clusters was able to self-organize into optic vesicle-like structure with an optic stalk (iv, inset) and migrating OSE cells (v). Suspension cultures of EFPs gave rise to RP and CP structures (vi,vii), which were isolated and cultured separately for further maturation (viii,ix). *n*=6. (B) TEM images of an 8-week-old minicornea (MC) showing epithelial microvilli (arrow) and tight junctions between cells (arrowheads), cell nuclei (N), microvesicles (v) and Descemet's-like membrane (DM). (C) RT-PCR profiles of 8-week-old MCs, as compared with undifferentiated iPSCs (F2-UD) and primary limbal epithelial cultures (LEC). (D) Representative images of MCs at different stages of development under suspension culture (i,ii) and adherent culture (iii,iv). H&E-stained sections of MCs analyzed (v-viii), showing limbus-like margin (arrows). Magnified view of adherent MC, with pigmented melanocytes (arrows) observed around the corneal periphery and spindle-shaped stromal cell infiltration seen within the transparent CP (ix,x). Scale bars: 1 mm, unless otherwise specified.

apical microvilli, which is a feature of corneal epithelium but not that of lens epithelial cells. The mucin-secreting goblet cells had numerous microvesicles on the apical surface. The middle stromal layer consisted of well-organized collagen fibrils interspersed with stromal cells. A monolayer of flat endothelium-like cells was observed on the inner surface, with a Descemet's-like basement membrane (Fig. 2B). About 10-15 MCs at 8 weeks of differentiation were pooled for the isolation of total RNA, and RT-PCR analysis revealed the expression of the cornea-specific markers *PAX6* and *P63*, but not *K12* (*KRT12*). Variant-specific PCR indicated *P63*α as the major variant expressed in the developing corneas (Fig. 2C).

Maturation of MCs *in vitro*

Hematoxylin and Eosin (H&E) staining of immunohistochemical (IHC) sections of MCs at 6, 8, 10 and 15 weeks of maturation revealed a stepwise process of tissue layer development and self-organization of cells. The transparent MCs grew from 1 to 4 mm in diameter until 10 weeks of differentiation and developed into

Development (2017) 144, 2338-2351 doi:10.1242/dev.143040

opaque structures (Fig. 2Di-iv). The 6-week-old transparent MCs under suspension culture (MC-1) consisted of a double-layered epithelium and a fluid-filled lumen, without any stroma. These structures collapsed immediately after fixation, with leakage of internal fluids (Fig. 2Dv). At ∼8-10 weeks of differentiation, the MCs became strengthened by the subepithelial infiltration of spindle-shaped cells (MC-2), resulting in the development of a thick stromal cell layer, which occupied the entire fluid-filled lumen (Fig. 2Dvi). Surprisingly, IHC examination of intact MCs developing *in situ* in adherent cultures revealed complex tissue patterns, with orderly layers of different cell types that constitute a normal cornea. The adherent MCs at 10 weeks of differentiation (MC-3) revealed the formation of anterior-segment-like structure, consisting of a thin lid-like structure above a cornea-like tissue (Fig. 2Dvii). At 15 weeks of differentiation the adherent MCs exhibited mature corneal features (MC-4), with well-formed corneal and conjunctiva-like surface epithelia, separated by a limbal crypt-like margin zone (Fig. 2Dviii). Pigmented NCCs marked the boundary between the clear corneal surface and the surrounding epithelium (Fig. 2Dix).

Cornea-specific marker expression patterns in floating corneal organoids

To confirm that the MCs are authentic ocular structures and to understand the spatiotemporal distribution of cells within complex tissues, we carried out IHC examinations on MCs at different stages of development (n=8). At 6 weeks, the fragile MC1-1 comprises a double-layered epithelium, with a fluid-filled lumen (Fig. 3Ai). The epithelial cells were VIM^+ $PAX6^-$ $P63^-$, suggesting an undifferentiated primitive state (data not shown). Interestingly, a pair of circular niche-like organizers was observed at the connecting base, and $Ki67^+$ proliferating cells emerged from there (Fig. 3Aii). At 8 weeks, the MC1-2 showed significant stromal cell expansion and stratification of surface epithelium. The basal epithelial cells expressed P63α and PAX6 (Fig. 3Bi,ii) and the entire stroma was populated by VIM^+ cells (Fig. 3Biii). At 10 weeks, the MC-2 developed a thick stratified epithelium, with highly ordered collagen-filled stroma. The epithelial cells expressed P63α, PAX6 and the cornea-specific cytokeratins K3/12 and the stromal cells expressed VIM (Fig. 3C).

Characterization of MCs developing *in situ* on adherent EFPs

At 10 weeks, the MC-3 that developed *in situ* was strikingly similar to a developing anterior segment, with lid-like structures connected by a periderm-like epithelial lining above the corneal surface, as described elsewhere (Findlater et al., 1993; Huang et al., 2009) (Fig. 4A). The stratified corneal surface epithelium expressed PAX6, P63α and low levels of K12; the stromal cells were VIM^+ and the endothelium-like cell layer was VIM^+, $CD200^+$ and $GPC4^+$ (Fig. 4B, Fig. S3A). Infiltrating αSMA^+ cells were observed within the anterior stroma (Fig. 4Biv) and the surrounding adnexal cell layers, possibly indicating the development of smooth muscle structures of limbal vasculatures and Schlemm's canal (Fig. S3B). The stromal, endothelial and lid surface epithelial cells were VIM^+, whereas the stratified corneal epithelial cells were VIM^- (Fig. 4Ci,ii). Interestingly, a pars plicata-like ciliary process with a pigmented epithelium was observed at the periphery of MC-3, as reported previously (Kuwahara et al., 2015; Kinoshita et al., 2016). VIM^+ cell clusters flanked the ciliary processes, suggesting the development of trabecular meshwork and choroid-like structures (Fig. 4Ciii,iv).

The 15-week-old MC-4 was morphologically identical to an adult ocular surface (Fig. 4D), with a distinct limbus-like transition zone separating the $PAX6^+$ $P63\alpha^+$ $K3/12^+$ $K10^-$ corneal epithelium on one side and the periodic acid-Schiff $(PAS)^+$ and Alcian $Blue^+$ goblet cell-enriched epithelium on the other (Fig. 4E, Fig. S3C). The cornea-like structure measured ∼2 mm in diameter (∼1/6th the size of an adult cornea) and expressed most of the cornea-specific markers observed in adult corneal tissues (Fig. S4). The goblet cells were $PAX6^-$ $P63^-$, which suggested their development from OSE independent of *PAX6* and *P63* regulation. Surprisingly, except for a few newly emerging cells, the majority of the goblet cells did not express the adult conjunctival goblet cell-specific mucin MUC5AC (Fig. 4Evi). Therefore, we further checked for expression of the other secretory mucin, MUC2. IHC examinations confirmed that the goblet cells were $MUC2^+$ (Fig. 4Ev). Interspersed between the goblet cells were a few brightly stained $PAX6^+$ and $K19^+$ epithelial cells (Fig. 4Ei, Fig. S5Bvii), which suggests the late emergence of conjunctival epithelium and its dependence on *PAX6* for development and maturation. Interestingly, a distinct vasculature-like structure with a central lumen and αSMA^+ cell lining was observed within the stroma of the transition zone. CD34 staining indicated the presence of vascular endothelium-like cells on the inner lining of the lumen, thus confirming the initiation of vascular network development along the conjunctival margin (Fig. S5Avii,viii). Another cluster of spindle-shaped $CD34^+$ cells in the peripheral stroma indicated the emergence of a mesenchymal cell wave (Fig. S5Bix).

A periderm lining in developing MC structures

The frequent detachment of an intact epithelial monolayer from the MC surface suggested that it constitutes a separate cell layer that is possibly embryonic periderm in origin. Mouse skin periderm cells are known to emerge from $P63^+$ surface epithelium during the early stratification events and are $P63^-$, $K17^+$ and $K6^+$ (Richardson et al., 2014). During development, the periderm layer plays an important role in preventing pathological cell adhesions between the epithelial linings of adjacent organs, thus ensuring normal tissue formation. Our IHC examinations confirmed that the limbal stem cell marker K15 was exclusively expressed by the basal epithelial cells and that K13 marked the surface and suprabasal epithelium, as reported previously (Ramirez-Miranda et al., 2011; Yoshida et al., 2006). Also, the entire epithelium of MC-2, including the loose surface layers, expressed K13 and the periderm markers K17 and K19 (Fig. 5A). In MC-3, the corneal surface, lid surface and the connecting periderm were lined by $K17^+$ and $K19^+$ cells (Fig. 5B). When we examined the adult tissues, we observed that the flat wing cells at the corneal epithelial surface retained K13 and K19 expression, while the entire adult ocular surface epithelium was $K17^-$ (Fig. S6).

Lid and corneal surface epithelial margins in developing organoids

The lid, forniceal and bulbar conjunctiva, limbal and corneal surfaces are lined by a contiguous sheet of epithelium and are distinguished based on minor differences in marker expression and the presence of additional cell types, such as the conjunctival goblet cells. It is well known that the basal cells of the entire epithelial lining express P63 (Fig. S7i). However, the eye-specific PAX6 is expressed only by the corneal and conjunctival epithelial cells (Fig. S7ii). To check if such higher-order cellular organization becomes established in mature corneal organoids, we examined 15-week-old MCs (MC-5) in long-term suspension cultures. As the organoids matured, the lid structures expanded simultaneously and occupied the major volume. The basally positioned corneal structure showed a remarkable cellular organization, with surface epithelium and orderly arranged, compact stromal cells, resembling

Development (2017) 144, 2338-2351 doi:10.1242/dev.143040

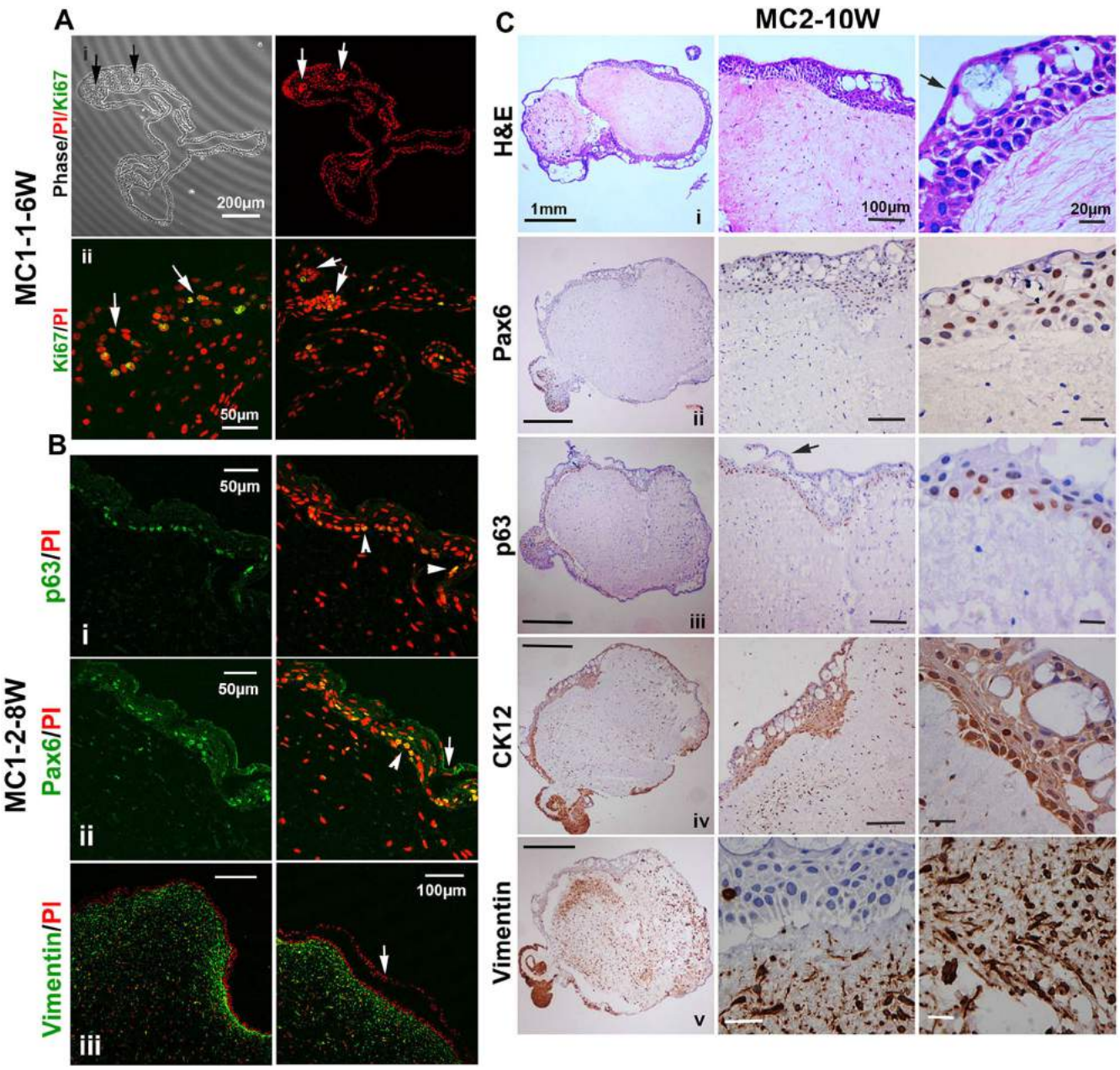

Fig. 3. IHC characterization of 6- to 10-week-old floating organoids. (A) IHC sections of 6-week-old MC1-1 showing a niche-like organizer region populated by Ki67$^+$ cells (i,ii). (B) IHC sections of 8-week-old MC1-2, immunostained for P63 (i), PAX6 (ii) and VIM (iii) (green) and counterstained with PI (red). Arrowheads point to P63$^+$ and PAX6$^+$ basal epithelium. Arrows indicate the loosely detaching surface epithelium. (C) Brightfield images of tissue sections of 10-week-old MC2 stained with H&E (i) or immunostained for PAX6 (ii), P63 (iii), K12 (iv) or VIM (v). DAB-stained sections (brown) were counterstained with Hematoxylin (blue).

that of a mature corneal tissue. Similar to MC1-1, a niche-like organizer formed the origin of P63$^+$ cells, which appeared to be migrating away from the center in an outward spiraling fashion, as a double-layered epithelium (Fig. 6i). The lid epithelium was stratified and the basal cells expressed P63. However, PAX6 expression was limited to the corneal surface epithelium, with very weak or no expression in epithelial cells along the lid margins (Fig. 6iii). Similarly, K10 expression was restricted to the lid surface epithelium, with negligible expression in the corneal epithelium (Fig. 6iv). The corneal epithelial basal cells were PAX6$^+$ P63$^+$, whereas the mature suprabasal cells were PAX6$^+$ P63$^-$ (Fig. 6v). Other adnexal structures, such as the lentoid bodies derived from OSE, could be identified as PAX6^{high} αA-crystallin$^+$ P63$^-$ cell clusters (Fig. 6ii,iii). In addition to the lens, the surface epithelial cells also expressed αA-crystallin, as observed in developing mouse eyes (Fig. S7iii).

Limbal margin establishment and delayed emergence of conjunctival epithelium

In 15-week-old adherent MC-4, P63$^+$ basal cells were restricted to the corneal side and MUC2$^+$ goblet cells were restricted to the conjunctival side, at the transition zone (Fig. 4Eii). In agreement with an earlier report (Richardson et al., 2014), upon epithelial stratification K17 expression became downregulated in the surface periderm cells, and the basal epithelial stem cells were P63$^+$ and K17$^+$ (Fig. 7Ai) and established a clear transition zone resembling that of a limbal margin. The abundance of Ki67$^+$ proliferating cells within the goblet cell-enriched epithelium indicates that the

Development (2017) 144, 2338-2351 doi:10.1242/dev.143040

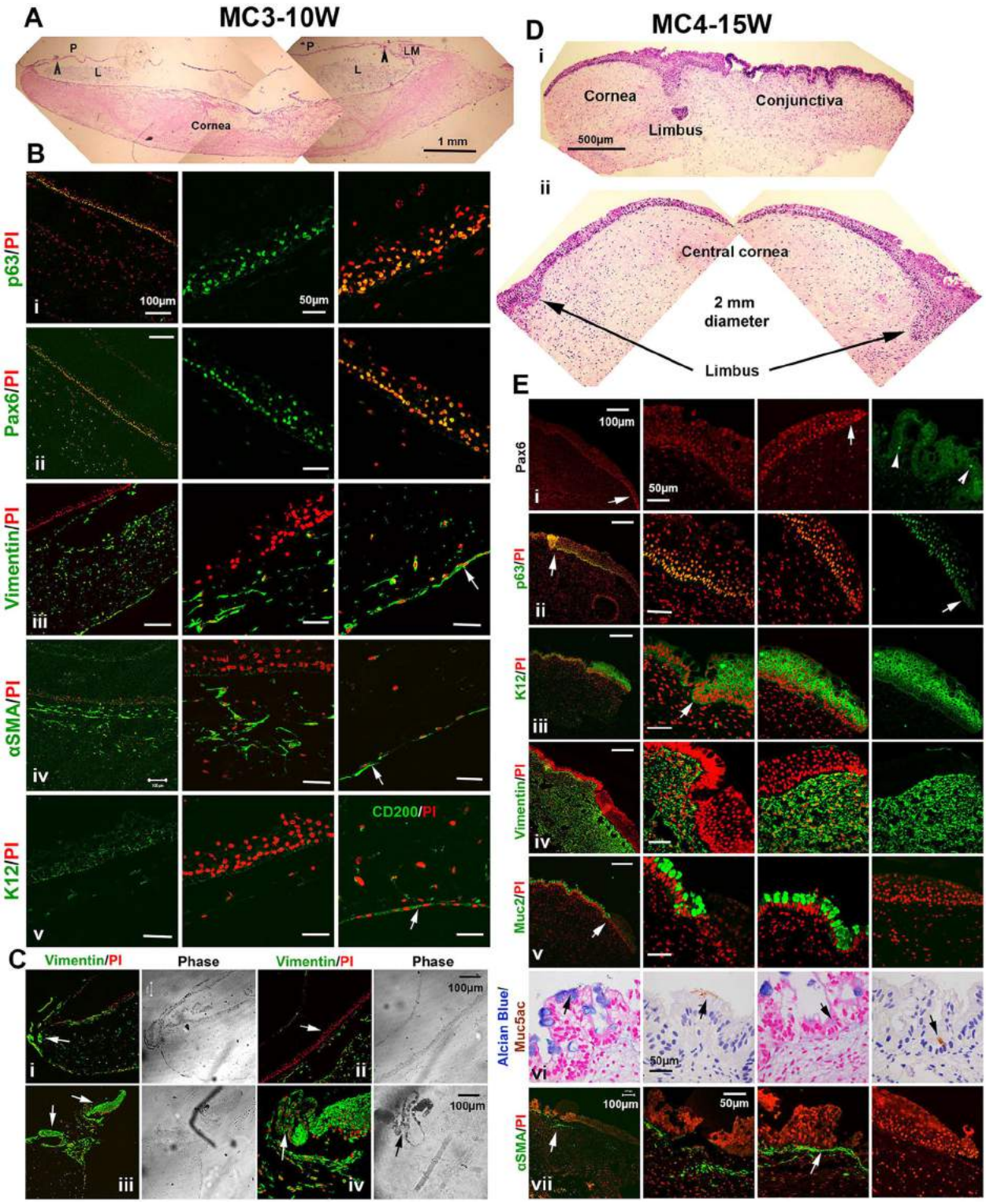

Fig. 4. IHC characterization of 10- to 15-week-old adherent MCs. (A) H&E-stained sections of 10-week-old MC3 shows a thick stroma lined by a thin monolayer of epithelium-like and endothelium-like cells on either side and a lid margin (LM) on the top (arrowhead), connected by a thin periderm-like (P) continuous epithelial lining covering the entire ocular surface, with a fluid-filled lumen (L) in between. (B) Confocal images of tissue sections of MC3, immunostained for P63 (i), PAX6 (ii), VIM (iii), αSMA (iv), K12 and CD200 (v) (green) and counterstained with PI (red). Arrows point to the endothelial cell layer. (C) The corneal surface epithelium (arrow) of MC3 is a VIM^{-} (ii), ciliary margin-like structure formed by ruffled pigmented epithelial cells (iv) and flanked by VIM^{+} ocular adnexal structures (iii). (D) H&E-stained sections of 15-week-old MC4 reveal mature cornea-like features, such as a thick stromal layer lined by a stratified squamous epithelium on the apical surface. A limbus-like structure separates the cornea-like epithelium and the goblet cell-enriched future conjunctiva. (E) Confocal images of tissue sections of MC4 immunostained with PAX6 antibody in red (i), or stained for P63 (ii), K12 (iii), VIM (iv), MUC2 (v) or αSMA (vii) in green and counterstained with PI in red. Brightfield IHC images are shown of sections stained with MUC5AC antibody (arrows) and Alcian Blue and counterstained with Hematoxylin or Nuclear Fast Red, respectively (vi).

Development (2017) 144, 2338-2351 doi:10.1242/dev.143040

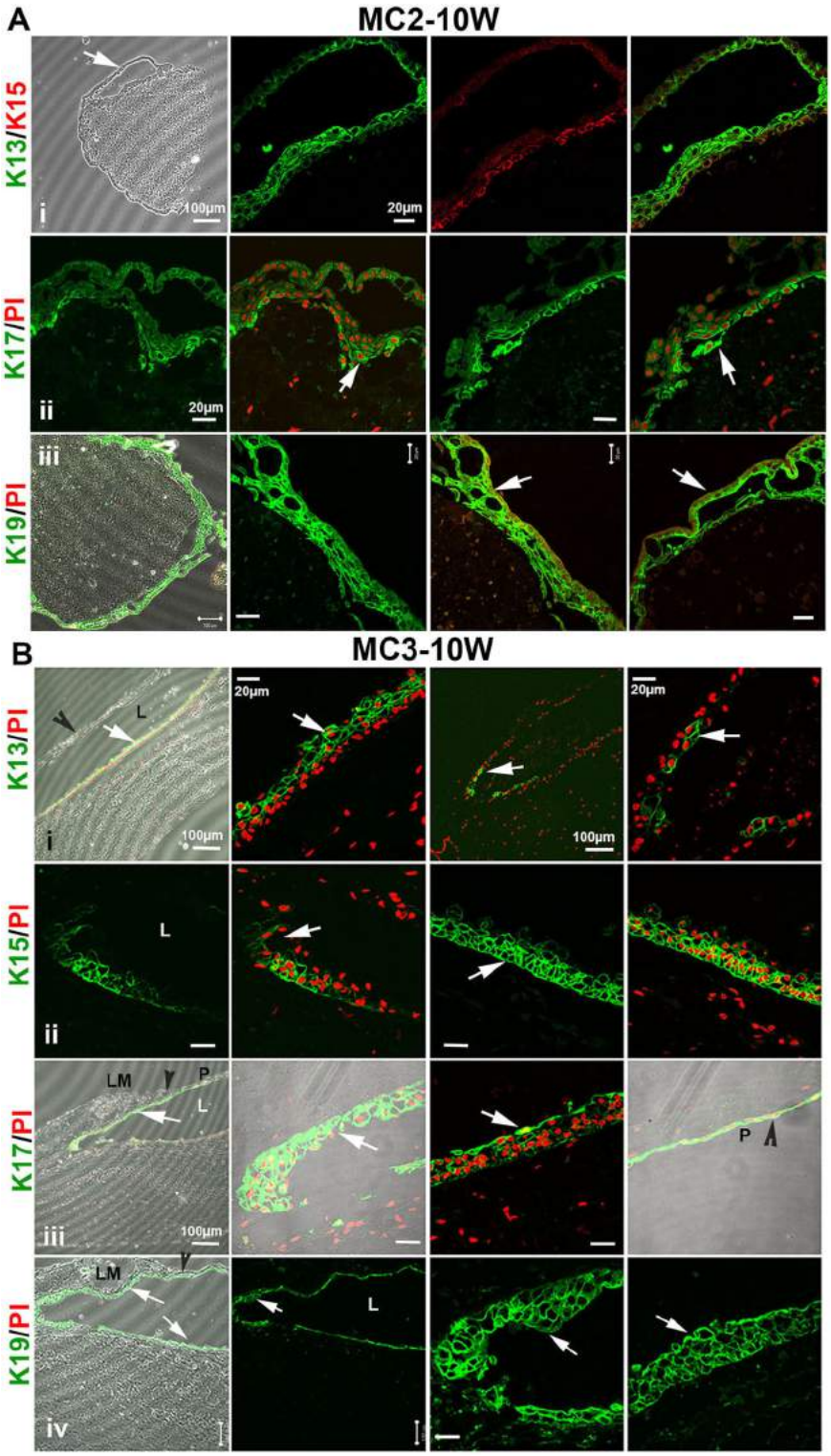

Fig. 5. Expression of periderm markers in floating and adherent MCs. (A) Confocal images of immunostained tissue sections of MC2 showing the expression of different keratins in green. The basal cells were $K15^+$, while the suprabasal cells and the apical lining were $K13^+$ (i). The basal cells also expressed K17 (arrows) (ii). However, the entire stratified epithelium and the loosely adhered, periderm-like flat surface lining cells (arrows) expressed K19 (iii). The sections were counterstained with PI to mark the nuclei in red. (B) The expression of cytokeratin markers shows a clear demarcation within the developing epithelium of a 10-week-old MC. The surface and suprabasal epithelium on the corneal surface express K13 and the expression disappears at the lid margin in the forniceal epithelium (i). K15 expression was observed in basal corneal epithelial cells and was absent at the corneal and lid surface junction (ii). The periderm, lid margin and the apical flat cell layer of the corneal epithelium showed intense K17 staining (iii). The entire epithelial lining of the developing ocular surface expressed K19 (iv). Lid margins (LM) are marked by arrowheads. The lid periderm (P) was observed as a thin continuous sheet of epithelium covering the entire corneal surface, with a fluid-filled lumen (L) in between.

progenitor cell proliferation, differentiation and tissue expansion proceed from the transition zone (Fig. 7Aii). Dual staining for MUC2 and P63 or K3/12 expression further confirmed the presence of a transition zone (Fig. 7Aiii,iv). The surface epithelium formed a collagen IV-enriched basement membrane, while the VIM^+ stromal cells laid out a well-organized collagen I-enriched extracellular matrix (Fig. 7Av,vi). When the expression patterns of other epithelial keratins were examined, we observed that $K13^+$, $K15^+$ and $K17^+$ cells were restricted to the limbal margin. Within the stratified corneal epithelium, K13 marked the surface and suprabasal cells, while K15 and K17 marked the basal and suprabasal cells (Fig. 7B). However, all of the surface epithelial cells expressed K19, with intense staining in the basal cells, surface periderm-like cells and in a few developing conjunctival epithelial cells, which suggested the late emergence of conjunctival epithelium.

Development (2017) 144, 2338-2351 doi:10.1242/dev.143040

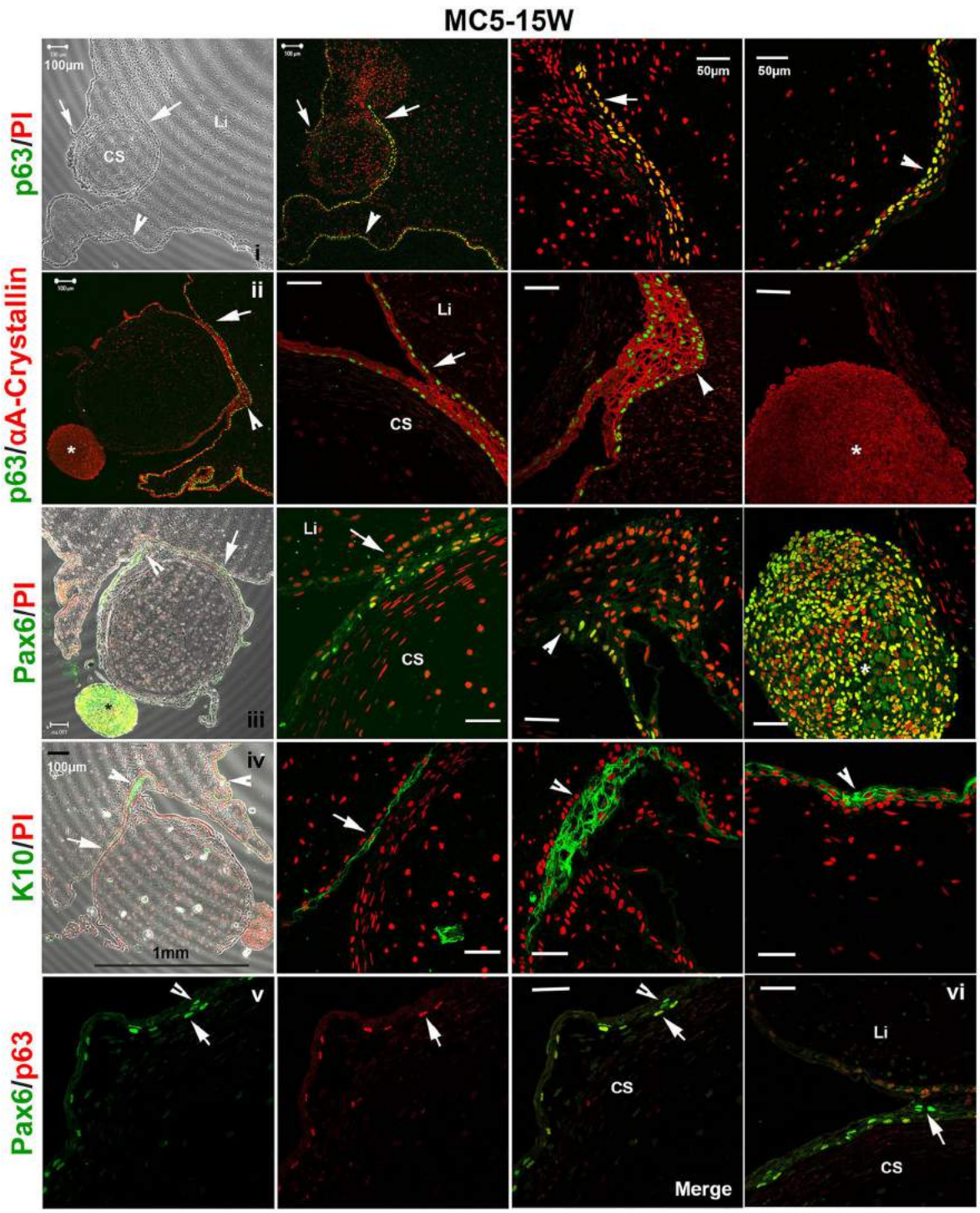

Fig. 6. IHC characterization of 15-week-old mature corneal organoid in suspension. Confocal images of tissue sections of MC5, showing a basally located MC with well-developed corneal stroma (CS) of ~1 mm diameter. The lid-like tissue (Li) became expanded on the apical surface. The first column of all panels (i-iv) represents a lower magnification view and columns 2-4 are higher magnification views of the regions marked by arrows, arrowheads and asterisks. The $P63^+$ epithelial cells seem to arise from a pair of niche-like organizers within the corneal stroma and formed the corneal and lid surface epithelium (i). The basal cells of the entire epithelial lining expressed P63 and co-expressed αA-crystallin. Lentoid clusters (asterisks) are distinguished as $P63^-$ αA-crystallin$^+$ cells (ii). Pax6 expression is limited to the corneal surface epithelium and the cells within the lentoid clusters. The anterior corneal stroma (CS) is well developed with flattened and compactly arranged stromal keratocytes, as observed in adult corneal tissues (iii). The epithelial lining on the lid surface adjoining the corneal surface showed weak PAX6 nuclear expression and was $K10^+$ (iv). The basal cells of the stratified corneal epithelium were $P63^+$ $PAX6^+$ (arrows), while the differentiated apical cells were $P63^-$ $PAX6^+$ (arrowhead). Columns 3 and 4 indicate two different merged images (v, vi).

Characterization of cell outgrowths from EFPs

When the cell outgrowths from EFPs were analyzed in adherent 2D cultures, we found that $SSEA4^+$ primordial cells tended to organize into ruffled structures resembling limbal crypts and gave rise to $P63^+$ and $PAX6^+$ ocular surface epithelial cells (Fig. 7Ci-iii, Movies 2 and 3) and waves of NES^+, $SOX10^+$ and $PAX6^{low}$ NCCs.

Development (2017) 144, 2338-2351 doi:10.1242/dev.143040

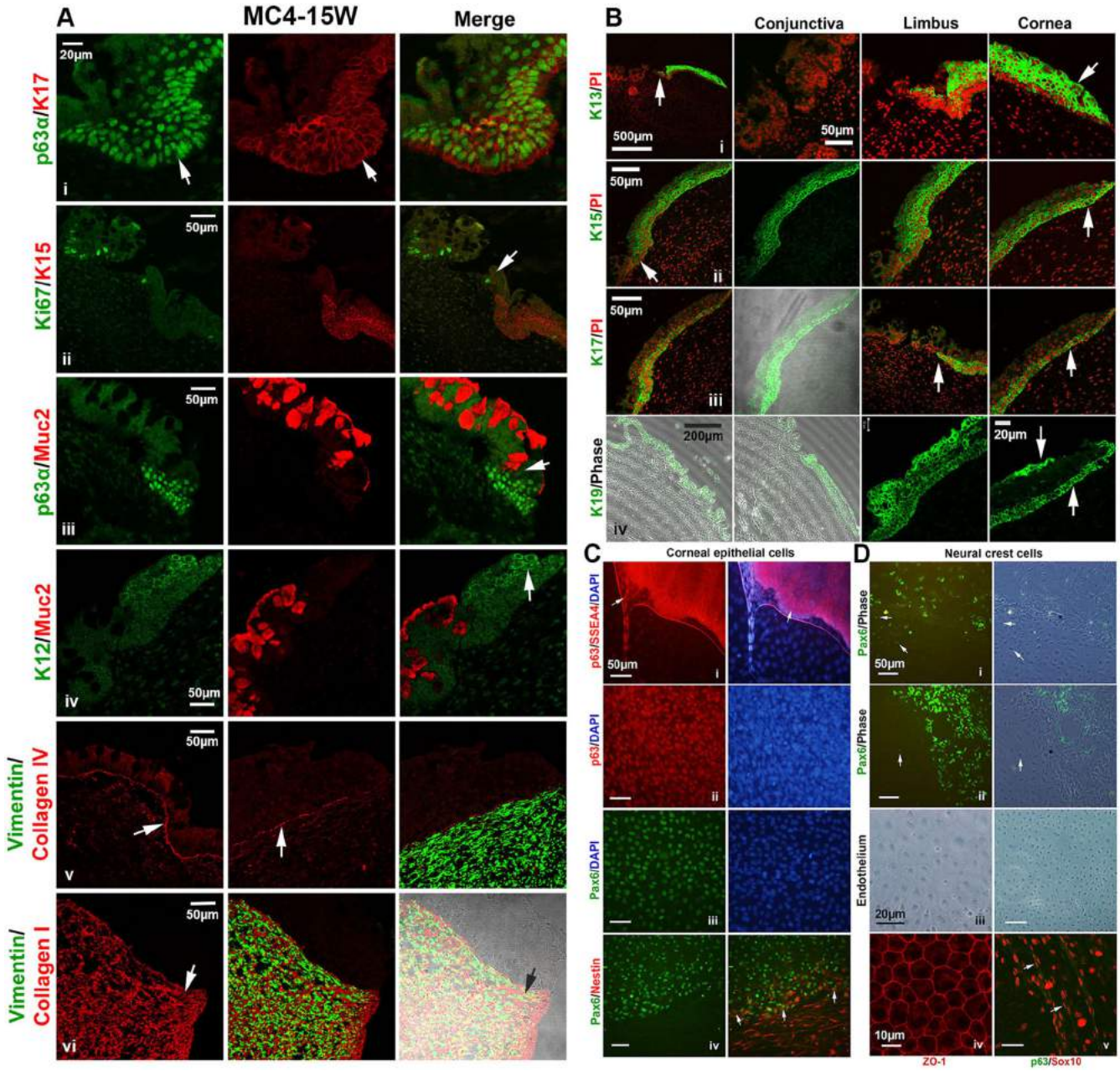

Fig. 7. Mature cornea-specific marker expression in MCs and cell outgrowths from tissue explants. (A) Confocal images of tissue sections of MC4 co-immunostained for P63α and K17 (i), KI67 and K15 (ii), P63α and MUC2 (iii), K12 and MUC2 (iv), VIM and COL4A1 (v), VIM and COL1A1 (vi). Arrows mark the limbus-like margins (i-iii), $K12^+$ corneal epithelium (iv), basement membrane (v) and the stromal matrix (vi). (B) Confocal images of tissue sections of MC4 immunostained for K13 (i), K15 (ii), K17 (iii) and K19 (iv). Note the surface epithelial expression patterns of K13 and K19, while K15 and K17 mark the basal epithelial stem cells. Apart from weak K19 expression, the conjunctival epithelium was negative for all the keratins tested. The limbus-like margins are indicated by arrows in the first column. $K13^+$ suprabasal cells (i), and $K15^+$ (ii), $K17^+$ (iii) and $K19^+$ (iv) basal cells of central corneal epithelium are indicated by arrows in the last column. (C) OSE outgrowths from EFPs formed a ruffled, limbal crypt-like arrangement of $SSEA4^+$ cells at the proximal end, giving rise to migrating $P63^+$ epithelial stem cells (arrows) (i). The outgrowths from explants result in uniform corneal epithelial sheets containing $P63^+$ (ii) and $PAX6^+$ (iii) cells. $PAX6^+$ epithelial sheets (green) are lined by NES^+ NCCs (red). Arrows indicate the double-positive cells at the boundaries (iv). (D) $PAX6^{low}$ NCC patches downregulate PAX6 expression (arrows) and morphologically differentiate into hexagonal, corneal endothelium-like cells (i,ii), with distinct $ZO\text{-}1^+$ tight junctions between the cells (iii,iv). The migratory NCCs are $SOX10^+$ $P63^-$ (arrows) (iv). DAPI (blue) and PI (red) were used as counterstains. Scale bars: 50 µm, unless otherwise specified.

NES^+ cells are a component of the native limbal niche (Fig. S4x) and we show that iPSC-derived $PAX6^+$ epithelial outgrowths are lined by NES^+ NCCs that co-express PAX6, as reported previously (Mariappan et al., 2014) (Fig. 7Civ). Patches of $PAX6^{low}$ neural crest-like cells differentiated into a corneal endothelium-like phenotype by downregulating PAX6 (Fig. 7Di,ii); they appeared as hexagonal, compactly arranged, non-pigmented flat cells with ZO-1 $(TJP1)^+$ tight junctions (Fig. 7Diii,iv). The migratory NCCs were found to be $SOX10^+$ $P63^-$ cells (Fig. 7Dv).

Characterization of corneal organoid-derived transplantable cell sheets

Explant cultures of 8- to 10-week-old MCs on glass coverslips resulted in a spiraling wave of $P63^-$ $K17^+$ OSE cells at the leading edge,

Development (2017) 144, 2338-2351 doi:10.1242/dev.143040

followed by a compactly arranged monolayer of P63^{+} K17^{+} corneal epithelial cells (Fig. S8). In an attempt to generate transplantable sheets of corneal epithelium, we established explant cultures on denuded human amniotic membrane (hAM) substrates, using mature cornea-like organoids at 8-10 weeks of maturation. IHC examination of 10-day-old cultures confirmed that the uniform sheets of PAX6^{+} K12^{+} epithelium generated using corneal organoids were comparable to those generated using adult limbal explants. The basal epithelial cells were PAX6^{+} P63^{+} P75 (NGFR)$^{+}$ and also expressed K17, K19 and VIM (Fig. 8). Interestingly, the resting corneal epithelium was found to

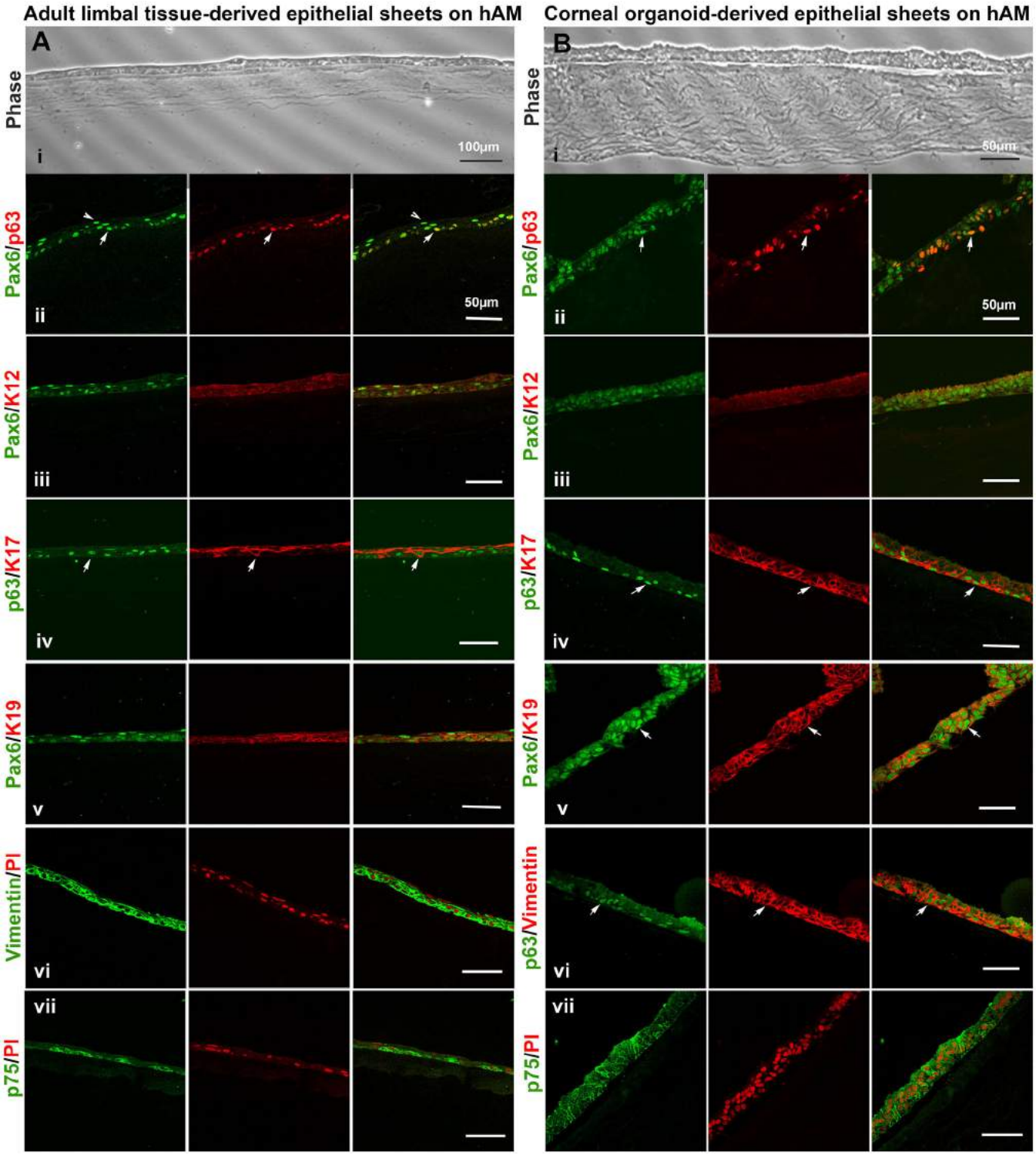

Fig. 8. Organoid-derived transplantable corneal epithelial grafts on human amniotic membrane substrate. (A) Confocal images of tissue sections of epithelial grafts generated using adult limbal tissues and (B) iPSC-derived corneal organoids on denuded hAM (i). Both the engineered grafts were comparable in terms of spatial distribution and expression patterns of corneal epithelium-specific markers such as PAX6, P63, K12 (ii-iii); cytoskeletal proteins such as K17 (iv), K19 (v) and VIM (vi); and of the basal stem cell marker P75 (vii). Arrows indicate the dual positive basal epithelial cells (ii-v). Arrowheads indicate the PAX6^{+}P63^{-} suprabasal cells (ii).

Development (2017) 144, 2338-2351 doi:10.1242/dev.143040

be VIM$^-$ K17$^-$ (Figs 4 and 6). However, the actively proliferating cells in both the limbal and organoid explant cultures were VIM$^+$ K17$^+$, suggesting a possible activation of these markers during acute regeneration and wound healing responses.

DISCUSSION

An autologous iPSC-derived corneal cell source will offer a promising alternative for the treatment of patients with bilateral LSCD. A few earlier reports have demonstrated the possibility of deriving PAX6$^+$ P63$^+$ K3/12$^+$ corneal epithelial cells from PSCs in 2D cultures. Here, we report for the first time an efficient method of generating complex 3D corneal organoids using iPSCs, which circumvents the need for complicated cell enrichment procedures as are involved in establishing limbal cultures.

The adoption of a simple differentiation protocol by the direct shifting of growing cultures to retinal differentiation conditions in the absence of noggin has resulted in successful induction of EFP clusters. We also emphasize that it is crucial to excise EFPs and initiate suspension cultures at 4 weeks of differentiation, before the commencement of surface ectodermal cell and NCC migration, in order to ensure successful induction of corneal organoids in ∼40% of the EFPs by 6 weeks. We believe that the inhibition of migration of proliferating progenitor cells away from EFPs in suspension culture enables the autonomous self-assembly of various cell types, resulting in the generation of complex 3D corneal organoids.

The bilayered epithelium of the newly emerged MCs was derived from the primitive periderm-like P63$^-$ PAX6$^-$ VIM$^+$ OSE cells. The presence of internal fluid appears to help in establishing a circular and convex shape for the developing corneas. The subsequent wave of VIM$^+$ stromal cells and the deposition of collagen matrix helped to strengthen the outer scaffold of OSE cells. The developing lid-like structure in MC-3 was lined and connected by a continuous periderm-like epithelium above the corneal surface. This observation is in agreement with the fact that the developing eyelids fuse and form a continuous covering over the developing cornea. The connecting periderm disintegrates and enables lid separation and eye opening during advanced stages of embryonic development in humans and at postnatal stages in rodents (Findlater et al., 1993; Huang et al., 2009). Unlike the developing skin periderm that is shed after birth (Richardson et al., 2014), the presence of K13$^+$ K17$^+$ K19$^+$ periderm-like surface epithelium in developing MCs and in adult corneas suggests their probable role in normal ocular surface development and in adult tissue homeostasis. We hypothesize that this unique surface lining may help in preventing abnormal cell fusions between the corneal and lid surface epithelium during embryonic eye development and in wound repair processes during adult tissue regeneration.

The presence of ciliary margin zone (CMZ)-like pigmented and ruffled epithelium, flanked by VIM$^+$ structures, at the corneal periphery prompted us to speculate that CMZ development might precede or coincide with ocular surface periderm formation (∼5-6 weeks). The secretions of the CMZ cells might contribute to setting the initial corneal shape, which becomes further strengthened by the infiltration of VIM$^+$ NCCs. The NCCs also contributed to the formation of a monolayer of VIM$^+$ CD200$^+$ GPC4$^+$ endothelium-like cells beneath the thick stroma, thus resulting in the generation of a complete anterior-segment-like structure.

As the MCs matured, the lid and the limbal margins became established by the spatiotemporal pattern of expression of P63, PAX6 and keratins. The P63$^+$ cells were restricted to the corneal and limbal basal epithelial cells, thus establishing a sharp boundary between the cornea and the future conjunctiva. Whereas the entire surface epithelium expressed PAX6 at low levels, well-differentiated central corneal cells and a subset of cells within the conjunctival region were brightly PAX6$^+$, confirming its key role in corneal maturation and the emergence of conjunctival epithelium. The majority of the goblet cells on the conjunctival side were MUC2$^+$ P63$^-$ PAX6$^-$, which suggests that the goblet cells emerge from the primitive OSE cells independently of P63 and PAX6 expression. However, the adult conjunctival goblet cells expressed very low levels of MUC2 (McKenzie et al., 2000) and were predominantly MUC5AC$^+$ (Fig. S4Av). An earlier report has confirmed that goblet cell development is normal in *Muc5ac*$^{-/-}$; *Muc5b*$^{-/-}$ mice (Marko et al., 2014). Taken together, we believe that MUC2 and MUC5AC are the developing and mature conjunctival goblet cell markers, respectively. The presence of niche-like organizing structures consisting of Ki67$^+$ P63$^+$ cells suggests that the tissue growth and expansion proceeds from such transition zones. Further anatomical maturation of corneal tissue was mediated by the infiltration of CD34$^+$ mesenchymal stem cells (Sidney et al., 2014) and other neural crest-derived cell types, such as the smooth muscle cells, which contributes to the formation of limbal and episcleral vasculatures.

Earlier evidence has confirmed the roles of *PAX6* in regulating NCC migration and their differentiation into ocular cell types (Baulmann et al., 2002; Kanakubo et al., 2006) and the involvement of NCC-dependent signaling in feedback regulation on *PAX6* (Grocott et al., 2011). Our observations indicate that the PAX6^{low} NCCs differentiated into flat, non-pigmented, endothelium-like hexagonal cells by downregulating PAX6 expression. Explant cultures of 8- to 10-week-old MCs on hAM has enabled the generation of transplantable sheets of PAX6$^+$ P63$^+$ K12$^+$ corneal epithelial sheets, similar to adult limbal tissue-derived grafts intended for regenerative applications. We further plan to use these tissue grafts in xenotransplantation studies in rabbit LSCD models, to test their clinical suitability in corneal surface reconstruction procedures.

Conclusions

In summary, we show for the first time that complex 3D corneal organoids can be generated from iPSCs and that the MCs undergo maturation *in vitro* and recapitulate the steps of normal corneal development, as depicted in Fig. 9. The availability of such MCs at 10 weeks of maturation circumvents the need for complicated cell enrichment protocols and offers a simpler method of establishing enriched cultures of corneal epithelial cell sheets for basic research needs and for regenerative applications.

MATERIALS AND METHODS

Ethics

This study was approved by our Institutional Review Board (IRB) of the LV Prasad Eye Institute, Hyderabad, India. All research involving human samples followed the tenets of the Declaration of Helsinki. Experiments involving animals were conducted in adherence to the ARVO statement for use of animals and with the approval of the Institutional Animal Ethics Committee (AEC) of the National Institute of Nutrition, Hyderabad, India.

Derivation and maintenance of human iPSCs

Full-thickness punch biopsies of skin were taken from volunteers with their informed consent. The biopsies were used to establish human dermal fibroblast (HDFs) cultures. A retroviral cocktail containing individual vectors expressing the *OCT4*, *SOX2*, *KLF4* and *cMYC* (OSKM) transgenes were used to transduce passage 3 HDFs at an MOI of ∼2. The cells were then split and cultured under standard human ESC culture conditions. The reprogrammed clones that emerged after 3 weeks were manually picked

Development (2017) 144, 2338-2351 doi:10.1242/dev.143040

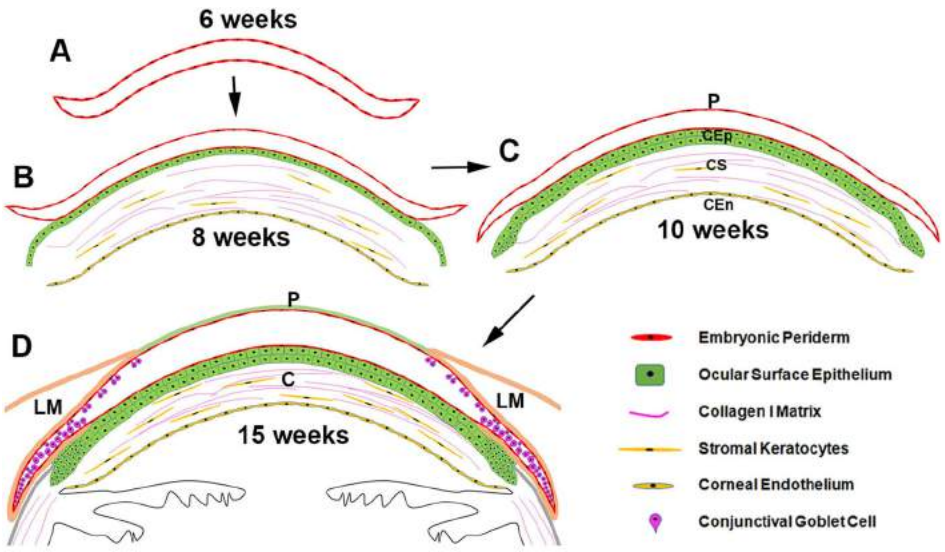

Fig. 9. Illustration of the different stages of MC development *in vitro*. (A) The transparent, bubble-like CP at 6 weeks of development consisted of a double-layered primitive embryonic periderm-like epithelium, with a fluid-filled lumen. (B) NCCs migrate into the subepithelial space at ∼8 weeks to form a thick stroma and an endothelium-like monolayer. This establishes and strengthens the corneal matrix. (C) The ocular surface epithelium (OSE) developed and stratified over the stably established stromal matrix at ∼10 weeks. The OSE remained sandwiched between the stroma and the periderm-like surface lining (P). P63α^{high} and PAX6^{low} cells appeared in the basal cell layers. The periderm lined the entire ocular surface and also formed a continuous outer covering for the developing anterior segment. (D) The lid-like structures developed on either side, connected by an intact periderm. Mature cell markers such as PAX6 and K12 became induced in the stratified OSE at ∼15 weeks. Goblet cells developed within the future conjunctival and forniceal surface epithelium, independently of PAX6 and P63 expression. C, cornea; CEp, corneal epithelium; CEn, corneal endothelium; CS, corneal stroma; LM, lid margin.

based on colony morphology and five clones were passaged for further expansion. The clones were also adapted to feeder-free culture conditions on Matrigel (Corning) coated plates using the mTeSR™1 kit, as per manufacturer's instructions (STEMCELL Technologies). The reprogramming efficiency was 0.005% and the clone hiPSC-F2-3F1 was expanded beyond 25 passages and characterized for stemness and pluripotency.

Eye field differentiation of human iPSCs and ESCs

Growing cultures of the human ESC line BJNhem20 and the normal human iPSC line hiPSC-F2-3F1 were differentiated towards eye field commitment as described below. When the cultures reached 70-80% confluence, the growth medium was replaced with differentiation medium [DM: DMEM/F12, 4% knockout serum replacement (KOSR), 4% fetal bovine serum (FBS), 1× non-essential amino acids (NEAA), 1× Glutamax, 1× Pen-Strep; Thermo Fisher Scientific] to induce spontaneous differentiation for 2 days. Subsequently, the cultures were shifted to retinal differentiation medium (RDM: DM plus 2% B27) and maintained for 1 month to induce eye field specification. Noggin was omitted from the RDM cocktail in order that uninhibited TGFβ and BMP intrinsic signals could direct OSE development. The distinct EFP clusters that emerged at 4 weeks were either continued as adherent cultures *in situ* or excised manually for suspension cultures as described below.

Corneal differentiation of eye field clusters

The EFPs were further continued *in situ* as adherent cultures in RDM for another 4 weeks to allow whole eyeball-like structure development, with transparent CP on the surface and NR cup on the basal side. These cultures were maintained in corneal differentiation medium (CDM: DM plus 1% N2, 5 µg/ml insulin, 5 ng/ml FGF, 10 ng/ml EGF; Thermo Fisher Scientific) for a further 6-8 weeks to enable maturation of the ocular surface structures. However, a majority of the EFPs gave rise to concentric cell outgrowths, as described previously (Hayashi et al., 2016). Alternatively, the EFPs were manually scooped out intact and cultured in RDM for 4 weeks in non-adherent plates. It is crucial to excise the EFPs at 4 weeks before the commencement of initial waves of surface ectodermal cell and NCC migration. Within 2 weeks of suspension culture, distinct RP and transparent, bubble-like CP structures emerged from the floating EFPs. At 6-8 weeks of differentiation, the delicate CP structures were dissected out of floating EFPs and cultured separately for a further 8-10 weeks in CDM for tissue maturation, as depicted in Fig. 1A. Alternatively, the MCs were processed directly for explant cultures or RNA isolation or fixed in 10% formalin for IHC examination.

Explant culture of MCs

MCs at different stages of maturation (6-10 weeks) were taken and the basal stalk that carries the niche-like organizer along with the adjoining epithelium was chopped out under a microscope and cut into fine pieces in a few drops of CDM. The tissue explants were picked using a needle and explanted on to the surface of de-epithelialized human amniotic membrane (hAM). Alternatively, the explants were placed on Matrigel-coated glass coverslips. The cultures were maintained in CDM and incubated at 37°C with 5% CO_2. The epithelial cells migrated out of the explants and formed growth zones that merged with each other to form uniform epithelial sheets within 10 days. The cell sheets were fixed and processed for IHC examination as described below.

Genomic PCR and semi-quantitative reverse-transcription PCR

Genomic DNA and total RNA were isolated from cell samples using standard procedures. cDNAs were prepared by reverse transcription using the SuperScript II reverse transcriptase kit (Invitrogen, Life Technologies). PCRs were performed using either genomic DNA or cDNA as the reaction template (n=3). Template concentrations were normalized based on *eEF1α* (*EEF1A1*) expression. Table S1 summarizes the primers used. The amplicons were resolved on 1% (w/v) agarose gels, stained with ethidium bromide and imaged using the Gel Doc XR+ system (Bio-Rad).

Immunohistochemistry and image analysis

The MCs were fixed in 10% formalin and paraffin embedded for further sectioning. Thin (4 µm) sections were processed for evaluation by H&E, PAS and Alcian Blue staining by standard procedures. For IHC examination, antigen retrieval was achieved by heating at 100°C with sodium citrate buffer (pH 6.2) and the slides were processed for blocking and antibody incubations. DAB staining of samples was performed as per the manufacturer's instructions (Super Sensitive One-Step Polymer-HRP

Development (2017) 144, 2338-2351 doi:10.1242/dev.143040

IHC detection system, Biogenex), with counterstaining with Hematoxylin, propidium iodide (PI) or DAPI (1 µg/ml each). Table S2 summarizes the antibodies used, including dilutions. Alkaline phosphatase staining was undertaken as per manufacturer's instruction (Chemicon, Millipore). The samples were finally mounted with DPX (SD Fine Chemicals) or glycerol and imaged using an epifluorescence (IX71, Olympus) or confocal (LSM 510, Carl Zeiss) microscope. The images were analyzed using ImagePro Express (Media Cybernetics) and LSM 510 Meta version 3.2 (Carl Zeiss) software, respectively, and the composites were prepared using Adobe Photoshop CS.

Teratoma formation assay

iPSCs at passage 25 were suspended in 20% Matrigel in DMEM/F12 and kept on ice. About 1×10^6 cells in 200 µl were aspirated into tuberculin syringes fitted with a 26 G needle and injected into the subcutaneous space above the rear right haunch of 6-week-old nude mice (n=8). Teratomas that developed at 6-8 weeks post-injection were surgically dissected after euthanizing the animals. The tissues were fixed overnight in 4% paraformaldehyde and processed for paraffin embedding. The tissue blocks were sectioned and processed for IHC examination as described above.

Karyotyping assay

The cells at passage 8 and 20 were grown under standard iPSC culture conditions. About 70-80% confluent cultures were treated with colcemid (0.1 µg/ml; Sigma-Aldrich) for 2-3 h to induce metaphase arrest and trypsinized to prepare single-cell suspensions. The cells were further treated with a hypotonic solution, fixed and then dropped onto clean glass slides (Fisher Scientific) and air dried. After a brief trypsin treatment, the chromosomes were G-banded by Giemsa staining. Well-spread metaphases were imaged and analyzed using CytoVision automated (Applied Imaging).

Transmission electron microscopy (TEM)

Tissues were fixed in 2.5% glutaraldehyde in 0.1 M phosphate buffer (pH 7.2) for 24 h at 4°C and then washed with 1× PBS thoroughly and post-fixed in 1% aqueous osmium tetroxide for 2 h. The samples were then washed, dehydrated through a graded alcohol series, embedded in Spurr's resin and incubated at 80°C for 72 h for complete polymerization. Ultra thin (60 nm) sections were prepared using an ultramicrotome (Leica Ultra Cut UCT-GA-D/E-1/00), mounted on copper grids and stained with saturated aqueous uranyl acetate and counterstained with Reynolds lead citrate. The sections were viewed using a Hitachi H-7500.

Statistics

The mean values of experimental repeats are given as ±s.d.

Acknowledgements

We thank Dr M. Lakshman of the RUSKA Lab, College of Veterinary Sciences, Prof. Jayshankar Telangana State Agricultural University (PJTSAU), Rajendranagar, Hyderabad, India, for providing TEM support; Dr Lakshmi Rao Kandukuri, Clinical Research Facility-Medical Biotechnology (CRF-MB), Centre for Cellular and Molecular Biology (CCMB), Hyderabad, India, for karyotyping; Dr Suresh Pothani, National Centre for Laboratory Animal Sciences, National Institute of Nutrition, Hyderabad, India, for providing animal facility support; and Prof. Dorairajan Balasubramanian, Dr S. Shivaji and Dr Gullapalli Nageshwara Rao for their critical review and useful suggestions in finalizing the manuscript.

Competing interests

The authors declare no competing or financial interests.

Author contributions

Conceptualization: P.J.S., S.M., I.M.; Methodology: P.J.S., S.M., V.K.P., S.R.B., R.R.N., M.N.N., G.B.R., I.M.; Software: I.M.; Validation: P.J.S., S.M., V.K.P., S.R.B., R.R.N., I.M.; Formal analysis: P.J.S., S.M., V.K.P., S.R.B., M.N.N., G.B.R., I.M.; Investigation: P.J.S., S.M., V.K.P., S.R.B., R.R.N., G.B.R., I.M.; Resources: V.K.P., S.R.B., R.R.N., M.N.N., G.B.R., V.S.S., I.M.; Data curation: P.J.S., V.K.P., I.M.; Writing - original draft: P.J.S., I.M.; Writing - review & editing: P.J.S., S.M., V.K.P., S.R.B., V.S.S., I.M.; Visualization: P.J.S., S.M., V.K.P., S.R.B., I.M.; Supervision: S.M., R.R.N., G.B.R., V.S.S., I.M.; Project administration: G.B.R., V.S.S., I.M.; Funding acquisition: V.S.S., I.M.

Funding

This study was supported by grants to I.M. and V.S.S. from the Department of Biotechnology, Ministry of Science and Technology, Government of India (BT/01/COE/06/02/10); Champalimaud Foundation; Tej Kohli Foundation; and the Hyderabad Eye Research Foundation.

Supplementary information

Supplementary information available online at
http://dev.biologists.org/lookup/doi/10.1242/dev.143040.supplemental

References

Ahmad, S., Stewart, R., Yung, S., Kolli, S., Armstrong, L., Stojkovic, M., Figueiredo, F. and Lako, M. (2007). Differentiation of human embryonic stem cells into corneal epithelial-like cells by in vitro replication of the corneal epithelial stem cell niche. *Stem Cells* **25**, 1145-1155.

Assawachananont, J., Mandai, M., Okamoto, S., Yamada, C., Eiraku, M., Yonemura, S., Sasai, Y. and Takahashi, M. (2014). Transplantation of embryonic and induced pluripotent stem cell-derived 3D retinal sheets into retinal degenerative mice. *Stem Cell Rep.* **2**, 662-674.

Basu, S., Sureka, S. P., Shanbhag, S. S., Kethiri, A. R., Singh, V. and Sangwan, V. S. (2016). Simple limbal epithelial transplantation: long-term clinical outcomes in 125 cases of unilateral chronic ocular surface burns. *Ophthalmology* **123**, 1000-1010.

Baulmann, D. C., Ohlmann, A., Flügel-Koch, C., Goswami, S., Cvekl, A. and Tamm, E. R. (2002). Pax6 heterozygous eyes show defects in chamber angle differentiation that are associated with a wide spectrum of other anterior eye segment abnormalities. *Mech. Dev.* **118**, 3-17.

Chan, A. A., Hertsenberg, A. J., Funderburgh, M. L., Mann, M. M., Du, Y., Davoli, K. A., Mich-Basso, J. D., Yang, L. and Funderburgh, J. L. (2013). Differentiation of human embryonic stem cells into cells with corneal keratocyte phenotype. *PLoS ONE* **8**, e56831.

Chen, P., Chen, J. Z., Shao, C. Y., Li, C. Y., Zhang, Y. D., Lu, W. J., Fu, Y., Gu, P. and Fan, X. (2015). Treatment with retinoic acid and lens epithelial cell-conditioned medium in vitro directed the differentiation of pluripotent stem cells towards corneal endothelial cell-like cells. *Exp. Ther. Med.* **29**, 351-360.

Cotsarelis, G., Cheng, S.-Z., Dong, G., Sun, T.-T. and Lavker, R. M. (1989). Existence of slow-cycling limbal epithelial basal cells that can be preferentially stimulated to proliferate: implications on epithelial stem cells. *Cell* **57**, 201-209.

Eiraku, M., Takata, N., Ishibashi, H., Kawada, M., Sakakura, E., Okuda, S., Sekiguchi, K., Adachi, T. and Sasai, Y. (2011). Self-organizing optic-cup morphogenesis in three-dimensional culture. *Nature* **472**, 51-56.

Findlater, G. S., McDougall, R. D. and Kaufman, M. H. (1993). Eyelid development, fusion and subsequent reopening in the mouse. *J. Anat.* **183**, 121-129.

Foster, J. W., Wahlin, K., Adams, S. M., Birk, D. E., Zack, D. J. and Chakravarti, S. (2017). Cornea organoids from human induced pluripotent stem cells. *Sci. Rep.* **7**, 41286.

Gonzalez-Cordero, A., West, E. L., Pearson, R. A., Duran, Y., Carvalho, L. S., Chu, C. J., Naeem, A., Blackford, S. J. I., Georgiadis, A., Lakowski, J. et al. (2013). Photoreceptor precursors derived from three-dimensional embryonic stem cell cultures integrate and mature within adult degenerate retina. *Nat. Biotechnol.* **31**, 741-747.

Grocott, T., Johnson, S., Bailey, A. P. and Streit, A. (2011). Neural crest cells organize the eye via TGF-β and canonical Wnt signalling. *Nat. Commun.* **2**, 265.

Hayashi, R., Ishikawa, Y., Ito, M., Kageyama, T., Takashiba, K., Fujioka, T., Tsujikawa, M., Miyoshi, H., Yamato, M., Nakamura, Y. et al. (2012). Generation of corneal epithelial cells from induced pluripotent stem cells derived from human dermal fibroblast and corneal limbal epithelium. *PLoS ONE* **7**, e45435.

Hayashi, R., Ishikawa, Y., Sasamoto, Y., Katori, R., Nomura, N., Ichikawa, T., Araki, S., Soma, T., Kawasaki, S., Sekiguchi, K. et al. (2016). Co-ordinated ocular development from human iPS cells and recovery of corneal function. *Nature* **531**, 376-380.

Hiler, D., Chen, X., Hazen, J., Kupriyanov, S., Carroll, P. A., Qu, C., Xu, B., Johnson, D., Griffiths, L., Frase, S. et al. (2015). Quantification of retinogenesis in 3D cultures reveals epigenetic memory and higher efficiency in ipscs derived from rod photoreceptors. *Cell Stem Cell* **17**, 101-115.

Huang, J., Dattilo, L. K., Rajagopal, R., Liu, Y., Kaartinen, V., Mishina, Y., Deng, C.-X., Umans, L., Zwijsen, A., Roberts, A. B. et al. (2009). FGF-regulated BMP signaling is required for eyelid closure and to specify conjunctival epithelial cell fate. *Development* **136**, 1741-1750.

Inamdar, M. S., Venu, P., Srinivas, M. S., Rao, K. and VijayRaghavan, K. (2009). Derivation and characterization of two sibling human embryonic stem cell lines from discarded grade III embryos. *Stem Cells Dev.* **18**, 423-434.

Kaewkhaw, R., Kaya, K. D., Brooks, M., Homma, K., Zou, J., Chaitankar, V., Rao, M. and Swaroop, A. (2015). Transcriptome dynamics of developing photoreceptors in three-dimensional retina cultures recapitulates temporal sequence of human cone and rod differentiation revealing cell surface markers and gene networks. *Stem Cells* **33**, 3504-3518.

Kanakubo, S., Nomura, T., Yamamura, K.-I., Miyazaki, J.-I., Tamai, M. and Osumi, N. (2006). Abnormal migration and distribution of neural crest cells in Pax6 heterozygous mutant eye, a model for human eye diseases. *Genes Cells* **11**, 919-933.

Kinoshita, H., Suzuma, K., Kaneko, J., Mandai, M., Kitaoka, T. and Takahashi, M. (2016). Induction of functional 3D ciliary epithelium-like structure from mouse induced pluripotent stem cells. *Invest. Ophthalmol. Vis. Sci.* **57**, 153-161.

Kuwahara, A., Ozone, C., Nakano, T., Saito, K., Eiraku, M. and Sasai, Y. (2015). Generation of a ciliary margin-like stem cell niche from self-organizing human retinal tissue. *Nat. Commun.* **6**, 6286.

Mariappan, I., Kacham, S., Purushotham, J., Maddileti, S., Siamwala, J. and Sangwan, V. S. (2014). Spatial distribution of niche and stem cells in ex vivo human limbal cultures. *Stem Cells Transl. Med.* **3**, 1331-1341.

Mariappan, I., Maddileti, S., Joseph, P., Siamwala, J. H. and Vauhini, V. (2015). Enriched cultures of retinal cells from BJNhem20 human embryonic stem cell line of Indian origin. *Invest. Ophthalmol. Vis. Sci.* **56**, 6714-6723.

Marko, C. K., Tisdale, A. S., Spurr-Michaud, S., Evans, C. and Gipson, I. K. (2014). The ocular surface phenotype of Muc5ac and Muc5b null mice. *Invest. Ophthalmol. Vis. Sci.* **55**, 291-300.

McCabe, K. L., Kunzevitzky, N. J., Chiswell, B. P., Xia, X., Goldberg, J. L. and Lanza, R. (2015). Efficient generation of human embryonic stem cell-derived corneal endothelial cells by directed differentiation. *PLoS ONE* **10**, e0145266.

McKenzie, R. W., Jumblatt, J. E. and Jumblatt, M. M. (2000). Quantification of MUC2 and MUC5AC transcripts in human conjunctiva. *Invest. Ophthalmol. Vis. Sci.* **41**, 703-708.

Mikhailova, A., Ilmarinen, T., Uusitalo, H. and Skottman, H. (2014). Small-molecule induction promotes corneal epithelial cell differentiation from human induced pluripotent stem cells. *Stem Cell Rep.* **2**, 219-231.

Rama, P., Matuska, S., Paganoni, G., Spinelli, A., De Luca, M. and Pellegrini, G. (2010). Limbal stem-cell therapy and long-term corneal regeneration. *N. Engl. J. Med.* **363**, 147-155.

Ramirez-Miranda, A., Nakatsu, M. N., Zarei-Ghanavati, S., Nguyen, C. V. and Deng, S. X. (2011). Keratin 13 is a more specific marker of conjunctival epithelium than keratin 19. *Mol. Vis.* **17**, 1652-1661.

Reichman, S., Terray, A., Slembrouck, A., Nanteau, C., Orieux, G., Habeler, W., Nandrot, E. F., Sahel, J.-A., Monville, C. and Goureau, O. (2014). From confluent human iPS cells to self-forming neural retina and retinal pigmented epithelium. *Proc. Natl. Acad. Sci. USA* **111**, 8518-8523.

Richardson, R. J., Hammond, N. L., Coulombe, P. A., Saloranta, C., Nousiainen, H. O., Salonen, R., Berry, A., Hanley, N., Headon, D., Karikoski, R. et al. (2014). Periderm prevents pathological epithelial adhesions during embryogenesis. *J. Clin. Invest.* **124**, 3891-3900.

Sangwan, V. S., Basu, S., Vemuganti, G. K., Sejpal, K., Subramaniam, S. V., Bandyopadhyay, S., Krishnaiah, S., Gaddipati, S., Tiwari, S. and Balasubramanian, D. (2011). Clinical outcomes of xeno-free autologous cultivated limbal epithelial transplantation: a 10-year study. *Br. J. Ophthalmol.* **95**, 1525-1529.

Sareen, D., Saghizadeh, M., Ornelas, L., Winkler, M. A., Narwani, K., Sahabian, A., Funari, V. A., Tang, J., Spurka, L., Punj, V. et al. (2014). Differentiation of human limbal-derived induced pluripotent stem cells into limbal-like epithelium. *Stem Cells Transl. Med.* **3**, 1002-1012.

Schermer, A., Galvin, S. and Sun, T. T. (1986). Differentiation-related expression of a major 64K corneal keratin in vivo and in culture suggests limbal location of corneal epithelial stem cells. *J. Cell Biol.* **103**, 49-62.

Shalom-Feuerstein, R., Serror, L., De La Forest Divonne, S., Petit, I., Aberdam, E., Camargo, L., Damour, O., Vigouroux, C., Solomon, A., Gaggioli, C. et al. (2012). Pluripotent stem cell model reveals essential roles for miR-450b-5p and miR-184 in embryonic corneal lineage specification. *Stem Cells* **30**, 898-909.

Sidney, L. E., Branch, M. J., Dunphy, S. E., Dua, H. S. and Hopkinson, A. (2014). Concise review: evidence for CD34 as a common marker for diverse progenitors. *Stem Cells* **32**, 1380-1389.

Takahashi, K., Tanabe, K., Ohnuki, M., Narita, M., Ichisaka, T., Tomoda, K. and Yamanaka, S. (2007). Induction of pluripotent stem cells from adult human fibroblasts by defined factors. *Cell* **131**, 861-872.

Völkner, M., Zschätzsch, M., Rostovskaya, M., Overall, R. W., Busskamp, V., Anastassiadis, K. and Karl, M. O. (2016). Retinal organoids from pluripotent stem cells efficiently recapitulate retinogenesis. *Stem Cell Rep.* **6**, 525-538.

Yoshida, S., Shimmura, S., Kawakita, T., Miyashita, H., Den, S., Shimazaki, J. and Tsubota, K. (2006). Cytokeratin 15 can be used to identify the limbal phenotype in normal and diseased ocular surfaces. *Invest. Ophthalmol. Vis. Sci.* **47**, 4780-4786.

Zhang, K., Pang, K. and Wu, X. (2014). Isolation and transplantation of corneal endothelial cell-like cells derived from *in-vitro*-differentiated human embryonic stem cells. *Stem Cells Dev.* **23**, 1340-1354.

Zhong, X., Gutierrez, C., Xue, T., Hampton, C., Vergara, M. N., Cao, L.-H., Peters, A., Park, T. S., Zambidis, E. T., Meyer, J. S. et al. (2014). Generation of three-dimensional retinal tissue with functional photoreceptors from human iPSCs. *Nat. Commun.* **5**, 4047.

Supplementary Information

Supplementary Figures

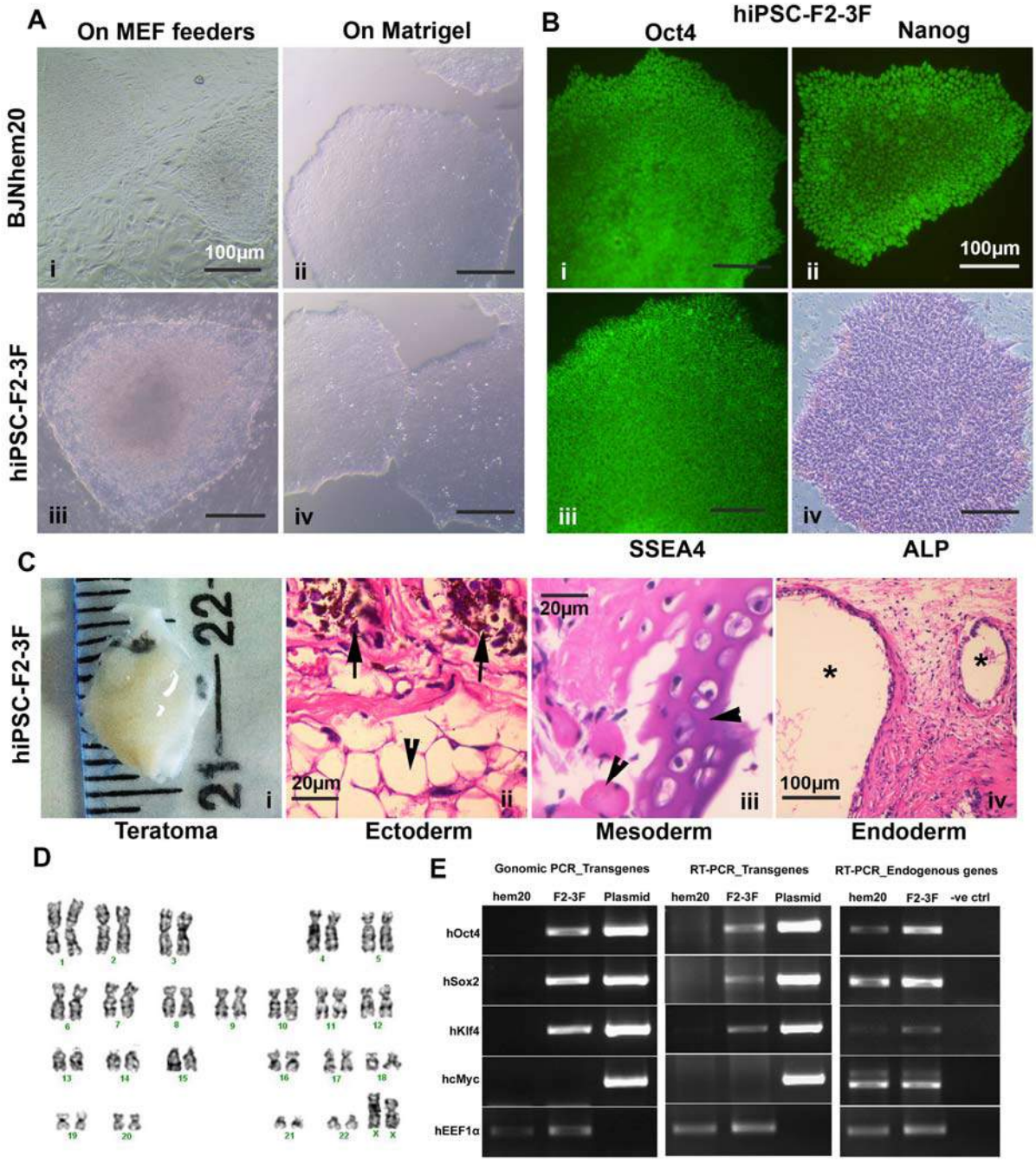

Figure S1. Derivation and characterization of a human induced pluripotent stem cell line. (A) Growing colony morphology of BJNhem20 cells (i-ii) and hiPSC-F2-3F1 cells at passage p0 on irradiated MEF feeders (iii) and at passage p20 on Matrigel coated plates (iv). (B) Immunocytochemistry of hiPSC-F2-3F1 cells at p20 on Matrigel coated chamber slides showing a homogenous expression of OCT4 (i), NANOG (ii), SSEA4 (iii) and alkaline phosphatase (iv). (C) A teratoma of about 8X8 mm, formed by hiPSC-F2-3F1 cells at p25, transplanted in the subcutaneous space of nude mice (i). H&E staining of tissue sections reveal the development of ectoderm derived RPE-like pigmented cell patches (arrow, ii), mesoderm derived adipose, cartilage and muscle tissues (arrow heads, iii) and endoderm derived gut epithelium like structures (asterisk, iv). (D) G-band karyotype of hiPSC-F2-3F1 cells at p20, confirmed a normal chromosomal pattern for this female line (n=2). (E) Genomic PCR profiles of transgene specific amplicons confirmed the genomic integration of human *OCT4, SOX2* and *KLF4* but not the *cMYC* transgenes (i). RT-PCR profiles of transgene-specific amplicons confirmed the expression of all transgenes except *cMYC,* at p20 (ii). RT-PCR profiles of endogenous gene specific amplicons confirmed the expression of all four transcripts, at levels comparable to that of BJNhem20, hESCs (iii). Plasmid DNA and no-RT samples were used as PCR controls. Genomic DNA and cDNA samples were normalized using eukaryotic elongation factor (*EEF1α*) as the loading control. Scale bars, 100 μm or as specified.

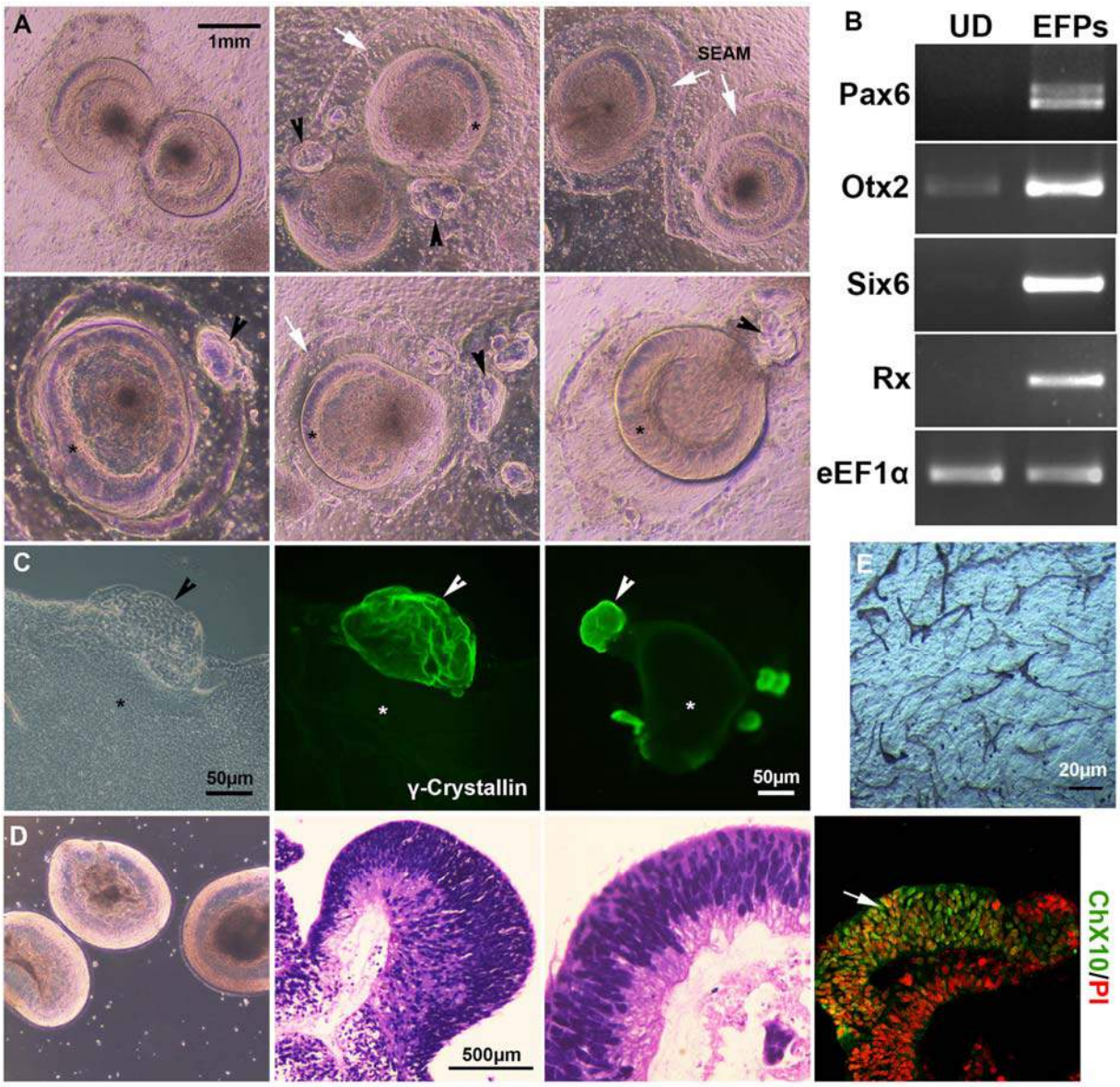

Figure S2. Morphology of adherent eye field clusters. (A) Distinct, oval to circular, three dimensional clusters of eye field primordial structures emerged at four weeks of differentiation. N=6. Upon continued adherent culture, the OSE cells migrate outwards to form a clear growth zone, as indicated by white arrows. Asterisks mark the central neuroretinal cups. OSE cells also gave rise to lens epithelium-like morphologically distinct clusters near the leading edge of the outgrowths as indicated by arrow heads. Scale bars, 1 mm. (B) RT-PCR profiles confirmed the

expression of early eye field commitment markers such as *PAX6, OTX2, SIX6* and *RX* in the cells that constitute EFP clusters. The cDNA samples were normalized using *EEF1α* as the loading control. (C) γ-Crystaline^{+} lentoid structures were observed adjacent to the neuroretinal cups. (D) NR clusters developed into optic vesicles, with layered arrangement of precursor cells in suspension cultures (H&E). They also formed double layered retinal cups, with Chx10^{+} neuroretinal layer (green) on the outer surface. (E) Spindle shaped, pigmented melanocytes were observed above the plane of epithelium in a bright field, confocal view.

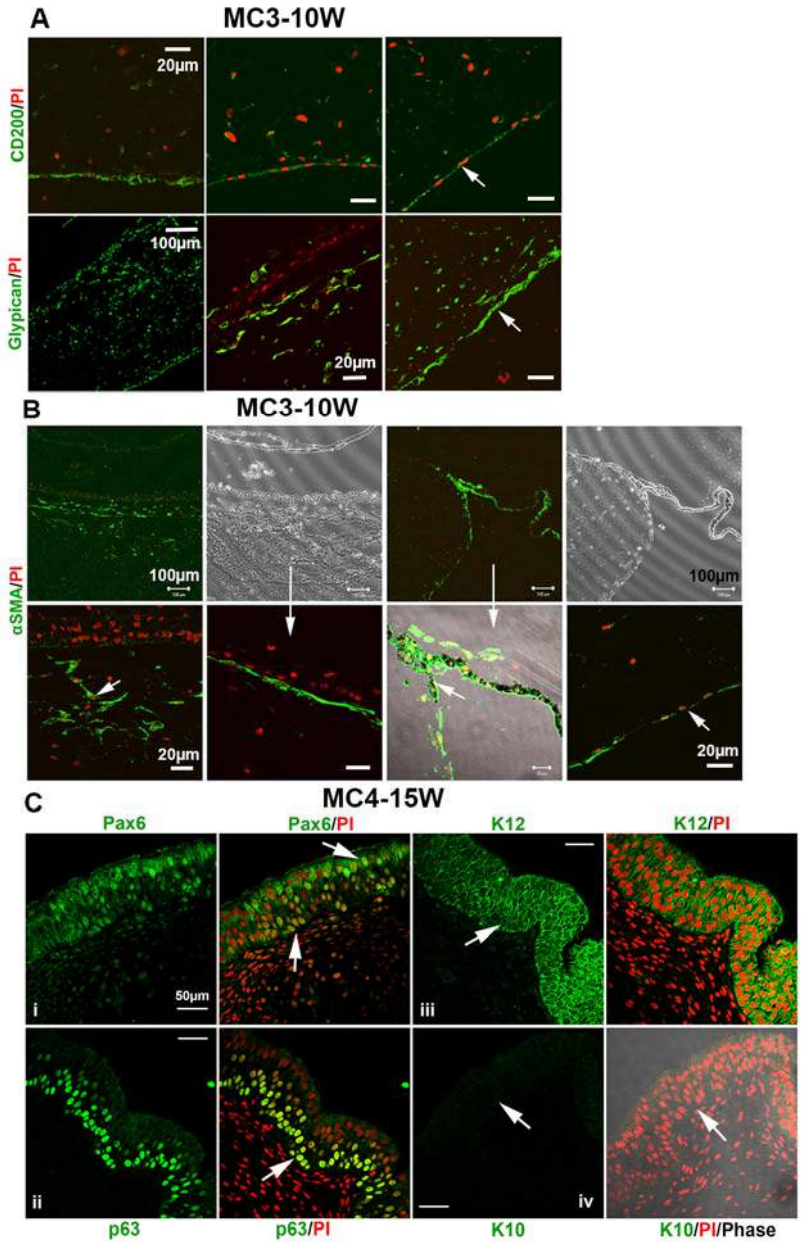

Figure S3. Expression of corneal endothelium and smooth muscle markers in minicorneas. (A) The endothelium like single cell lining on the basal side for the stroma expressed CD200 (i) and Glypican 4 (ii). (B) The peripheral and anterior stromal cell infiltrates were αSMA^{+} (i-ii). Peripheral endothelium and the surrounding adnexal tissues also expressed αSMA (arrows). PI counterstain marked the nuclei in red. (C) The surface epithelium of 15W old corneal organoids were Pax6^{+}, p63^{+}, K12^{+}, K10^{-}. Scale bars, 20 μm or as specified.

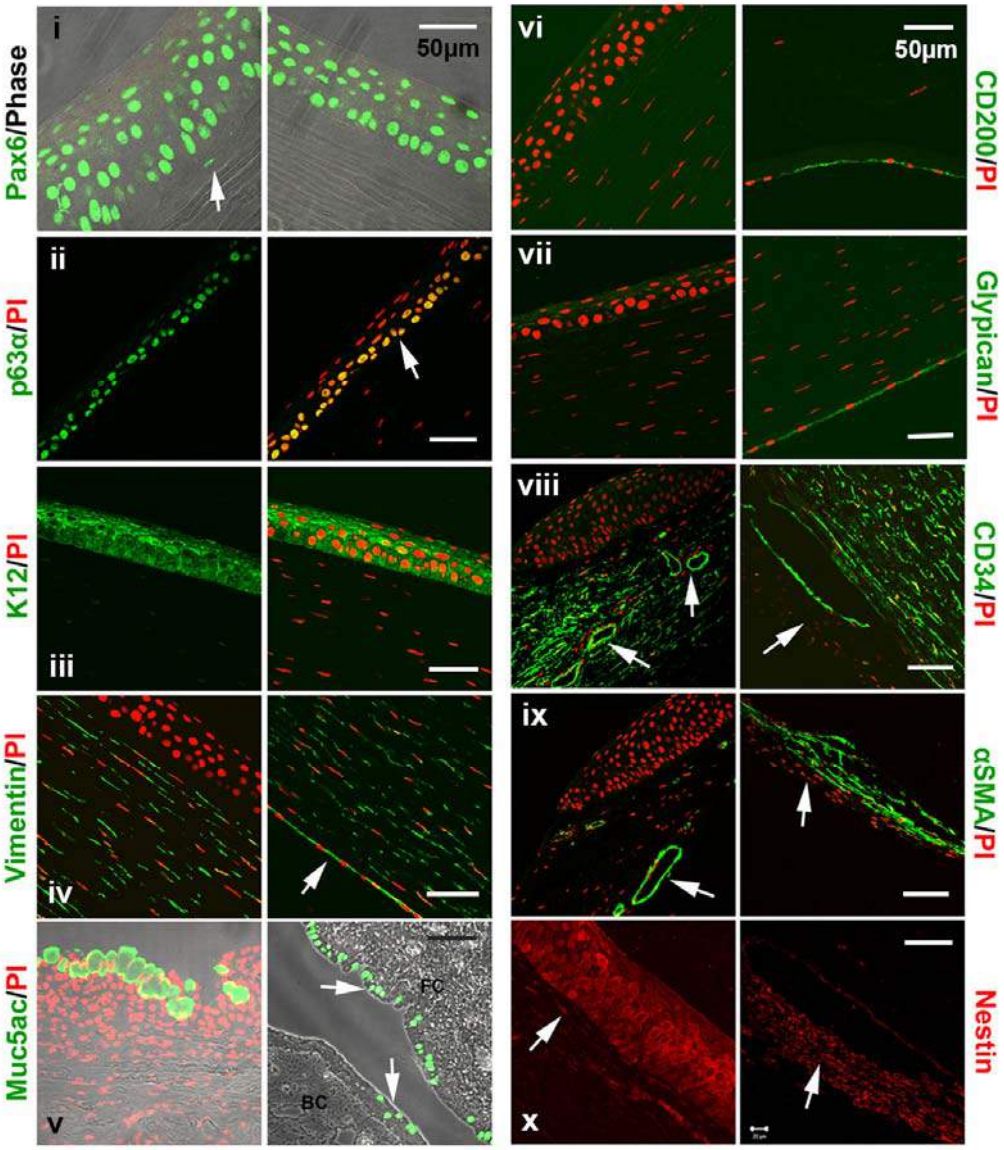

Figure S4. Tissue-specific marker expression profiles of adult corneas. Confocal images of adult donor corneal tissues sections showing the expression of various markers such as PAX6 (i), P63α (ii), K12 (ii), Vimentin (iv), MUC5AC (v), CD200 (vi), GPC4 (vii), CD34 (viii), αSMA (ix) and Nestin (x). The sections were counter stained with PI (red). Corneal epithelial cells were PAX6^{+} and K12^{+}. The basal epithelial cells were P63α^{+}. The VIM^{+} NCCs and CD34^{+} MSCs contribute equally to the corneal stroma. αSMA^{+} cells lines the lumen of Schlemm's canal. Trabecular meshwork cells were NES^{+}. Endothelial cells were CD200^{+}, GPC4^{+} and VIM^{+}. Scale bars are as indicated.

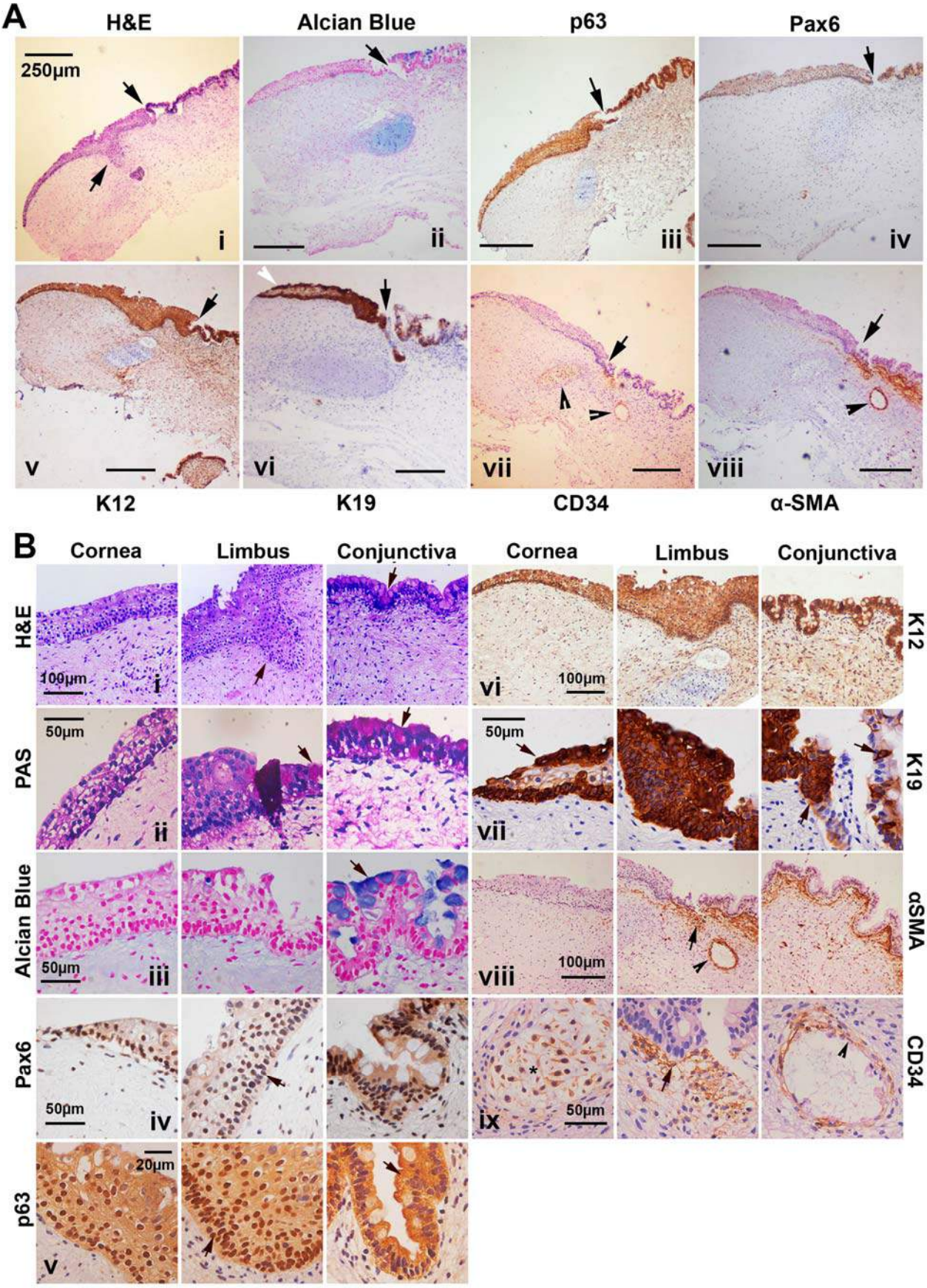

Figure S5. Gross morphology and IHC characterization of the minicornea, MC4. (A) Low magnification bright field IHC images of 15 weeks old MC4. Scale bars, 250 μm. (B) Higher magnification view of the sections shown above. H&E stained images displayed the gross tissue morphology (i) PAS and Alcian blue staining indicate the presence of goblet cells (ii-iii). Immunostained sections were labeled with DAB to mark the expression of different corneal markers such as the PAX6 (iv), P63 (v), K12 (vi), K19 (vii), αSMA (viii) and CD34 (ix). Limbal margins are marked by arrows. αSMA^{+}, $CD34^{+}$ vasculature like structures are marked by arrowheads. Another $CD34^{+}$ mesenchymal stromal cell patch is marked by asterisk. Note the intense expression of K19 in the basal and surface epithelium, separated by a layer of no expression. Scattered $K19^{+}$ cells were also found interspersed within the developing conjunctival epithelium (arrows). Hematoxylin and nuclear fast red were used as blue and pink counter stains respectively. Scale bars, 50 μm or as specified.

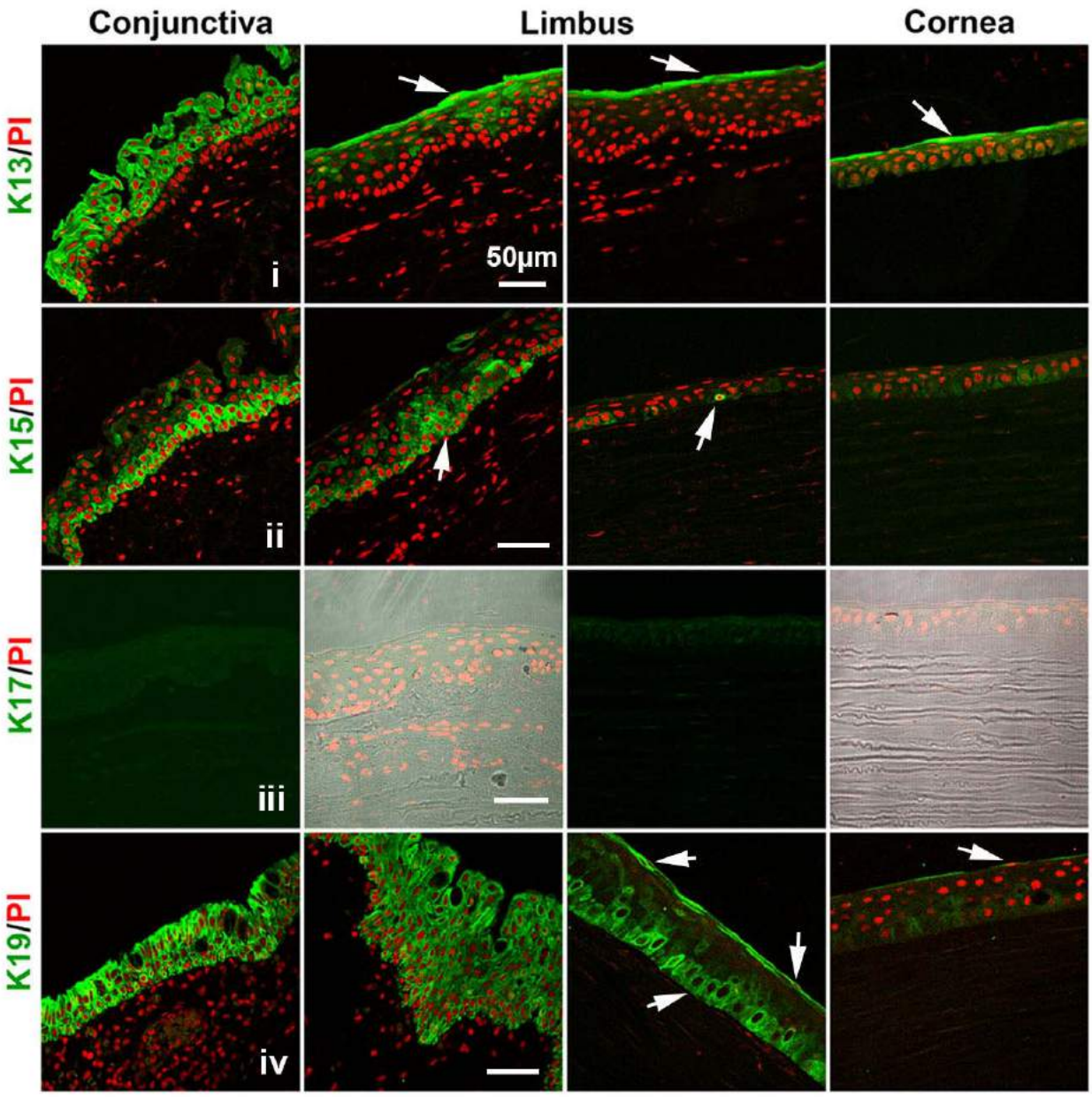

Figure S6.

Confocal images of tissues sections showing the expression of keratins such as K13 (i), K15 (ii), K17 (iii) and K19 (iv). Note the surface and suprabasal epithelial expression of K13, basal epithelial expression of K15, conjunctival, limbal basal and corneal surface epithelial staining of K19. K17 expression was found to be absent in adult corneal tissues. The sections were counterstained with PI (red). All scale bars, 50 µm.

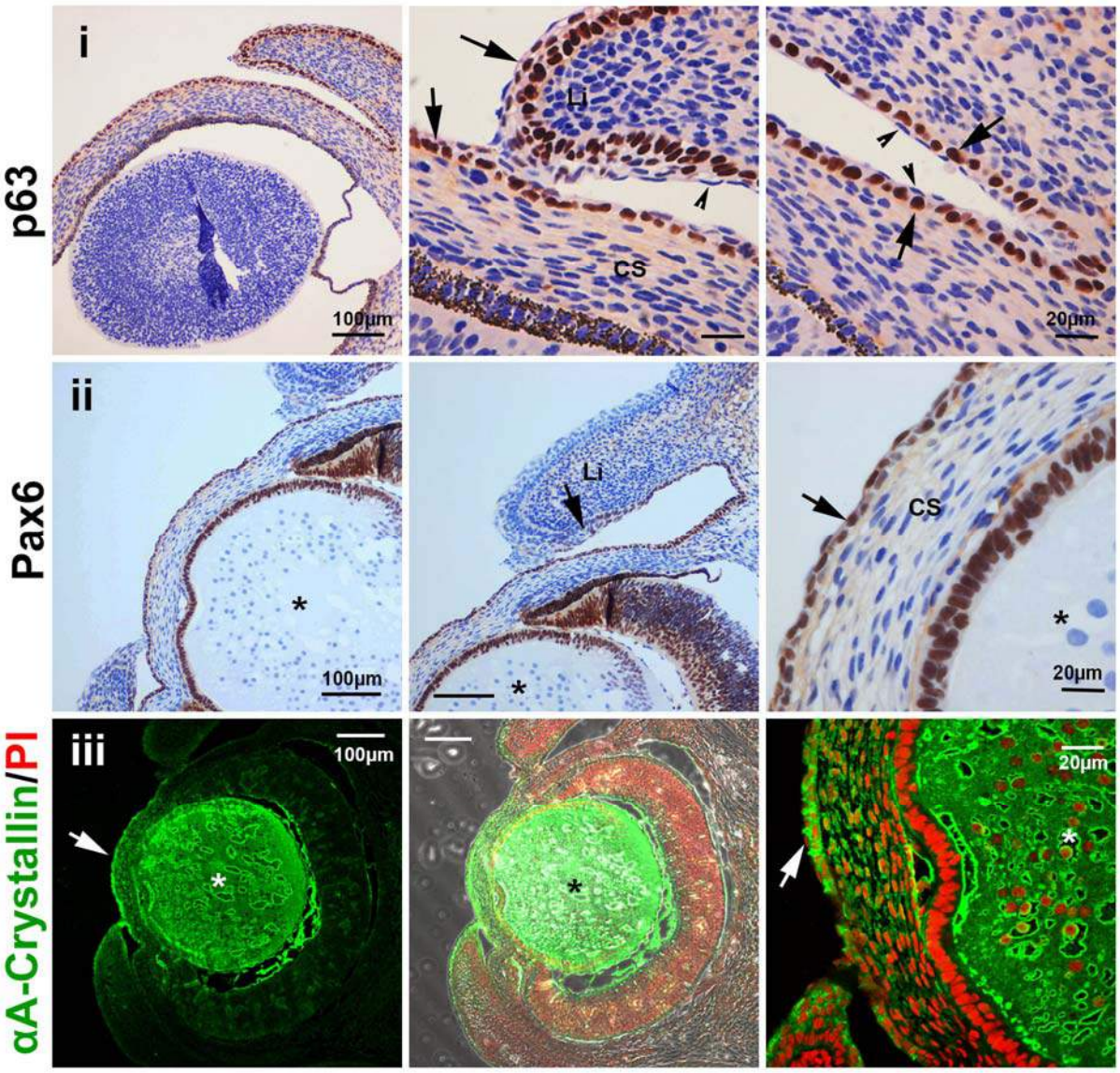

Figure S7. Marker expression patterns in developing eyes of mouse embryos.

IHC images of eye balls of E13.5 mouse embryos showing p63 expression in the basal epithelial cells of corneal, conjunctival and lid surface epithelium (i). PAX6 expression is limited to the corneal and conjunctival epithelium. Arrows points to the lip region of the lid epithelium (Li) showing diminished PAX6 expression (ii). αA-crystallin is expressed in the lens (asterisk) and the opposing surface ectoderm derived corneal epithelium (iii). Arrow heads point to PAX6$^-$ apical wing cells. CS indicates the corneal stroma. All scale bars, 20 μm or as specified.

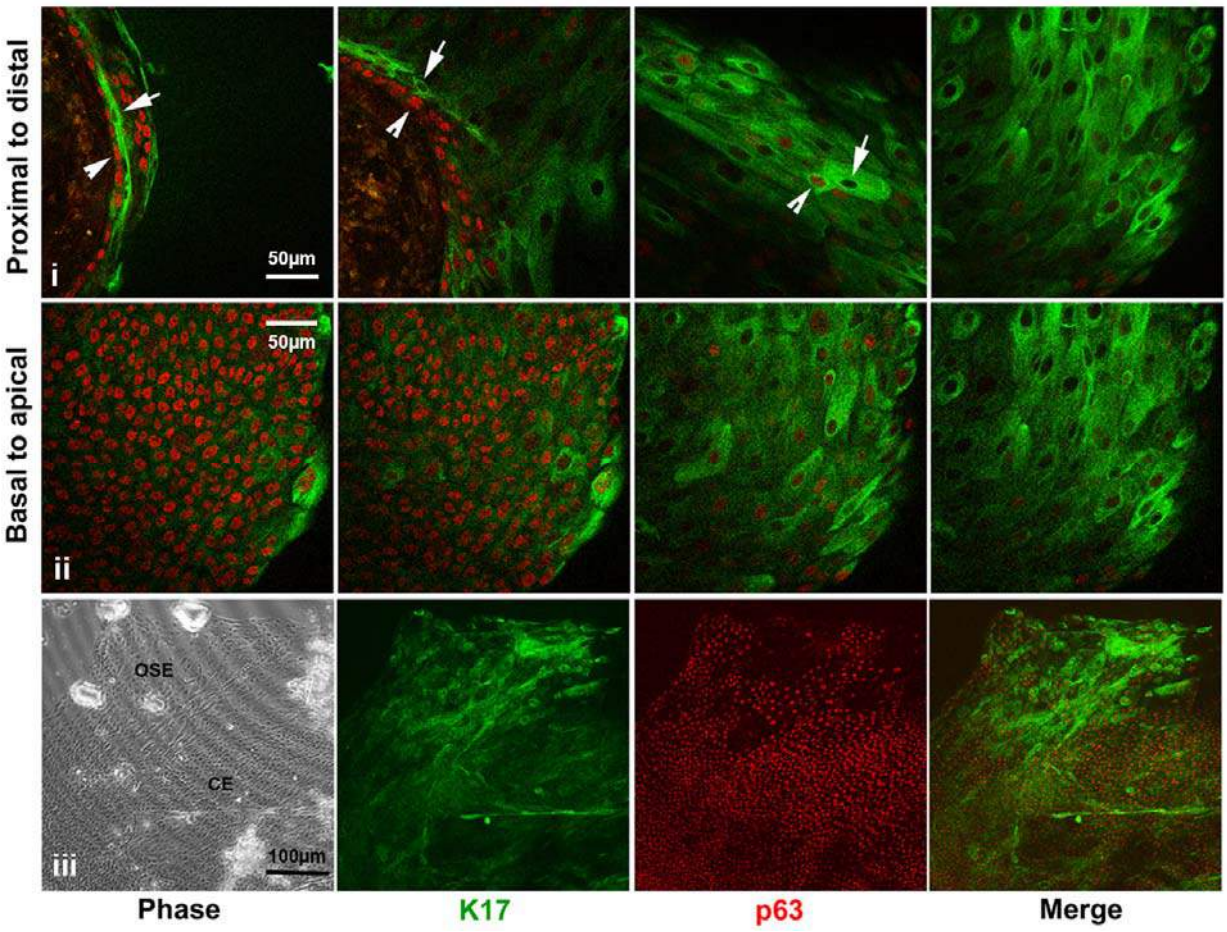

Figure S8. IHC characterization of cell outgrowth from corneal organoids on glass coverslips. Confocal images of 10 weeks old MC explants grown as confluent cultures on glass coverslips, showing the expression of K17 and P63. Serial images taken at proximal and distal positions from the explants show that $K17^{+}$, $P63^{-}$ cells (arrows) emerge first and forms the leading edge of the wave front, while $K17^{+}$, $P63^{+}$ cells (arrow heads) emerge later (i). Serial Z-sections from basal to apical surface of the outgrowths show $K17^{+}$, $P63^{+}$ cells on the basal side and $K17^{+}$, $P63^{-}$ cells (arrows) on the apical surface (ii). Low magnification images of epithelial outgrowth showing K17 and P63 expression, as described above (iii). Scale bars, 50 μm or as specified.

Supplementary Movies

Movie 1

Phase-contrast images of a minicornea at 8 weeks of development. A basal to apical view series.

Movie 2

Phase-contrast images of cell outgrowths from EFPs. A proximal to distal view series.

Movie 3

Fluorescence images of P63+ cell outgrowths from EFPs. A proximal to distal view series.

Supplementary Tables

Table S1. Details of primers used in the study

Human gene name	Primer Sequence 5'→ 3'	Amplicon size (bp)	NCBI Accession number
	RT-PCR primer sets		
P63	F: GCTGGAGACATGAATGGACT R: GGTGAATCGCACAGCATCAA	399 (α) 305 (β)	NM_003722 NM_001114978
K12	F- ATTGGAAATGCCCAGCTCCT R-TCTGCTCAGCGATGGTTTCA	352	NM_000223
PAX6	F1- ATAACCTGCCTATGCAACCC R1- GGAACTTGAACTGGAACTGAC	208	NM_000280
PAX6	F2: GAAGATTGTAGAGCTAGCTCACAGCG R2: TGTTGCTTTTCGCTAGCCAGGTTG	369 (5a) 327 (wt)	NM_001604 NM_000280
OTX2	F- ACTTCGGGTATGGACTTGCT R- GTTCCACTCTCTGAACTCAC	350 (a) 326 (b)	NM_021728 NM_172337
SIX6	F- ATTTGGGACGGCGAACAGAA R- TGGATGGGCAACTCAGATGT	381	NM_007374
RX	F- GCAAGGTCAACCTACCAGA R- TCGTCCAGCGGGAACTTGT	439	NM_013435
EEF1A	F- GAAGTCTGGTGATGCTGCCATTGT R- TTCTGAGCTTTCTGGGCAGACTTG	198	NM_001402
OCT3/4-endo	F3: TCCCTTCGCAAGCCCTCATTT R2- TCTGCAGAGCTTTGATGTCC	486	NM_002701
OCT3/4-transgene	F- CCTCACTTCACTGCACTGTACTC L3205- CCCTTTTTCTGGAGACTAAATAAA	335	
SOX2-endo	F- CCCAGCAGACTTCACATGTCC R- GCGTGAGTGTGGATGGGATTG	287	NM_003106
SOX2-transgene	F- CCCAGCAGACTTCACATGTCC L3205- CCCTTTTTCTGGAGACTAAATAAA	348	
KLF4-endo	F- GATCGTGGCCCCGGAAAAGGAC R- GATTGTAGTGCTTTCTGGCTGG	394	NM_004235
KLF4-transgene	F- GATCGTGGCCCCGGAAAAGGAC L3205- CCCTTTTTCTGGAGACTAAATAAA	455	
MYC- endo	F2- AGCTTGTACCTGCAGGATCT R2- CTGCGTAGTTGTGCTGATGT	409	NM_002467
MYC-transgene	F- GAACAGCTACGGAACTCTTGTGC L3205- CCCTTTTTCTGGAGACTAAATAAA	419	

Table S2. Details of antibodies used in the study

Click here to Download Table S2

Table S3. Dimensions of the minicorneas at different stages of *in vitro* development

Age of MCs	**Culture method**	**Tissue ID**	**Length/ Diameter**	**Total width/ thickness**	**Epithelial thickness**
6 weeks	Suspension	MC1-1	1.1 mm		15-25 µm
8 weeks	Suspension	MC1-2	2.7 mm		15-42 µm
10 weeks	Suspension	MC2	1.15 mm		70-80 µm
10 weeks	Adherent	MC3	7.2 mm	1.3 mm	46-51 µm
		MC3 (lid)	1.8-2.0 mm	150-220 µm	
15 weeks	Adherent	MC4	5.6 mm	1 mm	85-90 µm
		MC4 (Limbus to limbus)	**1.92 mm**	1 mm	
15 weeks	Suspension	MC5	1.5 mm		15-25 µm
Adult cornea		Limbus to limbus	**11-11.75 mm**	600 µm (central)	53 µm (central) 67 µm (limbal)

BJO Online First, published on June 10, 2015 as 10.1136/bjophthalmol-2014-306516

Effect of mitomycin-C on contraction and migration of human nasal mucosa fibroblasts: implications in dacryocystorhinostomy

Vinay Kumar,[1] Mohammad Javed Ali,[2] Charanya Ramachandran[1]

[1]Sudhakar and Sreekanth Ravi Stem Cell Biology Laboratory, L.V. Prasad Eye Institute, Hyderabad Eye Research Foundation, Hyderabad, Telangana, India
[2]Dacryology Service, L.V. Prasad Eye Institute, Hyderabad Eye Research Foundation, Hyderabad, Telangana, India

Correspondence to
Dr Charanya Ramachandran, Sudhakar and Sreekanth Ravi Stem Cell Biology Lab, Brien Holden Eye Research Institute, Hyderabad Eye Research Foundation, L.V. Prasad Eye Institute, Road No 2, Banjara Hills, Hyderabad, Telangana, 500034, India; charanya@lvpei.org

Received 13 December 2014
Revised 24 March 2015
Accepted 19 April 2015

ABSTRACT

Aim To determine the effect of mitomycin-C (MMC) on the contraction and migration of human nasal mucosal fibroblasts (HNMFs) in vitro in order to identify the least concentration of MMC required to prevent cicatrix development following dacryocystorhinostomy (DCR).

Methods Primary cultures of HNMFs were established from nasal mucosal tissues of patients undergoing DCR. Myofibroblast transformation of HNMFs was induced using transforming growth factor-β (TGF-β1) and confirmed by immunostaining for α-smooth muscle actin (α-SMA). Collagen gel contraction assay was employed to study contraction in the presence or absence of TGF-β1 (5 and 10 ng/mL) and MMC (0.2 and 0.4 mg/mL). Scratch wound assay was employed to determine the influence of MMC treatment on cell migration. Quantification of gel contraction and wound closure was done using Image J software.

Results α-SMA expression increased with TGF-β1 treatment in a time- and dose-dependent manner indicating myofibroblast transformation of HNMFs. MMC inhibited TGF-β1- induced collagen gel contraction in a dose-dependent manner (0.4 mg/mL>0.2 mg/mL). Further, there was a decrease in the migration of MMC-treated HNMFs, resulting in delayed wound closure that corroborated with the loss of actin stress fibres.

Conclusions MMC successfully inhibited TGF-β1-induced myofibroblast transformation, collagen gel contraction and significantly reduced the migration of HNMFs to cover the wound even at a low concentration of 0.2 mg/mL. This study provides evidence that low concentration and short duration of MMC treatment is efficient in reducing increased contraction and migration of HMNFs in response to injury.

INTRODUCTION

Dacryocystorhinostomy (DCR) is a commonly performed surgical procedure to treat nasolacrimal duct obstruction by creating an alternate drainage route through the bony ostium located between the lacrimal sac and nasal cavity.[1] The procedure has good outcome; however, failure reported in the literature ranges from 11% to 28%.[1–3] The most common cause for failure is the rhinostomy closure by cicatricial tissue during wound healing. It is therefore conceivable that preventing scar formation would improve the surgical outcomes.

Scar formation is a natural outcome of wound healing, a process that primarily involves the proliferation, transformation and migration of the fibroblast cells, resulting in tissue remodelling. The resident fibroblast cells, in response to an injury, undergo transient transformation into a more contractile and migratory phenotype called myofibroblast cells.[4] This transformation marks the onset of wound healing and is mediated by factors such as transforming growth factor-β family (TGF-β) of cytokines and other factors.[5–7] These cells have the ability to synthesise more extracellular matrix proteins, growth factors and receptors required for quick wound closure compared with the fibroblast cells.[4]

Mitomycin-C (MMC), an antineoplastic antibiotic, has been used extensively as adjuvant therapy to prevent excess scarring in several ophthalmic applications including pterygium excision, corneal surgeries, trabeculectomy and in DCR surgeries.[2 8–10] MMC acts by arresting new DNA and protein synthesis and thereby preventing cellular proliferation.[11] A recent meta-analysis of randomised control trials has shown that the use of MMC in conjunction with DCR surgery resulted in a significantly higher success rate and reduced the closure of osteomy site following surgery.[2 12] Even though MMC is commonly used in DCR surgeries and has been shown to be effective, there is a wide disparity and non-uniform use clinically in terms of the concentration (range 0.2–0.5 mg/mL) and duration of application (2–15 min). [2 3 12] Further, the mechanism of action of MMC on wound healing post-DCR surgery has not been addressed. Earlier studies have only shown that when exposed to higher concentrations of MMC the viability of human nasal mucosal fibroblasts (HNMFs) significantly reduces,[13 14] which clinically might present as mucosal burns. The need is therefore to understand the influence of MMC on the process of wound healing in order to arrive at an optimum concentration that would prevent scarring of the tissue without adversely affecting cell and tissue health.

Thus in this study, the functional aspects of wound healing such as cell contraction and migration have been studied in response to the application of MMC to HNMFs. The normal wound healing process has been simulated in vitro using the collagen contraction and wound healing assays, and to our best knowledge, this is the first study that addresses the influence of MMC treatment on wound healing in HNMFs.

METHODS

Normal nasal mucosa samples from four patients undergoing DCR surgery were obtained for conducting this study.

Material used and its sources

TGF-β1 recombinant human protein, fetal bovine serum (FBS) and rat tail collagen I were obtained from Invitrogen, Grand Island, New York, USA.

To cite: Kumar V, Ali MJ, Ramachandran C. *Br J Ophthalmol* Published Online First: [*please include* Day Month Year] doi:10.1136/bjophthalmol-2014-306516

Other materials used include MMC (Biochem Pharmaceutical Industries, UT, India), Dulbecco's modified Eagle's medium (DMEM) and penicillin-streptomycin antibiotics (Sigma Aldrich, Massachusetts, USA), phalloidin (Molecular Probes, Eugene, Oregon, USA) and α-smooth muscle actin (α-SMA) antibody (Abcam, Cambridge, UK).

Nasal mucosa harvesting and establishing cell cultures

Harvesting of the nasal mucosa and establishment of primary cultures of HNMFs using the explant culture technique was carried out as described earlier.[13] In brief, tissue pieces were washed with 1× phosphate buffered saline (PBS) containing 2× antibiotics and then cut into small pieces and enzymatically digested with 0.25% trypsin for 30 min. After digestion, equal volumes of culture medium (DMEM with 10% FBS) were added to inactivate the trypsin and the cell suspension was centrifuged at 100 *g* for 5 min. The pellet was resuspended in culture medium and cells cultured at 37°C with 5% CO_2 supply. Once 80% confluent, cells were subcultured at 1:3 ratio. Passage 2–3 cells were used for experiments.

Collagen gel contraction assay

Since the HNMFs are present within a three- dimensional mucosal tissue, we attempted to mimic the in vivo conditions by culturing the cells within collagen gels and assessing their contractility as opposed to on plastic dishes. About 70–80% confluent HNMF cells were released from T75 culture dish using 0.25% trypsin, 1 mM EDTA and the cell number was counted using a Neubaers chamber. Rat tail type I collagen (final concentration of 1.9 mg/mL), 10× DMEM, 10× reconstitution buffer (50 mM NaOH, 260 mM $NaHCO_3$ and 200 mM HEPES) and cell suspension (2×10^5 cells/mL) were mixed carefully on ice. Prior to adding the above mixture to a 24-well culture plate, each well was coated with 1% bovine serum albumin for 1 h. Following this, 500 μL of the mix was added to each well and incubated at 37°C for 1 h. After 1 h of incubation, the gel was flooded with fresh medium and was carefully detached from well wall using a needle. HNMFs embedded in the gels were treated with TGF-β1 and/or MMC to assess their contractility for 72 h at which time they were fixed with 4% paraformaldehyde and stained with rose bengal for quantification of gel area using Image J software (National Institutes of Health, Bethesda, Massachusetts, USA).

Immunostaining

HNMF cells were seeded on coverslips and allowed to adhere for 24 h. The cells were serum starved for 12 h following which they were treated with different concentrations of TGF-β1 (1 ng, 5 ng and 10 ng/mL) for up to 48 h to assess α-SMA expression using specific antibody. The number of α-SMA positive cells per 1000 cells, counterstained with propidium iodide, was counted at the end of the treatment period. In another set of experiments, the HNMFs were first subjected to 3 min of MMC (0.2 or 0.4 mg/mL) treatment following which the cells were treated with TGF-β1 (5 and 10 ng/mL) for 48 h to assess the change in α-SMA expression. The choice of MMC concentration and time duration of treatment was based on previous clinical and in vitro studies.[2 12–14] Phalloidin was used to stain the actin filaments. At the end of 48 h of treatment, the HNMFs were fixed in 4% paraformaldehyde, non-specific sites blocked using 10% fetal calf serum and incubated with primary antibody (1:50) followed by staining with Alexa-488 conjugated secondary antibody. The staining was visualised using the confocal microscope (LSM 510, Carl Zeiss, Jena, Germany).

Wound healing assay

For this assay, the cells were seeded in six-well plates and cultured as a monolayer until they reached 100% confluency. Scratch wounds were created using a blunt pipette tip. This was considered for analysis as time point 0 or T0. Following this, the cells were treated with MMC (0.2 and 0.4 mg/mL) for 3 and 5 min. Fresh culture medium was added to the cells after the removal of MMC and extensive rinsing with PBS. Images of wounds (three per well) were captured at different time points (T2, T4, T16, T24) until the wounds closed completely. The wound width in each picture was determined by outlining the two edges of the wounds and measuring the wound distance using Image J analysis software.

Data analysis

A two-factor analysis of variance was used to compare mean values for different treatments with Tukey's post-test analysis (Prism 6.0 GraphPad Software, San Diego, California, USA). A p value of <0.05 was considered statistically significant.

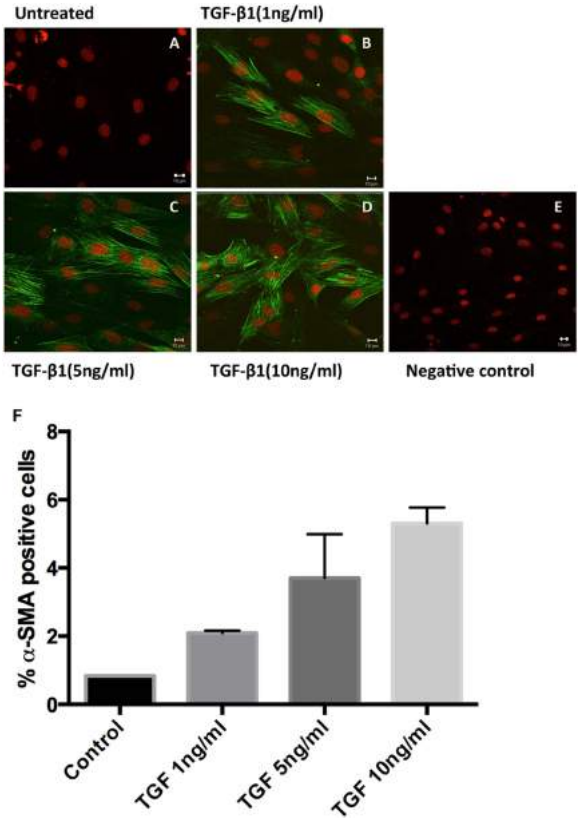

Figure 1 Effect of transforming growth factor-β (TGF-β1) on α-smooth muscle actin (α-SMA) expression by human nasal mucosal fibroblasts (HNMFs). HNMFs were treated with TGF-β of 1, 5 and 10 ng/mL for 24 h and stained for α-SMA using a specific antibody. A concentration-dependent increase in the expression of this protein can been seen in the figure ((B), (C) and (D) vs (A)) with 10 ng/mL≥5 ng/mL>1 ng/mL indicating that treatment with TGF-β induces fibroblast to myofibroblast transformation of HNMFs. (E) Negative control for α-SMA. (F) A graphical representation of data (mean±SD) analysed from two individual cultures. Green, α-SMA; red, propidium iodide; scale bar: 10 μm.

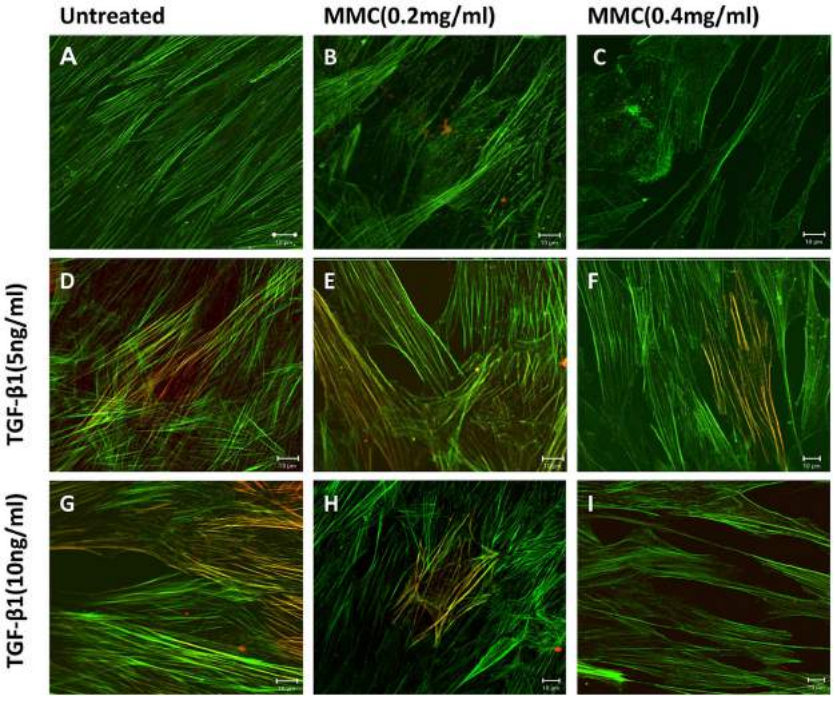

Figure 2 Mitomycin treatment reduces myofibroblast transformation of human nasal mucosal fibroblasts. There were very few, if any, α-smooth muscle actin (α-SMA)-positive cells in the untreated control as shown in (A) and the actin filaments showed uniform alignment. Treatment with mitomycin-C (MMC) alone (0.2 and 0.4 mg/mL) for 3 min led to the disruption and aggregation of the actin filaments. No staining for α-SMA was detected (B and C). Treatment of cells with 5 and 10 ng/mL of transforming growth factor-β (TGF-β), on the other hand, induced increased expression of α-SMA as can be seen in (D) and (G). Pretreatment of cells with MMC for 3 min before exposure to TGF-β reduced significantly the expression of α-SMA in these cells (E, F, H and I). Green, actin; red, α-SMA; scale bar: 10 μm.

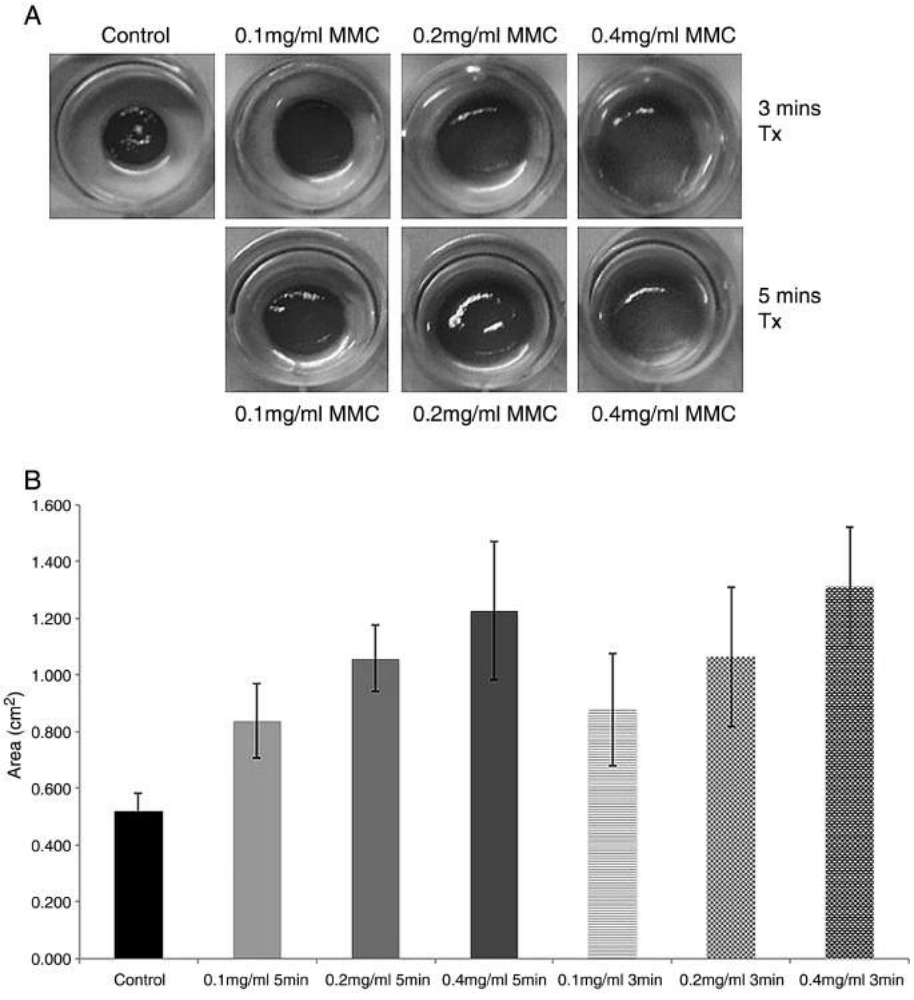

Figure 3 Effect of mitomycin-C (MMC) on collagen gel contraction. (A) A representation of the gel assay and shows the extent of gel contraction in the presence and absence of MMC treatment. The contraction measured in the untreated control was taken as the baseline and produced maximum contraction. Treatment with MMC for 3 min reduced gel contraction significantly compared with untreated control. Similarly, treatment with MMC for 5 min also reduced significantly the gel contraction. However, the gel contraction was not significantly different between the two durations of treatment for a given concentration of MMC (eg, 0.1 mg/mL treatment for 3 min vs 5 min). (B) A graphical representation of data as mean±SD with N=4.

Results are expressed as mean±SD. 'N' denotes the number of independent experiments.

RESULTS

TGF-β1 induced fibroblast to myofibroblast transformation

To determine the optimum concentration of TGF-β1 required for inducing the fibroblast to myofibroblast transformation, in order to simulate wound healing response in vitro, HNMFs were treated with TGF-β1 (1, 5 and 10 ng/mL) for 24 and 48 h. From figure 1A–D, it is clear that there is a concentration-dependent increase in α-SMA expression in the following order 10 ng/mL≥5 ng/mL>1 ng/mL. This difference was significant between 5 and 10 ng/mL TGF-β1-treated and TGF-β1-untreated cells (p=0.05 and 0.01, respectively). The α-SMA expression was not significantly different between 1 ng/mL TGF-β1-treated cells and TGF-β1-untreated cells (p>0.05). There was also a time-dependent difference noted (48 h >24 h); however, data only for 48 h are shown here. Thus in all further experiments, 5 and 10 ng/mL concentrations of TGF-β1 were employed.

MMC inhibited TGF-β1-induced expression of α-SMA

Cells were treated with 0.2 and 0.4 mg/mL of MMC for 3 min before the addition of TGF-β1 (5 and 10 ng/mL) for 48 h. As shown in figure 2, addition of MMC alone was seen to disrupt the actin filaments and cause their aggregation (figure 2B, C) compared with the arrangement of actin filaments in the control (figure 2A). Treatment with TGF-β1 alone increased the expression of α-SMA (figure 2D, G). Pretreatment with MMC reduced the expression of α-SMA in the HNMFs (figure 2E,F, H,I) with fewer cells staining positive for α-SMA compared with just TGF-β1-treated cells. Also, at 0.4 mg/mL concentration, MMC caused shrinking of HNMFs even in the presence of 10 ng/mL of TGF-β1.

Effect of MMC on gel contraction

When the cells cultured in collagen gels were treated with MMC (0.1, 0.2 and 0.4 mg/mL) for 3 or 5 min, there was a concentration-dependent reduction in gel contraction with 0.4 mg/mL concentration of MMC providing the maximum decrease compared with control and 0.1 mg/mL MMC (p=0.001; figure 3A, B). There was no significant difference in gel contraction produced by similar concentration of drug whether the treatment was for 3 or 5 min (eg, 0.1 mg/mL 3 min vs 0.1 mg/mL 5 min). Also, the difference in contraction produced by 0.2 and 0.4 mg/mL was not statistically significant (p>0.05).

The addition of TGF-β1 to cells in gels induced a greater contraction compared with control (figure 4A, B). Addition of MMC to the cells for 3 min before the addition of TGF-β1 for 72 h reduced significantly the contractility of the gels

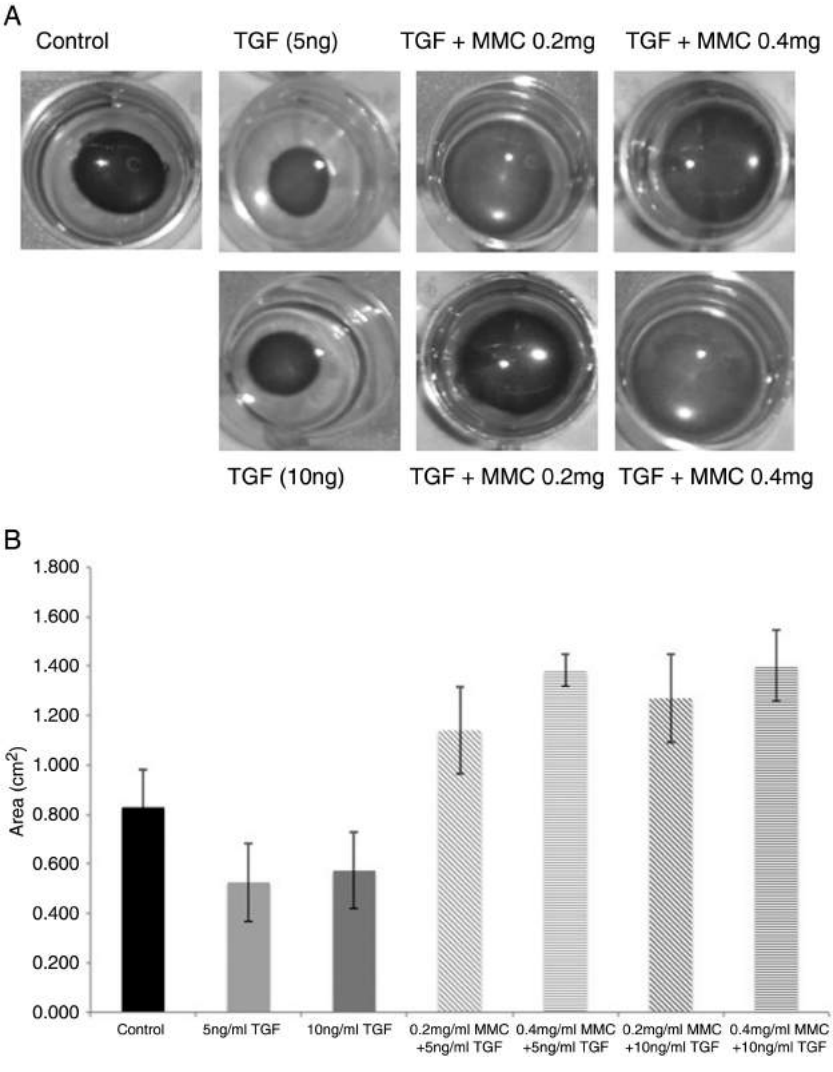

Figure 4 Effect of mitomycin-C (MMC) on transforming growth factor-β (TGF-β)-induced collagen gel contraction: (A) A representative gel picture of the contraction assay. As can be seen, the addition of TGF-β to cells increased significantly gel contraction compared with untreated control. Pretreatment of cells with MMC (for 3 min) was able to oppose TGF-β-induced increase in contraction. This reduction in gel contraction was significant. Data from four independent experiments (N=4) are represented as a graph in (B) as mean±SD.

(p=0.001). The contraction was more in 0.2 mg/mL treated cells than 0.4 mg/mL, but the difference was not significant (p>0.05), suggesting that even at lower concentration (0.2 mg/mL) and shorter treatment time (3 min) MMC significantly reduces cell contraction.

MMC treatment impedes cell migration

While it is clear from figure 1 that treatment with TGF-β1 induces the expression of α-SMA, we wanted to check whether creating wounds would also have the same effect on the cells. Scratch wounds were created and followed for up to 48 h to detect any change in α-SMA expression (figure 5A). At 4 h following injury, there were no α-SMA-positive cells (figure 5Ab) detectable similar to untreated control (figure 5Aa). However, at 24 h post injury, α-SMA-positive cells were found near the wound site (figure 5Ac) and at 48 h there was a further increase in the α-SMA-positive cells (figure 5Ad), indicating that creation of wounds in culture had an effect similar to TGF-β1 treatment.

In the next set of experiments, the influence of MMC treatment on cell migration was assessed. Shown in figure 5B is an example of how the wounds edges were marked for analysis until complete closure of the wound site was attained. When treated with MMC, there was an increase in the time taken for the cells to cover the wound completely compared with untreated cells (figure 5C). In the untreated cells, the average time taken for complete wound closure was 30 h. However, treatment for 3 min

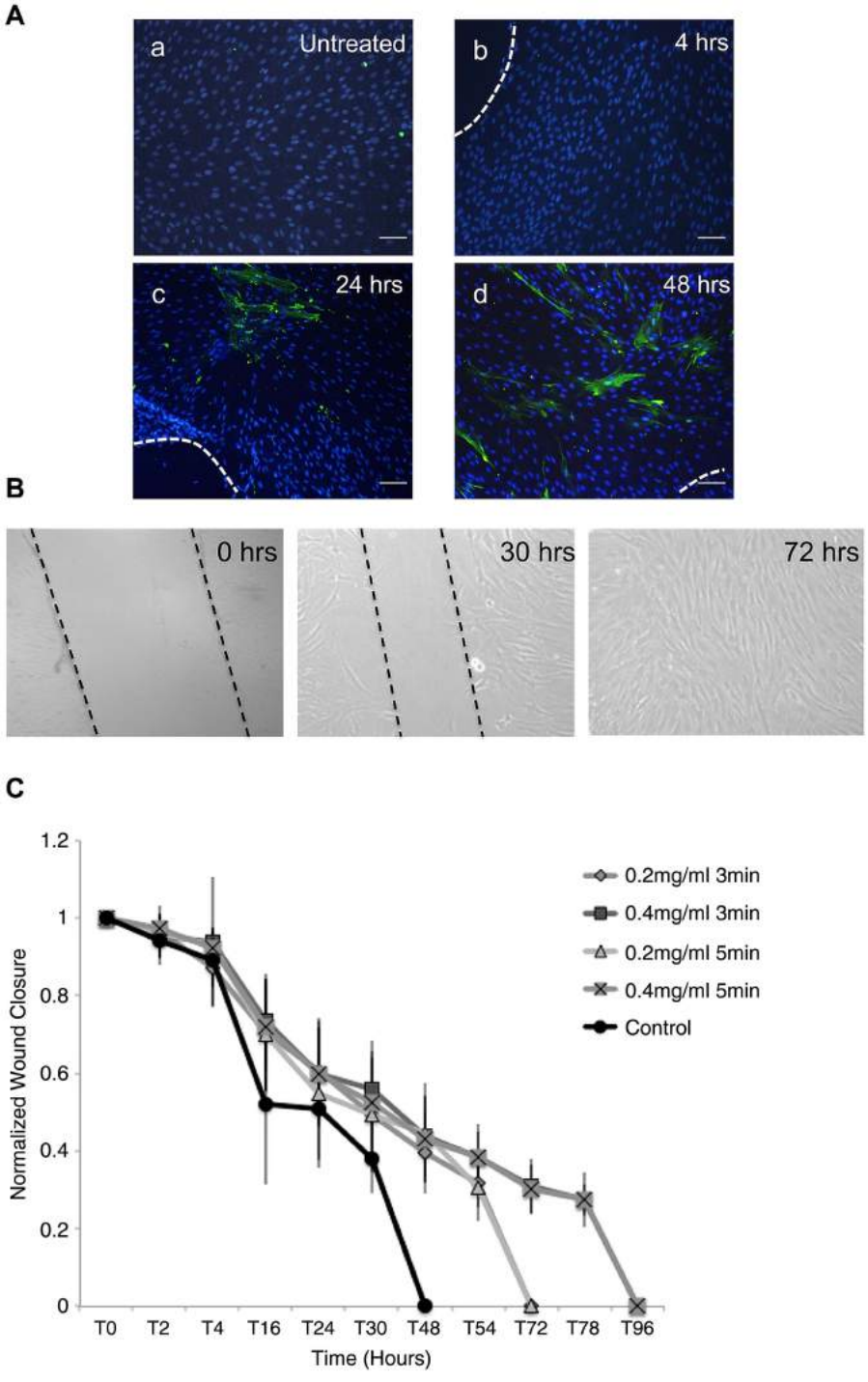

Figure 5 Mitomycin-C (MMC) delays wound healing in human nasal mucosal fibroblasts (HNMFs). (A) An increase in the expression of α-smooth muscle actin (α-SMA) following the creation of a scratch wound in confluent cultures of HNMFs indicating that the transformation of HNMFs to myofibroblast phenotype occurs as a normal response to wounding. There were no α-SMA-positive cells seen immediately after wounding and up to 4 h post wounding. Some positive cells were noted at 24 h and more cells were noted at 48 h (Ad). (B) How the quantitation of the rate of migration of cells in the presence or absence of MMC was done is shown. The distance between the wound edges (dashed black line) were marked until complete closure was attained. (C) A graphical representation of the rate of wound closure that shows that treatment with MMC (0.2 and 0.4 mg/mL) delays significantly the time taken for the cells to close the wound. The experiments were performed in three independent samples (N=3) and graph is represented as mean±SD. Scale bar: 10 μm.

with 0.2 mg/mL of MMC delayed the wound closure further by 24 h (p=0.01). The maximum delay was seen with 0.4 mg/mL MMC concentration wherein the wounds on an average took 96 h to fully close (p=0.001; figure 5C).

DISCUSSION

The present study shows that the use of MMC at a low concentration (0.2 mg/mL) is effective in preventing fibroblast to myofibroblast transformation, contraction and migration of HNMFs simulating in vitro the wound healing process post-DCR.

MMC has been shown to prevent cellular proliferation by cross-linking DNA.[15] The stalled replication fork then triggers several signalling pathways downstream that are involved in cell cycle arrest, repair or apoptosis.[16 17] The current study shows that treatment with MMC also affects other cellular functions such as contraction and migration of the HNMFs when applied at sublethal concentrations. To our best knowledge, this is the first study to look at these aspects of HNMF functions pertinent to wound healing post surgery.

Here, TGF-β was used to induce myofibroblast transformation and increase cell contraction, thereby simulating the wound healing response in vitro. When scratch wounds were created, there was a spontaneous increase in the myofibroblast (in the absence of exogenous TGF-β) population that became prominent around 24 h following wounding, suggesting that the models used in this study are representative of the normal wound healing process. When treated with MMC (0.2 mg/mL for 3 min), this transformation to a myofibroblast phenotype was arrested even in the continued presence of TGF-β. Similarly, the increased contraction induced by TGF-β was significantly reduced following treatment with MMC for just 3 min.

Although the exact mechanism of action is unclear, the data suggest that MMC is able to oppose TGF-β signalling, resulting in increased contraction and migration. At a higher concentration of 0.4 mg/mL, MMC induced extensive cell shrinking as was evident in the staining for actin filaments (figure 2). The concentration-dependent effect of MMC treatment was also noted in the significantly increased time taken for the wounds to close following the injury. Apoptosis could partly be the reason for the least contraction noted with 0.4 mg/mL (figure 3B) and also the delay in wound closure as has been reported in an earlier study.[13] This study showed that at higher concentrations of 0.4 or 0.5 mg/mL MMC induced extensive apoptosis of HNMFs even when treated for a short duration of 3 min. However, at 0.2 mg/mL, MMC was shown to induce minimal apoptosis but arrest significantly the proliferation of HNMFs while at 0.1 mg/mL the effect of MMC was found to be suboptimal in arresting even cell proliferation.[13] It could therefore be deduced that at 0.4 mg/mL concentration of MMC the reduced contraction and delayed migration of HNMFs might have a substantial component of apoptosis involved unlike the 0.2 mg/mL concentration.

In conclusion, this study shows that treatment with MMC can reduce increased cell contraction and delay migration without adversely affecting the health of the cells by inhibiting the TGF-β signalling pathway. Taken together, the results of the current study along with those of the previous in vitro[13 14] and clinical studies[2 3 18–20] show that there is now sufficient evidence to suggest that 0.2 mg/mL concentration of MMC when applied for 3 min might be sufficient to prevent the cicatricial closure without inducing extensive cell death or damage.

Acknowledgements We acknowledge Professor D. Balasubramanian for critical review and inputs on the manuscript and the Hyderabad Eye Research Foundation for the funding support.

Contributors VK: design and collection of data, data analysis and approval of manuscript; CR: conception and design, data analysis, manuscript writing and approval of manuscript; MJA: conception and design, manuscript writing and approval of manuscript.

Funding Hyderabad Eye Research Foundation.

Competing interests None declared.

Patient consent Obtained.

Ethics approval The institutional review board of LV Prasad Eye Institute.

Provenance and peer review Not commissioned; externally peer reviewed.

REFERENCES

1 Marcet MM, Kuk AK, Phelps PO. Evidence-based review of surgical practices in endoscopic endonasal dacryocystorhinostomy for primary acquired nasolacrimal duct obstruction and other new indications. *Curr Opin Ophthalmol* 2014;25:443–8.
2 Cheng SM, Feng YF, Xu L, *et al*. Efficacy of mitomycin C in endoscopic dacryocystorhinostomy: a systematic review and meta-analysis. *PLoS ONE* 2013;8:e62737.
3 Liao SL, Kao SC, Tseng JH, *et al*. Results of intraoperative mitomycin C application in dacryocystorhinostomy. *Br J Ophthalmol* 2000;84:903–6.
4 Hinz B. Formation and function of the myofibroblast during tissue repair. *J Invest Dermatol* 2007;127:526–37.
5 Funderburgh JL, Funderburgh ML, Mann MM, *et al*. Proteoglycan expression during transforming growth factor beta -induced keratocyte-myofibroblast transdifferentiation. *J Biol Chem* 2001;276:44173–8.
6 He J, Bazan HE. Epidermal growth factor synergism with TGF-beta1 via PI-3 kinase activity in corneal keratocyte differentiation. *Invest Ophthalmol Vis Sci* 2008;49:2936–45.
7 Jester JV, Petroll WM, Barry PA, *et al*. Expression of alpha-smooth muscle (alpha-SM) actin during corneal stromal wound healing. *Invest Ophthalmol Vis Sci* 1995;36:809–19.
8 Abraham LM, Selva D, Casson R, *et al*. Mitomycin: clinical applications in ophthalmic practice. *Drugs* 2006;66:321–40.
9 Cheng JW, Cai JP, Li Y, *et al*. Intraoperative mitomycin C for nonpenetrating glaucoma surgery: a systematic review and meta-analysis. *J Glaucoma* 2011;20:322–6.
10 Kaufman SC, Jacobs DS, Lee WB, *et al*. Options and adjuvants in surgery for pterygium: a report by the American Academy of Ophthalmology. *Ophthalmology* 2013;120:201–8.
11 Bass PD, Gubler DA, Judd TC, *et al*. Mitomycinoid alkaloids: mechanism of action, biosynthesis, total syntheses, and synthetic approaches. *Chem Rev* 2013;113:6816–63.
12 Feng YF, Yu JG, Shi JL, *et al*. A meta-analysis of primary external dacryocystorhinostomy with and without mitomycin C. *Ophthalmic Epidemiol* 2012;19:364–70.
13 Ali MJ, Mariappan I, Maddileti S, *et al*. Mitomycin C in dacryocystorhinostomy: the search for the right concentration and duration--a fundamental study on human nasal mucosa fibroblasts. *Ophthal Plast Reconstr Surg* 2013;29:469–74.
14 Hu D, Sires BS, Tong DC, *et al*. Effect of brief exposure to mitomycin C on cultured human nasal mucosa fibroblasts. *Ophthal Plast Reconstr Surg* 2000;16:119–25.
15 Tomasz M. Mitomycin C: small, fast and deadly (but very selective). *Chem Biol* 1995;2:575–9.
16 Boamah EK, White DE, Talbott KE, *et al*. Mitomycin-DNA adducts induce p53-dependent and p53-independent cell death pathways. *ACS Chem Biol* 2007;2:399–407.
17 Grillari J, Katinger H, Voglauer R. Contributions of DNA interstrand cross-links to aging of cells and organisms. *Nucleic Acids Res* 2007;35:7566–76.
18 Apuhan T, Yildirim YS, Eroglu F, *et al*. Effect of mitomycin C on endoscopic dacryocystorhinostomy. *J Craniofac Surg* 2011;22:2057–9.
19 Camara JG, Bengzon AU, Henson RD. The safety and efficacy of mitomycin C in endonasal endoscopic laser-assisted dacryocystorhinostomy. *Ophthal Plast Reconstr Surg* 2000;16:114–18.
20 Kamal S, Ali MJ, Naik MN. Circumostial injection of mitomycin C (COS-MMC) in external and endoscopic dacryocystorhinostomy: efficacy, safety profile, and outcomes. *Ophthal Plast Reconstr Surg* 2014;30:187–90.

Effect of mitomycin-C on contraction and migration of human nasal mucosa fibroblasts: implications in dacryocystorhinostomy

Vinay Kumar, Mohammad Javed Ali and Charanya Ramachandran

Br J Ophthalmol published online June 10, 2015

ADVANCES IN STEM CELL BIOLOGY

VOLUME 11

iPSCs in Tissue Engineering

Edited by Alexander Birbrair

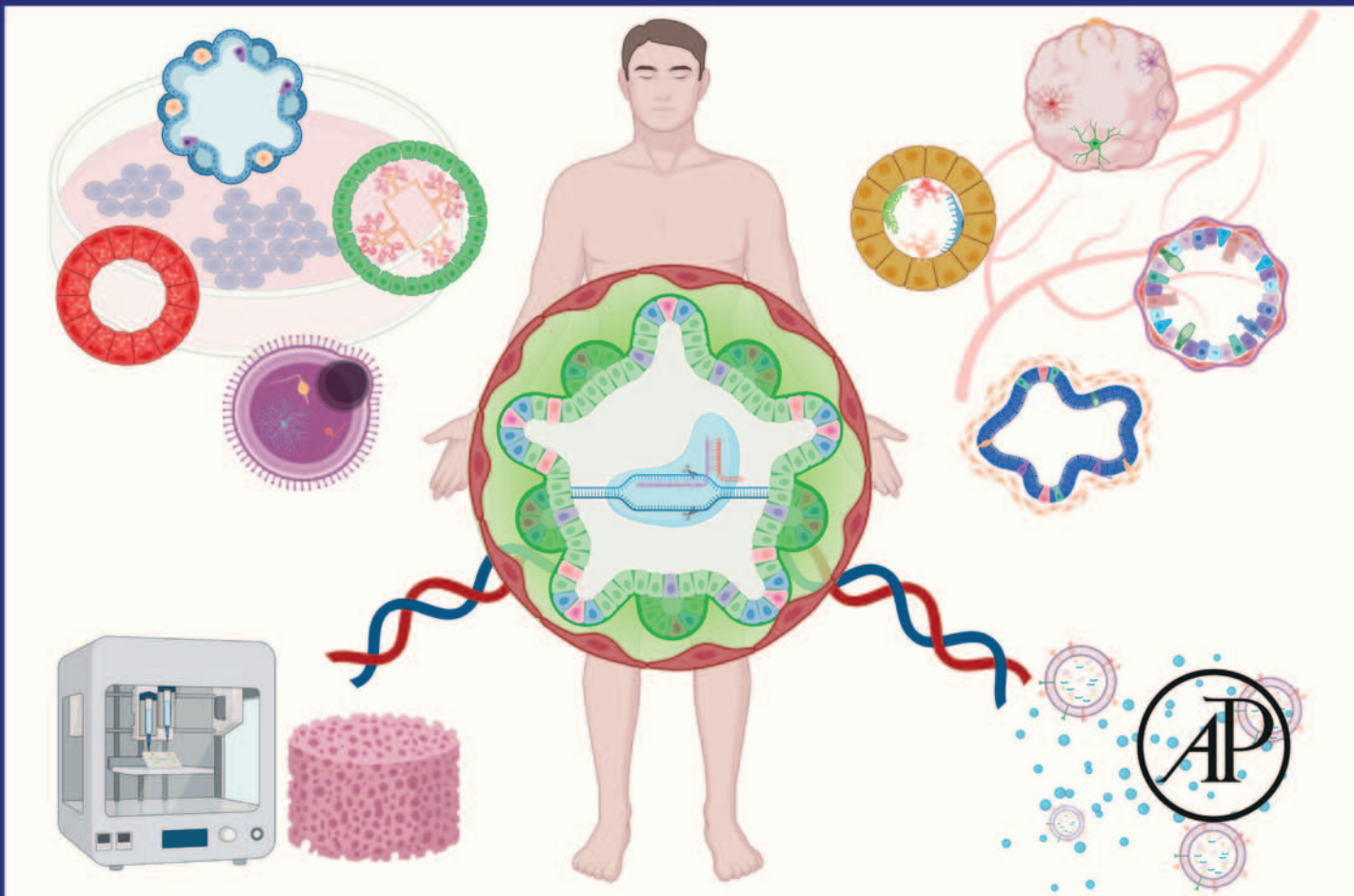

CHAPTER

Induced pluripotent stem-cell-derived corneal grafts and organoids

4

Vinay Kumar Pulimamidi[1,2], **Savitri Maddileti**[1], **Indumathi Mariappan**[1]

[1]*Center for Ocular Regeneration, Brien Holden Eye Research Centre, Hyderabad Eye Research Foundation, LV Prasad Eye Institute, Hyderabad, Telangana, India;* [2]*School of Life Sciences, University of Hyderabad, Hyderabad, Telangana, India*

Chapter outline

Abstract

The transparent cornea contributes to more than 60% of the refractive power of an eye. The corneal surface epithelial homeostasis is mediated by adult stem cells residing at the corneal periphery called the "limbal niche." Severe chemical or burn injuries or systemic Stevens–Johnson syndrome can cause limbal stem cell deficiency (LSCD) and result in altered light refraction and vision loss. Such LSCD eyes can be treated successfully by limbal stem cell transplantations. However, in

iPSCs in Tissue Engineering, Volume 11. https://doi.org/10.1016/B978-0-12-823809-7.00005-0

case of bilateral defects and due to limited availability of eye bank donor tissues, alternate stem-cell-derived corneal cells offer a great promise for regenerative needs. Pluripotent stem cells can be used to generate and mass produce corneal cells and three-dimensional organoids, for their applications in basic research, drug screening, and regenerative medicine. When combined with genome editing approaches, it is possible to generate tissue-engineered grafts for the treatment of certain inherited corneal disorders.

Keywords: Cornea; Corneal epithelium; Corneal organoids; Cultured limbal epithelial transplantation (CLET); Embryonic stem cells (ESCs); Eye field primordium (EFP); Induced pluripotent stem cells (iPSCs); Limbal stem cell deficiency (LSCD); Limbal stem cells (LSCs); Limbus; Neuroectoderm; Ocular regeneration; Ocular surface ectoderm (OSE); Retinal cups; Retinal organoids; Simple limbal epithelial transplantation (SLET).

Introduction

Visual perception is an important function of an eye, and is mediated by the combined involvement of different ocular parts such as the cornea, iris, lens, and retina. The transparent cornea on the ocular surface allows the light to enter into the eye and contributes to more than 60% of the refractive power. Iris and the lens together helps to focus the light onto the retina present at the back of the eye. The photoreceptor cells of the retina contain visual pigments that capture the photons of light and trigger a series of chemical reaction cascades called the "visual cycle" to generate membrane potentials that are converted into electrical signals and transmitted to the brain for visual perception. This chapter will elaborate on the corneal development and functions of different constituent cell types, currently available stem-cell-based therapeutics for the treatment of ocular surface defects, and will also highlight the emerging focus on induced pluripotent stem cells (iPSCs) and iPSC-derived corneal tissues in basic research and regenerative medicine.

Corneal structure and function

Cornea is a transparent, avascular tissue located at the front of the eye, which acts as a structural barrier and protects the eye against infections (DelMonte and Kim, 2011). It is a convex-shaped tissue with a refractive index of 1.376 and provides two-thirds of the refractive power of the eye (Fares et al., 2012). The cornea consists of five major layers: (1) the outermost nonkeratinized, stratified squamous epithelium, (2) the thick basement membrane or the Bowman's layer, (3) a dense connective tissue, containing a highly ordered arrangement of collagen fibrils and scattered keratocytes, together called the "corneal stroma," (4) the Descemet's membrane, and (5) a monolayer of corneal endothelium on the posterior side (Fig. 4.1). In normal eyes, the thickness of the cornea increases from the center to the periphery, with the central and peripheral thickness in the range of 551−565 μm and 612−640 μm, respectively (Feizi et al., 2014).

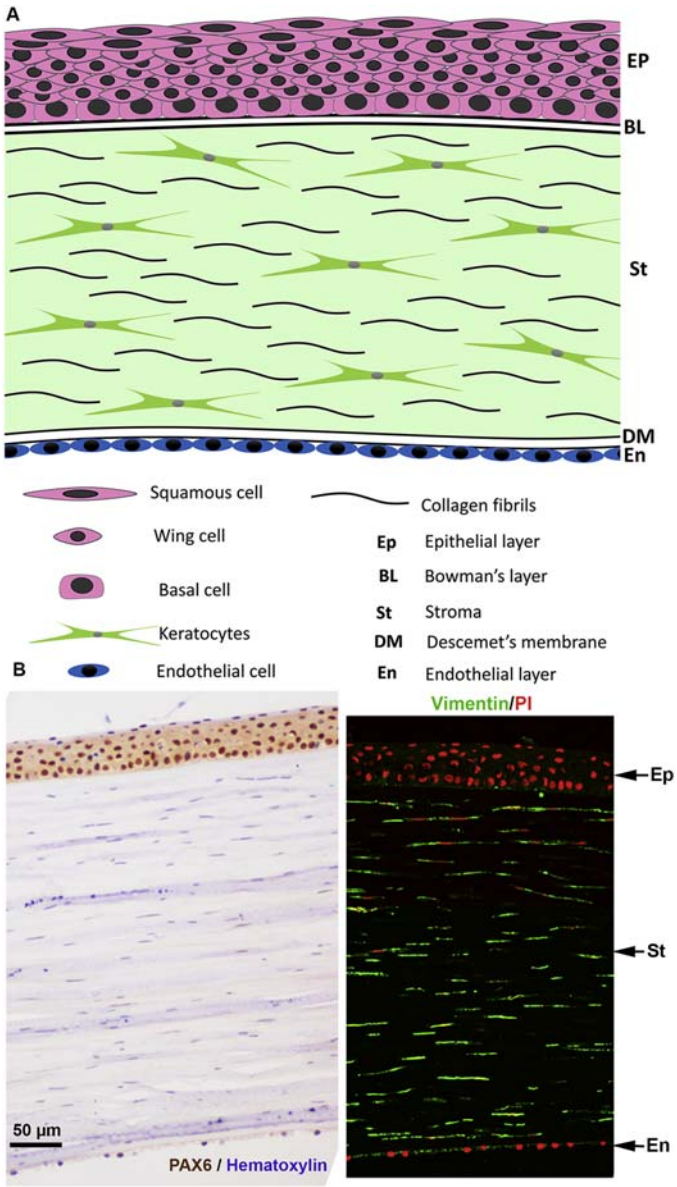

FIGURE 4.1 Cross-sectional view of a human cornea.

(A) Cartoonic representation of a corneal cross section. The cornea has a multilayered squamous epithelium (Ep) on the outer surface and a basement membrane called the Bowman's layer (BM). A highly ordered and densely packed collagenous stroma (St) with keratocytes in the middle. The Descemet's membrane (DM) acts as the basement membrane for the posterior monolayer of endothelium (En). (B) Immunohistochemistry of corneal sections stained with anti-PAX6 antibody (*brown*) and hematoxylin dye (*blue*) on the left; anti-Vimentin antibody (*green*) counterstained with the propidium iodide dye (*red*) on the right. Note the linear and compactly arranged collagen bundles in the corneal stroma and the neural crest origin of distinct Vimentin^{+} stromal keratocytes.

The corneal epithelium has around 5−7 layers of cells that make up approximately 10% of the total corneal thickness (∼50 μm) and contains three types of cells, namely the superficial squamous cells, central wing cells, and a single layer of basal cells. The superficial polygonal cells are the postmitotic mature cells and are arranged in 1−3 layers, followed by 2−3 layers of wing cells, which are polyhedral in shape. The wing cells rarely undergo division and migrate upward to become the superficial squamous cells. The basal cells are mitotically active and are arranged as a single layer of cuboidal or columnar cells. These cells can proliferate and differentiate to form the wing and superficial cells. The basal epithelial cells are tightly tethered to the basement membrane via hemidesmosomes, and the superficial and wing cells are interconnected by tight junctions to establish the epithelial barrier. The thick Bowman's membrane is about 12 μm in thickness and is rich in type I and III collagens and proteoglycans. It ensures the structural rigidity and maintains the corneal shape. The corneal epithelium is in contiguous with the adjacent conjunctival epithelium but is demarcated by a unique anatomical structure called the "Limbus." The limbal margin zone is about 2 mm wide, all around the cornea and has deep crypt-like structures called the "palisades of Vogt" that serve as the niche for the corneal epithelial stem cells. The Bowman's membrane disappears at the limbus and allows direct contact of the basal stem cells with the limbal stromal cells, peripheral neurons, melanocytes, and blood vessels and thereby establishes a unique microenvironment for stem cell regulation. It also acts as a physical barrier that prevents the inward migration of conjunctival epithelial cells and blood vessels and helps to maintain the transparent and avascular status of the cornea.

The stroma constitutes about 80%−85% of the corneal thickness and is made of stromal keratocytes, which are the source for a complex extracellular matrix (ECM) composed of different collagens (type I, III, V, and VI) and keratin sulfate glycosaminoglycans. The collagen fibrils are compactly arranged in a highly ordered fashion and contribute to the strength and transparency of the cornea (Meek and Boote, 2004). The corneal endothelium (CE) is the innermost lining of the cornea and is made of an orderly arranged monolayer of hexagonal to polygonal cells that are connected by tight junctions and display a typical cobble-stone phenotype, when observed under a specular microscope (Waring et al., 1982). The developing endothelium deposits its ECM and establishes a 7 μm thick Descemet's membrane, rich in type IV collagen and laminin.

The corneal endothelial cells are postmitotic and are not regenerated during adult life (Rio-Cristobal and Martin, 2014). The average endothelial cell density is about 3500−4000 cells/mm^2 in neonates, which gradually declines to about 2000 cells/mm^2 in adults. An average of about 0.6% of the cells is lost annually and is compensated by a corresponding increase in the size of the surviving cells. This contributes to the gradual reduction in cell density and is characterized by polymegathism and pleomorphism (Wilson and Roper-Hall, 1982). These cells express tight junctions and establish the inner corneal barrier. They also express Na^+K^+ATPases and bicarbonate pumps and support fluid and selective solute transport across the posterior surface of the cornea. The bidirectional fluid pumps ensure sufficient hydration

and also remove excess fluid from the stroma and drain it into the anterior chamber. The endothelium thus maintains the cornea in a slightly dehydrated state, to achieve optical transparency and prevents corneal edema (Maurice, 1957; Hirsch et al., 1977).

Corneal development and maintenance

The cornea, lens, ciliary body, iris, trabecular meshwork, and the aqueous humor form the anterior segment of the eye. The development of ocular surface and the anterior segment starts when the optic vesicles derived from the anterior neuroectoderm come in contact with the ocular surface ectoderm and with the migration of neural crest cells (NCCs) from the periocular mesenchyme. The surface ectoderm undergoes pseudo stratification, leading to the formation of a lens pit. At embryonic day 8.5 (E8.5−9.5) in mice, the lens pit develops into a vesicle and remains connected to the surface ectoderm via the lens stalk (Pei and Rhodin, 1970; Kaufman, 1992). Finally, the lens vesicle detaches from the surface ectoderm and invaginates into the optic cup. Further, the neural-crest-derived cells migrate between the lens epithelium and the surface ectoderm to form a thick corneal stroma and the endothelium.

The surface ectoderm overlaying the NCCs develop into corneal epithelium, which is 1−2 cells thick at birth. After birth, the surface epithelial cells undergo rapid division and form the 5−6 cells thick stratified squamous epithelium with a thick basement membrane called the Bowman's membrane. The NCCs present below the corneal epithelium undergo differentiation to form the stromal fibroblasts/keratocytes. In humans, a second wave of mesenchymal cells migrate into this region and together contributes to the development of a thick corneal stroma, consisting of keratocytes, embedded in a highly ordered collagenous matrix. In mice, 4−7 layers of flat mesenchymal cells with elongated, spindle-shaped morphology are seen at E12.5. At E14.5−15.5, the inner NCCs adjacent to the lens epithelium develop into corneal endothelium (Reneker et al., 2000). In reptiles, birds, and humans, the first wave of neural crest migration contributes to the formation the corneal endothelium (Wulle, 1972; Hay, 1980). Whereas in rodents, cats, and rabbits, a single wave of neural crest migration occurs and the cells immediately adjacent to the lens vesicle undergo mesenchymal-to-epithelial transition to form a monolayer of corneal endothelium (Bronner-Fraser et al., 1992).

The expression of the paired homeobox protein 6 or PAX6 and BMP signaling in the surface ectodermal cells is known to specify the presumptive lens and corneal epithelium during eye development (Robinson et al., 1998; Collomb et al., 2013). In adult corneal tissues, the surface epithelial cells undergo senescence and are regularly shed. This constant cell loss is compensated by the regenerating stem cells residing at the limbus and maintains adult tissue homeostasis.

Limbal stem cells (LSCs)

The limbus forms a junction between the transparent cornea and the opaque sclera. It serves as the niche for corneal epithelial stem cells and acts as a barrier for conjunctival vasculatures at the corneal boundary (Lavker et al., 2004). Severe damage to the limbus can breach this barrier function and trigger the migration of conjunctival cells onto the cornea, resulting in corneal neovascularization. The limbal epithelial stem cells (LESCs) divide asymmetrically to produce transient amplifying cells (TAC) and self-renewing stem cells, for tissue regeneration and normal homeostasis. The TACs in the basal layers divide and migrate centripetally from the limbus toward the central cornea. These proliferating TACs further undergo differentiation and migrate from basal to apical surface to form the fully mature, terminally differentiated, stratified corneal epithelium (Schermer et al., 1986). These terminally differentiated superficial squamous cells are shed regularly and replaced by the proliferating and differentiating TACs migrating from the limbus (Beebe and Masters, 1996). This mechanism of corneal epithelial homeostasis was explained by Thoft and Friend in their "XYZ hypothesis" wherein, X represents the proliferation and stratification of limbal basal cells, Y represents the centripetal migration of basal cells, and Z represents the superficial cell desquamation (Thoft and Friend, 1983). The anatomical structure of the limbal niche and the migration pattern of the proliferating LSCs are explained in Fig. 4.2.

The LESCs are slow cycling cells with high proliferation potential. They are small cells with high nuclear-to-cytoplasmic ratios and express the epithelial stem cell markers such as p63-alpha, C/EBP-delta, and TCF4 and are negative for the mature corneal epithelial markers such as K3 and K12 (Davanger and Evensen, 1971; Schermer et al., 1986; Barrandon and Green, 1987; Kurpakus et al., 1990; Romano et al., 2003; Barbaro et al., 2007). The corneal epithelial cells are shown to express the soluble vascular endothelial growth factor receptor 1 (VEGFR1 or sFlt1), a decoy receptor that blocks VEGF signaling and plays a vital role in maintaining the corneal avascularity (Ambati et al., 2006, 2007). Various signaling pathways such as the sonic hedgehog, Wnt/β-catenin, TGF-β, and Notch signaling have been implicated in the regulation of LESCs at the limbal niche. Dkk2-mediated repression of the Wnt/β-catenin signaling was shown to promote differentiation of limbal progenitor cells and Dkk2 knockout results in PAX6 downregulation and epidermal differentiation of corneal cells (Mukhopadhyay et al., 2006; Nakatsu et al., 2011). The limbal stromal fibroblasts closely interact with and regulate the LESCs. The pigmented melanocytes residing at the limbus act as tissue scavengers and protect the LESCs from ultraviolet radiation and other metabolic stress-induced damages (Li et al., 2007). A thorough understanding of the niche regulation of stem cells is therefore important for establishing successful corneal epithelial cultures (Blazejewska et al., 2009; Xie et al., 2011, 2012).

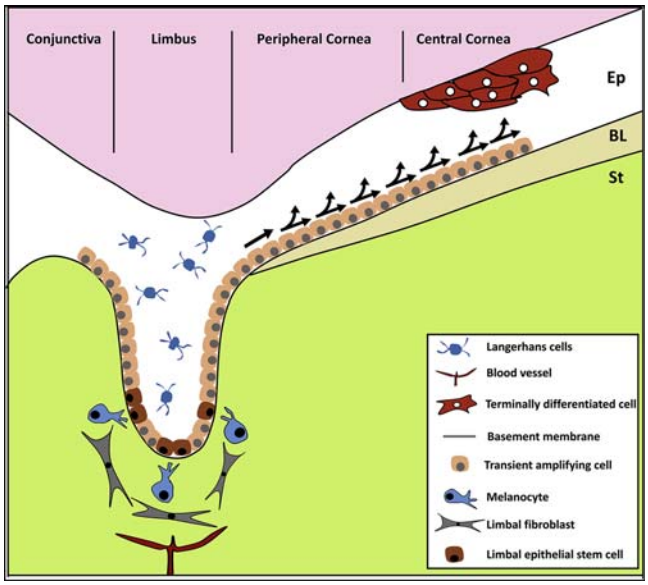

FIGURE 4.2 Anatomical structure of the human limbus.

LESCs are located within the deep crypts at the corneal periphery. The limbal crypts are supplied with blood vessels and are populated by stromal fibroblasts and pigmented melanocytes. LESCs proliferate and give rise to TACs. The TACs proliferate and migrate centripetally over the Bowman's layer (BL) and form the basal corneal epithelium. The basal cells differentiate and migrate apically to form the wing cells and mature superficial cells, together forming a stratified squamous epithelium on the corneal surface.

Limbal stem cell deficiency (LSCD)

LSCD is a pathological condition wherein the limbus and its barrier functions are lost and causes neovascularization and conjunctivalization of the cornea, leading to severe vision loss. Maintenance of corneal epithelium requires a healthy limbus with sufficient LSCs to regenerate the tissue. In some patients, the limbus gets severely damaged due to acid/alkali/burn injuries or due to systemic conditions affecting the epithelial linings of the body such as in aniridia, Steven–Johnson's syndrome, cicatricial pemphigoid, and chronic limbitis. These patients with dysfunctional LSCs display a total loss of corneal epithelial regeneration. This results in chronic ocular discomfort, with pain, irritation, and continuous watering of the eye. Such persistent inflammation triggers conjunctivalization and corneal neovascularization, leading to the formation of an opaque and vascular pannus tissue on the ocular surface. This affects the corneal transparency, leading to partial or complete blindness in LSCD patients (Dua et al., 2003).

Therapeutic strategies for the treatment of LSCD

LSCD can be either total or partial and can be either unilateral or bilateral, and the treatment modality depends on the extent of damage to the limbus and conjunctivalization seen on the ocular surface. In case of partial LSCD, the residual stem cells in the healthy parts of the limbus can proliferate and migrate to the neighboring regions and heal any defects. Therefore, mechanical debridement of the conjunctival epithelium on the corneal surface is sufficient to restore a stable ocular surface. In some cases, the conjunctival scrapping is also coupled with human amniotic membrane (hAM) transplantation, which allows faster healing of the ocular surface (Cauchi et al., 2008; Liang et al., 2009). In case of total LSCD, the treatment requires the replacement of healthy limbal stem cells. This could be achieved by transplanting a small portion of the healthy limbus biopsied from a donor eye. In case of unilateral LSCD, the fellow eye can serve as the limbal source for transplantation. However, in bilateral LSCDs with fully damaged limbus, an alternative limbal stem cell source is required for successful corneal surface reconstruction.

Conjunctival limbal autografts (CLAU)

This was one of the first few techniques originally reported for the treatment of LSCD by Barraquer and Strampelli in 1964 and later developed by Kenyon and Tseng (Kenyon and Tseng, 1989). This technique involves harvesting of about three clock hours sized conjunctival-limbal grafts from the healthy eye and its transplantation by suturing, at similar anatomical locations of the affected eye. This method was first tested in 26 cases of unilateral LSCD patients and significant regression of corneal neovascularization and improved visual acuity were observed after 6 months. Here, the donor graft seamlessly integrates into the host limbus without any risk of immune rejection or the need for immunosuppression. However, such autologous transplantations require a large limbal graft from the healthy eye and can cause the risk of LSCD at the donor site (Frucht-Pery et al., 1998).

Cultured limbal epithelial transplantations (CLET)

Skin epithelial cultures were originally described by Rheinwald and Green in 1975, wherein, they generated a sheet of stratified epithelium by culturing skin keratinocytes on a layer of mitotically inactivated NIH3T3 fibroblast feeder cells (Rheinwald and Green, 1975). Later, the same method was adopted for limbal cultures to generate donor grafts in autologous cultured limbal epithelial transplantations (CLET) (Pellegrini et al., 1997). In case of unilateral LSCDs, the fellow healthy eye serves as the donor tissue source for limbal transplantations. Unlike CLAU, this ex vivo culture technique is efficient and requires only a small limbal biopsy

(2×2 mm^2) that can be excised from the healthy donor eye and is cultured *in vitro* for stem cell proliferation and expansion. For *in vitro* expansion of limbal stem cells, various groups have used different substrates such as the fibrin gels, myogels, plasma polymer-coated surfaces, mitotically inactivated NIH-3T3 fibroblasts, hAM, and human limbal stromal fibroblasts, to generate transplantable sheets of corneal epithelium (Mariappan et al., 2010). For ocular surface reconstruction of LSCD eyes, the opaque and vascularized conjunctival pannus tissue on the corneal surface is first surgically removed. Later, the cultured limbal epithelial cell sheet is transplanted onto the cleared corneal surface and secured in place using biodegradable sutures or a fibrin glue. The limbal graft gradually integrates on the corneal stroma and stratifies *in vivo* to generate a stable ocular surface. The success rate for this therapeutic approach is around 60%−70% (Rama et al., 2010; Baylis et al., 2011; Basu et al., 2012; Pellegrini et al., 2013). In most cases, the clinical outcomes are directly correlated with the presence of sufficient limbal stem cells in the donor grafts (Rama et al., 2010). However, the technique is not widely practiced because of the need for state-of-the-art infrastructures such as the GMP-certified clean rooms for *in vitro* expansion of donor cell grafts and the associated costs, makes the therapeutic product greatly unaffordable.

Simple limbal epithelial cell transplantations (SLET)

SLET is a novel and innovative surgical technique developed for the treatment of unilateral LSCD (Sangwan et al., 2012). It is an autologous technique in which a small limbal tissue (2×2 mm) is excised from the unaffected fellow eye, typically from the superior quadrant and cut into 8−10 small pieces. The vascular and opaque pannus tissue on the recipient eye is surgically removed and a fresh hAM is placed over the corneal surface and secured with fibrin glue. The limbal tissue biopsy was cut into 8−10 small pieces and placed on hAM with epithelial side up and positioned in concentric ring patterns, with even spacing to spare the central visual axis and glued to corneal surface using a fibrin gel. A bandage contact lens is then applied to secure the hAM and the limbal explants on the corneal surface. The hAM gradually integrates into the corneal stroma postoperatively and epithelialization from limbal explants starts within 2 days and the explants usually disappear within 2−6 months (Mittal et al., 2015). SLET works in a similar mechanism as that of CLET and helps in limbal stem cell expansion in vivo. Our analysis of the long-term clinical outcomes of autologous SLET in 125 patients, including adults and children with unilateral LSCD revealed 76% success rate, in terms of stable corneal surface epithelialization and maintenance of avascular cornea at 1.5-year follow-up, and 67% of those eyes achieved a vision greater than 20/60 (Basu et al., 2016). Similar studies from other groups have also reported success rates of about 70%−80% at 1-year follow-up (Vazirani et al., 2016; Gupta et al., 2018). SLET is therefore a simpler, efficient and affordable surgical method for corneal surface reconstruction and vision restoration in case of unilateral LSCDs and does not require

any state-of-the-art stem cell culture facilities or specialized cell culture conditions. It has now evolved as a specialized surgical technique, widely practiced across the globe for the successful treatment of mild-to-moderate LSCD eyes.

Alternative strategies for the treatment of bilateral limbal stem cell deficiency

In case of bilateral LSCDs, keratolimbal allograft (KLAL) transplantations or allogeneic CLET procedures are considered using limbal biopsies from live-related donor eyes or using donor corneas sourced from eye banks. However, such allogeneic stem cell transplantations require continuous immune suppression for graft survival and to reduce host immune-response-mediated transplantation failures. Long-term studies on human allograft transplantations have reported limited success with immune complications and graft rejections (Tsai and Tseng, 1994). Other autologous or allogeneic and ectopic cell types such as the conjunctival epithelium, oral mucosal epithelium and mesenchymal stem cells were also explored in the past with limited success (Zannettino et al., 2008; Hirayama et al., 2012; Yao et al., 2012; Yao and Bai, 2013; Kolli et al., 2014; Silber et al., 2014; Holan et al., 2015; Utheim et al., 2016). Pluripotent stem cells (PSCs) such as the embryonic stem cells (ESCs) and iPSCs have an unlimited proliferation capacity *in vitro* and can differentiate into different cell types in the presence of suitable growth factors and culture conditions. Earlier reports have shown that ESCs could be successfully differentiated into corneal epithelial-like cells by the ectopic expression of PAX6 gene or by establishing cultures on limbal stromal cell feeders or on collagen type IV–coated surfaces for microenvironment simulation (Ueno et al., 2007; Zhang et al., 2017). However, ethical concerns associated with ESCs have restricted their widespread applications.

Induced pluripotent stem cells and their importance in ocular research and regenerative medicine

A landmark study in 2006 has reported that the somatic cells such as fibroblasts could be reprogrammed into ESC-like cells by the ectopic expression of four key transcription factors, namely OCT3/4, SOX2, cMYC, and KLF4 (Takahashi and Yamanaka, 2006). Similar to ESCs, these reprogrammed stem cells can differentiate into cell types of all three lineages and are therefore termed as induced pluripotent stem cells (iPSCs). Also, iPSCs can be maintained in culture and expanded over several passages, and their ability to sustain genetic manipulations makes it an ideal stem cell source for *in vitro* mutation corrections and disease modeling studies. Subsequently, robust and efficient protocols for differentiating PSCs into various ocular cell types such as the retinal cells (Ikeda et al., 2005; Lamba et al., 2006; Osakada

et al., 2008, 2009; Idelson et al., 2009; Lu et al., 2009; Meyer et al., 2009; Eiraku et al., 2011) corneal epithelial cells (Ahmad et al., 2007; Hayashi et al., 2012, 2016, 2018; Brzeszczynska et al., 2014; Mikhailova et al., 2014; Sareen et al., 2014; Hongisto et al., 2017), corneal stromal keratocytes (Chan et al., 2013; Naylor et al., 2016), corneal endothelium (Zhang et al., 2014; Chen et al., 2015; McCabe et al., 2015; Song et al., 2016; Zhao and Afshari, 2016; Wagoner et al., 2018), lens epithelial cells (Li et al., 2016), and different cell enrichment methods have been reported. This has opened up newer hopes for regenerating various ocular cells and tissues, which normally do not regenerate in adults such as, the retinal pigmented epithelium (RPE), photoreceptor cells, retinal ganglion cells (RGCs), corneal endothelium ….etc. Recent reports have also shown that transplantable sheets of corneal epithelium could be generated using iPSCs and provide a feasible treatment option for bilateral corneal surface defects (Hayashi et al., 2016; Susaimanickam et al., 2017; Hongisto et al., 2018). Such iPSC-derived ocular cells in 2D and 3D culture systems have greater importance in applications such as disease modeling, *in vitro* drug screening, and for developing stem-cell-based therapeutics for various ocular conditions.

Directed differentiation of iPSCs into eye field clusters and corneal specification

PSCs require unique culture conditions and stepwise differentiation signals for their efficient differentiation into desired cell types. In case of iPSCs, the epigenetic memory retained from the parental somatic cells is known to influence their differentiation efficiency and lineage preferences. Few groups have successfully derived iPSCs using limbal-derived epithelial cells and stromal fibroblasts (Chien et al., 2012; Hayashi et al., 2012; Sareen et al., 2014; Bikkuzin et al., 2019) and further differentiated them to make corneal cells. In order to replicate the limbal microenvironment and to trigger cornea-specific differentiation, PSCs were cultured using limbal stromal conditioned medium or grown on inactivated limbal keratocytes or PA6 murine stromal cells or NIH3T3 feeders or on different scaffolds and ECM such as hAM, deepithelialized porcine or human corneas, Matrigel, laminin-521, collagen IV, or fibronectin-coated surfaces (Ahmad et al., 2007; Yoshida et al., 2011; Zhu et al., 2013; Chan et al., 2013; Sareen et al., 2014; Hongisto et al., 2017). However, many reports have shown that iPSCs derived from human dermal fibroblasts (HDFs) or peripheral blood mononuclear cells (PBMCs) could be efficiently differentiated into retinal, corneal, and other ocular cell lineages (Mikhailova et al., 2014; Hayashi et al., 2016; Susaimanickam et al., 2017; Hongisto et al., 2018). The primordial eye field committed cells are known to originate from the ectoderm-derived anterior neural plate. They express a set of eye field transcription factors (EFTFs), namely ET, SIX3, PAX6, RX1, LHX2, TLL, and OPTX2, which together regulate eye development in vertebrates (Zuber et al., 2003). PAX6, RX1, or OTX2 gene

knockouts result in severe anterior segment anomalies and anophthalmia. Overexpression of either PAX6 alone or a cocktail of EFTFs along with OTX2 can induce ectopic eye formation in developing Drosophila and Xenopus (Halder et al., 1995; Chow et al., 1999). Similarly, overexpression of PAX6a was shown to be necessary and sufficient to induce neuro-ectoderm specification in human embryonic stem cells (Zhang et al., 2010). Antagonizing BMP signals in a subset of anterior neural plate cells was shown to induce retinal fate commitment (Zaghloul et al., 2005). Secreted inhibitor of BMP signaling such as noggin is known to strongly induce neural fate commitment (Lamb et al., 1993). This dual BMP/TGFβ signaling blockade has been efficiently utilized *in vitro* by using recombinant noggin and SB431542, a small molecule that blocks lefty/Activin/TGFβ signaling to trigger efficient differentiation of hESCs into neuro-ectodermal cells (Chambers et al., 2009). The eye field committed cells within the anterior neuro-ectoderm migrate to either sides of the neural axis to form the bilateral eye primordia. These neuro-ectodermal cells proliferate and evaginate to form the bilateral optic vesicles. The distal cells of the optic vesicles respond to high levels of FGF2 signals from the ocular surface ectoderm and get specified into future neuro-retina (Pittack et al., 1997). The low FGF signals at the proximal edge of the optic vesicle, combined with the Activin/TGFβ signaling from the surrounding periocular mesenchyme, induce the formation of future RPE layer (Fuhrmann et al., 2000). The neuro-retinal progenitors proliferate and invaginate to form the multilayered neuro-retina, resulting in optic cup development. Similarly, the development of the anterior segment or the ocular surface requires a coordinated interaction between the neuro-ectoderm, which forms the future retina, and the ocular surface ectoderm, which forms the future cornea and the lens. The ocular surface ectodermal cells proliferate and form the lens placode, which further invaginate into the retinal cavity to form the future lens. The remaining surface ectodermal cells expressing PAX6 develop into future corneal epithelium. The migrating, neural-crest-derived, periocular mesenchyme significantly contributes to the development of the corneal stroma and the endothelium.

To replicate the embryonic regulation and the early eye field developmental program *in vitro*, stepwise differentiation protocols have been developed to induce PSC differentiation into various ocular lineages (Ikeda et al., 2005; Meyer et al., 2009; Chambers et al., 2009; Osakada et al., 2009; Mikhailova et al., 2014; Hayashi et al., 2016). Broadly, the culture conditions involved the addition of different Wnt antagonists to induce the differentiation of proliferating stem cells (e.g., DKK1/DKK2 and IWP-2/IWR-1). Further, TGFβ signaling blockers such as Noggin/LeftyA and SB-505124/SB-431,542 (dual Smad inhibition) have been shown to be efficient in neuro-ectodermal lineage differentiation. Inclusion of recombinant bFGF promoted the differentiation of PSCs into both neuro-retinal and ocular surface ectodermal lineages. Similarly, recombinant Activin A induced the differentiation of retinal stem cells into retinal pigmented epithelium. BMP4 signaling and keratinocyte growth factor (KGF) were shown to mediate the differentiation and maturation of ocular surface ectodermal cells into limbal/corneal epithelium. Another elaborate study has demonstrated the differentiation of iPSCs into

different zones of cell types of ocular lineages such as the neuro-retina, retinal pigment epithelium, NCCs, lens epithelium, and ocular surface ectoderm to form a self-formed ectodermal autonomous multizone (SEAM) of ocular cells, in adherent two-dimensional cultures. The concentric arrangement of different cell types of the SEAM resembled the whole-eye development *in vitro* (Hayashi et al., 2016, 2017). For corneal endothelial cells, a two-step strategy has been adopted. Firstly, the PSCs are differentiated into NCCs using two small molecules, namely CHIR99021, a Wnt inducer and SB4315542, a TGFβ signaling blocker. The NCCs are further differentiated into corneal endothelial cells by culturing them in the presence of B27 neural growth supplement along with the recombinant growth factors such as DKK2, a Wnt antagonist, and PDGF-BB, an endothelial cell mitogen (Wagoner et al., 2018). Thus the existing knowledge on embryonic regulations and cell-type-specific signaling mechanisms is effectively used in developing robust *in vitro* culture conditions to generate various ocular cell types for research and regenerative applications.

iPSC-derived three-dimensional corneal organoids and their characteristics

The need for rigorous cell enrichment protocols is a major hurdle in PSC-derived, tissue-specific cell type expansion. This can be overcome by establishing three-dimensional (3D) culture systems to generate morphologically distinct and complex multicellular organoids. This method exploits the inherent self-organizing capacity of differentiating progenitor cells, together with the surrounding niche cells, to generate complex tissue structures *in vitro*. This has been demonstrated successfully with the generation of neuro-retinal tissues using PSCs (Eiraku et al., 2011; Gonzalez-Cordero et al., 2013; Assawachananont et al., 2014; Reichman et al., 2014; Zhong et al., 2014; Hiler et al., 2015; Kaewkhaw et al., 2015; Völkner et al., 2016). Our group has developed a combined adherent and suspension culture method for generating 3D retinal and corneal organoids from human PSCs. The eye field primordial clusters (EFP's) that emerged from differentiating PSCs at 3–4 weeks of differentiation are distinct circular clusters consisting of centrally positioned neuro-retina and a surrounding veil of migrating ocular surface ectodermal cells, which includes the corneal, conjunctival, and lens epithelial precursor cells (Fig. 4.3C). Upon further maturation *in situ*, a minor subset of EFPs developed into whole eye-ball-like, self-organized, 3D miniature structures consisting of retinal primordia (RP), corneal primordia (CP), primitive eye-lid-like outer covering, lens, and ciliary margin zone-like adnexal tissues in a stepwise maturation process within 15 weeks (Susaimanickam et al., 2017). However, when the EFPs are manually excised and cultured under suspension conditions, about 40% of the EFPs formed distinct retinal and corneal primordia that can be easily identified and excised for downstream applications. The CPs developed as fluid-filled and transparent

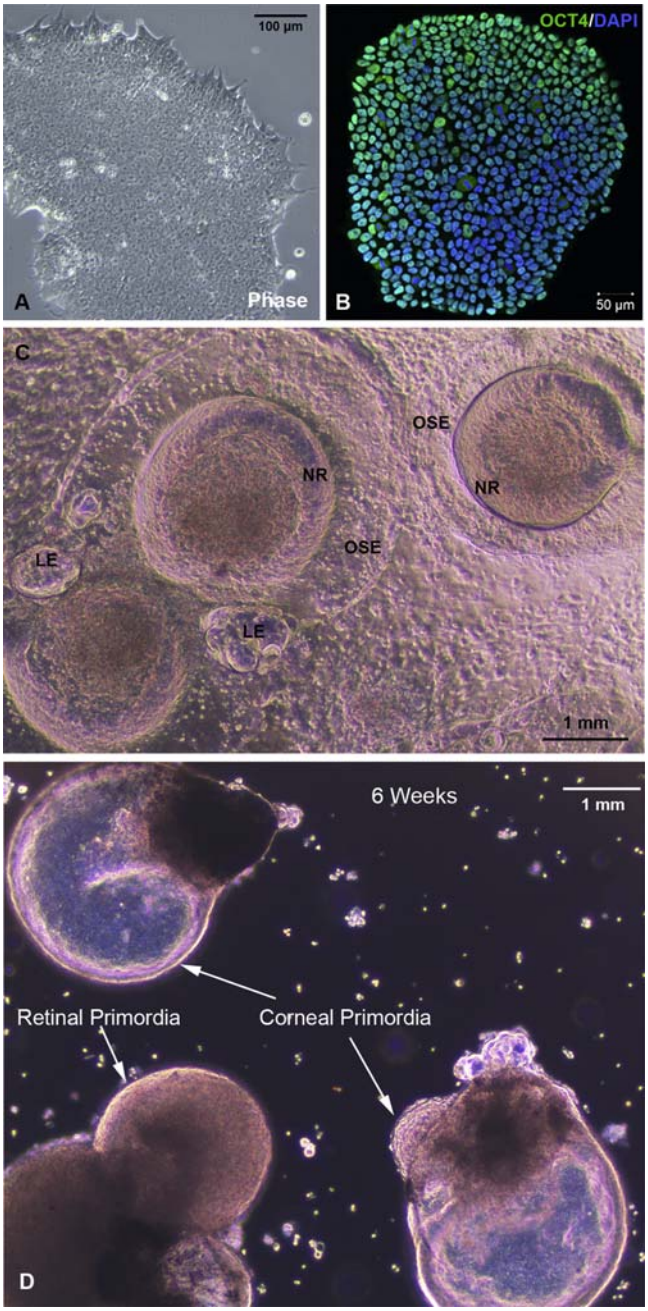

FIGURE 4.3 Differentiation of human iPSCs into eye field clusters (EFPs) and corneal primordia.

(A) Phase-contrast image of a growing iPSC colony, (B) Immunohistochemistry of a growing iPSC colony stained with anti-OCT4 antibody (*green*) and counterstained with the DAPI dye (*blue*), (C) Morphologically distinct eye field clusters (EFPs) that develop at around 3–4 weeks of neuro-ectodermal lineage differentiation of human iPSCs, showing the neuro retina (NR), ocular surface ectoderm (OSE), and lens epithelium (LE), (D) Developing corneal and retinal primordia in floating suspension cultures.

structures with single layer of epithelium (Fig. 4.3D). Upon maturation, these delicate structures are reinforced by the epithelial stratification and the thick stromal mesenchyme derived from the migrating neural crest cells. Such a complex, multilayered, cornea-like, 3D tissues are termed as "mini corneas" and consisted of a stratified squamous epithelium on the top, a thick collagen-enriched stroma in the middle, and a layer of endothelium at the bottom. Also, some mature corneal organoids developed crypt-like structures at the corneal margins and a lumen enclosed vasculature-like structure within the peripheral stroma, together resembling a rudimentary limbus. The developing conjunctival epithelium contained several mucin-filled goblet cells and was contiguous with primitive lid-like structures (Fig. 4.4A). Another study has reported the development of similar corneal organoids sharing some features of a developing cornea, by stepwise differentiation of human iPSCs (Foster et al., 2017). These complex organoids, containing most cell types of the ocular surface thus recapitulated the early corneal development *in vitro* and displayed similar anatomical features and marker expression profiles as that of adult tissues (Fig. 4.4B). It also offered an alternative tissue source for developing transplantable sheets of corneal epithelium, comparable to that of limbal grafts, and eliminated the need for complicated cell enrichment procedures.

iPSC-derived corneal epithelial grafts for regenerative applications

Unlike the applications of adult stem cell for tissue regeneration, PSC-derived cell therapeutic products have to undergo a more stringent process of quality checks to ensure cellular integrity and safety. More importantly, robust cell enrichment protocols are required to ensure absolute absence of undesirable cellular contaminants such as the undifferentiated stem cells and noncorneal cell types. Such contaminants can either increase the risk of tumor development or can render cell transplantations ineffective. In the study that reported the development of an SEAM of ocular cells in adherent cultures, the central clusters of neural and neural crest cells were first removed by manual pipetting. The remaining adherent cells of the SEAM are passaged enzymatically and FACS sorted based on the expression of limbal basal epithelial markers such as SSEA4 and ITGB4. Such positive cell sorting has enabled the enrichment of $PAX6^{+}/K12^{+}$ limbal cells that are required for preparing transplantable sheets of corneal epithelium (Hayashi et al., 2016, 2017). Also, the noncorneal epithelial cell contaminants could be negatively sorted and eliminated using CD200, a cell surface marker stably expressed by the undifferentiated iPSCs and also by most of the differentiated cells, except the corneal epithelium (Hayashi et al., 2018). The FACS sorted cells were grown on temperature-sensitive surfaces to prepare transplantable cell sheets that could successfully restore ocular surface integrity in rabbit LSCD models (Hayashi et al., 2016). Another study has reported the generation of clinically compatible limbal epithelial cells from iPSCs for

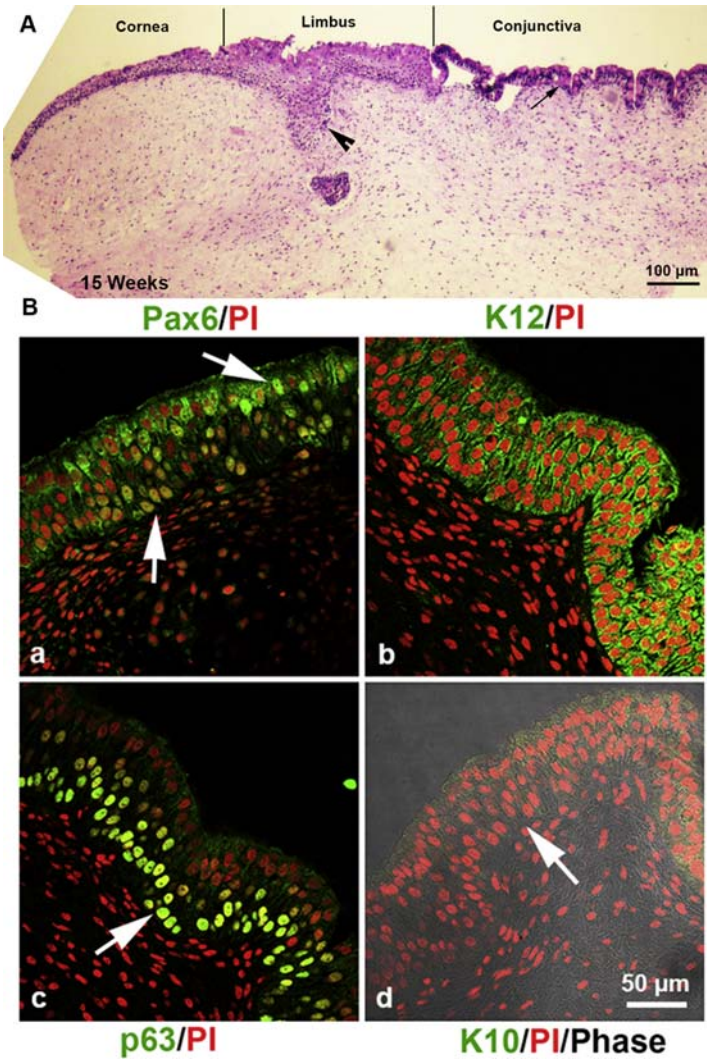

FIGURE 4.4 Immunohistochemical evaluation of human iPSC-derived corneal organoids.

(A) Hematoxylin and eosin-stained section of a mature corneal organoid at 15 weeks of development. Note the clear development of corneal, limbal, and conjunctival demarcations. The limbus region shows a rudimentary crypt-like structure and the conjunctival epithelium is interspersed with mucin-filled goblet cells, (B) Immunohistochemistry of a mature corneal organoid section stained with anti-PAX6 (a), anti-K12 (b), anti-p63 (c), and anti-K10 antibodies (*green*) counterstained with the propidium iodide dye (*red*).

scalable expansion, cryobanking, and for regenerative applications (Hongisto et al., 2018). Similarly, the NCCs are known to express the neural growth factor receptor (NGFR/p75NTR), a cell surface antigen that can be used for selective cell sorting to prepare enriched cultures (Chan et al., 2013). The limbal stromal keratocytes are also known to express the cell surface markers such as CD71, CD90, and CD105, which can be employed in cell enrichment strategies. However, the process of organoid development allowed the differentiation of stem cells and a coordinated self-organization of different cell types to form complex tissues. This has enabled simpler identification and isolation of morphologically distinct tissue parts for further cell expansion and greatly reduced the risk of undifferentiated stem cell contaminants. We have successfully adopted this strategy and used iPSC-derived corneal organoids as donor tissues for limbal stem cells, to establish simple explant cultures on denuded human amniotic membrane and generated transplantable sheets of corneal epithelial grafts that are comparable to those engineered using adult limbal tissues (Susaimanickam et al., 2017).

iPSC-derived corneal tissues for disease modeling and *in vitro* drug testing

To study human diseases and to understand the underlying pathobiology, it is important to use physiologically relevant *in vitro* or *in vivo* experimental models that are comparable to humans. Traditionally various immortalized cell lines, tissue-specific primary cell cultures, small and large animal models were used to evaluate basic research questions in cell biology and also for screening and testing chemicals and drugs under development. Most immortalized cell lines have lost their cellular identity and are transformed cells carrying greater levels of genomic aberrations and do not truly represent many tissue-specific phenomenon. While primary cultures are relevant for tissue-specific evaluations, they require specialized culture conditions and are hard to expand sufficiently for carrying out large-scale assays *in vitro*. Similarly, *in vivo* studies in animal models can convey meaningful tissue-specific information. However, serious ethical considerations and overwhelming costs associated with animal maintenance limit the feasibility of large-scale experimental planning. Also, the currently available animal models may not totally represent the human disease due to inherent differences in their anatomy, physiology, and the underlying genetics. For example, a total gene knockout model may not exactly replicate the pleiotropic effects of an array of missense and nonsense mutations seen in patients.

The development of PSCs such as ESCs and iPSCs and the availability of robust 2D and 3D culture protocols for tissue-specific differentiation have now opened up a large resource of human disease-relevant cells and tissues for large-scale experimentations. Recently, genome editing has evolved rapidly with the development of various editing tools such as the zinc finger nucleases (ZFNs), transcription activator-like effector nucleases (TALENs), and clusters of regularly interspaced

short palindromic repeats (CRISPRs). This has enabled in situ gene editing in cultured cells, developing embryos, and in adult tissues, for the development of human disease-relevant cell lines and animal models. The use of patient-specific iPSC-derived cells or organoids and the development of gene-edited isotype controls have allowed more precise understanding of mutation-specific cellular behaviors.

A study on human iPSC-derived corneal cells has identified miR-450b-5p as a molecular switch for PAX6 gene expression. It was found that miR-450b-5p inhibited PAX6 expression and triggered epidermal specification of the ocular surface ectoderm, while its absence allowed corneal epithelial development (Shalom-Feuerstein et al., 2012). Another study has shown that keratoconus patient-derived corneal fibroblasts can be successfully reprogrammed to generate disease-specific iPSCs. Transcriptome analysis of keratoconus iPSC-derived corneal keratocytes revealed that the FGFR2-Pi3-kinase signaling was downregulated and caused reduced AKT phosphorylation when compared to normal cells. This could result in reduced cell survival and increased apoptosis of mutant keratocytes, thus partly explaining the disease physiology (Joseph et al., 2016). Recently, corneal endothelium-like cells have been differentiated from iPSCs to assess the effect of a novel intronic mutation on SLC4A11 pre-mRNA splicing (Brejchova et al., 2019). Next-generation sequencing (NGS) analysis of target transcripts from iPSC-derived corneal endothelium-like cells of a heterozygous carrier, with a SLC4A11 variant, revealed multiple alternately spliced transcripts causing premature translational termination when compared to that of wild-type transcripts expressed in normal iPSC-derived corneal endothelium. This has opened up the possibility of modeling other genetic disorders such as the noncoding, trinucleotide repeat expansion in TCF4 and altered mRNA processing seen in Fuchs endothelial corneal dystrophy (FECD); pathological mutations in transforming growth factor β-induced gene (TGFBI)-linked corneal dystrophies such as granular corneal dystrophy (GCD), lattice corneal dystrophy (LCD), and more such corneal diseases in the future. Thus iPSC-derived cells are useful to elucidate the effects of unknown genetic variants on tissue-specific pre-mRNA splicing, protein expression, stability, subcellular localization, function, target gene regulation, and signaling.

Such tissue-specific cells, prepared in large numbers, are valuable resources for drug screening and toxicological testing *in vitro* and can replace physiologically irrelevant immortal cell lines and expensive large animal studies to some extent. This was validated in a study wherein, the iPSC-derived limbal epithelial cells are shown to behave very similar to that of adult limbus-derived primary cells in an *in vitro* drug toxicity assay (Aberdam et al., 2017). However, in case of PSC-derived organoids, it is important to note that they mostly lack vasculatures and immune cells and therefore may not be suitable for modeling inflammatory responses to infections or drugs. This may require the development of coculture systems, advanced bioengineering approaches, and microfluidics based bio-chip platforms to overcome such concerns. Thus, iPSC-derived ocular cells and organoids may become powerful, human-relevant, *in vitro* models for testing therapeutic drugs and cosmetics in the near future.

Major challenges in using iPSCs derived corneal cells and tissues for regeneration

While it is clear that the iPSCs have a great potential in disease modeling studies, there are few concerns and challenges that need more basic understanding and alternate strategies for the applications of iPSC-derived cells in regenerative medicine. The reprogramming process itself is a highly stochastic event and can lead to karyotype abnormalities, copy number variations, epigenetic alterations at certain imprinted regions of the genome, and this can lead to clonal variability in terms of their stemness and differentiation potential (Laurent et al., 2011; Taapken et al., 2011; Liang and Zhang, 2013). Such reprogramming-induced, epigenetic artifacts can alter iPSC characteristics and can negatively influence disease modeling studies involving epigenetic modification such as imprinting disorders or sex-linked disorders. Such reprogramming and culture-induced genomic instability and epigenetic concerns can be addressed by detailed molecular characterization of multiple clones per patient and careful selection of at least three best clones for lineage differentiation and preparation of therapeutic products. Transgene insertions, insertional activation or disruption of random genes, transgene reactivation after differentiation, and the risk of reversal to pluripotency (Choi et al., 2014) are sufficiently addressed by the use of nonintegrating constructs in latest somatic cell reprogramming strategies. The major concern of stem-cell-derived tumor formation can be avoided if well-differentiated and enriched populations of PSC-derived, tissue-specific cells are considered in transplantation studies. Therefore, apart from developing methods for directed differentiation, it is of paramount importance to establish robust protocols and strategies for the enrichment of desired cell types. This should ensure that the final cell therapeutic product is absolutely enriched with the desired cell type, without any contaminating undifferentiated stem cells and other differentiated, undesired cells that may cause the risk of tumorigenicity and poor transplantation outcomes.

Cell therapies involving autologous cells have greater chances of donor cell survival and *in vivo* integration. However, autologous therapies remain elusive in case of genetic disorders, unless the underlying the genetic defects are corrected. With the recent developments in CRISPR-Cas9-based, improved gene editing approaches, it is now possible to correct disease-causing gene mutations in patient-specific iPSCs, before differentiating them into desired cell types. This also requires extensive molecular characterizations to avoid any undesirable genomic alterations, while achieving the desired edits at the mutation site. The entire process involves long generation time, extended *in vitro* cultures with expensive reagents, elaborate quality assessments and validations. This can therefore render the final therapeutic product very expensive and unaffordable for most patients. However, with allogeneic therapies, well-characterized normal iPSCs and iPSC-derived tissue-specific cells can be produced in large numbers and validated for clinical use. A single batch of qualified cells may be useful to treat hundreds of patients, irrespective of the variable genetic

mutations they carry. This will render iPSC-based cell therapy affordable and widely accessible to a large number of needy patients. However, such allografts require systemic immune suppression to reduce the risk of graft rejections *in vivo.* A few centers have initiated efforts to establish HLA-typed iPSC banks to enable donor HLA-matching to reduce the risk of host immune response and allograft rejections (Turner et al., 2013; Solomon et al., 2015; Sugita et al., 2020). While this strategy may be feasible theoretically, it may require few tens to hundreds of iPSC lines, homozygous for all six major HLA alleles, depending on the population allele frequencies. Few groups have also initiated efforts toward developing universal iPSCs lacking the expression of both HLA class I and class II alleles by gene editing methods. Here, the CRISPRs are targeted to knock out the β_2-microglobulin (B2M) gene and the class II transactivator (CIITA) gene to abolish the expression of all MHC class I and II molecules respectively (Deuse et al., 2019; Xu et al., 2019). This strategy has been successfully utilized to generate universal corneal and retinal epithelial cells (Yang et al., 2018; Petrus-Reurer et al., 2020). However, the total lack of self HLA antigens can trigger NK-cell-mediated innate immune response. Various strategies such as the overexpression of chimeric HLA-E, HLA-G, or CD47 cell surface antigens in HLA class I and II null cells are currently being explored to suppress T-cell, NK-cell, and macrophage-cell-mediated allogeneic graft rejections. Such universal iPSCs and iPSC-derived donor cells need to be thoroughly tested in humanized animal models to confirm their immunogenicity and *in vivo* safety, before considering them for regenerative applications.

Future perspectives and conclusion

As discussed so far, successful translation of iPSC-based cell therapy from bench-to-bed side requires well-characterized, clinical-grade, autologous or universal allogeneic donor stem cells, combined with robust differentiation and cell enrichment protocols that ensures repeatable and reliable production of well-characterized donor cell grafts within shortest timelines possible. To reduce the developmental timelines, a study has directly trans-differentiated the fibroblast cells into limbal epithelial cells by overexpressing limbal-specific transcription factors such as ΔNp63α, TCF4, and C/EBPδ, along with either OCT4 or KLF4, and cultured the engineered cells under corneal growth conditions (Cieslar-Pobuda et al., 2016). Another group has reported overexpression of the core transcription factors such as PAX6, OVOL2, and KLF4 in human fibroblasts and induced "direct reprogramming" of fibroblast cells into corneal epithelial-like cells (Kitazawa et al., 2019). However, the stability of such ocular cells generated by direct reprogramming and their usefulness in regenerative applications need to be further evaluated. Similarly, the iPSC-derived organoids hold a great promise in disease modeling studies. These are currently miniature structures in the range of 1−2 mm in size and are devoid of vasculatures. As they grow bigger, the cells in the deeper layers are likely to face shortage of nutrient and growth factors, which in turn limits their long-term survival and maintenance *in vitro*.

Such limitations with stem-cell-derived and self-organized 3D organoids can be overcome with the use of bioreactors and the development of tissue-engineered corneal grafts and 3D printed corneas using iPSC-derived cell types, various biomaterials and scaffolds, ECMs, and bioinks. A recent study has used laser-assisted 3D bioprinting and functional bioinks and bioprinted corneal structures using hESC-derived limbal epithelial cells to form the stratified corneal epithelium and alternating layers of acellular bioink and human adipose tissue−derived stem cells (hASCs) to form the thick corneal stroma (Sorkio et al., 2018). Other approaches have incorporated stem-cell-derived corneal cells in micropatterns on dome-shaped 3D scaffolds to form eye-on-a-chip microfluidic devices for research and pharmaceutical applications. With the limited availability of human donor corneas and primary limbal stem cells, iPSC-derived corneal cells and organoid models offer a great promise for various applications in research and drug testing. Together with the recent developments in the area of gene editing and bioengineering, it may be possible to develop iPSC-based cell therapeutics for the treatment of some inherited corneal diseases and bilateral corneal surface defects in the near future.

References

Aberdam, E., Petit, I., Sangari, L., Aberdam, D., 2017. Induced pluripotent stem cell-derived limbal epithelial cells (LiPSC) as a cellular alternative for in vitro ocular toxicity testing. PLoS One 12, e0179913. https://doi.org/10.1371/journal.pone.0179913.

Ahmad, S., Stewart, R., Yung, S., Kolli, S., et al., 2007. Differentiation of human embryonic stem cells into corneal epithelial-like cells by in vitro replication of the corneal epithelial stem cell niche. Stem Cell. 25, 1145−1155. https://doi.org/10.1634/stemcells.2006-0516.

Ambati, B.K., Nozaki, M., Singh, N., Takeda, A., et al., 2006. Corneal avascularity is due to soluble VEGF receptor-1. Nature 443, 993−997. https://doi.org/10.1038/nature05249.

Ambati, B.K., Patterson, E., Jani, P., Jenkins, C., et al., 2007. Soluble vascular endothelial growth factor receptor-1 contributes to the corneal antiangiogenic barrier. Br. J. Ophthalmol. 91, 505−508. https://doi.org/10.1136/bjo.2006.107417.

Assawachananont, J., Mandai, M., Okamoto, S., Yamada, C., et al., 2014. Transplantation of embryonic and induced pluripotent stem cell-derived 3D retinal sheets into retinal degenerative mice. Stem Cell Rep. 2, 662−674. https://doi.org/10.1016/j.stemcr.2014.03.011.

Barbaro, V., Testa, A., Di Iorio, E., Mavilio, F., et al., 2007. C/EBPdelta regulates cell cycle and self-renewal of human limbal stem cells. J. Cell Biol. 177, 1037−1049. https://doi.org/10.1083/jcb.200703003.

Barrandon, Y., Green, H., 1987. Three clonal types of keratinocyte with different capacities for multiplication. Proc. Natl. Acad. Sci. U. S. A. 84, 2302−2306. https://doi.org/10.1073/pnas.84.8.2302.

Basu, S., Ali, H., Sangwan, V.S., 2012. Clinical outcomes of repeat autologous cultivated limbal epithelial transplantation for ocular surface burns. Am. J. Ophthalmol. 153, 643−650. https://doi.org/10.1016/j.ajo.2011.09.016, 650 e641−642.

Basu, S., Sureka, S.P., Shanbhag, S.S., Kethiri, A.R., et al., 2016. Simple limbal epithelial transplantation: long-term clinical outcomes in 125 cases of unilateral chronic ocular surface burns. Ophthalmology 123, 1000−1010. https://doi.org/10.1016/j.ophtha.2015.12.042.

Baylis, O., Figueiredo, F., Henein, C., Lako, M., et al., 2011. 13 years of cultured limbal epithelial cell therapy: a review of the outcomes. J. Cell. Biochem. 112, 993−1002. https://doi.org/10.1002/jcb.23028.

Beebe, D.C., Masters, B.R., 1996. Cell lineage and the differentiation of corneal epithelial cells. Invest. Ophthalmol. Vis. Sci. 37, 1815−1825.

Bikkuzin, T., Shi, Y., Sun, B., Guo, Y., et al., 2019. Human induced pluripotent stem cell line HMUi001-A derived from corneal stromal cells. Stem Cell Res. 37, 101409. https://doi.org/10.1016/j.scr.2019.101409.

Blazejewska, E.A., Schlotzer-Schrehardt, U., Zenkel, M., Bachmann, B., et al., 2009. Corneal limbal microenvironment can induce transdifferentiation of hair follicle stem cells into corneal epithelial-like cells. Stem Cell. 27, 642−652. https://doi.org/10.1634/stemcells.2008-0721.

Brejchova, K., Dudakova, L., Skalicka, P., Dobrovolny, R., et al., 2019. IPSC-derived corneal endothelial-like cells act as an appropriate model system to assess the impact of SLC4A11 variants on pre-mRNA splicing. Invest. Ophthalmol. Vis. Sci. 60, 3084−3090. https://doi.org/10.1167/iovs.19-26930.

Bronner-Fraser, M., Wolf, J.J., Murray, B.A., 1992. Effects of antibodies against N-cadherin and N-CAM on the cranial neural crest and neural tube. Dev. Biol. 153, 291−301. https://doi.org/10.1016/0012-1606(92)90114-v.

Brzeszczynska, J., Samuel, K., Greenhough, S., Ramaesh, K., et al., 2014. Differentiation and molecular profiling of human embryonic stem cell-derived corneal epithelial cells. Int. J. Mol. Med. 33, 1597−1606. https://doi.org/10.3892/ijmm.2014.1714.

Cauchi, P.A., Ang, G.S., Azuara-Blanco, A., Burr, J.M., 2008. A systematic literature review of surgical interventions for limbal stem cell deficiency in humans. Am. J. Ophthalmol. 146, 251−259. https://doi.org/10.1016/j.ajo.2008.03.018.

Chambers, S.M., Fasano, C.A., Papapetrou, E.P., Tomishima, M., et al., 2009. Highly efficient neural conversion of human ES and iPS cells by dual inhibition of SMAD signaling. Nat. Biotechnol. 27, 275−280. https://doi.org/10.1038/nbt.1529.

Chan, A.A., Hertsenberg, A.J., Funderburgh, M.L., Mann, M.M., et al., 2013. Differentiation of human embryonic stem cells into cells with corneal keratocyte phenotype. PLoS One 8, e56831. https://doi.org/10.1371/journal.pone.0056831.

Chen, P., Chen, J.Z., Shao, C.Y., Li, C.Y., et al., 2015. Treatment with retinoic acid and lens epithelial cell-conditioned medium in vitro directed the differentiation of pluripotent stem cells towards corneal endothelial cell-like cells. Exp. Ther. Med. 9, 351−360. https://doi.org/10.3892/etm.2014.2103.

Chien, Y., Liao, Y.W., Liu, D.M., Lin, H.L., et al., 2012. Corneal repair by human corneal keratocyte-reprogrammed iPSCs and amphiphatic carboxymethyl-hexanoyl chitosan hydrogel. Biomaterials 33, 8003−8016. https://doi.org/10.1016/j.biomaterials.2012.07.029.

Choi, H.W., Kim, J.S., Choi, S., Hong, Y.J., et al., 2014. Neural stem cells differentiated from iPS cells spontaneously regain pluripotency. Stem Cell. 32, 2596−2604. https://doi.org/10.1002/stem.1757.

Chow, R.L., Altmann, C.R., Lang, R.A., Hemmati-Brivanlou, A., 1999. Pax6 induces ectopic eyes in a vertebrate. Development 126, 4213−4222.

Cieslar-Pobuda, A., Rafat, M., Knoflach, V., Skonieczna, M., et al., 2016. Human induced pluripotent stem cell differentiation and direct transdifferentiation into corneal epithelial-like cells. Oncotarget 7, 42314−42329. https://doi.org/10.18632/oncotarget.9791.

Collomb, E., Yang, Y., Foriel, S., Cadau, S., et al., 2013. The corneal epithelium and lens develop independently from a common pool of precursors. Dev. Dynam. 242, 401–413. https://doi.org/10.1002/dvdy.23925.

Davanger, M., Evensen, A., 1971. Role of the pericorneal papillary structure in renewal of corneal epithelium. Nature 229, 560–561. https://doi.org/10.1038/229560a0.

DelMonte, D.W., Kim, T., 2011. Anatomy and physiology of the cornea. J. Cataract Refract. Surg. 37, 588–598. https://doi.org/10.1016/j.jcrs.2010.12.037.

Deuse, T., Hu, X., Gravina, A., Wang, D., et al., 2019. Hypoimmunogenic derivatives of induced pluripotent stem cells evade immune rejection in fully immunocompetent allogeneic recipients. Nat. Biotechnol. 37, 252–258. https://doi.org/10.1038/s41587-019-0016-3.

Dua, H.S., Joseph, A., Shanmuganathan, V.A., Jones, R.E., 2003. Stem cell differentiation and the effects of deficiency. Eye 17, 877–885. https://doi.org/10.1038/sj.eye.6700573.

Eiraku, M., Takata, N., Ishibashi, H., Kawada, M., et al., 2011. Self-organizing optic-cup morphogenesis in three-dimensional culture. Nature 472, 51–56. https://doi.org/10.1038/nature09941.

Fares, U., Otri, A.M., Al-Aqaba, M.A., Dua, H.S., 2012. Correlation of central and peripheral corneal thickness in healthy corneas. Contact Lens Anterior Eye 35, 39–45. https://doi.org/10.1016/j.clae.2011.07.004.

Feizi, S., Jafarinasab, M.R., Karimian, F., Hasanpour, H., et al., 2014. Central and peripheral corneal thickness measurement in normal and keratoconic eyes using three corneal pachymeters. J. Ophthalmic Vis. Res. 9, 296–304. https://doi.org/10.4103/2008-322X.143356.

Foster, J.W., Wahlin, K., Adams, S.M., Birk, D.E., et al., 2017. Cornea organoids from human induced pluripotent stem cells. Sci. Rep. 7, 41286. https://doi.org/10.1038/srep41286.

Frucht-Pery, J., Siganos, C.S., Solomon, A., Scheman, L., et al., 1998. Limbal cell autograft transplantation for severe ocular surface disorders. Graefes Arch. Clin. Exp. Ophthalmol. 236, 582–587. https://doi.org/10.1007/s004170050125.

Fuhrmann, S., Levine, E.M., Reh, T.A., 2000. Extraocular mesenchyme patterns the optic vesicle during early eye development in the embryonic chick. Development 127 (21), 4599–4609.

Gonzalez-Cordero, A., West, E.L., Pearson, R.A., Duran, Y., et al., 2013. Photoreceptor precursors derived from three-dimensional embryonic stem cell cultures integrate and mature within adult degenerate retina. Nat. Biotechnol. 31, 741–747. https://doi.org/10.1038/nbt.2643.

Gupta, N., Joshi, J., Farooqui, J.H., Mathur, U., 2018. Results of simple limbal epithelial transplantation in unilateral ocular surface burn. Indian J. Ophthalmol. 66, 45–52. https://doi.org/10.4103/ijo.IJO_602_17.

Halder, G., Callaerts, P., Gehring, W.J., 1995. Induction of ectopic eyes by targeted expression of the eyeless gene in Drosophila. Science 267, 1788–1792. https://doi.org/10.1126/science.7892602.

Hay, E.D., 1980. Development of the vertebrate cornea. Int. Rev. Cytol. 63, 263–322. https://doi.org/10.1016/s0074-7696(08)61760-x.

Hayashi, R., Ishikawa, Y., Ito, M., Kageyama, T., et al., 2012. Generation of corneal epithelial cells from induced pluripotent stem cells derived from human dermal fibroblast and corneal limbal epithelium. PLoS One 7, e45435. https://doi.org/10.1371/journal.pone.0045435.

Hayashi, R., Ishikawa, Y., Sasamoto, Y., Katori, R., et al., 2016. Co-ordinated ocular development from human iPS cells and recovery of corneal function. Nature 531, 376–380. https://doi.org/10.1038/nature17000.

Hayashi, R., Ishikawa, Y., Katori, R., Sasamoto, Y., et al., 2017. Coordinated generation of multiple ocular-like cell lineages and fabrication of functional corneal epithelial cell sheets from human iPS cells. Nat. Protoc. 12, 683–696. https://doi.org/10.1038/nprot.2017.007.

Hayashi, R., Ishikawa, Y., Katayama, T., Quantock, A.J., et al., 2018. CD200 facilitates the isolation of corneal epithelial cells derived from human pluripotent stem cells. Sci. Rep. 8, 16550. https://doi.org/10.1038/s41598-018-34845-2.

Hiler, D., Chen, X., Hazen, J., Kupriyanov, S., et al., 2015. Quantification of retinogenesis in 3D cultures reveals epigenetic memory and higher efficiency in iPSCs derived from rod photoreceptors. Cell Stem Cell 17, 101–115. https://doi.org/10.1016/j.stem.2015.05.015.

Hirayama, M., Satake, Y., Higa, K., Yamaguchi, T., et al., 2012. Transplantation of cultivated oral mucosal epithelium prepared in fibrin-coated culture dishes. Invest. Ophthalmol. Vis. Sci. 53, 1602–1609. https://doi.org/10.1167/iovs.11-7847.

Hirsch, M., Renard, G., Faure, J.P., Pouliquen, Y., 1977. Study of the ultrastructure of the rabbit corneal endothelium by the freeze-fracture technique: apical and lateral junctions. Exp. Eye Res. 25, 277–288. https://doi.org/10.1016/0014-4835(77)90094-x.

Holan, V., Trosan, P., Cejka, C., Javorkova, E., et al., 2015. A comparative study of the therapeutic potential of mesenchymal stem cells and limbal epithelial stem cells for ocular surface reconstruction. Stem Cell. Transl. Med. 4, 1052–1063. https://doi.org/10.5966/sctm.2015-0039.

Hongisto, H., Ilmarinen, T., Vattulainen, M., Mikhailova, A., et al., 2017. Xeno- and feeder-free differentiation of human pluripotent stem cells to two distinct ocular epithelial cell types using simple modifications of one method. Stem Cell Res. Ther. 8, 291. https://doi.org/10.1186/s13287-017-0738-4.

Hongisto, H., Vattulainen, M., Ilmarinen, T., Mikhailova, A., et al., 2018. Efficient and scalable directed differentiation of clinically compatible corneal limbal epithelial stem cells from human pluripotent stem cells. JoVE. https://doi.org/10.3791/58279.

Idelson, M., Alper, R., Obolensky, A., Ben-Shushan, E., et al., 2009. Directed differentiation of human embryonic stem cells into functional retinal pigment epithelium cells. Cell Stem Cell 5, 396–408. https://doi.org/10.1016/j.stem.2009.07.002.

Ikeda, H., Osakada, F., Watanabe, K., Mizuseki, K., et al., 2005. Generation of Rx+/Pax6+ neural retinal precursors from embryonic stem cells. Proc. Natl. Acad. Sci. U. S. A. 102, 11331–11336. https://doi.org/10.1073/pnas.0500010102.

Joseph, R., Srivastava, O.P., Pfister, R.R., 2016. Modeling keratoconus using induced pluripotent stem cells. Invest. Ophthalmol. Vis. Sci. 57, 3685–3697. https://doi.org/10.1167/iovs.16-19105.

Kaewkhaw, R., Kaya, K.D., Brooks, M., Homma, K., et al., 2015. Transcriptome dynamics of developing photoreceptors in three-dimensional retina cultures recapitulates temporal sequence of human cone and rod differentiation revealing cell surface markers and gene networks. Stem Cell. 33, 3504–3518. https://doi.org/10.1002/stem.2122.

Kaufman, M.H., 1992. Postcranial morphological features of homozygous tetraploid mouse embryos. J. Anat. 180 (Pt 3), 521–534.

Kenyon, K.R., Tseng, S.C., 1989. Limbal autograft transplantation for ocular surface disorders. Ophthalmology 96, 709–722. https://doi.org/10.1016/s0161-6420(89)32833-8. discussion 722–703.

Kitazawa, K., Hikichi, T., Nakamura, T., Nakamura, M., et al., 2019. Direct reprogramming into corneal epithelial cells using a transcriptional network comprising PAX6, OVOL2, and KLF4. Cornea 38 (Suppl. 1), S34−S41. https://doi.org/10.1097/ICO.0000000000002074.

Kolli, S., Ahmad, S., Mudhar, H.S., Meeny, A., et al., 2014. Successful application of ex vivo expanded human autologous oral mucosal epithelium for the treatment of total bilateral limbal stem cell deficiency. Stem Cell. 32, 2135−2146. https://doi.org/10.1002/stem.1694.

Kurpakus, M.A., Stock, E.L., Jones, J.C., 1990. Expression of the 55-kD/64-kD corneal keratins in ocular surface epithelium. Invest. Ophthalmol. Vis. Sci. 31, 448−456.

Lamb, T.M., Knecht, A.K., Smith, W.C., Stachel, S.E., et al., 1993. Neural induction by the secreted polypeptide noggin. Science 262, 713−718. https://doi.org/10.1126/science.8235591.

Lamba, D.A., Karl, M.O., Ware, C.B., Reh, T.A., 2006. Efficient generation of retinal progenitor cells from human embryonic stem cells. Proc. Natl. Acad. Sci. U. S. A. 103, 12769−12774. https://doi.org/10.1073/pnas.0601990103.

Laurent, L.C., Ulitsky, I., Slavin, I., Tran, H., et al., 2011. Dynamic changes in the copy number of pluripotency and cell proliferation genes in human ESCs and iPSCs during reprogramming and time in culture. Cell Stem Cell 8, 106−118. https://doi.org/10.1016/j.stem.2010.12.003.

Lavker, R.M., Tseng, S.C., Sun, T.T., 2004. Corneal epithelial stem cells at the limbus: looking at some old problems from a new angle. Exp. Eye Res. 78, 433−446. https://doi.org/10.1016/j.exer.2003.09.008.

Li, D., Qiu, X., Yang, J., Liu, T., et al., 2016. Generation of human lens epithelial-like cells from patient-specific induced pluripotent stem cells. J. Cell. Physiol. 231, 2555−2562. https://doi.org/10.1002/jcp.25374.

Li, W., Hayashida, Y., Chen, Y.T., Tseng, S.C., 2007. Niche regulation of corneal epithelial stem cells at the limbus. Cell Res. 17, 26−36. https://doi.org/10.1038/sj.cr.7310137.

Liang, G., Zhang, Y., 2013. Genetic and epigenetic variations in iPSCs: potential causes and implications for application. Cell Stem Cell 13, 149−159. https://doi.org/10.1016/j.stem.2013.07.001.

Liang, L., Sheha, H., Li, J., Tseng, S.C., 2009. Limbal stem cell transplantation: new progresses and challenges. Eye 23, 1946−1953. https://doi.org/10.1038/eye.2008.379.

Lu, B., Malcuit, C., Wang, S., Girman, S., et al., 2009. Long-term safety and function of RPE from human embryonic stem cells in preclinical models of macular degeneration. Stem Cell. 27, 2126−2135. https://doi.org/10.1002/stem.149.

Mariappan, I., Maddileti, S., Savy, S., Tiwari, S., et al., 2010. In vitro culture and expansion of human limbal epithelial cells. Nat. Protoc. 5, 1470−1479. https://doi.org/10.1038/nprot.2010.115.

Maurice, D.M., 1957. The structure and transparency of the cornea. J. Physiol. 136, 263−286. https://doi.org/10.1113/jphysiol.1957.sp005758.

McCabe, K.L., Kunzevitzky, N.J., Chiswell, B.P., Xia, X., et al., 2015. Efficient generation of human embryonic stem cell-derived corneal endothelial cells by directed differentiation. PLoS One 10, e0145266. https://doi.org/10.1371/journal.pone.0145266.

Meek, K.M., Boote, C., 2004. The organization of collagen in the corneal stroma. Exp. Eye Res. 78, 503−512. https://doi.org/10.1016/j.exer.2003.07.003.

Meyer, J.S., Shearer, R.L., Capowski, E.E., Wright, L.S., et al., 2009. Modeling early retinal development with human embryonic and induced pluripotent stem cells. Proc. Natl. Acad. Sci. U. S. A. 106, 16698−16703. https://doi.org/10.1073/pnas.0905245106.

Mikhailova, A., Ilmarinen, T., Uusitalo, H., Skottman, H., 2014. Small-molecule induction promotes corneal epithelial cell differentiation from human induced pluripotent stem cells. Stem Cell Rep. 2, 219−231. https://doi.org/10.1016/j.stemcr.2013.12.014.

Mittal, V., Jain, R., Mittal, R., 2015. Ocular surface epithelialization pattern after simple limbal epithelial transplantation: an in vivo observational study. Cornea 34, 1227−1232. https://doi.org/10.1097/ICO.0000000000000573.

Mukhopadhyay, M., Gorivodsky, M., Shtrom, S., Grinberg, A., et al., 2006. Dkk2 plays an essential role in the corneal fate of the ocular surface epithelium. Development 133, 2149−2154. https://doi.org/10.1242/dev.02381.

Nakatsu, M.N., Ding, Z., Ng, M.Y., Truong, T.T., et al., 2011. Wnt/beta-catenin signaling regulates proliferation of human cornea epithelial stem/progenitor cells. Invest. Ophthalmol. Vis. Sci. 52, 4734−4741. https://doi.org/10.1167/iovs.10-6486.

Naylor, R.W., McGhee, C.N., Cowan, C.A., Davidson, A.J., et al., 2016. Derivation of corneal keratocyte-like cells from human induced pluripotent stem cells. PLoS One 11, e0165464. https://doi.org/10.1371/journal.pone.0165464.

Osakada, F., Ikeda, H., Mandai, M., Wataya, T., et al., 2008. Toward the generation of rod and cone photoreceptors from mouse, monkey and human embryonic stem cells. Nat. Biotechnol. 26, 215−224. https://doi.org/10.1038/nbt1384.

Osakada, F., Jin, Z.B., Hirami, Y., Ikeda, H., et al., 2009. In vitro differentiation of retinal cells from human pluripotent stem cells by small-molecule induction. J. Cell Sci. 122, 3169−3179. https://doi.org/10.1242/jcs.050393.

Pei, Y.F., Rhodin, J.A., 1970. The prenatal development of the mouse eye. Anat. Rec. 168, 105−125. https://doi.org/10.1002/ar.1091680109.

Pellegrini, G., Traverso, C.E., Franzi, A.T., Zingirian, M., et al., 1997. Long-term restoration of damaged corneal surfaces with autologous cultivated corneal epithelium. Lancet 349, 990−993. https://doi.org/10.1016/S0140-6736(96)11188-0.

Pellegrini, G., Rama, P., Matuska, S., Lambiase, A., et al., 2013. Biological parameters determining the clinical outcome of autologous cultures of limbal stem cells. Regen. Med. 8, 553−567. https://doi.org/10.2217/rme.13.43.

Petrus-Reurer, S., Winblad, N., Kumar, P., Gorchs, L., et al., 2020. Generation of retinal pigment epithelial cells derived from human embryonic stem cells lacking human leukocyte antigen class I and II. Stem Cell Rep. 14, 648−662. https://doi.org/10.1016/j.stemcr.2020.02.006.

Pittack, C., Grunwald, G.B., Reh, T.A., 1997. Fibroblast growth factors are necessary for neural retina but not pigmented epithelium differentiation in chick embryos. Development 124, 805−816.

Rama, P., Matuska, S., Paganoni, G., Spinelli, A., et al., 2010. Limbal stem-cell therapy and long-term corneal regeneration. N. Engl. J. Med. 363, 147−155. https://doi.org/10.1056/NEJMoa0905955.

Reichman, S., Terray, A., Slembrouck, A., Nanteau, C., et al., 2014. From confluent human iPS cells to self-forming neural retina and retinal pigmented epithelium. Proc. Natl. Acad. Sci. U. S. A. 111, 8518−8523. https://doi.org/10.1073/pnas.1324212111.

Reneker, L.W., Silversides, D.W., Xu, L., Overbeek, P.A., 2000. Formation of corneal endothelium is essential for anterior segment development - a transgenic mouse model of anterior segment dysgenesis. Development 127, 533−542.

Rheinwald, J.G., Green, H., 1975. Serial cultivation of strains of human epidermal keratinocytes: the formation of keratinizing colonies from single cells. Cell 6, 331−343. https://doi.org/10.1016/s0092-8674(75)80001-8.

Rio-Cristobal, A., Martin, R., 2014. Corneal assessment technologies: current status. Surv. Ophthalmol. 59, 599−614. https://doi.org/10.1016/j.survophthal.2014.05.001.

Robinson, M.L., Ohtaka-Maruyama, C., Chan, C.C., Jamieson, S., et al., 1998. Disregulation of ocular morphogenesis by lens-specific expression of FGF-3/int-2 in transgenic mice. Dev. Biol. 198, 13−31. https://doi.org/10.1006/dbio.1998.8879.

Romano, A.C., Espana, E.M., Yoo, S.H., Budak, M.T., et al., 2003. Different cell sizes in human limbal and central corneal basal epithelia measured by confocal microscopy and flow cytometry. Invest. Ophthalmol. Vis. Sci. 44, 5125−5129. https://doi.org/10.1167/iovs.03-0628.

Sangwan, V.S., Basu, S., MacNeil, S., Balasubramanian, D., 2012. Simple limbal epithelial transplantation (SLET): a novel surgical technique for the treatment of unilateral limbal stem cell deficiency. Br. J. Ophthalmol. 96, 931−934. https://doi.org/10.1136/bjophthalmol-2011-301164.

Sareen, D., Saghizadeh, M., Ornelas, L., Winkler, M.A., et al., 2014. Differentiation of human limbal-derived induced pluripotent stem cells into limbal-like epithelium. Stem Cell. Transl. Med. 3, 1002−1012. https://doi.org/10.5966/sctm.2014-0076.

Schermer, A., Galvin, S., Sun, T.T., 1986. Differentiation-related expression of a major 64K corneal keratin in vivo and in culture suggests limbal location of corneal epithelial stem cells. J. Cell Biol. 103, 49−62. https://doi.org/10.1083/jcb.103.1.49.

Shalom-Feuerstein, R., Serror, L., De La Forest Divonne, S., Petit, I., et al., 2012. Pluripotent stem cell model reveals essential roles for miR-450b-5p and miR-184 in embryonic corneal lineage specification. Stem Cell. 30, 898−909. https://doi.org/10.1002/stem.1068.

Silber, P.C., Ricardo, J.R., Cristovam, P.C., Hazarbassanov, R.M., et al., 2014. Conjunctival epithelial cells cultivated ex vivo from patients with total limbal stem cell deficiency. Eur. J. Ophthalmol. https://doi.org/10.5301/ejo.5000511.

Solomon, S., Pitossi, F., Rao, M.S., 2015. Banking on iPSC–is it doable and is it worthwhile. Stem Cell Rev. Rep. 11, 1−10. https://doi.org/10.1007/s12015-014-9574-4.

Song, Q., Yuan, S., An, Q., Chen, Y., et al., 2016. Directed differentiation of human embryonic stem cells to corneal endothelial cell-like cells: a transcriptomic analysis. Exp. Eye Res. 151, 107−114. https://doi.org/10.1016/j.exer.2016.08.004.

Sorkio, A., Koch, L., Koivusalo, L., Deiwick, A., et al., 2018. Human stem cell based corneal tissue mimicking structures using laser-assisted 3D bioprinting and functional bioinks. Biomaterials 171, 57−71. https://doi.org/10.1016/j.biomaterials.2018.04.034.

Sugita, S., Mandai, M., Hirami, Y., Takagi, S., et al., 2020. HLA-matched allogeneic iPS cells-derived RPE transplantation for macular degeneration. J. Clin. Med. 9. https://doi.org/10.3390/jcm9072217.

Susaimanickam, P.J., Maddileti, S., Pulimamidi, V.K., Boyinpally, S.R., et al., 2017. Generating minicorneal organoids from human induced pluripotent stem cells. Development 144, 2338−2351. https://doi.org/10.1242/dev.143040.

Taapken, S.M., Nisler, B.S., Newton, M.A., Sampsell-Barron, T.L., et al., 2011. Karotypic abnormalities in human induced pluripotent stem cells and embryonic stem cells. Nat. Biotechnol. 29, 313−314. https://doi.org/10.1038/nbt.1835.

Takahashi, K., Yamanaka, S., 2006. Induction of pluripotent stem cells from mouse embryonic and adult fibroblast cultures by defined factors. Cell 126, 663−676. https://doi.org/10.1016/j.cell.2006.07.024.

Thoft, R.A., Friend, J., 1983. The X, Y, Z hypothesis of corneal epithelial maintenance. Invest. Ophthalmol. Vis. Sci. 24, 1442–1443.

Tsai, R.J., Tseng, S.C., 1994. Human allograft limbal transplantation for corneal surface reconstruction. Cornea 13, 389–400. https://doi.org/10.1097/00003226-199409000-00003.

Turner, M., Leslie, S., Martin, N.G., Peschanski, M., et al., 2013. Toward the development of a global induced pluripotent stem cell library. Cell Stem Cell 13, 382–384. https://doi.org/10.1016/j.stem.2013.08.003.

Ueno, H., Kurokawa, M.S., Kayama, M., Homma, R., et al., 2007. Experimental transplantation of corneal epithelium-like cells induced by Pax6 gene transfection of mouse embryonic stem cells. Cornea 26, 1220–1227. https://doi.org/10.1097/ICO.0b013e31814fa814.

Utheim, T.P., Utheim, O.A., Khan, Q.E., Sehic, A., 2016. Culture of oral mucosal epithelial cells for the purpose of treating limbal stem cell deficiency. J. Funct. Biomater. 7 https://doi.org/10.3390/jfb7010005.

Vazirani, J., Ali, M.H., Sharma, N., Gupta, N., et al., 2016. Autologous simple limbal epithelial transplantation for unilateral limbal stem cell deficiency: multicentre results. Br. J. Ophthalmol. 100, 1416–1420. https://doi.org/10.1136/bjophthalmol-2015-307348.

Volkner, M., Zschatzsch, M., Rostovskaya, M., Overall, R.W., et al., 2016. Retinal organoids from pluripotent stem cells efficiently recapitulate retinogenesis. Stem Cell Rep. 6, 525–538. https://doi.org/10.1016/j.stemcr.2016.03.001.

Wagoner, M.D., Bohrer, L.R., Aldrich, B.T., Greiner, M.A., et al., 2018. Feeder-free differentiation of cells exhibiting characteristics of corneal endothelium from human induced pluripotent stem cells. Biol. Open 7. https://doi.org/10.1242/bio.032102.

Waring 3rd, G.O., Bourne, W.M., Edelhauser, H.F., Kenyon, K.R., 1982. The corneal endothelium. Normal and pathologic structure and function. Ophthalmology 89, 531–590.

Wilson, R.S., Roper-Hall, M.J., 1982. Effect of age on the endothelial cell count in the normal eye. Br. J. Ophthalmol. 66, 513–515. https://doi.org/10.1136/bjo.66.8.513.

Wulle, K.G., 1972. Electron microscopy of the fetal development of the corneal endothelium and Descemet's membrane of the human eye. Invest. Ophthalmol. 11, 897–904.

Xie, H.T., Chen, S.Y., Li, G.G., Tseng, S.C., 2011. Limbal epithelial stem/progenitor cells attract stromal niche cells by SDF-1/CXCR4 signaling to prevent differentiation. Stem Cell. 29, 1874–1885. https://doi.org/10.1002/stem.743.

Xie, H.T., Chen, S.Y., Li, G.G., Tseng, S.C., 2012. Isolation and expansion of human limbal stromal niche cells. Invest. Ophthalmol. Vis. Sci. 53, 279–286. https://doi.org/10.1167/iovs.11-8441.

Xu, H., Wang, B., Ono, M., Kagita, A., et al., 2019. Targeted disruption of HLA genes via CRISPR-cas9 generates iPSCs with enhanced immune compatibility. Cell Stem Cell 24, 566–578 e567. https://doi.org/10.1016/j.stem.2019.02.005.

Yang, J., Park, J.W., Zheng, D., Xu, R.H., 2018. Universal corneal epithelial-like cells derived from human embryonic stem cells for cellularization of a corneal scaffold. Transl. Vis. Sci. Technol. 7, 23. https://doi.org/10.1167/tvst.7.5.23.

Yao, L., Bai, H., 2013. Review: mesenchymal stem cells and corneal reconstruction. Mol. Vis. 19, 2237–2243.

Yao, L., Li, Z.R., Su, W.R., Li, Y.P., et al., 2012. Role of mesenchymal stem cells on cornea wound healing induced by acute alkali burn. PLoS One 7, e30842. https://doi.org/10.1371/journal.pone.0030842.

Yoshida, S., Yasuda, M., Miyashita, H., Ogawa, Y., et al., 2011. Generation of stratified squamous epithelial progenitor cells from mouse induced pluripotent stem cells. PLoS One 6, e28856. https://doi.org/10.1371/journal.pone.0028856.

Zaghloul, N.A., Yan, B., Moody, S.A., 2005. Step-wise specification of retinal stem cells during normal embryogenesis. Biol. Cell. 97, 321−337. https://doi.org/10.1042/BC20040521.

Zannettino, A.C., Paton, S., Arthur, A., Khor, F., et al., 2008. Multipotential human adipose-derived stromal stem cells exhibit a perivascular phenotype in vitro and in vivo. J. Cell. Physiol. 214, 413−421. https://doi.org/10.1002/jcp.21210.

Zhang, C., Du, L., Pang, K., Wu, X., 2017. Differentiation of human embryonic stem cells into corneal epithelial progenitor cells under defined conditions. PLoS One 12, e0183303. https://doi.org/10.1371/journal.pone.0183303.

Zhang, K., Pang, K., Wu, X., 2014. Isolation and transplantation of corneal endothelial cell-like cells derived from in-vitro-differentiated human embryonic stem cells. Stem Cell. Dev. 23, 1340−1354. https://doi.org/10.1089/scd.2013.0510.

Zhang, X., Huang, C.T., Chen, J., Pankratz, M.T., et al., 2010. Pax6 is a human neuroectoderm cell fate determinant. Cell Stem Cell 7, 90−100. https://doi.org/10.1016/j.stem.2010.04.017.

Zhao, J.J., Afshari, N.A., 2016. Generation of human corneal endothelial cells via in vitro ocular lineage restriction of pluripotent stem cells. Invest. Ophthalmol. Vis. Sci. 57, 6878−6884. https://doi.org/10.1167/iovs.16-20024.

Zhong, X., Gutierrez, C., Xue, T., Hampton, C., et al., 2014. Generation of three-dimensional retinal tissue with functional photoreceptors from human iPSCs. Nat. Commun. 5, 4047. https://doi.org/10.1038/ncomms5047.

Zhu, J., Zhang, K., Sun, Y., Gao, X., et al., 2013. Reconstruction of functional ocular surface by acellular porcine cornea matrix scaffold and limbal stem cells derived from human embryonic stem cells. Tissue Eng. 19, 2412−2425. https://doi.org/10.1089/ten.TEA.2013.0097.

Zuber, M.E., Gestri, G., Viczian, A.S., Barsacchi, G., et al., 2003. Specification of the vertebrate eye by a network of eye field transcription factors. Development 130, 5155−5167. https://doi.org/10.1242/dev.00723.

Understanding the role of PAX6 in corneal epithelial regulation at the limbal niche

by P Vinay Kumar

Submission date: 15-Feb-2022 12:04PM (UTC+0530)
Submission ID: 1762803797
File name: 15LAPH13_Vinay_PhD_thesis_Final.docx (1.02M)
Word count: 42873
Character count: 234505

Understanding the role of PAX6 in corneal epithelial regulation at the limbal niche

ORIGINALITY REPORT

11%	6%	9%	4%
SIMILARITY INDEX	INTERNET SOURCES	PUBLICATIONS	STUDENT PAPERS

PRIMARY SOURCES

1	Submitted to University of Hyderabad, Hyderabad Student Paper	1%
2	Vinay Kumar Pulimamidi, Savitri Maddileti, Indumathi Mariappan. "Induced pluripotent stem-cell-derived corneal grafts and organoids", Elsevier BV, 2021 Publication	1%
3	Ohad Shaham, Yotam Menuchin, Chen Farhy, Ruth Ashery-Padan. "Pax6: A multi-level regulator of ocular development", Progress in Retinal and Eye Research, 2012 Publication	1%
4	reports.ias.ac.in Internet Source	<1%
5	Hassan Mubarak Ishqi, Mohammed Amir Husain, Sayeed Ur Rehman, Tarique Sarwar, Mohammad Tabish. "Identification and expression of alternatively spliced novel isoforms of cancer associated MYD88 lacking	<1%

HYDERABAD EYE RESEARCH FOUNDATION HYD.

This is to certify that No. 2 and 78 are published by the Student, P. Vinay Kumar, which are a part of his thesis. Thesis Supervisor. 17/2/2022.

	death domain in mouse", Molecular Biology Reports, 2018 Publication	
6	"Corneal Regeneration", Springer Science and Business Media LLC, 2019 Publication	<1 %
7	"In Situ Hybridization Protocols", Springer Science and Business Media LLC, 2020 Publication	<1 %
8	www.ncbi.nlm.nih.gov Internet Source	<1 %
9	core.ac.uk Internet Source	<1 %
10	Submitted to National University of Singapore Student Paper	<1 %
11	www.stem-cell-rejuvenation.com Internet Source	<1 %
12	hdl.handle.net Internet Source	<1 %
13	link.springer.com Internet Source	<1 %
14	Submitted to Mahidol University Student Paper	<1 %
15	Morita, Maresuke, Naoki Fujita, Ayaka Takahashi, Eun Ryel Nam, Sho Yui, Cheng Shu	<1 %

Chung, Naoya Kawahara, Hsing Yi Lin, Keiko Tsuzuki, Takayuki Nakagawa, and Ryohei Nishimura. "Evaluation of ABCG2 and p63 expression in canine cornea and cultivated corneal epithelial cells", Veterinary Ophthalmology, 2014.
Publication

16	Regenerative Medicine, 2013. Publication	<1 %
17	Submitted to Universiti Sains Malaysia Student Paper	<1 %
18	digitalcommons.unl.edu Internet Source	<1 %
19	www.advrehab.org Internet Source	<1 %
20	www.tandfonline.com Internet Source	<1 %
21	Nicole Haubst, Joachim Berger, Venugopal Radjendirane, Jochen Graw et al. "Molecular dissection of Pax6 function: the specific roles of the paired domain and homeodomain in brain development", Development, 2004 Publication	<1 %
22	epdf.pub Internet Source	<1 %
23	Submitted to University of Westminster	

	Student Paper	<1%
24	www.frontiersin.org Internet Source	<1%
25	www.molbiolcell.org Internet Source	<1%
26	"In Situ Hybridization Protocols", Springer Science and Business Media LLC, 2014 Publication	<1%
27	Dharma Pally, Mallar Banerjee, Shahid Hussain, Rekha V Kumar et al. "Galectin-9 signaling drives breast cancer invasion through matrix", Cold Spring Harbor Laboratory, 2021 Publication	<1%
28	jbiomedsci.biomedcentral.com Internet Source	<1%
29	"Stem Cell Aging: Mechanisms, Consequences, Rejuvenation", Springer Science and Business Media LLC, 2015 Publication	<1%
30	Basavaraj Mallikarjunayya Vastrad, Chanabasayya Mallikarjunayya Vastrad. "Investigation of the underlying hub genes and molexular pathogensis in gastric cancer	<1%

by integrated bioinformatic analyses", Cold Spring Harbor Laboratory, 2020
Publication

31	Melinda K. Duncan, Leike Xie, Larry L. David, Michael L. Robinson, Jennifer R. Taube, Wenwu Cui, Lixing W. Reneker. "Ectopic Pax6 Expression Disturbs Lens Fiber Cell Differentiation", Investigative Opthalmology & Visual Science, 2004 Publication	<1 %
32	Natalia Malek, Aleksandra Michrowska, Ewa Mazurkiewicz, Ewa Mrówczyńska, Paweł Mackiewicz, Antonina J. Mazur. "The origin of the expressed retrotransposed gene ACTBL2 and its influence on human melanoma cells' motility and focal adhesion formation", Scientific Reports, 2021 Publication	<1 %
33	etheses.bham.ac.uk Internet Source	<1 %
34	www.lenus.ie Internet Source	<1 %
35	mafiadoc.com Internet Source	<1 %
36	"Mouse Development", Springer Science and Business Media LLC, 2012 Publication	<1 %

37	Joseph Collin, Rachel Queen, Darin Zerti, Sanja Bojic et al. "A single cell atlas of human cornea that defines its development, limbal stem and progenitor cells and the interactions with the limbal niche", Cold Spring Harbor Laboratory, 2020 Publication	<1 %
38	d-nb.info Internet Source	<1 %
39	doras.dcu.ie Internet Source	<1 %
40	etheses.dur.ac.uk Internet Source	<1 %
41	idoc.pub Internet Source	<1 %
42	repository.kulib.kyoto-u.ac.jp Internet Source	<1 %
43	www.science.gov Internet Source	<1 %
44	Submitted to Indian Institute of Technology, Kharagpure Student Paper	<1 %
45	gyan.iitg.ac.in Internet Source	<1 %
46	www.hindawi.com Internet Source	

		<1 %
47	136.145.180.77:8080 Internet Source	<1 %
48	edoc.ub.uni-muenchen.de Internet Source	<1 %
49	portlandpress.com Internet Source	<1 %
50	sg.inflibnet.ac.in Internet Source	<1 %
51	"Regenerative Medicine: Laboratory to Clinic", Springer Science and Business Media LLC, 2017 Publication	<1 %
52	Ivan Milenkovic, Helaine Graziele Santos Vieira, Morghan C Lucas, Jorge Ruiz-Orera et al. "RPL3L-containing ribosomes modulate mitochondrial activity in the mammalian heart", Cold Spring Harbor Laboratory, 2021 Publication	<1 %
53	cyberleninka.org Internet Source	<1 %
54	elib.uni-stuttgart.de Internet Source	<1 %
55	www.jbc.org Internet Source	

		<1 %
56	Pharmacology of Ocular Therapeutics, 2016. Publication	<1 %
57	Philip J. Gage, Min Qian, Dianqing Wu, Kevin I. Rosenberg. "The canonical Wnt signaling antagonist DKK2 is an essential effector of PITX2 function during normal eye development", Developmental Biology, 2008 Publication	<1 %
58	krishikosh.egranth.ac.in Internet Source	<1 %
59	www.spandidos-publications.com Internet Source	<1 %
60	Methods in Molecular Biology, 2016. Publication	<1 %
61	W.W.-Y. Kao, C.-Y. Liu, H. Liu. "Knock-Out Mice Models: Cornea, Conjunctiva, Eyelids and Lacrimal Gland", Elsevier BV, 2010 Publication	<1 %
62	shodhganga.inflibnet.ac.in Internet Source	<1 %
63	Ji Yao Zhang, Xia Qin, Hui Gyu Park, Ellen Kim, Guowen Liu, Kumar S. D. Kothapalli, J. Thomas Brenna. "Alternative splicing generates novel	<1 %

Fads3 transcript in mice", Molecular Biology Reports, 2016
Publication

64	W Li, Y-T Chen, Y Hayashida, G Blanco, A Kheirkah, H He, S-Y Chen, C-Y Liu, SCG Tseng. "Down-regulation ofPax6 is associated with abnormal differentiation of corneal epithelial cells in severe ocular surface diseases", The Journal of Pathology, 2008 Publication	<1 %
65	ies.ijo.cn Internet Source	<1 %
66	Anil Tiwari, Sudha Swamynathan, Gregory Campbell, Vishal Jhanji, Shivalingappa K. Swamynathan. "BMP6 Regulates Corneal Epithelial Cell Stratification by Coordinating Their Proliferation and Differentiation and Is Upregulated in Pterygium", Investigative Opthalmology & Visual Science, 2020 Publication	<1 %
67	Clémence Bonnet, Sheyla González, JoAnn S. Roberts, Sarah Y.T. Robertson, Maxime Ruiz, Jie Zheng, Sophie X. Deng. "Human limbal epithelial stem cell regulation, bioengineering and function", Progress in Retinal and Eye Research, 2021 Publication	<1 %

68	Solomon S Merepa, Suzanne Broadgate, Sumathi Sekaran, Stephanie Halford. "Genetics of the Retinal Dystrophies", Wiley, 2018 Publication	<1 %
69	Yasuhiro Noda, Miruto Tanaka, Shinsuke Nakamura, Junko Ito, Akiyoshi Kakita, Hideaki Hara, Masamitsu Shimazawa. "Identification of VGF nerve growth factor inducible-producing cells in human spinal cords and expression change in patients with amyotrophic lateral sclerosis", International Journal of Medical Sciences, 2020 Publication	<1 %
70	kclpure.kcl.ac.uk Internet Source	<1 %
71	www.thno.org Internet Source	<1 %
72	Gang Li, Junyu Liu, Yingying Wang, Kun Yang, Manzhu Zhao, Yong Xiao, Xiujie Wen, Luchuan Liu. "LNGFR targets the Wnt/β-catenin pathway and promotes the osteogenic differentiation in rat ectomesenchymal stem cells", Scientific Reports, 2017 Publication	<1 %
73	Zheng Wang, Aritoshi Iida, Noriko Miyake, Koji M. Nishiguchi et al. "Axial	<1 %

	Spondylometaphyseal Dysplasia Is Caused by C21orf2 Mutations", PLOS ONE, 2016 Publication	
74	etd.ncsi.iisc.ernet.in Internet Source	<1 %
75	www.biorxiv.org Internet Source	<1 %
76	www.jneurosci.org Internet Source	<1 %
77	"Pathology of the Head and Neck", Springer Science and Business Media LLC, 2016 Publication	<1 %
78	Praveen Joseph Susaimanickam, Savitri Maddileti, Vinay Kumar Pulimamidi, Sreedhar Rao Boyinpally et al. "Generating minicorneal organoids from human induced pluripotent stem cells", Development, 2017 Publication	<1 %
79	Submitted to University College London Student Paper	<1 %
80	Wenkuan Xin, Tuan M. Tran, Wito Richter, Richard B. Clark, Thomas C. Rich. "Roles of GRK and PDE4 Activities in the Regulation of β2 Adrenergic Signaling", The Journal of General Physiology, 2008 Publication	<1 %

81	backend.orbit.dtu.dk Internet Source	<1 %
82	e-sciencecentral.org Internet Source	<1 %
83	worldwidescience.org Internet Source	<1 %
84	"Guidelines for Molecular Analysis in Archive Tissues", Springer Science and Business Media LLC, 2011 Publication	<1 %
85	Anandi Bhattacharya, Chih-Yu Chen, Sara Ho, Jennifer A. Mitchell. "Upstream Distal Regulatory Elements Contact the Lmo2 Promoter in Mouse Erythroid Cells", PLoS ONE, 2012 Publication	<1 %
86	Emily M. Dong, W. Ted Allison. " Vertebrate features revealed in the rudimentary eye of the Pacific hagfish ( ) ", Cold Spring Harbor Laboratory, 2020 Publication	<1 %
87	Konduri Ranjith, Kotakonda Arunasri, Gundlapally Sathyanarayana Reddy, HariKrishna Adicherla, Savitri Sharma, Sisinthy Shivaji. "Global gene expression in Escherichia coli, isolated from the diseased ocular surface	<1 %

	of the human eye with a potential to form biofilm", Gut Pathogens, 2017 Publication	
88	V. Oron-Karni, C. Farhy, M. Elgart, T. Marquardt, L. Remizova, O. Yaron, Q. Xie, A. Cvekl, R. Ashery-Padan. "Dual requirement for Pax6 in retinal progenitor cells", Development, 2008 Publication	<1 %
89	Yuki Kobayashi, Ryuhei Hayashi, Shun Shibata, Andrew J. Quantock, Kohji Nishida. "Ocular Surface Ectoderm Instigated by WNT inhibition and BMP4", Stem Cell Research, 2020 Publication	<1 %
90	igmlnet.uohyd.ac.in:8000 Internet Source	<1 %
91	insights.ovid.com Internet Source	<1 %
92	journals.physiology.org Internet Source	<1 %
93	jvi.asm.org Internet Source	<1 %
94	"OCT and Imaging in Central Nervous System Diseases", Springer Science and Business Media LLC, 2020 Publication	<1 %

95	Cecília G. Magalhães, Maraysa de Oliveira-Melo, C. Y. Irene Yan. "Morphogenesis of the lens placode", The International Journal of Developmental Biology, 2020 Publication	<1 %
96	Submitted to Chonnam National University Student Paper	<1 %
97	M BOULTON. "Stem cells in the eye", Principles of Tissue Engineering, 2007 Publication	<1 %
98	Rebecca M Beiter, Hannah E Ennerfelt, Courtney Rivet-Noor, Andrea Merchak et al. "Oligomeric amyloid beta prevents myelination in a clusterin-dependent manner", Cold Spring Harbor Laboratory, 2022 Publication	<1 %
99	Yury Kiselev, Tonje Engevik Eriksen, Siri Forsdahl, Lan Huong Thi Nguyen, Ingvild Mikkola. "3T3 Cell Lines Stably Expressing Pax6 or Pax6(5a) – A New Tool Used for Identification of Common and Isoform Specific Target Genes", PLoS ONE, 2012 Publication	<1 %
100	dc.uthsc.edu Internet Source	<1 %
101	onlinelibrary.wiley.com Internet Source	

		<1%
102	sjtrem.biomedcentral.com Internet Source	<1%
103	www.dovepress.com Internet Source	<1%
104	www.freepatentsonline.com Internet Source	<1%
105	A. Chantry. "The MH1 domain of Smad3 interacts with Pax6 and represses autoregulation of the Pax6 P1 promoter", Nucleic Acids Research, 01/26/2007 Publication	<1%
106	Claire L. Salzer, Justin P. Kumar. "Position dependent responses to discontinuities in the retinal determination network", Developmental Biology, 2009 Publication	<1%
107	N. Azuma. "The Pax6 isoform bearing an alternative spliced exon promotes the development of the neural retinal structure", Human Molecular Genetics, 01/27/2005 Publication	<1%
108	Sajjad Ahmad, Charles Osei-Bempong, Reza Dana, Ula Jurkunas. "The culture and	<1%

transplantation of human limbal stem cells", Journal of Cellular Physiology, 2010
Publication

109	Yuzuru Sasamoto, Ryuhei Hayashi, Sung-Joon Park, Mihoko Saito-Adachi et al. "PAX6 Isoforms, along with Reprogramming Factors, Differentially Regulate the Induction of Cornea-specific Genes", Scientific Reports, 2016 Publication	<1 %
110	documents.mx Internet Source	<1 %
111	journals.biologists.com Internet Source	<1 %
112	livrepository.liverpool.ac.uk Internet Source	<1 %
113	zfin.org Internet Source	<1 %
114	Babaei, Fatemeh, Tony Liu Chi Hong, Kelvin Yeung, Shuk Han Cheng, and Yun Wah Lam. "Contrast-Enhanced X-ray Micro-Computed Tomography as a Versatile Method for Anatomical Studies of Adult Zebrafish", Zebrafish, 2016. Publication	<1 %
115	Cristian Ferri, Michele Bianchini, Gustavo Icardi, Carolina Belli, Raquel Bengió, Irene	<1 %

Larripa. " Early detection and quantification of mutations in the tyrosine kinase domain of chimerical gene combining high-resolution melting analysis and mutant-allele specific quantitative polymerase chain reaction ", Leukemia & Lymphoma, 2012
Publication

116	Submitted to EDMC Student Paper	<1 %
117	S. Singh, R. Mishra, N. A. Arango, J. M. Deng, R. R. Behringer, G. F. Saunders. "Iris hypoplasia in mice that lack the alternatively spliced Pax6(5a) isoform", Proceedings of the National Academy of Sciences, 2002 Publication	<1 %
118	Submitted to University of Venda Student Paper	<1 %
119	ajprenal.physiology.org Internet Source	<1 %
120	digital.library.unt.edu Internet Source	<1 %
121	intl.jbc.org Internet Source	<1 %
122	ir.vanderbilt.edu Internet Source	<1 %
123	lipidworld.biomedcentral.com	

Internet Source

<1%

124	theses.ncl.ac.uk Internet Source	<1%
125	www.plantcell.org Internet Source	<1%
126	Chew-Li Soh. "Epithelial Stem Cells and the Development of the Thymus, Parathyroid, and Skin", Regulatory Networks in Stem Cells, 2009 Publication	<1%
127	Gina L. Griffith, Anne Kasus-Jacobi, H. Anne Pereira. "Bioactive Antimicrobial Peptides as Therapeutics for Corneal Wounds and Infections", Advances in Wound Care, 2017 Publication	<1%
128	K. Harada, A. B. Truong, T. Cai, P. A. Khavari. "The Class II Phosphoinositide 3-Kinase C2 Is Not Essential for Epidermal Differentiation", Molecular and Cellular Biology, 2005 Publication	<1%
129	Submitted to University of Auckland Student Paper	<1%
130	Submitted to University of Glasgow Student Paper	<1%
131	www.jove.com	

Internet Source

<1%

132 "News and Comment", Archives of Ophthalmology, 1989.
Publication

<1%

133 Balu Venugopal, Bernadette K. Madathil, Anil Kumar P.R.. "Stem cell–based therapeutic approaches toward corneal regeneration", Elsevier BV, 2020
Publication

<1%

134 Chen, Y.. "A role for Wnt/planar cell polarity signaling during lens fiber cell differentiation?", Seminars in Cell and Developmental Biology, 200612
Publication

<1%

135 Submitted to Indiana University
Student Paper

<1%

136 Submitted to Jawaharlal Nehru University (JNU)
Student Paper

<1%

137 La-ongsri Atchaneeyasakul, Adisak Trinavarat, Dhaivadee Dulayajinda, Kornphet Kumpornsin et al. " Novel and De-novo Truncating Mutations and Ocular Phenotypes in Thai Aniridia Patients ", Ophthalmic Genetics, 2009
Publication

<1%

138	Lina Zhang, Giacomo Lanzoni, Matteo Battarra, Luca Inverardi, Qibin Zhang. "Proteomic profiling of human islets collected from frozen pancreata using laser capture microdissection", Journal of Proteomics, 2017 Publication	<1 %
139	Submitted to University of Hong Kong Student Paper	<1 %
140	Submitted to University of Sydney Student Paper	<1 %
141	www.agingcare.com Internet Source	<1 %

Exclude quotes	On	Exclude matches	< 14 words
Exclude bibliography	On		